MICROBIAL SYNTHESIS, GAS-FERMENTATION AND BIOELECTROCONVERSION OF CO_2 AND OTHER GASEOUS STREAMS

EDITED BY: Andrea Schievano, Deepak Pant and Sebastià Puig

PUBLISHED IN: Frontiers in Energy Research and Frontiers in Chemistry

frontiers Research Topics

frontiers

ISSN 1664-8714
ISBN 978-2-88963-262-6
DOI 10.3389/978-2-88963-262-6

About Frontiers

Frontiers is more than just an open-access publisher of scholarly articles: it is a pioneering approach to the world of academia, radically improving the way scholarly research is managed. The grand vision of Frontiers is a world where all people have an equal opportunity to seek, share and generate knowledge. Frontiers provides immediate and permanent online open access to all its publications, but this alone is not enough to realize our grand goals.

Frontiers Journal Series

The Frontiers Journal Series is a multi-tier and interdisciplinary set of open-access, online journals, promising a paradigm shift from the current review, selection and dissemination processes in academic publishing. All Frontiers journals are driven by researchers for researchers; therefore, they constitute a service to the scholarly community. At the same time, the Frontiers Journal Series operates on a revolutionary invention, the tiered publishing system, initially addressing specific communities of scholars, and gradually climbing up to broader public understanding, thus serving the interests of the lay society, too.

Dedication to Quality

Each Frontiers article is a landmark of the highest quality, thanks to genuinely collaborative interactions between authors and review editors, who include some of the world's best academicians. Research must be certified by peers before entering a stream of knowledge that may eventually reach the public - and shape society; therefore, Frontiers only applies the most rigorous and unbiased reviews.
Frontiers revolutionizes research publishing by freely delivering the most outstanding research, evaluated with no bias from both the academic and social point of view. By applying the most advanced information technologies, Frontiers is catapulting scholarly publishing into a new generation.

What are Frontiers Research Topics?

Frontiers Research Topics are very popular trademarks of the Frontiers Journals Series: they are collections of at least ten articles, all centered on a particular subject. With their unique mix of varied contributions from Original Research to Review Articles, Frontiers Research Topics unify the most influential researchers, the latest key findings and historical advances in a hot research area! Find out more on how to host your own Frontiers Research Topic or contribute to one as an author by contacting the Frontiers Editorial Office: researchtopics@frontiersin.org

MICROBIAL SYNTHESIS, GAS-FERMENTATION AND BIOELECTROCONVERSION OF CO_2 AND OTHER GASEOUS STREAMS

Topic Editors:
Andrea Schievano, University of Milan, Italy
Deepak Pant, Flemish Institute for Technological Research (VITO), Belgium
Sebastià Puig, University of Girona, Spain

Citation: Schievano, A., Pant, D., Puig, S., eds. (2019). Microbial Synthesis, Gas-Fermentation and Bioelectroconversion of CO_2 and other Gaseous Streams. Lausanne: Frontiers Media SA. doi: 10.3389/978-2-88963-262-6

Table of Contents

frontiers in Energy Research

EDITORIAL
published: 18 October 2019
doi: 10.3389/fenrg.2019.00110

Editorial: Microbial Synthesis, Gas-Fermentation and Bioelectroconversion of CO_2 and Other Gaseous Streams

Andrea Schievano[1†], *Deepak Pant*[2*†] *and Sebastia Puig*[3†]

[1] e-BioCenter, Department of Environmental Science and Policy, University of Milan, Milan, Italy, [2] Separation and Conversion Technology, Flemish Institute for Technological Research (VITO), Mol, Belgium, [3] LEQUiA, Institute of the Environment, University of Girona, Girona, Spain

Keywords: bioelectrochemical system (BES), microbial electrosynthesis (MES), electrofermentation, gas fermentation, CO_2 fixation, microbial electrochemical technologies (MET), electromethanogenesis, biocathode

OPEN ACCESS

Edited by:
Sachin Kumar, Sardar Swaran Singh National Institute of Renewable Energy, India

Reviewed by:
Sunil A. Patil, Indian Institute of Science Education and Research Mohali, India
Elliot S. Friedman, University of Pennsylvania, United States

***Correspondence:**
Deepak Pant
deepak.pant@vito.be

These authors have contributed equally to this work

Specialty section:
This article was submitted to Bioenergy and Biofuels, a section of the journal Frontiers in Energy Research

Received: *30 July 2019*
Accepted: *26 September 2019*
Published: *18 October 2019*

Citation:
Schievano A, Pant D and Puig S (2019) Editorial: Microbial Synthesis, Gas-Fermentation and Bioelectroconversion of CO_2 and Other Gaseous Streams. Front. Energy Res. 7:110. doi: 10.3389/fenrg.2019.00110

Editorial on the Research Topic

Microbial Synthesis, Gas-Fermentation and Bioelectroconversion of CO_2 and Other Gaseous Streams

INTRODUCTION

The ongoing climate crisis, mainly caused by the emission of greenhouse gases (GHGs), gives rise to an urgent need for solutions to re-convert industrial waste gases and emissions into useful chemicals (Lal, 2005). Concentrated streams of carbon dioxide (CO_2) are continuously generated and emitted by a variety of anthropogenic activities. These include both biogenic sources (e.g., organic waste and wastewater treatment plants, biogas plants, landfills, waste and biomass combustion facilities, etc.) and fossil-carbon sources (e.g., centralized fossil-based energy production facilities, engines, etc.) In recent years, several efforts have been undertaken globally that are directed toward CO_2 capture and converting CO_2 into storable fuels and chemicals (ElMekawy et al., 2016). This conversion can be done via living bacteria as biocatalysts (Rojas et al., 2018a), via enzymes (Chiranjeevi et al., 2019), or electrocatalytically (Gutiérrez Sánchez et al., 2019).

In light of the different possibilities for efficiently utilizing such concentrated CO_2 streams, their dispersion in the atmosphere is a waste of an otherwise potentially valuable resource. In fact, only photosynthetic organisms can utilize CO_2 at atmospheric concentrations (around 400 ppm) (González Del Campo et al., 2013). Plants and photosynthetic microorganisms are known to significantly increase their growth rates under higher CO_2 concentrations (Brown et al., 2019). CO_2 fertilization in microalgae production facilities is widely recognized as a strategy for improving biomass yields and synthesizing a variety of bioproducts and food ingredients (Eustance et al., 2016).

Alternative pathways enabling the utilization of concentrated CO_2 streams to synthesize organic molecules have recently been developed using microorganisms (bacteria and archaea) as catalysts. In gas fermentation, reducing power is provided either within the gaseous stream or in the water solution. In microbial electrochemical technologies (METs), a biocatalyst (i.e., electroactive bacteria) exchanges electrons with an external circuit through a solid electrode.

GAS FERMENTATION

Gas fermentation is a process in which microorganisms can fix CO_2 if sources of reducing power and metabolic energy are available (Liew et al., 2016). Hydrogen (H_2) generated by electrochemical water-splitting is an example of an energy-rich electron carrier that can be utilized in co-fermentation with CO_2. Bio-syngas streams coming from biomass gasification or pyrolysis are mainly rich in H_2, carbon monoxide (CO), methane (CH_4), and CO_2. Their efficient utilization by gas fermentation has already been demonstrated at pilot scale for the production of high-value biocommodities (e.g., succinate, 2,3-butanediol, lactate, and acetone; Marcellin et al., 2016).

BIOELECTROCHEMICAL CO_2 REDUCTION

More recently, METs were proposed as a new strategy for furnishing electrons and metabolic energy for carbon fixation. In microbial electrosynthesis (MES) processes such as electromethanogenesis and electrofermentation, renewable electricity stimulates the metabolism of selected electro-active microbial communities to produce organic molecules [methane, short-chain fatty acids, alcohols, etc. (Kracke and Krömer, 2014; Sharma et al., 2014; Schievano et al., 2016)]. These molecules can undergo further carbon chain-elongation by heterotrophic communities to synthesize higher value biocommodities and biopolymers (Agler et al., 2012; Dennis et al., 2013).

The reduction of CO_2 to organics can occur through direct electron transfer (DET) or through the intermediate production of H_2, which acts as an electron transfer shuttle (as is the case with many acetogenic bacteria (Puig et al., 2017); Wenzel et al.). Until now, the main products of MES have been methane (electromethanogenesis) and acetate (homoacetogenesis), although the yield and product titers are still far from commercial application. During the last 10 years of research, several strategies have aimed at improving MES reactors and their production rates/yields. In the past 2 years, MES has been more intensively studied. Jourdin et al. proved that MES is progressing to becoming a robust clean CO_2 biorecycling process, producing higher-value chemicals at increasing rates while minimizing the cost of electrode materials. Verbeeck et al. presented a reactor setup that allowed the operation of MES reactors at higher current densities. An H_2/CO_2 gas-fermentation column was directly coupled to extraction, allowing pure product recovery in an acidic and clean liquid, achieving simultaneous stabilization of the pH in the fermentation broth.

Another key parameter affecting MES performance is the cathode material itself. Some key-properties are essential for superior cathodic performance: high conductivity, excellent chemical stability, high mechanical strength, good biocompatibility, high surface area, and low cost (Aryal et al., 2017). Aryal et al. reported the fabrication of a cathode coated with highly conductive polystyrene sulfonate polymer for acetate production in MES. This coating allowed increased acetate production while optimizing current consumption. The biofilm of *S. ovata* showed increased biomass presence as compared with the plain carbon cloth surface. Another strategy is the use of granular activated carbon (GAC) and graphite granules (GG) in a packed bed as the cathode electrode. Liu et al. showed that both GAC and GG are suitable cathode materials for high methane production rates in methane-producing MESs.

Gas diffusion electrodes (GDEs) have also represented a breakthrough in the current state of the art of MES. Srikanth et al. (2018) evaluated the impact of GDEs in enhancing CO_2 bioavailability for its transformation to C4-organics, especially to alcohols using selective mixed culture. A more stable current density was observed with GDE vs. submerged experiments, which significantly varied with pH and respective CO_2 solubility. An interesting synergy between METs and syngas fermentation is that the bio-char resulting from biomass pyrolysis can have interesting properties for the fabrication of bio-electrodes, such as electrical conductivity and a high surface area for microbial biofilm growth (Marzorati et al., 2018; Prado et al., 2019).

The chemical energy stored in the products of MES can be seen as a potential store of renewable energy surpluses (Schievano et al., 2018). However, solar and wind energy are typically characterized by a fluctuating regime, and this may represent a threat to microbial communities in MES biocathodes that rely on continuous polarization. Mateos et al. (2020) recently showed how MES could be resilient to long-term power interruptions (6 weeks). In the same line, Rojas et al. (2018b) demonstrated that the electro-autotrophic activity of an MES system could recover after power shortages, restoring acetic acid production while recovering sufficient electron transfer at current densities of -25 A m^{-2}.

CURRENT STATE OF ART (TOWARD UPSCALING AND INDUSTRIALIZATION)

In recent years, several developments have taken place to upscale the microbial gaseous conversion technologies, and both governments and industry have taken a lead in supporting such initiatives. One of the leaders in this field is the USA-based company LanzaTech, which has made rapid strides in syngas fermentation, with several demonstration plants operating globally (LanzaTech, 2019). Their core technology is based on the acetogen *Clostridium autoethanogenum*, with an estimated volumetric productivity of around 10 g l^{-1} h^{-1} (Takors et al., 2018). Within Europe, LanzaTech is involved in the Steelanol project funded by the European Commission, which aims at building a demonstrator for ethanol production at the Arcelor Mittal steel mill in Ghent to convert the gases produced during the steel production process by using fermentation by microbes that secrete ethanol (Steelanol, 2019). The plant is expected to have a capacity of 62,000 t/a (Carus et al., 2019). Their other operations are in China, India, and South Africa.

Upgrading of biogas by converting the CO_2 fraction of the biogas into gas-grid quality methane is also gaining significant momentum, and several pilot and industrial initiatives are currently being undertaken (Aryal et al., 2018). One of the main

players in this field is the Germany-based company Electrochaea, which recently announced the commissioning of a power-to-gas demonstration facility in Foulum, Denmark, based on a 10,000-liter bioreactor (Electrochaea, 2018).

Besides these industrial applications, research on this topic is also gaining momentum, and within Europe, several projects at different technology readiness levels (TRL) are being supported by the European Commission. One of these projects is BioRECO2VER, which aims at refining biotechnological processes that can turn CO_2 from industrial point sources into valuable platform chemicals such as lactate and isobutene (http://bioreco2ver.eu/). Another recently started project, Bac-To-Fuel, is developing a process to transform CO_2/H_2 into fuels by mimicking the photosynthetic process of plants. This approach uses novel inorganic photocatalysts that are capable of evolving H_2 from photocatalytic water splitting in the presence of sunlight and enhanced bacterial strains to convert CO_2 and the renewable hydrogen into biofuels (i.e., ethanol and butanol) in a novel electro-biocatalytic cell (http://bactofuel.eu/). The CelbiCon project, also funded by the European Commission under the H2020 program, attempts to combine CO_2 capture and electrochemical and biochemical conversion technologies for CO_2 conversion into chemicals (http://www.celbicon.org/). Yet another recent project on this topic is BIOCON-CO_2, which is developing biological processes to transform raw waste CO_2 from the iron, steel, cement, and electric power industries into value-added chemicals and plastics (https://biocon-co2.eu/). The above-mentioned projects are only representative examples of the research projects that are currently going on in the EU. There are several other initiatives being undertaken globally to harvest the potential of microorganisms in converting gaseous feedstocks into valuable chemicals.

CONCLUSIONS

To summarize, microbial conversion of waste gases, industrial off-gases, and CO_2-rich streams is gaining momentum, with interest coming from the industrial users, governments giving support, and researchers working toward upscaling these systems. A multidisciplinary approach is needed to develop new metabolic pathways and to optimize existing processes. Synthetic biology and microbial community selection should play a major role in constructing strains or communities for commercial operations. Metatranscriptomics, metabolomics, and proteomics, as well as metabolic engineering, are fundamental tools to understand and enhance microbial catalysis. Moreover, bioreactor engineering and material science are crucial for studying scalable process architectures and for optimizing microbial biofilm growth, gas solubilization, and product recovery.

This broad range of disciplines is also represented in the papers appearing on this Research Topic, which contribute toward advancing the basic research while moving to the next level of practical implementation. Theoretical and perspective insights into several possible metabolic pathways (Averesch and Kracke) and thermodynamic considerations (Scheller) have been presented regarding methane oxidation (and that of other alkanes) and toward the production of liquid biofuels or electricity. Also, fundamental experiments are being carried out, dealing with biofilm formation, microbial community structure on bioelectrodes (Jourdin et al.), and electrode materials optimization (Aryal et al., 2018; Liu et al.).

Innovative approaches are also being taken to biological CO_2 conversion, including an interesting experiment on the use of purple phototrophic bacteria for simultaneous bio-H_2 generation and carbon fixation (Vasiliadou et al.) and a mini-review on possible biocathodic CO_2-fixation pathways and applications by sulfate-reducing electroautotrophs (Agostino and Rosenbaum). Finally, practical approaches toward different configurations of reactors and process design have been reported (Ishii et al.; Lim et al.; Verbeeck et al.).

AUTHOR CONTRIBUTIONS

All authors listed have made a substantial, direct and intellectual contribution to the work, and approved it for publication.

FUNDING

AS was selected as the PI by the SIR 2014 Grant (PROJECT RBSI14JKU3—2015–2019), Italian Ministry of University and Research (MIUR). SP was a Serra Húnter Fellow (UdG-AG-575). LEQUiA has been recognized as a consolidated research group by the Generalitat de Catalunya (2017SGR-1552). DP was working on bacterial conversion of CO_2 and hydrogen into fuels in the project BAC-TO-FUEL funded by the European Union's Horizon 2020 Research and Innovation Program under Grant Agreement no. 825999.

REFERENCES

Agler, M. T., Spirito, C. M., Usack, J. G., Werner, J. J., and Angenent, L. T. (2012). Chain elongation with reactor microbiomes: upgrading dilute ethanol to medium-chain carboxylates. *Energy Environ. Sci.* 5, 8189–8192. doi: 10.1039/c2ee22101b

Aryal, N., Ammam, F., Patil, S. A., and Pant, D. (2017). An overview of cathode materials for microbial electrosynthesis of chemicals from carbon dioxide. *Green Chem.* 19, 5748–5760. doi: 10.1039/C7GC01801K

Aryal, N., Kvist, T., Ammam, F., Pant, D., and Ottosen, L. D. (2018). An overview of microbial biogas enrichment. *Bioresour. Technol.* 264, 359–369. doi: 10.1016/j.biortech.2018.06.013

Brown, T. W., Lajeunesse, M. J., and Scott, K. M. (2019). Strong effects of elevated CO_2 on freshwater microalgae and ecosystem chemistry. *Limnol. Oceanogr.* doi: 10.1002/lno.11298. [Epub ahead of print].

Carus, M., Skoczinski, P., Dammer, L., vom Berg, C., Raschka, A., and Breitmayer, E. (2019). *Hitchhiker's Guide to Carbon Capture and Utilisation*. Hürth 2019-02. Available online at: http://news.bio-based.eu/hitchhikers-guide-to-carbon-capture-utilisation/ (accessed August 30, 2019).

Chiranjeevi, P., Bulut, M., Breugelmans, T., Patil, S. A., and Pant, D. (2019). Current trends in enzymatic electrosynthesis for CO_2 reduction. *Curr. Opin. Green Sustain. Chem.* 16, 65–70. doi: 10.1016/j.cogsc.2019.02.007

Dennis, P. G., Harnisch, F., Yeoh, Y. K., Tyson, G. W., and Rabaey, K. (2013). Dynamics of cathode-associated microbial communities and metabolite

profiles in a glycerol-fed bioelectrochemical system. *Appl. Environ. Microbiol.* 79, 4008–4014. doi: 10.1128/AEM.00569-13

Electrochaea (2018). *Electrochaea Commissions World's Largest Power-to-Gas Demonstration Project*. Available online at: http://www.electrochaea.com/electrochaea-commissions-worlds-largest-power-to-gas-demonstration-project-based-on-biological-methanation/ (accessed August 30, 2019).

ElMekawy, A., Hegab, H. M., Mohanakrishna, G., Elbaz, A. F., Bulut, M., and Pant, D. (2016). Technological advances in CO_2 conversion electro-biorefinery: a step toward commercialization. *Bioresour. Technol.* 215, 357–370. doi: 10.1016/j.biortech.2016.03.023

Eustance, E. T., Wray, J., Badvipour, S. R., and Sommerfeld, M. (2016). Volatile nutrients - improving utilization of ammonia and carbon dioxide in microalgal cultivation: a review. *Curr. Biotechnol.* 5, 130–141. doi: 10.2174/2211550105666160120000606

González Del Campo, A., Cañizares, P., Rodrigo, M. A., Fernández, F. J., and Lobato, J. (2013). Microbial fuel cell with an algae-assisted cathode: a preliminary assessment. *J. Power Sour.* 242, 638–645. doi: 10.1016/j.jpowsour.2013.05.110

Gutiérrez Sánchez, O., Birdja, Y. Y., Bulut, M., Vaes, J., Breugelmans, T., and Pant, D. (2019). Recent advances in industrial CO_2 electroreduction. *Curr. Opin. Green Sustain. Chem.* 16, 47–56. doi: 10.1016/j.cogsc.2019.01.005

Kracke, F., and Krömer, J. O. (2014). Identifying target processes for microbial electrosynthesis by elementary mode analysis. *BMC Bioinformatics* 15:410. doi: 10.1186/s12859-014-0410-2

Lal, R. (2005). World crop residues production and implications of its use as a biofuel. *Environ. Int.* 31, 575–584. doi: 10.1016/j.envint.2004.09.005

LanzaTech (2019). Available online at: http://www.lanzatech.com/innovation/technical-overview/ (accessed August 30, 2019).

Liew, F., Martin, E., Tappel, R., Heijstra, B., Mihalcea, C., and Köpke, M. (2016). Gas fermentation – a flexible platform for commercial scale production of low carbon fuels and chemicals from waste and renewable feedstocks. *Front. Microbiol.* 7:694. doi: 10.3389/fmicb.2016.00694J

Marcellin, E., Behrendorff, J. B., Nagaraju, S., DeTissera, S., Segovia, S., Palfreyman, R., et al. (2016). Low carbon fuels and commodity chemicals from waste gases – Systematic approach to understand energy metabolism in a model acetogen. *Green Chem.* 18, 3020–3028. doi: 10.1039/C5GC02708

Marzorati, S., Goglio, A., Fest-Santini, S., Mombelli, D., Villa, F., Cristiani, P., et al. (2018). Air-breathing bio-cathodes based on electro-active biochar from pyrolysis of Giant Cane stalks. *Int. J. Hydrogen Energy*. 44, 4496–4507. doi: 10.1016/J.IJHYDENE.2018.07.167

Mateos, R., Escapa, A., San-Martín, M. I., De Wever, H., Sotres, A., and Pant, D. (2020). Long-term open circuit microbial electrosynthesis system promotes methanogenesis. *Journal of Energy Chemistry*, 41, 3–6.

Prado, A., Berenguer, R., and Esteve-Núñez, A. (2019). Electroactive biochar outperforms highly conductive carbon materials for biodegrading pollutants by enhancing microbial extracellular electron transfer. *Carbon* 146, 597–609. doi: 10.1016/J.CARBON.2019.02.03

Puig, S., Ganigu,é, R., Batlle-Vilanova, P., Balaguer, M. D., Bañeras, L., and Colprim, J. (2017). Tracking bio-hydrogen-mediated production of commodity chemicals from carbon dioxide and renewable electricity. *Bioresour. Technol.* 228, 201–209. doi: 10.1016/j.biortech.2016.12.035

Rojas, M. D. P. A., Mateos, R., Sotres, A., Zaiat, M., Gonzalez, E. R., Escapa, A., et al. (2018b). Microbial electrosynthesis (MES) from CO_2 is resilient to fluctuations in renewable energy supply. *Energy Conver. Manage.* 177, 272–279. doi: 10.1016/j.enconman.2018.09.064

Rojas, M. D. P. A., Zaiat, M., Gonzalez, E. R., De Wever, H., and Pant, D. (2018a). Effect of the electric supply interruption on a microbial electrosynthesis system converting inorganic carbon into acetate. *Bioresour. Technol.* 266, 203–210. doi: 10.1016/j.biortech.2018.06.074

Schievano, A., Goglio, A., Erckert, C., Marzorati, S., Rago, L., and Cristiani, P. (2018). Organic waste and bioelectrochemical systems: a future interface between electricity and methane distribution grids. *Detritus* 1, 57–63. doi: 10.26403/detritus/2018.6

Schievano, A., Sciarria, T. P., Vanbroekhoven, K., De Wever, H., Puig, S., Andersen, S. J., et al. (2016). Electro-fermentation–merging electrochemistry with fermentation in industrial applications. *Trends Biotechnol.* 34, 866–878. doi: 10.1016/j.tibtech.2016.04.007

Sharma, M., Bajracharya, S., Gildemyn, S., Patil, S. A., Alvarez-Gallego, Y., Pant, D., et al. (2014). A critical revisit of the key parameters used to describe microbial electrochemical systems. *Electrochim. Acta* 140, 191–208. doi: 10.1016/j.electacta.2014.02.111

Srikanth, S., Singh, D., Vanbroekhoven, K., Pant, D., Kumar, M., Puri, S. K., et al. (2018). Electro-biocatalytic conversion of carbon dioxide to alcohols using gas diffusion electrode. *Bioresour. Technol.* 265, 45–51. doi: 10.1016/j.biortech.2018.02.058

Steelanol (2019). Available online at: http://www.steelanol.eu/en (accessed August 30, 2019).

Takors, R., Kopf, M., Mampel, J., Bluemke, W., Blombach, B., Eikmanns, B., et al. (2018). Using gas mixtures of CO, CO_2 and H_2 as microbial substrates: the do's and don'ts of successful technology transfer from laboratory to production scale. *Microb. Biotechnol.* 11, 606–625. doi: 10.1111/1751-7915.13270

Conflict of Interest: The authors declare that the research was conducted in the absence of any commercial or financial relationships that could be construed as a potential conflict of interest.

The reviewer SP declared a past co-authorship with one of the authors DP to the handling editor.

frontiers in Energy Research

ORIGINAL RESEARCH
published: 01 March 2018
doi: 10.3389/fenrg.2018.00007

Critical Biofilm Growth throughout Unmodified Carbon Felts Allows Continuous Bioelectrochemical Chain Elongation from CO_2 up to Caproate at High Current Density

Ludovic Jourdin[1,2], Sanne M. T. Raes[1], Cees J. N. Buisman[1] and David P. B. T. B. Strik[1]**

[1] *Sub-Department of Environmental Technology, Wageningen University and Research, Wageningen, Netherlands,*
[2] *Advanced Water Management Centre, University of Queensland, Brisbane, QLD, Australia*

Current challenges for microbial electrosynthesis include the production of higher value chemicals than acetate, at high rates, using cheap electrode materials. We demonstrate here the continuous, biofilm-driven production of acetate (C2), *n*-butyrate (nC4), and *n*-caproate (nC6) from sole CO_2 on unmodified carbon felt electrodes. No other organics were detected. This is the first quantified continuous demonstration of *n*-caproate production from CO_2 using an electrode as sole electron donor. During continuous nutrients supply mode, a thick biofilm was developed covering the whole thickness of the felt (1.2-cm deep), which coincided with high current densities and organics production rates. Current density reached up to −14 kA $m^{-3}_{electrode}$ (−175 A m^{-2}). Maximum sustained production rates of 9.8 ± 0.65 g L^{-1} day^{-1} C2, 3.2 ± 0.1 g L^{-1} day^{-1} nC4, and 0.95 ± 0.05 g L^{-1} day^{-1} nC6 were achieved (averaged between duplicates), at electron recoveries of 60–100%. Scanning electron micrographs revealed a morphologically highly diverse biofilm with long filamentous microorganism assemblies (~400 μm). *n*-Caproate is a valuable chemical for various industrial application, e.g., it can be used as feed additives or serve as precursor for liquid biofuels production.

Keywords: bioelectrochemical chain elongation, microbial electrosynthesis, carbon dioxide utilization, biofilm, caproate, biocatalysis

OPEN ACCESS

Edited by:
Sebastià Puig,
University of Girona, Spain

Reviewed by:
Pascal E. Saikaly,
King Abdullah University of Science and Technology, Saudi Arabia
Mohanakrishna Gunda,
Flemish Institute for Technological Research (VITO), Belgium

****Correspondence:***
Ludovic Jourdin
ludovic.jourdin@wur.nl;
David P. B. T. B. Strik
david.strik@wur.nl

Specialty section:
This article was submitted to Bioenergy and Biofuels, a section of the journal Frontiers in Energy Research

Received: *15 December 2017*
Accepted: *14 February 2018*
Published: *01 March 2018*

Citation:
Jourdin L, Raes SMT, Buisman CJN and Strik DPBTB (2018) Critical Biofilm Growth throughout Unmodified Carbon Felts Allows Continuous Bioelectrochemical Chain Elongation from CO_2 up to Caproate at High Current Density. Front. Energy Res. 6:7. doi: 10.3389/fenrg.2018.00007

INTRODUCTION

The envisioned circular economy is depending on efficient raw materials (re)use without any harmful emissions into the environment (Sharon and Kamp, 2016). Water is already a scarce good while four billion people face severe water shortage at least 1 month per year (Mekonnen and Hoekstra, 2016). Evidently clean recycling technologies must be developed that are efficient in usage of water, nutrients, and carbon. Carbon building blocks can be recycled from biomass residues, organic wastes, and CO_2 sources. Microbial electrosynthesis is an emerging clean technology in which CO_2 can be converted into biochemicals like acetate, with an electrode as sole direct electron source (Rabaey and Rozendal, 2010). MES uses minimal amounts of water and naturally occurring microorganisms as cheap, robust, and self-repairing catalysts.

To date, mainly acetate or methane has been produced in MESs from CO_2. Other products such as *n*-butyrate, propionate, ethanol, butanol, and isopropanol were also produced in relatively small amounts and rates in MESs from CO_2 (Ganigue et al., 2015; Arends et al., 2017; Batlle-Vilanova

et al., 2017; LaBelle and May, 2017). *n*-Caproate formation in MES occurred incidental (at concentration of 0.739 g L^{-1}) from acetate (Van Eerten-Jansen et al., 2013) or was reported as a non-quantified trace compound (Sharma et al., 2013; Batlle-Vilanova et al., 2017). As such *n*-caproate formation in MES is principally feasible; though a continuous quantified production was never reported. Medium-chain fatty acids (MCFAs) like *n*-caproate can become important platform chemical while they can be used as feed additives after extraction or further converted into other products such as liquid biofuels, plastics, and lubricants (Agler et al., 2011). Once these latter products would reach their end-of-life time, they can conceptually be recycled by, e.g., incineration or digestion into methane which will release CO_2 that can be re-used as building block for the same products. We define the latter CO_2 as "circular CO_2."

Recently, Jourdin and co-workers developed novel electrodes which led to the highest acetate production rates to date when normalized to electrode dimension (Jourdin et al., 2014, 2015a,b, 2016a,b). These MES systems converted electrons and CO_2 into acetate at high rates, up to 133 kg $m^{-3}_{electrode}$ day^{-1} (Jourdin et al., 2015b, 2016a). It was shown that a well-developed biofilm over the whole surface of the electrode was an important prerequisite for a productive biocathode. The use of electrodes without a biofilm but relying on bacteria in suspension has achieved lower rates (Blanchet et al., 2015). Recently, LaBelle and May (2017) enhanced acetate volumetric productivity up to 18.7 g L^{-1} day^{-1} (when normalizing to catholyte volume) by optimizing the cathode to catholyte volume ratio (LaBelle and May, 2017).

An opportunity for practical implementation of MES is to produce continuously longer carbon-chain (>C2) organic compounds like *n*-caproate from CO_2 which have higher values than acetate (Jourdin and Strik, 2017; LaBelle and May, 2017). To date, MCFA production has been achieved by chain elongation fermentation with open cultures (i.e., reactor microbiome) or pure cultures, using organics as both electron and carbon sources (Angenent et al., 2016). Typically, acetate is fermentative elongated to MCFAs using ethanol (Grootscholten et al., 2013a), lactate (Kucek et al., 2016a), or methanol (Chen et al., 2016) as electron donor. A life cycle assessment on an ethanol and food waste chain elongation biorefinery process showed that the use of ethanol had a dominant impact on the environmental performance; specifically on the global warming potential, acidification potential, and eutrophication potential (Chen et al., 2017). Using electricity (i.e., MES coupled to solar or wind power) may present several advantages over supplying organics as electron donor, e.g., no biomass or (bio)waste source is needed and water is saved, of which huge amount is required during agricultural processes to produce, e.g., ethanol (Raes et al., 2017).

The focus of the present study was to investigate the feasibility of (i) elongating CO_2 to *n*-caproate with an electrode as sole electron source and (ii) reaching continuous production at high rates using a cheap commercially available electrode material. Accordingly, we report on the development of a microbial electrosynthesis process achieving elongation of CO_2 (sole carbon source) to *n*-butyrate (nC4) and *n*-caproate (nC6), using an electrode as electron donor and a carbon felt cathode with a densely populated multispecies microbiome as catalyst. For this study, duplicate bioelectrochemical reactors were operated in batch and consequently continuous nutrient supply mode. Bioelectrochemical performance and scanning electron microscopy (SEM) were applied to analyze the results.

RESULTS AND DISCUSSION

The results shown in **Figures 2–4** below were obtained from one of the two reactors. The results obtained on the duplicate reactor followed the same trends as discussed below, and are shown in the supporting information, as well as in **Figure 5**. Relevant reactor performance values are summarized in Table S1 in Supplementary Material for both reactors, normalized to projected surface area (psa) of the electrode, electrode volume, as well as to the catholyte volume in the cathode chamber. These ways of normalization have been extensively discussed previously (Patil et al., 2015b; Jourdin and Strik, 2017).

Continuous Supply of Nutrients Allowed for the Development of a Thick, Uniform, and Electroactive Biofilm throughout Unmodified Carbon Felt Electrode

During the first 133 days, while the reactors were operated in fed-batch mode, biofilm development was visually observed only on the carbon felt surface facing the membrane (Figures S1A–C in Supplementary Material). Within the first few days after the continuous nutrients supply started, biofilm growth could be observed with naked-eyes on the opposite side of the carbon felt (side not facing the membrane) as well as throughout the felt (Figures S1D–H in Supplementary Material). The continuous supply of nutrients supported the growth of a thick biofilm, which was seemingly more effective than adding nutrients in a fed-batch manner every 3–4 days. Macronutrients (N, P, C) were measured not to be limiting during the fed-batch period (data not shown). Micronutrients may have become limiting during this period, though 65% of the catholyte was replaced with fresh medium at day 50, which did not lead to an increase of biofilm coverage and electron uptake (see below). Further investigation into optimal nutrient requirement will be needed.

Scanning electron microscopy performed at the end of the experiment confirmed that the whole surface of the sampled carbon felt, on both sides was covered with a thick and uniform biofilm (**Figures 1A,B**). Figures S2A–E in Supplementary Material shows images of all locations. It can be observed that not only the fibers of the carbon felt were covered with biofilm but also the macro-pores between carbon fibers, bridging gaps of over several 100 micrometers. It raises the question as to how the electrons were transferred over such long distance, i.e., microorganisms far away from the supply source of electrons, namely the electrode surface, need to take up electrons to function. Furthermore, we observed that the biofilm was developed throughout the whole thickness of the carbon felt (1.2 cm; **Figures 1C–H**), with individual carbon fibres at different depths from the surface covered with biofilm, as well as their interspace (see Figures S2F–H in

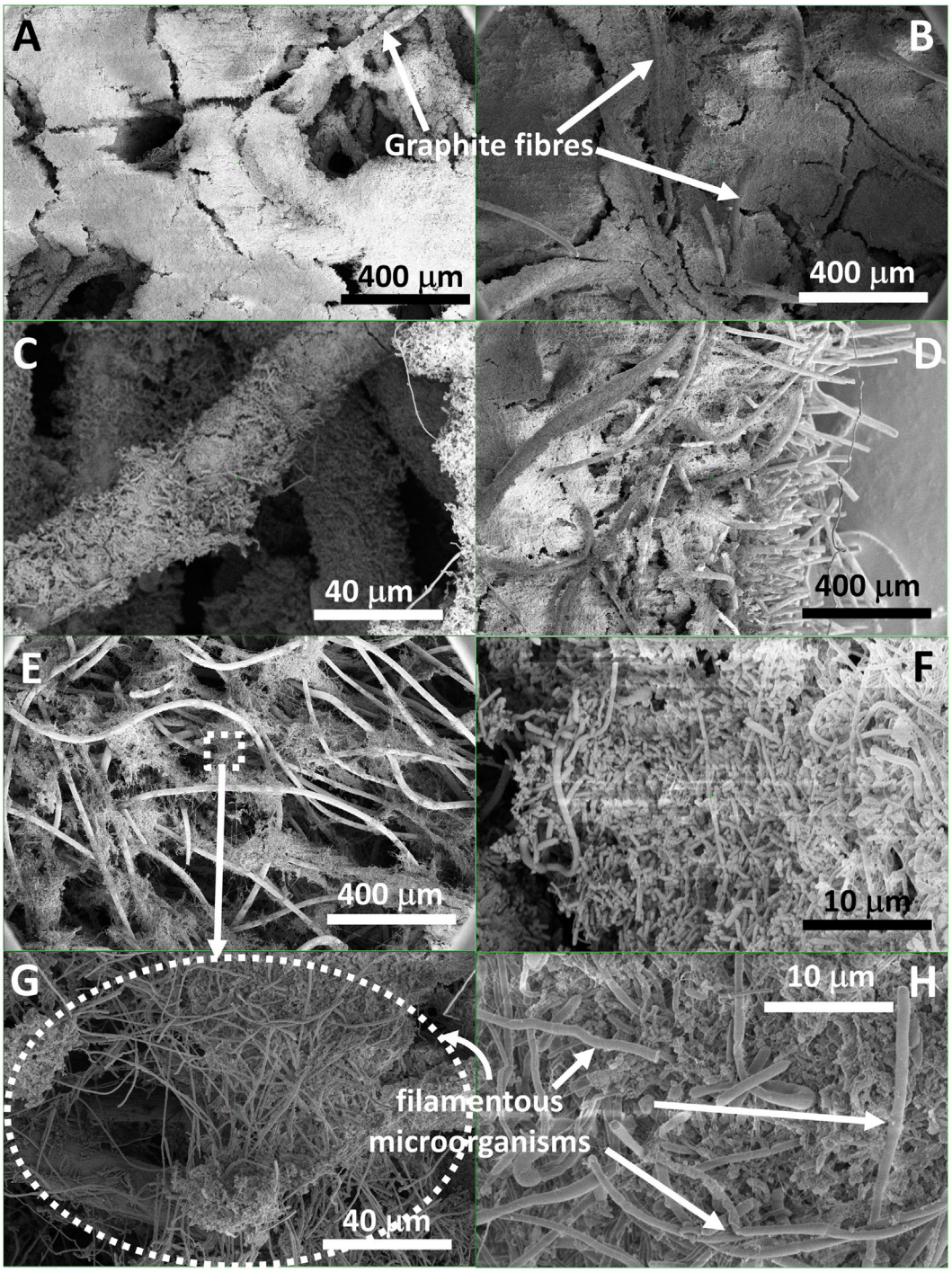

FIGURE 1 | Scanning electron micrograph images at different magnification of a biofilm developed **(A)** on the carbon felt surface facing the membrane (I–III, annotation used on Figure S3 in Supplementary Material), **(B)** on the felt surface facing the opposite side (VII–VIII), **(C)** on individual carbon fibers at different depth, **(D)** through the thickness of the carbon felt (side-view), **(E)** in the middle, width-wise, of the carbon felt electrode (i.e., ca. 0.6 cm deep; IV–V), and showing **(F–H)** a wide variety of shape and size of microorganisms colonizing the electrode, and **(G,H)** long filamentous microorganism assemblies.

Supplementary Material for more images, at different locations throughout the electrode).

Such biofilm coverage in the three directions, i.e., not only on the surface but also deeper in the carbon felt, has not been reported to date for microbial electrosynthesis studies using unmodified carbon felt as electrode material. Recently, Cui et al. (2017) reported the formation of a multi-layered biofilm around the carbon fibers of a metal-oxide-modified carbon felt electrode, using a pure

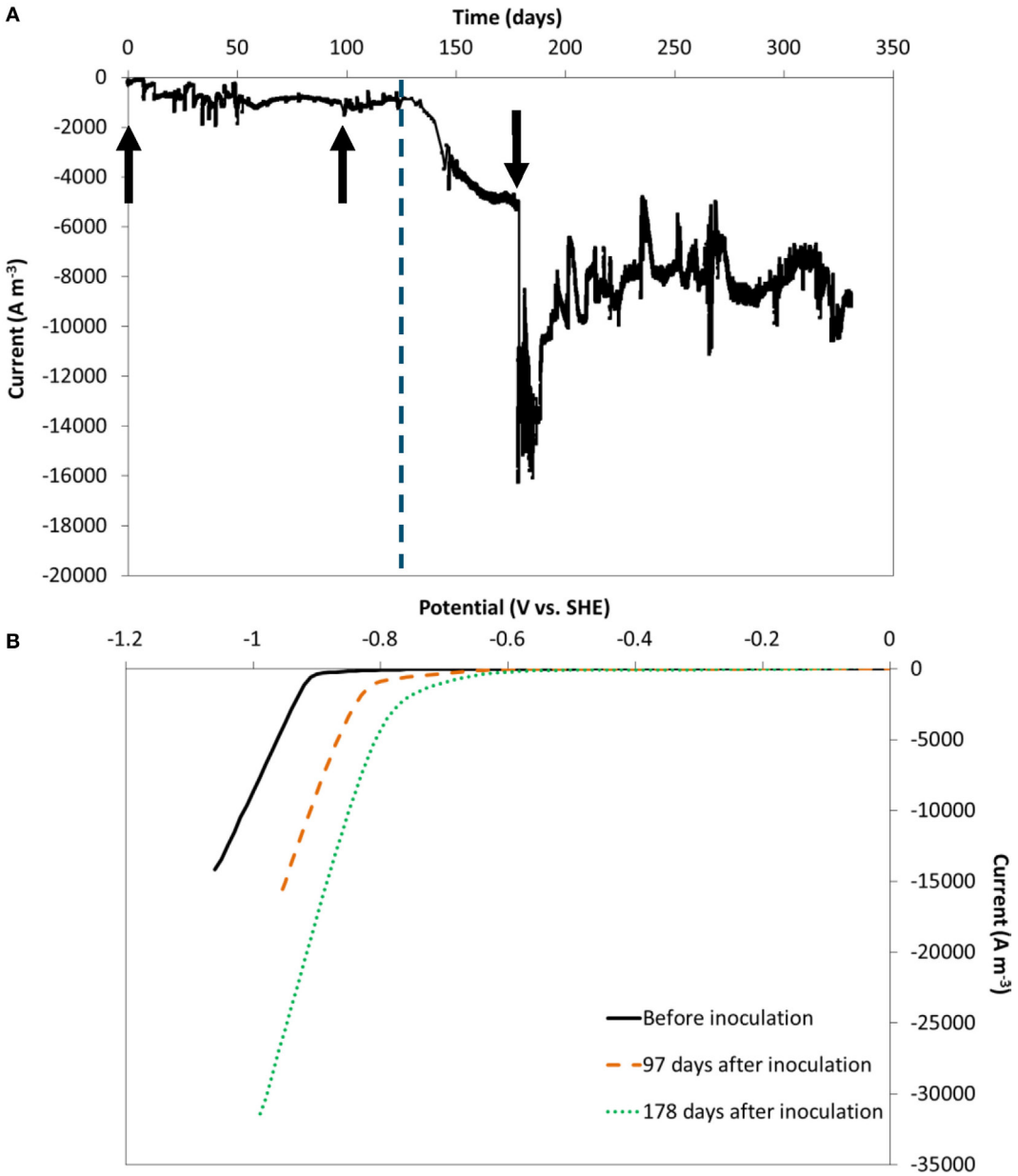

FIGURE 2 | **(A)** Current evolution over time, at an applied cathode potential of −0.85 V vs. standard hydrogen electrode (SHE), normalized to electrode volume. The vertical dashed line represents the time when nutrients addition was switched from fed-batch mode to continuous mode. **(B)** Reductive scan of CV recorded in the absence of microorganisms (black full line), 97 (orange dashed line) and 178 days after inoculation (green dotted line). The arrows indicate the moments chronoamperometry was momentarily stopped to run cyclic voltammetry.

culture of *Sporomusa ovata* (Cui et al., 2017). Relatively low current densities were achieved, between −1.8 and −2.5 A m^{-2}, at −0.7 V vs. standard hydrogen electrode (SHE). However, microorganisms only attached sporadically to unmodified carbon felt in that study. Similarly, Aryal et al. (2016) and Im et al. (2016) showed only few microorganisms attaching to the surface of unmodified carbon felt, while a more developed biofilm covered the surface of graphene-modified carbon felt (Aryal et al., 2016). All these studies were carried out in H-type reactors with magnetic stirring.

Unlike biofilm formation as observed here, Bajracharya et al. (2017a) and Arends et al. (2017) have both observed that microorganisms in suspension were responsible for most of the CO_2 reduction to reduced products, as biomass was washed out upon switching their systems from fed-batch to continuous mode. Once finding the optimal HRT to prevent biomass washout, Arends et al. (2017) suggested that the increased supply of trace elements and vitamins could be linked to the better performance of their MES systems, along with a higher growth rate imposed by the

shorter HRT, a better control of pH, and continuous removal of reduced products. Our work suggests that in addition of the positive effect of continuously adding nutrients, a combination of the following factors that were different than applied in the literature may also have played a role in the observed biofilm development: the forced-flow through regime, the long-term operation, and/or the microbial inoculum. A forced-flow through regime using graphite felt electrode was also adopted by Bajracharya et al. (2017a), though in that study it did not lead to biofilm development as observed here.

Oxygen transfer from the anode to the cathode likely did not play a significant role on the formation of the biofilm. To provide conditions for this, oxygen was actively flushed out with continuous CO_2 and CO_2/N_2 gas sparging of both anolyte and catholyte, respectively, as also suggested by Marshall et al. (2017). As such, it is expected that under the applied experimental conditions, the role of oxygen was minor; though we cannot fully exclude a potential role as shown by Marshall et al. (2017) that provided evidence that microaerobic conditions (due to oxygen cross-over) may provide a supportive role to develop the microbial community within mixed culture MES.

Electron Uptake Rate Significantly Enhanced with Dense Biofilm Development

Electron uptake rate (current) at a fixed cathode potential of −0.85 V vs. SHE was recorded during 314 days. The current normalized to electrode volume is depicted in **Figure 2A**. Because carbon felt is a three-dimensional electrode with pore diameters in the order of 10–100 μm, normalization to its volume is particularly relevant (Jourdin and Strik, 2017). The current evolution normalized to psa is shown in Figure S4A in Supplementary Material.

In the first 20 days after inoculation the current increased from ca. −200 A m^{-3} to ca. −1,000 A m^{-3} and remained largely constant during the remaining of the fed-batch period until 133 days. During this period, electron uptake rate was not affected by the change of carbon dioxide source (bicarbonate, periodic pure CO_2, or continuous CO_2:N_2 30–70%), as previously reported (Jourdin et al., 2016a,b).

From day 133 onward, the reactors were switched to continuous operation mode with an hydraulic retention time of 4 days. Within the first few days after the change, the electron uptake rate greatly increased, up to ca. −5.2 kA m^{-3} at day 178 and further to between −8 and −10 kA m^{-3} (−100 to 130 A m^{-2} psa) from day 194 to the end of the experiment. A similar significant increase was observed on the duplicate reactor, on which the current was recorded for 390 days (Figures S4B and S5A in Supplementary Material). The maximum current reached on the duplicate reactor was similar: ca. −7 to 10 kA m^{-3} at the end of the experiment (−90 to 130 A m^{-2} psa, days 369–390). These correspond to the highest biocathode current densities recorded on carbon felt to date, a relatively cheap electrode material (62 € m^{-2} from the provider of the carbon felt used here, for lab-use). The obtained current densities are of the same order of magnitude as the highest electron uptake rates reported using carbon nanotube-modified reticulated vitreous carbon electrodes for MES of acetate from CO_2 at the same applied potential (−10 kA m^{-3} to −102 A m^{-2} psa) (Jourdin et al., 2015b, 2016a,b). An overview of the performance indicators of most MES studies that used carbon felt as cathode material, in comparison to the highest performing MES systems, is shown in Table S2 in Supplementary Material. A more complete comparison of all MES studies up to 2016 has recently been reviewed (Jourdin and Strik, 2017).

Cyclic voltammetry experiments at day 0, at the end of the fed-batch period (day 97) and after 45 days of continuous operation (**Figure 2B**) confirmed (bio-)electrocatalytic activity. The onset potential of the reductive catalytic wave shifted from day 0 (ca. −0.9V vs. SHE) to higher potentials at day 97 (ca. −0.75V vs. SHE). Another increase in onset potential was observed at the last CV at day 178 (ca. −0.6V vs. SHE). The same trends were observed in the duplicate reactor (Figure S5B in Supplementary Material), in which the onset potential increased even further to −0.5 V vs. SHE at day 366. The increase in onset potential suggests an increase in biological catalytic activity in the systems over time, which is in line with the observed increase of biofilm coverage throughout the electrode (i.e., higher biocatalysts density) and the subsequent increase of electron uptake rate observed (**Figure 2A**).

Cyclic Voltammograms Triggered Further Increases of Biocatalytic Activity Which Was Sustained for Long Term

After the CV recorded on day 178, the electron uptake rate abruptly increased from −5.2 kA m^{-3} before the CV to between −11 and −14 kA m^{-3} (>210% increase) and sustained for over 12 days, after which the current stabilized between −8 and −10 kA m^{-3} for the remaining 124 days (**Figure 2A**). Similarly, the current on the duplicate reactor increased by 200% after the CV recorded on day 178, and again after the CV on day 366 (Figure S5 in Supplementary Material). However, the current was not influenced after the CVs ran before inoculation and on day 97 on both duplicates. The main difference was the biofilm coverage which was much less developed on day 97, as discussed above. This finding, though in need of more investigation, could present a novel and easy strategy to boost electron uptake rate, and sustain it for a long period of time.

Caproate (C6) and Butyrate (C4) Continuous Bioelectrochemical Production from CO_2

Short and MCFAs (C2–C8) as well as alcohols (C2–C6) production were followed for each reactor throughout the course of the experiments. The cumulative production, production rates, and electron recovery into acetate (C2), *n*-butyrate (nC4), and *n*-caproate (nC6), over time, are shown in **Figure 3**. Figure S6 in Supplementary Material shows these results obtained on the duplicate reactor. The production rates normalized to the other parameters mentioned earlier are also shown in Figure S7 and Table S1 in Supplementary Material for both duplicates. No

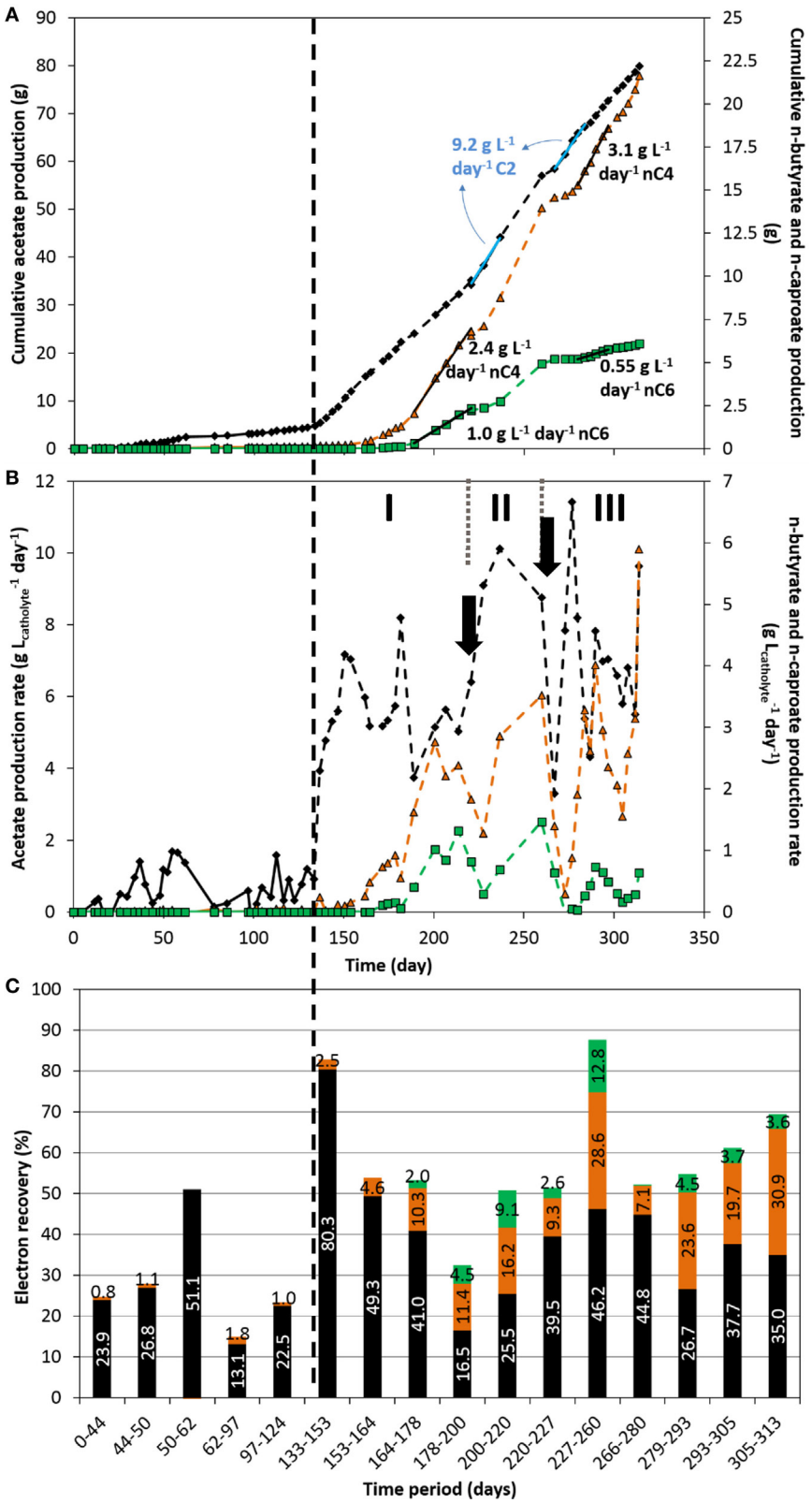

FIGURE 3 | Acetate (black diamond), *n*-butyrate (orange triangle), and *n*-caproate (green square) cumulative production **(A)**, production rate **(B)**, and electron recovery into each product **(C)** over time. The vertical dashed line represents the time when nutrients addition was switched from fed-batch mode to continuous mode. The two arrows indicate the time at which significant leakage of the catholyte occurred. The three periods I, II, and III indicate periods of interest discussed in the text.

alcohols or other organics were detected throughout the experiment in both reactors.

First, it can be observed that mostly acetate was produced in the fed-batch period, with a maximum production rate of about 1.83 ± 0.15 g L^{-1} day^{-1} (average and SD between both reactors) and a fairly low electron recovery into acetate. Technical issues (e.g., small leakages, gas mixture inflow instability) occurred between days 62 and 97 which affected the conversion of CO_2 to organics up to the end of the fed-batch period, as can be seen in **Figures 3B–C**. In line with the increase of electron uptake seen above directly after the switch from fed-batch to continuous mode (**Figure 2**), the production rate of acetate immediately and significantly increased up to 7.2 g L^{-1} day^{-1} just few days after the operational change (day 150, period I, **Figure 3B**). Maximum acetate production rates sustained for over 4–5 sampling dates (>17 days) of 9.85 ± 0.65 g L^{-1} day^{-1} were reached (average and SD between both reactors; days 220–237 and 267–284 (**Figure 3A**) and 373–390 (Figure S6A in Supplementary Material), respectively). Rates in the range from 5 to 9 g L^{-1} day^{-1} could be maintained throughout the period from day 133 to the end (**Figure 2B**), which are one order of magnitude higher than the highest rates ever reported on carbon felt-based MES (Table S2 in Supplementary Material). Our acetate production rates were comparable to rates achieved in industrial biological processes such as fermentation and anaerobic digestion (Angenent et al., 2002; Graves et al., 2006; Martin et al., 2013; Richter et al., 2013). If MES is to be implemented, productivity must at least be within the range of already industrially relevant bioproduction/bioconversion processes, such as bioethanol from starch plants (commercialized at 30–90 g L^{-1} day^{-1})(Graves et al., 2006; Richter et al., 2013), or biogas anaerobic digesters, with maximum productivities of 12 g L^{-1} day^{-1} using synthetic substrates, which will not easily be achieved with real substrate (Angenent et al., 2002; Martin et al., 2013; Kucek et al., 2016b).

About 10–15 days after the feeding strategy change, *n*-butyrate production started slowly and increased abruptly after day 153. Remarkably, 10 days later (around day 164), *n*-caproate production started as well, with a sharper increase in production rate after day 182. *n*-butyrate production in microbial electrosynthesis systems from carbon dioxide has been reported by couple of other groups recently (Ganigue et al., 2015; Arends et al., 2017; Bajracharya et al., 2017a; Batlle-Vilanova et al., 2017; LaBelle and May, 2017), but to the best of the authors' knowledge, continuous *n*-caproate has not been reported to date from CO_2-based MES. A maximum continuous production rate of *n*-butyrate of 3.2 ± 0.1 g L^{-1} day^{-1} was achieved here (averaged between both reactors; days 279–297, **Figure 2A**, and 374–390, Figure S6A in Supplementary Material), which is about 14 times higher than the highest rate reported to date in a similar system (LaBelle and May, 2017). In our study, a fairly high continuous production of 0.95 ± 0.05 g L^{-1} day^{-1} of *n*-caproate was also achieved, averaged between extended periods from both reactors, from days 188–220 (**Figure 3A**) and days 374–390 (Figure S6A in Supplementary Material). Though the production of organics was unstable (see explanations below in Section "Dense Biofilm-Based Carbon Biocathode Allowed Successive Production of Acetate, *n*-Butyrate, and *n*-Caproate from CO_2"), continuous production of *n*-butyrate and *n*-caproate was demonstrated from days 143 to 260 without interruption, and from day 272 to the end

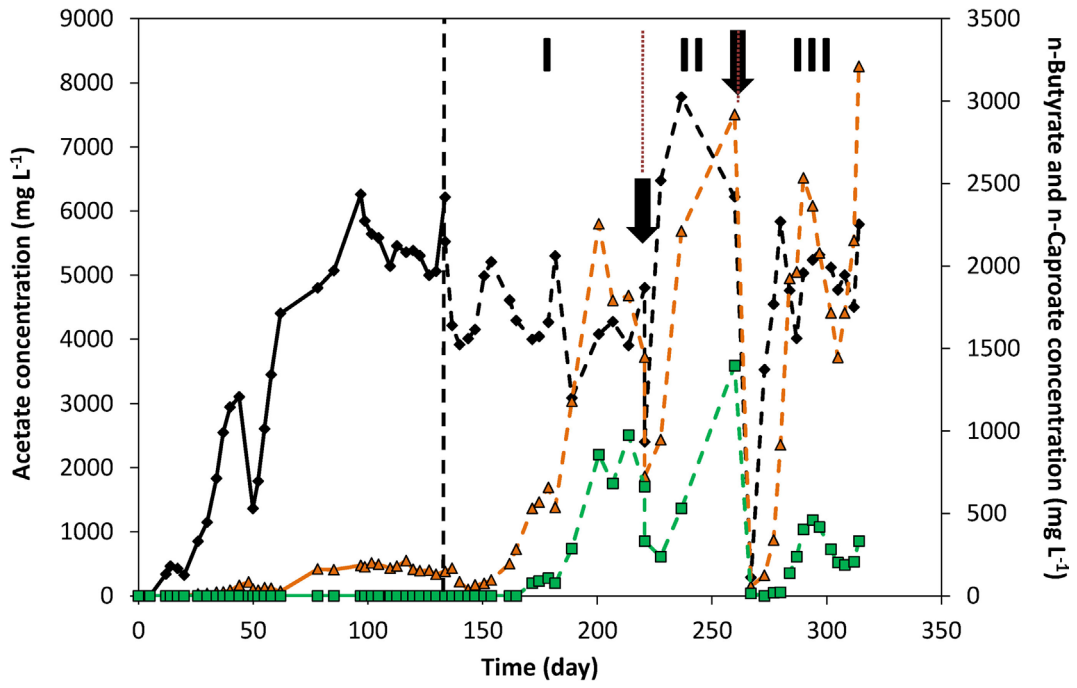

FIGURE 4 | Acetate (black diamond), *n*-butyrate (orange triangle), and *n*-caproate (green square) concentrations over time. The vertical dashed line represents the time when nutrients addition was switched from fed-batch mode to continuous mode. The two arrows indicate the time at which significant leakage of the catholyte occurred. The three periods I, II, and III indicate periods of interest discussed in the text.

of the experiment. We achieved here a total concomitant production of 6.65 g_C L^{-1} day^{-1} into C2, nC4, and nC6 (days 374–390, Figure S6A in Supplementary Material), which is similar to the highest rate (when normalized to catholyte volume) reported by LaBelle and May (2017) who recently reported a production rate of 7.61 g_C L^{-1} day^{-1} into sole acetate, at 35% electron recovery (see Table S2 in Supplementary Material).

A Biofilm-Driven Microbial Electrosynthesis System

Remarkably, electron recoveries into organics increased up to 83% after switching to continuous feeding, concomitantly with the increase in current densities (days 133–153, **Figure 3C**). The observed increase in biofilm coverage throughout the carbon felt over time (**Figure 1**; Figure S2 in Supplementary Material), could explain that more of the electrons converted ended up in organic products. Furthermore, the switch from fed-batch to continuous mode decreased the concentration of microorganisms in suspension (Optical $density_{660nm} < 0.1$). The increase in performance (rates and recoveries) while the concentration of microorganisms in suspension decreased highlight the activity of the biofilm in the conversion of CO_2 to products of interest, over the microorganisms in suspension, as previously reported by Jourdin et al. (2016a,b). A leakage of the catholyte on day 266 also removed all, or most of the microorganisms in suspension. Despite this, catalytic activity remained and organics production immediately restarted at similar rates after replenishing the system with fresh catholyte (**Figures 2** and **3**).

Up to 12.8% of the electrons were recovered in *n*-caproate in the most productive period (days 227 to 260, **Figure 3**), while 28.6 and 46.2% were recovered into *n*-butyrate and acetate, respectively, to a total of 87.6% coulombic efficiency. In our study, a small fraction of the electrons taken up were not recovered into identified soluble organics. The remaining electrons may have ended up in biomass or unused hydrogen for example (Jourdin et al., 2015a). Overall, higher electron recoveries from 65 to 100% were achieved on the duplicate reactor in the continuous-feeding phase (Figure S6C in Supplementary Material), which may be explained by less damaging events (e.g., leaks) occurring on this reactor (see below). The lower current density recorded for most of the duplicate reactor lifetime cannot explain the higher electron recoveries. Indeed, an electron recovery into organics of 89.7% was achieved in the last period on the duplicate reactor (days 369–390), during which the current density was the highest (-7 to 10 kA m^{-3}, -90 to 130 A m^{-2}, Figure S5A in Supplementary Material). A similar product distribution was achieved with 7.7, 28.4, and 53.6% of electron recovered into nC6, nC4, and acetate, respectively. These results demonstrate that high electron recoveries at high current densities can be achieved on unmodified carbon felt (Table S2 in Supplementary Material).

Dense Biofilm-Based Carbon Biocathode Allowed Successive Production of Acetate, *n*-Butyrate and *n*-Caproate from CO_2

Figure 4 and Figure S8 in Supplementary Material show the concentration profile of each of the products over time of both duplicates. On day 50, 65% of the catholyte was replaced, causing the decrease in concentrations observed. Apart from that, acetate concentration increased fairly quickly over the first 62 days. A maximum acetate concentration of 6.2 g L^{-1} was reached in fed-batch conditions.

From the switch to continuous addition of nutrients on day 133 to day 220 (period I in **Figure 4**), acetate concentrations around 4–5 g L^{-1} were maintained. During that period, *n*-butyrate and *n*-caproate were successively produced, as mentioned above, up to reaching concentrations from days 200 to 220 around 1.5–2.2 g L^{-1} for *n*-butyrate and ca. 0.7–1 g L^{-1} of *n*-caproate. From days 200 to 220 the current density was also constant around -8.5 kA m^{-3}, which led to define this period as a quasi-stable continuous reactor performance. After sampling on day 220 (first arrow in **Figure 4**), a leak in the recirculation pump tubing led to a loss of half of the catholyte which was immediately replaced with fresh catholyte. This led to C2, nC4, and nC6 concentrations to fall to 2.4, 0.6, and 0.3 g L^{-1} on day 220, respectively. In the 7 days that followed that leak (start of period II, **Figure 4**), acetate concentration significantly increased up to 6.5 g L^{-1}, corresponding to an increase of production rate from 6.4 to 9.1 g L^{-1} day^{-1} (see **Figure 3B**, period II), while current density remained constant (**Figure 2A**). In those 7 days, *n*-butyrate only slightly increased to 0.95 g L^{-1} while *n*-caproate decreased further to 0.24 g L^{-1}. In the following 9 days, *n*-butyrate concentration rose to 2.2 g L^{-1}, likely due to the higher acetate availability, which coincided with *n*-caproate production rising up again as well. The next 23 days (from days 237 to 260, end of period II, **Figure 4**) corresponded to the highest *n*-caproate production period reaching a maximum of 1.5 g L^{-1} and 1.5 g L^{-1} day^{-1} (**Figure 3B**), during which high acetate and *n*-butyrate concentrations were observed. During that period, it can be observed that acetate concentration decreased while both nC4 and nC6 concentrations increased. On day 266 (second arrow, **Figure 4**), all organics concentration fell to 0 due to another (complete) leakage of the catholyte. However, this allowed to observe the same phenomenon after adding fresh catholyte. First, acetate rapidly started being produced at similar rates right after the addition (day 266). Six days later (day 272), *n*-butyrate production rose rapidly as well up to 2.5 g L^{-1} on day 289 (max concentration of 3.2 g L^{-1} on day 313), followed by *n*–caproate production from day 280. This successive-production phenomenon can also be observed on the duplicate reactor (Figure S8 in Supplementary Material). From these observations, it would seem that an apparent C2 "threshold" concentration of 2–4 g L^{-1}, needed to be reached before nC4 production started, and a concentration of 0.5–2 g L^{-1} nC4 for nC6 to start being produced.

Figure 5 shows the current density and organics' concentration profiles over the period of continuous supply of nutrients recorded on the duplicate reactor, from days 133 to 390. It can be observed that lower products' concentrations and production rates were achieved up to day 368 (end of period III, **Figure 5B**). This can be explained by a process which performance and product spectrum was controlled by current density level and products' concentration. First of all, during most of periods I through III, a lower current density was recorded, ca. -3.5 ± 0.5 kA m^{-3}, than on the reactor presented above. This lower electron uptake rate led to a generally lower acetate concentration of around 2 to 4 g L^{-1} (**Figure 5**). As discussed above, this corresponds to the concentration range in which *n*-butyrate production was

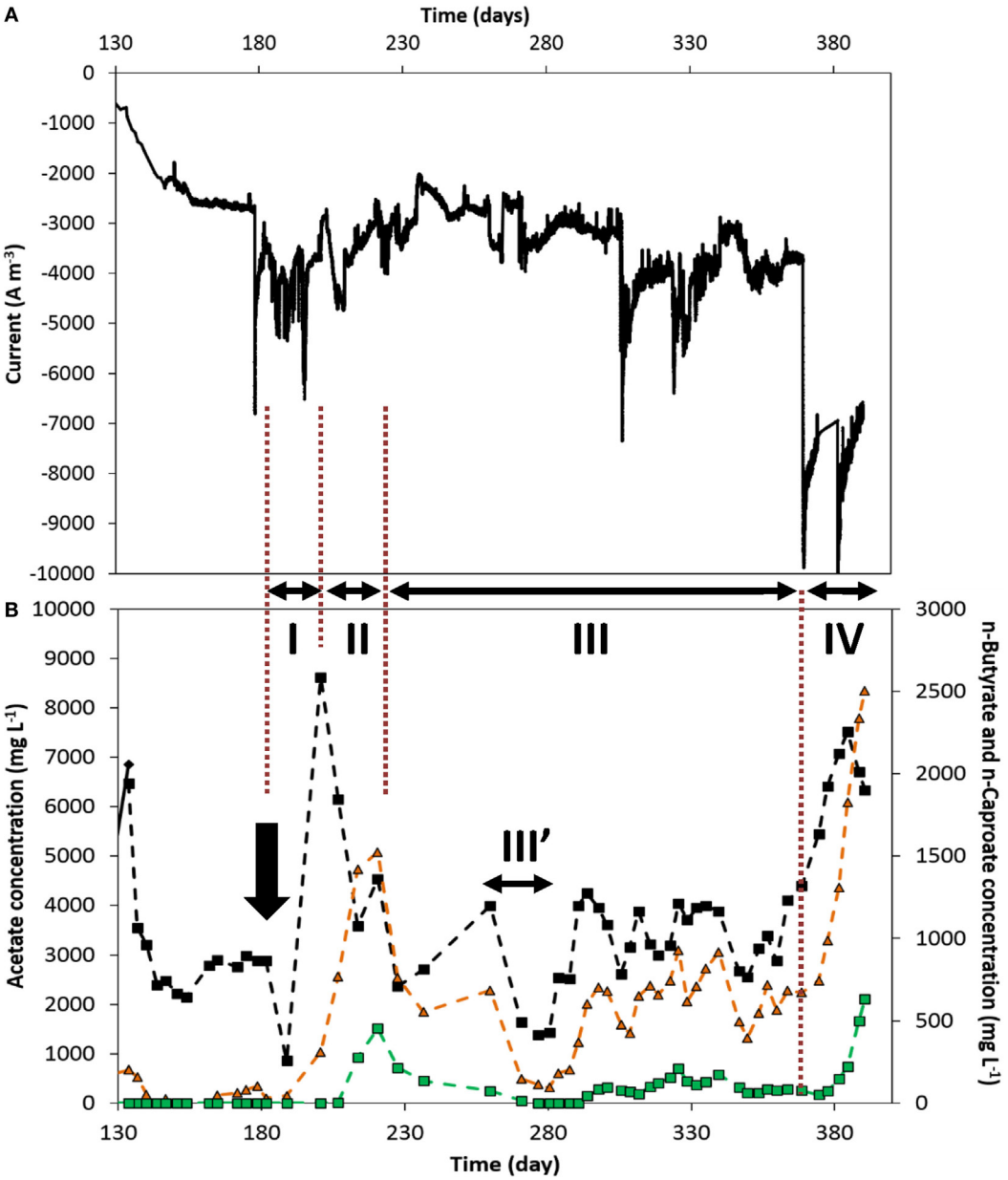

FIGURE 5 | Duplicate reactor: **(A)** current normalized to electrode volume and **(B)** acetate (black diamond), *n*-butyrate (orange triangle), and *n*-caproate (green square) concentration evolutions over time, from the switch to continuous addition of nutrients. The two arrows indicate the time at which significant leakage of the catholyte occurred. The three periods I, II, and III indicate periods of interest discussed in the text. III′: technical difficulties that led to multiple leakages. The whole period from inoculation can be seen in Figures S5 and S8 in Supplementary Material.

apparently triggered. However, this lower acetate concentration did not allow to steer the cathodic reaction to high *n*-butyrate concentration, which ranged around 0.4–0.9 g L^{-1} in that period (III, **Figure 5B**). Similarly, this allowed *n*-caproate production to only low concentrations of about 0.15 ± 0.05 g L^{-1} (period III, **Figure 5**), though being continuously produced over a long period (see production rates in Figure S6B in Supplementary Material). The first period in which current densities were higher, 5–6 kA m^{-3} from days 189 to 200 (period I, **Figure 5**), allowed to reach higher acetate concentration of up to 8.6 g L^{-1}. However, this could also be explained by a response to the CO_2-limitation stress the biofilm was subjected to during the 7 days prior (from day 182, arrow in **Figure 5**), due to a malfunction of the CO_2 supply, which explains the drop in products' concentrations. In the following 20 days (period II), *n*-butyrate and *n*-caproate concentrations successively increased to higher values, likely in response to a higher acetate availability, while acetate concentration decreased. This observation is in line with the concentration-driven production

described above. The link between current density and reactor performance can be observed in the last period of the experiment (IV, **Figure 5**). From day 369, current densities rose to and remained around 7–8 kA m^{-3} for 21 days until the experiment was stopped. Consequently, all products' concentration (**Figure 5**) and production rate (Figure S6B in Supplementary Material) increased significantly up to reaching similar performance as observed in **Figures 3** and **4**, when current densities were similar in both reactors (Table S1 in Supplementary Material).

Successive production of nC4 and nC6 were also observed in the start-up phase of typical chain elongation fermentation studies from acetate plus ethanol (Steinbusch et al., 2011; Grootscholten et al., 2013b). In those studies, a first elongation of C2 to nC4 can be observed, before longer chains are produced. Though, once short VFAs become limited (e.g., C2), longer VFAs (nC4) become primary available and are elongated to nC6. In the latter, upon addition of more soluble electron donor, i.e., ethanol, the higher reducing equivalent availability also typically leads to the production of more reduced compounds, i.e., longer carbon-chain compounds such as nC6, which quickly becomes the main product accumulating (Angenent et al., 2016).

Yeast extracts and vitamin B have been reported to be essential nutrients for chain elongating fermentative microorganisms (Barker, 1947; Grootscholten et al., 2013b; Angenent et al., 2016). It is worth noting that none of them were added at any time in our reactors. Addition of yeast extracts and vitamin solutions has often been linked to high operational costs for biological processes (Koutinas et al., 2016). While exact metabolic mechanisms remain to be elucidated in our systems, not adding these nutrients could lead to financial benefit and reduced costs. On the contrary, the addition of a chemical methanogenesis inhibitor, as used in our study, would negatively affect the application perspective. It is worth mentioning that tungsten and selenium-based nutrients were not added in our reactors. Both W and Se were reported to be essential for hydrogenotrophic methanogenic microorganisms to convert CO_2 into methane using H_2 as electron donor (Blaut, 1994). Additionally, acetoclastic methanogenesis would likely be inhibited at low pH such as applied in our study (pH 5.8) (Chen et al., 2002). Other strategies, such as inoculum pretreatment and several culture transfers, have showed successful at suppressing methanogenesis activity without adding an expensive chemical inhibitor (Patil et al., 2015a; Bajracharya et al., 2017b). Further experiments will need to be carried out without adding a chemical methanogenesis inhibitor in our MES systems, to verify whether methane production is inhibited.

High Microorganism Morphology Diversity with Filamentous Microorganism Assemblies

Figures 1F–H and Figure S9 in Supplementary Material are high magnification SEM images that show the electrodes were colonized by a high diverse-shaped microbial community. Both cocci and rod-shaped microorganisms can be observed, of which the size of the rod-shaped microbes vary from 1 to 10 µm. In most MES studies to date, the morphology of the microorganisms colonizing the cathode was shown to be fairly homogeneous, mainly small rods (ca. 1- to 2-µm long) (Jourdin et al., 2014, 2015b). The highly diverse morphology in our reactors may be attributed to the complexity of metabolic pathways and wider spectrum of reduced end-products obtained here, vs. only acetate and H_2 being produced in most MES studies (Table S2 in Supplementary Material).

The long rods (**Figures 1E–H**), 50 µm and longer (up to 300–400 µm, **Figure 1E**; Figures S2F–H in Supplementary Material) that can be observed throughout the biofilm are actually smaller rod-shaped microorganisms interconnected to each other length-wise forming long filaments (**Figure 1H**; Figure S9G–R in Supplementary Material). These filaments were observed to connect two or more far-apart carbon felt fibers, as well as to connect to other microorganisms. To the best of the authors' knowledge, such structures were never observed in biocathode biofilms to date. Microscopic observations of chain elongation fermentation reactor microbiomes have rarely been performed. Zhang et al. (2013) showed bacteria that were mainly rod-shaped of about 2-µm long, attached as biofilm on the outer surface of their CO_2:H_2 fed hollow-fiber membrane (Zhang et al., 2013). Rod-shaped microorganisms between 1 and 4 µm were also observed in other chain elongation fermentation studies (Liu et al., 2017; Zhu et al., 2017). Roghair et al. (2016) also showed a high diversity in morphologies in their granular chain elongation sludge that may be ascribed to the fundamentally different biological processes than granule formation requires, with rods up to 10 µm, and cocci (Roghair et al., 2016).

Our observation raises the question of the functionality of these filamentous microorganism assemblies in our systems. The filamentous morphology resembles that of so-called sulfur oxidizing filamentous "cable bacteria," which have mostly been found in marine and freshwater sediments, though the latter were observed to have a stripy morphology (Marzocchi et al., 2014; Schauer et al., 2014; Larsen et al., 2015; Risgaard-Petersen et al., 2015). These cable bacteria have been reported to conduct electrons over centimeter-long distances and thereby electrically couple sulfide oxidation and oxygen reduction (Schauer et al., 2014; Larsen et al., 2015; Risgaard-Petersen et al., 2015), as well as nitrate reduction (Marzocchi et al., 2014) in sediments. This raises the question whether the observed filamentous microorganism assemblies in our biofilm conducted intracellular electrons over long distance, which may have allowed the formation of such thick biofilm, i.e., delivering electrons to far-away microorganisms. However, at this stage, it also cannot be excluded that the filamentous microorganism assemblies were simply growing on the decay of the biofilm and its extracellular polymers and provided a structure to develop a thick biofilm. In addition, (bio)electrochemically produced hydrogen may also have diffused through the biofilm, and served as electron shuttle to microorganisms, e.g., for the CO_2 reduction to acetate, thus allowing the biofilm to grow thick. The role of H_2 as electron mediator in MES systems has been extensively discussed (Blanchet et al., 2015; Jourdin et al., 2016b; LaBelle and May, 2017; Puig et al., 2017) and some biofilms were showed to be very effective at capturing it before it could escape the biofilm (Jourdin et al., 2016b). Some methanogens belonging to genera such as *Methanosaeta* and *Methanospirillum* were also showed to

form long filaments over hundreds of micrometers in anaerobic granular sludge (Parshina et al., 2014; Li et al., 2015; Zhou et al., 2015). However, methanogenesis activity was inhibited in our reactors by continuously feeding a chemical inhibitor. Therefore, the filamentous microorganism assemblies observed in our reactors are unlikely methanogens.

Furthermore, thin filaments (nm diameter) were also observed everywhere throughout the biofilm (**Figure 1H**; Figure S9 in Supplementary Material), either between two or more microorganisms (Figures S9A–I in Supplementary Material) or between microorganism and the carbon fiber surface (Figures S9M–P in Supplementary Material). These filaments might be extracellular polymeric-like substance that hold the biofilm together. However, they possibly can also be electron-conductive nanowire filaments for long-range electron transfer, as observed in bioanode biofilms (Lovley, 2011).

Bioelectrochemical Chain Elongation Perspective

To the best of the authors' knowledge, only one study claimed to have elongated carbon dioxide to *n*-butyrate and *n*-caproate, using H_2 as electron donor, in a membrane biofilm reactor (Zhang et al., 2013). Production rates of 0.057 and 0.031 g L^{-1} day^{-1} of *n*-butyrate and *n*-caproate were achieved, respectively. However, subsequent reports in this field have argued the somewhat slower production rates achieved must have been due to the rate-limiting *in situ* production of ethanol which then acted as electron donor for elongation of acetate (Spirito et al., 2014; Angenent et al., 2016). In our reactors, CO_2 was used as sole carbon source, and a solid-state electrode as sole electron source. The acetate, *n*-butyrate, and *n*-caproate volumetric production rates (normalized to medium volume) obtained in our study were 51, 56, and 31 times higher than those obtained by Zhang et al. (2013). Remarkably though, ethanol, lactate, methanol, or other organics that could have acted as intermediate electron donor were not detected in our reactors. However, at this stage, it cannot be ruled out that an intermediate could have been produced and consumed immediately within the biofilm, before detection could be possible. Our findings seem to indicate conceptually different mechanisms than recently reported by Batlle-Vilanova et al. (2017). In that study, CO_2 was elongated to *n*-butyrate with an electrode as electron donor, in batch-mode bioelectrochemical reactors. However, it was demonstrated that CO_2 reduction to acetate and further elongation to *n*-butyrate occurred in the bulk catholyte and not in the biofilm. Furthermore, partial pressure of H_2 had to build up in the headspace, along with low enough pH (ca. pH 5) and low CO_2 availability, to allow acetate reduction to ethanol and further chain elongation of acetate to *n*-butyrate (Batlle-Vilanova et al., 2017). In our study, we show that CO_2 elongation to *n*-butyrate and *n*-caproate is possible within the biofilm, in continuous mode, while CO_2–N_2 is continuously flushed, i.e., no H_2 build up in the headspace. Most other microbial electrosynthesis studies reporting *n*-butyrate production also detected ethanol (Ganigue et al., 2015; Arends et al., 2017; Bajracharya et al., 2017a; Batlle-Vilanova et al., 2017). We kindly refer to Raes et al. (2017) for more in-depth discussions about the potential biological pathways and extracellular electron flows that may be occurring in bioelectrochemical chain elongation systems such as developed here. These potential electron transfer mechanisms are also graphically reproduced in Figure S10 in Supplementary Material. We still can suppose that, in our study, microorganisms responsible for bioelectrochemical chain elongation of produced organics (presumably done by bioelectrochemical chain elongators that elongate C2 to nC4 and nC6 *via* known or by Raes hypothesized pathways) did concurrently live in synergy with CO_2 reducers to acetate (presumably done by bioelectrochemical acetogens). Possible competition for electron donors between both functional microbial groups still needs to be uncovered. H_2 may be an electron mediator for the CO_2 reduction to acetate in our systems, as previously reported for MES from CO_2 to acetate studies (Blanchet et al., 2015; Jourdin et al., 2016b; LaBelle and May, 2017; Puig et al., 2017). However, a kinetic and thermodynamic modeling study predicted that direct acetate conversion to MCFAs by H_2 is most likely not feasible even under high H_2 partial pressures (González-Cabaleiro et al., 2013). Therefore, other electron transfer mechanisms than H_2-mediated electron transfer may also be at play in our systems (Raes et al., 2017).

The reduction of CO_2 to *n*-butyrate and *n*-caproate requires 20 and 32 electrons, respectively, while only 8 electrons are required to reduce CO_2 to acetate. However, we show that all these three products can be formed at the same applied potential. In our reactors, which were not optimized for this purpose, a cell voltage of about 3V was measured at the highest current density. The theoretical minimal electrical power required at the measured cell voltage is 10.9 kWh $kg_{acetate}^{-1}$, 18.4 kWh $kg_{butyrate}^{-1}$, and 22.3 kWh $kg_{caproate}^{-1}$ (see calculations in Supplementary materials). The latter represents the electrical power required to produce 1 kg of product if 100% of the electrons were recovered into that product. Therefore, only about 1.7 and 2 times more power is required to produce *n*-butyrate or *n*-caproate than acetate, while their market values are higher than of acetate (Kleerebezem et al., 2015). Taking the period from days 227 to 260 of the main reactor where *n*-caproate production was the highest (**Figures 3** and **4**), as a representative period (similar rates and recoveries were obtained in the last operating period of the duplicate reactor as well), the actual electrical power needed were calculated at 23.5 kWh $kg_{acetate}^{-1}$, 64.3 kWh $kg_{butyrate}^{-1}$, and 174 kWh $kg_{caproate}^{-1}$. These high electrical power requirement for *n*-butyrate and *n*-caproate were due to the relatively low electron recoveries into those products. The latter highlights the need for further research into increasing the selectivity of the process toward the most valuable product, which will in turn decrease the power requirement. The overall electrical energy efficiency for our microbial electrosynthesis systems (i.e., electricity and CO_2 to organics excluding energy need for pumping and other side equipment) was calculated at 38% (pH 5.8 cathode, pH 2 anode, and 32°C), showing efficient use of the applied power (see calculations in Supplementary material).

The findings presented here open up a new MES production platform and widen its product spectrum and potential implementations. Though the same products are generated as from chain elongation fermentation, MES does not use the same carbon and electron sources and could be complementary to that process.

MATERIALS AND METHODS

MES Reactor Setup

Two identical bioelectrochemical reactors were set up and used as duplicate. A photo of the reactor and a scheme of the reactor setup is shown in supporting information (Figure S11 in Supplementary Material). Each reactor consisted of two Plexiglas flow through compartments. The anode compartment had a volume of 31 cm^3 while the cathode compartment was wider (4.2 vs. 1.4 cm for the anode) and had an empty volume of 94 cm^3. Both compartments were separated by a cation exchange membrane of 19.8 cm^2 psa (Fumasep FKS, Fumatech BWT GmbH). Two Plexiglas support plates were used to close each compartment. A Pt/IrO_2 coated with Ti (Magneto Special Anodes, Schiedam, The Netherlands) was used as anode electrode (19.8 cm^2 psa). Carbon felt was used as cathode electrode material (4-mm thick, CTG Carbon GmbH, Germany). Three layers of felt (19.8 cm^2 psa, total volume of 25.5 cm^3) were stacked together and placed vertically in the center of the cathode compartment at about 1.65 cm of the membrane and 1.65 cm to the Plexiglas support on the other side (Figure S11B in Supplementary Material). A titanium wire (Salomon's Metalen, The Netherlands) was weaved through the carbon felt stack and used as current collector. The catholyte was forced to flow through the carbon felt, from the bottom of the reactor on the membrane-side of the felt, to the other side where it exited at the top (Figure S11 in Supplementary Material). This forced-flow through design was adapted from the hypothesis that it would promote biofilm coverage and improve performance throughout the carbon felt electrode, as earlier observed for bioanodes (Sleutels et al., 2009).

A pH probe (QMP108X, Q-is, Oosterhout, the Netherlandsg) was placed in the catholyte recirculation circuit and a pH controller (Ontwikkelwerkplaats, Elektronica ATV, the Netherlands) was used to control the pH of the catholyte at pH 5.8 (the applied potential was also confirmed not to influence the pH measurements). A recirculation bottle was also installed in the loop. The total catholyte volume in the whole setup was 360 mL, while the catholyte volume in the cathode chamber was 64 mL. The catholyte medium composition was identical to the one described in Jourdin et al. (2015a,b) and contained 0.2 g L^{-1} NH_4Cl, 0.04 g L^{-1} $MgCl_2{\cdot}6H_2O$, 0.015 g L^{-1} $CaCl_2$, 6 g L^{-1} Na_2HPO_4, 3 g L^{-1} KH_2PO_4, 1 mL L^{-1} of a mixed trace element solution, and 15 mM 2-bromoethanesulfonic acid to suppress methanogenic activity (Jourdin et al., 2015a). The trace element solution contained 1.5 g L^{-1} $FeCl_3{\cdot}6H_20$, 0.15 g L^{-1} H_3BO_3, 0.03 g L^{-1} $CuSO_4{\cdot}5H_2O$, 0.18 g L^{-1} KI, 0.12 g L^{-1} $MnCl_2{\cdot}4H_2O$, 0.06 g L^{-1} $Na_2MoO_4{\cdot}2H_2O$, 0.12 g L^{-1} $ZnSO_4{\cdot}7H_2O$, 0.15 g L^{-1} $CoCl_2{\cdot}6H_2O$, 0.023 g L^{-1} $NiCl_2{\cdot}6H_2O$, and 10 g L^{-1} EDTA. The anolyte composition was identical, but its pH was decreased to 2 by phosphoric acid addition at time 0, to favor proton crossing over the membrane over other cations, and the trace element solution was omitted. Due to the water oxidation reaction, the anolyte pH remained around 2 for the remaining of the experiments. The anolyte was operated in fed-batch and continuously sparged with CO_2 to prevent oxygen accumulation and possible crossover through the membrane. The setup was verified to be air tight before starting experiments. Both catholyte and anolyte were recirculated at 12 L h^{-1} using a recirculation pump. The reactors were operated in a temperature controlled cabin at 32°C. The experimental setup was covered from light to avoid phototrophic activity. The inoculum was taken from a running laboratory MES reactor which produced acetate from CO_2 (Jourdin et al., 2015b). The original source of the mixed microbial consortium was from both natural environments (stormwater pond sediments located on the University of Queensland, Saint Lucia campus, Brisbane, Australia) and engineered anaerobic systems (from the Luggage Point Wastewater Treatment Plant anaerobic digester, Brisbane, Australia) (Jourdin et al., 2015a). About 200 mg_{COD} L^{-1} of inoculum was added to each reactor.

MES Reactor Operation

One of the reactors was run for 314 days (results shown in the main text of the manuscript), while the other one was run for 390 days (results shown in the Supplementary materials, and **Figure 5**). Inoculation of the reactors was done on day 0. Different operational conditions were applied throughout the course of the experiments. From day 0 to 133, fed-batch conditions were applied, with replacement of about 5% of the catholyte every 3–4 days. 65% of the catholyte was also replaced on day 50. Different carbon source feeding strategies were applied during that period, with pure CO_2 gas flushed for 60 min every 4 days (days 0–44), sodium bicarbonate addition every 3–4 days (days 44–50, and 97–133), or continuous flushing of CO_2:N_2 30–70% (days 50–97). If applied, gases were flushed through the recirculation bottle (Figure S11 in Supplementary Material). From day 133 to the end of the experiments, fresh catholyte was added continuously at a flow rate of 90 mL day^{-1} corresponding to an hydraulic retention time of 4 days, while CO_2:N_2 30–70% was flushed continuously in the recirculation bottle. The bottle containing the fresh catholyte was stored in a fridge at 4°C and continuously flushed with pure N_2 to maintain anaerobic conditions and prevent microbial growth (no carbon source provided). Table S3 in Supplementary Material provides a summary of the operational conditions.

A multichannel potentiostat (n-stat, Ivium, the Netherlands) was connected to the three-electrode electrochemical reactors to control the cathode potential and record the current (electron uptake rate). The cathode was equipped with a 3 M Ag/AgCl reference electrode (QM710X, Q-is, Oosterhout, the Netherlands). Both reactors were controlled at −0.85 V vs. SHE throughout the course of the experiment. All potentials are reported vs. SHE unless stated otherwise. Cyclic voltammetry tests were performed at pH 6.7 by scanning potentials from 0 to −1.2 V vs. SHE at 1 mV s^{-1}, before, 97, 178, and 366 days after inoculation. Only the reductive scans were extracted and reported here (**Figure 2**; Figure S5 in Supplementary Material). Several "damaging" incidents occurred over the long-term life of these two reactors, e.g., leakage of the recirculation bottle. These events are further discussed in the Section "Results and Discussion" if relevant.

Analytical Methods

The concentrations of volatile and MCFAs (C2–C8) as well as alcohols (methanol to hexanol) in the liquid phase were determined in average every 3–4 days, by gas chromatography (Agilent 7890B, USA), with some occasional longer periods where samples were taken at longer intervals, e.g., 23 days from

days 237 to 260 (**Figures 3B** and **4**). An HP-FFAP column was used (25 m × 0.32 mm × 0.50 μm). The detector (FID) and injection temperatures were 240 and 250°C, respectively. The oven temperature was 60°C for 3 min, 21°C min^{-1} up to 140°C, 8°C min^{-1} up to 150°C and constant for 1.5 min, 120°C min^{-1} up to 200°C and constant for 1.25 min, and finally 120°C min^{-1} up to 240°C and constant for 3 min. Helium was used as carrier gas at a flow of 1.25 mL min^{-1} for the first 3 min and 2 mL min^{-1} until the end of the run. 1 μL of sample was injected in the column. The production of organics as well as the electron balance were calculated as described by Raes et al. (2017). The calculations are also explained in the Supplementary materials—Calculations. The productions rates were calculated between two consecutive sampling points, and represented as such in **Figure 3B** and Figure S6B in Supplementary Material.

To check whether all reduced components were identified, chemical oxygen demand (COD) was measured few times throughout the course of the experiments using the Hach Lange LCK014 cuvette test, according to fabricant's instructions.

Scanning Electron Microscopy

Carbon felt pieces were cut throughout the whole electrode as schematically represented in Figure S3 in Supplementary Material. Samples for SEM analysis were fixed within 2.5% glutaraldehyde in reactor matrix for 24 h at 4°C, washed with the original medium matrix and dehydrated in a graded series of ethanol. Removal of ethanol from the samples was done by critical point drying. Finally, the samples were sputter coated with tungsten prior to SEM analysis. SEM images were obtained with secondary electron detector. Applied acceleration voltage 2 kV and beam current of 6.3 pA.

CONCLUSION

MES is progressing to become a robust clean CO_2 biorecycling process producing higher value chemicals at increasing rates, while minimizing the cost of electrode materials. We first showed here that continuous mode operation (i.e., continuous nutrient supply) triggered a thick biofilm to form throughout the whole thickness (1.2 cm) of unmodified carbon felt. In turn, this biocatalytically active biofilm was demonstrated to significantly enhance electron uptake rates from the electrode (-110 ± 20 A m^{-2} or -8.5 ± 1.5 kA m^{-3}) and allowed elongation of CO_2 to higher value chemicals than acetate, namely *n*-butyrate and *n*-caproate. Bioelectrochemical biofilm-driven chain elongation to caproate was demonstrated for over 100 days continuously. Production rates and concentrations of 9.85 ± 0.65 g L^{-1} day^{-1} and 8.2 ± 0.4 g L^{-1} of acetate, 3.2 ± 0.1 g L^{-1} day^{-1} and 2.9 ± 0.3 g L^{-1} of *n*-butyrate, and 0.95 ± 0.05 g L^{-1} day^{-1} and 1.1 ± 0.03 g L^{-1} of *n*-caproate (average of two reactors) were achieved at electron recoveries of 60–100%. Cyclic voltammetry "treatment" was also shown to impact developed biocathodes into converting electrons into organics at twice higher rates after treatment, and sustained these rates over long term. Finally, a high diversity of microbial morphology was observed to colonize the electrode's carbon fibers and their interspace.

We showed that higher value chemicals can be produced from carbon dioxide, and that unmodified carbon felt, a relatively cheap electrode material (62 € m^{-2}), could be a good approach for high performance and economic viability of the technology. These results represent a step forward to practical implementation of the technology. Further research should focus into improving the selectivity of the process and understanding its mechanisms.

AUTHOR CONTRIBUTIONS

LJ designed and executed experiments, performed analyses, interpreted data, and drafted the manuscript. DS planned the study, contributed to experimental design and data interpretation, and revised the manuscript. SR contributed to data interpretation and revised the manuscript. CB participated in the planning of the study, data interpretation, and revised the manuscript. All authors read and approved the final manuscript.

ACKNOWLEDGMENTS

Financial support from the Dutch Technology Foundation NWO-TTW and the company Paques (project nr. STW-Paques 12999) is gratefully acknowledged. The authors thank Rene Rozendal and João Sousa for valuable discussions. The authors would like to thank the Wageningen Electron Microscopy Centre for equipment access. The authors thank Dainis Sudmalis for SEM samples preparation and imaging.

FUNDING

This work was supported by the Dutch Technology Foundation NWO-TTW and the company Paques (project nr. STW-Paques 12999).

SUPPLEMENTARY MATERIAL

The Supplementary Material for this article can be found online at http://www.frontiersin.org/articles/10.3389/fenrg.2018.00007/full#supplementary-material.

REFERENCES

Agler, M. T., Wrenn, B. A., Zinder, S. H., and Angenent, L. T. (2011). Waste to bioproduct conversion with undefined mixed cultures: the carboxylate platform. *Trends Biotechnol.* 29, 70–78. doi:10.1016/j.tibtech.2010.11.006

Angenent, L. T., Richter, H., Buckel, W., Spirito, C. M., Steinbusch, K. J. J., Plugge, C. M., et al. (2016). Chain elongation with reactor microbiomes: open-culture biotechnology to produce biochemicals. *Environ. Sci. Technol.* 50, 2796–2810. doi:10.1021/acs.est.5b04847

Angenent, L. T., Zheng, D., Sung, S., and Raskin, L. (2002). Microbial community structure and activity in a compartmentalized, anaerobic bioreactor. *Water Environ. Res.* 74, 450–461. doi:10.2175/106143002X140242

Arends, J. B. A., Patil, S. A., Roume, H., and Rabaey, K. (2017). Continuous long-term electricity-driven bioproduction of carboxylates and isopropanol from

CO_2 with a mixed microbial community. *J. CO2 Util.* 20, 141–149. doi:10.1016/j.jcou.2017.04.014

Aryal, N., Halder, A., Tremblay, P.-L., Chi, Q., and Zhang, T. (2016). Enhanced microbial electrosynthesis with three-dimensional graphene functionalized cathodes fabricated via solvothermal synthesis. *Electrochim. Acta* 217, 117–122. doi:10.1016/j.electacta.2016.09.063

Bajracharya, S., Vanbroekhoven, K., Buisman, C., Strik, D., and Deepak, P. (2017a). Bioelectrochemical conversion of CO_2 to chemicals: CO_2 as next generation feedstock for the electricity-driven bioproduction in batch and continuous mode. *Faraday Discuss.* 202, 433–449. doi:10.1039/C1037FD00050B

Bajracharya, S., Yuliasni, R., Vanbroekhoven, K., Buisman, C. J. N., Strik, D. P. B. T. B., and Pant, D. (2017b). Long-term operation of microbial electrosynthesis cell reducing CO_2 to multi-carbon chemicals with a mixed culture avoiding methanogenesis. *Bioelectrochemistry* 113, 26–34. doi:10.1016/j.bioelechem.2016.09.001

Barker, H. (1947). *Clostridium kluyveri*. *Antonie Van Leeuwenhoek* 12, 167–176. doi:10.1007/BF02272663

Batlle-Vilanova, P., Ganigué, R., Ramió-Pujol, S., Bañeras, L., Jiménez, G., Hidalgo, M., et al. (2017). Microbial electrosynthesis of butyrate from carbon dioxide: production and extraction. *Bioelectrochemistry* 117, 57–64. doi:10.1016/j.bioelechem.2017.06.004

Blanchet, E., Duquenne, F., Rafrafi, Y., Etcheverry, L., Erable, B., and Bergel, A. (2015). Importance of the hydrogen route in up-scaling electrosynthesis for microbial CO_2 reduction. *Energy Environ. Sci.* 8, 3731–3744. doi:10.1039/C5EE03088A

Blaut, M. (1994). Metabolism of methanogens. *Antonie Van Leeuwenhoek* 66, 187–208. doi:10.1007/BF00871639

Chen, C.-C., Lin, C.-Y., and Lin, M.-C. (2002). Acid–base enrichment enhances anaerobic hydrogen production process. *Appl. Microbiol. Biotechnol.* 58, 224–228. doi:10.1007/s002530100814

Chen, W.-S., Strik, D. P., Buisman, C. J., and Kroeze, C. (2017). Production of caproic acid from mixed organic waste – an environmental life cycle perspective. *Environ. Sci. Technol.* 51, 7159–7168. doi:10.1021/acs.est.6b06220

Chen, W. S., Ye, Y., Steinbusch, K. J. J., Strik, D. P. B. T. B., and Buisman, C. J. N. (2016). Methanol as an alternative electron donor in chain elongation for butyrate and caproate formation. *Biomass Bioenergy* 93, 201–208. doi:10.1016/j.biombioe.2016.07.008

Cui, M., Nie, H., Zhang, T., Lovley, D., and Russell, T. P. (2017). Three-dimensional hierarchical metal oxide-carbon electrode material for high efficient microbial electrosynthesis. *Sustainable Energy Fuels* 1, 1171–1176. doi:10.1039/C7SE00073A

Ganigue, R., Puig, S., Batlle-Vilanova, P., Balaguer, M. D., and Colprim, J. (2015). Microbial electrosynthesis of butyrate from carbon dioxide. *Chem. Commun.* 51, 3235–3238. doi:10.1039/C4CC10121A

González-Cabaleiro, R., Lema, J. M., Rodríguez, J., and Kleerebezem, R. (2013). Linking thermodynamics and kinetics to assess pathway reversibility in anaerobic bioprocesses. *Energy Environ. Sci.* 6, 3780–3789. doi:10.1039/c3ee42754d

Graves, T., Narendranath, N. V., Dawson, K., and Power, R. (2006). Effect of pH and lactic or acetic acid on ethanol productivity by *Saccharomyces cerevisiae* in corn mash. *J. Ind. Microbiol. Biotechnol.* 33, 469. doi:10.1007/s10295-006-0091-6

Grootscholten, T. I. M., Steinbusch, K. J. J., Hamelers, H. V. M., and Buisman, C. J. N. (2013a). Chain elongation of acetate and ethanol in an upflow anaerobic filter for high rate MCFA production. *Bioresour. Technol.* 135, 440–445. doi:10.1016/j.biortech.2012.10.165

Grootscholten, T. I. M., Steinbusch, K. J. J., Hamelers, H. V. M., and Buisman, C. J. N. (2013b). Improving medium chain fatty acid productivity using chain elongation by reducing the hydraulic retention time in an upflow anaerobic filter. *Bioresour. Technol.* 136, 735–738. doi:10.1016/j.biortech.2013.02.114

Im, C. H., Song, Y. E., Jeon, B.-H., and Kim, J. R. (2016). Biologically activated graphite fiber electrode for autotrophic acetate production from CO_2 in a bioelectrochemical system. *Carbon Lett.* 20, 76–80. doi:10.5714/CL.2016.20.076

Jourdin, L., Freguia, S., Donose, B. C., Chen, J., Wallace, G. G., Keller, J., et al. (2014). A novel carbon nanotube modified scaffold as an efficient biocathode material for improved microbial electrosynthesis. *J. Mater. Chem. A* 2, 13093–13102. doi:10.1039/C4TA03101F

Jourdin, L., Freguia, S., Donose, B. C., and Keller, J. (2015a). Autotrophic hydrogen-producing biofilm growth sustained by a cathode as the sole electron and energy source. *Bioelectrochemistry* 102, 56–63. doi:10.1016/j.bioelechem.2014.12.001

Jourdin, L., Grieger, T., Monetti, J., Flexer, V., Freguia, S., Lu, Y., et al. (2015b). High acetic acid production rate obtained by microbial electrosynthesis from carbon dioxide. *Environ. Sci. Technol.* 49, 13566–13574. doi:10.1021/acs.est.5b03821

Jourdin, L., Freguia, S., Flexer, V., and Keller, J. (2016a). Bringing high-rate, CO_2-based microbial electrosynthesis closer to practical implementation through improved design and operating conditions. *Environ. Sci. Technol.* 50, 1982–1989. doi:10.1021/acs.est.5b04431

Jourdin, L., Lu, Y., Flexer, V., Keller, J., and Freguia, S. (2016b). Biologically-induced hydrogen production drives high rate/high efficiency microbial electrosynthesis of acetate from carbon dioxide. *ChemElectroChem* 3, 581–591. doi:10.1002/celc.201500530

Jourdin, L., and Strik, D. P. B. T. B. (2017). "Electrodes for cathodic microbial electrosynthesis processes: key-developments and criteria for effective research & implementation," in *Functional Electrodes for Enzymatic and Microbial Bioelectrochemical Systems*, eds V. Flexer and N. Brun (Wageningen: World Scientific), 429–473.

Kleerebezem, R., Joosse, B., Rozendal, R., and Van Loosdrecht, M. C. M. (2015). Anaerobic digestion without biogas? *Rev. Environ. Sci. Biotechnol.* 14, 787–801. doi:10.1007/s11157-015-9374-6

Koutinas, A. A., Yepez, B., Kopsahelis, N., Freire, D. M. G., De Castro, A. M., Papanikolaou, S., et al. (2016). Techno-economic evaluation of a complete bioprocess for 2,3-butanediol production from renewable resources. *Bioresour. Technol.* 204, 55–64. doi:10.1016/j.biortech.2015.12.005

Kucek, L. A., Nguyen, M., and Angenent, L. T. (2016a). Conversion of l-lactate into n-caproate by a continuously fed reactor microbiome. *Water Res.* 93, 163–171. doi:10.1016/j.watres.2016.02.018

Kucek, L. A., Spirito, C. M., and Angenent, L. T. (2016b). High n-caprylate productivities and specificities from dilute ethanol and acetate: chain elongation with microbiomes to upgrade products from syngas fermentation. *Energy Environ. Sci.* 9, 3482–3494. doi:10.1039/C6EE01487A

LaBelle, E. V., and May, H. D. (2017). Energy efficiency and productivity enhancement of microbial electrosynthesis of acetate. *Front. Microbiol.* 8:756. doi:10.3389/fmicb.2017.00756

Larsen, S., Nielsen, L. P., and Schramm, A. (2015). Cable bacteria associated with long-distance electron transport in New England salt marsh sediment. *Environ. Microbiol. Rep.* 7, 175–179. doi:10.1111/1758-2229.12216

Li, L., Zheng, M., Ma, H., Gong, S., Ai, G., Liu, X., et al. (2015). Significant performance enhancement of a UASB reactor by using acyl homoserine lactones to facilitate the long filaments of *Methanosaeta harundinacea* 6Ac. *Appl. Microbiol. Biotechnol.* 99, 6471–6480. doi:10.1007/s00253-015-6478-4

Liu, Y., He, P., Shao, L., Zhang, H., and Lü, F. (2017). Significant enhancement by biochar of caproate production via chain elongation. *Water Res.* 119, 150–159. doi:10.1016/j.watres.2017.04.050

Lovley, D. R. (2011). Live wires: direct extracellular electron exchange for bioenergy and the bioremediation of energy-related contamination. *Energy Environ. Sci.* 4, 4896–4906. doi:10.1039/c1ee02229f

Marshall, C., Ross, D., Handley, K., Weisenhorn, P., Edirisinghe, J., Henry, C., et al. (2017). Metabolic Reconstruction and Modeling Microbial Electrosynthesis. *BioRxiv 059410*. 7. doi:10.1038/s41598-017-08877-z

Martin, M. R., Fornero, J. J., Stark, R., Mets, L., and Angenent, L. T. (2013). A single-culture bioprocess of *Methanothermobacter thermautotrophicus* to upgrade digester biogas by CO_2-to-CH_4 conversion with H_2. *Archaea* 2013, 157529. doi:10.1155/2013/157529

Marzocchi, U., Trojan, D., Larsen, S., Meyer, R. L., Revsbech, N. P., Schramm, A., et al. (2014). Electric coupling between distant nitrate reduction and sulfide oxidation in marine sediment. *ISME J.* 8, 1682–1690. doi:10.1038/ismej.2014.19

Mekonnen, M. M., and Hoekstra, A. Y. (2016). Four billion people facing severe water scarcity. *Sci. Adv.* 2, e1500323. doi:10.1126/sciadv.1500323

Parshina, S. N., Ermakova, A. V., Bomberg, M., and Detkova, E. N. (2014). *Methanospirillum stamsii* sp. nov., a psychrotolerant, hydrogenotrophic, methanogenic archaeon isolated from an anaerobic expanded granular sludge bed bioreactor operated at low temperature. *Int. J. Syst. Evol. Microbiol.* 64, 180–186. doi:10.1099/ijs.0.056218-0

Patil, S. A., Arends, J. B. A., Vanwonterghem, I., Van Meerbergen, J., Guo, K., Tyson, G. W., et al. (2015a). Selective enrichment establishes a stable performing community for microbial electrosynthesis of acetate from CO_2. *Environ. Sci. Technol.* 49, 8833–8843. doi:10.1021/es506149d

Patil, S. A., Gildemyn, S., Pant, D., Zengler, K., Logan, B. E., and Rabaey, K. (2015b). A logical data representation framework for electricity-driven bioproduction processes. *Biotechnol. Adv.* 33, 736–744. doi:10.1016/j.biotechadv.2015.03.002

Puig, S., Ganigué, R., Batlle-Vilanova, P., Balaguer, M. D., Bañeras, L., and Colprim, J. (2017). Tracking bio-hydrogen-mediated production of commodity chemicals from carbon dioxide and renewable electricity. *Bioresour. Technol.* 228, 201–209. doi:10.1016/j.biortech.2016.12.035

Rabaey, K., and Rozendal, R. A. (2010). Microbial electrosynthesis – revisiting the electrical route for microbial production. *Nat. Rev. Microbiol.* 8, 706–716. doi:10.1038/nrmicro2422

Raes, S. M. T., Jourdin, L., Buisman, C. J. N., and Strik, D. P. B. T. B. (2017). Continuous long-term bioelectrochemical chain elongation to butyrate. *ChemElectroChem* 4, 386–395. doi:10.1002/celc.201600587

Richter, H., Martin, M., and Angenent, L. (2013). A two-stage continuous fermentation system for conversion of syngas into ethanol. *Energies* 6, 3987–4000. doi:10.3390/en6083987

Risgaard-Petersen, N., Kristiansen, M., Frederiksen, R. B., Dittmer, A. L., Bjerg, J. T., Trojan, D., et al. (2015). Cable bacteria in freshwater sediments. *Appl. Environ. Microbiol.* 81, 6003–6011. doi:10.1128/AEM.01064-15

Roghair, M., Strik, D. P. B. T. B., Steinbusch, K. J. J., Weusthuis, R. A., Bruins, M. E., and Buisman, C. J. N. (2016). Granular sludge formation and characterization in a chain elongation process. *Process Biochem.* 51, 1594–1598. doi:10.1016/j.procbio.2016.06.012

Schauer, R., Risgaard-Petersen, N., Kjeldsen, K. U., Bjerg, J. J. T., Jørgensen, B. B., Schramm, A., et al. (2014). Succession of cable bacteria and electric currents in marine sediment. *ISME J.* 8, 1314–1322. doi:10.1038/ismej.2013.239

Sharma, M., Aryal, N., Sarma, P. M., Vanbroekhoven, K., Lal, B., Benetton, X. D., et al. (2013). Bioelectrocatalyzed reduction of acetic and butyric acids via direct electron transfer using a mixed culture of sulfate-reducers drives electrosynthesis of alcohols and acetone. *Chem. Commun.* 49, 6495–6497. doi:10.1039/c3cc42570c

Sharon, D. A. M., and Kamp, H. G. J. (2016). *A Circular Economy in the Netherlands by 2050*. The Hague: Government of the Netherlands.

Sleutels, T. H. J. A., Lodder, R., Hamelers, H. V. M., and Buisman, C. J. N. (2009). Improved performance of porous bio-anodes in microbial electrolysis cells by enhancing mass and charge transport. *Int. J. Hydrogen Energy* 34, 9655–9661. doi:10.1016/j.ijhydene.2009.09.089

Spirito, C. M., Richter, H., Rabaey, K., Stams, A. J. M., and Angenent, L. T. (2014). Chain elongation in anaerobic reactor microbiomes to recover resources from waste. *Curr. Opin. Biotechnol.* 27, 115–122. doi:10.1016/j.copbio.2014.01.003

Steinbusch, K. J., Hamelers, H. V., Plugge, C. M., and Buisman, C. J. (2011). Biological formation of caproate and caprylate from acetate: fuel and chemical production from low grade biomass. *Energy Environ. Sci.* 4, 216–224. doi:10.1039/C0EE00282H

Van Eerten-Jansen, M. C., Ter Heijne, A., Grootscholten, T. I., Steinbusch, K. J., Sleutels, T. H., Hamelers, H. V., et al. (2013). Bioelectrochemical production of caproate and caprylate from acetate by mixed cultures. *ACS Sustainable Chem. Eng.* 1, 513–518. doi:10.1021/sc300168z

Zhang, F., Ding, J., Zhang, Y., Chen, M., Ding, Z.-W., Van Loosdrecht, M. C. M., et al. (2013). Fatty acids production from hydrogen and carbon dioxide by mixed culture in the membrane biofilm reactor. *Water Res.* 47, 6122–6129. doi:10.1016/j.watres.2013.07.033

Zhou, L., Yu, H., Ai, G., Zhang, B., Hu, S., and Dong, X. (2015). Transcriptomic and physiological insights into the robustness of long filamentous cells of *Methanosaeta harundinacea*, prevalent in upflow anaerobic sludge blanket granules. *Appl. Environ. Microbiol.* 81, 831–839. doi:10.1128/AEM.03092-14

Zhu, X., Zhou, Y., Wang, Y., Wu, T., Li, X., Li, D., et al. (2017). Production of high-concentration n-caproic acid from lactate through fermentation using a newly isolated *Ruminococcaceae bacterium* CPB6. *Biotechnol. Biofuels* 10, 102. doi:10.1186/s13068-017-0788-y

Conflict of Interest Statement: The authors declare that the research was conducted in the absence of any commercial or financial relationships that could be construed as a potential conflict of interest.

frontiers in Energy Research

ORIGINAL RESEARCH
published: 13 April 2018
doi: 10.3389/fenrg.2018.00015

Microbial Community Pathways for the Production of Volatile Fatty Acids From CO_2 and Electricity

Jorge Wenzel[1], Erika Fiset[2,3], Pau Batlle-Vilanova[4], Angela Cabezas[1], Claudia Etchebehere[1], María D. Balaguer[2], Jesús Colprim[2] and Sebastià Puig[2]*

[1] *Microbial Ecology Laboratory, Microbial Biochemistry and Genomics Department, Biological Research Institute "Clemente Estable", Montevideo, Uruguay,* [2] *LEQUIA, Institute of the Environment, University of Girona, Girona, Spain,* [3] *Center for Microbial Ecology and Technology (CMET), Ghent University, Ghent, Belgium,* [4] *Department of Innovation and Technology, FCC Aqualia, Barcelona, Spain*

This study aims at elucidating the metabolic pathways involved in the production of volatile fatty acids from CO_2 and electricity. Two bioelectrochemical systems (BES) were fed with pure CO_2 (cells A and B). The cathode potential was first poised at −574 mV vs. standard hydrogen electrode (SHE) and then at −756 mV vs. SHE in order to ensure the required reducing power. Despite applying similar operation conditions to both BES, they responded differently. A mixture of organic compounds (1.87 mM acetic acid, 2.30 mM formic acid, 0.43 mM propionic acid, 0.15 mM butyric acid, 0.55 mM valeric acid, and 0.62 mM ethanol) was produced in cell A while mainly 1.82 mM acetic acid and 0.23 mM propionic acid were produced in cell B. The microbial community analysis performed by 16S rRNA gene pyrosequencing showed a predominance of *Clostridium* sp. and *Serratia* sp. in cell A whereas *Burkholderia* sp. and *Xanthobacter* sp. predominated in cell B. The coexistence of three metabolic pathways involved in carbon fixation was predicted. Calvin cycle was predicted in both cells during the whole experiment while Wood-Ljungdahl and Arnon-Buchanan pathways predominated in the period with higher coulombic efficiency. Metabolic pathways which transform organic acids into anabolic intermediaries were also predicted, indicating the occurrence of complex trophic interactions. These results further complicate the understanding of these mixed culture microbial processes but also expand the expectation of compounds that could potentially be produced with this technology.

Keywords: bioelectrochemical systems, carbon fixation pathways, 16S rRNA gene community analysis, PICRUSt, metagenome prediction

OPEN ACCESS

Edited by:
Youngjune Jason Park, Gwangju Institute of Science and Technology (GIST), South Korea

Reviewed by:
Francisco Jesus Fernandez Morales, Universidad de Castilla-La Mancha, Spain
Lucinda Elizabeth Doyle, Nanyang Technological University, Singapore

****Correspondence:***
Jorge Wenzel
jwenzel@iibce.edu.uy

Specialty section:
This article was submitted to Carbon Capture, Storage, and Utilization, a section of the journal Frontiers in Energy Research

Received: *08 December 2017*
Accepted: *02 March 2018*
Published: *13 April 2018*

Citation:
Wenzel J, Fiset E, Batlle-Vilanova P, Cabezas A, Etchebehere C, Balaguer MD, Colprim J and Puig S (2018) Microbial Community Pathways for the Production of Volatile Fatty Acids From CO_2 and Electricity. Front. Energy Res. 6:15. doi: 10.3389/fenrg.2018.00015

INTRODUCTION

Burning of fossil and biomass fuels is currently the primary energy source responsible for the increment of carbon gaseous emissions that arise during the industrialization period. In this regard, a variety of mitigation strategies have been implemented at different levels, from carbon fixation in planted forests to fine chemicals production (Mikkelsen et al., 2010). Bioelectrochemical systems (BES) have been proposed for CO_2 capture and transformation (Nevin et al., 2010). BES technology exploits the ability of certain microorganisms to exchange electrons with an electrode, under an applied electric potential or current, catalyzing either oxidation (at the anode) or reduction (at the cathode) reactions. In BES, CO_2 is reduced by electrotrophic microbial communities. These communities harbor microorganisms capable of performing extracellular electron transfer (EET) to

obtain electrons from the surface of the electrode (Choi and Sang, 2016). The electrons are transferred directly from the electrode by extracellular protein structures called nanowires or by cell wall cytochromes [direct electron transfer (DET)] as demonstrated for *Geobacter* and *Shewanella* genera, respectively. Alternatively, this transfer could be done by redox intermediaries such as molecular hydrogen or formate [mediated electron transfer (MET)] under an applied electric potential (Sharma et al., 2014).

Bioelectrochemical systems technology for CO_2 capture was first demonstrated by Nevin et al. (2010). CO_2 was transformed into acetate (up to 10 mM) using a pure culture of *Sporomusa ovata*. The production of acetate was explained by the fact that *S. ovata* performs Wood-Ljundahl pathway (WLP) to fix CO_2 probably using electrons directly from the cathode without intermediaries (Breznak, 2006). More recently, Marshall et al. (2012, 2013) demonstrated acetate production using mixed cultures (max. 175 mM) in two subsequent studies. *Acetobacterium* sp. was the predominant microorganism within the microbial community in the biocathode when the acetate production rate and concentration were maximum. As well as for *Sporomusa ovata*, it had already been shown that the genus *Acetobacterium* is capable of performing the WLP to fix CO_2, which explained acetate production (Ljungdahl, 1986). Ganigué et al. (2015) demonstrated for the first time that chain elongation could extend the product range to butyrate with small concomitant production of ethanol and butanol. Recently, the concept of fixing CO_2 in BES using a continuous system was tested on a small scale with promising results (Arends et al., 2017). Arends et al. obtained an acetate titer of up to 91 mM in long operation periods with isopropanol and butyrate as value-added coproducts. In this work, the genus *Acetobacterium* was also predominant.

Several previous investigations have been performed to elucidate the electronic transfer mechanisms between electrodes and bacteria (Tremblay et al., 2017). However, scarce information appears in the literature about the microbial carbon fixation pathways involved in BES as well as the microbial pathways and interactions that further transform the primary carbon fixation products. More recently, Marshall et al. (2017) went a step forward demonstrating acetate production through the Arnon Buchanan Cycle (ABC) (Evans et al., 1966) and also proposing a new pathway for CO_2 fixation, involving a formate dehydrogenase and cytochromes. In addition to this cycle other unreported carbon fixation pathways, such as 3-hydroxypropionate or the Calvin cycle are still unnoticed. The main products of these pathways are the internal metabolites pyruvate (Herter et al., 2002) and glyceraldehyde-3-phosphate (G3P) (Yeates et al., 2008). Meanwhile, Arends et al. (2017), Batlle-Vilanova et al. (2017), and Raes et al. (2017) also contributed to elucidate the microbial pathways proposing the route of reverse beta oxidation for the production of butyrate and isopropanol from acetyl CoA. However, there is still a lack of information on the metabolic routes and microorganisms that can convert short chain acids produced by carbon fixation to more complex (reduced or medium to long-chain) compounds. For example, the three mechanisms for propionate production (Reichardt et al., 2014) from short chain fatty acids as well as glycogen intermediates production through the glyoxylate cycle (Berg et al., 2002) remain unexplored in BES. The knowledge increase on metabolic potentials of cathode microbial communities will contribute to more accurate carbon fixation control strategies in BES and to the investigation of other alternative products, expanding the applications of this technology.

This study focused on elucidating the metabolic pathways associated with autotrophic bioelectrosynthesis of organic compounds in BESs inoculated with mixed cultures. The non-autotrophic metabolic pathways for propionate production and acetate uptake (glyoxylate cycle) were also evaluated. For that, two microbial electrosynthesis cells (MECs) fed with CO_2 and inoculated with adapted biomass were operated in parallel and the microbial communities developed were analyzed by 16S rRNA gene high throughput sequencing. Based on these datasets, the main metabolic pathways were predicted. This work also aimed to explain the bioelectrosynthesis performance of both MECs through its microbial community composition and its predicted metabolic pathways.

MATERIALS AND METHODS

BES Setup

Experiments were conducted in two-chambered H-type MECs (cells A and B) consisting of two 150 mL bottles (anodic and cathodic chambers) connected *via* a glass tube. The chambers were separated by a cationic exchange membrane (CMI-7000, Membranes International Inc., USA) to allow proton migration from the anode to the cathode and to prevent product diffusion into the anodic chamber. A modified carbon cloth with nitrogen functional groups was used as the cathode to improve the wettability of the material. To introduce nitrogen groups, the initial carbon cloths (3 cm × 3 cm) (NuVant's ELATs LT2400W, FuelCellsEtc, USA) were treated with melamine in methanol (20 g of melamine in 100 mL of methanol) and stirred at room temperature for 5 h. Then, the suspension was boiled to evaporate the alcohol and the carbon cloths were dried at 120°C. Carbon rods (5 mm in diameter and 100 mm in length) (Mersen Ibérica, Spain) were used as anodes. A mineral growth medium (100 mL) was used as electrolyte and supplied to the cells as described by Batlle-Vilanova et al. (2015). A methanogenic inhibitor (2-bromoethanesulfonate) was added to the medium at a concentration of 20 mM. The initial pH of the medium was set to 6.8. The cathode (working electrode) potential was controlled and monitored with a potentiostat (BioLogic, Model VSP, France) in a three-electrode arrangement cell with Ag/AgCl [+197 mV vs. standard hydrogen electrode (SHE); RE-5B, BASI, UK] as the reference electrode. A carbon rod placed in the anode chamber was set as the counter electrode.

MEC Operation

Both cells were operated under similar conditions. The cathodes were inoculated at 5% (in 100 mL of cathode working volume) with a mixed microbial community dominated by species of the genus *Clostridium* obtained from the cathode bulk solution of a parent MEC (Ganigué et al., 2015). The product composition in the parent MEC at inoculum extraction time was 9.80 mM of

acetate, 0.05 mM of propionate, and 0.40 mM butyrate. To provide a mineral carbon source and achieve anaerobic conditions in the chambers, CO_2 (99.9%, Praxair, Spain) was bubbled in the chamber for 20 min at the beginning of the experiment and then periodically when the observed current demand stopped increasing.

Cathode potentials of −574 mV vs. SHE were set from days 1 to 44 and from days 1 to 47 for cells A and B, respectively. As the response of the cells was not satisfactory, the availability of reducing power in the cathodes was increased by lowering the poised potential to −756 mV vs. SHE until the end of the experiment. The desired pH was adjusted using phosphoric acid (1 M) or NaOH (1 M) stock solutions. The cells were thermostatically controlled at 35°C.

During the experimental period, 10 mL of bulk cathode suspension were sampled periodically through two sampling ports in each chamber. After sampling, the same volume of fresh medium was added to the chamber. The pH was determined using a pH meter. After that, samples were centrifuged at 5,000 *g*, 5 min. The pellets were stored at −20°C for microbiological analysis and volatile fatty acids (VFAs) concentration was determined in the supernatant as described in Section "Chemical Analysis." At the end of the experiments, the electrodes were removed for microbiological analysis of the biofilm and stored at −20°C.

Chemical Analysis

Volatile fatty acid and alcohols in the samples were determined with a 7890A gas chromatograph (Agilent, USA) equipped with a DB-FFAP column (Agilent, USA) and a flame ionization detector. Prior to the analysis, samples were acidified with orthophosphoric acid (85%, Scharlau, Spain), and an internal standard (crotonic acid) was added. The composition of the gas phase (CH_4, H_2, CO_2, and O_2) was monitored daily using the same equipment in a second channel equipped with a HP-Molsieve column (Agilent, USA) and a thermal conductivity detector. Formate was quantified by ion chromatography using a Dionex CS-5000 DP (Thermo-Fisher Inc., USA).

Coulombic Efficiency (CE)

Current density was continuously monitored using EC-Lab software (Biologic, France). The CE was calculated as the ratio of the total charge delivered to the organic products obtained (VFA and alcohols). The charge in coulombs provided to the cathode by the potentiostat was calculated according to Batlle-Vilanova et al. (2015).

Cyclic Voltammetry (CV)

Cyclic voltammetry was performed at experimental periods II and VI after CO_2 bubbling, in experiments with the same three-electrode arrangement described in Section "BES Setup," to identify changes in the "bioelectrocatalysis" over time using an EC-Lab software controlled potentiostat (BioLogic, VSP model, France). The CV performed at the beginning of the experiment with fresh mineral medium was used as an abiotic control (pH 6.8). The scan window of the CV was from 400 to −600 mV vs. SHE when the poised potential was set in −547 mV and from 200 to −1,000 mV vs. SHE when the applied potential was shifted to −756 mV vs. SHE. Three voltamperometric cycles were performed in each routine at a scan rate of 1 mV/s. The cathode potentials from the CVs were corrected according to the pH and temperature conditions when the assay was performed using the Nernst equation.

Microbial Community Analysis

For DNA extraction from the biofilm attached to the carbon cloth, electrodes were washed exhaustively with sterile physiological serum (9 g/L NaCl in deionized water) to remove remaining planktonic cells. Aliquots of 250 mg of the finely chopped carbon cloth electrodes were used for DNA extraction. On the other hand, 150 mg of wet pellets were used for DNA extractions from the bulk biomass. The extractions were performed using the Power Soil DNA Kit (Mo Bio laboratories, Carlsbad, CA, USA) according to the manufacturer's instructions. After checking the extracted DNAs quality by agarose gel electrophoresis, it was dehydrated with 95% ethanol and sent to the Institute for Agrobiology Rosario (INDEAR, Argentina). The 16S rRNA genes were amplified using the primer sets V3-357F and V5-923R (Sim et al., 2012) and sequenced using a Roche Genome Sequencer FLX Titanium system. The raw sequences were analyzed using the QIIME software (Caporaso et al., 2010). *De novo* chimera detection was performed with Usearch 6.1 software (Edgar, 2010). *De novo* operational taxonomic units (OTUs) were chosen and their taxonomy assigned using the UClust tool on the basis of 97% sequence identity with Greengenes[1] reference sequences dataset. Sequence alignments were performed with PyNAST. To compare the microbial communities between samples a phylogenetic diversity index and a *jackknifed* (weighted and unweighted) UniFrac (Hamady et al., 2010) analysis were performed with QIIME software tools. Phylogenetic affiliations of the most prevalent OTUs obtained by the QIIME software were confirmed by the construction of a phylogenetic tree with reference sequences. The phylogenetic reconstructions were made using MEGA 6.0 software (Tamura et al., 2011).

The metabolic capabilities on a metagenomic scale were predicted with the PICRUSt software (Langille et al., 2013). This method uses the genomic information of the closest relative of the OTUs whose genome has been sequenced, annotated and deposited in the KEGG database.[2]

The sequences obtained were deposited at the National Center for Biotechnology Information SRA database (NCBI)[3] under the accession number SAMN04550871.

RESULTS AND DISCUSSION

Bioproduction of Carbon-Neutral Chemicals from CO_2 and Renewable Electricity

Several carbon chemicals were produced in both cells (**Table 1**). Initially, the cathode potential was set at −547 mV vs. SHE to promote DET mechanisms (Nevin et al., 2010). Formate and acetate were produced in both cells (**Table 1**) achieving similar maximum concentrations of formate (2.3 mM). The CEs during

[1] http://greengenes.lbl.gov (Accessed: September, 2015).
[2] http://www.genome.jp/kegg/ (Accessed: September, 2015).
[3] www.ncbi.nlm.nih.gov (Accessed: September, 2015).

TABLE 1 | Summary of the applied potential and response variables of cells A and B in each experimental period.

Cell	Period	Timespan (days)	Applied potential (mV)	Mean pH	Cumulative charge (C)	Charge to products (C)	CE (%)	Presence of H_2 in headspace	Maximum concentration of organic compounds (mM)					
									Formic acid	Acetic acid	Butyric acid	Propionic acid	Valeric acid	Ethanol
Cell A	1	0–14	−547	6.21 ± 0.46	738	136	18.4	No	2.32	0.59	0	0.10	0	0
	2	14–35	−547	2.20 ± 0.27	1,599	164	10.2	Yes	1.98	0.55	0	0	0	0
	3	35–44	−547	4.00 ± 1.00	1,752	101	5.8	No	2.18	0.10	0	0	0	0
	4	44–67	−756	5.25 ± 0.56	2,395	990	41.3	Yes	0.60	1.87	0.15	0.45	0.55	0.62
Cell B	1	0–21	−547	6.92 ± 0.26	1,290	94	7.3	No	2.36	0.35	0	0	0	0
	2	21–40	−547	2.32 ± 0.23	4,689	132	2.8	Yes	2.04	0.52	0	0.23	0	0
	3	40–47	−547	4.75 ± 1.00	4,751	113	2.4	No	0.28	0.05	0	0	0	0
	4	47–66	−756	5.88 ± 0.38	5,534	196	3.6	Yes	0.71	1.8	0	0	0	0

The pH values are mean values in each period ± SD.

this period were 18.4 and 7.3% for cells A and B, respectively (**Table 1**). Neither hydrogen nor methane were detected in the headspace. The product profiles obtained with the same microbial source in the parent MEC were not achieved, probably due to the lower reducing potential applied in the parent MEC (−800 mV vs. SHE) (Ganigué et al., 2015). In that work, a concentration of 3.8 mM of butyrate together with ethanol and acetate was achieved after 19 days of operation.

In order to reach product diversification according to the mentioned study by acidifying the cells, we decided to decrease the pH during the second operation period. The low buffer capacity of the medium made the pH control difficult and pH plummeted from 6.21 ± 0.46 and 6.92 ± 0.26 to 2.2 ± 0.3 and 2.3 ± 0.2 for cell A and B, respectively. As expected, at this low pH, hydrogen was detected in the cells headspace (**Table 1**) and carbon production ceased. During this period, CVs were performed for both cells. An increase was detected in the catalytic capability of the bioelectrode compared to the abiotic control, at the applied potential (**Figure 1**). The shape of the reductive current limit at low potential is usually reported as hydrogen evolution in non-noble electrodes, and the catalytic improvement is commonly linked to biofilm development in the electrode surface (Batlle-Vilanova et al., 2014).

As mentioned, hydrogen production was observed as well as an increase in the current limit at the applied potential, but the proton consumption was not enough to raise the pH. Therefore, NaOH was added, increasing the pH to mean values of 4.0 ± 1.0 and 4.8 ± 1.0 in cells A and B, respectively. In both cells, mainly formate was produced (up to 2.20 mM in cell A and 0.31 mM in cell B) with concomitant acetate production. The CE in this period decreased to 5.8 and 2.4% for cells A and B, respectively, and no hydrogen production was detected (**Table 1**).

During the fourth period, the applied potential was decreased to −756 mV vs. SHE. This strategy was used to convert the hydrogen ion excess to molecular hydrogen which would increase the pH. The presence of hydrogen explained the additional increase in the absolute reductive current limit at low potentials observed in the CVs (**Figure 1**). During this period, a diversification of organic compounds (1.87 mM acetate, 0.21 mM formate, 0.15 mM butyrate, 0.43 mM propionate, 0.55 mM valerate, and 0.62 mM ethanol were measured in the richest sample) as well as an increase in acetate concentration was observed in cell A. This organic compound production profile was in accordance to the inoculum potential demonstrated in the parent MEC (Ganigué et al., 2015). In cell B, acetic and formic acids were produced in a stable way, but did not exceed the amounts observed during earlier periods. An important improvement of the CE to a value of 41.3% was only observed in cell A (**Table 1**).

During the whole period, the organic acid production and the modification in the catalytic capability of the cathodes suggested the development of an electroactive community responsible for the bioelectrosynthesis of the organic compounds.

Microbiological Analysis

Microbial Community Structure and Diversity

Bulk solution samples from cathode chambers during experimental periods I, II, and IV were analyzed by 16S rRNA gene

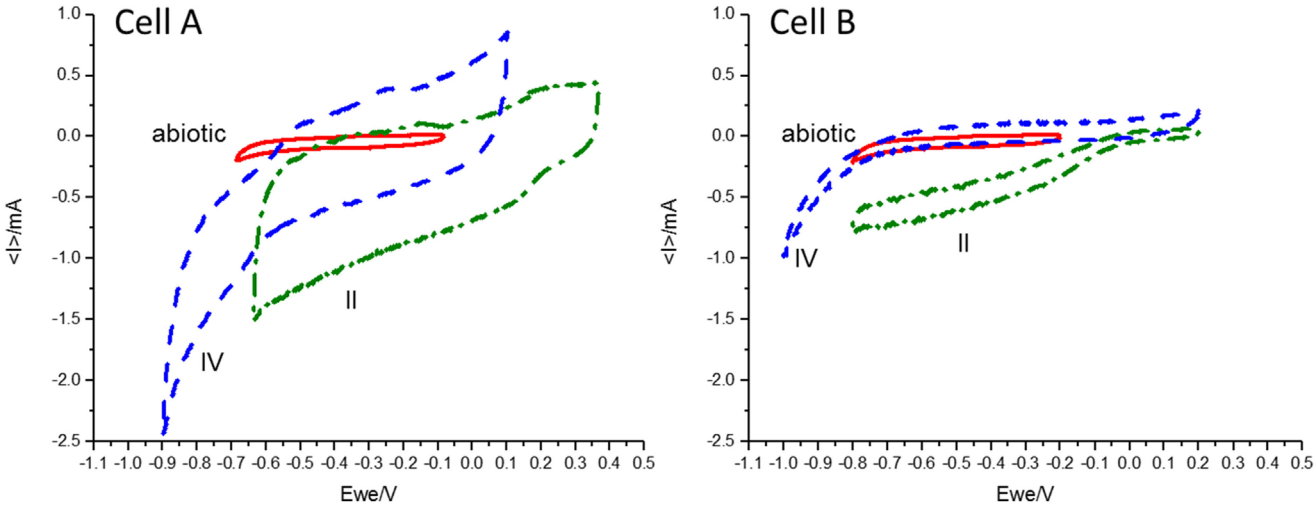

FIGURE 1 | Cyclic voltammetry results performed in the abiotic control (red, solid line), the second period (II, green dashed-dotted line) and the fourth period (IV, blue dashed line) for cells A and B at a scan rate of 1 mV/s under turnover conditions. Differences in the catalytic current for the different periods and between cells A and B at each potential can be observed.

pyrosequencing, together with samples from the biofilm attached to the cathodes at the end of experiments. A total of 101,344 high quality reads were obtained and grouped at 95% similarity into 63 and 146 OTUs in average for cells A and B, respectively. Rarefaction curves show that most of the sample diversity was contained in the datasets as the phylogenetic diversity index stabilized with increasing sample size (Figure S1 in Supplementary Material). The sample taken at day 34 from cell B presented higher diversity than the other samples as shown in the rarefaction curves. This sample contained a large number of sequences classified within minority microbial groups as will be seen further in the OTU level analysis. The sample taken during period I for cell B was not included in the analysis as no DNA was obtained probably due to low biomass concentration.

Principal component analysis (PCA) show that the microbial communities of cell A and cell B evolved divergently during operation time even though they were operated under similar conditions (**Figure 2**). This is in accordance with the differences observed in the VFA production profiles between both cells. Microbial communities attached to the cathodes and from bulk suspensions grouped together when PCA was performed without including OTU relative abundance (unweighted-UniFrac). This indicates a close phylogenetic relationship between microbial communities of both samples (suspension and biofilm) (**Figure 2A**). Differences in OTUs abundances were relevant as when including this variable in the analysis (weighted-UniFrac) the same samples from cell A did not group closely (**Figure 2B**). This allows us to point out that the phylogenetic groups associated with the attached biofilm are very similar to those that remain in suspension being the main difference their relative abundance.

The OTU level analysis showed that even though the microbial communities presented many OTUs, only a few OTUs were predominant, ranging from four to eight in the different samples (**Figure 3**). Moreover, high dominance of one, two, or three OTUs was observed in most of the samples as previously reported (Marshall et al., 2013, 2017; Arends et al., 2017). Although several OTUs were shared by both cells, their relative abundance was different explaining the divergence observed in the PCA. A very high dominance of OTUs 792 and 793 was detected in samples from cell B, especially at the end of the operation. On the contrary, samples taken from cell A presented codominace of OTUs 792, 960, and 834. The biofilm and bulk communities in cell B closely resemble each other. In contrast, in cell A the dominance between OTUs 792 and 960 changed; OTU 792 dominated the biofilm while OTU 960 dominated the bulk solution.

Classification of Predominant OTUs and Metabolic Potential of the Detected Microorganisms

Operational taxonomic unit sequences were classified mainly within the phyla *Firmicutes*, *Proteobacteria*, *Bacteroidetes*, and *Actinobacteria* (Figure S2 in Supplementary Material) with a high abundance of *Proteobateria*. According to the analysis at genus level, sequences from the most abundant OTUs were closely related to sequences from the genera *Clostridium, Burkholderia*, and *Serratia* in cell A and *Burkholderia* and *Xanthobacter* in cell B (**Table 2**; Figures S3 and S4 in Supplementary Material).

A literature review regarding the metabolic capabilities of the closest relatives of the predominant OTUs was performed. In relation to carbon fixation, the closest relatives presented known capacity to perform the WLP like *Clostridium* (OTU 960) (Schleifer 2009) in cell A and Calvin cycle (**Table 2**) like *Serratia* (OTU 834) (Octavia et al., 2014) in cell A, *Xanthobacter* (OTU 793) (Oren, 2014) and *Castellaniella* (OTU 970) in cell B. Interestingly, the most prevalent OTU in both cells was affiliated to the *Burkholderia* genus (OTU 792). Microorganisms belonging to this genus have the capability of short chain fatty acid uptake through the Glyoxylate cycle under microaerophilic conditions producing glycogenic intermediary compounds (Mira et al.,

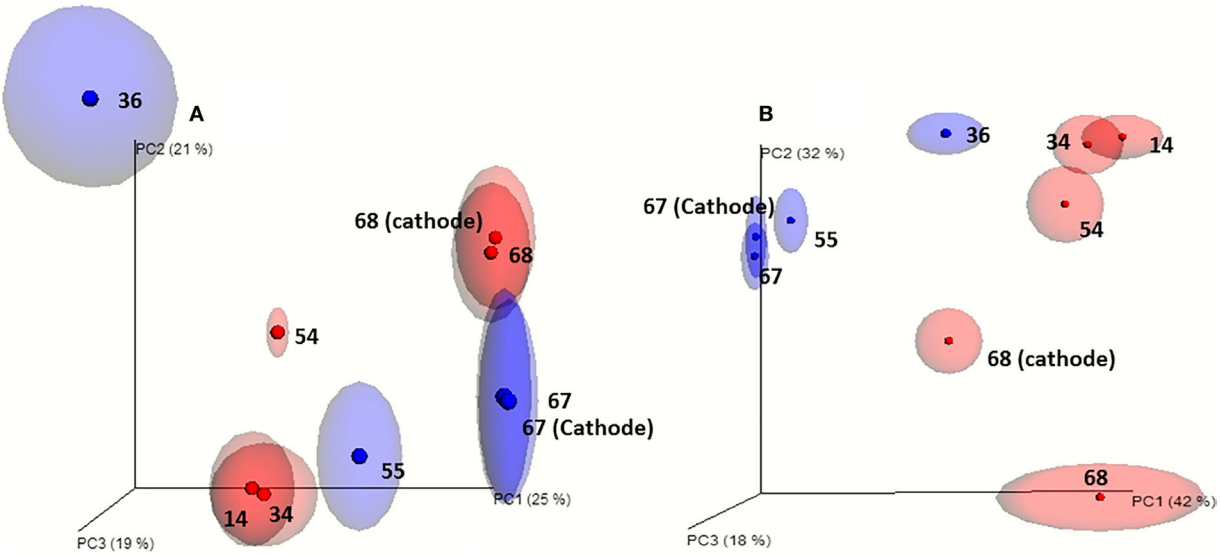

FIGURE 2 | Beta diversity analysis of the microbial communities based on the 16S rRNA gene pyrosequencing results. **(A)** Jack-knifed (even 500) unweighted-UniFrac and principal component analysis. **(B)** Jack-knifed (even 500) weighted-UniFrac and principal component analysis. Ellipses indicates the dispersion obtained for the Jack-knife analysis (red: cell A; blue: cell B). The samples obtained from the bulk solution are indicated by the day of sampling and the samples taken from the biofilm of the cathodes at the end of the experiments are indicated by the day of sampling and the word cathode.

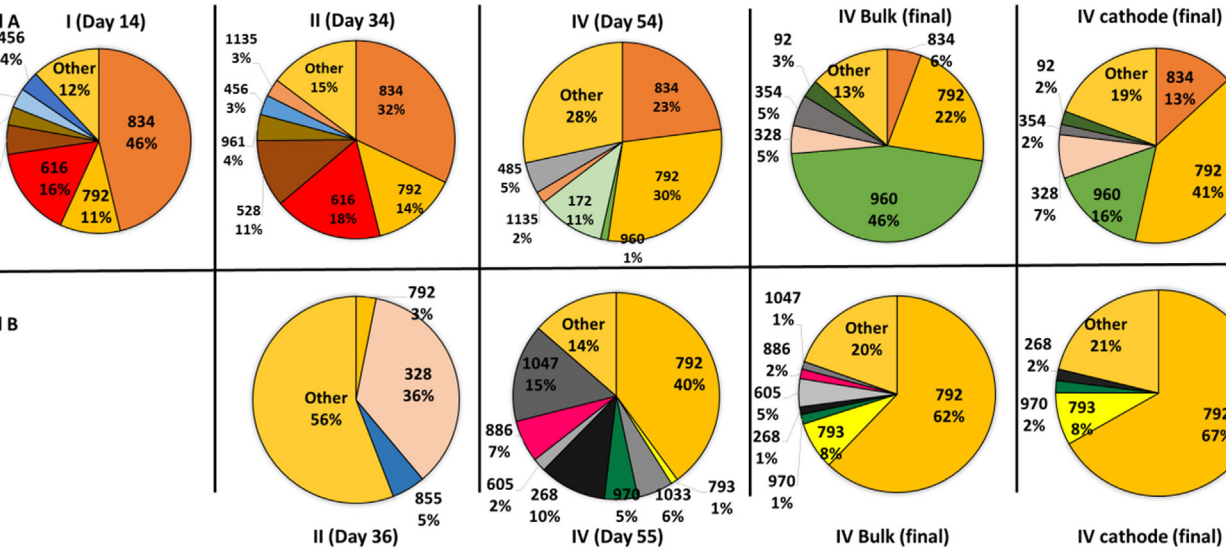

FIGURE 3 | Pie charts showing the relative abundance of the operational taxonomic units that contribute more than 1% to the total community according to 16S rRNA gene pyrosequencing analysis. The samples were taken during the four periods from the suspended cells. At the end of the operation, samples from the biofilm attached to the cathodes were also analyzed. The samples obtained from the bulk solution are indicated by the day of sampling and the samples taken from the biofilm of the cathodes at the end of the experiments are indicated by the day of sampling and the word cathode. The sample from cell B taken during the first period could not be analyzed due to the low biomass content.

2011; Van Acker et al., 2013) (**Table 2**). The presence of micro-aerophilic microorganisms might be helpful to decrease oxygen levels produced by diffusion from the anode chamber (Marshall et al., 2017). On the other hand, the production of propionic acid in cell A could be explained by the presence of organisms from the *Clostridium* genus and to the *Veillonellaceae* family. Both groups present species with the capacity to produce propionic acid (Tholozan et al., 1992; Reichardt et al., 2014). These groups were not found in high proportion in cell B where stable propionic production was not observed which then suggests that these microorganisms were involved in propionic acid production in cell A.

The WLP has been frequently reported and discussed in this type of systems. However, as far as we know, this is the first time

TABLE 2 | Classification of the predominant OTUs in the microbial communities according to 16S rRNA gene sequences analysis.

OTU	Abundance at final time in biofilm/suspension samples	Closer relative according to the phylogenetic tree	Metabolic capabilities	Reference
Cell A				
792	41/22%	*Burkholderia cepacia* [FJ169472.1]	Not reported CO_2 fixation. Glyoxylate cycle	Mira et al. (2011) and Van Acker et al. (2013)
960	16/46%	*Clostridium aciditolerans* JW/YJL-B3 [DQ114945.1]	Fix CO_2 by Wood-Ljungdahl pathway. VFA and alcohols producers (in genus)	Schleifer (2009)
834	13/6%	*Serratia marcescens* H14 [GU826156.1]	Fix CO_2 by Calvin cycle. Glyoxylate cycle	Bharti et al. (2014)
328	7/5%	Ideonella sp. B511 [AB049106.1]	Fix CO_2 unknown pathway	Garrity et al. (2005)
92	2/3%	*Haematobacter genomosp.* H2240 [DQ342319.1]	Not reported CO_2 fixation	Pujalte et al. (2014)
354	2/5%	*Sporomusa rhizae* RS [AM158322.1]; (*Veillonellaceae* family)	Fix CO_2 Wood-Ljungdahl pathway. Several propionate producers (in family)	Breznak (2006)
Cell B				
792	67/62%	*Burkholderia cepacia* [FJ169472.1]	Not reported CO_2 fixation. Glyoxylate cycle	Mira et al. (2011) and Van Acker et al. (2013)
793	8/8%	*Xanthobacter autotrophicus* [HQ025927.1]	Fix CO_2 by Calvin cycle. glyoxylate cycle	Oren (2014)
1,047	<1/1%	*Pandoraea pnomenusa B-356 [EF596910.1]*	Not reported CO_2 fixation	Coenye et al. (2000)
605	<1/5%	*Burkholderia* sp. kmd_168 [EU723147.1]	Not reported CO_2 fixation. Glyoxilate cycle	Mira et al. (2011) and Van Acker et al. (2013)
970	2/1%	*Castellaniella* sp. *Pyr24 [GU951458]*	Fix CO_2 by Calvin cycle	Hu et al. (2015)
886	<1/2%	*Cellulomonas gelida* DSM 20111^T [X83800.1]	Not reported CO_2 fixation	Goodfellow (2012)
268	<1/1%	*Dyella ginsengisoli str. LA-4* [EF191354.1]	Not reported CO_2 fixation	Jung et al. (2009)

Only the OTUs retrieved in the samples taken from the biocathodes at the end of the experiments were included. The closest relative to each OTU sequence was determined according to the phylogenetic trees showed in the supplementary material (Figures S3 and S4 in Supplementary Material). The metabolic capabilities of the microorganisms according to the bibliography were also included.

in which the presence of microorganisms capable of performing the Calvin cycle in MECs is reported. The primary product of this pathway is G3P, a compound found in the intermediary metabolism (Bharti et al., 2014). G3P can be further oxidized to pyruvate by glycolysis and then fermented to 2,3-butanediol, succinate, lactate, formate, glycerol, acetate, or acetoin by some *Serratia* species (Imhoff, 2005). G3P can also serve as a substrate for anabolic pathways such as gluconeogenesis, as well as for reserve product biosynthesis, such as polyhydroxyalcanoates or long chain fatty acids, in organic carbon limiting cultures (Lugg et al., 2008). The production of these compounds might contribute to explain the low CE observed in both cells during the whole experimental period.

In this context, glyoxylate cycle performing micoorganisms, like *Burkholderia cepacia* (OTU 792), might utilize acetate or formate produced by other microorganisms in the cell, suggesting interactions between primary producers (carbon fixing microorganisms) and organic acid consumers. The same behavior was observed by Hu et al. (2015) and the authors suggest that these trophic interactions were favorable for the carbon fixation flux rate.

Up to this point, the analysis has been based on the previous literature reporting the metabolic capabilities of the closest related microorganisms of those detected in the cells. These reports were based on experimental assays performed using cultured microorganisms. Nevertheless, not all metabolic pathways of the cultured microorganisms have been studied experimentally. The potential to perform these pathways could be found in the genomes of phylogenetically related microorganisms. Therefore, we decided to use a different approach to study the metabolic pathways involved in the production of organic compounds through bioelectrosynthesis.

Metabolic Capabilities at Community Level

The metabolic pathways were predicted from the 16S rRNA gene sequencing data using the tool PICRUSt. This tool enables to link 16S rRNA gene sequences with metabolic capabilities found in microbial genomes deposited in the KEGG database. The analysis was focused on searching key enzymes previously described in the literature for carbon fixation, propionic acid production and the Glyoxylate cycle (**Table 3**).

This approach showed that, in addition to the WLP and ABC reported in other MECs (Arends et al., 2017; Marshall et al., 2017), the Calvin cycle was also potentially relevant in the electrochemically assisted carbon fixation through the intermediary metabolism reactions, as suggested by Rabaey et al. (2011) (**Figure 4**). Calvin cycle was predicted in all samples in both cells without large differences in relative abundances over time, with the exception of the sample taken at day 36 (period II) from cell B, in which the Calvin cycle predicted genes presented very high abundance (**Figure 4**). The OTUs that strongly contribute to Calvin cycle were classified within the *Serratia* and *Xanthobacter* genera. In contrast, the WLP was absent at the beginning of the experiments in both cells, and became prevalent in cell A at the end of the experimental period where a diversification of the organic acids produced was observed. The main OTUs that contribute to the prediction of this pathway were classified within the *Clostridium* genus. A similar behavior was observed for the ABC (**Figure 5**), in which the OTUs contributing to this pathway, by its predicted content in *Kor*C gene, were classified mainly within the *Clostridiaceae* family, particularly within the *Clostridium* genus, and the *Veillonellaceae* family, in cell A. In the case of cell B, OTUs that represented individually less than 1% of the total amount of ARNr 16S gene sequences contributed to this pathway and were

TABLE 3 | Metabolic pathways (key enzymes) evaluated *via* PICRUSt.

Pathway	Enzyme	Definition	KEGG orthology
Calvin cycle	rbcL	Ribulosa biphosphate carboxylase long chain (RubisCo)	K01601
Calvin cycle	PRK	Phosphoribulokinase	K00855
Arnon-Buchanan	KorC	2-oxoglutarate ferredoxin oxidoreductase subunit gamma	K00177
Wood-Ljungdahl	acsB	Acetyl-CoA synthase	K14138
Wood-Ljungdahl	acsE	5-methyltetrahydrofolate corrinoid/iron sulfur protein methyltransferase	K15023
Wood-Ljungdahl	acdhD	Acetyl-CoA decarbonylase/synthase complex subunit delta	K00194
Wood-Ljungdahl	fhs	Formate-tetrahydrofolate ligase	K01938
Propionate (succinate pathway)	mmcD	Methylmalonyl-CoA decarboxylase	K11264
Propionate (propanediol pathway)	pduP	Propionaldehyde dehydrogenase	K01908
Propionate (propanediol pathway)	pct	Propionate CoA-transferase	K13922
Propionate (acrylate pathway)	prpE	Propionyl-CoA synthetase	K01026
Glyoxylate cycle	aceB	Malate synthase	K01638
Glyoxylate cycle	aceA	Isocitrate lyase	K01637

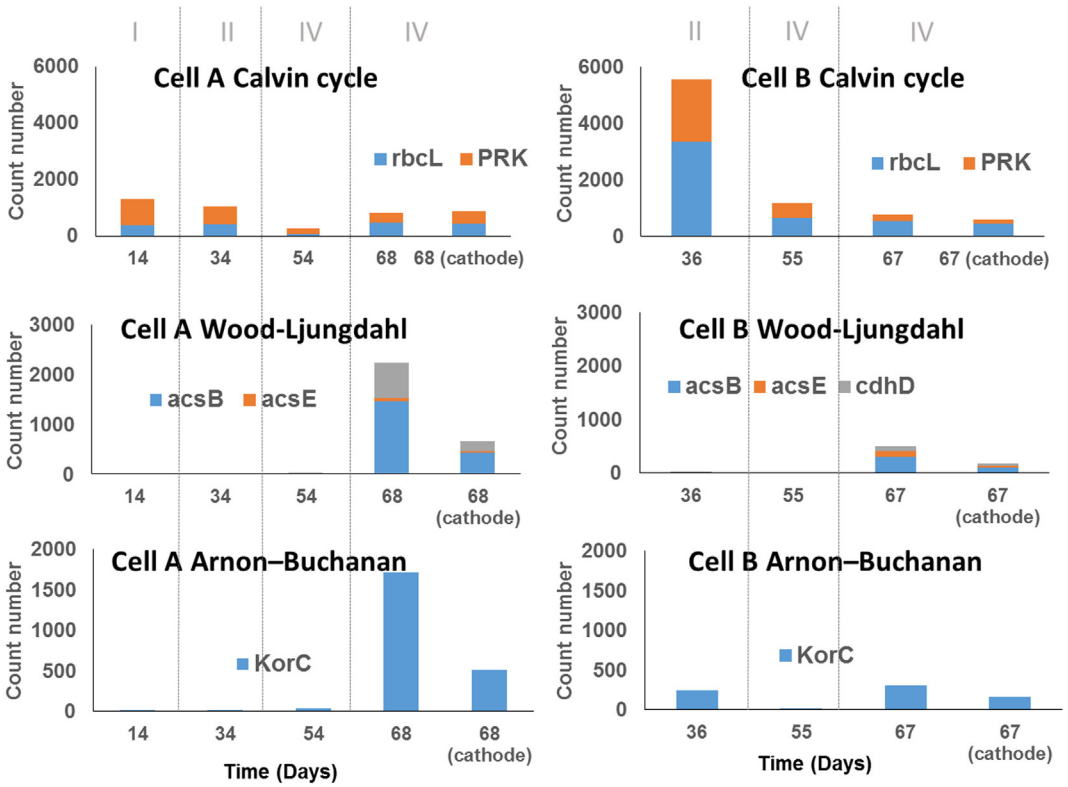

FIGURE 4 | Abundance of genes encoding key enzymes of three carbon fixation pathways according to PICRUSt analysis prediction. The samples taken from the biomass in the bulk solution are indicated by the day of sampling. The sample taken from the biocathodes at the end of the experiment were indicate as the day of sampling and the word cathode. The count number was calculated as the sum of the number of reads that were assigned to the species that contain the particular gene, divided by the number of copies of the gene encoding the 16S rRNA reported for the species to which the read was assigned and multiplied by the gene replicates number in the annotated genome of the closest relative.

classified within *Spirochaetaceae* and *Peptococcaceae* families (OTU table, Table S1 in Data Sheet 2 in Supplementary Material). Interestingly, the ABC had not been previously reported in bio-electrosynthesis until the metagenomics approach of Marshall et al. (2017) and was confirmed by Arends et al. (2017) and by this study.

In summary, the results from the PICRUSt prediction suggest that at least three CO_2 fixing mechanisms reported for *Bacteria* coexist in the cells. At the end of the experiment, where a diversification of the organic compounds production occurred, the WLP and ABC seemed to be more prevalent than the Calvin cycle, which was present in all periods.

The mechanisms by which propionic acid is produced in MECs remain unclear. In order to understand this process, the same approach was used. The key genes for the three reported pathways of propionic acid production were explored using

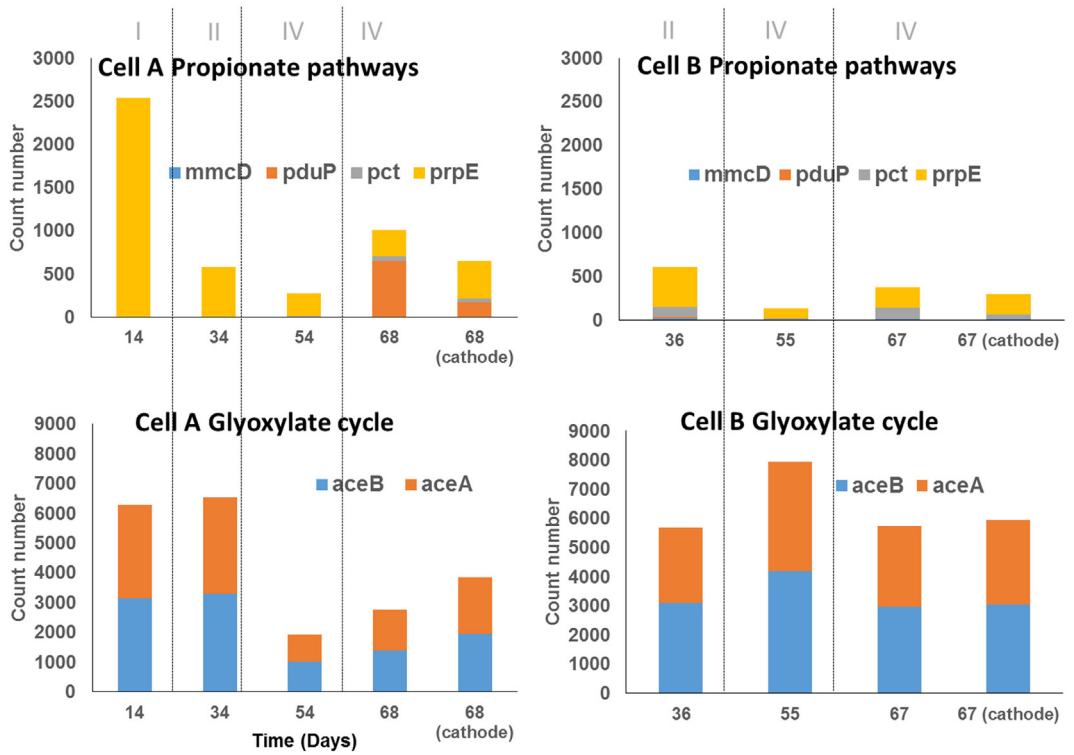

FIGURE 5 | Abundance of genes encoding key enzymes for propionate production and short-chain fatty acid uptake (glyoxylate cycle) in samples of cells A and B according to PICRUSt analysis. The samples taken from the biomass in the bulk solution are indicated by the day of sampling, the sample taken from the biocathodes at the end of the experiment were indicate as the day of sampling and the word cathode. The count number was calculated as the sum of the number of reads that are assigned to the specie that contains the particular gene, divided by the number of copies of the gene encoding the 16S rRNA reported for the specie to which read was assigned and multiplied by the gene replicates number in the annotated genome of the closest relative.

PICRUSt (**Table 3**). Key genes of the propanediol pathway (*pct* and *pdu*P) were predicted in all samples (**Figure 5**). The propanediol pathway allows bacteria to transform 2,3-propanediol, produced from sugars, lactate, or dihydroxyacetone phosphate (a glycogenic intermediary), into propionate and propanol (Reichardt et al., 2014). Specifically, the gene *pdu*P was predicted in high abundance in the two samples taken during period IV in cell A, in which propionic acid production was observed. The OTUs that mainly contributed to this predicted gene abundance in the samples were classified within the *Clostridium* genus in cell A and within the *Propionibacterium* genus in cell B, although in low abundance in the last case (within OTUs with less than 1% sequence abundances, Table S1 in Data Sheet 2 in Supplementary Material). Regarding the acrylate pathway for propionate production, the key gene *prp*E was also predicted in all samples but in low abundance. This pathway is characteristic of members belonging to the *Clostridium* genus and *Veillonellaceae* family allowing the utilization of lactate to produce propionate (Reichardt et al., 2014). Indeed, the OTUs found by PICRUSt which contribute with the *prp*E gene were classified within those phylogenetic groups. The succinate pathway uses succinate or lactate as inputs to produce propionate. The gene selected for this pathway (*mmc*D) was predicted in low proportion in all the samples, but interestingly, the OTUs that contributed to this gene abundance were classified in the *Burkholderia* genus.

Our results show that the organic acids produced might also be consumed producing glycogenic intermediates or reserve compounds by the Glyoxylate pathway. The Glyoxylate cycle was explored through this methodology focusing on two key genes: *ace*A and *ace*B (**Table 3**). These genes were predicted with high abundance in all samples (**Figure 5**). OTUs classified within *Burkholderia* genus found in both cells contributed strongly to this pathway, as well as *Serratia,* only in cell A, where the presence of both genes was predicted. In cell B, OTUs classified within *Xantomonadaceae* family and *Actinobacteria* phylum (including the OTUs classified as *Xantomonas* and *Cellulomonas*) also contributed to this pathway prediction. The presence of the glyoxylate pathway suggests that acetate transformation (produced by carbon fixation) into glycogenic intermediaries, gives the possibility for the fixed carbon to take anabolic or catabolic biochemical pathways. A metabolomics approach could contribute to elucidate the fixed carbon destination at community level. Interestingly, some observed OTUs for which a contribution to Calvin cycle was predicted, also contribute to the glyoxylate cycle. That is the case of the OTUs classified within the *Serratia* genus and the *Xantomonadaceae* family.

Based on the results obtained from the microbial community analysis, complex metabolic trophic interrelationships could be inferred (**Figure 6**). At least three pathways might be involved in carbon fixation (WLP, ABC, and Calvin cycle). The WLP and ABC

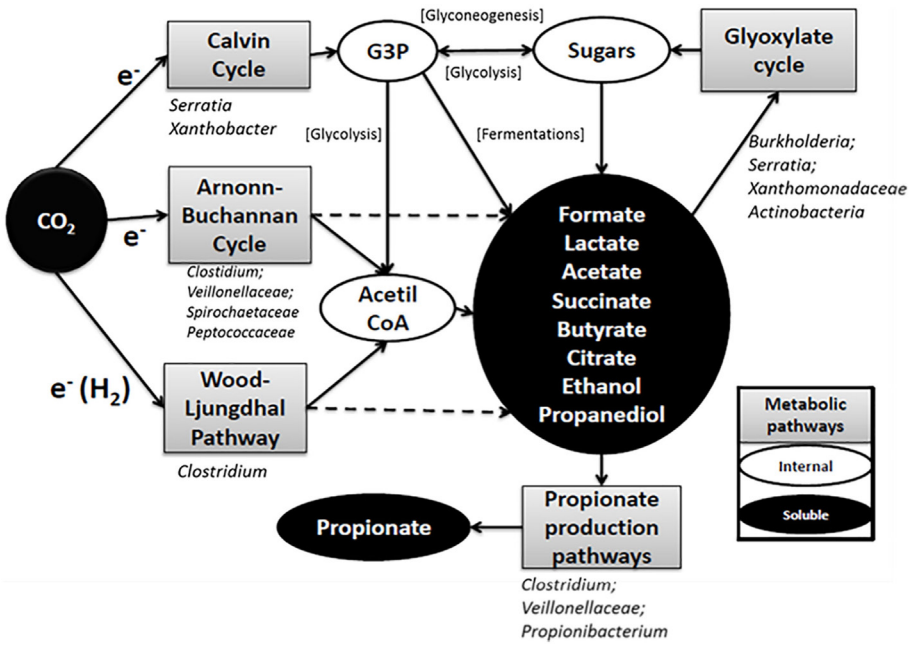

FIGURE 6 | General scheme of the metabolic pathways involved in the production of organic compounds in the electrosynthesis cells according to PICRUSt analysis. Bacterial groups included under the pathway boxes are groups of microorganisms who contribute to the predicted genes in the PICRUSt analysis according to the operational taxonomic units classification. Some groups of microorganisms contributed to the abundance of particular genes but their abundance in the community was less than 1% (Table S1 in Data Sheet 2 in Supplementary Material).

have acetate or acetil-CoA as a primary product, whereas Calvin cycle brings a glycogenic intermediary as G3P. This compound has the potential to be biologically converted to a wide range of intermediary metabolism compounds. The short chain fatty acids and alcohols observed during the primary production could be further converted to different organic compounds through different pathways by the same carbon fixing microorganisms or from their excretion products by other secondary microorganisms (Arends et al., 2017; Marshall et al., 2017; Raes et al., 2017). For example, in this work, a combination of propionic production pathways was predicted, and each one uses different simple substrates. In addition, short chain acid consumption through glyoxylate cycle was predicted suggesting, a complex process. It has to be taken into account that the analysis performed in this work was based on a 16S rRNA gene approach and has several limitations, such as bias in the PCR and the errors associated with the OTUs classification method. Moreover, this analysis was performed using DNA, and the activity of the microorganisms detected is not guaranteed. Therefore, the results presented should be taken as a first step, and further analysis should be carried out to fully understand the complexity of these systems. These results highlight the need of a deeper understanding of microbial processes in this type of systems in order to design control strategies and look for novel applications. For technical reasons, only two biological replicates were made in this study. Since the results for the two replicas differed, some hypotheses that emerge from the analysis should be elucidated with further biological replicates in future works.

In the last years, intense efforts have been done to improve the variety and quantity of products obtained in MECs with mixed cultures, as well as to elucidate the mechanisms of EET (Bajracharya et al., 2017). Elucidating EET mechanisms escapes the aim of this work, but our results have shown that a better MEC performance when the applied potential allowed electrochemical production of molecular hydrogen (Period 4). This fact allows us to speculate that electrochemically produced hydrogen served as electron shuttle for a *Clostridium* genera microorganism (OTU 960) that probably performs WLP using a MET mechanism. However, we cannot rule out the coexistence of DET in the systems, since both experimental devices showed organic compounds production at lower potentials in absolute terms (Period 1). This could be supported by previous reports that prove that some gram positive microorganisms have the capability to perform the DET mechanism (Choi and Sang, 2016). Improving experimental strategies in the future will allow elucidating the predominating EET mechanisms in this process.

However, there are very few works that emphasize on the knowledge of the metabolic pathways involved, in the trophic interactions between the microorganisms involved in the process based on the primary production of organic compounds from CO_2. This work contributes, together with the works of Marshall et al. (2017) and Arends et al. (2017), with different approaches to start to elucidate the complex intra or interspecies interactions, demonstrating metabolic pathways and possible products derived from currently unidentified metabolic and trophic interactions. Deepening into the biocatalyic processes present in these systems will contribute to develop the potential to exploit metabolic pathways and produce previously unexplored products.

Likewise, the understanding of the role of microorganisms present in these systems will provide, in the future, indicators of the functional status of this type of systems.

CONCLUSION

A mixture of volatile organic compounds was produced from CO_2 and electricity. Although the experiments were performed in similar conditions different behaviors were observed. Whereas a complex mixture of organic compounds was produced in cell A, only acetic and formic acids were produced in cell B. The differences between the performances of the cells were successfully explained through the analysis of the microbial communities present in the cathode biofilm and in the bulk solution.

Using the PICRUSt tool, three different metabolic pathways involved in carbon dioxide fixation were predicted. While the Calvin cycle was observed during the whole experiment, the WLP and the ABC predominated in the period with the highest CE and product diversification. Different pathways for propionate production coexist in these artificial environments.

Microorganisms that could indicate low performance were found, such as *Burkholderia* genus or the pathway such as glyoxylate cycle, but its detrimental role is relative regarding the target product of the system. These microorganisms might help to produce different highly reduced organic compounds in MECs.

The knowledge of the metabolic pathways present in MECs provides a better understanding about the biochemical reactions occurring and which products are feasible to achieve in this kind of systems.

AUTHOR CONTRIBUTIONS

JW assembled the experimental devices, executed the operations with the experimental devices, performed all the physicochemical, electrochemical and microbiological tests, analyzed, and integrated the results and wrote the manuscript. EF made the modified carbon felt anodes, contributed with the experimental design, collaborated in analytical workflow, discussed the results, and collaborated in the manuscript writing. PB-V contributed to the experimental design, collaborated in the analytical workflow, discussed the results, and collaborated in the manuscript writing. AC contributed to the microbial community analysis with microbial ecology tools, discussed the results, and collaborated in the manuscript writing. CE directed the analysis of microbial communities, discussed the results, and collaborated with the writing of the manuscript. MB contributed with the experimental design, discussed the results, and collaborated in the manuscript writing. JC advised in the experimental procedures, discussed the results, and critically read the manuscript. SP designed and directed the experiments and collaborated in manuscript writing.

ACKNOWLEDGMENTS

This research was financially supported by the Spanish Government (CTQ 2014-53718-R) and the National Agency of Research and Innovation of Uruguay (ANII; FSE6437 and FSE102488). JW was funded by the ANII-PhD grant (SNB). LEQUIA has been recognized as a consolidated research group by the Catalan Government under the code 2014-SGR-1168. The authors also wish to thank Dr. Hector Romero for a critical reading of the manuscript.

SUPPLEMENTARY MATERIAL

The Supplementary Material for this article can be found online at https://www.frontiersin.org/articles/10.3389/fenrg.2018.00015/full#supplementary-material.

REFERENCES

Arends, J. B. A., Patil, S. A., Roume, H., and Rabaey, K. (2017). Continuous long-term electricity-driven bioproduction of carboxylates and isopropanol from CO2 with a mixed microbial community. *J. CO_2 Util.* 20, 141–149. doi:10.1016/j.jcou.2017.04.014

Bajracharya, S., Srikanth, S., Mohanakrishna, G., Zacharia, R., Strik, D. P. B. T. B., and Pant, D. (2017). Biotransformation of carbon dioxide in bioelectrochemical systems: state of the art and future prospects. *J. Power Sources* 356, 256–273. doi:10.1016/j.jpowsour.2017.04.024

Batlle-Vilanova, P., Puig, S., Gonzalez-Olmos, R., Vilajeliu-Pons, A., Bañeras, L., Balaguer, M. D., et al. (2014). Assessment of biotic and abiotic graphite cathodes for hydrogen production in microbial electrolysis cells. *Int. J. Hydrogen Energy* 39, 1297–1305. doi:10.1016/j.ijhydene.2013.11.017

Batlle-Vilanova, P., Ganigué, R., Ramió-Pujol, S., Bañeras, L., Jiménez, G., Hidalgo, M., et al. (2017). Microbial electrosynthesis of butyrate from carbon dioxide: production and extraction. *Bioelectrochemistry* 117, 57–64. doi:10.1016/j.bioelechem.2017.06.004

Batlle-Vilanova, P., Puig, S., Gonzalez-Olmos, R., Dolors Balaguer, M., and Colprim, J. (2016). Continuous acetate production through microbial electrosynthesis from CO_2 with microbial mixed culture. *J. Chem. Technol. Biotechnol.* 91(4), 921–927. doi:10.1002/jctb.4657

Berg, J. M., Tymoczko, J. L., and Stryer, L. (2002). "Section 17.4 The glyoxylate cycle enables plants and bacteria to grow on acetate," in *Biochemistry*, 5th Edn (New York: W H Freeman), 723-725.

Bharti, R. K., Srivastava, S., and Thakur, I. S. (2014). Proteomic analysis of carbon concentrating chemolithotrophic bacteria *Serratia* Sp. for sequestration of carbon dioxide. *PLoS ONE* 9:e91300. doi:10.1371/journal.pone.0091300

Breznak, J. A. (2006). "The Genus *Sporomusa*," in *The Prokaryotes*, eds M. Dworkin, S. Falkow, E. Rosenberg, KH. Schleifer, E. Stackebrandt, (New York, NY: Springer US), 991–1001.

Caporaso, J. G., Kuczynski, J., Stombaugh, J., Bittinger, K., Bushman, F. D., Costello, E. K., et al. (2010). QIIME allows analysis of high-throughput community sequencing data. *Nat. Methods* 7, 335–336. doi:10.1038/nmeth0510-335

Choi, O., and Sang, B. I. (2016). Extracellular electron transfer from cathode to microbes: application for biofuel production. *Biotechnol. Biofuels* 9, 11. doi:10.1186/s13068-016-0426-0

Coenye, T., Falsen, E., Hoste, B., Ohlen, M., Goris, J., Govan, J., et al. (2000). Description of *Pandoraea* Gen. Nov. with *Pandoraea apista* Sp. Nov., *Pandoraea pulmonicola* Sp. Nov., *Pandoraea pnomenusa* Sp. Nov., *Pandoraea sputorum* Sp. Nov. and *Pandoraea norimbergensis* Comb. Nov. *Int. J. Syst. Evol. Microbiol.* 50, 887–899. doi:10.1099/00207713-50-2-887

Edgar, R. C. (2010). Search and clustering orders of magnitude faster than BLAST. *Bioinformatics* 26, 2460–2461. doi:10.1093/bioinformatics/btq461

Evans, M. C., Buchanan, B. B., and Arnon, D. I. (1966). A new ferredoxin-dependent carbon reduction cycle in a photosynthetic bacterium. *Proc. Natl. Acad. Sci. U.S.A.* 55, 928–934. doi:10.1073/pnas.55.4.928

Ganigué, R., Puig, S., Batlle-Vilanova, P., Balaguer, M. D., and Colprim, J. (2015). Microbial electrosynthesis of butyrate from carbon dioxide. *Chem. Commun.* 51, 3235–3238. doi:10.1039/C4CC10121A

Garrity, G. M., Bell, J. A., and Lilburn, T. (2005). "Class II. Betaproteobacteria Class. Nov," in *Bergey's Manual® of Systematic Bacteriology* eds D.J. Brenner, N.R. Krieg, J.T. Staley (Boston, MA: Springer US), 609–620.

Goodfellow, M. (2012). "Phylum XXVI. Actinobacteria Phyl. Nov," in *Bergey's Manual of Systematic Bacteriology*, Vol. 3, 33–34.

Hamady, M., Lozupone, C., and Knight, R. (2010). Fast UniFrac: facilitating high-throughput phylogenetic analyses of microbial communities including analysis of pyrosequencing and PhyloChip data. *ISME J.* 4, 17–27. doi:10.1038/ismej.2009.97

Herter, S., Fuchs, G., Bacher, A., and Eisenreich, W. (2002). A bicyclic autotrophic CO_2 fixation pathway in *Chloroflexus aurantiacus*. *J. Biol. Chem.* 277, 20277–20283. doi:10.1074/jbc.M201030200

Hu, J., Wang, L., Zhang, S., Xi, X., Le, Y., Fu, X., et al. (2015). Interactions between autotrophic and heterotrophic strains improve CO_2 fixing efficiency of non-photosynthetic microbial communities. *Appl. Biochem. Biotechnol.* 176, 1459–1471. doi:10.1007/s12010-015-1657-4

Imhoff, J. F. (2005). "Enterobacteriales," in *Bergey's Manual® of Systematic Bacteriology*, eds D. J. Brenner, N. R. Krieg, J. T. Staley, G. M. Garrity, D. R. Boone, P. De Vos, et al. (Boston, MA: Springer US), 587–850.

Jung, H.-M., Ten, L. N., Kim, K.-H., An, D. S., Im, W.-T., and Lee, S.-T. (2009). *Dyella ginsengisoli* Sp. Nov., isolated from soil of a ginseng field in South Korea. *Int. J. Syst. Evol. Microbiol.* 59, 460–465. doi:10.1099/ijs.0.64514-0

Langille, M. G., Zaneveld, J., Caporaso, J. G., McDonald, D., Knights, D., Reyes, J. A., et al. (2013). Predictive functional profiling of microbial communities using 16S rRNA marker gene sequences. *Nat. Biotechnol.* 31, 814–821. doi:10.1038/nbt.2676

Ljungdahl, L. G. (1986). The autotrophic pathway of acetate synthesis in acetogenic bacteria. *Annu. Rev. Microbiol.* 40, 415–450. doi:10.1146/annurev.mi.40.100186.002215

Lugg, H., Sammons, R. L., Marquis, P. M., Hewitt, C. J., Yong, P., Paterson-Beedle, M., et al. (2008). Polyhydroxybutyrate accumulation by a *Serratia* Sp. *Biotechnol. Lett.* 30, 481–491. doi:10.1007/s10529-007-9561-9

Marshall, C. W., Ross, D. E., Fichot, E. B., Norman, R. S., and May, H. D. (2012). Electrosynthesis of commodity chemicals by an autotrophic microbial community. *Appl. Environ. Microbiol.* 78, 8412–8420. doi:10.1128/AEM.02401-12

Marshall, C. W., Ross, D. E., Fichot, E. B., Norman, R. S., and May, H. D. (2013). Long-term operation of microbial electrosynthesis systems improves acetate production by autotrophic microbiomes. *Environ. Sci. Technol.* 47, 6023–6029. doi:10.1021/es400341b

Marshall, C. W., Ross, D. E., Handley, K. M., Weisenhorn, P. B., Edirisinghe, J. N., Henry, C. S., et al. (2017). Metabolic reconstruction and modeling microbial electrosynthesis. *Sci. Rep.* 7, Article number: 8391. doi:10.1038/s41598-017-08877-z

Mikkelsen, M., Jørgensen, M., and Krebs, F. C. (2010). The teraton challenge. A review of fixation and transformation of carbon dioxide. *Energy Environ. Sci.* 3, 43–81. doi:10.1039/B912904A

Mira, N. P., Madeira, A., Sílvia Moreira, A., Coutinho, C. P., and Sá-Correia, I. (2011). Genomic expression analysis reveals strategies of *Burkholderia cenocepacia* to adapt to cystic fibrosis patients' airways and antimicrobial therapy. *PLoS ONE* 6(12): e28831. doi:10.1371/journal.pone.0028831

Nevin, K. P., Woodard, T. L., and Franks, A. E. (2010). Microbial electrosynthesis: feeding microbes electricity to convert carbon dioxide and water to multicarbon extracellular organic. *Am. Soc. Microbiol.* 1, 1–4. doi:10.1128/mBio.00103-10. Editor

Octavia, S., and Lan, R. (2014). "The family *Enterobacteriaceae*," in *The Prokaryotes* eds E. Rosenberg, E. F. DeLong, S. Lory, E. Stackebrandt and F. Thompson (Berlin, Heidelberg: Springer), 226–273.

Oren, A. (2014). "The family *Xanthobacteraceae*," in *The Prokaryotes* eds E. Rosenberg, E. F. DeLong, S. Lory, E. Stackebrandt, F. Thompson (Berlin, Heidelberg: Springer), 709–726.

Pujalte, M. J., Lucena, T., Ruvira, M. A., Arahal, D. R., and Macián, M. C. (2014). "The family *Rhodobacteraceae*," in *The Prokaryotes* eds E. Rosenberg, E. F. DeLong, S. Lory, E. Stackebrandt, F. Thompson (Berlin, Heidelberg: Springer), 439–512.

Rabaey, K., Girguis, P., and Nielsen, L. K. (2011). Metabolic and practical considerations on microbial electrosynthesis. *Curr. Opin. Biotechnol.* 22, 371–377. doi:10.1016/j.copbio.2011.01.010

Raes, S. M. T., Jourdin, L., Buisman, C. J. N., and Strik, D. P. B. T. B. (2017). Continuous long-term bioelectrochemical chain elongation to butyrate. *ChemElectroChem* 4, 386–395. doi:10.1002/celc.201600587

Reichardt, N., Duncan, S. H., Young, P., Belenguer, A., McWilliam, LC, Scott, K. P., et al. (2014). Phylogenetic distribution of three pathways for propionate production within the human gut microbiota. *ISME J.* 8, 1323–1335. doi:10.1038/ismej.2014.14

Schleifer, K. H. (2009). "Phylum XIII. Firmicutes Gibbons and Murray 1978, 5 (Firmacutes [sic] Gibbons and Murray 1978, 5)," in *Bergey's Manual® of Systematic Bacteriology*, ed. P. De Vos (New York, NY: Springer), 734-828.

Sharma, M., Bajracharya, S., Gildemyn, S., Patil, S. A., Alvarez-Gallego, Y., Pant, D., et al. (2014). A critical revisit of the key parameters used to describe microbial electrochemical systems. *Electrochim. Acta* 140, 191–208. doi:10.1016/j.electacta.2014.02.111

Sim, K., Cox, M. J., Wopereis, H., Martin, R., Knol, J., Li, M. S., et al. (2012). Improved detection of bifidobacteria with optimised 16S rRNA-gene based pyrosequencing. *PLoS ONE* 7:e32543. doi:10.1371/journal.pone.0032543

Tamura, K., Peterson, D., Peterson, N., Stecher, G., Nei, M., and Kumar, S. (2011). MEGA5: molecular evolutionary genetics analysis using maximum likelihood, evolutionary distance, and maximum parsimony methods. *Mol. Biol. Evol.* 28, 2731–2739. doi:10.1093/molbev/msr121

Tholozan, J. L., Touzel, J. P., Samain, E., Grivet, J. P., Prensier, G., and Albagnac, G. (1992). *Clostridium neopropionicum* Sp. Nov., a strict anaerobic bacterium fermenting ethanol to propionate through acrylate pathway. *Arch. Microbiol.* 157, 249–257. doi:10.1007/BF00245158

Tremblay, P. L., Angenent, L. T., and Zhang, T. (2017). Extracellular electron uptake: among autotrophs and mediated by surfaces. *Trends Biotechnol.* 35, 360–371. doi:10.1016/j.tibtech.2016.10.004

Van Acker, H., Sass, A., Bazzini, S., De Roy, K., Udine, C., Messiaen, T., et al. (2013). Biofilm-grown *Burkholderia cepacia* complex cells survive antibiotic treatment by avoiding production of reactive oxygen species. *PLoS ONE* 8:e58943. doi:10.1371/journal.pone.0058943

Yeates, T. O., Kerfeld, C. A., Heinhorst, S., Cannon, G. C., and Shively, J. M. (2008). Protein-based organelles in bacteria: carboxysomes and related microcompartments. *Nat. Rev. Microbiol.* 6, 681–691. doi:10.1038/nrmicro1913

Conflict of Interest Statement: The authors declare that the research was conducted in the absence of any commercial or financial relationships that could be construed as a potential conflict of interest.

frontiers in Energy Research

ORIGINAL RESEARCH
published: 02 May 2018
doi: 10.3389/fenrg.2018.00027

Photosynthetic and Lipogenic Response Under Elevated CO_2 and H_2 Conditions—High Carbon Uptake and Fatty Acids Unsaturation

Sai Kishore Butti [1,2] *and S. Venkata Mohan* [1,2]*

[1] *Bioengineering and Environmental Sciences Lab, Centre for EEFF, CSIR-Indian Institute of Chemical Technology, Hyderabad, India,* [2] *Academy of Scientific and Innovative Research, Chennai, India*

Microalgae are most versatile organisms having ability to grow under diverse conditions and utilize both organic and inorganic carbon sources. Microalgal photosynthesis can be employed to transform carbon dioxide (CO_2) into essential bioactives and photofuels. In this study, microalgal growth under modified headspace gas compositions which are CO_2 + H_2 (1:1), CO_2, H_2 and Air was evaluated to determine the photosynthetic efficiency and bioactives production. A marked enhancement was observed in quantum yield (Fv/Fm: 0.77) and CO_2 biosequestration rate (0.39 $g.L^{-1}d^{-1}$) under CO_2 + H_2 headspace gas condition as compared to the other experimental variations. The chemoselective functioning of Rubisco under varying gas concentrations was determined, where elevated CO_2 conditions negate the oxygenase activity under a high CO_2/O_2 ratio which enabled higher CO_2 sequestration. The enhanced CO_2 sequestration and altered redox conditions through H_2 addition under the monophasic operation have also led to a higher average degree of unsaturation (DU) and carbon chain length (CCL) of the fatty acids produced. This study provides an approach to augment photosynthetic efficiency and lipogenesis through non-genetic modifications along with the feasibility to cultivate microalgae in integration with industrial flue gases. Exploiting the true potential of microalgae would provide sustenance from climatic changes and environmental pollution concurrently producing biobased products analogous to the fossil-derived products.

Keywords: photoautotrophy, quantum yield, CO_2 biosequestration, biorefinery, FAME, CO_2 fixation rate, biohydrogen

OPEN ACCESS

Edited by:
Deepak Pant,
Flemish Institute for Technological Research, Belgium

Reviewed by:
Ahmed ElMekawy,
University of Sadat City, Egypt
Laura Rago,
Università degli Studi di Milano, Italy

***Correspondence:**
S. Venkata Mohan
svmohan@iict.res.in;
vmohan_s@yahoo.com

Specialty section:
This article was submitted to Bioenergy and Biofuels, a section of the journal Frontiers in Energy Research

Received: *22 October 2017*
Accepted: *28 March 2018*
Published: *02 May 2018*

Citation:
Butti SK and Venkata Mohan S (2018) Photosynthetic and Lipogenic Response Under Elevated CO_2 and H_2 Conditions—High Carbon Uptake and Fatty Acids Unsaturation. Front. Energy Res. 6:27. doi: 10.3389/fenrg.2018.00027

INTRODUCTION

Continuously converting the fossilized carbon into atmospheric CO_2 through expeditious extraction and consumption has left the carbon loop unbalancd leading to adverse climate changes and a dearth of raw material (fossils) (Hoornweg et al., 2013; Dowson and Styring, 2017). With substantial increase in the world population, need for sustainable feedstocks has also increased. In the lookout for alternative feedstocks, CO_2 has gained ground as a virtuous feedstock for the production of chemicals, fuels, and energy (Venkata Mohan et al., 2016a). Utilizing CO_2 as feedstock through biotechnological routes has the potential to sustainably solve the problem

of global climate change primarily occuring due to increase in atmospheric CO_2 levels (Butti and Mohan, 2017; Kant, 2017). Increase in the atmospheric CO_2 concentration has a harmful influence on the environment like acidification of oceans which develops a higher homeostasis stress on the phytoplaktons to maintain their redox conditions, acidification of soil, and acid rains (Rodrigues et al., 2016). Photosynthesis provides a possible solution with its natural ability to biocapture CO_2 using solar energy and produce valuable chemicals along with several other advantages to mitigate environmental pollution (Benemann et al., 1977; Demars et al., 2016; Keenan et al., 2016).

Amongst the photosynthetic organisms microalgae have achieved higher significance as the primary responders to the climate change with their efficient carbon assimilation mechanism, high growth rate, bioactive, and biofuels production and the ability to grow on non-arable lands. Microalgae can grow under different trophic modes of nutrition and hence can be cultivated using both inorganic and organic carbon in light and dark conditions under photoautotrophic, mixotrophic, and heterotrophic modes (Venkata Mohan et al., 2014; Rohit and Mohan, 2015). Understanding these resourceful abilities several researchers have progressed toward microalgal photo-biotechnology encompassing biosequestration of CO_2, wastewater treatment and biobased products synthesis. Different microalgal strains have robust capabilities to overcome climatic changes by CO_2 sequestration and production of diverse products owing to their competent metabolism. However, through an integrated approach or genetic modifications the spectrum of products synthesized can be expanded like biocrude through hydrothermal liquefaction, bioalcohols through anaerobic digestion, bioelectricity through microbial electrochemical technologies, biohydrogen/biomethane through acidogenic fermentation, biofertilizers through pyrolysis (Perez-Garcia et al., 2011; Ooms et al., 2016; Venkata Mohan et al., 2016b). Under autotrophic mode of nutrition, substrate (CO_2) availability governs the photosynthetic efficiency and biomass productivity at optimum operational parameters. The incidence of a positive influence on the biomass growth and lipogenesis under higher CO_2 for different microalgal strains like *Chlorella, Scenedesmus, Nannochloropsis, Dunaliella, Botryococcus,* and plants has been previously discussed in different studies (Riebesell et al., 1993; Hein and Sand-Jensen, 1997; Chiu et al., 2009; Yoo et al., 2010; Price and Howitt, 2014; Peng et al., 2016a; Watson-Lazowski et al., 2016). Improving the energy conversion efficiency in photosynthesis is a multivariable problem, where, it is greatly influenced by an array of operational and physiological parameters like phases of operation, nutrients/substrate availability, photosynthetically active radiation (PAR) exposure, temperature, pH, the source of essential compounds and gases (industrial exhausts; Stewart et al., 2015; Chiranjeevi and Mohan, 2016).

We hypothesize that microalgae can be optimized to selectively enhance the carbon dioxide uptake and the photo-biocommodities productivity at an economic scale under photoautotrophic cultivation by regulating the inlet gas concentrations (10% CO_2 + 10% H_2, 20% CO_2, 20% H_2, 0.04% CO_2) at an elevated pressure. The varying headspace gas concentrations would ensure controlled compartmentalization of essential metabolites and determine the possibility of selective photo-products synthesis. Also, in this study a monophasic cultivation strategy with a synergistic role of CO_2 and H_2 was incorporated taking lead from Gaffron who suggested the possibility of CO_2 reduction by molecular hydrogen in microalgae (Gaffron, 1940). While most of the preceding studies in this domain have largely focused on varying the inlet concentrations of CO_2 and operating in two phases with growth and stress phase separately. The present study has the potential to provide a holistic solution to the climate change and feedstock limitation through microalgal CO_2 biosequestration and pave a sustainable path for the future generation.

MATERIALS AND METHODS

Microalgal Isolation and Cultivation

The freshwater microalgae *Chlorella* sp. was isolated from a local ecological water body (Hussain Sagar, Hyderabad, 17.4239°N, 78.4738°E—India). Water samples were collected from five different locations around the banks of the lake, each sample was filtered through a 0.2 μm hydrophilic nylon membrane filter (Spin-pure, India), and the leftover residue was washed to remove non-biological components and it was suspended into BG11 culture media. Equal aliquots of the grown culture were sub-cultured in tapered opening glass screw-cap bottles (2 l, Borosil) tightly sealed to prevent contamination. The cultures were domesticated by providing a periodic input of sterile CO_2 enriched air (0.4 $l.min^{-1}$) at atmospheric pressure for 4 weeks enabling the adaptive evolution at the laboratory scale. Effective illumination was continuously provided by non-heating fluorescent white lights (95 $\mu mol.m^{-2}.s^{-1}$) measured by photon density lux meter (Extech LT-300 Light meter) with a photoperiod of 12 h. The reactors were operated in an open top reciprocal shaker (120 rpm) maintained at 25 ± 2°C and initial pH 8, this culture was labeled as pre-culture. A total of 10 ml pre-culture from suspension in log phase was added into autoclaved screw cap glass bioreactors (500 ml, Borosil) prefilled with modified BG11 growth medium which has the concentrations of nitrates (1.1 $g.L^{-1}$), phosphates (0.03 $g.L^{-1}$), and sulfates (0.060 $g.L^{-1}$) with the other components same as the BG11 media. Pre-filled bioreactors were operated at the same operational conditions with a stepping increase in CO_2 enriched air input (0.03–20% V/V) monitored by gas flow meter to acclimatize the pre-culture for high CO_2 tolerance and uptake conditions for 4 weeks (only for CO_2 and CO_2 + H_2 conditions). Homogeneity of species was confirmed microscopically (Nikon Eclipse-80i) and the images were captured on digital camera (YIM-smt, 5 MP) using NIS-elements (D3.0) software, primary observations suggest the occurrence of *Chlorella* sp.

Experimental Setup and Operational Parameters

The specifically designed photobioreactor (height 25 cm, base diameter 11 cm, opening diameter 5 cm, glass thickness 3 mm, equipped with separate sampling and gas exchange ports i.d/o.d-−0.9/1.1 and 0.4/0.64 mm, respectively) with the ability to sustain

pressures of upto 2 bar and having maximum light penetration. The working volume of the reactor was 400 ml with an effective headspace of 100 ml. Four identical reactor setups were evaluated with specific sterile gases; CO_2 (20% v/v), H_2 (20% v/v), CO_2 + H_2 (20% v/v + 20% v/v), and Air (as control with 0.03% CO_2 v/v) input with initial pH 8 (**Table 1**). The gas inputs were provided from GC grade gas cylinders through pneumatic pressure and flow control values to maintain constant pressure and flowrate in the reactors. The different inlet CO_2, H_2, and N_2 gases concentrations in the reactors were monitored using gas chromatography with a thermal conductivity detector (Nucon-5765, Centurion Scientific, India) operated under specific conditions: packed ($1/8'' \times 2$ m Heysep Q) column, injection volume 0.5 ml, argon as a carrier gas (47 ml.min^{-1}), the injector and detector temperatures were maintained at 60°C and the oven was operated at 40°C isothermally. Culture and gas sampling were done through specifically provided ports using sterile needles on alternate days to determine the exponential growth, cellular components, carbon dioxide fixation, and occurrence of contamination was preventively monitored.

Dry Weight and Growth Kinetics

Microalgal samples were collected at every 48 h interval to evaluate growth by measuring optical density at 750 nm using a UV-Vis Spectrophotometer (Thermo Electron). Dry cell weight (g.L^{-1}) was determined after the biomass was centrifuged twice at 10,000 rpm at 4°C for 5 min (XT/XF centrifuge, Thermo Scientific) the resulting pellet was washed twice with Milli-Q water and dried in hot air oven at 65°C for 24 h. The resulting biomass dry cell weight was used to calculate growth rate μ (g.L^{-1}.d^{-1}) as mentioned in Equation (1) (Cabanelas et al., 2016).

$$\mu = \frac{\ln (DW_{tf} - DW_{to})}{tf - to} \quad (1)$$

Where, DW_{tf} and DW_{to} represent dry cell weight of biomass (g.L^{-1}), at time tf (the final sample time) and to (the initial sample time) in days respectively. Mean of the biomass concentrations was considered for measurement at specific time intervals.

Photosynthetic Efficiency

The microalgal photosynthetic efficiency was evaluated using pulse-amplitude modulated fluorometry employing AquaPen-C (AP-C 100, Photon System Instruments, Czech Republic) which was monitored and controlled through PC using FluorPen software (PSI, Czech Republic). Chlorophyll fluorescence of PSII Quantum yield (Fv/Fm) was evaluated for samples directly withdrawn from the reactors after the biomass density was adjusted to 0.025 g.L^{-1} using MilliQ water and placed in a closed chamber for dark adaptation (10 min). The maximum quantum yield was calculated using Equation (2),

$$\frac{F_v}{F_m} = \frac{F_m - F_o}{F_m} \quad (2)$$

Where, the minimum fluorescence (F_0) and maximum fluorescence (F_m) were determined after the samples were dark adapted and variable fluorescence (F_v) was determined according to calculation $F_v = F_m - F_0$ which gives the fluorescence difference between the closed and open reaction centers in PSII under real time photosynthetic active radiation (PAR) (de Mooij et al., 2016).

TABLE 1 | Experimental setups with the operational parameters in batch mode.

Experimental condition	Head space gas composition		
	CO_2 (% v/v)	H_2 (% v/v)	N_2 (% v/v)
CO_2	20	–	80
H_2	0.036	20	80
$CO_2 + H_2$	10	10	80
Air (Control)	0.036	0.001	71

Carbon Dioxide Fixation Rate

The biomass at the end of the cycle was collected (10 ml), washed with MilliQ water twice and left overnight for drying in a glass crucible. The carbon content in the biomass was determined by the CHNS analyser (vario MICRO cube, Elementar). The relation between biomass productivity and carbon fixation rates (g.d^{-1}.L^{-1}), when cultivated under different CO_2 concentrations, was determined by the Equation (3), average biomass productivities were considered (Gonçalves et al., 2016).

$$R_{CO_2} = C_c P_{max} (M_{CO_2}/M_c) \quad (3)$$

Where C_C was the carbon content of the microalgal cells (% w/w), P_{max} was the maximum biomass productivity (g.L^{-1}.d^{-1}), M_{CO2} was the molar mass of CO_2 (44 g.mol^{-1}), and M_C was the molar mass of carbon (12 g.mol^{-1}).

Cellular Components Analysis

Lipids and Fatty Acids Composition

The total lipid content in the dry algal biomass was determined by the modified Bligh and Dyer method (Bligh and Dyer, 1959), where, 10 ml of 2:1 chloroform: methanol was added to 100 mg of dry biomass and sonicated at 40 KHz using probe Sonicator (Qsonica, Q55) for 2 min. Later, the solution is centrifuged at 8,000 rpm for 10 min and the supernatant was transferred into pre-weighed tubes and left overnight at 50°C in hot air oven. The neutral lipid content was determined using the same method with n-Hexane as the solvent (Venkata Mohan and Prathima Devi, 2012). The percentage gain in weight determined by the gravimetric means was used to conventionally quantify the total and neutral lipid content in the biomass. The lipid productivity in the batch culture was calculated using Equation (4) (Han et al., 2013).

$$\text{Lipid productivity } \left(mg.g^{-1}.d^{-1}\right) = (C_t.L_t - C_o.L_o).1000/T \quad (4)$$

Where, T was the culture time in days, C_t and L_t were the biomass concentration and lipid content at T and C_0 and L_0 were the initial biomass concentration and initial lipid content. Fatty acid composition was determined by acidic transesterification of the lipids using acid saturated methanol. The dried lipid was refluxed with acidified methanol for 2 h in hot water bath at 80°C. The

esterified mixture was washed with ethyl acetate and water until the solution became alkaline. Later, it was filtered through an anhydrous Na_2SO_3 impregnated filter paper to remove moisture. The solvent recovery is done using rotary evaporator (Hei-VAP, Heidolph) and the pooled fame mix obtained is dissolved in chloroform and injected into GC for compositional analysis. The quantification of fatty acid methyl esters is done by GC-FID (Nucon-5765) with a capillary wax column (Valcobond 30 mm) using hydrogen as fuel and nitrogen as carrier gas. The oven temperature was initially maintained at 140°C later ramped to 240°C with 4°C/min increase, the detector and injector were maintained at 300 and 280°C, respectively with a split ratio of 1:10. Obtained FAME composition was compared to the standard FAME mix (C8-C22; LB66766, SUPELCO; Rohit and Mohan, 2015). The average carbon chain length (CCL) and average degree of unsaturation (DU) observed in the fatty acid profile were calculated using the equations

$$\text{Avg CCL} = \sum_{i=0}^{n} \left(\frac{FA_i}{100}\right) * C_i \quad (5)$$

$$\text{Avg DU} = \sum_{i=0}^{n} \left(\frac{FA_i}{100}\right) * D_i \quad (6)$$

Where, CCL and DU represent the CCL and DU observed in the fatty acids synthesized, C_i and D_i are the chain lengths and unsaturation of the particular fatty acid and FA_i is the fatty acid abundance (Hoekman et al., 2012).

Carbohydrates Estimation

The carbohydrate content was determined by a phenol-sulfuric acid method where the pelleted biomass after centrifugation was powdered and dried (DuBois et al., 1956). The dry powder (10 mg) was acid hydrolyzed with 5 ml 2.5N HCl in a boiling water bath for 30 min. The solution volume is made upto 10 ml with distil-water, then centrifuged at 5,000 rpm for 5 min. To 0.2 ml of supernatant 1 ml 5% phenol solution and 5 ml 96% sulfuric acid is added. The contents are vortexed and placed in water bath for 20 min at 30°C later optical density was measured at 490 nm to determine the carbohydrate concentration.

Proteins, Nitrates, and Chlorophyll Estimation

Proteins were extracted from the microalgal cells using 0.5N NaOH for 24 h followed by heating upto 40°C followed by lysis buffer (Rausch, 1981; Fernández-Reiriz et al., 1989). Quantitative estimation of protein content in the biomass is determined by the Lowry's method (Lowry et al., 1951) and the nitrate removal is determined by the standard APHA methods (Chandra et al., 2015). Chlorophyll was estimated using spectrophotometry, the 10 ml of cell biomass was pelleted using a centrifuge at 5,000 rpm for 5 min. To the pellet 10 ml of acetone and ethanol (in 1:1 ratio) were added and sonicated at 40 kHz for 2 min using probes sonicator (Qsonica, Q55). The cell debris was separated by centrifugation at 8,000 rpm for 5 min, the resulting supernatant was used to quantify chlorophyll a and chlorophyll b by measuring the OD at 647 and 664 nm respectively using Equations (7–9) (Chiranjeevi and Mohan, 2016).

$$\text{Chla} = (-1.93^{*}OD_{647}) + (11.93^{*}OD_{664}) \quad (7)$$

$$\text{Chl b} = (20.36^{*}OD_{647}) - (5.5^{*}OD_{664}) \quad (8)$$

$$\text{Total Chlorophyll} = \text{Chl a} + \text{chl b} \quad (9)$$

Bioprocess Monitoring Redox Conditions

Redox conditions (pH) was continuously monitored (Eutech, Thermo Scientific) to determine the effective CO_2 uptake and the dissolved inorganic carbon fraction in the media under elevated pressure and gas inputs.

RESULTS AND DISCUSSION

The different experimental conditions are given codes for ease of understanding and are uniformly followed throughout the manuscript. Where, experimental variations with Air, CO_2, CO_2 + H_2, and H_2 are coded as AI, CC, CH, and HY, respectively based on the gas provided in the headspace. Correlative analysis of the photosynthetic activity and the cellular metabolite synthesis are delineated to understand the functional role of the specific gas inlets.

Photosynthetic Efficiency vs. CO_2 Biofixation

Biomass growth, quantum yield, CO_2 fixation rate and chlorophyll pigment were monitored for all the experimental variations to assess the photosynthetic efficiency and understand the influence of controlled gas composition. CH condition has resulted in relatively higher biomass productivity of 2.5 $g.L^{-1}$ with a positive growth rate of 0.3 $g.L^{-1}d^{-1}$ on the 2nd day of cultivation. The maximum biomass growth was followed by CC, AI and HY with 2.3 $g.L^{-1}$ (0.27 $g.L^{-1}d^{-1}$), 1.9 $g.L^{-1}$ (0.21 $g.L^{-1}d^{-1}$), and 1.5 $g.L^{-1}$ (0.17 $g.L^{-1}d^{-1}$), respectively (**Figure 1**).

Biosequestration of CO_2 was evaluated in correlation with the quantum yield for all the experimental conditions. Rate of CO_2 sequestration was observed to be higher in the CH condition with 0.39 $g.L^{-1}d^{-1}$ followed by CC (0.37 $g.L^{-1}d^{-1}$), AI (0.33 $g.L^{-1}d^{-1}$), and HY (0.30 $g.L^{-1}d^{-1}$) conditions respectively. The rate of CO_2 sequestration is well in correlation with the biomass growth were higher CO_2 uptake under the photoautotrophic conditions has led to higher biomass productivity. Efficiency of the photosynthetic machinery responsible for light energy harvestation is quantified by monitoring the quantum yield (Fv/Fm). Higher quantum yield was observed in CH- 0.77 followed by CC (0.75), AI (0.66), and HY (0.61) which supports the higher biomass growth and CO_2 fixation rate (**Figure 2**). The marked increment in biomass productivity with CH condition might be attributed to the enhanced photosynthetic activity with the function of key photoautotrophic enzymes (carbonic anhydrase and Rubisco) associated with light reactions (Sun et al., 2016b). Enzymatic catalysis of CO_2 into usable form is catalyzed by carbonic anhydrase which increases the dissolved

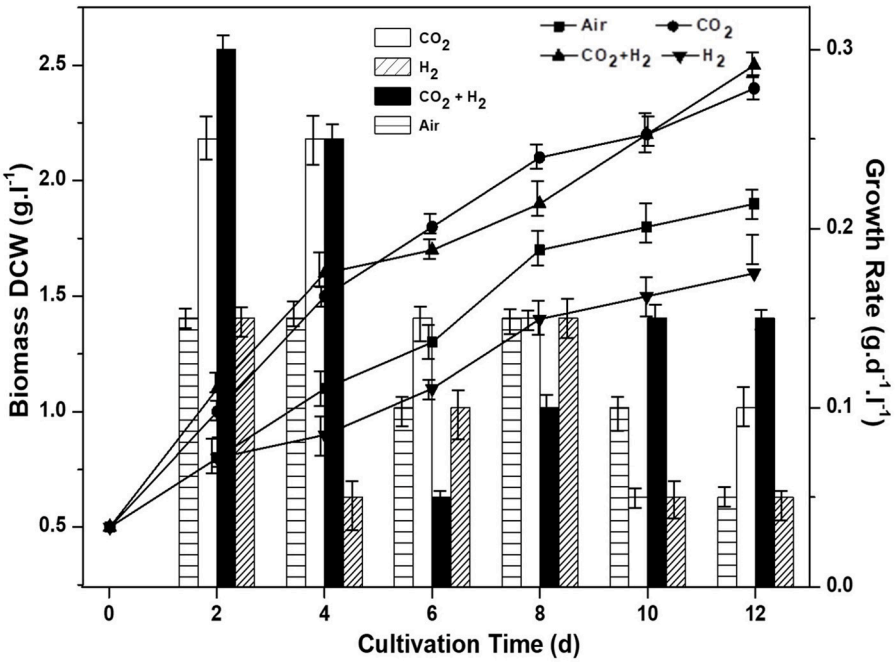

FIGURE 1 | Influence of specific gas inlet in the headspace on biomass concentration ($g.L^{-1}$) and biomass productivity ($g.L^{-1}.d^{-1}$) of the microalgal cultures.

inorganic carbon, augmenting its accessibility for the cellular metabolism under CH condition followed by CC, AI, and HY (Moroney and Ynalvez, 2007). Calvin cycle operates by utilizing the reducing energy generated during the light reactions (in form of NADH and ATP) for the reduction of CO_2 catalyzed by Rubisco to form carbohydrates (Blankenship, 2002). Maintaining elevated CO_2 gas concentrations in the CH and CC conditions, the CO_2/O_2 ratio gets escalated (compared to the ambient condition) thereby negating the oxygenase activity which has a detrimental effect on the CO_2 uptake (Kitaya et al., 2003; Lohman et al., 2015; Mortensen and Gislerod, 2015). The improved uptake of CO_2 through photocatalytic carbon fixation releases ADP and NAD^+ rapidly making them readily available for accepting inorganic phosphorous and electrons by the electron transport chain thereby increasing the photosynthetic efficiency (correlating well with the quantum yields). The addition of H_2 gas along with elevated CO_2 maintains the cellular redox conditions with abundant proton concentrations that reduce the reactive oxygen species thereby increasing the photosynthetic efficiency as observed in CH condition. The increment in biomass productivity with elevated CO_2 gas has been reported in different studies (Bowes, 1991; Hu and Gao, 2006; Mohammadi, 2016; Sun et al., 2016a). The supplementation of hydrogen along with higher CO_2 also has a governing influence on higher biomass productivity and photosynthetic efficiency where hydrogen could be acting as an energy source as reported by Gaffron (1940). Apart from being an energy source it also maintains cellular redox conditions which allows the effective availability of dissolved inorganic carbon for uptake and reduces the reactive oxygen species (Gaffron, 1940; Cuellar-Bermudez et al., 2015). On the contrary, much higher levels of CO_2 or H_2 causes acidification below the optimal level thus causing decrement in microalgal growth. However, in the HY conditions the non-availability of carbon as compared to other conditions has resulted in lower biomass yields.

Chlorophyll content (both a and b) was estimated for all the experimental variations, as the primary light harvesting pigment it correlates with the photosynthetic efficiency. The total chlorophyll quantified was observed to be higher in CH followed by CC, AI, and HY conditions (**Figure 3**). High chlorophyll a concentration was observed in CH conditions during the eighth day of operation with $5.1\,\mu.mg^{-1}$ followed by CC, AI, and HY with 4.1, 2.9, and $0.66\,\mu.mg^{-1}$ respectively. Similar trends were observed in the case of chlorophyll b where CH ($1.8\,\mu.mg^{-1}$) was quantified to be higher followed by CC ($1.5\,\mu.mg^{-1}$), AI ($1.3\,\mu.mg^{-1}$), and HY ($0.58\,\mu.mg^{-1}$). Based on the mode of operation and nutrient availability the concentration of chlorophyll varies. Hence, the chlorophyll content showed a decremental trend toward the end of the cycle as the result of nitrate limitation and lower pH (Matich et al., 2016). The photosynthetic efficiency also correlates with the Chl a/b ratio as the chlorophyll a is the primary light harvesting pigment and chlorophyll b is the accessory pigment. Positive and higher chl a/b ratio symbolizes the effective photosynthetic activity and light conversion efficiency (Karpagam et al., 2015; Li et al., 2015). CH and CC showed ratio above 2, whereas, AI and HY showed ratio in between 1 and 2 correlating to the biomass productivity and quantum yields.

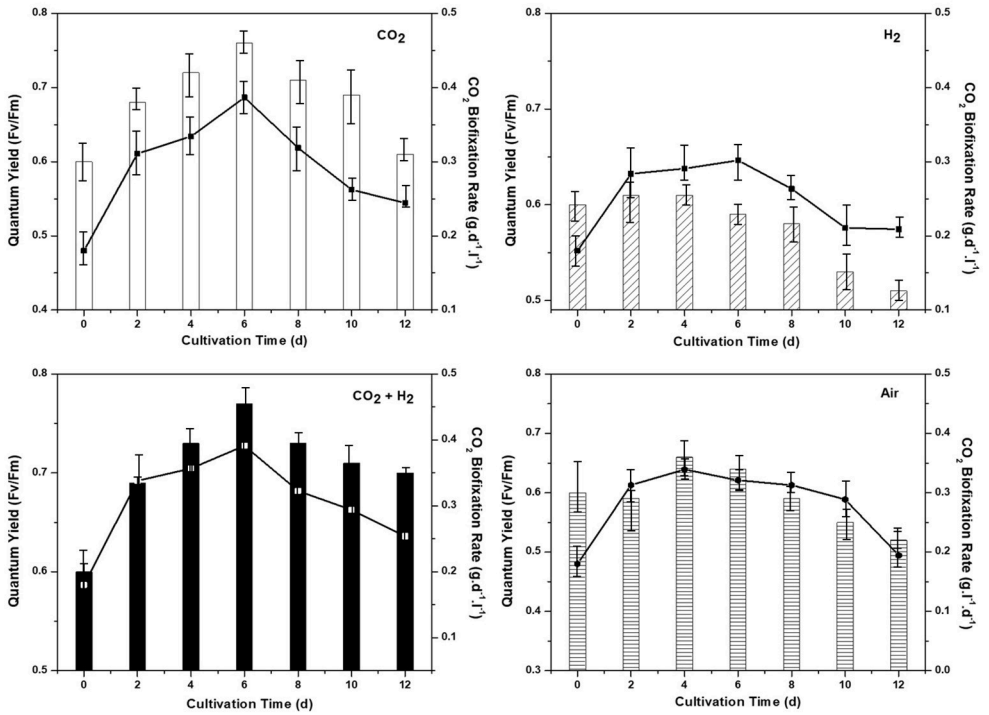

FIGURE 2 | Quantum yield (Fv/Fm) of the dark adapted samples along with the chronological CO_2 biofixation rate ($g.l^{-1}.d^{-1}$) for all the experimental conditions AI, CC, HY, and CH represent clockwise from top left.

Lipogenesis Under Nutrient and Redox Stress Conditions

To understand the role of varying gas conditions (CH, AI, CC, and HY) on lipid biosynthesis. Total lipids, neutral lipids, and lipid productivity are evaluated in correlation with nitrate utilization and pH variation. The elevated CO_2 levels enhanced the overall lipogenesis, possibly thorough the upregulated activities of acetyl CoA carboxylase and the fatty acid synthase complexes (Yasmin Anum Mohd Yusof et al., 2011; Yu et al., 2011; Peng et al., 2016b). The total lipid content was observed to be higher in CH condition with 26% followed by CC, AI, and HY with 21, 19, and 13%, respectively. The trend of higher total lipids positively correlated with sufficient carbon supply and nitrate stress in the case of CH and CC compared to AI and HY. Single stage non-replete nitrogen conditions were employed in all the experimental conditions where, lower nitrogen (120 mg/l) was provided which enables simultaneous biomass growth and lipogenesis (Klok et al., 2013; Benavente-Valdés et al., 2016). The maximum lipid productivity of 29, 19, 12, and 9 $mg.g^{-1}.d^{-1}$ were observed in CH, CC, AI, and HY conditions, respectively. The nitrate removal showed a steady decremental trend in the CH, CC, and AI conditions compared to HY condition where the nitrate utilization was relatively lower (Velmurugan et al., 2014). The nitrates concentrations dropped from 120 mg/l at the initial day of operation to 10 $\pm$ 1 mg/l at the end of operation in CH, CC, and AI conditions, whereas in the HY condition the concentration has only dropped to 70 mg/l which explains the lower biomass as well as lipid productivity. Carbon availability has played the major role in lipid synthesis under CH condition followed by CC and AI as the nitrate utilization trend is similar (**Figure 4**). Initial pH was setup at 8.0 to increase the system buffering at elevated CO_2 and H_2 conditions. The pH was observed to drop in all the conditions from 8 to 6.89, 6.99, 7.09, and 7.38 in HY, CH, CC, and AI, respectively (**Figure 4**). The nutrient stress in the form nitrogen limitation and pH variations governed the lipogenesis along with carbon availability.

The elevated CO_2 gas concentrations have a governing influence on the lipogenic enzymes (phosphoenolpyruvate carboxylase, carbamoyl-phosphate synthase, and pyruvate carboxylase) along with anaplerotic carbon assimilation reactions which could have catalyzed the enhanced lipid synthesis (Peng et al., 2016b). The intracellular and extracellular redox conditions have a marked influence on the neutral lipids synthesis which are primarily storage lipids (TAGs and esters; Juneja et al., 2013). The neutral lipids were dominant under the CH condition followed by CC, AI, and HY condition with 14, 11, 9, and 6%, respectively. Under acidic conditions, to limit the proton gradient across the cell membrane, the microalgal cells discontinue the membrane polar lipid synthesis, and surge the storage lipid synthesis which are primarily neutral lipids (Juneja et al., 2013). The role of pH apart from governing the lipogenesis is also to regulate the carbonaceous species availability for cellular metabolism, where at high alkaline pH

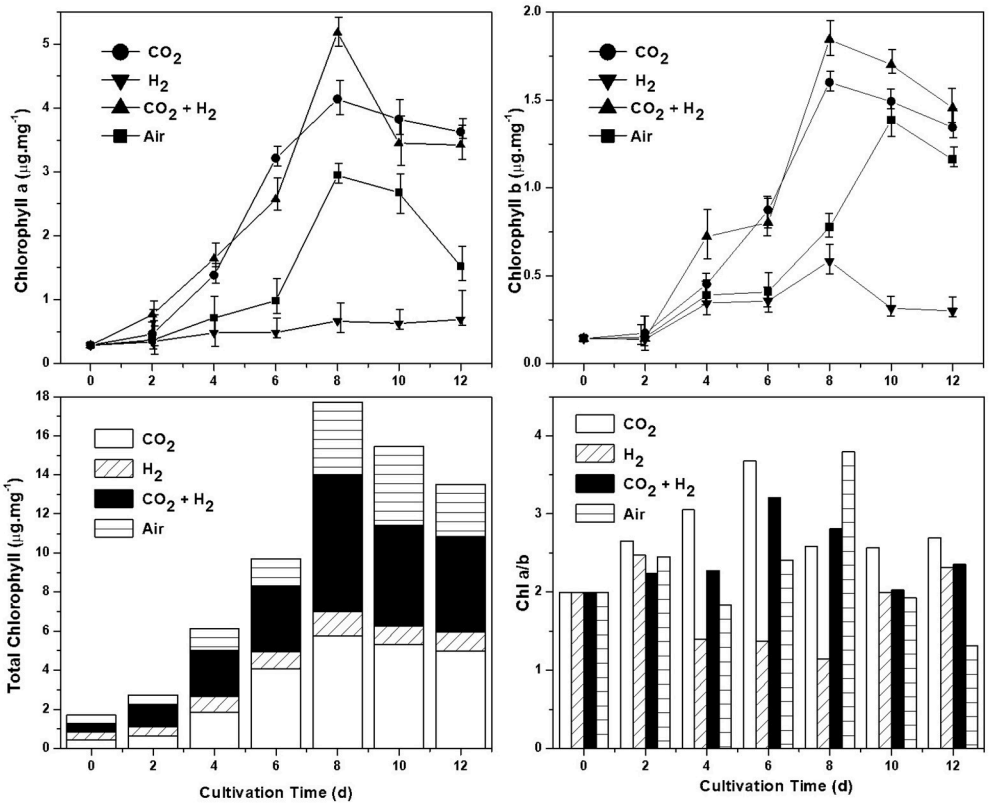

FIGURE 3 | Chlorophyll estimation under different gas conditions determining the photosynthetic activity. Chlorophyll a ($\mu g.mg^{-1}$), chlorophyll b ($\mu g.mg^{-1}$), Chlorophyll a/b ratio, and total chlorophyll ($\mu g.mg^{-1}$) are depicted clockwise from the top left.

the carbon is in the inaccessible form of carbonates (Azov, 1982).

Photofuels and Bioactives

Transesterified fatty acid profile of the lipids produced in all the experimental conditions were quantified to determine the photofuels and bioactive compounds production under each experimental variation. The Fatty Acid Methyl Esters (FAME) composition showed synthesis of fatty acids with CCL ranging from C10 to C20 and having unsaturation (mono/poly). Polyunsaturated fatty acids (PUFA; C18:3 and C18:2) were observed with relative abundance of 17 and 15%, 14 and 13%, 10 and 14%, and 8 and 9% in CH, CC, AI, and HY conditions, respectively (**Figure 5**). PUFA have a multitude of applications as bioactive compounds that are of high nutrient value, edible oil supplements, pharmaceutical precursors which help in lowering cardiovascular diseases apart from being used as a intermediates for various industrial chemicals. Monounsaturated Fatty Acids (MUFA; C18:1, C16:1, and C15:1) were observed, amongst which C18:1 was quantitatively higher in the case of CH and AI (11%) followed by HY (10%) and lowest was observed in CC (8%). C18:1 fatty acids has a property of being used as a food and dietary supplement and pharmaceutical ingredient. C16:1 and C15:1 were observed to have relative abundance of 11 and 5%, 7 and 3%, 6 and 2%, and 5 and 2% in the case of CH, AI, CC, and HY, respectively which have fuel properties and is applied in detergent industries as emulsifiers and also as a cosmetics for topical application. Saturated Fatty Acids (SFA; C18:0, C16:0, and C20:0) are relatively higher along with low concentrations of fatty acids like C14:0, C13:0, C12:0, and C10:0. The quantitative variations in C18:0, C16:0, and C20:0 are 11, 16, and 15% in the case of CC, 13, 16, and 11% in the case of HY, 10, 15, and 17% in the case of CH and 11, 17, and 8% in the case of AI, respectively. SFAs find application as biofuels, soaps, medicines, military lubricants and photographic plates. The lipogenic potential of microalgae is observed to be regulated through CO_2 and H_2 variation enabling the selective production of photofuels and bioactive compounds which have a significant role in developing a sustainable future analogous to the petroleum based precursor chemicals.

Fatty Acid Chain Length and Saturation

The average CCL was observed to be higher in the case of CH condition with 17.58 followed by CC with 17.33, HY with 17 and AI with 16.84. Along with the variations in chain length the additional CO_2 and H_2 influenced the DU observed in the fatty acids. Average DU was quantified, which portrayed higher unsaturation in the case of CH (0.99) followed by CC (0.88), AI (0.85), and HY (0.73). Though the variations in the average CCL is modest, a noteworthy influence of elevated CO_2 and H_2 was observed on the DU. The supplementation of CO_2 influenced the shift of saturated fatty acids toward unsaturation which could be

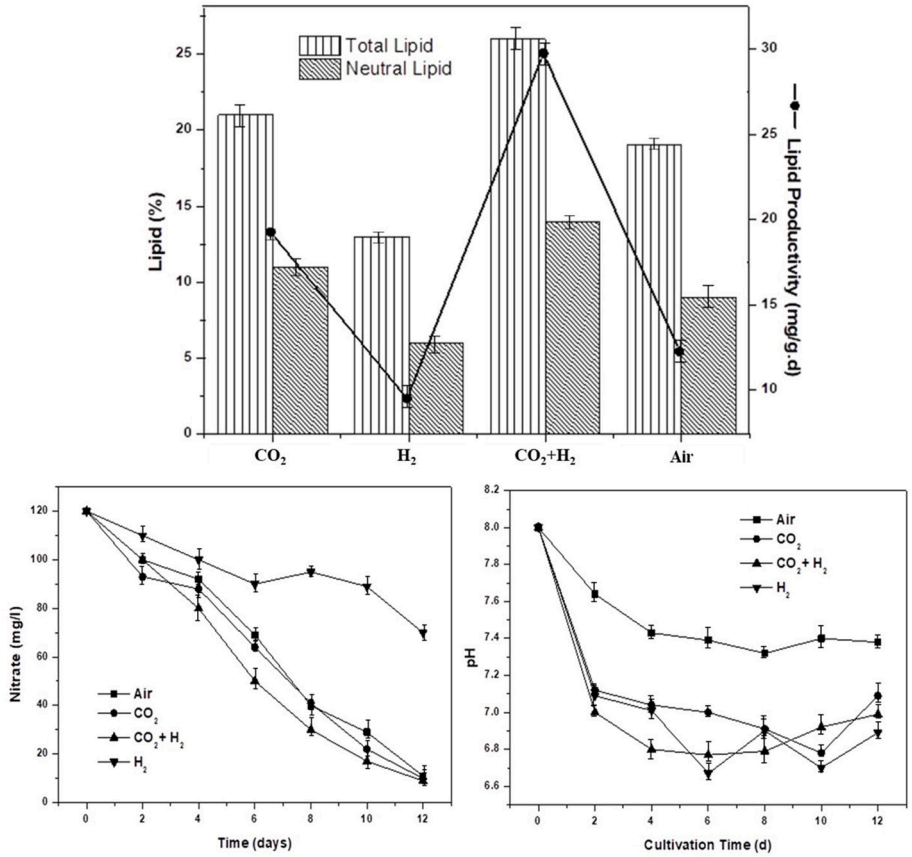

FIGURE 4 | The total lipid and neutral lipid contents in the dry biomass at the end of the cycle along with specific lipid productivity ($mg.g^{-1}.d^{-1}$) under nutrient and redox stress are depicted for the varied gas concentrations in the headspace.

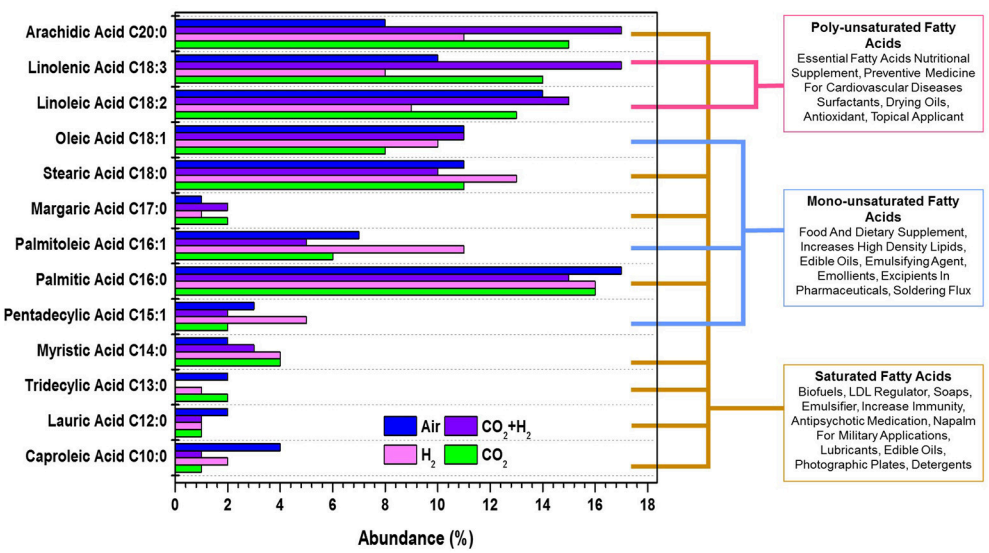

FIGURE 5 | Fatty acid methyl esters profile showing the variations in the photofuels and bioactive compounds synthesis abundance with the function of varying gas compositions is presented for all experimental variations.

to maintain the membrane fluidity allowing efficient CO_2 uptake. Most of the unsaturated fatty acids are membrane bound lipids and hence the increase in unsaturation could be observed in the CH, HY, and CC conditions sequentially as compared to AI. The predominant shifts of saturated fatty acid to unsaturated fatty acids was observed in C18:0 fatty acid to C18:1, C18:2, and C18:3 fatty acids (**Table 2**). Similar trends of unsaturation under elevated CO_2 conditions were reported in different studies with microalgae, which suggested the upregulation of desaturase enzymes catalytic activity that results in more of unsaturation (Tsuzuki et al., 1990; Nagaich et al., 2014; Cuellar-Bermudez et al., 2015). However, the lowering of pH has shown an increase in the saturated fatty acids that is specifically observed in the change of C18 and C16 fatty acids which could protect the cells from the extracellular low pH (Santos et al., 2014). Total SFA:MUFA:PUFA was observed to be 47:18:32 in the case of CH, 49:21:17 in the case of HY, 51:16:27 in the case of CC and 47:14:24 in the case of AI depicting an increased chain length and unsaturation of fatty acids in the case of CH (Yasmin Anum Mohd Yusof et al., 2011; Yu et al., 2011).

Essential Cellular Metabolites Synthesis

Under photoautotrophy the primary metabolites synthesized are carbohydrates and proteins which serve as the energy source for cellular metabolism in dark/stress conditions. The carbohydrate synthesis has shown a linear increase with time correlating to the photosynthetic activity, as the energy for CO_2 hydrogenation catalyzed by Rubisco is drawn from the light reactions and supplemented hydrogen. Relatively higher carbohydrates synthesis was observed in CH conditions (274 $mg.g^{-1}$; 8th day) followed by CC (243 $mg.g^{-1}$; 9th day), AI (197 $mg.g^{-1}$; 9th day), and HY (120 $mg.g^{-1}$; 8th day) which has correlating trends with photosynthetic activities and CO_2 fixation. Post the maximum productivity carbohydrate concentration showed a decremental trend in all the conditions with 231, 180, 174, and 101 $mg.g^{-1}$ in CH, CC, AI, and HY conditions, respectively. The decrease in carbohydrate concentration maybe due to its consumption for lipids synthesis under stress conditions correlating with nutrient uptake and lowering of pH conditions (**Figure 6**). Proteins are synthesized during biomass growth most of which are essential enzymes, membrane bound electron shuttlers and redox mediators required for the cellular functioning. The higher protein levels were observed in CH followed by AI, CC, and HY conditions with 48, 46, 45, and 26 $mg.g^{-1}$, respectively. Owing to the reduced biomass growth during the nutrient stress conditions the protein concentrations have also shown a decrement in concentrations toward the end of the operation reaching 24, 37, 43, and 44 $mg.g^{-1}$ in HY, CC, AI, and CH conditions, respectively.

TABLE 2 | FAME compositional distribution with desaturation, average carbon chain length, average degree of unsaturation for lipids extracted from samples grown under different headspace gas concentrations.

FAME composition	CO_2	H_2	$CO_2 + H_2$	Air
	% Abundance			
C10:0	1	2	1	4
C12:0	1	1	1	2
C13:0	2	1	0	2
C14:0	4	4	3	2
C15:1	2	5	2	3
C16:0	16	16	15	17
C16:1	6	11	5	7
C17:0	2	1	2	1
C18:0	11	13	10	11
C18:1	8	10	11	11
C18:2	13	9	15	14
C18:3	14	8	17	10
C20:0	15	11	17	8
Total SFA	51	49	47	47
Total MUFA	16	21	18	14
Total PUFA	27	17	32	24
Average DU	0.884	0.739	0.99	0.859
Average CCL	17.337	17	17.58	16.85

Elemental Distribution in Biomass

The dry algal biomass at the end of the experiment was analyzed to determine the carbon, hydrogen, nitrogen, and sulfur distribution for all the experimental conditions (**Figure 7**). The carbon and hydrogen distribution correlates with the carbohydrate synthesis and CO_2 fixation as the reactors are operated in photoautotrophic mode of nutrition amounting to 85 $\pm$ 1% of the total elemental composition in all the experimental conditions. The distribution of nitrogen was modestly varying in CH (12.82%) compared to the other CC, AI, and HY (11 $\pm$ 0.5%) conditions which could be the result of enhanced protein synthesis in CH condition supporting the hypothesis that elevated CO_2 inlets under photoautotrophic mode resemble the heterotrophic mode of nutrition. The sulfur content showed similar distribution (1.5 $\pm$ 0.2%) amongst all the experimental variations (Gonçalves et al., 2016). The increase in CO_2 uptake had the influence on the carbon accumulation along with the protein synthesis which govern the C:N distribution of the biomass.

CONCLUSIONS

Present study shows the possibilities of selectively producing microalgal based bioactives and photofuels from industrial effluent gasses. The influence of elevated CO_2 and H_2 gas concentrations on both biomass growth and lipogenesis was specifically evident from the fatty acids compositions and the quantum yield. This study unwraps the possibility of cultivating microalgae in integration with industrial effluent treatment by utilizing the flue gases with low investments and also help in generating additional revenue, making the process economically feasible. However, deeper insights for growth and metabolite regulation in photosynthesis can be determined through molecular level quantification and transcriptomics of the targeted proteins/enzymes. The recent advances in photosynthetic research provide a ray of hope to overcome climate change and progress toward sustainable development with the multifaceted applications of microalgae.

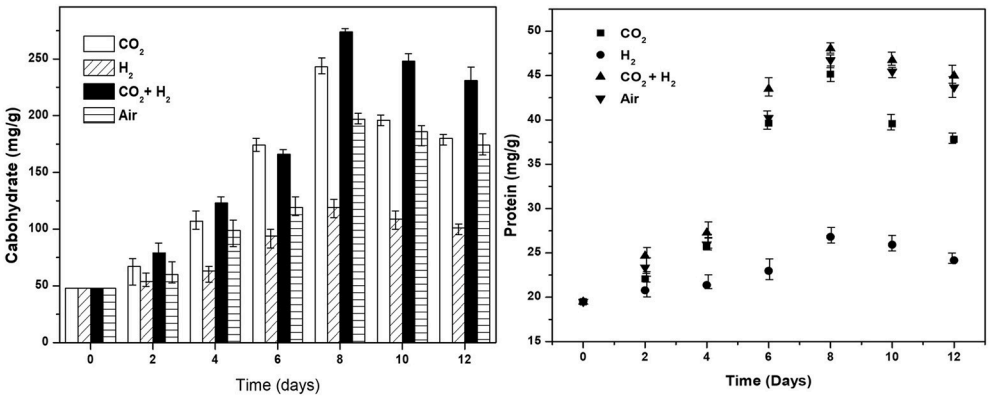

FIGURE 6 | Cellular biochemicals carbohydrates (mg.g^{-1}) and proteins (mg.g^{-1}) synthesis under different gas concentrations is depicted for all the experimental variations.

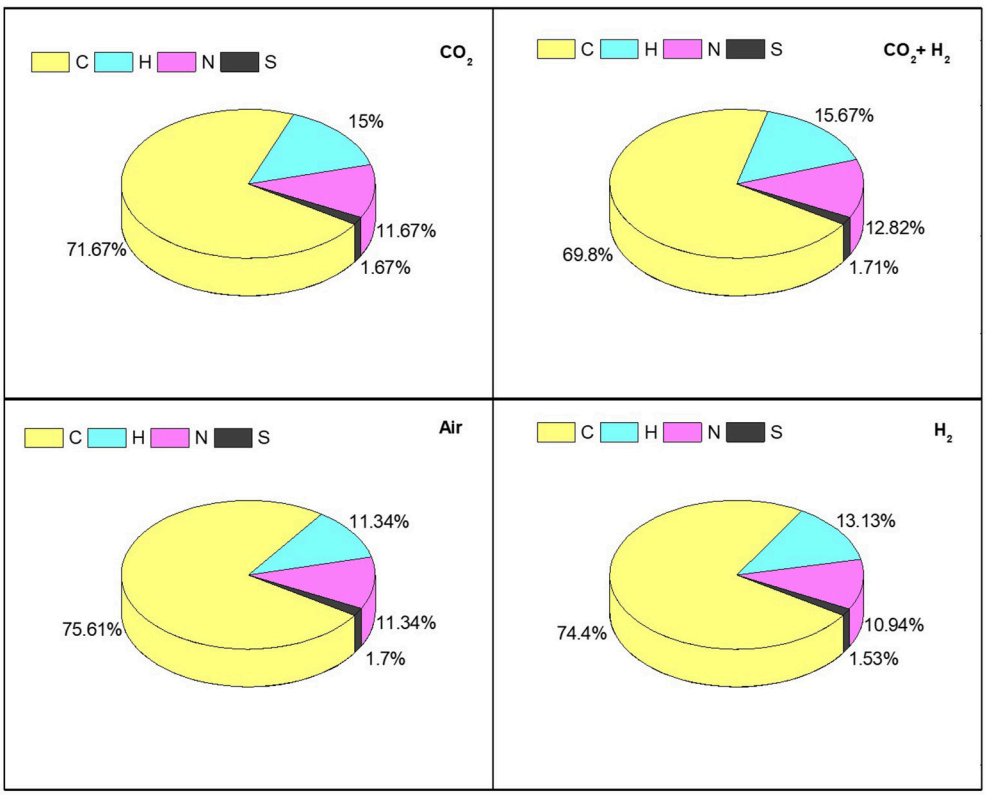

FIGURE 7 | Determining the relative abundance of CHNS influenced by photosynthetic activity and CO_2 sequestration trough elemental composition analysis for individual specific gas inlet variations.

AUTHOR CONTRIBUTIONS

All authors listed have made a substantial, direct and intellectual contribution to the work, and approved it for publication.

ACKNOWLEDGMENTS

SKB acknowledges University Grants Commission (UGC) for providing research fellowship.

REFERENCES

Azov, Y. (1982). Effect of pH on inorganic carbon uptake in algal cultures. *Appl. Environ. Microbiol.* 43, 1300–1306.

Benavente-Valdés, J. R., Aguilar, C., Contreras-Esquivel, J. C., Méndez-Zavala, A., and Montañez, J. (2016). Strategies to enhance the production of photosynthetic pigments and lipids in chlorophycae species. *Biotechnol. Rep.* 10, 117–125. doi: 10.1016/j.btre.2016.04.001

Benemann, J. R., Weissman, J. C., Koopman, B. L., and Oswald, W. J. (1977). Energy production by microbial photosynthesis. *Nature* 268, 19–23. doi: 10.1038/268019a0

Blankenship, R. E. (2002). "The basic principles of photosynthetic energy storage," in *Molecular Mechanisms of Photosynthesis* (Oxford, UK: Blackwell Science Ltd.), 1–10.

Bligh, E. G., and Dyer, W. J. (1959). A rapid method of total lipid extraction and purification. *Can. J. Biochem. Physiol.* 37, 911–917. doi: 10.1139/y59-099

Bowes, G. (1991). Growth at elevated CO_2: photosynthetic responses mediated through Rubisco. *Plant. Cell Environ.* 14, 795–806. doi: 10.1111/j.1365-3040.1991.tb01443.x

Butti, S. K., and Mohan, S. V. (2017). Autotrophic biorefinery: dawn of the gaseous carbon feedstock. *FEMS Microbiol. Lett.* 364, 1–8. doi: 10.1093/femsle/fnx166

Cabanelas, I. T., van der Zwart, M., Kleinegris, D. M., Wijffels, R. H., and Barbosa, M. J. (2016). Sorting cells of the microalga Chlorococcum littorale with increased triacylglycerol productivity. *Biotechnol. Biofuels* 9:183. doi: 10.1186/s13068-016-0595-x

Chandra, R., Arora, S., Rohit, M. V., and Venkata Mohan, S. (2015). Lipid metabolism in response to individual short chain fatty acids during mixotrophic mode of microalgal cultivation: influence on biodiesel saturation and protein profile. *Bioresour. Technol.* 188, 169–176. doi: 10.1016/j.biortech.2015.01.088

Chiranjeevi, P., and Mohan, S. V. (2016). Critical parametric influence on microalgae cultivation towards maximizing biomass growth with simultaneous lipid productivity. *Renew. Energy* 98, 64–71. doi: 10.1016/j.renene.2016.03.063

Chiu, S.-Y., Kao, C.-Y., Tsai, M.-T., Ong, S.-C., Chen, C.-H., and Lin, C.-S. (2009). Lipid accumulation and CO_2 utilization of Nannochloropsis oculata in response to CO_2 aeration. *Bioresour. Technol.* 100, 833–838. doi: 10.1016/j.biortech.2008.06.061

Cuellar-Bermudez, S. P., Romero-Ogawa, M. A., Vannela, R., Lai, Y. S., Rittmann, B. E., and Parra-Saldivar, R. (2015). Effects of light intensity and carbon dioxide on lipids and fatty acids produced by *Synechocystis* sp. PCC6803 during continuous flow. *Algal Res.* 12, 10–16. doi: 10.1016/j.algal.2015.07.018

Demars, B. O. L., Gislason, G. M., Olafsson, J. S., Manson, J. R., Friberg, N., Hood, J. M., et al. (2016). Impact of warming on CO_2 emissions from streams countered by aquatic photosynthesis. *Nat. Geosci.* 9, 758–761. doi: 10.1038/ngeo2807

de Mooij, T., de Vries, G., Latsos, C., Wijffels, R. H., and Janssen, M. (2016). Impact of light color on photobioreactor productivity. *Algal Res.* 15, 32–42. doi: 10.1016/j.algal.2016.01.015

Dowson, G. R. M., and Styring, P. (2017). Demonstration of CO_2 conversion to synthetic transport fuel at flue gas concentrations. *Front. Energy Res.* 5:26. doi: 10.3389/fenrg.2017.00026

DuBois, M., Gilles, K. A., Hamilton, J. K., Rebers, P. A., and Smith, F. (1956). Colorimetric method for determination of sugars and related substances. *Anal. Chem.* 28, 350–356. doi: 10.1021/ac60111a017

Fernández-Reiriz, M. J., Perez-Camacho, A., Ferreiro, M. J., Blanco, J., Planas, M., Campos, M. J., et al. (1989). Biomass production and variation in the biochemical profile (total protein, carbohydrates, RNA, lipids and fatty acids) of seven species of marine microalgae. *Aquaculture* 83, 17–37. doi: 10.1016/0044-8486(89)90057-4

Gaffron, H. (1940). Carbon dioxide reduction with molecular hydrogen in green algae. *Am. J. Bot.* 27, 273–283. doi: 10.1002/j.1537-2197.1940.tb14683.x

Gonçalves, A. L., Rodrigues, C. M., Pires, J. C. M., and Simões, M. (2016). The effect of increasing CO_2 concentrations on its capture, biomass production and wastewater bioremediation by microalgae and cyanobacteria. *Algal Res.* 14, 127–136. doi: 10.1016/j.algal.2016.01.008

Han, F., Huang, J., Li, Y., Wang, W., Wan, M., Shen, G., et al. (2013). Enhanced lipid productivity of *Chlorella pyrenoidosa* through the culture strategy of semi-continuous cultivation with nitrogen limitation and pH control by CO_2. *Bioresour. Technol.* 136, 418–424. doi: 10.1016/j.biortech.2013.03.017

Hein, M., and Sand-Jensen, K. (1997). CO_2 increases oceanic primary production. *Nature* 388, 526–527. doi: 10.1038/41457

Hoekman, S. K., Broch, A., Robbins, C., Ceniceros, E., and Natarajan, M. (2012). Review of biodiesel composition, properties, and specifications. *Renew. Sustain. Energy Rev.* 16, 143–169. doi: 10.1016/j.rser.2011.07.143

Hoornweg, D., Bhada-tata, P., and Kennedy, C. (2013). Waste production must peak this century. *Nature* 502, 615–617. doi: 10.1038/502615a

Hu, H., and Gao, K. (2006). Response of growth and fatty acid compositions of *Nannochloropsis* sp. to environmental factors under elevated CO_2 concentration. *Biotechnol. Lett.* 28, 987–992. doi: 10.1007/s10529-006-9026-6

Juneja, A., Ceballos, R., and Murthy, G. (2013). Effects of environmental factors and nutrient availability on the biochemical composition of algae for biofuels production: a review. *Energies* 6, 4607–4638. doi: 10.3390/en6094607

Kant, M. (2017). Overcoming barriers to successfully commercializing carbon dioxide utilization. *Front. Energy Res.* 5:22. doi: 10.3389/fenrg.2017.00022

Karpagam, R., Preeti, R., Ashokkumar, B., and Varalakshmi, P. (2015). Enhancement of lipid production and fatty acid profiling in *Chlamydomonas reinhardtii*, CC1010 for biodiesel production. *Ecotoxicol. Environ. Saf.* 121, 253–257. doi: 10.1016/j.ecoenv.2015.03.015

Keenan, T. F., Prentice, I. C., Canadell, J. G., Williams, C., Wang, H., Raupach, M. R., et al. (2016). Recent pause in the growth rate of atmospheric CO_2 due to enhanced terrestrial carbon uptake. *Nat. Commun.* 7:13428. doi: 10.1038/ncomms13428

Kitaya, Y., Okayama, T., Murakami, K., and Takeuchi, T. (2003). Effects of CO_2 concentration and light intensity on photosynthesis of a rootless submerged plant, *Ceratophyllum demersum* L., used for aquatic food production in bioregenerative life support systems. *Adv. Space Res.* 31, 1743–1749. doi: 10.1016/S0273-1177(03)00113-3

Klok, A. J., Martens, D. E., Wijffels, R. H., and Lamers, P. P. (2013). Simultaneous growth and neutral lipid accumulation in microalgae. *Bioresour. Technol.* 134, 233–243. doi: 10.1016/j.biortech.2013.02.006

Li, D., Wang, L., Zhao, Q., Wei, W., and Sun, Y. (2015). Improving high carbon dioxide tolerance and carbon dioxide fixation capability of *Chlorella* sp. by adaptive laboratory evolution. *Bioresour. Technol.* 185, 269–275. doi: 10.1016/j.biortech.2015.03.011

Lohman, E. J., Gardner, R. D., Pedersen, T., Peyton, B. M., Cooksey, K. E., and Gerlach, R. (2015). Optimized inorganic carbon regime for enhanced growth and lipid accumulation in *Chlorella vulgaris*. *Biotechnol. Biofuels* 8:82. doi: 10.1186/s13068-015-0265-4

Lowry, O. H., Rosebrough, N. J., Farr, A. L., and Randall, R. J. (1951). Protein measurement with the folin phenol reagent. *J. Biol. Chem.* 193, 265–275.

Matich, E. K., Butryn, D. M., Ghafari, M., del Solar, V., Camgoz, E., Pfeifer, B. A., et al. (2016). Mass spectrometry-based metabolomics of value-added biochemicals from Ettlia oleoabundans. *Algal Res.* 19, 146–154. doi: 10.1016/j.algal.2016.08.009

Mohammadi, F. S. (2016). Investigation of effective parameters on biomass and lipid productivity of *Chlorella vulgaris*. *Period. Biol.* 118, 123–129. doi: 10.18054/pb.2016.118.2.3197

Moroney, J. V., and Ynalvez, R. A. (2007). Proposed carbon dioxide concentrating mechanism in *Chlamydomonas reinhardtii*. *Eukaryot. Cell* 6, 1251–1259. doi: 10.1128/EC.00064-07

Mortensen, L. M., and Gislerod, H. R. (2015). The growth of as influenced by high CO and low O in flue gas from a silicomanganese smelter. *J. Appl. Phycol.* 27, 633–638. doi: 10.1007/s10811-014-0357-8

Nagaich, V., Dongre, S. K., Singh, P., Yadav, M., and Tiwari, A. (2014). Maximum-CO_2 tolerance in microalgae : possible mechanisms and higher lipid accumulation. *Int. J. Adv. Res.* 2, 101–106.

Ooms, M. D., Dinh, C. T., Sargent, E. H., and Sinton, D. (2016). Photon management for augmented photosynthesis. *Nat. Commun.* 7:12699. doi: 10.1038/ncomms12699

Peng, H., Wei, D., Chen, F., and Chen, G. (2016a). Regulation of carbon metabolic fluxes in response to CO_2 supplementation in phototrophic *Chlorella vulgaris*: a cytomic and biochemical study. *J. Appl. Phycol.* 28, 737–745. doi: 10.1007/s10811-015-0542-4

Peng, H., Wei, D., Chen, G., and Chen, F. (2016b). Transcriptome analysis reveals global regulation in response to CO_2 supplementation in oleaginous

microalga Coccomyxa subellipsoidea C-169. *Biotechnol. Biofuels* 9, 1–17. doi: 10.1186/s13068-016-0571-5

Perez-Garcia, O., Escalante, F. M., de-Bashan, L. E., and Bashan, Y. (2011). Heterotrophic cultures of microalgae: metabolism and potential products. *Water Res.* 45, 11–36. doi: 10.1016/j.watres.2010.08.037

Price, G. D., and Howitt, S. M. (2014). Plant science: towards turbocharged photosynthesis. *Nature* 513, 497–498. doi: 10.1038/nature13749

Rausch, T. (1981). The estimation of micro-algal protein content and its meaning to the evaluation of algal biomass I. Comparison of methods for extracting protein. *Hydrobiologia* 78, 237–251. doi: 10.1007/BF00008520

Riebesell, U., Wolf-Gladrow, D. A., and Smetacek, V. (1993). Carbon dioxide limitation of marine phytoplankton growth rates. *Nature* 361, 249–251. doi: 10.1038/361249a0

Rodrigues, W. P., Martins, M. Q., Fortunato, A. S., Rodrigues, A. P., Semedo, J. N., Simões-Costa, M. C., et al. (2016). Long-term elevated air [CO_2] strengthens photosynthetic functioning and mitigates the impact of supra-optimal temperatures in tropical *Coffea arabica* and *C. canephora* species. *Glob. Chang. Biol.* 22, 415–431. doi: 10.1111/gcb.13088

Rohit, M. V., and Mohan, S. V. (2015). Tropho-metabolic transition during *Chlorella sp*. cultivation on synthesis of biodiesel. *Renew. Energy* 98, 84–91. doi: 10.1016/j.renene.2016.03.041

Santos, A. M., Wijffels, R. H., and Lamers, P. P. (2014). PH-upshock yields more lipids in nitrogen-starved *Neochloris oleoabundans*. *Bioresour. Technol.* 152, 299–306. doi: 10.1016/j.biortech.2013.10.079

Stewart, J. J., Bianco, C. M., Miller, K. R., and Coyne, K. J. (2015). The marine microalga, heterosigma akashiwo, converts industrial waste gases into valuable biomass. *Front. Energy Res.* 3:12. doi: 10.3389/fenrg.2015.00012

Sun, Z., Chen, Y. F., and Du, J. (2016a). Elevated CO_2 improves lipid accumulation by increasing carbon metabolism in Chlorella sorokiniana. *Plant Biotechnol. J.* 14, 557–566. doi: 10.1111/pbi.12398

Sun, Z., Dou, X., Wu, J., He, B., Wang, Y., and Chen, Y. F. (2016b). Enhanced lipid accumulation of photoautotrophic microalgae by high-dose CO_2 mimics a heterotrophic characterization. *World J. Microbiol. Biotechnol.* 32, 1–11. doi: 10.1007/s11274-015-1963-6

Tsuzuki, M., Ohnuma, E., Sato, N., Takaku, T., and Kawaguchi, A. (1990). Effects of CO_2 concentration during growth on fatty acid composition in microalgae. *Plant Physiol.* 93, 851–856. doi: 10.1104/pp.93.3.851

Velmurugan, N., Sung, M., Yim, S. S., Park, M. S., Yang, J. W., and Jeong, K. J. (2014). Systematically programmed adaptive evolution reveals potential role of carbon and nitrogen pathways during lipid accumulation in *Chlamydomonas reinhardtii*. *Biotechnol. Biofuels* 7:117. doi: 10.1186/s13068-014-0117-7

Venkata Mohan, S., Modestra, J. A., Amulya, K., Butti, S. K., and Velvizhi, G. (2016a). A circular bioeconomy with biobased products from CO_2 sequestration. *Trends Biotechnol.* 34, 506–519. doi: 10.1016/j.tibtech.2016.02.012

Venkata Mohan, S., Nikhil, G. N., Chiranjeevi, P., Nagendranatha Reddy, C., Rohit, M. V., Kumar, A. N., et al. (2016b). Waste biorefinery models towards sustainable circular bioeconomy: critical review and future perspectives. *Bioresour. Technol.* 215, 2–12. doi: 10.1016/j.biortech.2016.03.130

Venkata Mohan, S., and Prathima Devi, M. (2012). Fatty acid rich effluent from acidogenic biohydrogen reactor as substrate for lipid accumulation in heterotrophic microalgae with simultaneous treatment. *Bioresour. Technol.* 123, 627–635. doi: 10.1016/j.biortech.2012.07.004

Venkata Mohan, S., Rohit, M. V., Chiranjeevi, P., Chandra, R., and Navaneeth, B. (2014). Heterotrophic microalgae cultivation to synergize biodiesel production with waste remediation: progress and perspectives. *Bioresour. Technol.* 184, 169–178. doi: 10.1016/j.biortech.2014.10.056

Watson-Lazowski, A., Lin, Y., Miglietta, F., Edwards, R. J., Chapman, M. A., and Taylor, G. (2016). Plant adaptation or acclimation to rising CO_2? Insight from first multigenerational RNA-Seq transcriptome. *Glob. Chang. Biol.* 22, 3760–3773. doi: 10.1111/gcb.13322

Yasmin Anum Mohd Yusof, Y. A. M., Basari, J. H., Mukti, N. A., Sabuddin, R., Muda, A. R., Sulaiman, S., et al. (2011). Fatty acids composition of microalgae *Chlorella vulgaris* can be modulated by varying carbon dioxide concentration in outdoor culture. *Afr. J. Biotechnol.* 10, 13536–13542. doi: 10.5897/AJB11.1602

Yoo, C., Jun, S.-Y., Lee, J.-Y., Ahn, C.-Y., and Oh, H.-M. (2010). Selection of microalgae for lipid production under high levels carbon dioxide. *Bioresour. Technol.* 101, S71–S74. doi: 10.1016/j.biortech.2009.03.030

Yu, W.-L., Ansari, W., Schoepp, N. G., Hannon, M. J., Mayfield, S. P., and Burkart, M. D. (2011). Modifications of the metabolic pathways of lipid and triacylglycerol production in microalgae. *Microb. Cell Fact.* 10:91. doi: 10.1186/1475-2859-10-91

Conflict of Interest Statement: The authors declare that the research was conducted in the absence of any commercial or financial relationships that could be construed as a potential conflict of interest.

frontiers in Bioengineering and Biotechnology

ORIGINAL RESEARCH
published: 12 June 2018
doi: 10.3389/fbioe.2018.00078

Granular Carbon-Based Electrodes as Cathodes in Methane-Producing Bioelectrochemical Systems

*Dandan Liu[1], Marta Roca-Puigros[1], Florian Geppert[2], Leire Caizán-Juanarena[1], Susakul P. Na Ayudthaya[3], Cees Buisman[1] and Annemiek ter Heijne[1]**

[1] Sub-Department of Environmental Technology, Wageningen University & Research, Wageningen, Netherlands, [2] Fraunhofer Institute for Environmental, Safety, and Energy Technology UMSICHT, Oberhausen, Germany, [3] Laboratory of Microbiology, Wageningen University & Research, Wageningen, Netherlands

OPEN ACCESS

Edited by:
Andrea Schievano, Università degli Studi di Milano, Italy

Reviewed by:
Sunil A. Patil, Indian Institute of Science Education and Research Mohali, India
Matteo Grattieri, University of Utah, United States
Miriam A. Rosenbaum, Leibniz-Institut für Naturstoff-Forschung und Infektionsbiologie, Hans Knöll Institut, Germany

***Correspondence:**
Annemiek ter Heijne
annemiek.terheijne@wur.nl

Specialty section:
This article was submitted to Bioenergy and Biofuels, a section of the journal Frontiers in Bioengineering and Biotechnology

Received: *29 March 2018*
Accepted: *29 May 2018*
Published: *12 June 2018*

Citation:
Liu D, Roca-Puigros M, Geppert F, Caizán-Juanarena L, Na Ayudthaya SP, Buisman C and ter Heijne A (2018) Granular Carbon-Based Electrodes as Cathodes in Methane-Producing Bioelectrochemical Systems. Front. Bioeng. Biotechnol. 6:78. doi: 10.3389/fbioe.2018.00078

Methane-producing bioelectrochemical systems generate methane by using microorganisms to reduce carbon dioxide at the cathode with external electricity supply. This technology provides an innovative approach for renewable electricity conversion and storage. Two key factors that need further attention are production of methane at high rate, and stable performance under intermittent electricity supply. To study these key factors, we have used two electrode materials: granular activated carbon (GAC) and graphite granules (GG). Under galvanostatic control, the biocathodes achieved methane production rates of around 65 L $CH_4/m^2cat_{proj}/d$ at 35 A/m^2cat_{proj}, which is 3.8 times higher than reported so far. We also operated all biocathodes with intermittent current supply (time-ON/time-OFF: 4–2′, 3–3′, 2–4′). Current-to-methane efficiencies of all biocathodes were stable around 60% at 10 A/m^2cat_{proj} and slightly decreased with increasing OFF time at 35 A/m^2cat_{proj}, but original performance of all biocathodes was recovered soon after intermittent operation. Interestingly, the GAC biocathodes had a lower overpotential than the GG biocathodes, with methane generation occurring at −0.52 V vs. Ag/AgCl for GAC and at −0.92 V for GG at a current density of 10 A/m^2cat_{proj}. 16S rRNA gene analysis showed that *Methanobacterium* was the dominant methanogen and that the GAC biocathodes experienced a higher abundance of proteobacteria than the GG biocathodes. Both cathode materials show promise for the practical application of methane-producing BESs.

Keywords: methane production, intermittent current supply, low cathode overpotential, bioelectrochemical system (BES), granular carbon-based electrode

INTRODUCTION

The expansion of global energy demand results in an increasing utilization of fossil fuels, which leads to unwanted CO_2 emissions (Rogelj et al., 2016). To mitigate CO_2 emissions, the energy transition from fossil fuels to renewable energy is necessary. In the Energy Roadmap 2050 released by European Commission in 2011, the share of renewable energy in the final gross energy consumption will grow from 10% of today, to 30% in 2030, and at least 55% in 2050 (Commission, 2011). The substantial rise of renewable electricity demand requires new technologies for electricity storage, because the renewable electricity produced is fluctuating and intermittent due to the intermittent nature of wind and sun (Hu et al., 2018).

Power to Gas (PtG) technologies have been reported as a flexible option to convert and store excess renewable electricity from the power grid (electricity) into the gas grid (CH_4) (Bailera et al., 2017). CH_4 can be generated by reduction of CO_2 through thermochemical or biological methanation. Methane-producing bioelectrochemical systems (BESs) are one form of biological methanation (Geppert et al., 2016). In methane-producing BESs, H_2O is typically used as an electron donor, and oxidized at the anode (Van Eerten-Jansen et al., 2012). At the cathode, CO_2 is reduced to CH_4 by microorganisms. This assembly of cathode and microorganisms is called a biocathode.

Since the concept of methane-producing BESs has been shown in 2009 (Cheng et al., 2009), methane-producing BESs have mainly been studied at constant external electricity supply. The electricity generated by the renewable sources is, however, intermittent. So far, performance of biocathodes under intermittent electricity supply has not been studied. Intermittent operation has been performed with capacitive anode electrode materials in the form of activated carbon granules (GAC) for wastewater microbial fuel cells (MFCs) (Borsje et al., 2016; Santoro et al., 2017). These capacitive bioanodes can store electrons generated by electroactive microorganisms in the charging period (open circuit), and afterwards, these stored electrons could be harvested in the discharging cell (closed circuit) (Deeke et al., 2015). Use of granular electrodes with this capacitive property (storage of electrons) might benefit methane-producing BESs operated with intermittent electricity supply, so that the capacitance can act as an electron buffer when current peaks occur.

Besides the capacitance property of GAC, use of granular carbon-based electrodes is in general beneficial to the performance of biocathodes. The reason behind this may be that carbon-based materials have good biocompatibility, and the 3D granular structure can provide benefits for the attachment of microorganisms and increase mass transfer between the bulk solution and the electrode (Guo et al., 2015; Jourdin et al., 2015). In addition, GAC has been proven to stimulate methane production in anaerobic digestion, as it probably promotes direct interspecies electron transfer from *Geobacter* (Liu et al., 2012), *Sporanaerobacter, and Enterococcus* (Dang et al., 2016) species to methanogens. Addition of pre-acclimated GAC as inoculum has also been shown to enhance methane production and decrease startup time in the methane-producing BESs, although carbon brushes were used as cathode electrode (LaBarge et al., 2017).

In this paper, we report the use of GAC and graphite granules (GG) in a packed bed as the cathode electrode. Three intermittent current supply modes with time-ON/time-OFF (4–2′, 3–3′, and 2–4′) were performed at two different current densities (10 and 35 A/m^2 cat_{proj}). The effect of intermittent current supply with different time intervals was studied. We tested both granule types in duplicate reactors for 137 days and assessed performance in terms of methane production rate and current-to-methane efficiency. We also analyzed the microbial community composition.

MATERIALS AND METHODS

Experimental Setup

We operated four bioelectrochemical reactors (see Figure S1 in the Supporting Information). Each reactor contained an anodic and cathodic chamber, each with a volume of 33 cm^3 (11 × 2 × 1.5 cm). A cation exchange membrane (FumaTech GmbH, Ingbert, Germany) was used with a projected surface area of 22 cm^2 (11 × 2 cm). As cathode materials, we used GAC with a specific surface area of 764 m^2/g (Cabot Norit Nederland B.V., Zaandam, the Netherlands; 1–3 mm diameter) and GG with a specific surface area of 0.438 m^2/g (Carbone Lorraine Benelux BV, Wemmel, Belgium; 3–5 mm), leading to a substantially higher capacitance property in GAC compared with GG (Borsje et al., 2016).

Two cathodic chambers were packed with GAC granules (GAC_1 with 8.5 g and GAC_2 with 8.4 g). The other two cathodic chambers were packed with GG granules (GG_1 with 26 g and GG_2 with 29.2 g). All the granules were washed by distilled water before use. The current collector at the cathode was a plain graphite plate. The projected cathode surface area was 22 cm^2 (11 × 2 cm), and was equal to the membrane surface area. The granule bed was tightly packed to ensure good contact between granules and current collector. The anodic chambers contained a 22-cm^2 platinum-iridium-coated titanium plate as electrode (Magneto Special Anodes BV, Schiedam, the Netherlands). The anodic chambers were filled with glass beads with a 7-mm diameter (Hecht-Assistent, Sondheim v. d. Rhön, Germany) to further ensure tight packing of the carbon granules. The reference electrodes (3 M KCl Ag/AgCl, QM710X, QIS, Oosterhout, the Netherlands, +0.205 V vs. standard hydrogen electrode) were connected to the anolyte and catholyte solutions. Throughout this paper, all potentials are expressed against Ag/AgCl reference electrode.

Each cathodic chamber was connected to a liquid-gas separation bottle (60 mL) with a gas bag of 2 L (Cali-5-Bond^{TM}). After the separation bottle, the catholyte was channeled into the recirculation bottle (500 mL), where CO_2 was sparged. The excess CO_2 went through a water lock and was released into the environment. All four anode chambers shared the same anolyte that was pumped via a recirculation bottle (5 L). Anolyte and catholyte flow rates were 7 mL/min.

Electrolytes and Microorganisms

The catholyte consisted of a 50 mM phosphate buffer (2.77 g/L $NaH_2PO_4 \cdot 2H_2O$ and 4.58 g/L Na_2HPO_4) with 0.2 g/L NH_4Cl, 0.13 g/L KCl, 10 mL/L Wolfe's vitamin solution and 10 mL/L Wolfe's modified mineral solution (Wolin et al., 1963). Catholyte pH was 7.1. The fresh catholyte was flushed with N_2 gas for 30 min before each use. In order to keep the catholyte with sufficient CO_2 and stable pH simultaneously, the catholyte in the recirculation bottle was sparged with CO_2 for 2 h/day during weekdays. After day 71, the catholyte was sparged with CO_2 continuously.

All cathode chambers were inoculated with 10 mL of an anaerobic mixed culture (volatile suspended solids = 12.9 ±

1.3 g/L), which contained 50% anaerobic granular sludge from the paper industry wastewater treatment facility in Eerbeek (the Netherlands) and 50% anaerobic sludge from the municipal wastewater treatment facility in Ede (the Netherlands).

The anolyte consisted of a 50 mM phosphate buffer at pH 7. The anolyte was continuously flushed with N_2 gas in the recirculation bottle to keep O_2 levels at a minimum.

System Operation

Experimental conditions are shown in **Figure 1**. All reactors were galvanostatically controlled (fixed current) by a potentiostat (Ivium n-Stat, Eindhoven, the Netherlands), which collected the cathode potential data from all reactors at intervals of 1 min. In this way, methane production rates can be regulated more directly than with cathode potential control, as the current determines the electrochemical reaction rate (Jörissen and Speiser, 2015). After inoculation, all reactors were operated at a fixed current of 5 A/m^{2}cat$_{proj}$ as startup period. The current of all reactors was increased from 5 to 10 A/m^{2}cat$_{proj}$ on day 37 and from 10 to 35 A/m^{2}cat$_{proj}$ on day 71. All cathodes were operated in batch. Half of the catholyte was replaced on days 31 and 70 to replenish buffer, nutrients and vitamins. The pH of each reactor was monitored daily by pH measurement of liquid samples (0.5 mL per sample) taken from anode and cathode chamber. All reactors were operated inside a temperature-controlled cabinet at 30°C.

For intermittent operation, a cycle time of 6 min (′) was used at three different current time-ON/time-OFF ratios: 4–2′, 3–3′, and 2–4′. Each ratio was tested for 20 h and was performed twice. After intermittent operation, all biocathodes were supplied with constant current for 20 h to investigate recovery after intermittent operation.

Electrochemical Analysis

Polarization curves were recorded before inoculation and on day 30 and day 90 after inoculation. For the polarization curve before inoculation, the cathode potential was controlled from −0.5 to −1.0 V with steps of 0.1 V; for the polarization curve after inoculation, the cathode potential was controlled from −0.1 to −0.7 V with steps of 0.05 V. Each potential step lasted 600 s for the GAC biocathodes, and 300 s for the GG biocathodes, as the latter required a shorter equilibrium time.

Chemical Analyses

The liquid and gas samples were taken from each reactor twice a week. Volatile fatty acids (VFAs), including formate, acetate and lactate, were determined in the liquid phase by high-performance liquid chromatography (HPLC) (Lindeboom et al., 2016), whereas the gas composition was measured by gas chromatography (GC) (Liu et al., 2016). The gas volume was quantified by emptying the gas bags with a syringe. The methane production rate was calculated and normalized to the projected surface area of the cathode (Equation 1) and the volume of the cathodic chamber (Equation 2), as follows:

$$\gamma_{CH4-A} = \frac{V_T \times C_{CH4}}{A_{proj} \times t} \quad (1)$$

$$\gamma_{CH4-V} = \frac{V_T \times C_{CH4}}{V_{electrode} \times t} \quad (2)$$

Here, γ_{CH4-A} (L CH$_4$/m^2 cat$_{proj}$ /d) and γ_{CH4-V} (L CH$_4$/m^3 cat /d) represent methane production rates; V_T (L) is the total volume by summing up the volume of the gas bag and the headspace (0.015 L); C_{CH_4}(%) is the methane fraction in the headspace; $A_{proj}(m^2)$ is the projected surface area of the graphite plate current collector and membrane; $V_{electrode}(m^3)$ is the cathodic chamber volume; t (d) is the experimental time between each headspace measurement (d).

Current-to-Methane Efficiency

This indicates which percentage of the electrons ended up in the form of methane and is calculated as Equation 3.

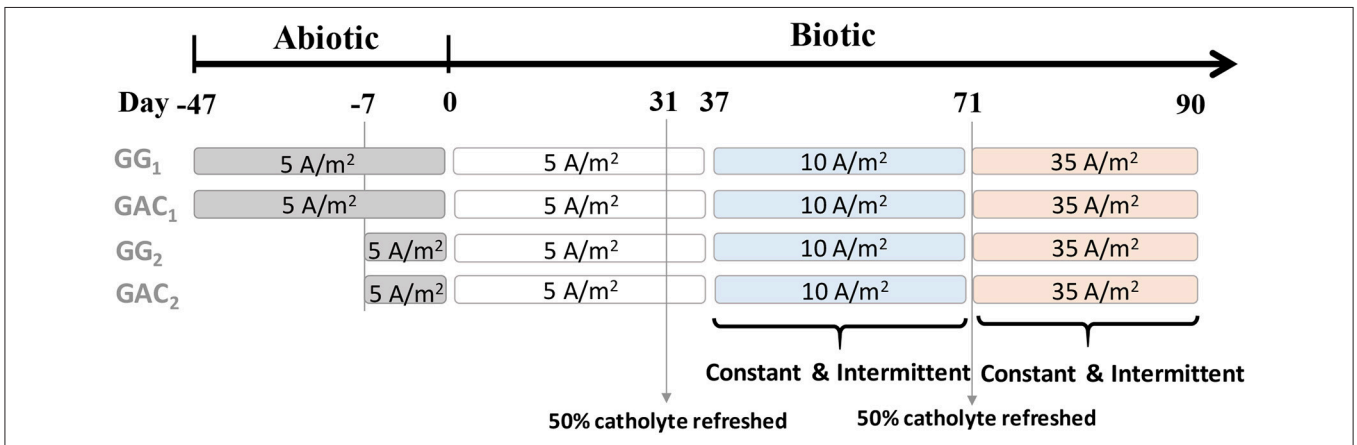

FIGURE 1 | Overview of experimental conditions that were carried out for four methane-producing BES reactors. At day 0, all catholytes were inoculated. Days before inoculation are indicated as negative, days after inoculation are indicated as positive. During the phases of 10 and 35 A/m^{2}cat$_{proj}$, both constant and intermittent current supply modes were performed.

$$\eta_{CH4} = \frac{n_{CH4} \times z_{CH4} \times F}{\int_{t=0}^{t} I\, dt} \quad (3)$$

F is the Faraday constant (96485 C/mol e^-); n_{CH4} (mol) is total moles of CH_4 produced; z_{CH4} is moles of electrons per mole of CH_4 (8); I (A) is the current.

Microbial Community Analysis

After operation at a current density of 35 A/$m^2$$cat_{proj}$, all reactors were disassembled inside an anaerobic chamber, and 0.5 g (wet weight) of the granules was taken from each cathode. In addition, 300 mL of the catholyte was taken from each reactor and filtered it over a 0.22 μm MF-MilliPore filter. Genomic DNA was extracted from each reactor samples with a Mo Bio PowerSoil DNA isolation kit for 0.5 g of the granular electrode and a Mo Bio PowerWater DNA isolation kit for the filter, according to the manufacturer's instructions. To investigate both bacteria and archaea, firstly amplification of 16S rRNA gene fragments was carried out by using a two-step PCR protocol, and then DNA was quantified using a Qubit® dsDNA BR Assay Kit and a DeNovix DS-11 FX spectrophotometer/fluorometer (DENovix Inc., Wilmington, DE, USA), finally the 16S rRNA gene Miseq sequencing data were analyzed using Galaxy/NG-Tax, an in-house pipeline (see detailed information in Supportive Information, under B). Bray-Curtis similarities were calculated between reactors (biocathodes and used catholytes) from the microbial community relative abundance data with Primer-E software, version 7 (LaBarge et al., 2017).

RESULTS AND DISCUSSION

High Methane Production Rates Directly Linked to Current Density

We determined methane production rates at two different current densities of 10 and 35 A/$m^2$$cat_{proj}$. At the current density of 35 A/$m^2$$cat_{proj}$, the methane production rates were around 65 L CH_4 /$m^2$$cat_{porj}$/d for both cathode materials (**Figure 2A**). As methane production rates were directly related to current density, they were almost four times higher than at 10 A/$m^2$$cat_{proj}$. The current-to-methane efficiencies for the GAC and GG reactors (**Figure 2B** increased from 55% at 10 A/$m^2$$cat_{proj}$ to 67% at 35 A/$m^2$$cat_{proj}$. No H_2 and volatile fatty acids were detected in any of the reactors at these two current densities, which suggests that during the stable performance period, the methanogenic activity was high enough to utilize these components if they were produced. Possible other electron sinks are biomass growth (Geppert et al., 2016), or loss of methane via membrane, tubes, and connections within the reactor (Skovsgaard and Jacobsen, 2017), especially considering our relatively long sampling intervals (3–4 days). Also, reduction of oxygen generated at the anode could play a role (Van Eerten-Jansen et al., 2012). The methane production rates achieved with GAC and GG at constant current in this study were compared with similar carbon-based electrodes in other studies (Geppert et al., 2016; **Table 1**). One the one hand, methane production rate at 35 A/m^2 were several times higher than those in other studies. On the other hand, methane production rate at 10 was similar with other studies, but it is interesting to note that the cathode potentials of GAC biocathodes were quite different in this case, −0.55 V for GAC biocathodes compared to −1.1 V for biocathodes, i.e., Villano et al.

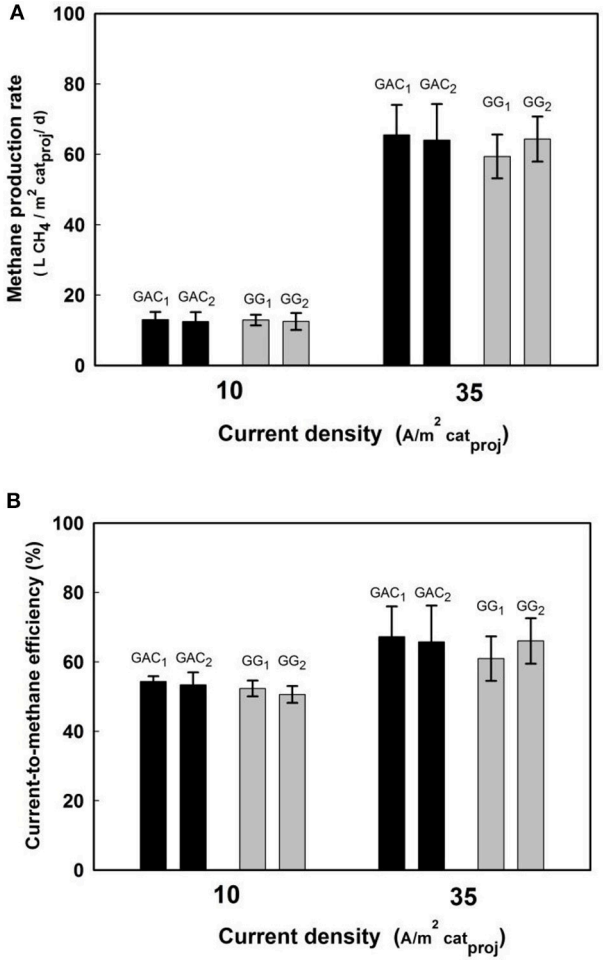

FIGURE 2 | Methane production rates **(A)** and current-to-methane efficiencies **(B)** at current densities of 10 A/$m^2$$cat_{proj}$ and 35 A/$m^2$$cat_{proj}$ for GAC and GG biocathodes. Data were collected throughout a period of 2 weeks with stable performance for every reactor. Shown are the average value and standard deviation of four samples for each reactor and current density.

Methane Production Was Related to Total Charge Also in Intermittent Mode

After all the biocathodes achieved a stable methane production rates at a constant current supply of 10 A/$m^2$$cat_{proj}$, intermittent current (at the same current density) was supplied to all biocathodes with three different time intervals: 4–2′, 3–3′, and 2–4′. Methane production rate of each biocathode is shown in **Figure 4A**, calculations based on the 20 h period for each time interval. Higher current time-ON/time-OFF interval supplied to the biocathodes resulted in higher methane production

TABLE 1 | Comparison of methane production rates for similar 3D carbon-based electrodes in methane-producing BESs when water was used as electron donor.

Electrode material	Current density		Methane production rate		Current-to-CH_4 Efficiency (%)	Cathode potential (V vs. Ag/AgCl)	Reference
	(A/m^2cat_{proj})	(kA/m^3cat)	($LCH_4/m^2cat_{proj}/d$)	($m^3CH_4/m^3cat/d$)			
GAC	10	0.67	15	1.0	54	-0.52	This study
GAC	35	2.3	65	4.3	66	-0.58	This study
GF	0.21	0.070	0.13	0.045	23	-0.75	Van Eerten-Jansen et al., 2012
GF	2.9	0.97	5.1	1.7	73	-0.9	van Eerten-Jansen et al., 2015
GF	7.1	2.5	8.8	3.1	69	-1.3	Liu et al., 2017
GG	10	0.67	15	0.97	52	-0.9	This study
GG	35	2.3	62	4.1	67	-1.1	This study
GG	3.8	0.13	17	0.56	79	-1.1	Villano et al., 2013

rates, with 9.5 L CH_4/m^2 cat_{proj}/d at 4–2′, 5.5 L CH_4/m^2 cat_{proj}/d at 3–3′ and 4.0 L CH_4/m^2 cat_{proj}/d at 2–4′, meaning that charge provided during ON-time was used to generate methane.

When the current density was increased from 10 to 35 $A/m^2cat_{proj,}$ the methane production rate at continuous current supply increased from 15 L CH_4/m^2 cat_{proj}/d at 10 A/m^2 (**Figure 3A**) to 90 L CH_4/m^2 cat_{proj}/d at 35 A/m^2 (**Figure 3B**). Again, an increase in methane production rate was observed along with increasing time-ON/time-OFF ratios. Moreover, we compared our experimental data with the theoretical methane production calculated for the different current time-ON/time-OFF ratios (Figure S4 in Supporting Information, under D). The close fit between measured and calculated data shows that methane generation is closely linked to the charge provided to the biocathode, for both GG and GAC.

Intermittent Current Operation Does Not Influence Biocathode Activity

Studies on bioanodes have shown that GAC can store charge in the electric double layer when used in Microbial Fuel Cells (Deeke et al., 2015; Lu et al., 2015), whereas GG with low capacitance does not show this charge storage behavior. This higher capacitance of GAC biocathodes was expected to result in smaller fluctuations in cathode potential, and as a possible electron buffer, compared to GG biocathodes during intermittent operation (Borsje et al., 2016). As shown in Figure S5, the cathode potentials of GAC biocathodes during intermittent current indeed kept stable around −0.5 V, whereas the cathode potentials of GG biocathodes changed in the range from −0.6 to −1.0 V. These results might indicate that intermittent current operation would affect GAC biocathodes less than GG biocathodes. However, at a current density of 10 A/m^2cat_{proj}, all biocathodes, operated under different current time-ON/time-OFF intervals, had a similar current-to-methane efficiency of 50–60% (**Figure 4A**). When the current density was increased from 10 to 35 $A/m^2cat_{proj,}$ the current-to-methane efficiency was also constant with a slight decrease along with the longer time-OFF intervals (**Figure 4B**). After these intermittent operations, an additional constant current supply for 20 h was operated for all biocathodes to verify if the initial activity was restored after intermittent operation. As shown in **Figure 4**, the current-to-methane efficiencies of all biocathodes after intermittent operations were similar to those at constant current supply, indicating that biocathodes were not affected by the intermittent operation at these two current densities of 10 and 35 A/m^2cat_{proj}, for both materials. In addition, the methane production rate of all biocathodes in our study kept stable, even though all biocathodes had experienced around 60 min of open circuit period during each headspace and pH sampling time. Our results are, however, different from those results found in the previous study that the methane production rate decreased by 87% after an open circuit period of 45 min, and it took 4 months before performance was back at the original level (Bretschger et al., 2015). The discrepancy could be due to that the quantity and/or bioactivity of biofilm growth on our granular carbon-based electrodes is higher than those on the carbon cloth electrode used in that study, as higher current density was found on our biocathodes (5 A/m^2) compared with their biocathodes (0.06 A/m^2). To conclude, current-to-methane efficiency (%) remained quite stable under the different current supply modes at 10 A/m^2, and showed a slight decrease with increasing OFF-time at 35 A/m^2.

It is worth notifying that current-to-methane efficiencies obtained at continuous current density of 35 A/m^2cat_{proj} in **Figure 4B**, are even higher than those achieved at the same current density reported in **Figure 2B**. This discrepancy could be due to the different durations between headspace sampling: 20 h for **Figure 5** and 3–4 days for **Figure 3**. Shorter duration between headspace sampling could mitigate losses via H_2 or O_2 leakage from the joints of the experimental set-up.

Biocathodes With Granular Activated Carbon Produced Methane at Low Overpotentials

Although there is no difference between GAC and GG biocathodes during constant and intermittent operation in terms

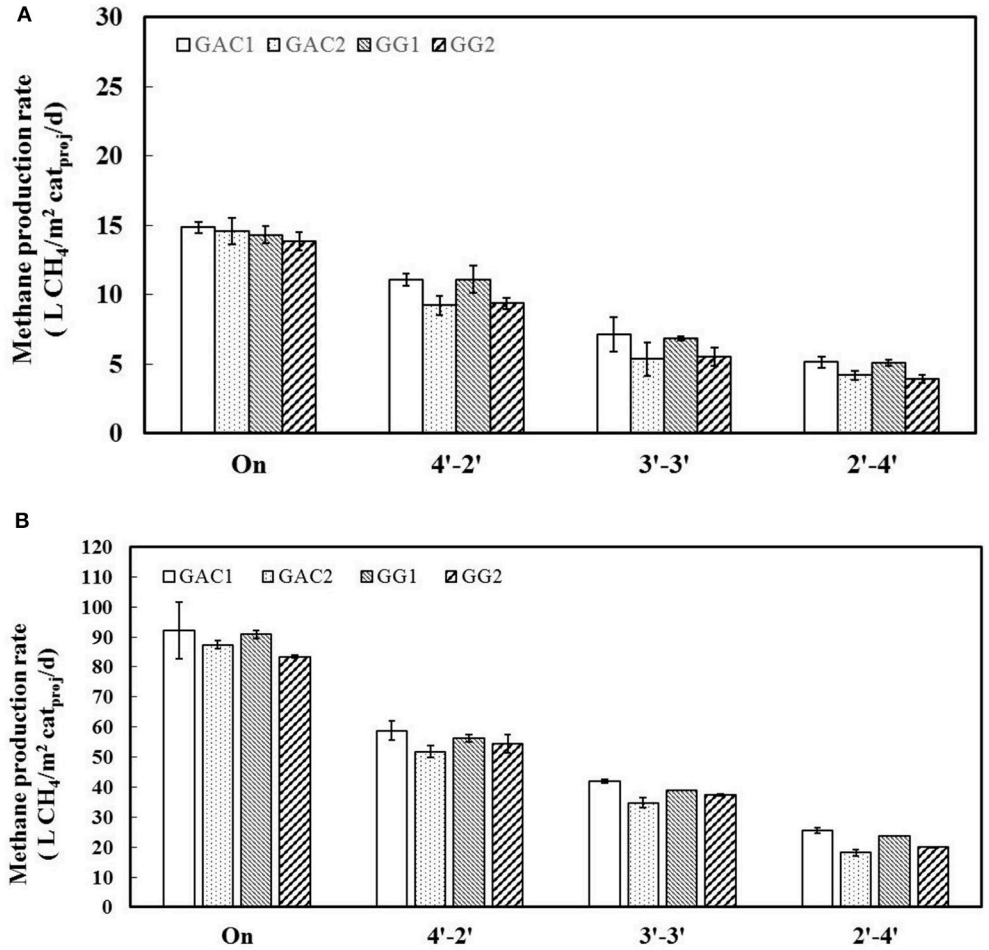

FIGURE 3 | Methane production rates for all biocathodes when they were supplied with constant current and intermittent current. Three different current time-ON/time-OFF intervals (4–2′, 3–3′, and 2–4′) were carried out. The current density during the current time-ON was 10 A/$m^2$$cat_{proj}$ **(A)** and 35 A/$m^2$$cat_{proj}$ **(B)**. For each operational condition, duplicate experiments were performed. The standard deviations are shown as an error bar, whereas the average value is shown as a column.

of methane production rate (**Figures 2A**, **3**) and current-to-methane efficiency (**Figures 2B**, **4**). Interestingly, the cathode potentials of the GAC biocathodes were different from the GG biocathodes.

Directly after inoculation, all the reactors had similar cathode potentials of about −0.90 V (**Figure 5**). The cathode potential of GAC_1 changed from −0.90 to −0.52 V between day 7 and 10, whereas the cathode potential of GAC_2 changed from −0.80 to −0.52 V between day 30 and 37. The cathode potentials of the GG reactors remained stable around −0.92 V long after inoculation and became slightly more negative around day 37 and day 70 due to the increases in current density. These potential differences between GAC and GG biocathodes were also seen in the polarization curves at day 30 (Figure S2B in the Supporting Information, under C) and day 90 (Figure S2C in the Supporting Information, under C). These polarization curves show that the onset of current for GAC biocathodes occurred at a more positive potential from −0.5 V to even −0.4 V, whereas the current densities of GG biocathodes were negligible in the whole range of cathode potentials tested (−0.7 to −0.3 V). For the current obtained in GAC at −0.5 V during the polarization experiment, other possible secondary reactions, e.g., hydrogen, acetate or formate, could play a role. As with these intermediates, quick consumption by methanogens could lead to undetectable levels of these intermediates. Nevertheless, the onset potentials of the bare GAC electrodes (Figure S2A in the Supporting Information, under C) were around −0.7 V, the difference indicating the catalytic effect of the cathodic microorganisms growth on the GAC electrodes.

To exclude that the measurement of cathode potential was influenced by the fact that the reference electrode was placed outside the cathode compartment, we inserted a new Ag/AgCl reference electrode into one of GAC cathodic chamber as close as possible to the granular bed. The cathode potential was around −0.43 V, which was 100 mV less negative than the cathode

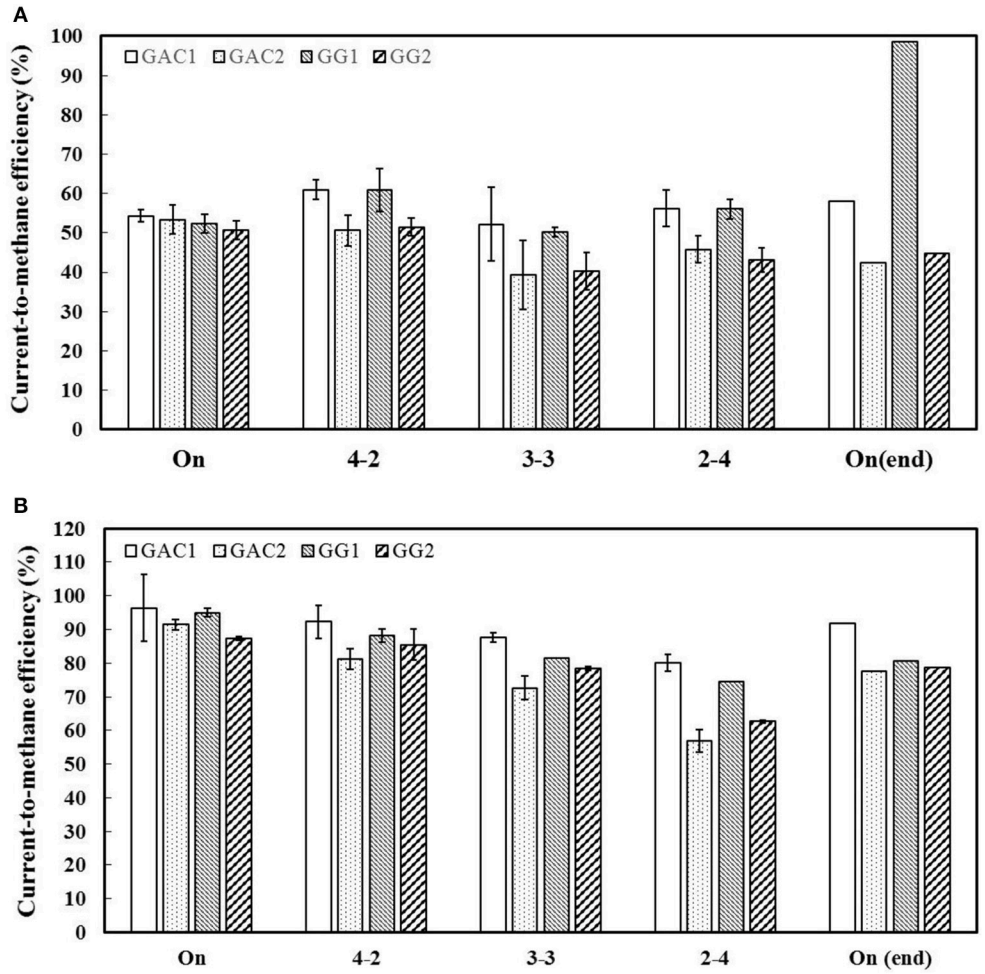

FIGURE 4 | Current-to-methane efficiencies (%) for all reactors when they were supplied with constant and intermittent current. Three different current time-ON/time-OFF ratios (4–2′, 3–3′ and 2–4′) were carried out. The current density during the current time-ON was 10 A/$m^2$$cat_{proj}$ **(A)** and 35 A/$m^2$$cat_{proj}$ **(B)**. For each operational condition, duplicate operations were performed. The maximum and minimum values are shown as an error bar, whereas the average value is shown as a column.

potential (−0.52 V) measured outside the cathode chamber, pointing out that the actual cathode potential was even less negative than that was measured. To our knowledge, these cathode potentials for GAC are the least negative ones (i.e., lowest overpotential) reported in the literature for methane-producing BESs (Geppert et al., 2016). It is likely that methane production at a cathode potential of −0.52 V has not been reported before due to the fact that all methane-producing biocathodes in other studies were operated at a constant potential rather than at a constant current. Actually, most of the studies have used cathode potentials more negative than −0.7 V vs. Ag/AgCl to supply a sufficiently high overpotential for methane generation (Siegert et al., 2014; Villano et al., 2016; LaBarge et al., 2017). Switching from galvanostatic control to potentiostatic control with an active biocathode resulted in similar rates and efficiencies (results are shown as Figure S6 in the Supporting Information, under F). Galvanostatic control is thus useful to achieve methane production at low overpotential, but can be changed to potentiostatic control once an active biocathode is present, without loss in activity.

At this point, it is unclear why the cathode potential of GAC changed to −0.52 V, while cathode potential of GG remained at −0.90 V. The high specific surface area and average smaller size of GAC (764 m^2/g, 1–3 mm) relative to GG (0.438 m^2/g, 3–5 mm) may have played a role, but does not explain the mechanism of methane formation. It is worth notifying that similar phenomenon had been shown in a previous study where the presence of GAC in anaerobic digestion stimulated methane production rate, whereas graphite electrode did not affect the performance, for reasons not yet understood (Dang et al., 2016). In our study, the cathode potential of −0.52 V is 0.1 V more positive than the thermodynamic equilibrium potential for hydrogen evolution (−0.62 V) under the biological conditions (T = 30°C, P = 1 bar, pH = 7) (Beese-Vasbender et al., 2015). Such less negative cathode potential and the

undetectable hydrogen in GAC biocathodes suggests that the change in potential for methane production on GAC biocathodes observed here could be related to direct electron transfer. However, hydrogen as an intermediate for methane production at GAC biocathode cannot be excluded as the local hydrogen pressures and local pH values are not known. Additional research is needed to measure the actual values of local pH and hydrogen pressure on the biocathode by using microsensor, and therefore, providing insight into the relationship between mechanisms of electron transfer and different conductive materials.

The changes in the biocathode potentials of the GAC reactors occurred on different days (**Figure 5**). The reason for that may be that in GAC_1, which had been operated and adjusted during 2 months before inoculation to perform electrochemical measurements, the catholyte and/or electrode may already have contained methanogens before inoculation. Indeed, a minor amount of CH_4 was already detected in the headspace of GAC_1 during the phase before inoculation (data not shown). The fluctuations of the cathode potentials, especially at current densities of 5 A/m^2cat_{proj} and 10 A/m^2cat_{proj}, were probably the result of fluctuations in catholyte pH due to intermittent CO_2 supply (Jourdin et al., 2015). After changing to continuous CO_2 supply and a current density of 35 A/m^2cat_{proj} on day 71, the pH of the catholyte and the cathode potentials remained more stable (Figure S3, supporting information, under C).

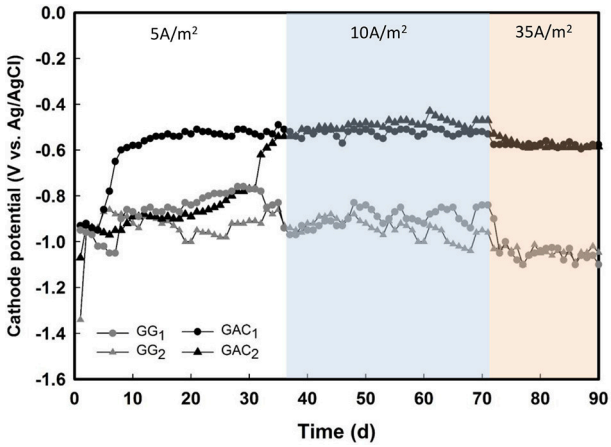

FIGURE 5 | Average daily cathode potentials of all the reactors after inoculation. Both GAC biocathodes showed a steep increase in cathode potential, whereas the cathode potential for both GG biocathodes remained constant, and decreased with increased current density.

Microbial Community Analysis Revealed *Methanobacterium* as Dominant Species

Microbial communities of biofilm and catholyte were characterized for all reactors to investigate whether different microbial communities developed on the two cathode materials. Table S1 in the Supporting Information shows the community similarity results for all granules. All cathodic communities (both in biofilm and catholyte) were dominated by hydrogenotrophic methanogens (*Methanobacterium*), which has been found in many other studies (Van Eerten-Jansen et al., 2013; Cai et al., 2016; LaBarge et al., 2017) regardless of electrode material and inoculum source (**Figure 6**). Another hydrogenotrophic methanogen, namely *Mthanocorposculum*, was detected 21% in the catholyte of GG_1. The GAC electrode samples showed a greater relative abundance of Proteobacteria (*Deltaproteobacteria and Betaproteobacteria*) with 14% for GAC_1 and 47% for GAC_2, relative to 8.7% for GG_1 and 3.4% for GG_2. As exoelectrogens like *Geobacter* sp. belong to the proteobacteria, the most common phylum of bacteria found on the anode of microbial fuel cells (Hasany et al., 2016), this may be related to the lower overpotentials measured for GAC.

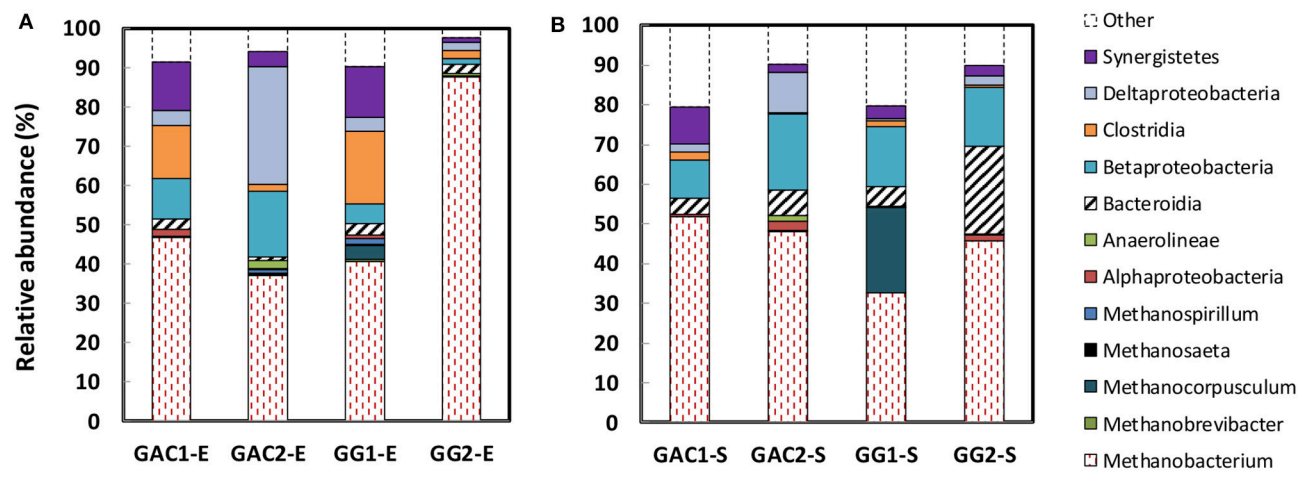

FIGURE 6 | Taxonomic distribution of microbial populations with >2% relative abundance by 16S rRNA gene sequences. Samples from all four reactors were taken from: **(A)** biofilm on granular biocathodes (GAC_1-E, GAC_2-E, GG_1-E, GG_2-E); **(B)** suspended cells within the catholyte (GAC_1-S, GAC_2-S, GG_1-S, GG_2-S).

CONCLUSION

In this paper, we have shown that both GAC and GG are suitable cathode materials for high methane production rates in methane-producing BESs. Intermittent current operation resulted in stable methane production for both materials, and original performance was restored directly after intermittent operation. GAC biocathodes showed lower overpotentials than GG; the mechanism behind this needs to be further investigated. Granular biocathodes thus hold promise for the practical application of methane-producing BESs for renewable electricity storage.

AUTHOR CONTRIBUTIONS

AtH conceived the original idea and together with CB supervised the project. DL and MR-P carried out the experiment. DL wrote the manuscript with support from MR-P, SN. LC-J, and FG, helped supervise the project. SN helped conducted the microbial community analysis.

ACKNOWLEDGMENTS

The authors thank Nurul Azyyati Sabri for her help with DNA extraction, and Caroline Plugge for facilitating the microbial community analyses. The authors are also grateful for financial support from Dutch companies (Alliander, DMT Environmental Technology), the Chinese Scholarship Council (File No. 201306120043) and the Cluster of Excellence RESOLV (EXC 1069), which is funded by the Deutsche Forschungsgemeinschaft.

SUPPLEMENTARY MATERIAL

The Supplementary Material for this article can be found online at: https://www.frontiersin.org/articles/10.3389/fbioe.2018.00078/full#supplementary-material

REFERENCES

Bailera, M., Lisbona, P., Romeo, L. M., and Espatolero, S. (2017). Power to gas projects review: lab, pilot and demo plants for storing renewable energy and CO_2. *Renew. Sustain. Energy Rev.* 69, 292–312. doi: 10.1016/j.rser.2016.11.130

Beese-Vasbender, P. F., Grote, J.-P., Garrelfs, J., Stratmann, M., and Mayrhofer, K. J. J. (2015). Selective microbial electrosynthesis of methane by a pure culture of a marine lithoautotrophic archaeon. *Bioelectrochem.* 102, 50–55. doi: 10.1016/j.bioelechem.2014.11.004

Borsje, C., Liu, D., Sleutels, T. H. J. A., Buisman, C. J. N., and ter Heijne, A. (2016). Performance of single carbon granules as perspective for larger scale capacitive bioanodes. *J. Power Sources* 325, 690–696. doi: 10.1016/j.jpowsour.2016.06.092

Bretschger, O., Carpenter, K., Phan, T., Suzuki, S., Ishii, S.,i., Grossi-Soyster, E., et al. (2015). Functional and taxonomic dynamics of an electricity-consuming methane-producing microbial community. *Bioresour. Technol.* 195, 254–264. doi: 10.1016/j.biortech.2015.06.129

Cai, W., Liu, W., Yang, C., Wang, L., Liang, B., Thangavel, S., et al. (2016). Biocathodic methanogenic community in an integrated anaerobic digestion and microbial electrolysis system for enhancement of me thane production from waste sludge. *ACS Sustain. Chem. Eng.* 4, 4913–4921. doi: 10.1021/acssuschemeng.6b01221

Cheng, S., Xing, D., Call, D. F., and Logan, B. E. (2009). Direct biological conversion of electrical current into methane by electromethanogenesis. *Environ. Sci. Technol.* 43, 3953–3958. doi: 10.1021/es803531g

Commission, E. E. (2011). *Energy Roadmap 2050*. COM 885:15. Luxembourg: Publications Office of the European Union.

Dang, Y., Holmes, D. E., Zhao, Z., Woodard, T. L., Zhang, Y., Sun, D., et al. (2016). Enhancing anaerobic digestion of complex organic waste with carbon-based conductive materials. *Bioresour. Technol.* 220, 516–522. doi: 10.1016/j.biortech.2016.08.114

Deeke, A., Sleutels, T. H. J. A., Donkers, T. F. W., Hamelers, H. V. M., Buisman, C. J. N., and Ter Heijne, A. (2015). Fluidized capacitive bioanode as a novel reactor concept for the microbial fuel cell. *Environ. Sci. Technol.* 49, 1929–1935. doi: 10.1021/es503063n

Geppert, F., Liu, D., van Eerten-Jansen, M., Weidner, E., Buisman, C., and ter Heijne, A. (2016). Bioelectrochemical power-to-gas: state of the art and future perspectives. *Trends Biotechnol.* 34, 879–894. doi: 10.1016/j.tibtech.2016.08.010

Guo, K., Prévoteau, A., Patil, S. A., and Rabaey, K. (2015). Engineering electrodes for microbial electrocatalysis. *Curr. Opin. Biotechnol.* 33, 149–156. doi: 10.1016/j.copbio.2015.02.014

Hasany, M., Mardanpour, M. M., and Yaghmaei, S. (2016). Biocatalysts in microbial electrolysis cells: a review. *Int. J. Hydrogen Energy* 41, 1477–1493. doi: 10.1016/j.ijhydene.2015.10.097

Hu, J., Harmsen, R., Crijns-Graus, W., Worrell, E., and van den Broek, M. (2018). Identifying barriers to large-scale integration of variable renewable electricity into the electricity market: a literature review of market design. *Renew. Sustain. Energy Rev.* 81, 2181–2195. doi: 10.1016/j.rser.2017.06.028

Jörissen, J., and Speiser, B. (2015). *Organic Electrochemistry, 5th Edn*. Boca Raton, FL: CRC Press.

Jourdin, L., Grieger, T., Monetti, J., Flexer, V., Freguia, S., Lu, Y., et al. (2015). High acetic acid production rate obtained by microbial electrosynthesis from carbon dioxide. *Environ. Sci. Technol.* 49, 13566–13574. doi: 10.1021/acs.est.5b03821

LaBarge, N., Yilmazel, Y. D., Hong, P.-Y., and Logan, B. E. (2017). Effect of pre-acclimation of granular activated carbon on microbial electrolysis cell startup and performance. *Bioelectrochemistry* 113, 20–25. doi: 10.1016/j.bioelechem.2016.08.003

Lindeboom, R. E. F., Shin, S. G., Weijma, J., van Lier, J. B., and Plugge, C. M. (2016). Piezo-tolerant natural gas-producing microbes under accumulating pCO_2. *Biotechnol. Biofuels* 9:236. doi: 10.1186/s13068-016-0634-7

Liu, D., Zhang, L., Chen, S., Buisman, C., and ter Heijne, A. (2016). Bioelectrochemical enhancement of methane production in low temperature anaerobic digestion at 10°C. *Water Res.* 99, 281–287. doi: 10.1016/j.watres.2016.04.020

Liu, D., Zheng, T., Buisman, C., and ter Heijne, A. (2017). Heat-treated stainless steel felt as a new cathode material in a methane-producing bioelectrochemical system. *ACS Sustain. Chem. Eng.* 5, 11346–11353. doi: 10.1021/acssuschemeng.7b02367

Liu, F., Rotaru, A.-E., Shrestha, P. M., Malvankar, N. S., Nevin, K. P., and Lovley, D. R. (2012). Promoting direct interspecies electron transfer with activated carbon. *Energy Environ. Sci.* 5, 8982–8989. doi: 10.1039/c2ee22459c

Lu, Z., Girguis, P., Liang, P., Shi, H., Huang, G., Cai, L., et al. (2015). Biological capacitance studies of anodes in microbial fuel cells using electrochemical impedance spectroscopy. *Bioprocess Biosyst. Eng.* 38, 1325–1333. doi: 10.1007/s00449-015-1373-z

Rogelj, J., den Elzen, M., Höhne, N., Fransen, T., Fekete, H., Winkler, H., et al. (2016). Paris Agreement climate proposals need a boost to keep warming well below 2°C. *Nature* 534, 631–639. doi: 10.1038/nature18307

Santoro, C., Arbizzani, C., Erable, B., and Ieropoulos, I. (2017). Microbial fuel cells: from fundamentals to applications. a review. *J. Pow. Sources* 356, 225–244. doi: 10.1016/j.jpowsour.2017.03.109

Siegert, M., Yates, M. D., Call, D. F., Zhu, X., Spormann, A., and Logan, B. E. (2014). Comparison of nonprecious metal cathode materials for methane production by electromethanogenesis. *ACS Sustain. Chem. Eng.* 2, 910–917. doi: 10.1021/sc400520x

Skovsgaard, L., and Jacobsen, H. K. (2017). Economies of scale in biogas production and the significance of flexible regulation. *Energy Policy* 101, 77–89. doi: 10.1016/j.enpol.2016.11.021

Van Eerten-Jansen, M. C. A. A., Heijne, A. T., Buisman, C. J. N., and Hamelers, H. V. M. (2012). Microbial electrolysis cells for production of methane from CO_2: long-term performance and perspectives. *Int. J. Energy Res.* 36, 809–819. doi: 10.1002/er.1954

van Eerten-Jansen, M. C. A. A., Jansen, N. C., Plugge, C. M., de Wilde, V., Buisman, C. J. N., and ter Heijne, A. (2015). Analysis of the mechanisms of bioelectrochemical methane production by mixed cultures. *J. Chem. Technol. Biotechn.* 90, 963–970. doi: 10.1002/jctb.4413

Van Eerten-Jansen, M. C. A. A., Veldhoen, A. B., Plugge, C. M., Stams, A. J. M., Buisman, C. J. N., and Ter Heijne, A. (2013). Microbial community analysis of a methane-producing biocathode in a bioelectrochemical system. *Archaea* 2013:12. doi: 10.1155/2013/481784

Villano, M., Ralo, C., Zeppilli, M., Aulenta, F., and Majone, M. (2016). Influence of the set anode potential on the performance and internal energy losses of a methane-producing microbial electrolysis cell. *Bioelectrochemistry* 107, 1–6. doi: 10.1016/j.bioelechem.2015.07.008

Villano, M., Scardala, S., Aulenta, F., and Majone, M. (2013). Carbon and nitrogen removal and enhanced methane production in a microbial electrolysis cell. *Bioresour. Technol.* 130, 366–371. doi: 10.1016/j.biortech.2012.11.080

Wolin, E. A., Wolin, M. J., and Wolfe, R. S. (1963). Formation of methane by bacterial extracts. *J. Biol. Chem.* 238, 2882–2886.

Conflict of Interest Statement: The authors declare that the research was conducted in the absence of any commercial or financial relationships that could be construed as a potential conflict of interest.

frontiers in Energy Research

MINI REVIEW
published: 20 June 2018
doi: 10.3389/fenrg.2018.00055

Sulfate-Reducing ElectroAutotrophs and Their Applications in Bioelectrochemical Systems

Valeria Agostino[1] *and Miriam A. Rosenbaum*[1,2,3]*

[1] *Institute of Applied Microbiology, Aachen Biology and Biotechnology, RWTH Aachen University, Aachen, Germany,* [2] *Bio Pilot Plant, Leibniz Institute for Natural Product Research and Infection Biology – Hans-Knöll-Institute, Jena, Germany,* [3] *Faculty of Biological Sciences, Friedrich Schiller University, Jena, Germany*

Electroautotrophs are microbes able to perform different biocathodic reactions by using CO_2 as sole carbon source and electrochemical reducing power as a sole energy source. Electroautotrophy has been discovered in several groups of microorganisms, including iron-oxidizing bacteria, iron-reducing bacteria, nitrate-reducing bacteria, acetogens, methanogens and sulfate-reducing bacteria. The high diversity of electroautrophs results in a wide range of Bioelectrochemical Systems (BES) applications, ranging from bioproduction to bioremediation. In the last decade, particular research attention has been devoted toward the discovery, characterization and application of acetogenic and methanogenic electroautotrophs. Less attention has been given to autotrophic sulfate-reducing microorganisms, which are extremely interesting biocatalysts for multiple BES technologies, with concomitant CO_2 fixation. They can accomplish water sulfate removal, hydrogen production and, in some case, even biochemicals production. This mini-review gives a journey into electroautotrophic ability of sulfate-reducing bacteria and highlights their possible importance for biosustainable applications. More specifically, general metabolic features of autotrophic sulfate reducers are introduced. Recently discovered strains able to perform extracellular electron uptake and possible molecular mechanisms behind this electron transfer capacity are explored. Finally, BES technologies based on sulfate-reducing electroautotrophs are illustrated.

Keywords: bioelectrochemical systems, electroautotrophs, sulfate-reducing microorganisms, biocathodes, bioremediation, bioproduction

OPEN ACCESS

Edited by:
Deepak Pant,
Flemish Institute for Technological Research, Belgium

Reviewed by:
Mirella Di Lorenzo,
University of Bath, United Kingdom
Feng Zhao,
Institute of Urban Environment (CAS), China
Mohita Sharma,
University of Calgary, Canada

***Correspondence:**
Miriam A. Rosenbaum
miriam.rosenbaum@leibniz-hki.de

Specialty section:
This article was submitted to Bioenergy and Biofuels, a section of the journal Frontiers in Energy Research

Received: *03 April 2018*
Accepted: *04 June 2018*
Published: *20 June 2018*

Citation:
Agostino V and Rosenbaum MA (2018) Sulfate-Reducing ElectroAutotrophs and Their Applications in Bioelectrochemical Systems. Front. Energy Res. 6:55. doi: 10.3389/fenrg.2018.00055

INTRODUCTION

During the last decade, much research focused toward the use of electroautotrophic microorganisms in Bioelectrochemical Systems (BES). While exoelectrogens have evolved to use extracellular insoluble minerals or electrodes as terminal electron acceptors, electroautotrophs are able to acquire energy by taking up electrons from extracellular solid compounds or electrodes, while using carbon dioxide (CO_2) as inorganic carbon source (Tremblay et al., 2017).

Electroautotrophy was first discovered in the model exoelectrogen genus *Geobacter* (Gregory et al., 2004; Gregory and Lovley, 2005). As the majority of exoelectrogenic biocatalysts are dissimilatory iron-reducing bacteria, researchers hypothesized that iron-oxidizing bacteria could be able to accept electrons from a cathodic electrode. Indeed, *Acidithiobacillus ferrooxidans*, *Mariprofundus ferrooxydans* PV-1, and *Rhodopseudomonas palustris* have been designated

as electroautotrophs (Carbajosa et al., 2010; Summers et al., 2013; Bose et al., 2014). Moreover, the chemolithoautotrophic archea *Methanococcus maripaludis* and *Methanobacterium*-like archaeon strain IM1, isolated with metallic iron as sole electron donor, are able to perform electromethanogenesis (Lohner et al., 2014; Beese-Vasbender et al., 2015a). Several acetogenic bacteria, including *Sporomusa ovata*, *Sporomusa silvacetica*, *Sporomusa sphaeroides*, *Sporumosa acidovorans*, *Sporumosa malonica*, *Clostridium ljungdahlii*, *Clostridium aceticum*, and *Moorella thermoacetica*, can utilize the cathodic current for CO_2 reduction to organic acids (Nevin et al., 2011; Aryal et al., 2017). Also, some autotrophic sulfate-reducing microorganisms (SRM) have shown the ability to consume electrons from the cathode to accomplish sulfate reduction and hydrogen (H_2) production (Rodrigues and Rosenbaum, 2014; Beese-Vasbender et al., 2015b). However, overall fairly little research has been devoted toward this last group of electroautotrophic biocatalysts.

Pioneering discoveries regarding cathodic electron consumption of SRM are related to anaerobic microbial induced corrosion (MIC) studies (Widdel, 1992). SRM can stimulate not only a chemically-influenced corrosion of iron through the production of corrosive hydrogen sulfide (Widdel, 1992), but also an electrochemical-induced corrosion by the consumption of "cathodic hydrogen" formed on iron in contact with water (von Wolzogen Kühr and van der Vlugt, 1934; Pankhania, 1988), or by directly uptaking electrons from iron (Dinh et al., 2004; Gu et al., 2009; Gu and Xu, 2010; Xu and Gu, 2011). The readers are referred to several excellent reviews on to role of SRM in MIC (Enning and Garrelfs, 2014; Anandkumar et al., 2016; Li et al., in press).

It should be noticed that early BES studies with SRM have been focused on their anodic exploitation for electricity generation and sulfate removal using organic substrates (Habermann and Pommer, 1991; Liang et al., 2013; Zheng et al., 2014). However, it was soon clarified that the production of electricity with SRM-based anodes was mainly due to the abiotic oxidation of biologically produced sulfide to elemental sulfur (Zhao et al., 2008). Consequently, sulfur-oxidizing bacteria have started to be applied in anodic oxidation processes for current generation (Sun et al., 2009; Gong et al., 2013; Lee et al., 2014; Zhang et al., 2014).

Another very recent and promising BES application of SRM is the cathodic electrofermentation of short chain organic acids into more valuable compounds as alcohols and acetone (Sharma et al., 2013a,b, 2014, 2015).

Figure 1A summarizes the application of the different metabolic capabilities of SRM in various BES. Despite these different attractive SRM-based BES technologies, the specific focus of this mini-review is to summarize the current understanding and trends in biocathodic applications of electroautotrophic SRM, using CO_2 as inorganic carbon source (highlighted with a red box in **Figure 1A**).

SULFATE REDUCING MICROORGANISMS

SRM are a heterogeneous group of anaerobic microorganisms, widely distributed in anoxic environments with essential roles in the global cycling of carbon and sulfur (Jørgensen, 1982). Most cultured SRM belong to four bacterial (Deltaproteobacteria, Nitrospirae, Firmicutes, Thermodesulfobacteria) and two archaeal phyla (Euryarchaeota, Crenarchaeota) (Rabus et al., 2006; Muyzer and Stams, 2008). SRM have the ability to use sulfate, the most oxidized sulfur specie, as terminal electron acceptor for the oxidation of organic compounds or hydrogen in a process named dissimilatory sulfate reduction (Widdel and Hansen, 1991). This is an intracellular pathway that requires an eight-electron reaction for the reduction of sulfate to sulfide, with sulfite as intermediate. After crossing microbial membranes, sulfate is "activated" to form adenosine 5′-phosphosulfate (APS) by the enzyme Adenosine Triphosphate (ATP) sulfurylase (Peck, 1959). APS is then reduced to sulfite in a two-electron reaction performed by the enzyme APS reductase (AprBA) (Lampreia et al., 1994). The final step of sulfite reduction to sulfide is catalyzed by the dissimilatory sulfite reductase complex (Dsr), with the involvement of an energy-conserving membrane complex (DsrMKJOP or DsrMK) (Fike et al., 2016).

Carbon Assimilation and Electron Donors

SRM can grow on more than one hundred organic compounds, including monocarboxylic acids, dicarboxylic acids, sugars, alcohols, ketones, amino acids, aromatic compounds, and hydrocarbons (Barton and Fauque, 2009).

SRM can either perform incomplete or complete oxidation of organic compounds (Rabus et al., 2006). Incomplete oxidation of organic substrates results in the excretion of acetate as main product, due to a deficiency for the terminal oxidation of acetyl-CoA (Widdel, 1988). On the contrary, complete oxidizers degrade organic compounds to CO_2, oxidizing acetate with two different pathways: a modified citric acid cycle (e.g., *Desulfobacter* spp., Brandis-Heep et al., 1983), or the acetyl-CoA pathway (e.g., *Desulfobacterium* spp., Schauder et al., 1986). Both of these groups can also utilize H_2 as electron donor during sulfate reduction. Despite the prospects for chemolithoautotrophic growth on H_2, most SRM require acetate in addition to CO_2 for growth (Badziong et al., 1979). Nevertheless, true autotrophic growth with H_2 as electron donor was discovered in some SRM (Pfennig et al., 1981; Jansen et al., 1985; Klemps et al., 1985; Brysch et al., 1987; Rozanova et al., 1988; Schauder et al., 1989). Of these facultative chemolithoautotrophic SRM all but *Desulfosporosinus orientis* are complete oxidizers (Brysch et al., 1987). Thereby, CO_2-fixation proceeds through reverse reactions of the pathways used by SRM for acetyl-CoA oxidation during heterotrophic growth. *D. hydrogenophilus* assimilates CO_2 via a reductive citric acid cycle (Schauder et al., 1987), while *D. autotrophicum* and *D. orientis* use the reductive acetyl-CoA pathway (Wood Ljungdahl–pathway) (Schauder et al., 1989), the only autotrophic microbial route able to simultaneously fix CO_2 and yield ATP by converting acetyl-CoA to acetate (Wood et al., 1986; Fuchs, 2011). This pathway consists of two separate branches: one molecule of CO_2 is reduced to carbon monoxide (CO) in the carbonyl branch and another CO_2 molecule is reduced to a methyl group in the methyl branch. The acetyl-CoA is generated from the combination of the CO and methyl group with the coenzyme A (Wood et al., 1986). Recent reviews

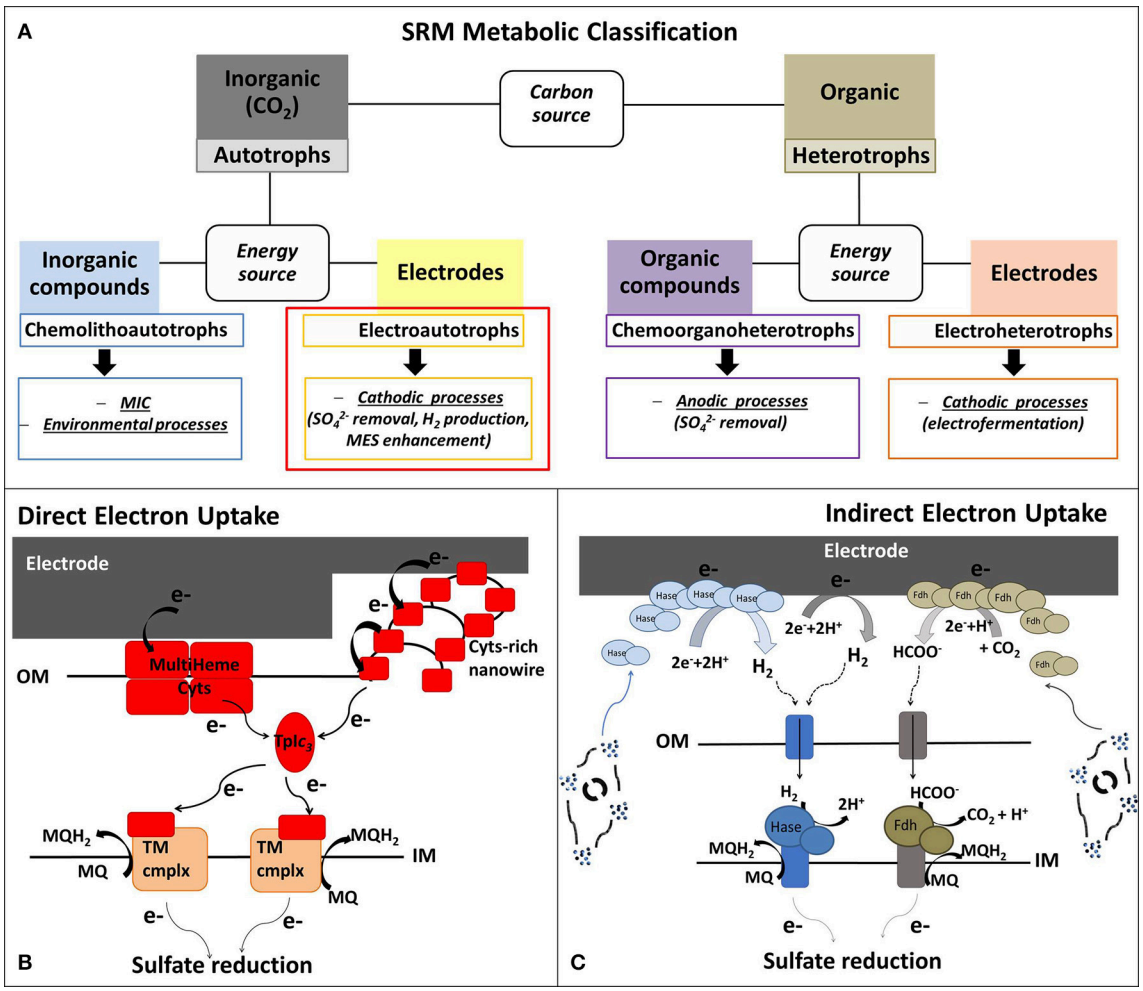

FIGURE 1 | (A) Metabolic classification of the sulfate-reducing microorganisms (SRM) presented in this Mini-Review, whereby the review focus is on electroautotrophic SRM. **(B,C)** Schematic model of possible extracellular electron uptake (EEU) mechanisms in electroautotrophic SRM with **(B)** Direct EEU: the cathodic electrons can enter SRM cells through outer membrane (OM) multiheme cytochromes (Cyts) or via Cyt-covered nanowires (Deng et al., 2018). Cyt-rich group of SRM (Deltaproteobacteria and Nitrospirae) are characterized by periplasmatic tetraheme Type I cytochrome *c3* (Tplc*3*) that could act as periplasmatic electron shuttle component, like cytochrome Cyc-1 in *A. ferroxidans* (Ishii et al., 2015) and the monoheme *c*-Cyt PccH in *Geobacter sulfurreducens* (Strycharz et al., 2011). Tplc*3* serves then as electron donor for several inner membrane redox complexes that reduce the menaquinone pool or are involved in transmembrane electron transfer; and **(C)** Indirect EEU: SRM belonging to Cyt-poor group (Archaea and Clostridia) have no periplasmatic multiheme *c*-Cyts and they most probably perform a mediated electron transfer, using H_2 and formate as soluble electron donors for their hydrogenases (Hase) and formate dehydrogenases (Fdh) associated to the inner membrane (IM). The abiotic electrochemical production of H_2 and formate can be enhanced by extracellular Hase and Fdh, excreted by viable cells or released after microbial death (Deutzmann et al., 2015). MES, Microbial electrosynthesis; MIC, microbial induced corrosion; MQ/MQH_2, menaquinone/menaquinol; TM cmplx, transmembrane complex.

give an exhaustive biochemical description of these CO_2-fixation pathways (Berg, 2011; Fuchs, 2011; Schuchmann and Müller, 2014).

Energy-Conservation and Electron Transport Pathways

In chemolithoautotrophic SRM, sulfate reduction must be coupled to energy conservation by oxidative phosphorylation. This implies an electron transport chain that allows the production of a transmembrane proton motive force for the chemiosmotic synthesis of ATP (Thauer et al., 2007; Grein et al., 2013). While APS and sulfite reduction are two strongly exoergonic reactions, the enzymes responsible, AprBA and DsrAB/DsrC, are cytoplasmic soluble reductases and, thus, cannot be directly involved in the formation of a transmembrane proton gradient. Instead, the quinone-interacting membrane-bound oxidoreductase complex (QmoABC) (Pires et al., 2003) and the DsrMKJOP complex (Pires et al., 2006) represent the membrane complex candidates that can act as electron donor for AprBA and DsrAB/DsrC, respectively (Ramos et al., 2012; Grein et al., 2013). Both complexes are strictly conserved across

SRM (Pereira et al., 2011). Other energy-conserving membrane complexes, capable of ion translocation, are present in SRM, but they are less conserved (Pereira et al., 2011).

Due to the high variability of organic and inorganic electron donors used by SRM, there is no unifying theory for their electron transport chain. However, one classification method is based on the content of periplasmic *c*-type cytochromes (*c*-Cyt) (Rabus et al., 2015). The cytochrome-rich group has numerous multiheme *c*-Cyt and includes SRM belonging to Deltaproteobacteria (e.g., *Desulfovibrio* spp., *Desulfobulbus* spp., *Desulfomicrobium* spp.) and Nitrospira (e.g., *Thermodesulfovibrio* spp.), while the cytochrome-poor group has few or no *c*-Cyt and comprises Archaea (e.g., *Archaeoglobus* spp.) and Clostridia SRM (e.g., *Desulfosporosinus* spp., *Desulfotomaculum* spp.) (Pereira et al., 2011; Rabus et al., 2015). Cytochrome-rich SRM have soluble periplasmatic hydrogenases and formate dehydrogenases that lack an integral membrane subunit. These soluble enzymes use a periplasmatic multiheme *c*-Cyt, usually the tetraheme cytochrome *c3* (TpI*c3*), as electron acceptor (Louro, 2007; da Silva et al., 2012; Romaõ et al., 2012) (**Figure 1B**). These SRM also contain a set of inner membrane redox complexes that reduce the menaquinone pool (Qrc, Nhc and Ohc) or are involved in transmembrane electron transfer (Tmc and Hmc) (Rabus et al., 2015). On the contrary, cytochrome-poor SRM have membrane-bound hydrogenases and formate dehydrogenases associated to the inner membrane through a *b*-type cytochrome that directly reduce the menaquinone pool (Pereira et al., 2011) (**Figure 1C**).

Electroautotrophic SRM

The discovery of direct electron uptake capacity of some Fe(0)-corroding SRM (Dinh et al., 2004; Gu et al., 2009; Gu and Xu, 2010; Xu and Gu, 2011) suggested the researchers to start employing these microorganisms for biocathodic BES applications, turning, thus, this negative metabolic feature into positive and sustainable biotechnological solutions. However, so far only few pure culture SRM are elucidated as electroautotrophs.

In 2008, *Desulfovibrio desulfuricans* ATCC 27774 was shown to form an electroactive cathodic biofilm at an applied cathodic potential (E_{cath}) of −0.169 V vs. SHE. A stable negative current was obtained after 20 days, but lactate was supplied as carbon source, not CO_2 (Cordas et al., 2008). Subsequently, other species of the genus *Desulfovibrio* were tested for cathodic current generation and H_2 production, using bicarbonate or lactate as carbon source and E_{cath} that allow abiotic H_2 evolution: *D. paquesii* and *D. caledoniensis* (Yu et al., 2011; Aulenta et al., 2012).

As first pure culture SRM to really show electroautotrophy, we identified *Desulfosporosinus orientis* and *Desulfovibrio piger* at $E_{cath} = -0.31$ V vs. SHE, which is much more positive than the H_2 evolution redox potential at neutral conditions ($E^{0'}_{H+/H2} = -0.41$ V vs. SHE), with gaseous CO_2 as sole inorganic growth substrate (Rodrigues and Rosenbaum, 2014). *D. orientis* is a spore-forming SRM in the class Clostridia and is able to perform anaerobic sulfate respiration but also acetogenesis. It can utilize a wide range of energy sources, such as H_2/CO_2, CO, formate, lactate, pyruvate, methanol, ethanol, and medium chain fatty acids (Klemps et al., 1985; Robertson et al., 2001), and different terminal electron acceptors, such as sulfate, thiosulfate, sulfite, sulfur dioxide (Cypionka and Pfennig, 1986).

D. piger is a non-spore-forming, H_2-oxidizing Gram-negative SRM Deltaproteobacterium. It can oxidize organic compounds, such as ethanol, lactate, and pyruvate, incompletely to acetate. Like for the other *Desulfovibrio* species, autotrophic growth on CO_2 was not reported before.

Desulfopila corrodens strain IS4 is the first Fe(0)-corroding SRM characterized in BES (Beese-Vasbender et al., 2015b). This Gram-negative Deltaproteobacterium was isolated from marine sediment using metallic iron as the sole electron donor. Using iron as energy source, this strain is able to perform very rapid sulfate reduction and hydrogen production compared to the conventional hydrogen-scavenging *Desulfovibrio* species (Dinh et al., 2004). In BES, direct electron uptake was achieved at $E_{cath} = -0.4$ V vs. SHE with CO_2 in the headspace as carbon substrate (Beese-Vasbender et al., 2015b).

Very recently, electroautotrophic activity was reported also in the fully sequenced sulfate-reducing bacterium *Desulfobacterium autotrophicu*m HRM2, using a $E_{cath} = -0.5$ V vs. SHE (Zaybak et al., 2018). This Deltaproteobacterium, isolated from marine mud, is a complete oxidizer SRM belonging to the *c*-Cyt rich group and harboring a bidirectional Wood-Ljungdahl pathway (Brysch et al., 1987; Strittmatter et al., 2009). *D. autotrophicu*m HRM2 exhibited acetate bioelectrosynthesis ability, with an extremely high coulombic efficiency of 83 ± 6% (Zaybak et al., 2018).

EXTRACELLULAR ELECTRON UPTAKE IN SRM

Little is known about the molecular mechanisms beyond extracellular electron uptake (EEU) in SRM and in electroautotrophic microorganisms in general. As for the extracellular electron transfer (EET) from microbes to the anode, direct and indirect pathways can be employed. So far, direct EEU mechanisms have been elucidated in the oxygen-reducers *Shewanella oneidensis*, which directly uses electrons from the cathode via the reversed anodic Mtr pathway (Ross et al., 2011), and *Acidithiobacillus ferroxidans*, which utilizes a cascade of outer membrane (OM) cytochrome reductases (Ishii et al., 2015). Indirect electron transfer pathway has been demonstrated for the anaerobic methanogen *Methanococcus maripaludis* (Choi and Sang, 2016). Here, the electron uptake seems dependent on extracellular formate dehydrogenases and hydrogenases that catalyze the cathodic production of hydrogen and formate, which act as soluble electron donors for microbial activity (Deutzmann et al., 2015).

Indirect Mechanism

Generally, in BES for bioremediation and bioproduction a power input is given to reduce cathodic potential and drive thermodynamically unfavorable bioelectrochemical reductions. If the E_{cath} is more negative that the standard redox potential of the H^+/H_2 couple, molecular H_2 is generated at the

cathode. The majority of acetogens, methanogens as well as SRM are able to use H_2 as electron donor. Consequently, abiotic H_2 can easily mediate the EET from cathode to hydrogenotrophic microorganisms. In addition, similar to the case of *M. maripaludis*, solubles enzymes, released by SRM after cell lysis, could increase the abiotic production rate of H_2 and even formate by decreasing the overpotentials of these abiotic electroreduction processes (**Figure 1C**). Indeed, SRM are characterized by a high amount of soluble periplasmatic and cytoplasmatic hydrogenases and formate dehydrogenases (Rabus et al., 2006).

Direct Mechanism

As discussed above, *D. orientis*, *D. piger*, and *D. corrodens* strain IS4 have shown ability to grow in cathodic environments with applied potentials too positive for the abiotic H_2 evolution, suggesting a direct EEU requiring a physical interaction between the electrode and the microbial cells (**Figure 1B**).

D. piger and *D. corrodens* strain IS4 belong to the cytochrome-rich group of SRM, both having the periplasmatic TpI*c3*, but not *D. orientis* (Rabus et al., 2006). Nevertheless, the OM proteins that permit the entrance of extracellular electrons inside SRM cells and the subsequent reduction of periplasmatic redox components have yet to be elucidated. Electrochemical and infrared spectroelectrochemical analyses identified *c*-Cyt as redox active components associated with the OM of *D. corrodens* strain IS4 and are, thus, possibly involved in direct EEU (Beese-Vasbender et al., 2015b). These results are supported by the very recent study of the electron uptake mechanism of another iron-corroding SRM, *Desulfovibrio ferrophilus* IS5 (Deng et al., 2018). This strain was isolated from marine sediment with *D. corrodens* IS4 (Dinh et al., 2004). Biochemical, transcriptomic, and microscopic analyses of *D. ferrophilus* IS5 pointed out a high expression of different OM multiheme cytochromes in response to organic electron donor limitation. Moreover, transmission electron microscopy revealed segmented nanowire structures, strongly positive for cytochrome staining and very similar to the ones of *S. oneidensis*, suggesting that also *D. ferrophilus* IS5 can use nanowires for EEU (Deng et al., 2018).

BES TECHNOLOGIES BASED ON ELECTROAUTOTROPHIC SRM

With growing interest in Microbial Electrolysis Cell (MEC) (Logan and Rabaey, 2012), SRM have started to be applied in biocathodic systems. This section outlines the recent applications of electroautotrophic SRM-based biocathodes, using CO_2 as inorganic carbon source.

Sulfate-Rich Waters Treatment

Sulfate-rich wastewaters require treatment before being discharged to the environment, as this anion may create acute laxative effects in humans and it may increase dissolution of metals in water resources (Gomez et al., 1995). Biological sulfate removal technologies are based on the exploitation of SRM. Sulfate-rich wastewaters are usually deficient in organic matter and, thus, external electron donors are required to achieve complete sulfate reduction in bioreactors (Liamleam and Annachhatre, 2007). While methanogens are generally more competitive to use organic electron donors, autotrophic SRM are generally more efficient in H_2 utilization. However, the application of hydrogen reports several disadvantages, like cost and safety aspects of H_2 storage. BES can overcome some of these limitations since the production/consumption of H_2 occur in the same reactor, without H_2 waste, and with operations at atmospheric temperature and pressure. Electricity-driven autotrophic sulfate-reduction has been reported by several authors (Su et al., 2012; Coma et al., 2013; Luo et al., 2014; Pozo et al., 2015, 2017a; Blázquez et al., 2017) and an overview is presented in **Table 1**. The first sulfate-reducing biocathode used a mixed culture originated from wastewater and at $E_{cath} = -0.2$ V vs. SHE a maximum sulfate reduction rate of 0.02 g L^{-1} day^{-1} was achieved (Su et al., 2012). Thereafter, many studies, mostly with *Desulfovibrio*, have investigated different E_{cath}, BES operation conditions cathodic electrode materials, inoculum source and start-up strategies (**Table 1**). To date, the highest bioelectrochemical sulfate reduction rate of 5.6 g L^{-1} day^{-1} was obtained with a mixed microbial community collected from previous sulfate-reducing BES reactors at an E_{cath} of −1.1 V vs. SHE (Pozo et al., 2017a).

Sulfide is the principal product of biological sulfate respiration and it may lead to significant issues such as corrosion, bad odors and human health toxicity. For real application of BES in sulfate-rich water treatment, a second step of sulfide transformation to elemental sulfur should be integrated. Two recent studies have combined the bioelectroreduction of sulfate to sulfide with the recovery of elemental sulfur (S^0) through the use of sulfur-oxidizing bacteria in the anodic chamber of a separate BES, resulting in a S^0 recovery of 74% (Pozo et al., 2017b), or in the same biocathodic system by using part of the anodic-produced oxygen that partially diffuse to the cathode through the ion exchange membrane (Blázquez et al., 2016).

Hydrogen Production

H_2 was the first value product generated through BES technology (Liu et al., 2005; Rozendal et al., 2006). Compared to conventional methods (dark fermentation, biophotolysis, water electrolysis and water photolysis), H_2 production with MECs shows multiple advantages. Firstly, MECs can theoretically produce hydrogen with an energy input much lower than for industrial electrolyzers, 1 kWh $m^{-3}H_2$ (Rozendal et al., 2008) vs. 4.5–5 kWh $m^{-3}H_2$ (Wang et al., 2014). Secondly, no precious metals catalysts are needed since both anodic and cathodic reactions can be catalyzed by electroactive microorganisms (Jafary et al., in press). Thirdly, cathodic biocatalysts can use the CO_2 originating from organic matter as inorganic carbon source for cathodic H_2 production. MEC biocathodes are usually inoculated with the effluent of running BES or by directly transferring used bioanodes or biocathodes to new cathodic chambers (Hasany et al., 2016). Microbial community analysis of several H_2-producing biocathodes revealed SRM as amongst the dominant bacteria (**Table 1**). SRM, indeed, have an extremely high hydrogenase activity and in sulfate limitation conditions can produce H_2

TABLE 1 | Overview of mixed-community electroautotrophic SRM-based biocathodes for sulfate removal and H_2 production.

SRM-Biocathodes for sulfate-rich water treatment						
Inoculum	**Dominant species**	**Operation mode**	**E_{cath} (V vs. SHE)**	**SO_4^{2-} reduction rate (g L^{-1} day^{-1})**	**CE sulfate%**	**References**
Enriched WWT sludge	*Desulfobulbus propionicus, Geobacter* spp.	Fed-batch	−0.2	0.015	72	Su et al., 2012
MFC effluent	–	Continuous	−0.26	0.06	–	Coma et al., 2013
Enriched WWT sludge	–	Continuous	−0.6	0.19	47	Luo et al., 2014
Non-acclimated consortia + autotrophic acetate-producing biocathode	*Methanobacterium Desulfovibrio Desulfomicrobium*	Fed-batch Continuous	−0.9 −1.1	0.19 5.6	5 78	Pozo et al., 2015 Pozo et al., 2017a
Acclimated sediment	*Desulfovibrio*	Fed-batch	−0.7	0.03	16	Teng et al., 2016
Lab-scale sewer	*Desulfovibrio*	Fed-batch	−1	0.7	85	Blázquez et al., 2017
Sediment	*Desulfovibrio*	Fed-batch	−0.7	0.06	25	Luo et al., 2017
Enriched river sediment	*Desulfovibrio Acetobacterium*	Fed-batch	−0.85	0.15	56	Hu et al., 2018
SRM-Rich Biocathodes for H_2 production						
Inoculum	**Dominat species**	**Operation mode**	**E_{cath} (V vs. SHE)**	**H_2 production rate (m^3 m^{-3} day^{-1})**	**CE H_2%**	**References**
Marine sediment MFC	*Eubacterium limosum, Desulfovibrio* sp.A2, *Rhodococcus*	Batch	−0.54	0.08 mmoles	–	Pisciotta et al., 2012
Effluent of 4 year old MFC and MEC	*Desulfovibrio vulgaris*	Continuous	−0.7	0.63	–	Croese et al., 2011
MEC effluent	*Hydrogenophaga Desulfovibrio*	Continuous	−0.7	2.7	–	Croese et al., 2014
Palm oil mill effluent enriched in SRM	–	Batch	R_{ext} 1Ω	1.85	–	Jafary et al., 2017

Except for the work of Jafary et al. (2017), all the BES studies reported in the table operated in MEC mode.
CE, coulombic efficiency; R_{ext}, external resistance.

fermentatively (Rabus et al., 2006). Very recently, Jafary and co-workers have purposely enriched a palm oil mill effluent sample for autotrophic SRM and then used this as inoculum source for biocathodic H_2 production. The SRM enriched-biocathode was able to generate 1.85 m^3 H_2/ (m^3·d) in acidic catholyte conditions (pH = 4) (Jafary et al., 2017).

It should be highlighted that the sulfate concentration in the catholyte of SRM-based MEC has to be limited not only to encourage SRM fermentative metabolism, but also to avoid the generation of a harmful off-gas mixture of H_2S and H_2. Researchers should start to focus their attention on the purification of the produced H_2, especially in the case of mixed-community biocathodes.

Microbial Electrosynthesis Enhancement

BES research on biocathodic production of alternative fuels and higher value chemicals from CO_2 has caught much attention in the last years. Methane and acetate are, usually, the main products of this microbial electrosynthesis (MES), particularly in pure culture-based systems (Tremblay and Zhang, 2015). For practical implementation, the generation of molecules with higher value than acetate, such as longer carbon-chain organic compounds and alcohols, is desirable. Approaches with mixed-culture MES that exploit intermediate metabolite transfer and microbial cooperation show some success to extend the product spectrum to *n*-butyrate, propionate, ethanol, isopropanol and caproate (Ganigué et al., 2015; Arends et al., 2017; Batlle-Vilanova et al., 2017; Jourdin et al., 2018). In addition, the low rate EEU of electroautotrophic acetogens and methanogens still constitute a big limit for application on a commercial scale. Especially in undefined mixed community biocathodes, high negative potentials are applied to allow H_2-mediated bioproduction processes, resulting in high energetic efficiency losses.

Very recently, researchers have evaluated the enhancement of MES rates through syntrophic growth of SRM with acetogens or methanogens (Deutzmann and Spormann, 2017; Song et al., 2017; Xiang et al., 2017). By adding low concentration of sulfate in the catholyte of a MES, Xiang et al. enriched the

biocathodic community in *Desulfovibrionaceae* (37%), resulting in a 2.7-fold increase in acetate production in comparison to a MES with lower abundance of SRM (*Desulfovibrionaceae* 7.3%). As proof of concept, the Spormann group evaluated two defined co-culture biocathodes: *D. corrodens* strain IS4 as high rate electron uptaking and H_2 producing strain was combined with *Acetobacterium woodi,* as acetogenic biocatalyst, or with *M. maripaludis,* as methane producer (Deutzmann and Spormann, 2017). *A. woodi* is not able to directly consume electrons from the cathode to produce acetate (Nevin et al., 2011), but in this case the co-culture showed acetate production rate of 0.21–0.23 μmol cm^{-2} h^{-1} at $E_{cath} = -0.4$ V vs. SHE. The *D. corrodens-M. maripaludis* co-culture exhibited a methane production 20-times higher (0.6–1.2 μmol h^{-1} cm^{-2}) (Deutzmann and Spormann, 2017) compared to a pure culture *M. maripaludis* cathode poised at -0.6 V (0.05 μmol h^{-1} cm^{-2}) (Lohner et al., 2014). This study opens the door for the exploitation of defined co-cultures for microbial electrosynthesis of higher value chemicals from CO_2. Thereby, naturally efficient electroautotrophic strains, can be coupled with acetogenic engineered strains. Importantly, this combination of an efficient cathodic EEU catalyst with an efficient bioproduction catalyst in the bulk liquid allows for a better use of the entire volume of the cathodic reactor. For the real scale-up of the MES process using SRM, researchers should consider also undesired MIC activities of these biocatalysts and, thus, avoid the use of metallic materials in the reactor design.

CONCLUDING REMARKS AND OUTLOOK

With the aim to mitigate climate change, much research efforts have been initiated toward the development of new biotechnologies able to convert CO_2-rich waste gases into valuable products. MES represents one of these technologies. Thereby, the exploitation of autotrophic SRM in CO_2-based cathodic bioprocesses has just begun. With this mini-review, we highlight that SRM-based biocathodes represent a very promising technology for sustainable and environmentally friendly bioremediation and bioproduction applications. Further understanding and characterization of these electroautotrophic biocatalysts will enable successful realization of SRM-based BES technologies. First of all, more effort should be addressed toward the screening of other Fe(0)-corroding strains, in order to likely discover SRM with superior EEU rate capacity. Moreover, the complete elucidation of the molecular mechanisms beyond the EEU transport chain will allow genetic and metabolic engineering of these biocatalysts for the incrementation of their natural electron uptake rate and to extend the product spectrum. From an engineering point of view, the most critical challenge to achieve the commercialization of BES technologies is the development of a cost-effective and scalable reactor design. The combination of the recovery of multiple value-added products could possibly help to cut down the implementation cost. The versatility of electroautotrophic SRM could positively contribute in accomplishing this goal. For example, the sulfide produced by SMR biocathodes can be exploited for the precipitation of heavy metals, combining, thus, the treatment of sulfate-rich wastewaters and metal-rich industrial effluents with the recovery of precious metals. Thus, with the highlighted new developments and emerging technologies the formerly considered destructive process of MIC might open new ways to biotechnological productions and environmental engineering strategies.

AUTHOR CONTRIBUTIONS

VA performed the literature search for this review and prepared the first draft of the manuscript. MR discussed the content and structure and revised the review manuscript.

ACKNOWLEDGMENTS

The authors acknowledge financial support through the Cluster of Excellence Tailor-Made Fuels from Biomass EXC 236, which is funded by the Excellence Initiative of the German federal and state governments to promote science and research at German universities.

REFERENCES

Anandkumar, B., George, R., Maruthamuthu, S., Parvathavarthini, N., and Mudali, U. (2016). Corrosion characteristics of sulfate-reducing bacteria (SRB) and the role of molecular biology in SRB studies: an overview. *Corr. Rev.* 34, 41–63. doi: 10.1515/corrrev-2015-0055

Arends, J. B. A., Patil, S. A., Roume, H., and Rabaey, K. (2017). Continuous long- term electricity-driven bioproduction of carboxylates and isopropanol from CO_2 with a mixed microbial community. *J. CO2 Util.* 20, 141–149. doi: 10.1016/j.jcou.2017.04.014

Aryal, N., Tremblay, P. L., Lizak, D. M., and Zhang, T. (2017). Performance of different Sporomusa species for the microbial electrosynthesis of acetate from carbon dioxide. *Biores. Technol.* 233, 184–190. doi: 10.1016/j.biortech.2017.02.128

Aulenta, F., Catapano, L., Snip, L., Villano, M., and Majone, M. (2012). Linking bacterial metabolism to graphite cathodes: electrochemical insights into the H2-producing capability of *Desulfovibrio* sp. *Chemsuschem* 5, 1080–1085. doi: 10.1002/cssc.201100720

Badziong, W., Ditter, B., and Thauer, R. K. (1979). Acetate and carbon dioxide assimilation by *Desulfovibrio vulgaris* (Marburg), growing on hydrogen and sulfate as sole energy source. *Arch. Microbiol.*123, 301–305. doi: 10.1007/BF00406665

Barton, L. L., and Fauque, G., D. (2009). Biochemistry, physiology and biotechnology of sulfate-reducing bacteria. *Adv. Appl. Microbiol.* 68, 41–98. doi: 10.1016/S0065-2164(09)01202-7

Batlle-Vilanova, P., Ganigué, R., Ramió-Pujol, S., Ba-eras, L., Jiménez, G., Hidalgo, M., et al. (2017). Microbial electrosynthesis of butyrate from carbon dioxide: production and extraction. *Bioelectrochemistry* 117, 57–64. doi: 10.1016/j.bioelechem.2017.06.004

Beese-Vasbender, P. F., Grote, J. P., Garrelfs, J., Stratmann, M., and Mayrhofer, K. (2015a). Selective microbial electrosynthesis of methane by a pure culture of a marine lithoautotrophic archaeon. *Bioelectrochemistry* 102, 50–55. doi: 10.1016/j.bioelechem.2014.11.004

Beese-Vasbender, P. F., Nayak, S., Erbe, A., Stratmann, M., and Mayrhofer, K. (2015b). Electrochemical characterization of direct electron uptake in electrical microbially influenced corrosion of iron by the lithoautotrophic

SRB Desulfopila corrodens strain IS4. *Electrochim. Acta* 167, 321–329. doi: 10.1016/j.electacta.2015.03.184

Berg, I. (2011). Ecological aspects of the distribution of different autotrophic CO_2 fixation pathways. *Appl. Environ. Microbiol.* 77, 1925–1936. doi: 10.1128/AEM.02473-10

Blázquez, E., Gabriel, D., Baeza, J. A., and Guisasola, A. (2016). Treatment of high-strength sulfate wastewater using an autotrophic biocathode in view of elemental sulfur recovery. *Water Res.* 105, 395–405. doi: 10.1016/j.watres.2016.09.014

Blázquez, E., Gabriel, D., Baeza, J. A., and Guisasola, A. (2017). Evaluation of key parameters on simultaneous sulfate reduction and sulfide oxidation in an autotrophic biocathode. *Water Res.* 123, 301–310. doi: 10.1016/j.watres.2017.06.050

Bose, A., Gardel, E., Vidoudez, C., Parra, E., and Girguis, P. (2014). Electron uptake by iron-oxidizing phototrophic bacteria. *Nat. Commun.* 5:3391. doi: 10.1038/ncomms4391

Brandis-Heep, A., Gebhardt, N. A., Thauer, R. K., Widdel, F., and Pfennig, N. (1983). Anaerobic acetate oxidation to CO_2 by Desulfobacter postgatei. I. Demonstration of all enzymes required for the operation of the citric acid cycle. *Arch. Microbiol.* 136, 222–229. doi: 10.1007/BF00409849

Brysch, K., Schneider, C., Fuchs, G., and Widdel, F. (1987). Lithoautotrophic growth of sulfate-reducing bacteria, and description of *Desulfobacterium autotrophicum* gen. nov., sp. nov. *Arch. Microbiol.* 148, 264–274. doi: 10.1007/BF00456703

Carbajosa, S., Malki, M., Caillard, R., Lopez, M. F., Palomares, F. J., and Martín-Gago, J. A., et al. (2010). Electrochemical growth of *Acidithiobacillus ferrooxidans* on a graphite electrode for obtaining a biocathode for direct electrocatalytic reduction of oxygen. *Biosens. Bioelectron.* 26, 877–880. doi: 10.1016/j.bios.2010.07.037

Choi, O., and Sang, B. (2016). Extracellular electron transfer from cathode to microbes: application for biofuel production. *Biotechnol. Biofuels* 9:11. doi: 10.1186/s13068-016-0426-0

Coma, M., Puig, S., Pous, N., Balaguer, M. D., and Colprim, J. (2013). Biocatalysed sulphate removal in a BES cathode. *Bioresour. Technol.* 130, 218–223. doi: 10.1016/j.biortech.2012.12.050

Cordas, C., Guerra, L., Xavier, C., and Moura, J. (2008). Electroactive biofilms of sulphate reducing bacteria. *Electrochim. Acta* 54, 29–34. doi: 10.1016/j.electacta.2008.02.041

Croese, E., Jeremiasse, A. W., Marshall, I. P., Spormann, A. M., Euverink, G. J. W.,Geelhoed, J. S., et al. (2014). Influence of setup and carbon source on the bacterial community of biocathodes in microbial electrolysis cells. *Enzyme Microb. Technol.* 61-62, 67–75. doi: 10.1016/j.enzmictec.2014.04.019

Croese, E., Pereira, M., Euverink, G. J. W., Stams, A. M., and Geelhoed, J. S. (2011). Analysis of the microbial community of the biocathode of a hydrogen-producing microbial electrolysis cell. *Appl. Microbiol. Biotechnol.* 92, 1083–1093. doi: 10.1007/s00253-011-3583-x

Cypionka, H., and Pfennig, N. (1986). Growth yields of Desulfotomaculum orientis with hydrogen in chemostat culture. *Arch. Microbiol.* 143, 396–399. doi: 10.1007/BF00412808

da Silva, S. M., Pacheco, I., and Pereira, I. A. C. (2012). Electron transfer between periplasmic formate dehydrogenase and cytochromes c in *Desulfovibrio desulfuricans* ATCC 27774. *J. Biol. Inorg. Chem.* 17, 831–838. doi: 10.1007/s00775-012-0900-5

Deng, X., Dohmae, N., Nealson, K., Hashimoto, K., and Okamoto, A. (2018). Multi-heme cytochromes provide a pathway for survival in energy-limited environments. *Sci. Adv.* 4:eaao5682. doi: 10.1126/sciadv.aao5682

Deutzmann, J. S., and Spormann, A. M. (2017). Enhanced microbial electrosynthesis by using defined co-cultures. *ISME J.* 11, 704–714. doi: 10.1038/ismej.2016.149

Deutzmann, J. S., Sahin, M., and Spormann, A. (2015). Extracellular enzymes facilitate electron uptake in biocorrosion and bioelectrosynthesis. *mBio* 6:e00496–e00415. doi: 10.1128/mBio.00496-15

Dinh, H., Kuever, J., Mußmann, M., Hassel, A., Stratmann, M., and Widdel, F. (2004). Iron corrosion by novel anaerobic microorganisms. *Nature*, 427, 829–832. doi: 10.1038/nature02321

Enning, D., and Garrelfs, J. (2014). Corrosion of iron by sulfate-reducing bacteria: new views of an old problem. *Appl. Environ. Microbiol.* 80, 1226–1236. doi: 10.1128/AEM.02848-13

Fike, D. A., Bradley, A. S., and Leavitt, W. D. (2016). "Geomicrobiology of sulfur," in *Ehrlich's Geomicrobiology, 6th Edn.* eds H. L. Ehrlich, D. K. Newman and A. Kappler (Boca Raton, FL: Taylor & Francis), 479–515.

Fuchs, G. (2011). Alternative pathways of carbon dioxide fixation: insights into the early evolution of life? *Annu. Rev. Microbiol.* 65, 631–658. doi: 10.1146/annurev-micro-090110-102801

Ganigué, R., Puig, S., Batlle-Vilanova, P., Balaguer, M. D., and Colprim, J. (2015). Microbial electrosynthesis of butyrate from carbon dioxide. *Chem. Commun.* 51, 3235–3238. doi: 10.1039/C4CC10121A

Gomez, G. G., Sandler, R. S., and Seal, E. J. (1995). High levels of inorganic sulfate cause diarrhea in neonatal piglets. *J. Nutr.* 125, 2325–2332. doi: 10.1093/jn/125.9.2325

Gong, Y., Ebrahim, A., Feist, A., Embree, M., Zhang, T., Lovley, D., et al. (2013). Sulfide-driven microbial electrosynthesis. *Environ. Sci. Technol.* 47, 568–573. doi: 10.1021/es303837j

Gregory, K., and Lovley, D. (2005). Remediation and recovery of uranium from contaminated subsurface environments with electrodes. *Environ. Sci. Technol.* 39, 8943–8947. doi: 10.1021/es050457e

Gregory, K., Bond, D., and Lovley, D. (2004). Graphite electrodes as electron donors for anaerobic respiration. *Environ. Microbiol.* 6, 596–604. doi: 10.1111/j.1462-2920.2004.00593.x

Grein, F., Ramos, A. R., Venceslau, S. S., and Pereira, I. A. (2013). Unifying concepts in anaerobic respiration: insights from dissimilatory sulfur metabolism. *Biochim. Biophys. Acta* 1827, 145–160. doi: 10.1016/j.bbabio.2012.09.001

Gu, T., and Xu, D. (2010). Demystifying MIC mechanisms. *Corrosion/2010, NACE International, PaperNo. 10213*. Houston, TX.

Gu, T., Zhao, K., and Nesic, S. (2009). A new mechanistic model for MIC based on a biocatalytic cathodic sulfate reduction theory. *Corrosion/2009, NACE International, Atlanta, Georgia, 2009, Paper No. 09390.*

Habermann, W., and Pommer, E. (1991). Biological fuel cells with sulphide storage capacity. *Appl. Microbiol. Biotechnol.* 35, 128–133. doi: 10.1007/BF00180650

Hasany, M., Mardanpour, M., and Yaghmaei, S. (2016). Biocatalysts in microbial electrolysis cells: a review. *Int. J. Hydrogen Energ.* 41, 1477–1493. doi: 10.1016/j.ijhydene.2015.10.097

Hu, J., Zeng, C., Liu, G., Luo, H., Qu, L., and Zhang, R. (2018). Magnetite nanoparticles accelerate the autotrophic sulfate reduction in biocathode microbial electrolysis cells. *Biochem. Eng. J.* 133, 96–105. doi: 10.1016/j.bej.2018.01.036

Ishii, T., Kawaichi, S., Nakagawa, H., Hashimoto, K., and Nakamura, R. (2015). From chemolithoautotrophs to electrolithoautotrophs: CO_2 fixation by Fe(II)-oxidizing bacteria coupled with direct uptake of electrons from solid electron sources. *Front. Microbiol.* 6:994. doi: 10.3389/fmicb.2015.00994

Jafary, T., Daud, W., Ghasemi, M., Kim, B., Carmona-Martínez, A., and Bakar, M., et al. (2017). A comprehensive study on development of a biocathode for cleaner production of hydrogen in a microbial electrolysis cell. *J. Clean. Prod.* 164, 1135–1144. doi: 10.1016/j.jclepro.2017.07.033

Jafary, T., Wan Daud, W., Ghasemi, M., Abu Bakar, M., Sedighi, M., and Kim, B., et al. (in press). Clean hydrogen production in a full biological microbial electrolysis cell. *Int. J. Hydrogen Energ.* doi: 10.1016/j.ijhydene.2018.01.010

Jansen, K., G., Fuchs, and R. K., Thauer (1985). Autotrophic CO_2 fixation by *Desulfovibrio baarsii*: demonstration of enzyme activities characteristics for the acetyl-CoA pathway. *FEMS Microbiol. Lett.* 28, 311–315. doi: 10.1111/j.1574-6968.1985.tb00812.x

Jørgensen, B. (1982). Mineralization of organic matter in the sea bed—the role of sulphate reduction. *Nature* 296, 643–645. doi: 10.1038/296643a0

Jourdin, L., Raes, S. M. T., Buisman, C. J. N., and Strik, D. P. B. T. B. (2018). Critical biofilm growth throughout unmodified carbon felts allows continuous bioelectrochemical chain elongation from CO_2 up to caproate at high current density. *Front. Energ. Res.* 6:7. doi: 10.3389/fenrg.2018.00007

Klemps, R., Cypionka, H., Widdel, F., and Pfennig, N. (1985). Growth with hydrogen, and further physiological characteristics of Desulfotomaculum species. *Arch. Microbiol.* 143, 203–208. doi: 10.1007/BF00411048

Lampreia, J., Pereira, A. S., and Moura, J. J. G. (1994). "Adenylsulfate reductases from sulfate-reducing bacteria," in *Methods in Enzymology,* Vol. 243. eds H. D. Peck, Jr., and J. LeGall (San Diego,CA: Academic Press), 241–260.

Lee, D. J., Liu, X., and Weng, H. L. (2014). Sulfate and organic carbon removal by Microbial Fuel Cell with sulfate-reducing bacteria and

sulfide-oxidising bacteria anodic biofilm. *Bioresour. Technol.* 156, 14–19. doi: 10.1016/j.biortech.2013.12.129

Li, Y., Xu, D., Chen, C., Li, X., Jia, R., Zhang, D., et al. (in press). Anaerobic microbiologically influenced corrosion mechanisms interpreted using bioenergetics and bioelectrochemistry: a review. *J. Mater. Sci. Technol.* doi: 10.1016/j.jmst.2018.02.023

Liamleam, W., and Annachhatre, A. P. (2007). Electron donors for biological sulfate reduction. *Biotechnol. Adv.* 25, 452–463. doi: 10.1016/j.biotechadv.2007.05.002

Liang, F., Xiao, Y., and Zhao, F. (2013). Effect of pH on sulfate removal from wastewater using a bioelectrochemical system. *Chem. Eng. J.* 218, 147–153. doi: 10.1016/j.cej.2012.12.021

Liu, H., Grot, S., and Logan, B. E. (2005). Electrochemically assisted microbial production of hydrogen from acetate. *Environ. Sci. Technol.* 39, 4317–4320. doi: 10.1021/es050244p

Logan, B. E., and Rabaey, K. (2012). Conversion of wastes into bioelectricity and chemicals by using microbial electrochemical technologies. *Science* 337, 686–690. doi: 10.1126/science.1217412

Lohner, S. T., Deutzmann, J. S., Logan, B. E., Leigh, J., and Spormann, A. M.(2014). Hydrogenase-independent uptake and metabolism of electrons by the archaeon *Methanococcus maripaludis*. *ISME J.* 8, 1673–1681. doi: 10.1038/ismej.2014.82

Louro, R. O. (2007). Proton thrusters: overview of the structural and functional features of soluble tetrahaem cytochromes c3. *J. Biol. Inorg. Chem.* 12, 1–10. doi: 10.1007/s00775-006-0165-y

Luo, H., Fu, S., Liu, G., et al. (2014). Autotrophic biocathode for high efficient sulfate reduction in microbial electrolysis cells. *Bioresour. Technol.* 167, 462–468. doi: 10.1016/j.biortech.2014.06.058

Luo, H., Teng, W., Liu, G., Zhang, R., and Lu, Y. (2017). Sulfate reduction and microbial community of autotrophic biocathode in response to acidity. *Process Biochem.* 54, 120–127. doi: 10.1016/j.procbio.2016.12.025

Muyzer, G., and Stams, A. (2008). The ecology and biotechnology of sulphate-reducing bacteria. *Nat. Rev. Microbiol.* 6, 441–454. doi: 10.1038/nrmicro1892

Nevin, K. P., Hensley, S., Franks, A., Summers, Z., Ou, J., Woodard, T., et al. (2011). Electrosynthesis of organic compounds from carbon dioxide is catalyzed by a diversity of acetogenic microorganisms. *Appl. Environ. Microbiol.* 77, 2882–2886. doi: 10.1128/AEM.02642-10

Pankhania, I. P. (1988). Hydrogen metabolism in sulphate-reducing bacteria and its role in anaerobic corrosion. *Biofouling* 1, 27–47. doi: 10.1080/08927018809378094

Peck, H. (1959). The ATP-dependent reduction of sulfate with hydrogen in extracts of *Desulfovibrio desulfuricans*. *Proc. Natl. Acad. Sci.* 45, 701–708. doi: 10.1073/pnas.45.5.701

Pereira, I. A., Ramos, A. R., Grein, F., Marques, M. C., da Silva, S. M., and Venceslau, S. S. (2011). A comparative genomic analysis of energy metabolism in sulfate reducing bacteriaand archaea. *Front. Microbiol.* 2:69. doi: 10.3389/fmicb.2011.00069

Pfennig, N., Widdel, F., and Trüper, H. G. (1981). "The dissimilatory sulfate-reducing bacteria," in *The Prokaryotes: aHandbook of Habitats, Isolation and Identification of Bacteria,* eds M.P. Starr, H. Stolp, H. G. Trüper, A. Balows, and H.Schlegel (Berlin: Springer) 926–940.

Pires, R. H., Lourenço, A. I. C., Morais, F., Teixeira, M., Xavier, A. V., Saraiva, L. M., et al. (2003). A novel membrane-bound respiratory complex from *Desulfovibrio desulfuricans* ATCC 27774. *Biochim. Biophys. Acta* 1605, 67–82. doi: 10.1016/S0005-2728(03)00065-3

Pires, R. H., Venceslau, S. S., Morais, F., Teixeira, M., Xavier, A. V., and Pereira, I. A. (2006). Characterization of the *Desulfovibrio desulfuricans* ATCC 27774 DsrMKJOP complex—A membrane-bound redox complex involved in the sulfate respiratory pathway. *Biochemistry* 45, 249–262. doi: 10.1021/bi0515265

Pisciotta, J. M., Zaybak, Z., Call, D. F., Nam, J. Y., and Logan, B. E. (2012). Enrichment of microbial electrolysis cell biocathodes from sediment microbial fuel cell bioanodes. *Appl. Environ. Microbiol.* 78, 5212–5219. doi: 10.1128/AEM.00480-12

Pozo, G., Jourdin, L., Lu, Y., et al. (2015). Methanobacterium enables high rate electricity-driven autotrophic sulfate reduction. *RSC Adv.* 5, 89368–89374. doi: 10.1039/C5RA18444D

Pozo, G., Lu, Y., Pongy, S., Keller, J., Ledezma, P., and Freguia, S. (2017a). Selective cathodic microbial biofilm retention allows a high current-to-sulfide efficiency in sulfate-reducing microbial electrolysis cells. *Bioelectrochemistry* 118, 62–69. doi: 10.1016/j.bioelechem.2017.07.001

Pozo, G., Pongy, S., Keller, J., Ledezma, P., and Freguia, S. (2017b). A novel bioelectrochemical system for chemical-free permanent treatment of acid mine drainage. *Water Res.* 126, 411–420. doi: 10.1016/j.watres.2017.09.058

Rabus, R., Hansen, T., and Widdel, F. (2006). "Dissimilatory sulfate- and sulfur-reducing Prokaryotes," in *The Prokaryotes*, Vol. 2. eds M. Dworkin, S. Falkow, E. Rosenberg, K. H. Schleifer, and E. Stackebrandt (New York, NY: Springer-Verlag) 659–768.

Rabus, R., Venceslau, S., Wöhlbrand, L., Voordouw, G., Wall, J., and Pereira, I. (2015). A post-genomic view of the ecophysiology, catabolism and biotechnological relevance of sulphate-reducing prokaryotes. *Adv. Microb. Physiol.* 66, 55–321. doi: 10.1016/bs.ampbs.2015.05.002

Ramos, A. R., Keller, K. L., Wall, J. D., and Pereira, I. A. C. (2012). The membrane QmoABC complex interacts directly with the dissimilatory adenosine 5'-phosphosulfate reductase in sulfate reducing bacteria. *Front. Microbiol.* 3:137. doi: 10.3389/fmicb.2012.00137

Robertson, W., Bowman, J., Mee, B., and Franzmann, P. (2001). Desulfosporosinus meridiei sp. nov., a spore-forming sulfate-reducing bacterium isolated from gasolene-contaminated groundwater. *Int. J. Syst. Evol. Microbiol.* 51, 133–140. doi: 10.1099/00207713-51-1-133

Rodrigues, T., d, C., and Rosenbaum, M. (2014). Microbial electroreduction: screening for new cathodic biocatalysts. *Chemelectrochem* 1, 1916–1922. doi: 10.1002/celc.201402239

Romaõ, C. V., Archer, M., Lobo, S. A., Louro, R. O., Pereira, I. A. C., Saraiva, L. M., et al. (2012). "Diversity of heme proteins in sulfate reducing bacteria," in *Handbook of Porphyrin Science*, Vol. 19. eds K. M. Kadish, K. M. Smith, and R. Guilard (Singapore: World Scientific Publishing Co), 139–230.

Ross, D. E., Flynn, J. M., Baron, D. B., Gralnick, J. A., and Bond, D. R. (2011). Towards electrosynthesis in Shewanella: energetics of reversing the Mtr Pathway for reductive metabolism. *PLoS ONE* 6:e16649. doi: 10.1371/journal.pone.0016649

Rozanova, E. P., Nazina, T. N., and Galushko, A. S. (1988). Isolation of a new genus of sulfate-reducing bacteria and description of a new species of this genus, Desulfomicrobium apsheronum gen. nov., sp. nov. *Mikrobiologiya* 57, 634–641.

Rozendal, R. A., Hamelers, H. V. M., Euverink, G. J. W., Metz, S. J., and Buisman, C. J. (2006). Principle and perspectives of hydrogen production through biocatalyzed electrolysis. *Int. J. Hydrogen Energ.* 31, 1632–1640. doi: 10.1016/j.ijhydene.2005.12.006

Rozendal, R. A., Jeremiasse, A. W., Hamelers, H. V., and Buisman, C. J. (2008). Hydrogen production with a microbial biocathode. *Environ. Sci. Technol.* 42, 629–634. doi: 10.1021/es071720+

Schauder, R., Eikmanns, B., Thauer, T. K., Widdel, F., and Fuchs, G. (1986). Acetate oxidation to CO_2 in anaerobic bacteria via a novel pathway not involving reactions of the citric acid cycle. *Arch. Microbiol.* 145, 162–172. doi: 10.1007/BF00446775

Schauder, R., Preuß, A., Jetten, M., and Fuchs, G. (1989). Oxidative and reductive acetyl CoA/carbon monoxide dehydrogenase pathway in *Desulfobacterium autotrophicum*. *Arch. Microbiol.* 151,84–89. doi: 10.1007/BF00444674

Schauder, R., Widdel, F., and Fuchs, G. (1987). Carbon assimilation pathways in sulfate-reducing bacteria. II. Enzymes of a reductive citric acid cycle in the autotrophic *Desulfobacter hydrogenophilus*. *Arch. Microbiol.* 148, 218–225. doi: 10.1007/BF00414815

Schuchmann, K., and Müller, V. (2014). Autotrophy at the thermodynamic limit of life: a model for energy conservation in acetogenic bacteria. *Nat. Rev. Microbiol.* 12, 809–821. doi: 10.1038/nrmicro3365

Sharma, M., Aryal, N., Sarma, P., Vanbroekhoven, K., Lal, B., Benetton, X., et al. (2013a). Bioelectrocatalyzed reduction of acetic and butyric acids via direct electron transfer using a mixed culture of sulfate-reducers drives electrosynthesis of alcohols and acetone. *Chem. Commun.* 49:6495. doi: 10.1039/c3cc42570c

Sharma, M., Jain, P., Varanasi, J., Lal, B., Rodríguez, J., Lema, J., et al. (2013b). Enhanced performance of sulfate reducing bacteria based biocathode using stainless steel mesh on activated carbon fabric electrode. *Bioresour. Technol.* 150, 172–180. doi: 10.1016/j.biortech.2013.09.069

Sharma, M., Sarma, P., Pant, D., and Dominguez-Benetton, X. (2015). Optimization of electrochemical parameters for sulfate-reducing bacteria (SRB) based biocathode. *RSC Adv.* 5, 39601–39611. doi: 10.1039/C5RA04120A

Sharma, M., Varanasi, J., Jain, P., Dureja, P., Lal, B., Dominguez-Benetton, X., et al. (2014). Influence of headspace composition on product diversity by sulphate reducing bacteria biocathode. *Bioresour. Technol.* 165, 365–371. doi: 10.1016/j.biortech.2014.03.075

Song, T., Fei, K., Zhang, H., Yuan, H., Yang, Y., Ouyang, P., et al. (2017). High efficiency microbial electrosynthesis of acetate from carbon dioxide using a novel graphene-nickel foam as cathode. *J. Chem. Technol. Biotechnol.* 93, 457–466. doi: 10.1002/jctb.5376

Strittmatter, A. W., Liesegang, H., Rabus, R., Decker, I., Amann, J., Andres, S., et al. (2009). Genome sequence of Desulfobacterium autotrophicum HRM2, a marine sulfate reducer oxidizing organic carbon completely to carbon dioxide. *Environ. Microbiol.* 11, 1038–1055. doi: 10.1111/j.1462-2920.2008.01825.x

Strycharz, S., Glaven, R., Coppi, M., Gannon, S., Perpetua, L., Liu, A., et al. (2011). Gene expression and deletion analysis of mechanisms for electron transfer from electrodes to *Geobacter sulfurreducens*. *Bioelectrochemistry* 80, 142–150. doi: 10.1016/j.bioelechem.2010.07.005

Su, W., Zhang, L., Tao, Y., Zhan, G., Li, D., and Li, D. (2012). Sulfate reduction with electrons directly derived from electrodes in bioelectrochemical systems. *Electrochem. Commun.* 22, 37–40. doi: 10.1016/j.elecom.2012.04.030

Summers, Z. M., Gralnick, J. A., and Bond, D. R. (2013). Cultivation of an obligate Fe(II)-oxidizing lithoautotrophic bacterium using electrodes. *mBio* 4:e00420-12-e00420-12. doi: 10.1128/mBio.00420-12

Sun, M., Mu, Z., Chen, Y., Sheng, G., Liu, X., Chen, Y., et al. (2009). Microbe-assisted sulfide oxidation in the anode of a microbial fuel cell. *Environ. Sci. Technol.* 43, 3372–3377. doi: 10.1021/es802809m

Teng, W., Liu, G., Luo, H., Zhang, R., and Xiang, Y. (2016). Simultaneous sulfate and zinc removal from acid wastewater using an acidophilic and autotrophic biocathode. *J. Hazard. Mater.* 304, 159–116. doi: 10.1016/j.jhazmat.2015.10.050

Thauer, R. K., Stackebrandt, E., and Hamilton, W. A. (2007). "Energy metabolism and phylogenetic diversity of sulphate-reducing bacteria," in *Sulphate-Reducing Bacteria: Environmental and Engineered Systems*, eds L. L. Barton and W. A. Hamilton (Cambridge: Cambridge University Press), 1–37.

Tremblay, P. L., and Zhang, T. (2015). Electrifying microbes for the production of chemicals. *Front. Microbiol.* 6:201. doi: 10.3389/fmicb.2015.00201

Tremblay, P. L., Angenent, L. T., and Zhang, T. (2017). Extracellular electron uptake: among autotrophs and mediated by surfaces. *Trends Biotechnol.* 35, 360–371. doi: 10.1016/j.tibtech.2016.10.004

von Wolzogen Kühr, C. A. H., and van der Vlugt, L. S. (1934). The graphitization of cast iron as an electrobiochemical process in anaerobic soil. *Water* 18,147–165.

Wang, M., Wang, Z., Gong, X., and Guo, Z. (2014). The intensification technologies to water electrolysis for hydrogen production – a review. *Renew. Sustain. Energ. Rev.* 29, 573–588. doi: 10.1016/j.rser.2013.08.090

Widdel, F. (1988). "Microbiology and ecology of sulphate-reducing bacteria," in *Biology of Anaerobic Microorganisms,* ed A. J. B. Zehnder (Munich: Carl Hanser Verlag), 469–585.

Widdel, F. (1992). "Microbial corrosion," in *Biotechnology Focus,*Vol. 3, eds R. K. Finn, P. Prave, M. Schlingmann, W. Crueger, K. Esser, R. Thauer and F. Wagner (Munich: Carl Hanser Verlag), 277–318.

Widdel, F., and Hansen, T. A. (1991). "The sulphate and sulphur-reducing prokaryotes," in *The Prokaryotes,* 2nd ed. Vol. 2, eds M. Dworkin, S. Falkow, E. Rosenberg, K.H. Schleifer, and E. Stackebrandt (New York, NY: Springer), 583–624.

Wood, H. G., Ragsdale, S. W., and Pezacka, E. (1986). The acetyl-CoA pathway of autotrophic growth. *FEMS Microbiol. Rev.* 39, 345–362. doi: 10.1111/j.1574-6968.1986.tb01865.x

Xiang, Y., Liu, G., Zhang, R., Lu, Y., and Luo, H. (2017). Acetate production and electron utilization facilitated by sulfate-reducing bacteria in a microbial electrosynthesis system. *Bioresour. Technol.* 241, 821–829. doi: 10.1016/j.biortech.2017.06.017

Xu, D., and Gu, T. (2011). Bioenergetics explains when and why more severe MIC pitting by SRB can occur. *Corrosion/2011, NACE International, Houston, Texas, 2011, Paper No. 11426.*

Yu, L., Duan, J., Zhao, W., Huang, Y., and Hou, B. (2011). Characteristics of hydrogen evolution and oxidation catalyzed by *Desulfovibrio caledoniensis* biofilm on pyrolytic graphite electrode. *Electrochim. Acta* 56, 9041–9047. doi: 10.1016/j.electacta.2011.05.086

Zaybak, Z., Logan, B. E., and Pisciotta, J. (2018). Electrotrophic activity and electrosynthetic acetate production by *Desulfobacterium autotrophicum* HRM2. *Bioelectrochemistry* 123, 150–155. doi: 10.1016/j.bioelechem.2018.04.019

Zhang, T., Bain, T., Barlett, M., Dar, S., Snoeyenbos-West, O., Nevin, K., et al. (2014). Sulfur oxidation to sulfate coupled with electron transfer to electrodes by Desulfuromonas strain TZ1. *Microbiology* 160, 123–129. doi: 10.1099/mic.0.069930-0

Zhao, F., Rahunen, N., Varcoe, J., Chandra, A., Avignone-Rossa, C., Thumser, A., et al. (2008). Activated carbon cloth as anode for culfate removal in a microbial fuel cell. *Environ. Sci. Technol.* 42, 4971–4976. doi: 10.1021/es8003766

Zheng, Y., Xiao, Y., Yang, Z., Wu, S., Xu, H., Liang, F., et al. (2014). The bacterial communities of bioelectrochemical systems associated with the sulfate removal under different pHs. *Process Biochem.* 49, 1345–1351. doi: 10.1016/j.procbio.2014.04.019

Conflict of Interest Statement: The authors declare that the research was conducted in the absence of any commercial or financial relationships that could be construed as a potential conflict of interest.

frontiers in Energy Research

ORIGINAL RESEARCH
published: 20 July 2018
doi: 10.3389/fenrg.2018.00072

Highly Conductive Poly(3,4-ethylenedioxythiophene) Polystyrene Sulfonate Polymer Coated Cathode for the Microbial Electrosynthesis of Acetate From Carbon Dioxide

Nabin Aryal[1,2†], *Pier-Luc Tremblay*[1], *Mengying Xu*[1], *Anders E. Daugaard*[3] *and Tian Zhang*[1,2*]

[1] School of Chemistry, Chemical Engineering and Life Science, Wuhan University of Technology, Wuhan, China, [2] The Novo Nordisk Foundation Center for Biosustainability, Technical University of Denmark, Kongens Lyngby, Denmark, [3] Department of Chemical and Biochemical Engineering, Danish Polymer Centre, Kongens Lyngby, Denmark

OPEN ACCESS

Edited by:
Andrea Schievano,
Università degli Studi di Milano, Italy

Reviewed by:
Pascal E. Saikaly,
King Abdullah University of Science and Technology, Saudi Arabia
Matteo Grattieri,
University of Utah, United States

***Correspondence:**
Tian Zhang
tzhang@whut.edu.cn

†Present Address:
Nabin Aryal,
Biological and Chemical Engineering, Anaerobic Digestion Technologies, Aarhus University, Aarhus N, Denmark

Specialty section:
This article was submitted to Bioenergy and Biofuels, a section of the journal Frontiers in Energy Research

Received: *14 April 2018*
Accepted: *03 July 2018*
Published: *20 July 2018*

Citation:
Aryal N, Tremblay P-L, Xu M, Daugaard AE and Zhang T (2018) Highly Conductive Poly(3,4-ethylenedioxythiophene) Polystyrene Sulfonate Polymer Coated Cathode for the Microbial Electrosynthesis of Acetate From Carbon Dioxide. Front. Energy Res. 6:72. doi: 10.3389/fenrg.2018.00072

Microbial electrosynthesis (MES) is a bioelectrochemical technology developed for the conversion of carbon dioxide and electric energy into multicarbon chemicals of interest. As with other biotechnologies, achieving high production rate is a prerequisite for scaling up. In this study, we report the development of a novel cathode for MES, which was fabricated by coating carbon cloth with conductive poly(3,4-ethylenedioxythiophene):polystyrene sulfonate (PEDOT:PSS) polymer. *Sporomusa ovata*-driven MES reactors equipped with PEDOT:PSS-carbon cloth cathodes produced 252.5 ± 23.6 mmol d^{-1} acetate per m^2 of electrode over a period of 14 days, which was 9.3 fold higher than the production rate observed with uncoated carbon cloth cathodes. Concomitantly, current density was increased to −3.2 ± 0.8 A m^{-2}, which was 10.7-fold higher than the untreated cathode. The coulombic efficiency with the PEDOT: PSS-carbon cloth cathodes was 78.6 ± 5.6%. Confocal laser scanning microscopy and scanning electron microscopy showed denser bacterial population on the PEDOT:PSS-carbon cloth cathodes. This suggested that PEDOT:PSS is more suitable for colonization by *S. ovata* during the bioelectrochemical process. The results demonstrated that PEDOT: PSS is a promising cathode material for MES.

Keywords: microbial electrosynthesis, carbon dioxide, PEDOT:PSS, acetogens, acetate

INTRODUCTION

Reductive bioelectrochemical reactions rely on the transfer of electrons from a cathode to a microbial catalyst for the reduction of a substrate with protons coming from an anodic reaction (Rabaey and Rozendal, 2010; Tremblay and Zhang, 2015). The substrate can be inorganic carbon molecules such as CO_2 that will be reduced to multicarbon compounds or CH_4 *via* microbial electrosynthesis (MES) (Cheng et al., 2009; Nevin et al., 2010; Lovley, 2012; Ganigué et al., 2015; Bajracharya et al., 2016, 2017; Tremblay et al., 2017). The MES process requires electric energy that could be generated by a combination of renewable sources such as wind and solar with biological

oxidation reactions at the anode (Villano et al., 2010, 2013; Tremblay and Zhang, 2015). In the actual energetic and environmental context, MES could become a flexible approach for the capture of the greenhouse gas CO_2 and the storage of intermittent clean energy into compounds of interest such as biofuels and commodity chemicals (Zhang and Tremblay, 2017).

Since the beginning of the decade, multiple strategies have been deployed to increase the productivity of MES reactors. For instance, better microbial catalysts capable of synthesizing a wider range of products have been developed and electrolyte solution have been optimized (Ganigué et al., 2015; Tremblay et al., 2015; Ammam et al., 2016; May et al., 2016; Aryal et al., 2017b; Lehtinen et al., 2017; Krieg et al., 2018). Additionally, several research groups have focused their effort on the development of optimal cathode materials to establish highly efficient electron transfer to microbes (Aryal et al., 2017c). Most commonly-used materials for MES cathodes are carbon base such as graphite, carbon cloth and carbon felt as well as metals including stainless steel and nickel (Nie et al., 2013; Soussan et al., 2013; Tremblay and Zhang, 2015; Cui et al., 2017). More recently, a highly performant MES cathode made of multiwalled carbon nanotube coated onto reticulated vitreous carbon was developed (Jourdin et al., 2014, 2015, 2016). The potential of graphene, a robust, cheap and highly conductive material, was also explored for MES (Aryal et al., 2016, 2017a; Chen et al., 2016; Song et al., 2017).

The ideal cathode material for MES application should have some critical properties such as high conductivity, excellent chemical stability, high mechanical strength, good biocompatibility, high surface area and low cost (Aryal et al., 2017c). The poly(3,4-ethylenedioxythiophene):polystyrene sulfonate (PEDOT:PSS) polymer and its derivatives, which have high conductivity at room temperature, are electrochemically stable, flexible and easy to process as well as relatively inexpensive could be interesting materials for the fabrication of performant MES electrodes (Groenendaal et al., 2000; Kirchmeyer and Reuter, 2005; Song et al., 2014). PEDOT:PSS consists of polycationic PEDOT chains incorporated into a polyanionic PSS matrix (Nardes et al., 2008). Combining PEDOT with PSS enables the formation of aqueous dispersion that can be cast into thin, optically transparent, conductive films. PEDOT:PSS films have been used for many applications including photovoltaics, circuits, field-effect transistors and light-emitting diodes (Chen et al., 2003; Kok et al., 2004; Ko et al., 2007; Yoo and Dodabalapur, 2007). PEDOT:PSS alone or in combination with other materials has also been employed in the fabrication of anodes to improve the performance of microbial fuel cell (MFC), a technology developed for the production of electric energy from the microbial oxidation of organic carbon (Wang et al., 2013; Chou et al., 2014; Antolini, 2015; Jiang et al., 2015; Webb et al., 2015; Pang et al., 2018).

This work reports the fabrication of a cathode made of carbon cloth coated with PEDOT:PSS. The PEDOT:PSS-carbon cloth cathode was tested in MES reactors with the well-characterized electroautotrophic bacteria *Sporomusa ovata* as microbial catalyst (Nevin et al., 2010). The composite cathode covered with the conductive polymer was shown to be suitable for bacterial colonization resulting in microbial acetate production from CO_2 and current density nearly one order of magnitude higher than the unmodified electrode.

EXPERIMENTAL PROCEDURE

Bacterial Strain and Growth Condition

S. ovata DSM 2662 was ordered from the Deutsche Sammlung Mikroorganismen und Zellkulturen (DSMZ) and grown in 311 medium with 40 mM betaine as substrate under a N_2:CO_2 (80:20) atmosphere (Möller et al., 1984). Bacteria were successively transferred four times in autotrophic condition with H_2 as the electron source and CO_2 as the carbon source omitting yeast extract, betaine, casitone, sodium sulfide, and resazurin from 311 medium. Cultures from the fourth transfer were used to inoculate the cathode chamber of MES reactors. Cysteine was omitted from 311 medium during MES experiments (Aryal et al., 2017b).

PEDOT:PSS-Carbon Cloth Electrode Fabrication

Carbon cloth (Jiangsu Tongkang Special Activated Carbon Fiber & Fabric Co., Ltd, China) was first pretreated by immersion into 3M HNO_3 during 12 h before being extensively washed with ultrapure water (Aryal et al., 2016). The conductivity of carbon cloth is ca. 110 S cm^{-1} (Stolten et al., 2016). The acid-treated electrode was then dried under nitrogen gas. The dip and dry method described by Hou et al. (2012) was used to coat carbon cloth with PEDOT:PSS. Briefly, the carbon cloth material was dipped into an aqueous solution of commercially available PEDOT:PSS (3.0–4.0% in H_2O, high-conductivity grade above 200 S cm^{-1}, Sigma-Aldrich, USA) for 2 h to ensure that the porous carbon substrate was completely soaked. Then, the electrode was taken out of the solution and left at room temperature in air for 15 min to remove excess PEDOT:PSS. The process was repeated a second time before drying the electrode in an oven at 105°C for 5 h. In the last step, the PEDOT:PSS carbon cloth electrode was cleaned continuously for 15 min with running ultrapure water (Hou et al., 2012).

Operation of MES Reactor

Dual-chambered three-electrode system bioreactors were operated at room temperature with *S. ovata* grown in the cathode chamber as described previously (Nevin et al., 2010; Tremblay et al., 2015). Unmodified or PEDOT:PSS-coated carbon cloth cathodes (20.25 cm^2) and the graphite stick anode (36 cm^2) were both immerged into 250 ml of 311 medium and were separated by a Nafion 115 ion-exchange membrane (Ion Power, Inc., New Castle, DE, USA). A platinum wire and a marine wire were used as current collector for the cathode and the anode, respectively. Platinum wires were not in contact with the electrolyte solution to avoid unwanted H_2 evolution reaction. An Ag/AgCl electrode model ET072 (eDAQ, Denmark) was used as reference electrode and the cathode potential was set at −690 mV versus Standard Hydrogen Electrode (SHE) during MES with a CH Instrument potentiostat (CH Instruments, Inc, USA). The cathode potential was chosen because it works well for *S. ovata*-driven MES and it enables performance comparison

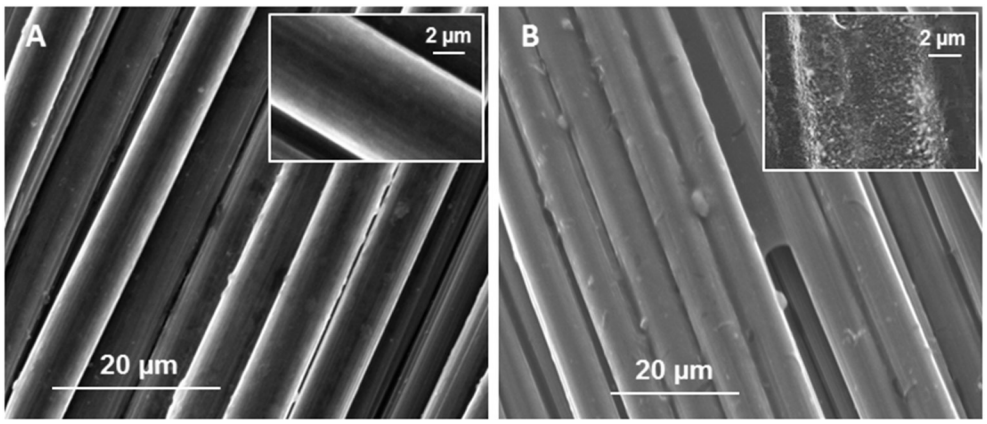

FIGURE 1 | SEM images of (**A**) sterile carbon cloth and sterile (**B**) carbon cloth coated with PEDOT:PSS.

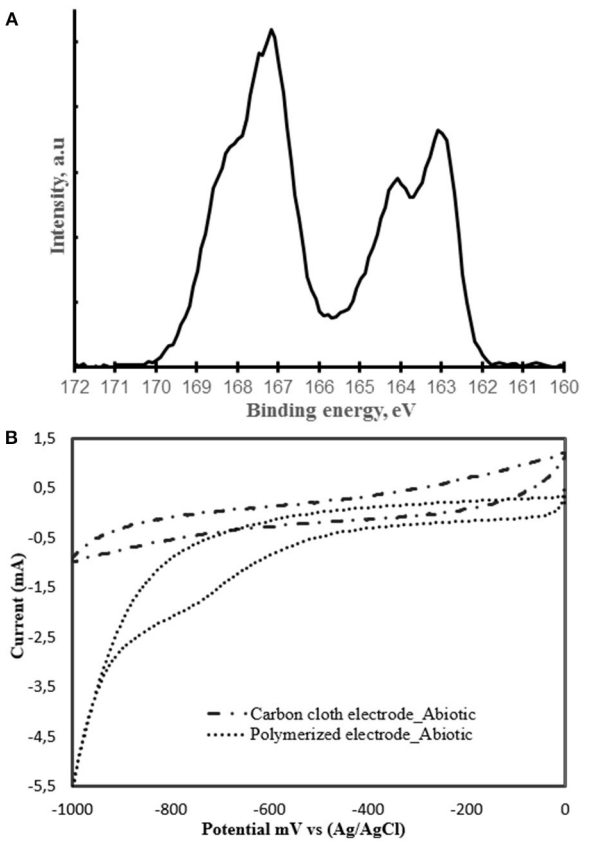

FIGURE 2 | (A) S(2p) XPS spectrum of PEDOT:PSS-carbon cloth electrode. **(B)** Cyclic voltammograms of carbon cloth and PEDOT:PSS-carbon cloth electrode (polymerized) in sterile 311 medium. Scan rate of 1 mV s^{-1}.

with other electrodes tested under the same MES operational conditions (Tremblay et al., 2015; Ammam et al., 2016; Aryal et al., 2017a,b; Lehtinen et al., 2017). After the inoculation of MES reactors with *S. ovata*, bacterial population were established with a N_2:CO_2:H_2 (83:10:7) gas mix. After three fresh medium swaps, the gas mix was switched to N_2:CO_2 (80:20) and acetate production as well as current data started being collected (Aryal et al., 2017a). All MES experiments were done in triplicate.

Cyclic Voltammetry

The cyclic voltammetry (CV) experiments were performed with a Gamry potentiostat (Gamry Instruments, Warminster, PA). Electrochemical data for both MES and CV experiments were analyzed with the EC-Lab v.10.2 software (BioLogic, France) as described previously (Sharma et al., 2013; Lepage et al., 2014) CV of tested electrodes was performed at a scan rate of 1 mV s^{-1} within a potential range of 0 to −1000mV vs. Ag/AgCl.

High Performance Liquid Chromatography and Gas Chromatography

High Performance Liquid Chromatography (HPLC) was used for the quantification of acetate as previously described (Tremblay et al., 2015). Gas chromatography (GC) was used for the quantification of H_2 in the MES reactor headspace. Briefly, gas samples were collected in N_2-flushed serum bottles and H_2 was measured with a Trace 1300 gas chromatograph (ThermoFisher Scientific, Denmark). Argon was the carrier gas with a HP-PLOT Molesieve column (Agilent). The GC oven temperature was 130°C. H_2 was detected with a thermal conductivity detector (TCD).

Microscopy

Confocal Laser Scanning Microscopy (CLSM) images and Scanning Electron Microscopy (SEM) images were taken after 14 days of MES operation to study bacterial population at the surface of the different cathodes. For CLSM, *S. ovata* cells present on cathodes were stained with the LIVE/DEAD® BacLight™ Bacterial Viability Kit (ThermoFisher Scientific). Images were taken with a Zeiss LSM 5 Pascal microscope and analyzed with the ZEN imaging software (Zeiss, Germany) (Aryal et al., 2016). For SEM images, cathodes from MES reactors were fixed with 0.1M buffer solution at pH 7.0 containing 2.5% glutaraldehyde

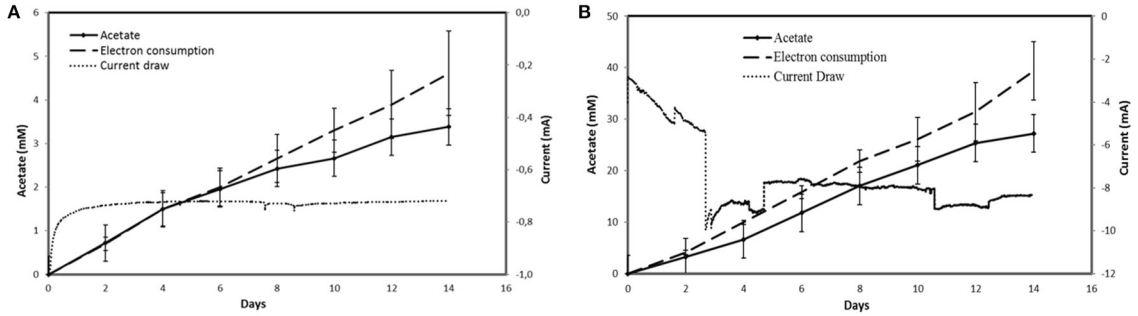

FIGURE 3 | Acetate production, electron consumption and current draw with **(A)** unmodified carbon cloth cathode and **(B)** PEDOT:PSS-carbon cloth cathode. Electron consumption curves correspond to the acetate concentration in mM if all the electrons transferred were converted to acetate. Acetate production curves in mM correspond to the real progression of acetate concentration in the MES reactor detected by HPLC. Results shown for acetate production and electron consumption are in triplicate. Current draw curves are from a representative example of three replicate MES reactors.

TABLE 1 | MES performance with PEDOT:PSS-carbon cloth cathode [a].

Cathode	Microbial catalyst[b]	Acetate production rate (mmol m^{-2} d^{-1})[c]	Current density (A m^{-2})[c]	Coulombic efficiency for acetate (%)[c]
Carbon Cloth	Sterile	N.D.[d]	-0.0 ± 0.2	N.A.[e]
Carbon Cloth	*S. ovata*	27.3 ± 4.5	-0.3 ± 0.1	87.2 ± 7.1
PEDOT:PSS-carbon cloth	Sterile	N.D.	-2.7 ± 1.2	N.A.
PEDOT:PSS-carbon cloth	*S. ovata*	252.3 ± 17.7	-3.2 ± 0.8	78.6 ± 5.6

[a] *Cathode potential set at −690 mV vs. SHE.*
[b] *S. ovata is the wild type strain DSM-2662.*
[c] *Each value is the mean and standard deviation of three replicates.*
[d] *Not detected.*
[e] *Not applicable.*

for 5 h at room temperature. Fixed samples were washed with the same buffer without glutaraldehyde and then immersed successively in acetonitrile and ethanol before being dried under nitrogen as described previously (Zhang et al., 2013). SEM images were taken with a Quanta 200 FEG scanning electron microscope (FEI) at an accelerating voltage of 10 V under high vacuum condition (Aryal et al., 2016).

Analytical Methods

Specific surface area of carbon cloth and PEDOT:PSS-carbon cloth cathodes was measured with the Brunauer–Emmett–Teller (BET) method as previously described (Poreddy et al., 2015). X-ray photoelectron spectroscopy (XPS) was performed with an ESCALAB 250Xi XPS system (ThermoFisher Scientific) with an aluminum K-alpha (1486.6 eV) source. X-ray spot area measurement was set at 500 μM.

RESULTS AND DISCUSSION

The PEDOT:PSS-Carbon Cloth Electrode

The novel PEDOT:PSS-carbon cloth electrode tested here for MES activities was fabricated *via* the dip dry method (Hou et al., 2012). SEM image showed that the coating of the carbon cloth cathode electrode with the PEDOT:PSS polymer was successful (**Figure 1**). After treatment, a PEDOT:PSS layer significantly increasing surface roughness could be observed on the carbon fibers comprised in the carbon cloth electrode (**Figure 1B** inset). This layer was not present on the untreated electrode (**Figure 1A** inset). XPS also confirmed the presence of PEDOT:PSS at the surface of carbon cloth. Characteristic S(2p) peaks were observed corresponding to the sulfur signal from PEDOT at a binding energy of 164.1 and 163.1 eV and to the sulfur signal from PSS at 167.2 eV (**Figure 2A**) (Crispin et al., 2006). Electrochemical performance of the PEDOT:PSS-modified carbon cloth electrode was investigated by CV with sterile 311 medium as the electrolyte (**Figure 2B**). Interestingly, the reductive current response with the sterile medium was improved from −0.988 to −5.506 mA after coating with PEDOT:PSS. Furthermore, PEDOT:PSS increased the specific surface area of the electrode from 0.5 to 1.1 m^2 g^{-1}. This is consistent with results published before by Guzman *et al.* also showing a doubled specific surface area when carbon cloth material is coated with PEDOT (Guzman et al., 2017).

MES With PEDOT:PSS-Carbon Cloth Cathode

MES systems equipped with a PEDOT:PSS-carbon cloth cathode poised at −690 mV vs SHE had an acetate production rate of 252.3 ± 17.7 mmol m^{-2} d^{-1} ($n = 3$) over a period of 14 days with a current density of -3.2 ± 0.8 A m^{-2} and a coulombic efficiency

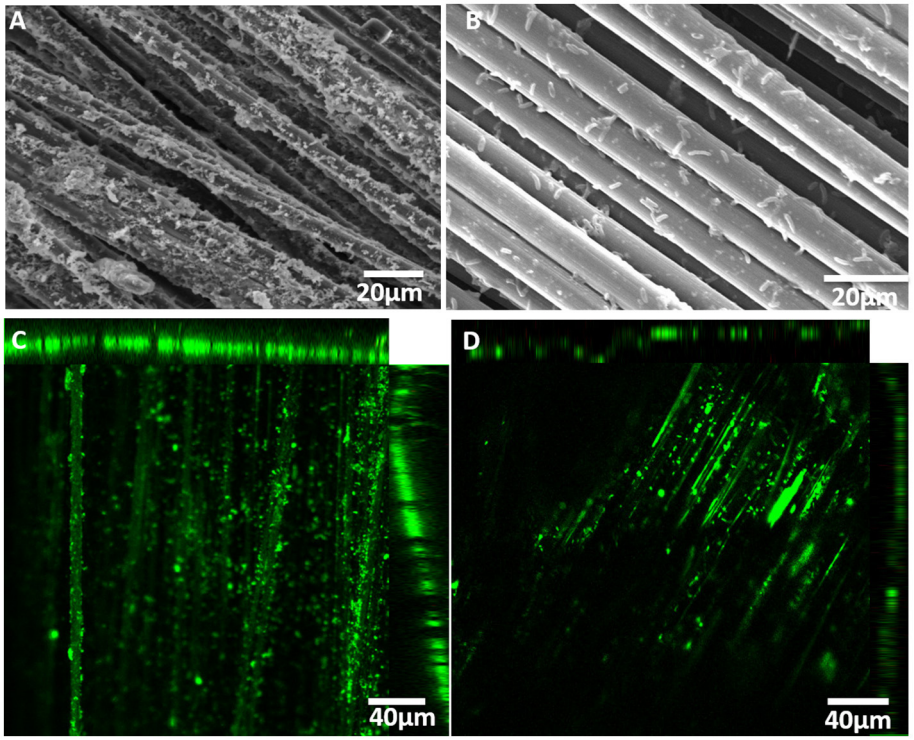

FIGURE 4 | SEM and CLSM images of **(A, C)** a PEDOT:PSS-carbon cloth and **(B, D)** of a carbon cloth cathode in *S. ovata*-driven MES reactors.

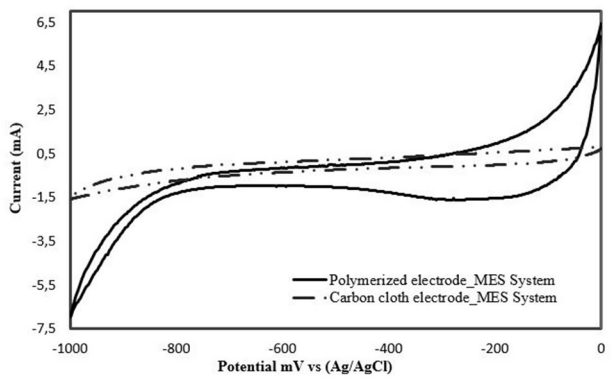

FIGURE 5 | Cyclic voltammograms obtained at a carbon cloth and a PEDOT:PSS-carbon cloth electrode (polymerized) in *S. ovata*-driven MES reactors. Scan rate of 1 mV s^{-1}.

of 78.6 ± 5.6% (**Figure 3**,**Table 1**). Acetate production rate was 9.2-fold faster and current density was 10.7-fold higher with the modified electrode compared to the untreated electrode. No H_2 was detected in the headspace of MES reactors equipped with the PEDOT:PSS-carbon cloth cathode. In combination with the good coulombic efficiency, this suggested that most electrons coming from the cathode were harvested by the microbial catalyst.

To understand further the impact of PEDOT:PSS on MES productivity, SEM and CLSM images were taken after 14 days of reactor operation. The bacterial population found on the modified cathode was significantly denser than on the untreated electrode with the presence of numerous characteristic rod-shaped *S. ovata* cells (**Figure 4**). The higher number of bacteria attached to the PEDOT:PSS-carbon cloth cathode electrode suggested that this material is more suitable for colonization by electroautotrophic bacteria than carbon cloth. As with other MES systems, this increase in the bacterial population density may correspond to a higher number of electric contacts between microbial catalysts and the modified cathode, which is probably one of the main reasons for the observed higher rates of current consumption and acetate production (Chen et al., 2016; Aryal et al., 2017a).

Until now, the three-dimensional graphene carbon felt electrode (3D-G-CF) was the best reported cathode material for MES with wild type *S. ovata* as microbial catalyst and a cathode potential set at −690 mV versus SHE. The PEDOT:PSS-carbon cloth cathode performance was similar to the 3D-G-CF, which had an acetate production rate of 231.4 ± 7.4 mmol d^{-1} per m^2 of electrode (Aryal et al., 2016). The PEDOT:PSS-carbon cloth electrode is more performant than other carbon-based cathodes tested at the same potential with *S. ovata* wild type including carbon cloth, carbon paper, carbon felt and reduced graphene oxide (RGO) paper (Aryal et al., 2017a). Within this group, RGO paper cathode achieved the highest acetate production rate of 168.5 ± 22.4 mmol d^{-1} per m^2 of electrode, which was ca. 1.37 times lower than with PEDOT:PSS-carbon cloth electrode. These comparisons showed the potential of PEDOT:PSS as an electrode material for MES.

Electrochemical Performance of the PEDOT:PSS-Carbon Cloth Biocathode

The PEDOT:PSS-modified biocathode was further characterized *via* CV (**Figure 5**). The cathodic current of the PEDOT:PSS-carbon cloth biocathode was significantly improved compared to the unmodified biocathode, showing that the PEDOT:PSS modification increased bioelectrocatalytic activity. No reversible redox peaks were detected on the current–potential curves before and after colonization by *S. ovata* during MES (**Figures 2**, **5**). This suggested that no electroactive species were present in the medium or excreted by *S. ovata*, acting as electron shuttles between the bacterial cells and the cathodes.

CONCLUSION

The results presented here demonstrate that PEDOT:PSS is a suitable conductive polymer for the development of performant MES biocathode. The results of acetate production as well as current consumption were improved significantly in the presence of PEDOT:PSS. *S. ovata* population at the surface of PEDOT:PSS was more substantial when compared with the uncoated carbon cloth electrode, which demonstrated that PEDOT:PSS is biocompatible and suitable for the development of robust bioelectrocatalyst. Beside its good conductivity, PEDOT:PSS has other interesting properties such as low cost, good mechanical flexibility and high environmental stability that could be harnessed in the future for the fabrication of more performant and robust MES reactor (Groenendaal et al., 2000; Wang, 2009).

AUTHOR CONTRIBUTIONS

NA, TZ, and AD designed the study. MX and NA fabricated the cathodes and did the microscopy characterization. NA performed the bioelectrochemical experiments and did the analytical chemistry. MX did the XPS analysis. NA, TZ, and P-LT analyzed the data and wrote the manuscript.

ACKNOWLEDGMENTS

TZ acknowledges the financial support of the Chinese Thousand Talents Plan Program and the Novo Nordisk Foundation.

REFERENCES

Ammam, F., Tremblay, P. -L., Lizak, D. M., and Zhang, T. (2016). Effect of tungstate on acetate and ethanol production by the electrosynthetic bacterium *Sporomusa ovata*. *Biotechnol. Biofuels* 9:163. doi: 10.1186/s13068-016-0576-0

Antolini, E. (2015). Composite mateials for polymer electrolyte membrane microbial fuel cells. *Biosens. Bioelectron.* 69, 54–70. doi: 10.1016/j.bios.2015.02.013

Aryal, N., Ammam, F., Patil, S. A., and Pant, D. (2017c). An overview of cathode materials for microbial electrosynthesis of chemicals from carbon dioxide. *Green Chem.* 19, 5748–5760. doi: 10.1039/C7GC01801K

Aryal, N., Halder, A., Tremblay, P. -L., Chi, Q., and Zhang, T. (2016). Enhanced microbial electrosynthesis with three-dimensional graphene functionalized cathodes fabricated via solvothermal synthesis. *Electrochim. Acta* 217, 117–122. doi: 10.1016/j.electacta.2016.09.063

Aryal, N., Halder, A., Zhang, M., Whelan, P. R., and Tremblay, P. -L., Chi, Q., et al. (2017a). Freestanding and flexible graphene papers as bioelectrochemical cathode for selective and efficient CO_2 conversion. *Sci. Rep.* 7:9107. doi: 10.1038/s41598-017-09841-7

Aryal, N., Tremblay, P. -L., Lizak, D. M., and Zhang, T. (2017b). Performance of different Sporomusa species for the microbial electrosynthesis of acetate from carbon dioxide. *Bioresour. Technol.* 233, 184–190. doi: 10.1016/j.biortech.2017.02.128

Bajracharya, S., Vanbroekhoven, K., Buisman, C. J. N., Pant, D., and Strik, D. P. (2016). Application of gas diffusion biocathode in microbial electrosynthesis from carbon dioxide. *Enviro. Sci. Pollut. Res.* 23, 22292–22308. doi: 10.1007/s11356-016-7196-x

Bajracharya, S., Yuliasni, R., Vanbroekhoven, K., Buisman, C. J. N., Strik, D. P., and Pant, D. (2017). Long-term operation of microbial electrosynthesis cell reducing CO2 to multi-carbon chemicals with a mixed culture avoiding methanogenesis. *Bioelectrochemistry* 113, 26–34. doi: 10.1016/j.bioelechem.2016.09.001

Chen, B., Cui, T., Liu, Y., and Varahramyan, K. (2003). All-polymer RC filter circuits fabricated with inkjet printing technology. *Solid State Electron.* 47, 841–847. doi: 10.1016/S0038-1101(02)00443-4

Chen, L., Tremblay, P. -L., Mohanty, S., Xu, K., and Zhang, T. (2016). Electrosynthesis of acetate from CO_2 by a highly structured biofilm assembled with reduced graphene oxide–tetraethylene pentamine. *J. Mater. Chem. A* 4, 8395–8401. doi: 10.1039/C6TA02036D

Cheng, S., Xing, D., Call, D. F., and Logan, B. E. (2009). Direct biological conversion of electrical current into methane by electromethanogenesis. *Environ. Sci. Technol.* 43, 3953–3958. doi: 10.1021/es803531g

Chou, H. T., Lee, H. J., Lee, C. Y., Tai, N. H., and Chang, H. Y. (2014). Highly durable anodes of microbial fuel cells using a reduced graphene oxide/carbon nanotube-coated scaffold. *Bioresour. Technol.* 169, 532–536. doi: 10.1016/j.biortech.2014.07.027

Crispin, X., Jakobsson, F. L. E., Crispin, A., Grim, P. C. M., Andersson, P., Volodin, A., et al. (2006). The origin of the high conductivity of poly(3,4-ethylenedioxythiophene)–poly(styrenesulfonate) (PEDOT–PSS) plastic electrodes. *Chem. Mater.* 18, 4354–4360. doi: 10.1021/cm061032+

Cui, M., Nie, H., Zhang, T., Lovley, D., and Russell, T. P. (2017). Three-dimensional hierarchical metal oxide-carbon electrode material for high efficient microbial electrosynthesis. *Sustain. Energ. Fuels* 1, 1171–1176. doi: 10.1039/C7SE00073A

Ganigué, R., Puig, S., Batlle-Vilanova, P., Dolors Balaguer, M., and Colprim, J. (2015). Microbial electrosynthesis of butyrate from carbon dioxide. *Chem. Comm.* 51, 3235–3238. doi: 10.1039/C4CC10121A

Groenendaal, L., Jonas, F., Freitag, D., Pielartzik, H., and Reynolds, J. R. (2000). Poly(3,4-ethylenedioxythiophene) and its derivatives: past, present, and future. *Adv. Mater. Weinheim.* 12, 481–494. doi: 10.1002/(SICI)1521-4095(200004)12:7<481::AID-ADMA481>3.0.CO;2-C

Guzman, J. J. L., Pehlivaner, M. O., Frey, M. W., and Angenent, L. T. (2017). Performance of electro-spun carbon nanofiber electrodes with conductive poly(3,4-ethylenedioxythiophene) coatings in bioelectrochemical systems. *J. Power Sources* 356, 331–337. doi: 10.1016/j.jpowsour.2017.03.133

Hou, S., Cai, X., Wu, H., Lv, Z., Wang, D., Fu, Y., et al. (2012). Flexible, metal-free composite counter electrodes for efficient fiber-shaped dye-sensitized solar cells. *J. Power Sources* 215, 164–169. doi: 10.1016/j.jpowsour.2012.05.002

Jiang, H., Halverson, J. L., and Dong, L. (2015). A miniature microbial fuel cell with conducting nanofibers-based 3D porous biofilm Manuscript version. *J. Micromech. Microeng.* 25:125017. doi: 10.1088/0960-1317/25/12/125017

Jourdin, L., Freguia, S., Donose, B. C., Chen, J., Wallace, G. G., Keller, J., et al. (2014). A novel carbon nanotube modified scaffold as an efficient biocathode material for improved microbial electrosynthesis. *J. Mater Chem. A* 2:13093. doi: 10.1039/C4TA03101F

Jourdin, L., Freguia, S., Flexer, V., and Keller, J. (2016). Bringing High-Rate, CO_2-Based microbial electrosynthesis closer to practical implementation through

improved electrode design and operating conditions. *Enviro. Sci. Technol.* 50, 1982–1989. doi: 10.1021/acs.est.5b04431

Jourdin, L., Grieger, T., Monetti, J., Flexer, V., Freguia, S., Lu, Y., et al. (2015). High acetic acid production rate obtained by microbial electrosynthesis from carbon dioxide. *Environ. Sci.Technol.* 49, 13566–13574. doi: 10.1021/acs.est.5b03821

Kirchmeyer, S., and Reuter, K. (2005). Scientific importance, properties and growing applications of poly(3,4-ethylenedioxythiophene). *J. Mater. Chem.* 15, 2077–2088. doi: 10.1039/b417803n

Ko, C., Lin, Y., Chen, F., Chu, C., and Ko, C. (2007). Modified buffer layers for polymer photovoltaic devices. *Appl. Phys. Lett.* 90:063509. doi: 10.1063/1.2437703

Kok, M. M., De Buechel, M., Vulto, S. I. E., Weijer, P., Van De Meulenkamp, E. A., and Winter, S. H. P. M., et al. (2004). Modification of PEDOT:PSS as hole injection layer in polymer LEDs. *Physica Status Solidi A* 201, 1342–1359. doi: 10.1002/pssa.200404338

Krieg, T., Sydow, A., Faust, S., Huth, I., and Holtmann, D. (2018). CO_2 to terpenes: autotrophic and electroautotrophic a-humulene production with *Cupriavidus necator*. *Angew. Chem. Int. Ed Engl.* 57, 1879–1882. doi: 10.1002/anie.201711302

Lehtinen, T., Efimova, E., Tremblay, P., Santala, S., Zhang, T., and Santala, V. (2017). Bioresource technology production of long chain alkyl esters from carbon dioxide and electricity by a two-stage bacterial process. *Bioresour. Technol.* 243, 30–36. doi: 10.1016/j.biortech.2017.06.073

Lepage, G., Perrier, G., Merlin, G., Aryal, N., and Dominguez-Benetton, X. (2014). Multifactorial evaluation of the electrochemical response of a microbial fuel cell. *RSC Adv.* 4, 23815–23825. doi: 10.1039/C4RA03879G

Lovley, D. R. (2012). Electromicrobiology. *Annu. Rev. Microbiol.* 66, 391–409. doi: 10.1146/annurev-micro-092611-150104

May, H. D., Evans, P. J., and LaBelle, E. V. (2016). The bioelectrosynthesis of acetate. *Curr. Opin. Biotechnol.* 42, 225–233. doi: 10.1016/j.copbio.2016.09.004

Möller, B., Rolf, O., Howard, B. H., Gottsehalk, G., and Hippe, H. (1984). Sporomusa, a new genus of gram-negative anaerobic bacteria including *Sporomusa sphaeroides* spec. nov. and *Sporomusa ovata* spec. nov. *Arch Mierobiol.* 139, 388–396. doi: 10.1007/BF00408385

Nardes, A. M., Kemerink, M., de Kok, M. M., Vinken, E., Maturova, K., and Janssen, R. A. J. (2008). Conductivity, work function, and environmental stability of PEDOT:PSS thin films treated with sorbitol. *Org. Electron.* 9, 727–734. doi: 10.1016/j.orgel.2008.05.006

Nevin, K. P., Woodard, T. L., Franks, A. E., Summers, Z. M., and Lovley, D. R. (2010). Microbial electrosynthesis: feeding microbes electricity to convert carbon dioxide and water to multicarbon extracellular organic compounds. *MBio* 1, e00103–e00110. doi: 10.1128/mBio.00103-10

Nie, H., Zhang, T., Cui, M., Lu, H., Lovley, D. R., and Russell, T. P. (2013). Improved cathode for high efficient microbial-catalyzed reduction in microbial electrosynthesis cells. *Phys. Chem. Chem. Phys.* 15, 14290–14294. doi: 10.1039/c3cp52697f

Pang, S., Gao, Y., and Choi, S. (2018). Flexible and stretchable microbial fuel cells with modified conductive and hydrophilic textile. *Biosens. Bioelectron.* 100, 504–511. doi: 10.1016/j.bios.2017.09.044

Poreddy, R., Engelbrekt, C., and Riisager, A. (2015). Copper oxide as efficient catalyst for oxidative dehydrogenation of alcohols with air. *Catal. Sci. Technol.* 5, 2467–2477.

Rabaey, K., and Rozendal, R. A. (2010). Microbial electrosynthesis - revisiting the electrical route for microbial production. *Nat. Rev. Microbiol.* 8, 706–716. doi: 10.1038/nrmicro2422

Sharma, M., Aryal, N., Sarma, P. M., Vanbroekhoven, K., Lal, B., Benetton, X. D., et al. (2013). Bioelectrocatalyzed reduction of acetic and butyric acids via direct electron transfer using a mixed culture of sulfate-reducers drives electrosynthesis of alcohols and acetone. *Chem. Comm.* 49, 6495–6497. doi: 10.1039/c3cc42570c

Song, D., Li, M., Jiang, Y., Chen, Z., Bai, F., Li, Y., et al. (2014). Facile fabrication of MoS_2 / PEDOT–PSS composites as low-cost and efficient counter electrodes for dye-sensitized solar cells. *J. Photochem. Photobiol. A Chem.* 279, 47–51. doi: 10.1016/j.jphotochem.2014.01.009

Song, T., Fei, K., Zhang, H., and Yuan, H. (2017). High efficiency microbial electrosynthesis of acetate from carbon dioxide using a novel graphene–nickel foam as cathode. *J. Chem. Technol. Biotechnol.* 93, 457–466. doi: 10.1002/jctb.5376

Soussan, L., Riess, J., Erable, B., Delia, M. L., and Bergel, A. (2013). Electrochemical reduction of CO_2 catalysed by geobacter sulfurreducens grown on polarized stainless steel cathodes. *Electrochem. commun.* 28, 27–30. doi: 10.1016/j.elecom.2012.11.033

Stolten, D., Samsun, R. C., and Garland, N. (2016). *Fuel Cells: Data, Facts, and Figures*. New york, NY: Wiley.

Tremblay, P. L., and Zhang, T. (2015). Electrifying microbes for the production of chemicals. *Front. Microbiol.* 6:201. doi: 10.3389/fmicb.2015.00201

Tremblay, P. L., Angenent, L. T., and Zhang, T. (2017). Extracellular electron uptake: among autotrophs and mediated by surfaces. *Trends Biotechnol.* 35, 360–371. doi: 10.1016/j.tibtech.2016.10.004

Tremblay, P. L., Höglund, D., Koza, A., Bonde, I., and Zhang, T. (2015). Adaptation of the autotrophic acetogen *Sporomusa ovata* to methanol accelerates the conversion of CO_2 to organic products. *Sci. Rep.* 5:16168. doi: 10.1038/srep16168

Villano, M., Aulenta, F., Ciucci, C., Ferri, T., Giuliano, A., and Majone, M. (2010). Bioelectrochemical reduction of CO_2 to CH_4 via direct and indirect extracellular electron transfer by a hydrogenophilic methanogenic culture. *Bioresour. Technol.* 101, 3085–3090. doi: 10.1016/j.biortech.2009.12.077

Villano, M., Scardala, S., Aulenta, F., and Majone, M. (2013). Bioresource Technology Carbon and nitrogen removal and enhanced methane production in a microbial electrolysis cell. *Bioresour. Technol.* 130, 366–371. doi: 10.1016/j.biortech.2012.11.080

Wang, Y. (2009). Research progress on a novel conductive Research progress on a novel conductive polymer — poly (3,4- ethylenedioxythiophene) (PEDOT). *J. Phys. Conf. Ser.* 152:012023. doi: 10.1088/1742-6596/152/1/012023

Wang, Y., Zhao, C. E., Sun, D., Zhang, J. R., and Zhu, J. J. (2013). A graphene/poly(3,4-ethylenedioxythiophene) hybrid as an anode for high-performance microbial fuel cells. *Chempluschem* 78, 823–829. doi: 10.1002/cplu.201300102

Webb, H. K., Notley, S. M., and Evans, D. R. (2015). Observation of electron transfer between bacteria and high conductivity graphene–PEDOT composites. *RSC Adv.* 5, 45642–45645. doi: 10.1039/C5RA08720A

Yoo, B., and Dodabalapur, A. (2007). Germanium nanowire transistors with ethylene glycol treated poly (3,4- ethylenedioxythiophene):poly(styrene sulfonate) contacts. *Appl. Phys. Lett.* 90:072106. doi: 10.1063/1.2535710

Zhang, T., and Tremblay, P. L. (2017). Hybrid photosynthesis - powering biocatalysts with solar energy captured by inorganic devices. *Biotechnol. Biofuels* 10:249. doi: 10.1186/s13068-017-0943-5

Zhang, T., Nie, H., Bain, T. S., Lu, H., Cui, M., Snoeyenbos-West, O. L., et al. (2013). Improved cathode materials for microbial electrosynthesis. *Energ. Environ. Sci.* 6, 217–224. doi: 10.1039/C2EE23350A

Conflict of Interest Statement: The authors declare that the research was conducted in the absence of any commercial or financial relationships that could be construed as a potential conflict of interest.

frontiers in Chemistry

ORIGINAL RESEARCH
published: 15 August 2018
doi: 10.3389/fchem.2018.00318

Effects of Applied Potential and Reactants to Hydrogen-Producing Biocathode in a Microbial Electrolysis Cell

*Swee Su Lim[1,2], Byung Hong Kim[2,3], Da Li[4], Yujie Feng[4], Wan Ramli Wan Daud[2], Keith Scott[1] and Eileen Hao Yu[1]**

[1] School of Engineering, Newcastle University, Newcastle Upon Tyne, United Kingdom, [2] Fuel Cell Institute, Universiti Kebangsaan Malaysia, Bangi, Malaysia, [3] Bioelectrochemistry Laboratory, Water Environment and Remediation Research Centre, Korea Institute of Science and Technology, Bongdong-eup, South Korea, [4] State Key Laboratory of Urban Water Resource and Environment, School of Environment, Harbin Institute of Technology, Harbin, China

OPEN ACCESS

Edited by:
Deepak Pant,
Flemish Institute for Technological Research, Belgium

Reviewed by:
Jung Rae Kim,
Pusan National University, South Korea
Mohanakrishna Gunda,
Qatar University, Qatar

***Correspondence:**
Eileen Hao Yu
eileen.yu@newcastle.ac.uk

Specialty section:
This article was submitted to Green and Sustainable Chemistry, a section of the journal Frontiers in Chemistry

Received: 21 February 2018
Accepted: 10 July 2018
Published: 15 August 2018

Citation:
Lim SS, Kim BH, Li D, Feng Y, Daud WRW, Scott K and Yu EH (2018) Effects of Applied Potential and Reactants to Hydrogen-Producing Biocathode in a Microbial Electrolysis Cell. Front. Chem. 6:318. doi: 10.3389/fchem.2018.00318

Understanding the mechanism of electron transfer between the cathode and microorganisms in cathode biofilms in microbial electrolysis cells (MECs) for hydrogen production is important. In this study, biocathodes of MECs were successfully re-enriched and subjected to different operating parameters: applied potential, sulfate use and inorganic carbon consumption. It was hypothesized that biocathode catalytic activity would be affected by the applied potentials that initiate electron transfer. While inorganic carbon, in the form of bicarbonate, could be a main carbon source for biocathode growth, sulfate could be a terminal electron acceptor and thus reduced to elemental sulfurs. It was found that potentials more negative than −0.8 V (vs. standard hydrogen electrode) were required for hydrogen production by the biocathode. In additional, a maximum hydrogen production was observed at sulfate and bicarbonate concentrations of 288 and 610 mg/L respectively. Organic carbons were found in the cathode effluents, suggesting that microbial interactions probably happen between acetogens and sulfate reducing bacteria (SRB). The hydrogen-producing biocathode was sulfate-dependent and hydrogen production could be inhibited by excessive sulfate because more energy was directed to reduce sulfate (E° $SO_4^{2-}/H_2S = -0.35$ V) than proton (E° $H^+/H_2 = -0.41$ V). This resulted in a restriction to the hydrogen production when sulfate concentration was high. Domestic wastewaters contain low amounts of organic compounds and sulfate would be a better medium to enrich and maintain a hydrogen-producing biocathode dominated by SRB. Besides the risks of limited mass transport and precipitation caused by low potential, methane contamination in the hydrogen-rich environment was inevitable in the biocathode after long term operation due to methanogenic activities.

Keywords: hydrogen-producing biocathode, microbial electrolysis cell, electron bifurcation, sulfate reduction, bicarbonate conversion

INTRODUCTION

Since hydrogen-producing biocathode was first introduced by Rozendal et al. (2008), biocathode activities in microbial electrolysis cells (MECs) were extensively studied. Combining wastewater treatment and production of hydrogen as energy carrier makes MECs an attractive technology. As the catalysts used in the cathode are living microorganisms, the associated microbiological knowledge is important for systematic optimisation MECs (Kim et al., 2015). Rozendal et al. (2008) used three phase start-up procedures to enrich hydrogen-producing biocathodes in a bioelectrochemical system (BES). A biocathode was obtained by reversing a bioanode. The whole process took less than a month to achieve a fully developed biocathode. Community analysis confirmed that sulfate-reducing bacteria (SRB) belonging to the genus, *Desulfovibrio,* were the key players in the hydrogen-producing biocathode (Croese et al., 2011, 2014). *Desulfovibrio sp*. conserve energy through a hydrogen cycling mechanism, that involves different types of hydrogenases which are involved in hydrogen production and consumption. A decade after, Jourdin et al. (2015) successfully grew an autotrophic biocathode and operated it for 9 months. They claimed that a sustainable autotrophic biocathode was involved in hydrogen evolution, when suitable cathodic condition were applied with inorganic carbon as the carbon source. The bacteria communities on the biocathode changed over the biofilm enrichment period; a significant increase on *proteobacteria* distribution between initial inoculum and enriched biocathode from 10 to 57% at the end of the experiment. Initial *Archaea* distribution disappeared completely from 30.3% to less than 0.1% of population. In additional to carbonates serving as the carbon source, both studies added a trace amount of sulfate into the catholyte to grow and maintain their biocathodes. SRB thrived and their domination could be due to the availability and quantity of sulfate present in the catholyte. It also been showed that sulfate was an important final electron terminal accepter in SRB hydrogen cycling mechanism (Kim and Gadd, 2008; Keller and Wall, 2011; Madigan et al., 2014). Nevertheless hydrogen production in a SRB dominated biocathode was the main purpose of the studies. Considering the standard reduction potentials of hydrogen and sulfate, hydrogen (E° $H^{+}/H_2 = -0.41$ V) requires more energy than sulfate reduction (E° $SO_4^{2-}/H_2S = -0.35$ V). Furthermore, as the reduction potentials are relatively close (−0.06 V), indicates that sulfate reduction could take place in conjunction with hydrogen evolution, and the concentration of sulfate present may impact hydrogen production. Regardless of the standard reduction potential, many studies used much lower potential than −0.41 V in practical condition for biological hydrogen evolution (Geelhoed et al., 2010; Jeremiasse et al., 2012; Batlle-Vilanova et al., 2014; Jourdin et al., 2015). If SRB play an important role in electrochemical hydrogen production, sulfate concentration and its availability should be taken consideration as it will not only affect the current density of BES but also the working potential applied to the cathode. Bicarbonate (carbon source) and ammonium (nitrogen source) were commonly used in the biocathode study which have direct link to the growth of biocathode but not the case where sulfate is the responsible as electron acceptor and sulfur source. Therefore, sulfate could be the third important parameter after the carbon and nitrogen sources. Some studies presented results where additional acetate could enhance the start-up process of biocathode (Jeremiasse et al., 2012) or by using lactate as organic carbon with high sulfate concentration in pure culture tests (Aulenta et al., 2012). Due to the fact that SRB especially *Desulfovibrio* sp. cannot use inorganic carbon directly as a carbon source, there must be an active interaction between the species and other autotrophic bacteria in the hydrogen-producing biocathode to use the inorganic carbon as organic carbon. The community interaction between SRB and autotroph acetogens actually happened where only inorganic carbon, such as carbonates were in the solution (Muyzer and Stams, 2008; Mand et al., 2014). Even though SRB specifically *Desulfovibrio* sp. were found responsible for hydrogen production in BES biocathode, questions on optimum operational conditions and the feasibility of the biocathode in real applications still remain unanswered. The changes of influent content in varies inorganic carbon, nitrogen source and sulfate concentrations could shift microbial metabolism and the community and affect whole BES performance.

To fully understand the operational conditions of hydrogen-producing biocathode in a microbial electrolysis cell (MEC), the study of essential parameters and community interaction need to be integrated. Mand et al. (2014) proposed that sulfate-reducing bacteria and acetogen's interaction were responsible for steel pipe corrosion. However, other evidence showed that the form of ferrous sulfide layer on an iron sheet due to SRB corrosion was more severe without the sources of organic carbons or presence of acetogens (Venzlaff et al., 2013). The deposited ferrous sulfide works as a semiconductor in anaerobic corrosion by mediating electron flow from metal to the cells and by by-passing the slow reduction of proton to free hydrogen. The mechanisms of electron transfer are similar to a biocathode enriched from a mixed culture aimed for hydrogen production and could serve as a model for biocathode community interactions. Meanwhile Keller and Wall (2011) studied genetics and molecular level of electron flow in *Desulfovibrio* sp. for sulfate respiration. They reported how the respiration could assist in hydrogen production while reducing sulfate to sulfides. The results also inferred that periplasm hydrogenases plays an important role in hydrogen evolution. However, no experiment has been conducted to further examine the hypothesis. In addition, Geelhoed et al. (2010) discussed how the key enzymes, [Fe-Fe]- and [NiFe]-hydrogenases, from *Desulfovibrio vulgaris* were involved in hydrogen production. They stressed that utilization of immobilized whole cells were better and more robust than using only enzymes and therefore co-culture should be considered. As the whole cells and community should be focused, electron transfer within syntrophic partners become important and, from a thermodynamic point of view, hydrogen production via reduction of proton has to be coupled with energy conservation from hydrogenases. The balance between the conservation energy and hydrogen production indicated that microbial communities in a biocathode are able to grow and maintain their catalytic activity. It was also suggested that

studying the correct growth conditions with a carbon source and applied voltage, longevity of the biocathode could be the key issues for further understanding the electron transport mechanism. Later, Rosenbaum et al. (2011) proposed possible direct and indirect electron transfer mechanisms by analyzing the literature on hydrogen producing biocathodes. On one hand, direct mechanisms were involved in direct electron transfer through *c*-type cytochromes either coupled with or without hydrogenases. On the other hand, indirect electron transfer mechanism relied on natural redox mediators shuttling between cathode and hydrogenases. Surprisingly, they suggested that the biocatalysed reactions was not necessarily an energy conservation process for microorganisms (Rosenbaum et al., 2011). Recently, Kim et al. (2015) proposed another electron transfer mechanism, similar to those in microbial influenced corrosion (MIC) and showed a sound reason that biocathode should conserve energy during electron consuming reactions, i.e., microbes performed proton reduction and should grow and be maintained under the given cathodic condition for sustainable function and thermodynamically balance.

The objective of the study was to re-culture biocathodes to optimize operational conditions and increase biocathode performance for hydrogen production, by manipulating the cathode potential, inorganic carbon and sulfate concentrations. The study will help to determine what kind of wastewaters will be suitable for biocathode formation and assist in establishing potential electron transfer mechanisms. It will also indicate the possible wastewater treatments that could be performed using this technology.

MATERIALS AND METHODS

Experimental Setup and Biocathode Enrichment

Double-chamber electrochemical cells, 25 cm^3 (mL) in volume (each chamber) were used as described in Lim et al. (2017). **Figure 1** is the schematic of the experimental setup in this study. The enrichment of hydrogen-producing biocathode was performed as stated in Rozendal et al. (2008). A three step start-up procedure and polarity reversal method was exploited to obtain the desired biocathode. An abiotic anode (RVG-2000, Mersen, USA) coated with 0.5 mg/cm^2 platinum catalyst was used. Anolyte was a mixture of sodium chloride and phosphate buffer consisted of (g/L): $NaH_2PO_4{\cdot}2H_2O$ 3.30; $Na_2HPO_4{\cdot}2H_2O$ 5.14; NaCl 2.92. The anolyte was circulated from a 250 mL reservoir to anodic chamber at flowrate 8.7 mL/min. Once a stable current was observed, the biocathode potential was further increased and fixed at −1.0 V versus standard hydrogen electrode (SHE) for all the experiments unless stated otherwise. The catholyte medium contained (g/L): $NaH_2PO_4{\cdot}2H_2O$ 0.66; $Na_2HPO_4{\cdot}2H_2O$ 1.03, $KHCO_3$ 1.0, NH4Cl 0.27, $MgSO_4{\cdot}7H_2O$ 1.23, $CaCl_2{\cdot}2H_2O$ 0.01 and trace element mixture 1.0 mL/L (Rozendal et al., 2008). The medium consisted of only phosphate buffer was first prepared and autoclaved. The remaining ingredients were filter-added then after. The amount of $KHCO_3$ and $MgSO_4{\cdot}7H_2O$ was added into the medium as stated above except if mentioned otherwise. The medium was then fed continuously into the cathodic chamber at 0.2 mL/min. The anolyte consisted 5 times higher concentration of phosphate buffer than in catholyte when the solutions were prepared. It is to ensure anolyte pH was maintained in neutral under recycle condition. Ion balance could affect conductivity value in the electrolytes and performance of MEC due to different phosphate buffer concentration. However, the effect was insignificant in our study as small operation volume (25 mL each chamber with half of the volume filled with carbon felt electrode) and a closer electrode gap ($\leq$1.0 cm) was used. During the enrichment process, hydrogen was filled in cathode headspace and recycled by a peristaltic pump into the cathode chamber and then bubbled through the catholyte. The headspace hydrogen was refilled every day.

Experimental Parameter

Enriched biocathodes were subjected to three main experiments to examine optimum conditions for better performance especially in producing hydrogen. The experiments include manipulating applied potentials and various sulfate and bicarbonate concentrations to the cathodes. **Table 1** shows the experiment parameters used in this study. The applied potential experiments were done using chronoamperometry to check the biocathode performance in term of hydrogen production and their energy requirement in term of current. All experiments were conducted in duplicate. The average values with the maximum and minimum are presented.

Electrochemical Analysis

Cyclic voltammetry (CV) was carried out after each experiment to compile the information how the catalytic activity responses to the experimental parameters. Four channel potentiostat (Quad, Whistonbrook Technologies, UK) was used to conduct the analysis. Start and end potentials were 0 and 1.0 V with scan rate 0.001 V/s and repeated for at least 3 cycles to obtain a stable voltammogram. Only the last voltammograms from the last cycles of each experiment are reported in this study. All potential values were reported as vs. SHE unless stated otherwise.

Samples Analysis and Calculations

Influent and effluent samples were collected for each parameter test. Ph and conductivity are the simpler indication of the change liquid properties through bioelectrochemical reactions. For instance, substrate oxidation or proton reduction in anode or cathode could result the decrease or increase of pH value. While ionic conductivity may influence the efficiency of whole system when the reactant and product contents vary in electrolytes. pH (HI 9025 Microcomputer pH meter, Hanna Instruments, UK) and conductivity (HI 8733 Conductivity meter, Hanna Instruments, UK) values were measured for each sample before the sample was filtered through a 0.2 μm PES membrane [VWR (514-0072), UK]. The filtered samples were then kept in refrigerator under 4°C prior analysis.

Sulfate and total soluble carbon were the two main parameter in this study. It is important to monitor the changes of the sample contents and the effect of applied cathode potential. Anions

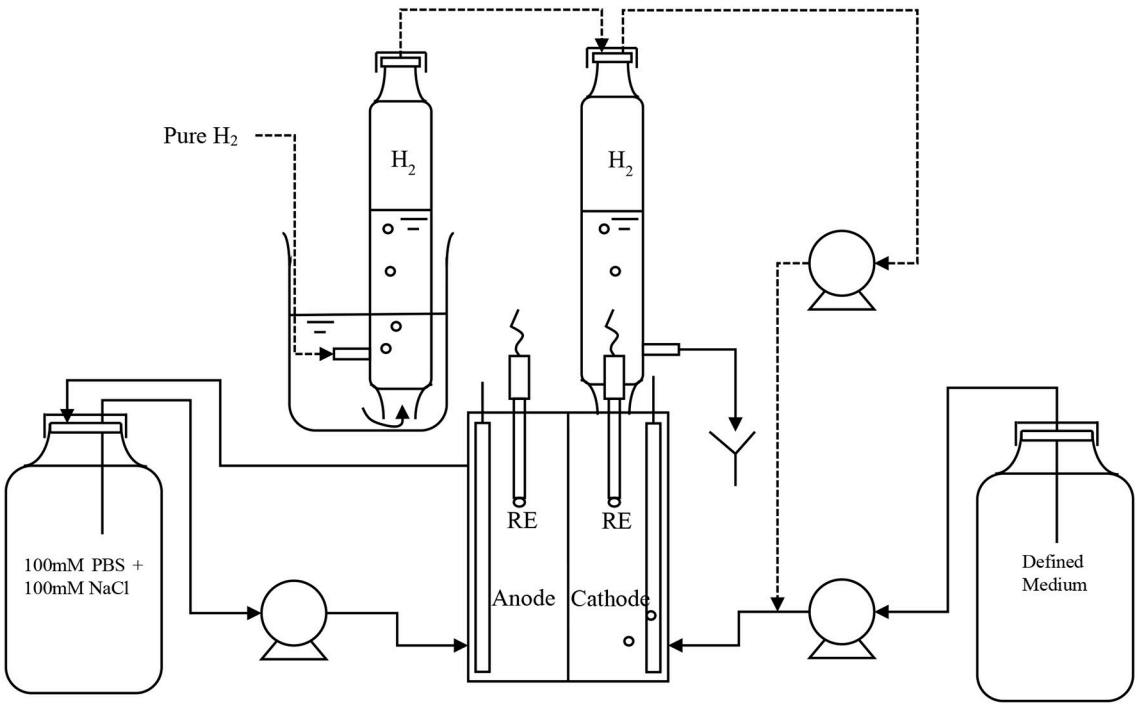

FIGURE 1 | Schematic of the experimental setup.

compounds included sulfate (SO_4^{2-}) and phosphate (PO_4^{3-}) were determined by ion chromatography (Interrion HPIC, Dionex, USA) equipped with autosampler (AS-AP, Dionex, USA) while inorganic and organic carbon measured by total carbon analyzer (TOC-5050A, Shimadzu, UK) equipped with autosampler (ASI-5000A, Shimadzu, UK). The pH of TOC samples were maintained as they were collected. The alkaline condition of the samples avoid dissolution of carbonates to CO_2 which could affect the results of total carbon.

Ammonium ion could contribute to the ionic strength of the medium while acted as nitrogen source to bioanode. Therefore, it was included in the analysis apart from the main parameter analysis. Ammonium (NH4-N) contain was determined by using the cell test kits (14559: 4.0–80.0 mg/L NH4-N) supplied by Merck, UK. The samples were prepared and added into the reagent vials according to the manufacture's procedures and then measured by a spectrophotometer (Spectroquant® Pharo 300, Merck, UK).

Hydrogen is the main product in this study. In order to calculate the hydrogen production rate, gas evolution from the biocathode was measured using a water replacement method. A gas collection tube with marked volume was placed on the top of cathodic chamber and then filled with catholyte from the top opening. Gas bubble produced from cathodic was evolved to the top of the tube and replaced the catholyte by pushing it out from a side outlet. The effluent channel was filled with catholyte all the time to maintain anaerobic condition and atmospheric pressure inside the chamber (Lim et al., 2017). The gas samples then were analyzed using a gas chromatography (GC-8A, Shimadzu, UK). Two columns molecular sieve 5A (mesh range 40-60) and Chromosorb 101 (mesh range 80–100) were equipped and operated at isothermal temperature 40°C. The carrier gas was research grade 99.99% N_2 (BOC, UK) at a pressure of 100 kPa. A thermal conductivity detector was used to detect the gas based on their retention times. The actual hydrogen volume was calculated as

$$V_{H2} = V_h \cdot X_{H2} \quad (1)$$

where V_{H2} (L) is pure hydrogen volume, V_h (L) is the headspace volume of the gas captured in the glass collection tube, X_{H2} is fraction of hydrogen in the gas samples determined from the GC analysis. The actual hydrogen volume was then used to

TABLE 1 | Experimental matrix.

Parameter 1	Parameter 2	Parameter 3
Cathodic potential (V vs. SHE)	**[Sulfate] mg/L (mM)**	**[Bicarbonate] mg/L (mM)**
0.5	0 (0)	0 (0)
0.7	96 (1)	61 (1)
0.8	288 (3)	183 (3)
0.9	768 (8)	305 (5)
1.0	–	610 (10)
–	–	3051 (50)

determined hydrogen production rate as

$$Q_{H2} = V_{H2}/(A_{cat} \cdot t) \quad (2)$$

where Q_{H2} (L H_2/m^2 cathode/day) is hydrogen production rate, A_{cat} (m^2) is cathode surface area and t (day) is production time.

Faraday's law of electrolysis equation was obtained to compute hydrogen recovery efficiency from cathode

$$r_{cat}(\%) = Q_{recovery}/Q_{supply} \quad (3)$$

where $Q_{recovery}$ (C) = $\eta \cdot F \cdot z$ is charge use to reduce proton to hydrogen, η is hydrogen recovery in mole, F is faraday constant (96,485 C/mol), z is the valency number of hydrogen formation which is 2. Q_{supply} (C) = $\int$ I (t) dt is total charge supplied from a power supply within specific time of recovery.

And, energy yield from hydrogen relatives to electrical input is calculated based on

$$\eta_e(\%) = W_h/W_e \times 100\% \quad (4)$$

where W_h and W_e (J) are energy content of H_2 and electrical energy.

RESULTS AND DISCUSSION

Enrichment of Hydrogen-Producing Biocathode

The enrichment of biocathodes in this study was performed by following the method reported in Rozendal et al. (2008). Cathode chamber was cultivated with inoculum collected from bioanode effluent operated in microbial fuel cell mode for over a year (Spurr, 2016). The inoculum was dominated by *Deltaproteobacteria* (∼60%), followed by Clostridia (∼20%) and *Bacteroidia* (∼10%). The *Geobacter* sp. (∼50%) was found as dominated ribotype in *Deltaproteobacteria* cluster and sulfate-reducing bacteria only consisted around 2%. A defined medium was prepared as described in Rozendal et al. (2008). **Figure 2** shows the monitored current density during enrichment process. Target electrode was fixed at −0.1 V and was left for overnight without any inoculum. Acetate was used as electron donor to grow the bioelectrode. Significant current increase was observed after day 2 and a stable current was achieved after day 4. After 6.5 days, the potential was further reduced to −0.2 V and acetate was removed and replaced by hydrogen on the headspace. Hydrogen recycle rate was reduced and then increased in between 5.05 and 26.86 mL/min after 8 days of enrichment to check whether the bioelectrode was actively growth under hydrogen as electron donor. **Figure 3** shows the relationship between hydrogen consumption and the rate of recycle between headspace and bioelectrodes. The optimum recycle rate was determined as 13 mL/min and was used throughout the rest of experiments. The biocathode test was continued by replacing hydrogen with nitrogen between 12 and 13 day. This is to confirm that the biocathode was relied and grew on hydrogen. After the test, carbon dioxide was filled instead of hydrogen. As the current value changed from positive to negative between 14 and 15.5 day, it justified that the polarity could be reversed from electron-producing bioanode to electron-accepting biocathode. A polarity reversal scan was performed at 15.5 day and the result is shown in **Figure 4**. Based on the graph, the minimum starting potential that could be applied to the bioelectrode was determined as −0.80 V. Therefore, −0.80 V was fixed for further enrichment of the electron-consuming biocathode. Bicarbonate was used as carbon source starting from 16.5 day. A stable current was observed after 23.5 day. Sulfate test was performed at 26 day to check whether the biocathode was dominated by sulfate-reducing bacteria and depended on the compound to perform anaerobic respiration (Jeremiasse et al., 2012; Croese et al., 2014). The results showed little or no significant effect of the sulfate when the concentration was reduced from 5 mM to zero. Therefore, the cathode potential was further reduced to −0.9 V and a remarkably current density dropped was noticed between 32 and 34 day. The current was resumed after 5 mM SO_4^{2-} was reintroduced to the biocathode.

Effects of Cathodic Potential on Hydrogen Production

The reactors were operated under different cathode conditions and performance between biocathode and abiotic cathode were compared. The cathode potentials was first fixed at −0.5 V before moving toward more negative potential until −1.0 V where a significant amount of gas was collected in the headspace. Each applied potential was fixed and applied for at least 2–3 days to obtain a stable current and hydrogen production. **Figure 5A** represents current density and hydrogen production rate from both control and biocathode. As shown in **Figure 5A**, biocathode hydrogen production was higher than control when the cathode potential was fixed at −0.8 V or below. No significant hydrogen production was observed in both biocathode and control when the potential was higher than −0.8 V. The biocathode produced almost 10 L/m^2/day compared with the control cathode production of 3 L/m^2/day at −1.0 V, evidencing biotic activity. The hydrogen production increased consistently with the external energy requirement for hydrogen evolution at lower potentials. The current density achieved was −1.10 A/m^2 for biocathode compared to −0.45 A/m^2 for the control, at a cathode potential of −1.0 V. Even though the reduction potential for hydrogen evolution from proton at standard condition is −0.41 V, the real operational reduction potentials are much more lower than the theoretical value (Lim et al., 2017). Potentials as low as −0.7 V and below were used to produce hydrogen as a result of overcoming overpotentials during the electron transfer to microbes (Rozendal et al., 2008; Jeremiasse et al., 2012; Jourdin et al., 2015). In additional, some studies applied even lower potentials than −0.7 V due to the different designs and configurations that possibly increased the overpotentials (Aulenta et al., 2012; Batlle-Vilanova et al., 2014; Liang et al., 2014; Luo et al., 2014; Lim et al., 2017).

Figure 5B shows the catalytic activity between biocathode and control (without inoculum) under the potential range of 0 to −1.0 V. Significant reduction activity was observed from

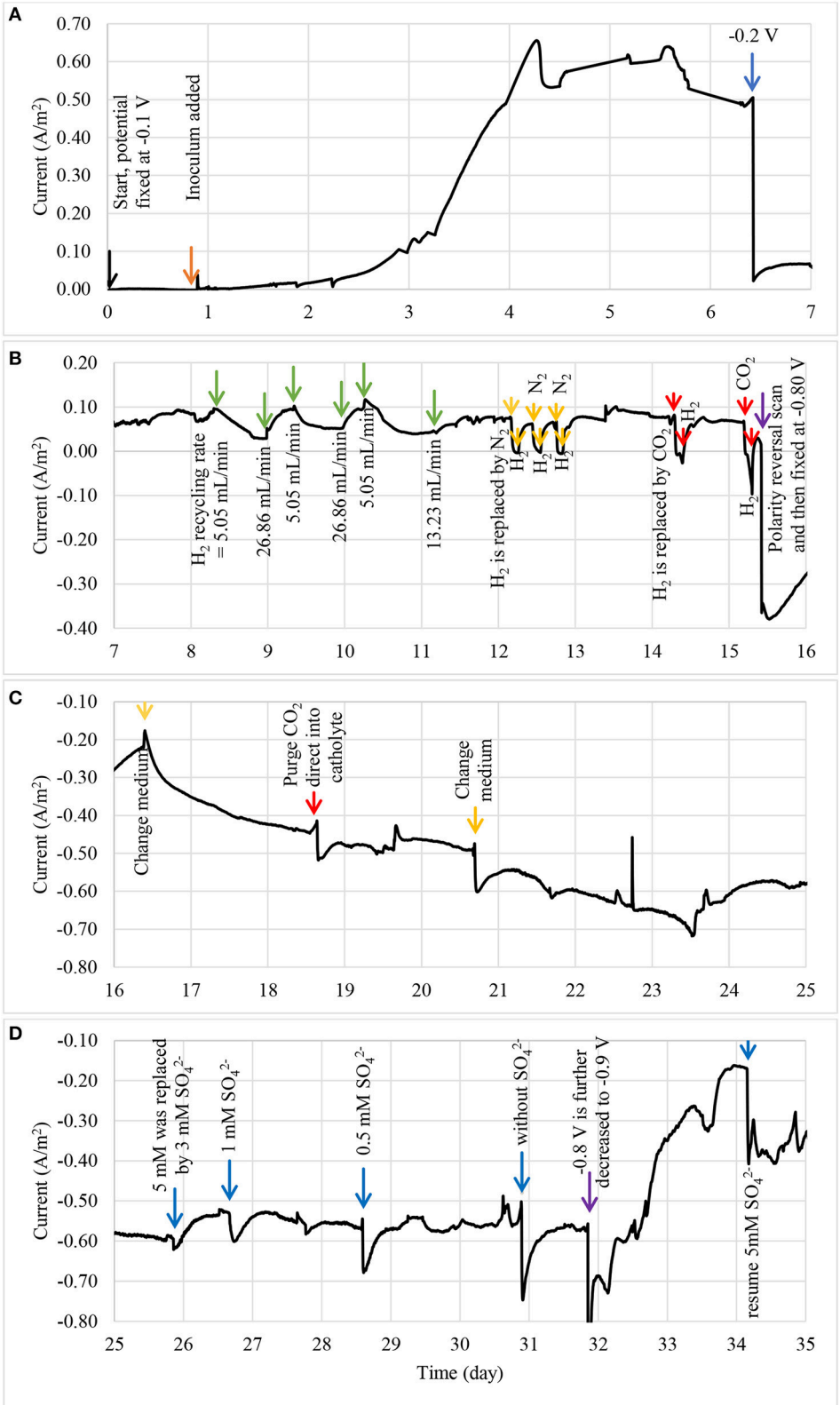

FIGURE 2 | The current density profile of enriched bioelectrode using three step start-up procedure: **(A)** bioelectrode was enriched as bioanode between 0 and 7 day, and **(B)** subjected to series of bioanode confirmation tests between 7 and 16 day, **(C)** the bioanode was then switched to biocathode and grew under a fixed potential of −0.8 V between 16 and 25 day, and **(D)** subjected to sulphate tests after a stable current was observed between 25 and 35 day.

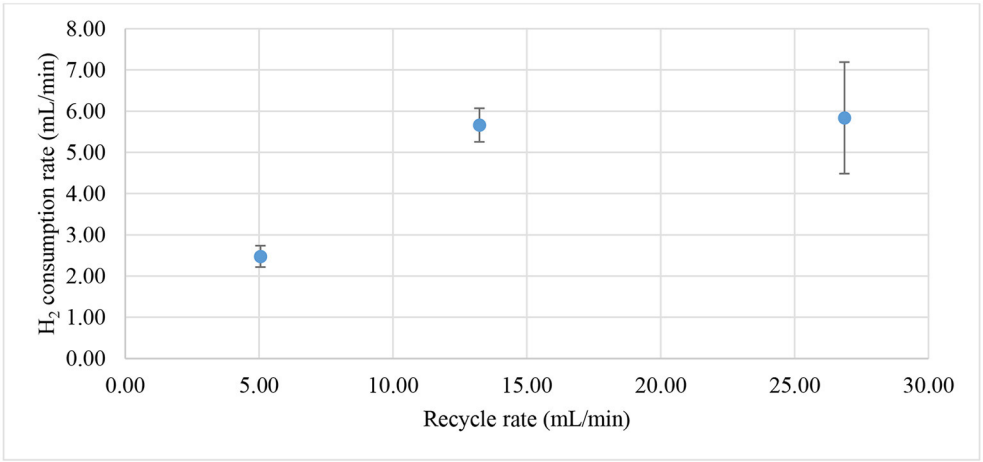

FIGURE 3 | Hydrogen consumption rate based on hydrogen recycling rate from the headspace. Maximum hydrogen consumption was observed after the recycle rate was higher than 13 mL/min.

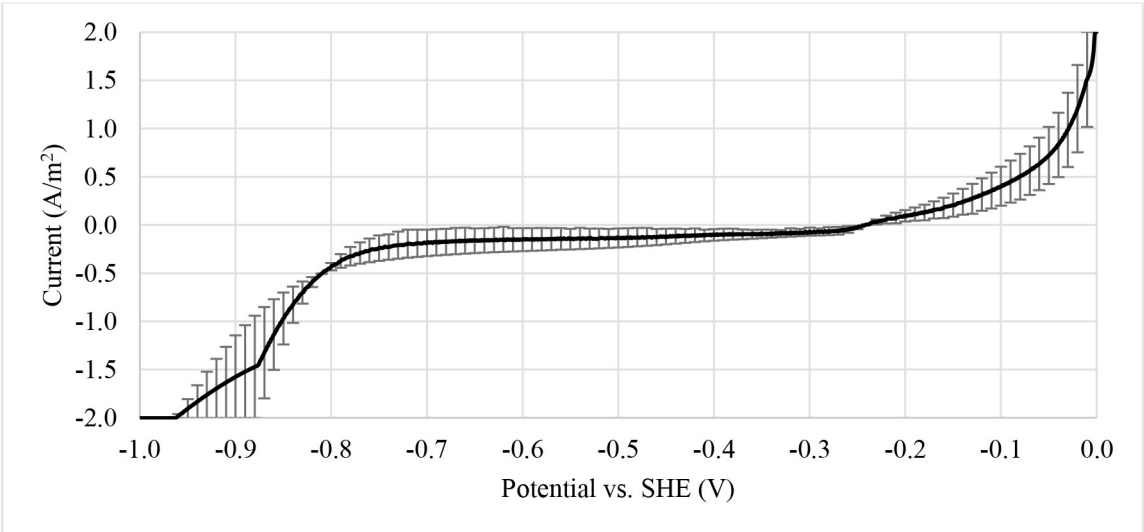

FIGURE 4 | Polarity reversal scan from 0 to −1.0 V vs. SHE at scan rate of 0.2 mV/s. The information was obtained to determine the minimum potential to be fixed on bioelectrode for hydrogen production.

−0.8 V and below. A small oxidation peak at −0.6 V was noticed when the voltammetry was scanned from −1.0 to 0 V. The peak was asserted as hydrogen oxidation reaction where the generated hydrogen (near −1.0 V) was re-oxidized under the outer membrane enzymes called hydrogenases (Aulenta et al., 2012). Furthermore, a small reduction curve at −0.3 V was also noticed and proved to be related to the process of inorganic to organic carbon conversion. Similar reduction peak was found in other CO_2 conversion studies especially those for acetate production at the range between −0.3 and −0.6 V (Marshall et al., 2012; Blanchet et al., 2015; Patil et al., 2015; Bajracharya et al., 2017; Wenzel et al., 2018). Meanwhile, the control only showed reduction activity at −0.8 V and below and the activity was significantly lower than the biocathode. The catalytic properties proved biocathode growth on the electrode surface (Aulenta et al., 2012; Jourdin et al., 2015). Data suggests that hydrogen production was significant after cathodic potentials more negative than −0.8 V.

Figure 5C shows the variation in sulfate and ammonium content at different applied potentials. Lower potential was not necessary to increase the sulfate removal rate as fresh medium was continuously fed into the chamber (Jeremiasse et al., 2012; Luo et al., 2014). However, ammonium removal slightly increased at potentials lower than −0.8 V as ammonium acted as nitrogen source for microbial cell construction which could be much more important than sulfate as electron terminal acceptor.

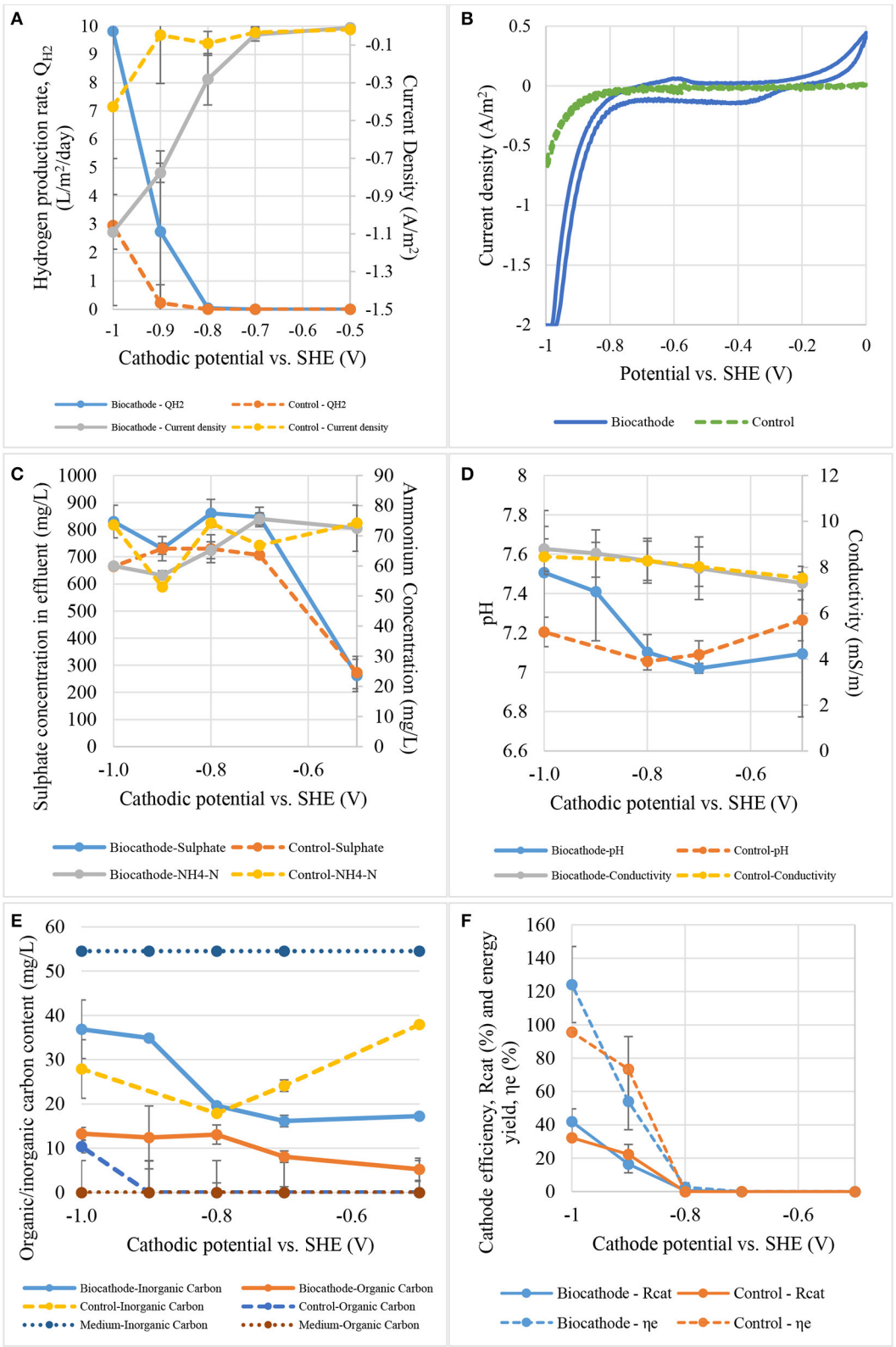

FIGURE 5 | The effect of cathode potential on: **(A)** hydrogen production rate and current density, **(B)** catalytic activity, **(C)** sulfate and ammonium contents, **(D)** pH and conductivity, **(E)** total carbon content, and **(F)** cathode efficiency and energy yield.

Ph and conductivity are simpler indicators to biocathode activities. **Figure 5D** presents the pH and conductivity according to cathodic applied potentials. The pH of catholyte in biocathode remained at 7.0 between −0.5 and −0.8 V but start to increase to 7.5 when the potential was further decreased to −1.0 V depending on hydrogen evolution. The rate of pH increases was disproportional to the applied potential. However, catholyte pH in control fluctuated slightly between 7.0 and 7.3. Conductivity for both biocathode and control was increased vaguely from 8.0 to 9.0 mS/m when potential was dropped from −0.5 to −1.0 V. It is crucial to control the pH at neutral or slightly acidic to maintain the biocathode performance in producing hydrogen (Rozendal et al., 2008; Jeremiasse et al., 2010). This is because proton was continuously removed to produce hydrogen causing the increases of pH value.

Figure 5E shows inorganic and organic carbon contents of biocathode and control effluents. Bicarbonate as an inorganic carbon can be converted to acetate by homoacetogens to generate energy for growth (Bar-Even, 2013; Schuchmann and Muller, 2014; Mohanakrishna et al., 2015). Acetate was then could be used by SRB as the carbon source (Aulenta et al., 2012; Jeremiasse et al., 2012). This means that bicarbonate was converted to cell materials of homoacetogens and SRB, and to acetate. As observed from the **Figure 5E**, inorganic carbon content went up faster than organic carbon when more negative potential was applied to biocathode. It might due to external energy supply shifted the metabolic pathways from acetogenic energy conversion to direct electron uptake from high potential cathode or because of the excessive external energy at lower potential was more favored in SRB compared to acetate (Venzlaff et al., 2013). As a results, inorganic carbon was not in used causing the accumulation of inorganic carbon at lower applied potentials. However, cell yield is usually low in this system and the conversion to cell materials can be ignored. There was a 20–45% increase compared to fresh medium indicated a formation of organic carbon generated in the biocathode (data not shown). Interestingly organic carbon content from biocathode was higher compared to control with the same applied potential. While the potentials were low, the differential of the content was significant but start to converge when reaching −1.0 V which showing the shift of CO_2 to electron uptake dependent and favored the SRB instead of acetogens. However, there was no consistent pattern in inorganic carbon removal in controls. Standard reduction potential for hydrogen evolution at neutral pH is −0.41 V while acetate is higher around −0.28 V (Geelhoed et al., 2010; Rabaey and Rozendal, 2010; Lim et al., 2017). Due to thermodynamic considerations, hydrogen-producing biocathode not only produce hydrogen but they could promote acetate production as well. In our experiments, more negative potentials were used starting from −0.5 to −1.0 V and not only inducing abiotic reduction of bicarbonate to organic carbon but also hydrogen evolution. Nevertheless, the reduction potentials favored the biocathode compared to control because the rate of hydrogen production and current density were much higher in biocathode.

Figure 5F shows cathode efficiency and energy yield of biocathode under different applied potentials. The values of cathodic efficiency between control and biocathode were almost similar within the tested applied potentials. Nevertheless, significant difference was only observed below −0.8 V rising from 0 to about 40% at −1.0 V. The energy yield also showed the same trend as cathodic efficiency with dramatically rise below −0.8 V. However, the energy yield for biocathode (120%) was slightly higher than control (100%) at −1.0 V. The value of energy yield was more than 100% as the calculation taking account of external power rather than both anode and external power contributions (Lim et al., 2017). Besides, the experiments were focused on cathode reaction which were conducted in half-cell setup instead of whole cell causing inaccuracy in the calculation. Even though the values were overestimated, they provided quantitative comparisons between the control and biocathode.

Effects of Sulfate Concentration on Hydrogen Production

Figure 6A shows the effect of sulfate concentration to current density and hydrogen production rate at cathodic potential of −1.0 V. In the test, both peak hydrogen production rate and current density occurred at a sulfate concentration of 288 mg SO_4^{2-}/L. The peak hydrogen production rate and current density were 5.3 L/m^2/day and −0.81 A/m^2 respectively. Meanwhile the control remained almost stagnant throughout this test. Hydrogen production rate could be highly depended on the sulfate concentration due to fact that the sulfate might favor certain microorganisms like SRB. It is commonly known that high substrate concentration could limit or saturate metabolic reactions in living cells. The sulfate reduction in this case was limited by low sulfate concertation (< 288 mg SO_4^{2-}/L). The effect of sulfate inhibition began to observe after 288 mg SO_4^{2-}/L where the current density and hydrogen production rate started to plummet. At this stage, SRB would reduce sulfate preferentially over proton under unlimited bicarbonate source. Extra reducing power or lower cathodic potential was needed to support the reduction of sulfate. Therefore, the hydrogen production was disproportional to the sulfate concentration as more electrons are used to reduce sulfate rather than protons at high sulfate concentration. The present of sulfate is important for SRB to outcompete other anaerobes, including methanogens and fermentative bacteria in the anaerobic environments (Muyzer and Stams, 2008; Madigan et al., 2014). When the sulfate is quantitatively low, methanogens could dominant in the community. However, SRB could survive at very low amount of acetate as carbon source compared to the methanogens, and therefore, they will coexist with homoacetogens when acetate is not available (Singleton, 1993; Muyzer and Stams, 2008).

Figure 6B shows the cyclic voltammograms of the biocathode on the sulfate concentration. Based on the results, we believe sulfate could be considered as one of the key parameters in this study. It can be seen from the figure that the evolvement of specific catalytic peaks at −0.6 and −1.0 V was actually affected by the sulfate concentration. Both peaks were postulated catalyzing hydrogen oxidation and hydrogen evolution related to the species of sulfate-reducing bacteria (Aulenta et al., 2012; Lim et al., 2017). Moreover, significant hydrogen oxidation and reduction peaks were observed at 288 mg SO_4^{2-}/L. The oxidation

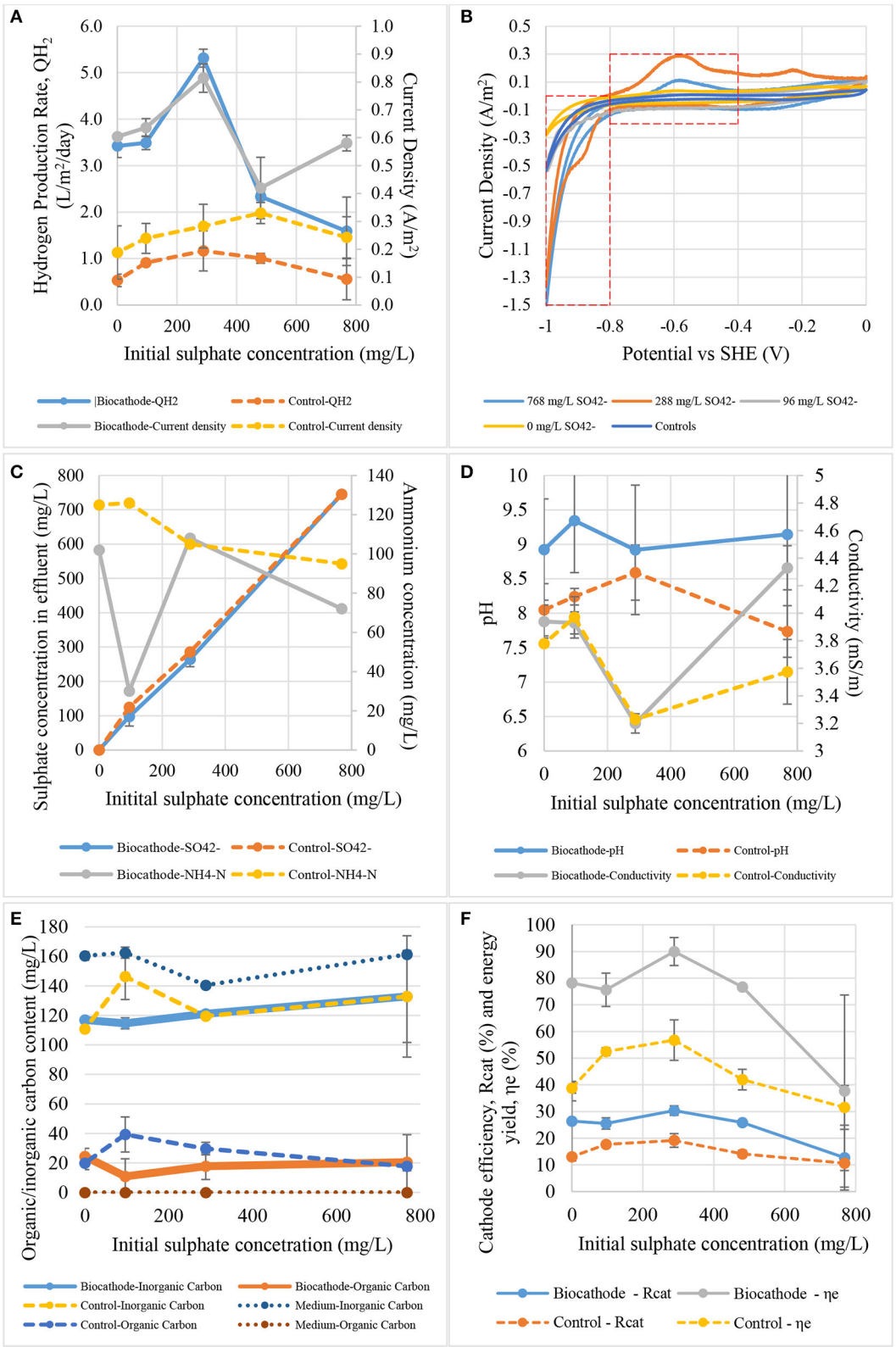

FIGURE 6 | The effect of initial sulfate concentration on: **(A)** hydrogen production rate and current density, **(B)** catalytic activity, **(C)** sulfate and ammonium contents, **(D)** pH and conductivity, **(E)** total carbon content, and **(F)** cathode efficiency and energy yield.

peak was believed to be related to reversible electrochemically active periplasm enzymes or proteins called hydrogenases. Hydrogenase can be found in many microorganisms included SRB, acetogens and methanogens and catalyze hydrogen production and/or utilization. The higher oxidation peak at 288 mg SO_4^{2-}/L was due to the increased hydrogenase content on the biocathode. In the cyclic voltammogram, the hydrogenases performed instant hydrogen oxidation around −0.6 V which was generated at −1.0 V when the applied potential moved from −1.0 to 0 V. The increases in hydrogenase activity was also supported by the evidence that the maximum hydrogen production rate was at the same sulfate concentration. Even though hydrogen catalysis (by comparing the CV tails at −1.0 V) was slightly higher at 768 compared to 288 mg SO_4^{2-}/L, the hydrogen oxidation peak at −0.6 V was not as high as at 288 mg SO_4^{2-}/L. This could be due to the substrate inhibition on the hydrogenases (Aulenta et al., 2012; Batlle-Vilanova et al., 2014). It was believed that this enzyme posed an on set potential at least at −0.6 V while an extra −0.4 V (standard reduction potential for hydrogen evolution) should be invested to produce hydrogen (Lim et al., 2017).

Figure 6C exhibits sulfate and ammonium concentration in the effluent depend on initial sulfate concentrations. Sulfate concentration as low as 96 mg/L was actually good for ammonium removal. It means that sulfate and ammonium should be presented in the same time but not in high concentrations for a better biocathode reactions. Ammonium was depleting faster at 96 mg SO_4^{2-}/L that the other concentrations and became a limiting factor to block the current and hydrogen production as shown in **Figure 6A**. Surprisingly, the current and hydrogen production rate reached a peak at 288 mg SO_4^{2-}/L but decrease after higher sulfate concentration. Substrate inhibition could be the main factor restricting the activities and not necessary for better hydrogen production as long as the sulfate was presented in the environments (Jeremiasse et al., 2012).

Ph and conductivity values were plotted relatively to sulfate concentration in **Figure 6D**. The pH increased in biocathode explains protons were utilized and removed from the catholyte to produce hydrogen. The biocathode pH fluctuated between 8.9 and 9.3 which was higher than initial medium pH around 7.0. However, the control pH was slightly lower than the biocathode pH with the value in between 7.7 and 8.6. The higher the pH values indicated that more protons were removed during reduction process and biocathode activity. At this point the pH values were increased remarkably from neutral to about 9.0. This means the added 50 mM phosphate buffer (PBS) in the medium wasn't the best option for controlling but managed to prevent a dramatically changes of pH. LaBelle et al. (2014) lowered catholyte pH to around 5.0 in order to increase hydrogen production in acetogen and SRB dominated mixed community. Acetogen domination in biocathode could be a problem as they ceased the production of hydrogen. Therefore, *Acetobacterium* dominated biocathode was controlled at certain level in repeatedly exposure to acidic condition to increase hydrogen production rate (LaBelle et al., 2014; LaBelle and May, 2017). Meanwhile, lower pH could also mean to provide more proton for hydrogen and acetate production. Surprisingly, conductivity values followed the trend of hydrogen production and current density. This is different from the effect of applied potentials where the conductivity and pH values did not change dramatically.

Figure 6E shows the inorganic/organic content relatively to sulfate concentration. The organic carbon content in control and biocathode effluent was remained almost the same without any significant different when the sulfate concentration was increased. The main purpose of this results was to notice any relevant connection between bicarbonate and sulfate roles in the biocathode. From the results, there was no clear connection between the tested parameter. Either bicarbonate or sulfate was required by two different community and no competitions was exist between them for sulfate and bicarbonate in the same time. The evidence concretes the idea that bicarbonate was necessary for some autotroph community in biocathode to produce organic carbons (Mohanakrishna et al., 2015). The organic carbons were then utilized by SRB to produce hydrogen with external reducing power for cathode (Jeremiasse et al., 2012; Zaybak et al., 2013).

Figure 6F shows the effects of sulphate concentration to hydrogen recovery efficiency and energy yield for biocathode and control. Overall, the efficiency and yield values of biocathode were higher than control and peaked at 288 mg SO_4^{2-}/L. The biocathode efficiency and energy yield were calculated as 30 and 90%, which are higher compared to the control that only achieved up to 20 and 56% at the peak. The biocathode energy yield dropped faster than the control might be due to the lower hydrogen production when large portion of supplied energy was utilised by the biocathode to reduce sulphate instead of proton. In contrast, low sulphate concentration (<288 mg SO_4^{2-}/L) limited the hydrogen production indicated sulphate is one of the important reactants or compounds for the biocathode in the proton reduction reaction.

Effects of Bicarbonate Content on Hydrogen Production

The effect of bicarbonate concentration to current density and hydrogen production rate is shown in **Figure 7A**. The bicarbonate test showed that a concentration of 610 mg HCO_3^-/L gave the maximum hydrogen production rate of 3.6 L/m^2/day and the maximum current density of −0.67 A/m^2. The control hydrogen production rate in this test was almost the same after 305 mg HCO_3^-/L. One of the speculation is that there is no biofilm was growth or attached on the surface of control cathode. Hence, the transportation of protons from bulk solution to control cathode surface was faster than in biocathode. Abiotic hydrogen production rate was remained stagnant at 3.6 L/m^2/day after 305 mg HCO_3^-/L. Meanwhile, hydrogen production in biocathode peaked at 305 mg HCO_3^-/L with the production rate equal to 3.6 L/m^2/day.

Figure 7B shows the cyclic voltammograms of the biocathode in different bicarbonate concentrations. Low bicarbonate concentration (61 and 183 mg HCO_3^-/L) was actually good for biocathode catalytic activity as they induced the highest hydrogen oxidation peak. However, only 610 mg/L HCO_3^-/L

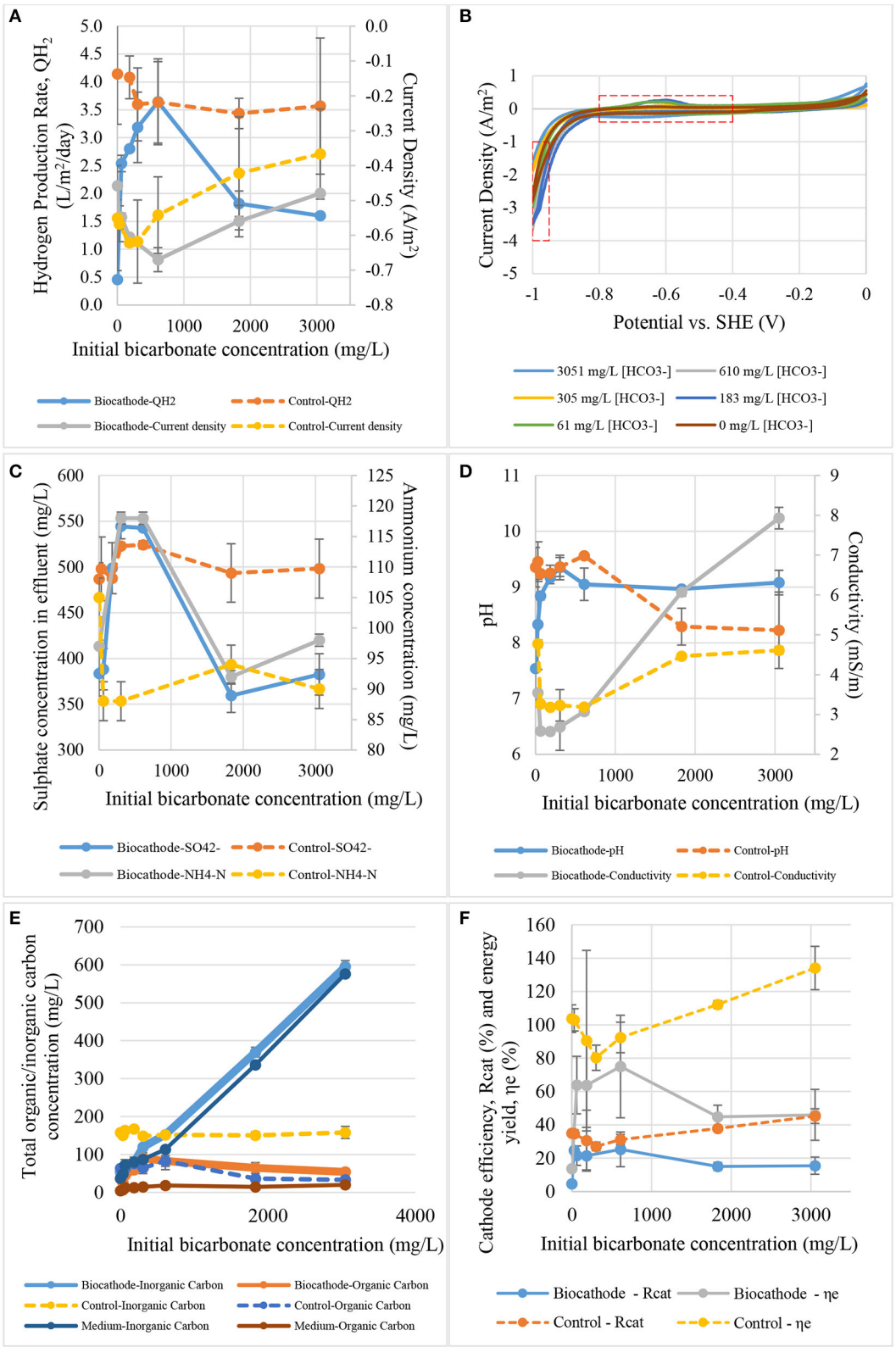

FIGURE 7 | The effect of initial bicarbonate concentration on: **(A)** hydrogen production rate and current density, **(B)** catalytic activity, **(C)** sulfate and ammonium contents, **(D)** pH and conductivity, **(E)** total carbon content, and **(F)** cathode efficiency and energy yield.

promoted the highest hydrogen production rate and current density as shown in **Figure 7A**. If the interaction of microbial community in the biocathode was true, acetogens that produced short-chain fatty acids for the hydrogen producing bacteria could be saturated with the inorganic carbon concentration at 610 mg HCO_3^-/L or higher (Su et al., 2013; LaBelle and May, 2017). Maximum fatty acid was converted at this concentration. Thus, the hydrogen production rate and current density were the highest at this bicarbonate concentration. Higher catalytic activity at −0.6 V did not necessary means it could promote high hydrogen evolution and the interaction of biocathode microbes should be taking into consideration.

Figure 7C illustrates the profile of effluent sulfate and ammonium concentration to initial sulfate concentration. Bicarbonate worked as carbon source is crucial to support biocathode growth. The quantity could affect sulfate and ammonium removal especially at 610 mg HCO_3^-/L. The value is the optimum concentration because it gave the maximum current and hydrogen production. As we could see in **Figure 7C** the sulfate removal in biocathode was gone up at low bicarbonate concentration but decreased after reaching the peak. It was revealed that either the fixed sulfate concentration was not sufficient to support the rate of biocathode activities when bicarbonate concentration was high. More sulfate was required for the reactions.

The effect of bicarbonate to pH and conductivity value is presented in **Figure 7D**. Carbonate species could act as buffer system to maintain the pH as observed in control. The pH was maintained after 1,831 mg HCO_3^-/L. For the biocathode, bacterial growth in biofilm usually is much lower than free-living bacteria and cell yield is low in anaerobic bacteria. These mean that the effects of carbonate might not be related to the bacterial growth. Therefore, the hydrogen production rate between control and biocathode was not significantly different between each other. The only comparable performance was the current density where the biocathode required lower energy that the control. About 0.15 A/m^2 different between both control and biocathode after 305 mg HCO_3^-/L. Second explanation is that at least two biotic steps was need to produce hydrogen. As we known that SRB which responsible for the hydrogen production are chemoorganotrophs and could not use inorganic carbon to growth (Muyzer and Stams, 2008). Therefore, autotrophic acetogens become important to in the community to produce acetate from bicarbonate which in turn consumed by SRB. Some literature also suggested that the hydrogen and acetate production were coexistent in hydrogen-producing biocathode (Su et al., 2013; LaBelle et al., 2014; LaBelle and May, 2017). In additional to the PBS, Liang et al. (2014) suggested that bicarbonate could also enhances electric migration of proton when more H^+ was release from HCO_3^- and accelerated hydrogen evolution. This explained why the conductivity was getting lower at peak hydrogen production rate. Bicarbonate may contribute to the conductivity values. Catalytic activity of hydrogen production could actually utilized the proton and CO_2 derived from HCO_3^-, driving the conductivity value low as HCO_3^- was consumed.

Figure 7E shows the inorganic/organic carbon conversion from different bicarbonate concentration. Bicarbonate concentration was increased constantly to monitor the effect on the biocathode. Organic carbon concentration increased until it reached a peak at 305 mg HCO_3^-/L. The bicarbonate was essential in this study as a carbon source for microbial growth (Luo et al., 2014; Jourdin et al., 2015; Mohanakrishna et al., 2016). Hydrogen production also reached a maximum point at this concentration. This postulated that possibly of carbonates consumed by autotrophs such as acetogens to produce organic carbons which in turn used by SRB to produce hydrogen. Once the bicarbonate concentration excess 305 mg HCO_3^-/L, the hydrogen production rate dropped dramatically as shown in **Figure 7A**. Substrate inhibition may occurred within the biofilm when acetogens produce excessive organics carbons and decrease hydrogen production in SRB (Croese et al., 2014; Bajracharya et al., 2017; LaBelle and May, 2017). On one hand, organic carbons content and removal in biocathode seems to peak at 305 mg HCO_3^-/L which is proportional to hydrogen production rate. On the other hand, the organic carbon content and removal in control were remarkably lower compared to the biocathode. The trend of changing was negligible and lightly shifted relative to the bicarbonate concentrations.

Figure 7F presents the effects of bicarbonate concentration to hydrogen recovery efficiency and energy yield for biocathode and control. Surprisingly, both efficiency and yield values for biocathode were lower than control. Higher bicarbonate concentration did not assist the biocathode in hydrogen production. Instead, the efficiency and yield decreased after the bicarbonate concentration was more than 610 mg HCO_3^-/L. This is because higher bicarbonate concentration could inhibit the biocathode reaction activities as discussed in the paragraphs above. Meanwhile, the efficiency and yield values increased proportional to bicarbonate concentration in abiotic control probably of the buffering properties of bicarbonate (Liang et al., 2014).

Bottlenecks and Beneficial Applications of Hydrogen-Producing Biocathode

It is believed that microbial community in hydrogen-producing biocathode should contain key enzyme, hydrogenases in order to catalyst hydrogen evolution from protons (Geelhoed et al., 2010; Croese et al., 2011; Rosenbaum et al., 2011; Jourdin et al., 2015; Kim et al., 2015). Sulfate-reducing bacteria (SRB) belong to *Desulfovibrio* sp. was then found abundant in the biocathode which contain active hydrogenase enzymes in its cytoplasm and periplasm (Croese et al., 2014). According to the conventional information, SRB poses energy conservation mechanism called hydrogen cycling mechanism in sulfate reduction (Kim and Gadd, 2008; Madigan et al., 2014). The mechanism happens in anaerobic condition by oxidizing organic compounds like lactate and ethanol as electron donors for sulfate reduction. However, there was no organic matter only inorganic carbon like carbonates introduced to hydrogen-producing biocathode. To replace the organic matter, external energy source was required to provide the reducing power to the biocathode. In our study,

it was found that at least −0.8 V vs. SHE was required to make the biocathode feasible for hydrogen evolution (**Figure 5A**). The potentials provided sufficient exergonic energy to overcome overpotentials in the system and to facilitate electron transfer from electrode to electrochemically-active microbes. These microbes normally contain membrane-bound complexes such as cytochrome C, Fe-S protein, oxidoreductase and periplasm enzymes that could receive the electrons (Choi and Sang, 2016). As a result, the microbes could perform the metabolic process and initialize the electron transport-chain reactions and generate hydrogen included trace amount of organic carbon.

From thermodynamic point of view, standard reduction potential, $E^{\circ\prime}$ for hydrogen evolution from proton, H^+/H_2 is −0.41 V at neutral pH. In real case scenario, potentials lower than this value were normally applied to biocathode to overcome overpotential and activation loss (Rozendal et al., 2008; Aulenta et al., 2012; Batlle-Vilanova et al., 2014; Jourdin et al., 2015; Lim et al., 2017). In additional to the proton reduction under energy conserving hydrogenases in *Desulfovibrio* sp. respiration, sulfate is also an important element as final terminal electron acceptor. The $E^{\circ\prime}$ of SO_4^{2-}/H_2S is −0.35 V which the potential is slightly higher than reduction of protons to hydrogen [$E^{\circ\prime}$ SO_4^{2-}/H_2S −0.35 V is calculated based on $E^{\circ\prime}$ SO_4^{2-}/HSO_3^- −0.52 V and $E^{\circ\prime}$ SO_3^{2-}/H_2S −0.17 V] (Madigan et al., 2014). Sulfate reduction will be dominated in the present of high sulfate concertation as less energy is required and causing less hydrogen evolution. Even in real environmental concentration is considered, the couple of H^+/H_2 is still more negative than SO_4^{2-}/HS^- ($E^{\circ\prime}$ of H^+/H_2 is −0.27 V at 1 Pa of H_2 and SO_4^{2-}/HS^- is −0.20 V at 0.1 mM HS^-; Keller and Wall, 2011). In recent development, it has been proven that the potentials required of bioelectrochemically hydrogen evolution is lower than sulfate reduction (Luo et al., 2014; Zheng et al., 2014). Under fed-batch mode,the cathode potentials for sulfate reduction ranged between −0.6 to −1.0 V (Luo et al., 2014). Meanwhile, significant hydrogen evolution potentials were around −0.8 to −1.2 V (Aulenta et al., 2012; Batlle-Vilanova et al., 2014; Lim et al., 2017). Slightly more positive potential around −0.7 V were also used to generate hydrogen from biocathode but under a feed-controlled system in the anode and cathode. The purpose of the system is to eliminate mass transport limitation and overpotential losses that occurred in a batch system (Rozendal et al., 2008; Jeremiasse et al., 2010).

In this study, it is interesting to show that bioelectrochemically hydrogen production was sulfate-dependent. The hydrogen production rate was recorded by varying the cathode potentials, sulfate and bicarbonate concentrations as shown in this study. In spite of that, operational potentials have been well studied in hydrogen-producing biocathode and are predictable using the thermodynamic information (Geelhoed et al., 2010; Keller and Wall, 2011; Jafary et al., 2015; Choi and Sang, 2016). In addition to the potential, carbonate concentration might not literally affected by the BES performance in this study. This is because of anaerobic bacteria normally grow slowly on biocathode compared to free-living bacteria or in aerobic condition (Kim and Gadd, 2008; Madigan et al., 2014). SRB are chemolithotrophic bacteria that required organic matters like acetate to growth. Some studies reported the requirement of organic matter in hydrogen-producing biocathode by adding acetate in carbonate-containing medium (Liu et al., 2005; Jeremiasse et al., 2012; LaBelle et al., 2014). It is suspected that this bacteria actually live syntrophically with acetogens which are autotrophs. The growth of these autotrophs were even lower if they involved in the biocathode activities such as acetogens and the accumulation of biomass would be redundant (Su et al., 2013; Mand et al., 2014). Jeremiasse et al. (2012) tried to test the acetate and sulfate effects on hydrogen-producing biocathode by feeding the medium with and without acetate or sulfate. It is interesting to point out that the current density supplied to the system was slightly lower at the beginning for sulfate-fed biocathode but overtook the control biocathode after 20 days (Jeremiasse et al., 2012). Based on this reason, it is believed that electron bifurcation couple process occurred from both protons and sulfate reduction simultaneously. Electron bifurcation has been emerged and recognized as the third important biological energy conservation mechanism in the last decades after the two fundamental mechanisms, substrate level phosphorylation and electron transport-linked phosphorylation were unable to explain thermodynamically unfavorable reactions (Buckel and Thauer, 2013; Peters et al., 2016).

In the review, Keller and Wall (2011) claimed that *Desulfovibrio* sp. produce hydrogen during sulfate reduction with ethanol. This involves electron bifurcation and *Desulfovibrio* sp. have energy conserving hydrogenases As *Desulfovibrio* sp. oxidize ethanol reducing NAD^+ to NADH ($E^{\circ\prime} = -0.320$ V), NADH is bifurcated to reduce sulfate and proton (Ramos et al., 2015). In the paper, Ramos et al. (2015) found hdrCBA-flxDCBA gene cluster is presented in many different phyla including electrochemically active microbes, *Desulfovibrio* sp. and *Geobacter* sp. This gene is responsible for transcribing flavin oxidoreductase (FlxABCD) and heterodisulfide reductase (HdrABC) to perform flavin-based electron bifurcation (FBEB). Both enzymes are involved in producing reducing carriers for hydrogen evolution and sulfate reduction. Proton reduction to hydrogen is catalyzed by energy-conserving hydrogenase with the reducing carriers. It is hypothesized that at low cathode potential sulfate is reduced without hydrogen production, and if hydrogen is produced it is not sulfate-dependent. When the cathode potential was not low enough to reduce proton, electrons were bifurcated reducing both high and low redox potential electron carriers. The former is used to reduce sulfate and the latter to reduce proton conserving in both reduction reactions. Based on these facts, it is believed that hydrogen production would be inhibited in the presence of sulfate or sulfate-dependent because SRB conserve more energy reducing sulfate than reducing proton as shown in **Figure 6**. **Figure 8** describes the possible electron bifurcation flow for SRB growth on cathode used to reduce proton and sulfate. Lower sulfate concentration is actually good for SRB respiration (<288 mg/L) and promoted proton reduction. The hydrogen evolution decrease dramatically when more sulfate was added (>288 mg/L) as more electrons were utilized by reducing sulfate instead of protons.

Last but not least, the finding of the sulfate-dependent hydrogen-producing biocathode has raised the question; what type of wastewaters can be treated by using this technology?

The sulfate dependency was due to the SRB domination in the biocathode and a specific range of sulfate concentration was required to maintain the balance and functionality of the biocathode to produce hydrogen while reducing sulfate. Domestic wastewater usually contain low amount of sulfate between 20 and 60 mg/L, although the concentration can be

A

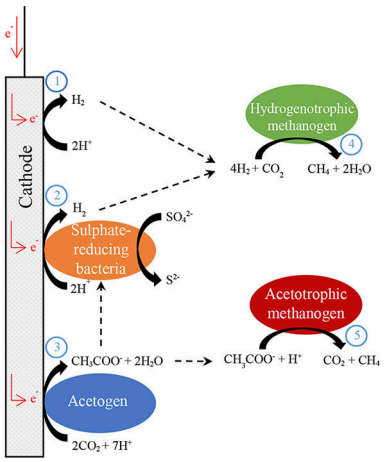

Legend:
Catalytic reaction either occurred at periplasm, cytoplasm, or electrode surface
End product is consumed by
Electron flow

Mechanism	Mass balance	Potential vs. SHE (V)	Reaction type
1	$2H^+ + 2e^- \rightarrow H_2$ (Abiotic H_2 production)	- 0.41	Electrochemical
2	$2H^+ + 2e^- \rightarrow H_2$ $CH_3COO^- + 4H_2O \rightarrow 2HCO_3^- + 9H^+ + 8e^-$ $SO_4^{2-} + 6H^+ + 8e^- \rightarrow S^{2-} + 2OH^- + 2H_2O$ (Biotic H_2 production; acetate and low potential are served as carbon source and reducing power while sulphate is utilised as final electron acceptor in SRB)	- 0.41 +0.28 - 0.35	Bioelectrochemical
3	$2HCO_3^- + 9H^+ + 8e^- \rightarrow CH_3COO^- + 4H_2O$ (Biotic organic carbon production)	- 0.28	Bioelectrochemical
4	$HCO_3^- + 4H_2 + H^+ \rightarrow CH_4 + 3H_2O$ (Hydrogen is consumed by methanogens)	Not available	Biochemical
5	$CH_3COO^- + H_2O \rightarrow CH_4 + HCO_3^-$ (Acetate is consumed by methanogens)	Not available	Biochemical

B

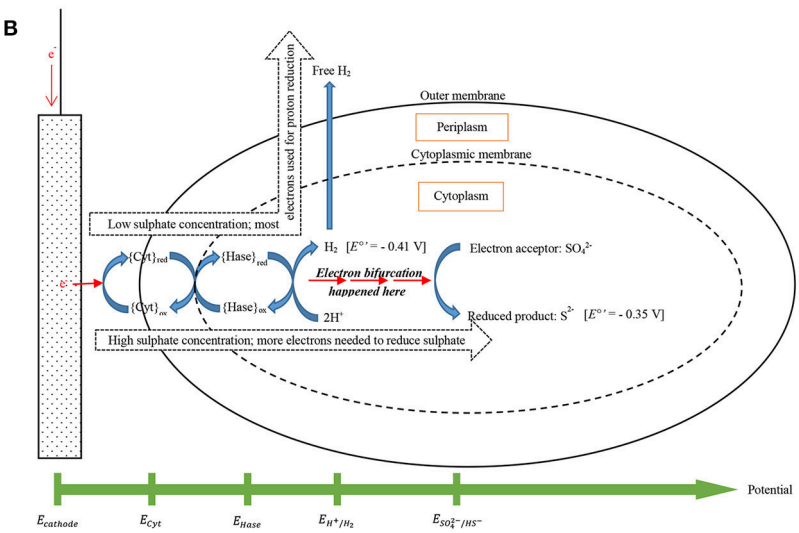

FIGURE 8 | (A) Proposed electron flow and possible final destinations of the supplied electrons being utilized in producing various end products (modified after Mand et al., 2014), **(B)** description of electron bifurcation flow in sulfate-reducing bacteria-dominated biocathode to generate hydrogen and reduce sulfate.

up to 500 mg/L for industrial wastewater (Lens et al., 1998; Moussa et al., 2006). Conventional sulfate removal technology benefits from the presence of SRB to treat domestic and industrial wastewaters. The benefits include reducing sludge accumulation and pathogen content (if present), removing heavy metals and as anaerobic digestion pre-treatment (van den Brand et al., 2015). In the present study, an "optimum" sulfate concentration was 288 mg/L which generated the maximum hydrogen volume. It is recommended to use domestic wastewater to enrich and maintain a hydrogen-producing biocathode, because low amounts of organic compounds and sulfate make it a better medium to enhance the growth of SRB. (Jeremiasse et al., 2012; Lee et al., 2014).

Drawbacks on Low Potential, Mass Transport Limitation and Long Term Operation

At the end of experiments, white precipitations could be observed from cathodic chamber (**Figure 9A**). The precipitated compounds were attached along with biomass on the surface of cathode and caused the biocathode performance drop over time. We believe the precipitations that crystallized on the cathode surface was a form of alkali phosphates due to low reduction potentials (Jeremiasse et al., 2010). Moreover, recycle flow was connected between outlet and inlet in order to reduce mass transport limitation between bulk solution and the biocathode. **Figure 9B** shows the relationship between current density and the flow rate. Four flow rates were used to test the mass transport limitation: 0, 2.8, 7.1, and 11.4 mL/min. When zero flow rate was applied to the chamber, the current density reduced significantly. Flow rate 7.1 mL/min was selected to use in the experiments as it generated almost similar current density compared to the higher flow rate 11.4 mL/min.

The risk of enriched biocathode contaminated by methanogens under a hydrogen-rich environment after a long time operation have been previously reported (Wagner et al., 2009; Kyazze et al., 2010; van Eerten-Jansen et al., 2015; Bajracharya et al., 2017). **Figure 10A** shows performance dropped when methane was first detected

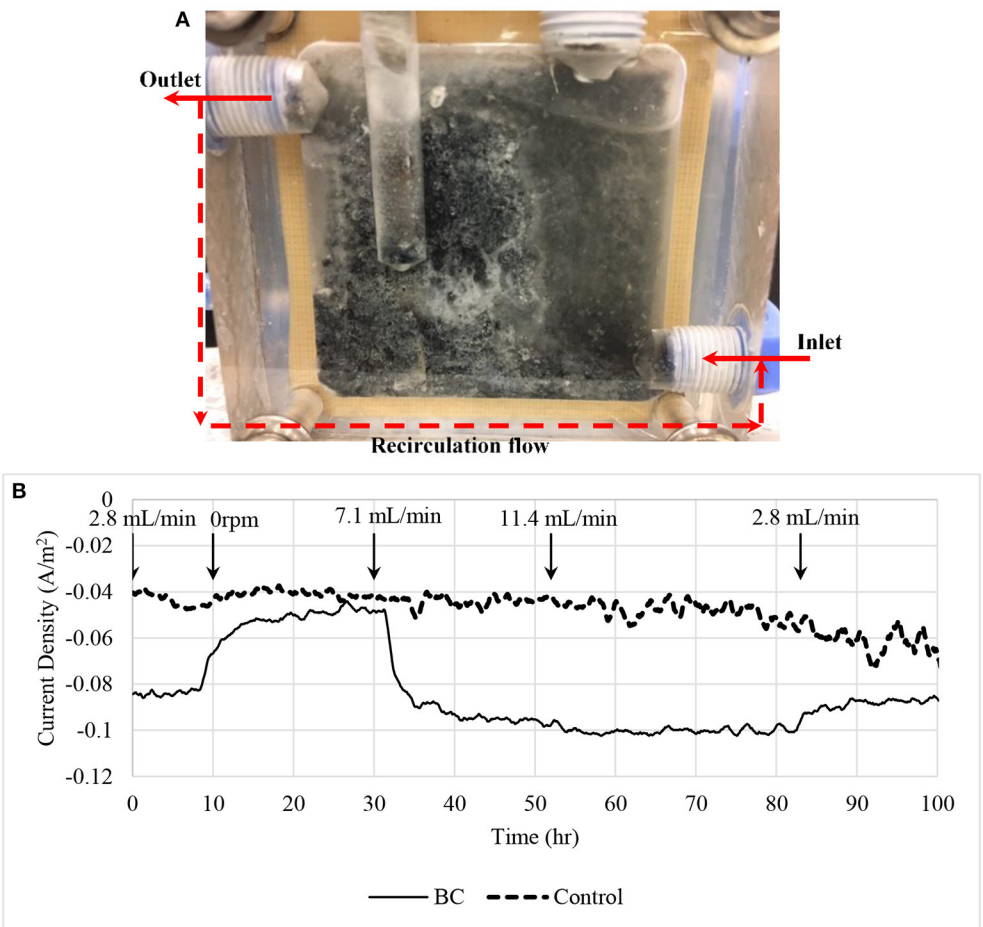

FIGURE 9 | (A) Biocathode after the experiments. White crystallization and black biomass were appeared on the surface of the electrode causing current density dropped. **(B)** Current density affected by mass transport limitation. A recirculation flow line was connected between inlet and outlet to recycle the catholyte in order to reduce the mass transfer limitation. A control using 7.1 mL/min recycle flow rate was included in the figure for comparison purpose.

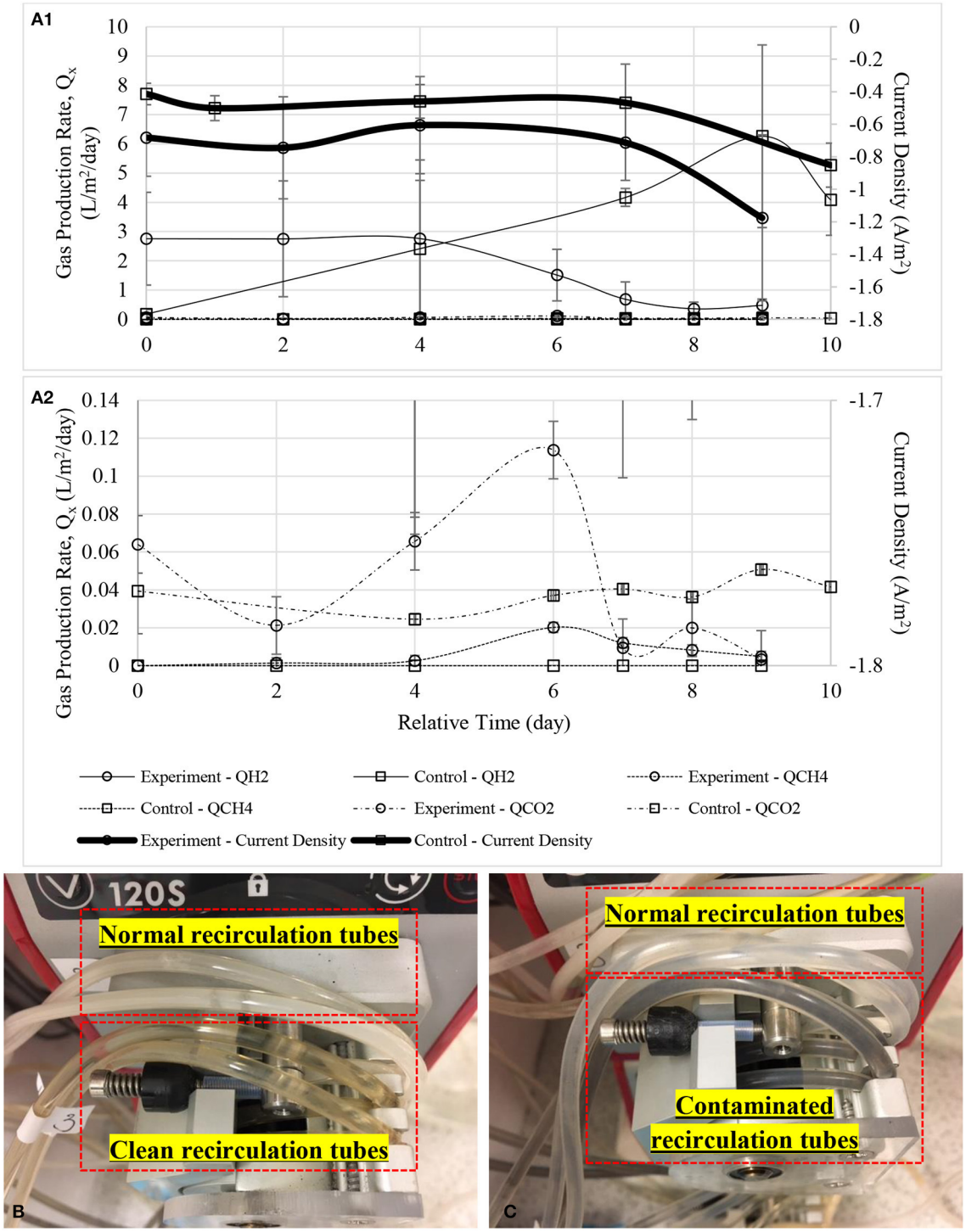

FIGURE 10 | (A1) Gas production rate of the defected MECs with a zoom-in figure **(A2)**. Noted that hydrogen production dropped dramatically even when CH_4 was first detected at a very low concentration at day 6. Small amount of bicarbonate was probably released as CO_2 or consumed by methanogens. Timeline was adjusted to zero for comparison purpose. **(B)** Upper tubes show white biofilm grew on the inner surface of the tubes while lower tubes were after cleaned and soaked with disinfectant, Virkon, and **(C)** upper tubes were the normal biocathode recirculation tubes while black color biofilm was observed in the lower tubes when methane started to detect in gas samples.

in biocathode after 120 days of operation (further data not shown). Hydrogen production dropped remarkably after methane was detected in the biocathode at day 4. Current demand was also increased as more energy was required to support both hydrogen and methane production. **Figure 10B** shows the clean and normal recirculation tubes while **Figure 10C** shows the comparison between the normal and contaminated recirculation tubes when methane was first detected.

CONCLUSION

This study revealed that applied potential, sulfate and inorganic carbon are vital parameters to promote hydrogen production in a biocathode of electrolysis cell. The optimum ratio of PBS: HCO_3^-: NH_4^+: SO_4^{2-} in this study was determined as 950:610:90:288 mg/L (10:10:5:3 mM) for a biocathode sized 0.005 m^2, operation volume 0.0025 m^3 and applied potential −1.0 V vs. SHE in a continuous flow rate 0.1 mL/min. The information provided the first insight of how much carbon, nitrogen and sulfate sources that must be presented in the influent in order to provide better operational conditions. Even though the ratio may slightly vary according to the size of reactor, cell configuration and controlling system, the basic principle of how a biocathode catalyzes hydrogen under the influences of those main sources would still remain the same. Besides the ratio, external power supply was required to provide initial energy under low potential electrons to start the biocathode catalytic activity while sulfate served as final terminal electron acceptor to dispose the exhausted electrons. Inorganic carbon in the form of carbonates was added to the influent and worked as carbon backbone to support the growth of biocathode community. As organic carbon compounds were found in the biocathode effluents, it is believed that within the microbial community the inorganic carbon was consumed by acetogens to produce organic carbons such as acetate and then consumed by SRB as carbon source. Another significant finding is the present and quantity of sulfate did affect the hydrogen production in SRB-dominated biocathode. At high sulfate concentration, it could inhibit hydrogen production if the cathode potential was not low enough to reduce both sulfate and proton. The phenomena is similar to those electron bifurcation.

SUPPLEMENTARY DATA STATEMENT

Data supporting this publication is openly available under an 'Open Data Commons Open Database License'. (Lim et al., 2018) Additional metadata are available at: https://doi.org/10.17634/150659-2. Please contact Newcastle Research Data Service at rdm@ncl.ac.uk for access instructions.

AUTHOR CONTRIBUTIONS

SL carried out the experiment and wrote the manuscript with support from EY and KS. BK conceived the original idea and suggested on the experiment framework. All authors provided critical feedback and helped shape the research, analysis and manuscript.

ACKNOWLEDGMENTS

This research was financially supported by EPSRC (EP/N009746/1), NERC (NE/L01422X/1), The International Cooperating Project between China and European Union (2014DFE90110) and UKIERI Department of Science & Technology Partnerships (2014-15 S. No. 16). SL was sponsored by Skim Latihan Akedemik IPTA (SLAI) under the Malaysian Ministry of Education (MoE).

REFERENCES

Aulenta, F., Catapano, L., Snip, L., Villano, M., and Majone, M. (2012). Linking bacterial metabolism to graphite cathodes: electrochemical insights into the H2-producing capability of *Desulfovibrio* sp. *ChemSusChem* 5, 1080–1085. doi: 10.1002/cssc.201100720

Bajracharya, S., Yuliasni, R., Vanbroekhoven, K., Buisman, C. J., Strik, D. P., and Pant, D. (2017). Long-term operation of microbial electrosynthesis cell reducing CO2 to multi-carbon chemicals with a mixed culture avoiding methanogenesis. *Bioelectrochemistry* 113, 26–34. doi: 10.1016/j.bioelechem.2016.09.001

Bar-Even, A. (2013). Does acetogenesis really require especially low reduction potential? *Biochim. Biophys. Acta* 1827, 395–400. doi: 10.1016/j.bbabio.2012.10.007

Batlle-Vilanova, P., Puig, S., Gonzalez-Olmos, R., Vilajeliu-Pons, A., Bañeras, L., Balaguer, M. D., et al. (2014). Assessment of biotic and abiotic graphite cathodes for hydrogen production in microbial electrolysis cells. *Int. J. Hydrogen Energy* 39, 1297–1305. doi: 10.1016/j.ijhydene.2013.11.017

Blanchet, E., Duquenne, F., Rafrafi, Y., Etcheverry, L., Erable, B., and Bergel, A. (2015). Importance of the hydrogen route in up-scaling electrosynthesis for microbial CO2 reduction. *Energy Environ. Sci.* 8, 3731–3744. doi: 10.1039/C5EE03088A

Buckel, W., and Thauer, R. K. (2013). Energy conservation via electron bifurcating ferredoxin reduction and proton/Na+ translocating ferredoxin oxidation. *Biochim. Biophys. Acta* 1827, 94–113. doi: 10.1016/j.bbabio.2012.07.002

Choi, O., and Sang, B. I. (2016). Extracellular electron transfer from cathode to microbes: application for biofuel production. *Biotechnol. Biofuels* 9:11. doi: 10.1186/s13068-016-0426-0

Croese, E., Jeremiasse, A. W., Marshall, I. P., Spormann, A. M., Euverink, G.-J. W., Geelhoed, J. S., et al. (2014). Influence of setup and carbon source on the bacterial community of biocathodes in microbial electrolysis cells. *Enzyme Microbial Technol.* 61–62, 67–75. doi: 10.1016/j.enzmictec.2014.04.019

Croese, E., Pereira, M. A., Euverink, G. J., Stams, A. J., and Geelhoed, J. S. (2011). Analysis of the microbial community of the biocathode of a hydrogen-producing microbial electrolysis cell. *Appl. Microbiol. Biotechnol.* 92, 1083–1093. doi: 10.1007/s00253-011-3583-x

Geelhoed, J. S., Hamelers, H. V., and Stams, A. J. (2010). Electricity-mediated biological hydrogen production. *Curr. Opin. Microbiol.* 13, 307–315. doi: 10.1016/j.mib.2010.02.002

Jafary, T., Daud, W. R. W., Ghasemi, M., Kim, B. H., Md Jahim, J., Ismail, M., et al. (2015).. Biocathode in microbial electrolysis cell; present status and future prospects. *Renewable and Sustain. Energy Rev.* 47, 23–33. doi: 10.1016/j.rser.2015.03.003

Jeremiasse, A. W., Hamelers, H. V., and Buisman, C. J. (2010). Microbial electrolysis cell with a microbial biocathode. *Bioelectrochemistry* 78, 39–43. doi: 10.1016/j.bioelechem.2009.05.005

Jeremiasse, A. W., Hamelers, H. V. M., Croese, E., and Buisman, C. J. N. (2012). Acetate enhances startup of a H2-producing microbial biocathode. *Biotechnol. Bioeng.* 109, 657–664. doi: 10.1002/bit.24338

Jourdin, L., Freguia, S., Donose, B. C., and Keller, J. (2015). Autotrophic hydrogen-producing biofilm growth sustained by a cathode as the sole electron and energy source. *Bioelectrochemistry* 102, 56–63. doi: 10.1016/j.bioelechem.2014.12.001

Keller, K., and Wall, J. (2011). Genetics and molecular biology of the electron flow for sulfate respiration in desulfovibrio. *Front. Microbiol.* 2:135. doi: 10.3389/fmicb.2011.00135

Kim, B. H., and Gadd, G. M. (2008). *Bacterial Physiology and Metabolism*. New York, NY: Cambridge University Press.

Kim, B. H., Lim, S. S., Daud, W. R. W., Gadd, G. M., and Chang, I. S. (2015). The biocathode of microbial electrochemical systems and microbially-influenced corrosion. *Bioresour. Technol.* 190, 395–401. doi: 10.1016/j.biortech.2015.04.084

Kyazze, G., Popov, A., Dinsdale, R., Esteves, S., Hawkes, F., Premier, G., et al. (2010). Influence of catholyte pH and temperature on hydrogen production from acetate using a two chamber concentric tubular microbial electrolysis cell. *Int. J. Hydrogen Energy* 35, 7716–7722. doi: 10.1016/j.ijhydene.2010.05.036

LaBelle, E. V., Marshall, C. W., Gilbert, J. A., and May, H. D. (2014). Influence of acidic pH on hydrogen and acetate production by an electrosynthetic microbiome. *PLoS ONE* 9:e109935. doi: 10.1371/journal.pone.0109935

LaBelle, E. V., and May, H. D. (2017). Energy efficiency and productivity enhancement of microbial electrosynthesis of acetate. *Front. Microbiol.* 8:756. doi: 10.3389/fmicb.2017.00756

Lee, D. J., Liu, X., and Weng, H. L. (2014). Sulfate and organic carbon removal by microbial fuel cell with sulfate-reducing bacteria and sulfide-oxidising bacteria anodic biofilm. *Bioresour. Technol.* 156, 14–19. doi: 10.1016/j.biortech.2013.12.129

Lens, P. N. L., Visser, A., Janssen, A. J. H., Pol, L. W. H., and Lettinga, G. (1998). Biotechnological treatment of sulfate-rich wastewaters. *Crit. Rev. Environ. Sci. Technol.* 28, 41–88. doi: 10.1080/10643389891254160

Liang, D., Liu, Y., Peng, S., Lan, F., Lu, S., and Xiang, Y. (2014). Effects of bicarbonate and cathode potential on hydrogen production in a biocathode electrolysis cell. *Front. Environ. Sci. Eng.* 8, 624–630. doi: 10.1007/s11783-013-0584-2

Lim, S. S., Scott, K., Yu, E., Kim, B. H., and Daud, W. R. W. (2018). *Experimental Data of a Hydrogen-Producing Biocathode to the Responses of Applied Potential and Reactants in a Microbial Electrolysis Cell*. Newcastle University.

Lim, S. S., Yu, E. H., Daud, W. R. W., Kim, B. H., and Scott, K. (2017). Bioanode as a limiting factor to biocathode performance in microbial electrolysis cells. *Bioresour. Technol.* 238, 313–324. doi: 10.1016/j.biortech.2017.03.127

Liu, H., Grot, S., and Logan, B. E. (2005). Electrochemically assisted microbial production of hydrogen from acetate. *Environ. Sci. Technol.* 39, 4317–4320. doi: 10.1021/es050244p

Luo, H., Fu, S., Liu, G., Zhang, R., Bai, Y., and Luo, X. (2014).. Autotrophic biocathode for high efficient sulfate reduction in microbial electrolysis cells. *Bioresour. Technol.* 167, 462–468. doi: 10.1016/j.biortech.2014.06.058

Madigan, M. T., Martinko, J. M., Bender, K. S., Buckley, D. H., Stahl, D. A., and Brock, T. (2014). *Brock Biology of Microorganisms.* London: Pearson.

Mand, J., Park, H. S., Jack, T. R., and Voordouw, G., (2014). The role of acetogens in microbially influenced corrosion of steel. *Front. Microbiol.* 5:268. doi: 10.3389/fmicb.2014.00268

Marshall, C. W., Ross, D. E., Fichot, E. B., Norman, R. S., and May, H. D. (2012). Electrosynthesis of commodity chemicals by an autotrophic microbial community. *Appl. Environ. Microbiol.* 78, 8412–8420. doi: 10.1128/AEM.02401-12

Mohanakrishna, G., Seelam, J. S., Vanbroekhoven, K., and Pant, D. (2015). An enriched electroactive homoacetogenic biocathode for the microbial electrosynthesis of acetate through carbon dioxide reduction. *Faraday Discuss.* 183, 445–462. doi: 10.1039/C5FD00041F

Mohanakrishna, G., Vanbroekhoven, K., and Pant, D. (2016). Imperative role of applied potential and inorganic carbon source on acetate production through microbial electrosynthesis. *J. CO2 Utiliz.* 15, 57–64. doi: 10.1016/j.jcou.2016.03.003

Moussa, M. S., Fuentes, O. G., Lubberding, H. J., Hooijmans, C. M., van Loosdrecht, M. C. M., and Gijzen, H. J. (2006). Nitrification activities in full-scale treatment plants with varying salt loads. *Environ. Technol.* 27, 635–643. doi: 10.1080/09593332708618673

Muyzer, G., and Stams, A. J. (2008). The ecology and biotechnology of sulphate-reducing bacteria. *Nat. Rev. Micro.* 6, 441–454. doi: 10.1038/nrmicro1892

Patil, S. A., Arends, J. B. A., Vanwonterghem, I., van Meerbergen, J., Guo, K., Tyson, G. W., et al. (2015). Selective enrichment establishes a stable performing community for microbial electrosynthesis of acetate from CO_2. *Environ. Sci. Technol.* 49, 8833–8843. doi: 10.1021/es506149d

Peters, J. W., Miller, A. F., Jones, A. K., King, P. W., and Adams, M. W. (2016). Electron bifurcation. *Curr. Opin. Chem. Biol.* 31, 146–152. doi: 10.1016/j.cbpa.2016.03.007

Rabaey, K., and Rozendal, R. A. (2010). Microbial electrosynthesis — revisiting the electrical route for microbial production. *Nat. Rev. Micro.* 8, 706–716. doi: 10.1038/nrmicro2422

Ramos, A. R., Grein, F., Oliveira, G. P., Venceslau, S. S., Keller, K. L., Wall, J. D., et al. (2015). The FlxABCD-HdrABC proteins correspond to a novel NADH dehydrogenase/heterodisulfide reductase widespread in anaerobic bacteria and involved in ethanol metabolism in Desulfovibrio vulgaris Hildenborough. *Environ. Microbiol.* 17, 2288–2305. doi: 10.1111/1462-2920.12689

Rosenbaum, M., Aulenta, F., Villano, M., and Angenent, L. T. (2011). Cathodes as electron donors for microbial metabolism: Which extracellular electron transfer mechanisms are involved? *Bioresour. Technol.* 102, 324–333. doi: 10.1016/j.biortech.2010.07.008

Rozendal, R. A., Jeremiasse, A. W., Hamelers, H. V. M., and Buisman, C. J. N. (2008). Hydrogen production with a microbial biocathode. *Environ. Sci. Technol.* 42, 629–634. doi: 10.1021/es071720+

Schuchmann, K., and Muller, V. (2014). Autotrophy at the thermodynamic limit of life: a model for energy conservation in acetogenic bacteria. *Nat. Rev. Micro.* 12, 809–821. doi: 10.1038/nrmicro3365

Singleton, R. J. (1993). *The Sulfate-Reducing Bacteria*. Contemporary Perspectives. New York, NY: Springer.

Spurr, M. W. A. (2016). *Microbial Fuel Cell-based Biosensors for Estimation of Biochemical Oxygen Demand and Detection of Toxicity*.

Su, M., Jiang, Y., and Li, D. (2013). Production of acetate from carbon dioxide in bioelectrochemical systems based on autotrophic mixed culture. *J. Microbiol. Biotechnol.* 23, 1400–1146. doi: 10.4014/jmb.1304.04039

van den Brand, T. P., Roest, K., Chen, G. H., Brdjanovic, D., and van Loosdrecht, M. C. M. (2015). Potential for beneficial application of sulfate reducing bacteria in sulfate containing domestic wastewater treatment. *World J. Microbiol. Biotechnol.* 31, 1675–1681. doi: 10.1007/s11274-015-1935-x

van Eerten-Jansen, M. C. A. A., Jansen, N. C., Plugge, C. M., de Wilde, V., Buisman, C. J. N., and ter Heijne, A. (2015). Analysis of the mechanisms of bioelectrochemical methane production by mixed cultures. *J. Chem. Technol. Biotechnol.* 90, 963–970. doi: 10.1002/jctb.4413

Venzlaff, H., Enning, D., Srinivasan, J., Mayrhofer, K. J. J., Hassel, A. W., Widdel, F., et al. (2013). Accelerated cathodic reaction in microbial corrosion of iron due to direct electron uptake by sulfate-reducing bacteria. *Corros. Sci.* 66, 88–96. doi: 10.1016/j.corsci.2012.09.006

Wagner, R. C., Regan, J. M., Oh, S. E., Zuo, Y., and Logan, B. E. (2009). Hydrogen and methane production from swine wastewater using microbial electrolysis cells. *Water Res.* 43, 1480–1488. doi: 10.1016/j.watres.2008.12.037

Wenzel, J., Fiset, E., Batlle-Vilanova, P., Cabezas, A., Etchebehere, C., Balaguer, M. D., et al. (2018). Microbial community pathways for the production of volatile fatty acids from CO_2 and electricity. *Front. Energy Res.* 6:15. doi: 10.3389/fenrg.2018.00015

Zaybak, Z., Pisciotta, J. M., Tokash, J. C., and Logan, B. E. (2013). Enhanced start-up of anaerobic facultatively autotrophic biocathodes in bioelectrochemical systems. *J. Biotechnol.* 168, 478–485. doi: 10.1016/j.jbiotec.2013.10.001

Zheng, Y., Xiao, Y., Yang, Z.-H., Wu, S., Xu, H.-J., Liang, F.-Y., et al. (2014). The bacterial communities of bioelectrochemical systems associated with the sulfate removal under different pHs. *Proc. Biochem.* 49, 1345–1351. doi: 10.1016/j.procbio.2014.04.019

Conflict of Interest Statement: The authors declare that the research was conducted in the absence of any commercial or financial relationships that could be construed as a potential conflict of interest.

frontiers in Energy Research

ORIGINAL RESEARCH
published: 04 September 2018
doi: 10.3389/fenrg.2018.00088

Membrane Electrolysis Assisted Gas Fermentation for Enhanced Acetic Acid Production

*Kristof Verbeeck, Sylvia Gildemyn† and Korneel Rabaey**

Center for Microbial Ecology and Technology (CMET), Ghent University, Ghent, Belgium

Gas fermentation has rapidly emerged as a commercial technology for the production of low-carbon fuels and chemicals from (industrial) CO and/or CO_2-rich feedstock gas. Recent advances in using CO_2 and H_2 for acetic acid production demonstrated that high productivity and substrate utilization are achievable. However, the costly constant addition of base and the energy-intensive nature of conventional recovery options (e.g., distillation) need to be overcome to drive organic acid production forward. Recently, membrane electrolysis has been presented as a technology that enables for the direct extraction of carboxylates across an anion exchange membrane (AEM) into a clean and low pH concentrate stream. Continuous *in-situ* extraction of acetate directly from the catholyte of a microbial electrosynthesis reactor showed that membrane electrolysis allows pure product recovery while improving productivity. Here we demonstrate that the system can be further enhanced through additional input of electrolytic hydrogen, produced at higher energetic efficiency while improving the overall extraction efficiency. A gas-lift reactor was used to investigate the hydrogen uptake efficiency at high hydrogen loading rates. During stable operation acetate transport across the membrane accounted for 31% of the charge balancing, indicating that the use of external H_2 can lead to a more efficient use of the extraction across the membrane. By coupling membrane electrolysis with the gas fermentation reactor the pH decrease associated with H_2/CO_2 fermentations could be prevented, resulting in a stable and zero-chemical input process (except for the CO_2). This now enables us to produce more than 0.6 M of acetic acid, a more attractive starting point toward further processing.

Keywords: microbial electrosynthesis, anion exchange membrane, bioproduction, CO_2 utilization, bioelectrochemical systems

OPEN ACCESS

Edited by:
Sebastià Puig,
University of Girona, Spain

Reviewed by:
Juan Antonio Baeza,
Autonomous University of Barcelona, Spain
Nabin Aryal,
Aarhus University, Denmark

****Correspondence:***
Korneel Rabaey
korneel.rabaey@ugent.be

†Present Address:
Sylvia Gildemyn,
OWS nv, Ghent, Belgium

Specialty section:
This article was submitted to Bioenergy and Biofuels, a section of the journal Frontiers in Energy Research

Received: *01 June 2018*
Accepted: *15 August 2018*
Published: *04 September 2018*

Citation:
Verbeeck K, Gildemyn S and Rabaey K (2018) Membrane Electrolysis Assisted Gas Fermentation for Enhanced Acetic Acid Production. Front. Energy Res. 6:88. doi: 10.3389/fenrg.2018.00088

INTRODUCTION

In recent years, microbial electrosynthesis (MES) has emerged as a promising bioreactor technology for the production of multi-carbon compounds from CO_2 and renewable electricity (Rabaey and Rozendal, 2010; Logan and Rabaey, 2012). This electricity-driven CO_2-conversion process uses the cathode of a so-called bio-electrochemical system to supply the reducing equivalents (in the form of electrons and/or H_2) for reducing CO_2 in the Wood-Ljungdahl pathway (May et al., 2016). Thus far acetic acid has been the main natural end-product of acetogenic metabolism in MES (Nevin et al., 2010, 2011; Marshall et al., 2012; Jourdin et al., 2015, 2016b; Patil et al., 2015; Bajracharya et al., 2016; Chen et al., 2016; Song et al., 2018), but recent reports have demonstrated

the production of higher-value organics like isopropanol (C3) (Batlle-Vilanova et al., 2017), butyric acid (C4) (Arends et al., 2017), and caproic acid (Vassilev et al., 2018) from CO_2 feed. Since its first description in 2010 (Nevin et al., 2010), considerable advancements in MES performance have been achieved, but today production rates, energy efficiencies and product titers are far too low to push MES forward as an industrial relevant platform for CO_2-based bioproduction (Desloover et al., 2012). Since production rates are ultimately limited by the applied current, it is essential to engineer MES systems that have the ability to deal with high electron supply rates at a high conversion efficiency and low power input (Gildemyn, 2016).

Gildemyn and co-workers have already demonstrated the advantages of using membrane electrolysis (ME) for MES. This approach can uniquely couple the production and recovery of acetic acid through *in-situ* product extraction across an anion exchange membrane (AEM) using nothing but an electrical current (Andersen et al., 2014; Gildemyn et al., 2015). The use of an AEM for MES can simultaneously separate, concentrate and acidify the product as a single organic acid in a solid-free extraction liquid, while enhancing performance through the combined effect of product recovery and *in-situ* pH control (Gildemyn et al., 2017). To date, the integrated MES approach for production and extraction is limited in terms of: (i) production rate; (ii) efficiency for electrons used for acetic acid recovery; and (iii) energy input requirements for acetic acid production. At best 40% of the electrons ended up in residual H_2 during MES experiments at 5 A m^{-2} applied current density, indicating that the transfer of reducing power to the homoacetogenic culture needs optimization (Gildemyn et al., 2015; Patil et al., 2015;). At 100% efficiency for production and extraction, acetate transport can at most account for 12.5% of the charge balance, as 8 moles electrons are required per mole of acetic acid produced, while extraction of the monovalent acetate ion (theoretically) only requires one electron. Since the extraction efficiency is limited by the production rate, acetate experimentally accounts for only 5–8% of the charge balancing (Gildemyn et al., 2015, 2017). Most of the charge is thus balanced by other anions, mainly HCO_3^-. It should be recognized that the full extraction capacity of the reactor can only be utilized if additional acetic acid is produced with externally supplied reducing equivalents (as hydrogen gas). We thus proposed an improved design where acetate production from an external H_2 source is linked to an extraction reactor providing only 12.5% of the total load of reducing equivalents, aimed at enhancing extraction efficiency at a lower power input. An alternative embodiment for this would be the extraction of acetate from an organic sidestream in combination with additional acetate production using the cathodic hydrogen.

Considering the aforementioned aspects, the focus of the present study was to investigate the impact of additional H_2 injection in an external fermenter on: (i) the current efficiency for acetate extraction; (ii) the final acetic acid concentration in the extraction liquid; (iii) the acetic acid production rate of the integrated MES-extraction approach; and (iv) the energy input for acetic acid production. Operation of the MES reactor was modified by coupling it to a bubble-column fermenter and adding externally produced H_2 to the reactor system to increase both H_2 retention time in the aqueous medium and productivity. Accordingly, this work reports on the development of a platform for CO_2 conversion based on existing gas fermentation technology coupled to membrane electrolysis as a tool for product recovery and pH control. Use of CO_2 as a raw material for large scale bioproduction will require proper integration of autotrophic biotechnology to fully exploit the intrinsic power of CO_2-based bioproduction.

MATERIALS AND METHODS

Reactor Setup and Operation

The experimental setup included a three-chambered electrochemical cell, a two-chambered water electrolyzer and a custom-made glass bubble-column reactor (**Figure 1**). The three-chambered reactor consisted of three identical Perspex frames with a working volume of 0.2 L per chamber (20 × 5 × 2 cm inner dimensions). The anode compartment contained a 50 mM Na_2SO_4 solution as electrolyte (adjusted to pH 2 with sulfuric acid) and a 20 × 5 cm MMO-coated titanium mesh electrode (Magneto Special Anodes BV, The Netherlands). The cathode compartment contained a modified homoacetogenic medium (pH 7.7) as described by Gildemyn et al. (2015) and a carbon felt electrode (100 cm^2 projected surface area, thickness of 3.18 mm, Alfa Aesar, Germany) with a stainless steel frame current collector. The initial volume of the catholyte was 1 L with the bubble-column reactor positioned in the recirculation loop op the cathode chamber. The electrolyte in the extraction compartment consisted of a 4-fold concentrated salt solution containing the same salts as the catholyte, adjusted to pH 2 with H_2SO_4. The initial working volume of the acolyte and extraction medium was 0.35 L, including an external recirculation flask. The anode and extraction compartments were separated by a cation exchange membrane (Fumatech FKB, Fumasep, Germany), while an AEM (Fumatech FAB, Fumasep, Germany) was placed in between the cathode and extraction chambers. All compartments were operated in batch mode during the entire experimental period (86 days) and recirculated at approximately 50 mL min^{-1}. A N_2/CO_2 mixture (90/10%, v/v) was continuously bubbled into the cathode compartment at a flow rate of 28.5 ± 12.4 L d^{-1}. The reactor was operated as a three-electrode setup using the cathode as working electrode and placement of a reference electrode (Ag/AgCl, 3 M KCl, + 210 mV vs. SHE, BASi) in the catholyte. A fixed reductive current of −50 mA (corresponding to a current density of −5 A m^{-2}) was used to facilitate electrosynthesis by means of potentiostatic control (VSP, BioLogic, France).

An additional two-chambered electrochemical cell was constructed using identical materials except that a stainless steel mesh was used as cathode material and a 0.5 M Na_2SO_4 solution was used as electrolyte in both reactor chambers. Both electrolytes were recirculated over a buffer vessel at high speed (∼100 mL min^{-1}) to ensure proper mixing. The cell was operated as a water electrolyzer (with CEM) at a fixed current density of −35 A m^{-2} (0.35 A), producing H_2 gas that was sparged into the bubble column through anaerobic tubing.

The bubble-column was a cylindrical reactor with a volume of 2 L (1 m height, 5 cm internal diameter) and an integrated

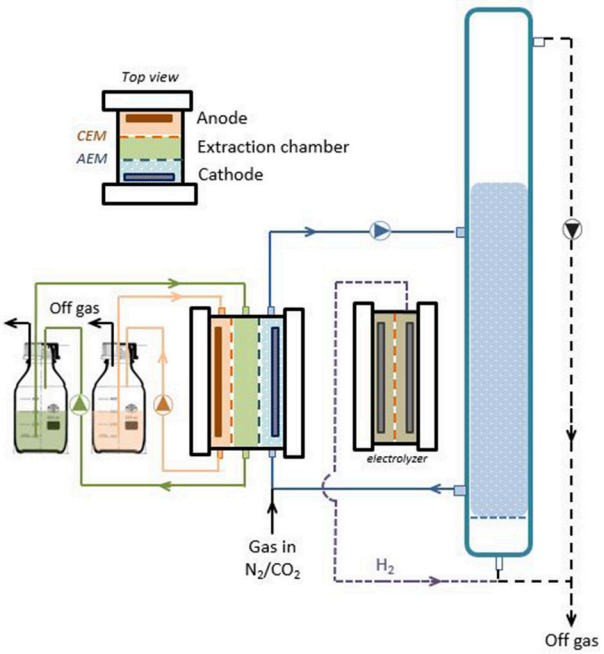

FIGURE 1 | Bubble column reactor setup for simultaneous biological production and extraction of acetic acid from CO_2 and electrical current through a hybrid microbial electrosynthesis-gas fermentation approach. An external fermenter is fed with additional hydrogen from a water electrolyzer to increase acetate production rates. Full black lines show liquid streams, dotted lines gas streams.

sintered glass to allow fine bubble dispersion. Connection to the MES cell was established through glass nipples on the side of the column. An ATEX gas pump (KNF Verder, Belgium) was installed to intensively recirculate the headspace gas through the fermentation medium ($\sim$ 15 L min^{-1}). The same experimental procedures as described in Gildemyn et al. (2015) were used. Any liquid removed during sampling as well as liquid lost via electro-osmosis was replaced with an equal amount of sterile anaerobic stock solution. The experiments were conducted under anaerobic conditions, at room temperature (21 $\pm$ 2°C). The reactor setup (electrochemical cell + column) was inoculated at the start of the experiment up to a final cell density of $\sim 10^5$ viable cells $mL^{-1}_{fermentation\ broth}$ with a pre-enriched autotrophic acetate-producing mixed microbial community that was used in previous MES experiments (Patil et al., 2015; Gildemyn et al., 2017). Gas and liquid samples were taken three times per week from each reactor compartment for monitoring gas composition, VFAs, alcohols, anions, cations, pH, conductivity and bicarbonate. Water transfer was estimated based on the volume changes in the different recirculation vessels. The flow rate of N_2/CO_2 was monitored by water displacement measurements prior to sampling. For abiotic control experiments (current but no bacteria as well as bacteria but no current) we refer to Gildemyn et al. (2015) and Patil et al. (2015) since these studies showed that in both control experiments no production of organic products or biomass was detected.

Analytical Procedures

Conductivity and pH were determined according to standard methods. VFAs, alcohols and inorganic anions were measured using ion chromatography as described in Gildemyn et al. (2015). Sodium, ammonium, potassium, magnesium, and calcium were determined on a 761 Compact Ion Chromatograph (Metrohm, Switzerland) using a conductivity detector. The device was equipped with a Metrosep C6 – 250/4 column and a Metrosep C4 Guard/4.0 guard column. The eluent was 1,7 mM HNO_3, 1.7 mM dipicolinic acid. Gas samples were analyzed for the presence of N_2, O_2, H_2, and CH_4 by gas chromatography using a Compact GC (Global Analyser Solutions, Breda, The Netherlands) equipped with a thermal conductivity detector.

Data Representation

The calculations for the volumetric acetic acid production rate [based on the fermentation broth volume (g L^{-1} d^{-1})], electron recovery and energy efficiency are based on the methods described in (Patil et al., 2015). The calculation of electron recovery in unutilized H_2 is based on the residual H_2 concentration in the off-gas from the bubble column reactor. The extraction efficiency is defined as the ratio of extraction rate to production rate (of the whole system, electrolyzer + MES), while the charge balancing efficiency is defined as the ratio of the charge transported as a specific ion through a membrane and the total electrical charge of the extraction cell. Only the power input for electrochemical reactions (water splitting) is taken into account for specific energy input calculations.

In an abiotic test preceding the inoculation, the hydrogen production rate of both the MES cell (operated at a fixed current density of -5 A m^{-2}) and the electrolyzer (operated at a fixed current density of -35 A m^{-2}) was quantified. With a combined hydrogen gas flow rate of 3.5 $\pm$ 0.2 L day^{-1} leaving the reactor, the electron balance could be closed for 86.4 $\pm$ 0.1%, indicating some loss through tubing, connectors and sampling ports (provided 100% current efficiency for H_2 production).

RESULTS AND DISCUSSION

Additional Hydrogen Injection Enhances Acetic Acid Productivity

Production of acetic acid by the microbial community in a galvanostatic operated MES reactor started 10 days after inoculation. The longer lag-phase in this study (3–5 days in our previous studies) could potentially be attributed to the lower initial biomass concentration and the larger reactor volume. Once acetogenic activity started, gas recirculation was activated to improve the H_2 mass transfer to the fermentation broth. A cathode potential of -1.21 $\pm$ 0.07 V vs. SHE was recorded during the experiment. Carbon fixation via homoacetogenesis allowed for a sustained increase in the concentration of acetic acid throughout the test. Acetic acid gradually accumulated in the extraction chamber, reaching 37.0 g L^{-1} (617 mM) on day 86 (**Figure 2A**). This is the highest titer of acetic acid reported so far for MES from CO_2 feed. From day 56, acetate concentration in the catholyte remained fairly constant (4.1 $\pm$ 0.6 g L^{-1}), while the concentration in the anolyte rose to reach 13.7 g L^{-1} by the

end of the cycle. For the whole 86 days operation, the average acetic acid production rate was 0.76 $g_{acetate}$ L^{-1} d^{-1}. Higher carbon fixation rates (1.48 g L^{-1} d^{-1}) were observed during stable operation (from day 37 to 65), whereas a maximum value of 3.54 g L^{-1} d^{-1} can be reported. These results confirm that an 8 times higher H_2 feeding rate and a higher H_2 retention time (∼ 1 h by continuous recirculation of the H_2 headspace through the fermentation medium) resulted in 2.6–4.1 times higher acetic acid concentration and 2.1–2.7 times higher volumetric productivity compared to our previous studies (Gildemyn et al., 2015, 2017). Acetic acid accounted for 99.8% of all organic compounds present at the end of the experiment (as carbon, sum of products in all reactor compartments). Other carboxylates such as formate, propionate and butyrate were present but only in low concentrations (<50 mg L^{-1}). Just as in our previous work, product diversification to alcohols was not observed and methane was not consistently detected in the off-gas. The batch cycle resulted in a total acetic acid production of 42.9 g acetic acid by day 86 (**Figure 2B**), resulting in an overall electron recovery in acetic acid of 21% (**Figure 2C**). When only taking into account the stable operation period, the coulombic efficiency (CE) was 41%. CE increased throughout the test, probably due to a higher biomass density in the fermentation broth, and reached a plateau from day 75 (**Figure 2C**). Unutilized H_2 in the reactor off-gas resulted in an overall electron recovery in H_2 of 45%. The electron balance can be further closed with the presence of other products (short-chain carboxylic acids and methane; <1%), losses of H_2 gas through tubing, connectors and stoppers (13.6% based on abiotic quantification), and biomass production. The concentrations in the different reactor compartments did not reflect the real productivity of the system because water displacement between the compartments caused a change in the volumes throughout the reactor run. An average water flow across the AEM of 0.75 L $m^{-2}_{membrane}$ d^{-1} was observed (from cathode to extraction compartment), which was 11 times higher than the flow across the CEM (0.07 L $m^{-2}_{membrane}$ d^{-1}). The water flux through the AEM is diluting the acetic acid stream, limiting the product titer in the extraction liquid so that a final concentration of 37 g L^{-1} (in 1.20 L) instead of 108 g L^{-1} (in 0.35 L) was achieved. It was observed that the water flux showed a linear dependency on current in the range of current densities tested (data not shown), and seems to be related to the hydration shell of the anions crossing the membrane (electro-osmosis) (Lakshminarayanaiah, 1969; Giorno et al., 2016).

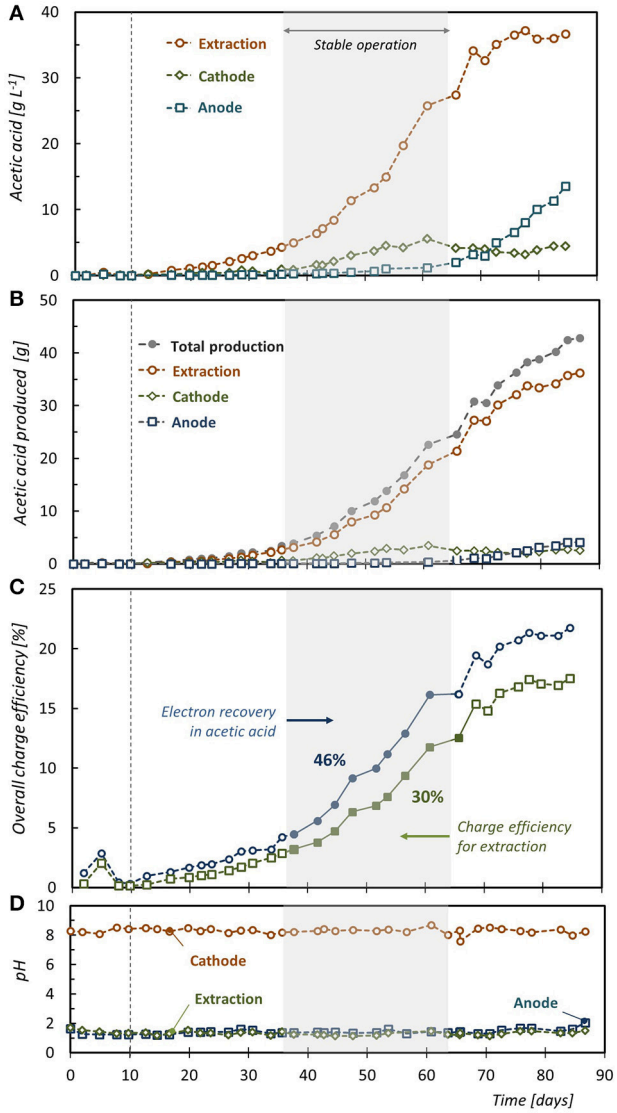

FIGURE 2 | (A) Acetic acid concentration in the catholyte, middle compartment and anolyte. **(B)** Total mass of acetic acid produced, extracted across the AEM and present in the extraction liquid. **(C)** Overall charge efficiency for production and extration. **(D)** pH in the different reactor chambers. Dotted vertical lines represent the start of gas recirculation.

MES offers the intrinsic advantage to directly supply bacteria with electrons, however there is more and more evidence that production via MES is mainly driven by an indirect electron flow from the cathode to the acetogens, occurring via abiotically or biologically induced H_2 production (Patil et al., 2015; Jourdin et al., 2016b). The crucial role of H_2 in the conversion of CO_2 to organics is thus creating the need for a MES reactor design that can work at high current density and consume high H_2 fluxes. As discussed in previous reports, MES reactor design (often H-type, cylindrical or plate and frame type reactors) is not optimized for *in-situ* H_2 conversion, leading to high losses of residual H_2. Efforts to increase CEs have been focusing on 3D electrodes that supply H_2 in the whole cathode chamber (Jourdin et al., 2016a; Song et al., 2018), but the scalability of these systems is questionable and channeling issues may arise when microbial growth completely fills the electrode pores (Klasson et al., 1991). Due to the fact that electrosynthesis is limited to the surface (and close surroundings) of the cathode reactor, scalability of this 2D system is more challenging compared to 3D gas fermentation systems. For the first time coupling MES to the gas fermentation platform is demonstrated as a strategy to achieve higher electron supply rates for CO_2-based bioproduction. As a CO_2-based bioproduction platform MES is still far behind H_2/CO_2 or syngas based fermentation in

terms of production rates, energy efficiencies, scalability, and maturity, so integration within the gas fermentation platform could push MES forward as an elegant way to control/steer fermentation and achieve *in-situ* product recovery (see further). The coupling of MES to a bubble column reactor is also a promising strategy to increase the H_2 retention in the reactor, thereby increasing the H_2 conversion efficiency. However, more optimization will be needed to boost production and achieve high H_2 uptake efficiencies typically obtained in optimized gas fermentation reactors (El-Gammal et al., 2017; Steger et al., 2017). The continuous supply of N_2:CO_2 gas mixture resulted in a relatively low H_2 partial pressure of 0.07 ± 0.03 bar, limiting the driving force for H_2 mass transfer from gas to liquid. The low gas-to-liquid mass transfer of H_2 has been identified previously as the rate-limiting factor in gas fermentation processes (De Tissera et al., 2017). It could be expected that production rates will increase when H_2 is not flushed out permanently, but accumulates in the headspace of a pressurized reactor system, increasing the pH_2. The use of pure CO_2 (limiting the dilution of H_2/CO_2 with N_2) or intermittent sparging of CO_2 (for example pH or $[CO_2]_{dissolved}$ controlled) could be exploited as gas feeding strategies to increase pH_2. Efforts to increase the volumetric mass transfer coefficient (k_La) mainly focus on increasing the interfacial surface area for mass transfer via mixing, microbubble sparging, or the use of packing material (Orgill et al., 2013). Bioreactor designs such as bubble, immobilized cell and trickle bed columns are proposed as low-cost reactor platforms for gas fermentation (De Tissera et al., 2017). Although the design and operation of gas fermentation reactors has reached industrial scale, energy efficient recovery of the water-soluble products from the aqueous broth still presents an engineering challenge. For the first time interlinking of different autotrophic bioprocesses is proposed as a way to overcome the limitations of separate technologies. Furthermore, additional value could be created by coupling different production platforms to upgrade the low-value products typically produced in MES as well as gas fermentations and produce higher value chemicals. The further conversion of acetic acid to caproic and caprylic acid through chain elongation has been proposed as an efficient way to increase the product value of primary fermentation products (Gildemyn, 2016).

Membrane Electrolysis as a Tool to Assist Gas Fermentation: *in-situ* Product Recovery and pH Control

As the result of charge balancing, an electrochemical reactor with an AEM has the intrinsic ability to extract *in-situ* the produced acetic acid as the negatively charged acetate ion, into the acidic extraction compartment (termed membrane electrolysis, ME) (Andersen et al., 2014; Gildemyn et al., 2015). Since acetate synthesis from CO_2 requires 8 electrons per mole acetate (at 100% current efficiency), and since the electricity-driven extraction of one mole of acetate theoretically requires only one electron, the current use for acetate extraction (limited to a maximum of 12.5%) can only be improved by linking an external H_2 source to the MES reactor (increasing the theoretical production rate and thus the membrane availability for extraction). Acetate transport from the cathode to the extraction compartment accounted for 17.5% of the charge balancing through the AEM (**Figure 2C**), while in a MES cell without external H_2 injection, acetate accounted for only 8.1 ± 0.8% of the charge passing through the AEM (Gildemyn et al., 2015). This result clearly indicates that through external H_2 supply, a more efficient use of the intrinsic extraction capacity of the reactor can be achieved, but also that the charge efficiency for extraction is limited by the efficiency for production. During stable operation, a charge balancing efficiency for acetate production of 31% was achieved. Calculated on a mass balance, 94% of the produced acetic acid was extracted and 85% of the product was present in the extraction solution (**Figure 2B**). Diffusion of uncharged acetic acid molecules through the CEM resulted in an acetic acid loss of 9% toward the anode compartment although principally in time this should stabilize. From day 75, the extraction efficiency was 100%, as no product build-up in the catholyte took place. Membrane electrolysis can avoid product build-up in the fermentation broth, and thus allows a batch mode operation without the occurrence of product inhibition or product diversification. Separation of the fermentation product from the broth in a cost- and energy- efficient recovery process is envisaged as a crucial feature for scaling up gas fermentation processes to commercial-scale production plants. Distillation has been the traditional recovery technology for low boiling point fermentation products (Liew et al., 2013), but its energy-intensive nature has led to the development of alternative and potentially less expensive separation techniques (Ezeji et al., 2010), of which membrane electrolysis is of particular interest for charged metabolites that have the tendency to lower broth pH. ME stabilized the pH of the fermentation medium throughout the operation at a pH value of 8.30 ± 0.19 (**Figure 2D**), while typically a pH drop in the broth of MES and gas fermentation reactors is observed unless a chemical pH control mechanism is applied (Liew et al., 2013; Arends et al., 2017). pH control is an effective strategy to achieve long-term stable acetate production and high product concentrations (Drake et al., 2006; De Tissera et al., 2017), but the addition of large amounts of base is costly and adds salts to the broth (Gildemyn et al., 2017). Base (to prevent product inhibition) and acid dosage (to acidify the product stream) are fully replaced by OH^- and H^+ production at the cathode and anode of the ME reactor, respectively, highlighting that integration of ME in gas fermentation technology enables operation of a bioproduction reactor without addition of chemicals. This confirms earlier observations that an AEM can stabilize MES operation (Gildemyn et al., 2017). The results suggest that the *in-situ* extraction of the acetic acid produced in a gas fermenter can enhance productivity through the combined effect of product removal and *in-situ* pH control. The ME technology would be more efficient as "secondary" microbial electrochemical technology (MET), assisting H_2/CO_2 fermentation, rather than as a electrosynthesis approach itself. In this way a larger fraction of the intrinsic extraction capacity of the system can be used, and the power input of this cell can be lowered as only part of the reducing equivalents

will be supplied by this reactor. As secondary MET, the extraction through ME supports H_2/CO_2 fermentation by: (i) extracting the produced acetic acid (avoiding product build-up and inhibition); (ii) balancing the pH of the fermentation broth (avoiding caustic addition); and (iii) providing additional reducing equivalents in the form of *in-situ* electrochemically produced hydrogen (generating high pH_2 close to the electrode surface) (**Figure 3**). Periodic (ON-OFF) extraction could be exploited as a way to make fully use of the capabilities of ME during gas fermentation as it allows to recover the product more efficiently at higher product concentrations in the broth. It could thus be implemented as a recovery approach that intermittently extracts the product when pH stabilization is needed, or when acetic acid accumulates above a set concentration. Fine-tuning of this ON-OFF strategy could results in an optimized energy investment and reduction of water displacement across the membrane. By lowering the current density applied to the three-chambered reactor (and increasing the availability of acetate ions at the membrane surface) the electro-osmotic water transport per kilogram product can be reduced (compared a system where all H_2 is produced *in-situ*). HCO_3^- transport over the AEM is of high importance for charge balancing and is a major contributor of the (electro-osmotic) water transport (Gildemyn et al., 2017). Intermittent extraction could result in short periods of very efficient extraction with limited water drag.

Membrane Electrolysis Assisted Gas Fermentation as Future Scenario to Reduce Power Input

Increasing productivity at a lower power input is crucial for the economics of both MES and H_2/CO_2 fermentation processes. The power input for the system presented here required 15 kWh kg^{-1} for the production of 3.7% acetic acid (only taking into account the electricity input of the electrochemical cells), which is 19–43% lower compared to the energy input in MES-extraction reactors without additional H_2 (max. 1.35% acetic acid), but still, undeniably, too high to compete with current production standards (98% acetic acid production via methanol carbonylation at 4 kWh kg^{-1}) (Althaus et al., 2007). The power consumption per kilogram product can be decreased by: (i) increasing the H_2 conversion efficiency (getting more product with the same power input), or (ii) reducing the cell voltage of the system (getting the same amount of product at a lower power input). For an industrial process it is critically important to operate a production process at high volumetric production rates, so for MES this means that current densities will need to increase drastically. It is however highly debatable whether H_2 can be produced at high energy efficiencies in a MES cell at high current densities when using the conventional (rather unconducive) bacterial growth media as electrolyte, while alkaline or polymer electrolyte membrane (PEM) electrolyzers are optimized for efficient H_2 generation. Due to the fact that biological compatibility needs to be guaranteed during electrolyte selection, the low conductivity will make these systems not competitive with abiotic electrolyzers considering only H_2 production. During stable reactor operation, cell voltages of 3.91 ± 0.10 V were recorded for the MES cell (5 A m^{-2}), while conventional water electrolyzers are operated under current densities ranging from 1,000 to 3,000 A m^{-2} and stable cell voltages of 1.7–1.9 V (Zeng and Zhang, 2010). With an energy efficiency ranging from 65 to 82%, current industrial PEM electrolyzers are much more efficient in producing H_2 than MES systems currently do (35% energy efficiency at only 5 A m^{-2}). Projecting forward to a fully realized system, the power input of acetic acid production via the ME-assisted gas fermentation pipeline should be calculated based on realistic rather than experimental and non-optimized cell voltages. The economics of the proposed concept is briefly demonstrated for a 10,000 L gas fermentation reactor. At 2,000 A m^{-2} and 1.8 V, the power cost of water electrolysis is calculated at 4.3 kWh per Nm^3 of H_2 produced, which corresponds to € 4.8 per kg H_2 (at an energy cost of € 0.1 per kWh). Considering a gas fermentation reactor fixing CO_2 into acetic acid at a volumetric productivity of 148 g $L_{reactor}^{-1}$ d^{-1} (experimentally achieved by Kantzow et al., 2015) and 90% electron recovery, H_2 gas should be supplied at a flow rate of 106 Nm^3 per hour. If coupled to continuous

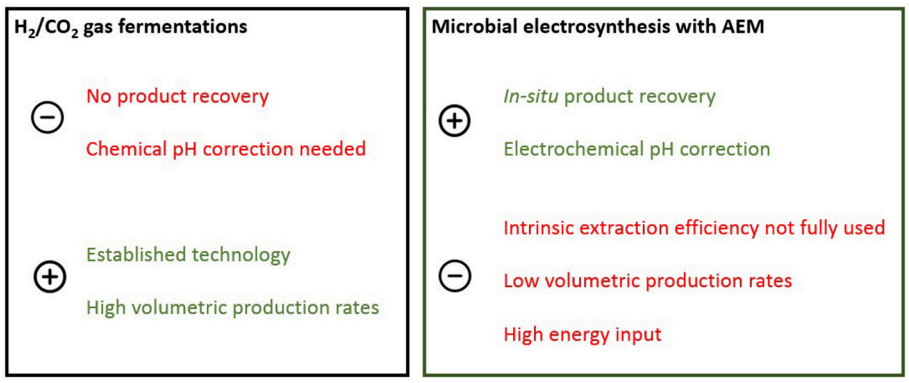

FIGURE 3 | Benefits and drawbacks of gas fermentation and microbial electrosynthesis as CO_2-based production platforms. The coupling of both technologies results in a hybrid reactor configuration that combines the product recovery and pH stabilizing ability with the maturity and productivity of gas fermentation.

extraction in a ME unit operated at 1000 A m^{-2}, 42 m^2 membrane surface is needed to allow for a stable broth concentration. At 5 V and a charge balancing efficiency by acetate of 65%, 17% of the total H_2 load is produced in the ME cell and ME is able to recover 1.48 ton acetic acid per day (extraction rate is set equal to production rate). Based on these assumptions a power input for acetic acid production and extraction of 9.56 kWh per kg acetic acid is calculated, of which 36% can be attributed to the electrochemical extraction. Assuming 40 m^2 membrane electrode assembly per cubic meter reactor (Desloover et al., 2015), a ME setup of 1.06 m^2 would be sufficient to control fermentation. Potentially the power input can be further decreased if the system is operated with an intermittent rather than continuous extraction (for example 10% of the time ON, 90% OFF), since a higher molecular availability for flux results in a higher charge efficiency for carboxylate extraction and thus a potentially lower current use by the ME system. Assuming a charge balancing efficiency by acetate of 80% when acetate concentration in the broth is 20 g L^{-1}, the power input can be lowered to 8.76 kWh per kg product. This demonstrates that the ME extraction would fit ideally with a high concentration fermentation to obtain an effective and cost-optimized ME step. To lower the energy input per kilogram acetic acid extracted, it is clear that a maximal use of the "expensive" charge for target ion recovery in the ME cell should be targeted. Furthermore, off-gases from industrial processes, such as steel production and reformed biogas, as well as syngas from biomass gasification can serve as substrate gas in the flexible/hybrid MES-gas fermentation approach.

CONCLUSION

Since its first demonstration, MES has been intensively studied in terms of microbiology (Nevin et al., 2011), electron transfer (Marshall et al., 2012; Jourdin et al., 2016b), electrode materials (Zhang et al., 2013; Jourdin et al., 2016a), CO_2 supply (Bajracharya et al., 2016), media modification (Ammam et al., 2016), and product outcome (Ganigué et al., 2015; Vassilev et al., 2018), but engineering of the system has only been studied in terms of product recovery. This study presents an reactor setup that allows operation of MES reactors at higher current densities, thereby increasing the availability of reducing equivalents and, thus, increasing the (theoretical) production rates (provided that the kinetics of the acetogens are not the rate-limiting factor). Coupling direct extraction to an H_2/CO_2 gas fermentation column allows for recovery of the pure product in an acid and clean extraction liquid while simultaneously stabilizing the pH in the fermentation broth. The external hydrogen injection allows acetic acid production from CO_2 at a lower power input and cost. We therefore believe that ME-assisted gas fermentation offers opportunities for the scalability of acetic acid production from CO_2.

AUTHOR CONTRIBUTIONS

All authors listed have made a substantial, direct and intellectual contribution to the work, and approved it for publication.

FUNDING

KV is supported by FWO Vlaanderen through a Ph.D. scholarship. KR acknowledges support by the European Research Council (StG ELECTROTALK) and Interreg grant EnOP.

ACKNOWLEDGMENTS

The authors thank Amanda K. Luther for critically reading the manuscript.

REFERENCES

Althaus, H.-J., Doka, G., Dones, R., Heck, T., Hellweg, S., Hischier, R., et al. (2007). "The Ecoinvent reference is the Swiss center for life cycle inventories," in *Overview and Methodology. Ecoinvent Report No. 1*, eds R. Frischknecht and N. Jungbluth (Dübendorf). Available online at: https://www.ecoinvent.org/files/200712_frischknecht_jungbluth_overview_methodology_ecoinvent2.pdf.

Ammam, F., Tremblay, P.-L., Lizak, D. M., and Zhang, T. (2016). Effect of tungstate on acetate and ethanol production by the electrosynthetic bacterium *Sporomusa ovata. Biotechnol. Biofuels* 9:163. doi: 10.1186/s13068-016-0576-0

Andersen, S. J., Hennebel, T., Gildemyn, S., Coma, M., Desloover, J., Berton, J., et al. (2014). Electrolytic membrane extraction enables production of fine chemicals from biorefinery sidestreams. *Environ. Sci. Technol.* 48, 7135–7142. doi: 10.1021/es500483w

Arends, J. B. A., Patil, S. A., Roume, H., and Rabaey, K. (2017). Continuous long-term electricity-driven bioproduction of carboxylates and isopropanol from Co_2 with a mixed microbial community. *J. CO_2 Util.* 20, 141–149. doi: 10.1016/j.jcou.2017.04.014

Bajracharya, S., Vanbroekhoven, K., Buisman, C. J. N., Pant, D., and Strik, D. P. (2016). Application of gas diffusion biocathode in microbial electrosynthesis from carbon dioxide. *Environ. Sci. Pollut.Res.* 23, 22292–22308. doi: 10.1007/s11356-016-7196-x

Batlle-Vilanova, P., Ganigué, R., Ramió-Pujol, S., Bañeras, L., Jiménez, G., Hidalgo, M., et al. (2017). Microbial electrosynthesis of butyrate from carbon dioxide: production and extraction. *Bioelectrochemistry* 117, 57–64. doi: 10.1016/j.bioelechem.2017.06.004

Chen, L., Tremblay, P.-L., Mohanty, S., Xu, K., and Zhang, T. (2016). Electrosynthesis of acetate from CO_2 by a highly structured biofilm assembled with reduced graphene oxide-tetraethylene pentamine. *J. Mater. Chem. A* 4, 8395–8401. doi: 10.1039/C6TA02036D

De Tissera, S., Köpke, M., Simpson, S. D., Humphreys, C., Minton, N. P., and Dürre, P.(2017). *Syngas Biorefinery and Syngas Utilization*. Berlin; Heidelberg: Springer Berlin Heidelberg.

Desloover, J., Arends, J. B. A., Hennebel, T., and Rabaey, K. (2012). Operational and technical considerations for microbial electrosynthesis. *Biochem. Soc. Trans.* 40, 1233–1238. doi: 10.1042/BST20120111

Desloover, J., De Vrieze, J., Van de Vijver, M., Mortelmans, J., Rozendal, R., and Rabaey, K. (2015). Electrochemical nutrient recovery enables ammonia toxicity control and biogas desulfurization in anaerobic digestion. *Environ. Sci. Technol.* 49, 948–955. doi: 10.1021/es504811a

Drake, H. L., Küsel, K., Matthies, C., Dworkin, M., Falkow, S., Rosenberg, E., et al. (Eds). (2006). "Acetogenic prokaryotes," in *The Prokaryotes,* Vol. 2, *Ecophysiology and Biochemistry,* eds M. Dworkin, S. Falkow, E. Rosenberg, K.-H. Schleifer, and E. Stackebrandt (New York, NY: Springer), 354–420.

El-Gammal, M., Abou-Shanab, R., Angelidaki, I., Omar, B., Sveding, P. V., Karakashev, D. B., et al. (2017). High efficient ethanol and vfa production from gas fermentation: effect of acetate, gas and inoculum microbial composition. *Biomass Bioenergy* 105, 32–40. doi: 10.1016/j.biombioe.2017.06.020

Ezeji, T. C., Li, Y. A. A., Vertès, N., Qureshi, Blaschek, H. P., and Yukawa H (Eds). (2010). "Advanced product recovery technologies," in *Biomass to Biofuels,* eds A. A. Vertès, N. Qureshi, H. P. Blaschek, and H. Yukawa (Chichester: John Wiley & Sons Ltd), 331–346.

Ganigué, R., Puig, S., Batlle-Vilanova, P., Balaguer, M., and Colprim, J. (2015). Microbial electrosynthesis of butyrate from carbon dioxide. *Chem. Commun.* 51, 3235–3238. doi: 10.1039/c4cc10121a

Gildemyn, S. (2016). *Technology and Tools for Bioelectrochemical Production of Short- and Medium-Chain Carboxylic Acids from CO_2*. Ghent: Ghent University; Faculty of Bioscience Engineering.

Gildemyn, S., Verbeeck, K., Jansen, R., and Rabaey, K. (2017). The type of ion selective membrane determines stability and production levels of microbial electrosynthesis. *Bioresour. Technol.* 224, 358–364. doi: 10.1016/j.biortech.2016.11.088

Gildemyn, S., Verbeeck, K., Slabbinck, R., Andersen, S. J., Prevoteau, A., and Rabaey, K. (2015). Integrated production, extraction, and concentration of acetic acid from CO_2 through microbial electrosynthesis. *Environ. Sci. Tech. Let.* 2, 325–328. doi: 10.1021/acs.estlett.5b00212

Giorno, L., Drioli, E., Strathmann, H., Drioli, E., and Giorno, L. (Eds). (2016). "Water transport in ion-exchange membranes," in *Encyclopedia of Membranes,* eds E. Drioli and L. Giorno (Berlin; Heidelberg: Springer), 968–989.

Jourdin, L., Freguia, S., Flexer, V., and Keller, J. (2016a). Bringing high-rate, CO_2-based microbial electrosynthesis closer to practical implementation through improved electrode design and operating conditions. *Environ. Sci. Technol.* 50, 1982–1989. doi: 10.1021/acs.est.5b04431

Jourdin, L., Grieger, T., Monetti, J., Flexer, V., Freguia, S., Lu, Y., et al. (2015). High acetic acid production rate obtained by microbial electrosynthesis from carbon dioxide. *Environ. Sci. Technol.* 49, 13566–13574. doi: 10.1021/acs.est.5b03821

Jourdin, L., Lu, Y., Flexer, V., Keller, J., and Freguia, S. (2016b). Biologically induced hydrogen production drives high rate/high efficiency microbial electrosynthesis of acetate from carbon dioxide. *Chem. Electro. Chem.* 3, 581–591. doi: 10.1002/celc.201500530

Kantzow, C., Mayer, A., and Weuster-Botz, D. (2015). Continuous gas fermentation by Acetobacterium woodii in a submerged membrane reactor with full cell retention. *J. Biotechnol.* 212, 11–18. doi: 10.1016/j.jbiotec.2015.07.020

Klasson, K. T., Ackerson, M. D., Clausen, E. C., and Gaddy, J. L. (1991). Bioreactor design for synthesis gas fermentations. *Fuel* 70, 605–614. doi: 10.1016/0016-2361(91)90174-9

Lakshminarayanaiah, N. (1969). Electroosmosis in ion-exchange membranes. *J. Electrochem. Soc.* 116, 338–342. doi: 10.1006/jcis.2000.7063

Liew, F. M., Köpke, M., Simpson Sa, D., and Fang, Z. (ed). (2013). "Gas fermentation for commercial biofuels production," in *Liquid, Gaseous and Solid Biofuels - Conversion Techniques,* ed Z. Fang (Rijeka: InTech), 125–173.

Logan, B. E., and Rabaey, K. (2012). Conversion of wastes into bioelectricity and chemicals by using microbial electrochemical technologies *Science* 337, 686–690. doi: 10.1126/science.1217412

Marshall, C. W., Ross, D. E., Fichot, E. B., Norman, R. S., and May, H. D. (2012). Electrosynthesis of commodity chemicals by an autotrophic microbial community. *Appl. Environ. Microbiol.* 78, 8412–8420. doi: 10.1128/AEM.02401-12

May, H. D., Evans, P. J., and LaBelle, E. V. (2016). The bioelectrosynthesis of acetate. *Curr. Opin. Biotechnol.* 42, 225–233. doi: 10.1016/j.copbio.2016.09.004

Nevin, K. P., Hensley, S. A., Franks, A. E., Summers, Z. M., Ou, J., Woodard, T. L., et al. (2011). Electrosynthesis of organic compounds from carbon dioxide is catalyzed by a diversity of acetogenic microorganisms. *Appl. Environ. Microbiol.* 77, 2882–2886. doi: 10.1128/AEM.02642-10

Nevin, K. P., Woodard, T. L., Franks, A. E., Summers, Z. M., and Lovley, D. R. (2010). Microbial electrosynthesis: feeding microbes electricity to convert carbon dioxide and water to multicarbon extracellular organic compounds. *MBio* 1:e00103-10. doi: 10.1128/mBio.00103-10

Orgill, J. J., Atiyeh, H. K., Devarapalli, M., Phillips, J. R., Lewis, R. S., and Huhnke, R. L. (2013). A comparison of mass transfer coefficients between trickle-bed, hollow fiber membrane and stirred tank reactors. *Bioresour. Technol.* 133, 340–346. doi: 10.1016/j.biortech.2013.01.124

Patil, S. A., Arends, J. B., Vanwonterghem, I., Van Meerbergen, J., Guo, K., Tyson, G. W., et al. (2015). Selective enrichment establishes a stable performing community for microbial electrosynthesis of acetate from CO_2. *Environ. Sci. Technol.* 49, 8833–8843. doi: 10.1021/es506149d

Rabaey, K., and Rozendal, R. A. (2010). Microbial electrosynthesis—revisiting the electrical route for microbial production. *Nat. Rev. Microbiol.* 8, 706–716. doi: 10.1038/nrmicro2422

Song, T. S., Fei, K. Q., Zhang, H. K., Yuan, H., Yang, Y., Ouyang, P. K., et al. (2018). High efficiency microbial electrosynthesis of acetate from carbon dioxide using a novel graphene-nickel foam as cathode. *J. Chem. Technol. Biotechnol.* 93, 457–466. doi: 10.1002/jctb.5376

Steger, F., Rachbauer, L., Windhagauer, M., Montgomery, L. F. R., and Bochmann, G. (2017). Optimisation of continuous gas fermentation by immobilisation of acetate-producing acetobacterium woodii. *Anaerobe* 46, 96–103. doi: 10.1016/j.anaerobe.2017.06.010

Vassilev, I., Hernandez, P. A., Batlle-Vilanova, P., Freguia, S., Krömer, J. O., Keller, J., et al. (2018). Microbial electrosynthesis of isobutyric, butyric, caproic acids, and corresponding alcohols from carbon dioxide ACS Sustainable. *Chem. Eng.* 6, 8485–8493. doi: 10.1021/acssuschemeng.8b00739

Zeng, K., and Zhang, D. (2010). Recent progress in alkaline water electrolysis for hydrogen production and applications. *Progr. Energy. Combust. Sci.* 36, 307–326. doi: 10.1016/j.pecs.2009.11.002

Zhang, T., Nie, H., Bain, T. S., Lu, H., Cui, M., Snoeyenbos-West, O. L., et al. (2013). Improved cathode materials for microbial electrosynthesis. *Energy Environ. Sci.* 6, 217–224. doi: 10.1039/C2EE23350A

Conflict of Interest Statement: The authors declare that the research was conducted in the absence of any commercial or financial relationships that could be construed as a potential conflict of interest.

frontiers in Energy Research

ORIGINAL RESEARCH
published: 15 October 2018
doi: 10.3389/fenrg.2018.00106

Metabolic Network Analysis of Microbial Methane Utilization for Biomass Formation and Upgrading to Bio-Fuels

Nils J. H. Averesch[1*†] *and Frauke Kracke*[2†]

[1] *Universities Space Research Association at NASA Ames Research Center, Mountain View, CA, United States,* [2] *Department of Civil & Environmental Engineering, Stanford University, Stanford, CA, United States*

OPEN ACCESS

Edited by:
Andrea Schievano, Università degli Studi di Milano, Italy

Reviewed by:
Andrea Franzetti, Università degli studi di Milano Bicocca, Italy
Mohanakrishna Gunda, Qatar University, Qatar

***Correspondence:**
Nils J. H. Averesch
nils.averesch@uq.net.au

†These authors have contributed equally to this work

Specialty section:
This article was submitted to Bioenergy and Biofuels, a section of the journal Frontiers in Energy Research

Received: *02 June 2018*
Accepted: *24 September 2018*
Published: *15 October 2018*

Citation:
Averesch NJH and Kracke F (2018) Metabolic Network Analysis of Microbial Methane Utilization for Biomass Formation and Upgrading to Bio-Fuels. Front. Energy Res. 6:106. doi: 10.3389/fenrg.2018.00106

The potent greenhouse gas methane presents a widely accessible resource, being the primary component in natural gas as well as in bio-gas from anaerobic digesters. Given its relatively low heating-value and several issues concerning its storage and transportation, methane upgrading to liquid fuels is of particular interest. Microbial methane conversion/utilization and upgrading is gaining increasing interest due to its high conversion efficiency. In this study we computationally compare aerobic and anaerobic microbial pathways for CH_4-oxidation and discuss theoretically achievable biomass yields as well as the possibility for building synthetic biological production platforms for liquid fuels. Specifically, the presented *in-silico* work investigates the potential of microbial methane upgrading in a metabolic network analysis by means of elementary flux modes. Aerobic fixation of methane via conversion of methane to methanol by a methane monooxygenase (MMO) and different subsequent formaldehyde assimilation pathways (Serine-cycle, RuMP, XMP/DHA-pathway) is compared with anaerobic pathways for oxidation of methane (AOM) by means of reverse-methanogenesis or via a presumed glycyl-radical enzyme, which uses fumarate for activation of methane. The different pathways for aerobic and anaerobic methane oxidation are compared in different central carbon-metabolism envelopes in order to identify highest achievable carbon yields. The capability of efficient CO_2 fixation, as well as energy preservation in form of reducing equivalents is identified as crucial to enable high yields, which ranged from 22 100%. The potential of the different microbes to grow on these gas streams is assessed by means of the maximum achievable biomass yield and the CO_2/CH_4 uptake ratio. CO_2 co-utilization, by transferring reducing power between the two co-substrates, is highest, when combining reverse-methanogenesis with the Wood-Ljungdahl pathway, effectively replacing the need for H_2 with CH_4. Further, the possibility to upgrade methane into liquid (drop-in) bio-fuels is investigated. Established routes to methanol, ethanol, C4-alcoholes and farnesene are evaluated in the most promising substrate-pathway/organism combinations. Stoichiometric, thermodynamic

and kinetic limitations are assessed and recommendations regarding potential industrial feasibility are given. The results presented here should guide future research efforts in search for feasible ways of (co)utilizing novel carbon substrates for sustainable production of fuels and chemicals.

Keywords: gas fermentation, methane upgrading, bio-GTL, elementary flux mode analysis, metabolic modeling, anaerobic methane oxidation, microbial CO_2 fixation

INTRODUCTION

Two of the greatest challenges of today's society are represented by the development of sustainable replacement processes to produce chemicals and fuels from non-fossil resources while simultaneously reducing greenhouse gas emissions. Microbial gas fermentation offers a solution to both issues via organisms with the ability to utilize gaseous C1-compounds, such as CH_4, CO_2 and CO as feedstock for production of chemicals. Here, we propose, analyse and discuss different strategies for microbial methane upgrading, a challenging but auspicious approach.

Methane, the main component of natural gas, has several shortcomings as an energy carrier. It has low energy content (MJ/L) and economical storage requires liquefaction or at least compression (which is expensive, because energy intensive). The same applies to biogas, which is further often contaminated with large amounts of carbon dioxide (up to 50%), making it an even less efficient energy carrier (Miltner et al., 2017). Methane is also a very potent greenhouse gas; therefore, it is often flared when logistics are (economically) infeasible (Haynes and Gonzalez, 2014). An estimated amount of 5 quadrillion BTU, around 5% of the global natural gas production, is flared or vented annually (Fei et al., 2014). This "lost" methane does not only contribute to greenhouse gas emissions but also represents a considerable market value of around $13 billion per annum, which alone could satisfy 27% of the US electricity market if made accessible (Fei et al., 2014). Therefore, the industrial interest in methane upgrading is high and different approaches for its conversion into better energy carriers have been developed. The chemical transformation of methane into fuels is mainly realized in the Fischer-Tropsch process via activation with syngas. However, this process achieves maximum carbon efficiencies of <50% and is further limited by its intensive energy requirements for the generation and conversion of syngas as well as hydro-processing steps and has proven economically viable only at very large scale (Steynberg, 2004). Seeking more efficient and sustainable alternatives, biological conversion of methane into more readily transportable and valuable fuels via biocatalysts at ambient temperatures and pressures, termed "Bio-GTL," receives increasing interest (biological gas-to-liquid).

The most extensively studied microorganisms for methane utilization are methanotrophic, aerobic α- and γ-proteobacteria, which are known to naturally metabolize methane as their only carbon and energy source. In these organisms the metabolism of methane starts with oxidation by O_2 to methanol, which is assimilated after further oxidation to formaldehyde via different pathways, depending on the organism (serine-cycle in α-proteobacteria/type II methanotrophs; ribulose-monophosphate pathway in γ-proteobacteria/type I methanotrophs). Although extensively studied, most methanotrophs are genetically not very tractable, so that to date their industrial use remains limited to the production biomass (single-cell protein), which is used as a feedstock for livestock in agriculture (Kalyuzhnaya et al., 2015). The production of more valuable target compounds, such as methanol, formaldehyde, organic acids, ectoine, lipids and vitamin B12 has been demonstrated in natural and synthetically engineered methanotrophs (Strong et al., 2015). However, the industrial use of microbial methane oxidation via aerobic pathways has several major limitations. Genetic engineering approaches in natural hosts are challenging and the expression of the key enzyme, methane- monooxygenase (MMO) in heterologous hosts has had only limited success to date (Hwang et al., 2018). Further, the requirement of O_2 as electron donor for methane oxidation has certain safety concerns at industrial scale due to explosive gas-mixtures. Additionally, the aerobic pathway via MMO has a limited maximum achievable carbon yield (67%) due to every third carbon being "lost" as CO_2 in a decarboxylation reaction of the pathway (Conrado and Gonzalez, 2014).

Opposing to the aerobic pathways, a second, less-studied option for microbial oxidation of methane is based on anaerobic metabolism. Anaerobic oxidation of methane (AOM) requires a suitable electron acceptor, such as iron(III), nitrate or sulfate and has been observed as natural occurring phenomenon in several environments often including syntrophic consortia (Boetius et al., 2000; Valentine and Reeburgh, 2000). Majorly hindered by the unavailability of pure cultures, AOM has been significantly less studied compared to aerobic methane oxidation and as a result the exact pathways of AOM still involve several knowledge gaps (Scheller et al., 2017; Hwang et al., 2018). However,

Abbreviations: ANME, anaerobic methanotrophic archaea; AOM, anaerobic oxidation of methane; BDO, butanediol; Bio-GTL, biological gas-to-liquid (microbial conversion of methane into liquid fuels); BMY, biomass carbon yield; BTU, British thermal unit; DHA, dihydroxyacetone; DXP, 1-deoxy-D-xylulose 5-phosphate; EFM, elementary flux mode; GSH, glutathione; H_4MPT, tetrahydromethanopterin; MCR, methyl-coenzyme M reductase; MDH, methanol dehydrogenase; MEP, 2-C-methylerythritol 4-phosphate; MMO, methane monooxygenase; MSS, methyl-succinate synthase; PY, product carbon yield; RuBisCO, ribulose-1,5-bisphosphate carboxylase/oxygenase; RuMP, ribulose mmonophosphate pathway; THF, tetrahydrofolate; XMP, xylulose-monophosphate; Δ_rG, Gibbs free energy of a chemical reaction; Δ_rG°, Gibbs free energy of a chemical reaction at standard conditions (not accounting for pH or ionic strength); $\Delta_rG'^\circ$, Gibbs free energy of a chemical reaction at a particular pH and ionic strength at 1 M standard concentrations; $\Delta_rG'^m$, Gibbs free energy of a chemical reaction at a particular pH and ionic strength at 1 mM (physiologically relevant) concentrations

there is evidence that anaerobic methane oxidation coupled to the reduction of sulfate, iron(III), manganese, or nitrate is found in anaerobic methanotrophic archaea (ANME) and proceeds at least in part via reversed-methanogenesis involving the nickel enzyme methyl-coenzyme M reductase (Mcr) for methane activation (Thauer and Shima, 2008; Beal et al., 2009; Shima et al., 2011; Haroon et al., 2013; Ettwig et al., 2016; Scheller et al., 2017). At standard conditions this presents an endergonic reaction, and therefore will proceed inherently slow. Nevertheless, this pathway has higher conservation of energy and may thus achieve a carbon efficiency advantage over aerobic pathways.

A second, MCR-independent AOM pathway coupled to nitrite reduction was observed in bacteria (Ettwig et al., 2010; Scheller et al., 2017). The first step in this pathway is most likely the exergonic formation of 2-methyl-succinate from fumarate and methane catalyzed by a glycyl-radical activating enzyme (Thauer and Shima, 2008). The involvement of a radical enzyme in this first step would not allow a direct coupling to energy conservation, so that most, if not all, energy generated during methane activation would dissipate as heat in the first step of the pathway. Therefore, this would not leave enough energy to drive ADP phosphorylation in reactions further downstream if coupled to sulfate reduction. However, with nitrate or nitrite as electron acceptor the free energy change would be sufficient to allow formation of 2-methyl-succinate (Thauer and Shima, 2008). And indeed, the (k_{cat}/K_m) of AOM with nitrate was found more than 1,000 times higher than that of AOM with sulfate (Raghoebarsing et al., 2006). With no pure culture isolate available, the details of the proposed pathway for anaerobic methane oxidation via 2-methyl-succinate remain unknown to date.

Several synthetic biology and metabolic engineering approaches present new pieces to the puzzles of anaerobic methane oxidation pathways. Yan et al. successfully introduced the MCR of an unculturable ANME into *Methanosarcina acetivorans*, which enabled the genetically modified strain of anaerobic methanotrophic growth dependent on reduction of iron(III) resulting in a pathway remarkably similar to AOM pathways hypothesized for uncultured anaerobic methanotrophic archaea (Yan et al., 2018). Another recent study followed an enrichment approach, which identified an archaeon capable of iron-dependent AOM via reverse-methanogenesis (Cai et al., 2018). Interestingly, a high abundance of multi-heme *c*-type cytochromes was found in this culture, which are hypothesized to facilitate dissimilatory iron(III) reduction. The fast development of ∼omics platforms and tools for genetic modification of non-model organisms gives reason to believe that significant progress regarding the fundamentals of aerobic and anaerobic oxidation of methane can be expected in the near future (Kalyuzhnaya et al., 2015). This system-level understanding of methanotrophic metabolism will lay the groundwork for metabolic engineering to generate value-added products from methane (Strong et al., 2015). However, it remains unknown which metabolic pathway for methane oxidation will prove most suitable for the development of this platform technology.

Here, we present a computational study to assess the potential of different pathways for the microbial oxidation of methane for formation of biomass and production of value added compounds. Using an *in silico* approach to calculate the metabolic capability of organisms to grow and produce chemicals from CH_4 as only carbon and energy source, enables to theoretically evaluate the most promising routes while current knowledge gaps remain. First, the different discussed pathways for aerobic and anaerobic methane oxidation are implemented in a metabolic network of the model organisms for biotechnology, *Escherichia coli.* Based on stoichiometry, we compare the theoretical maximum achievable biomass yields of each pathway. In a second part, the possibility of simultaneous CO_2 fixation enabled by the accumulation of reducing equivalents from the methane oxidizing pathway is discussed for different heterological host organisms. Finally, the different metabolic pathways for methane oxidation are paired with synthetic pathways for production of different (drop-in) fuels to evaluate most promising production routes. Benefits and limitations of the theoretical proposed scenarios are discussed critically.

MATERIALS AND METHODS

Construction of Metabolic Networks

Metabolic networks of the different organisms (Komagataella phaffii formerly Pichia pastoris, Saccharomyces cerevisiae, Escherichia coli, Bacillus subtilis, Corynebacterium glutamicum, Cupriavidus necator formerly Ralstonia eutropha and Clostridium autoethanogenum) were modified from published stoichiometric network analyses (Melzer et al., 2009; Lopar et al., 2013, 2014; Ternon et al., 2014; Unrean, 2014; Kracke et al., 2016; Koch et al., 2017; Averesch and Krömer, 2018; Averesch et al., 2018) to fulfill the requirements of this elementary flux mode analysis. Specifically, the networks were integrated with methane assimilation pathways, compiled as follows:

The methanol/formaldehyde assimilation pathways Serine-cycle, Ribulose-Monophosphate Pathway (RuMP) and Xylulose-Monophosphate Pathway (XMP)/Dihydroxyacetone- (DHA-) pathway, as described in Fei et al. (2014), Hwang et al. (2018), and on MetaCyc (Caspi et al., 2014), were compiled into stoichiometric reactions. The DHA-pathway corresponds to the XMP where instead of the DHA synthase a formolase is used (Siegel et al., 2015). Further, an NAD dependent methanol dehydrogenase (MDH) (Bennett et al., 2018) was evaluated in comparison to O_2 as electron acceptor for oxidation of methanol to formaldehyde, to determine the potential for increased carbon efficiency and energy conservation. NADH and NADPH dependent MMOs, which allow the initial oxidation of methane, completed the three fundamentally different pathways. Co-factor recycling allowed redox power to be derived from the oxidation of formaldehyde to CO_2 and proceeded with tetrahydrofolate (THF) for the Serine-cycle, with tetrahydromethanopterin (H_4MPT) in the RuMP and via glutathione (GSH) in the XMP/DHA-pathway (Marx et al., 2003). **Figure 1** shows the three pathways for aerobic methane catabolism in detail.

The proposed AOM by means of a glycyl-radical enzyme via methyl-succinate (Mss-AOM) was defined as proposed by

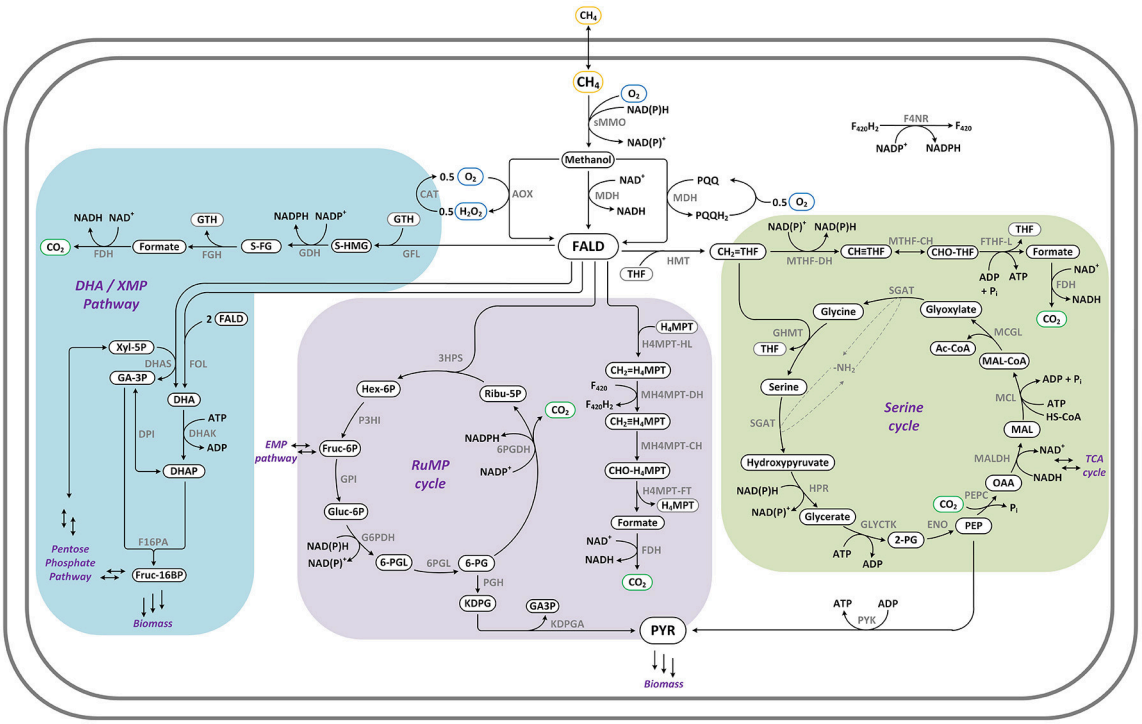

FIGURE 1 | Pathways for aerobic methane oxidation via methane monooxygenase (MMO): Serine-cycle (green), RuMP (purple), XMP/DHA-pathway (blue). Enzymes: 3HPS: 3-hexulose-6-phosphate synthase; 6PGD: 6-phosphogluconate dehydrogenase; 6PGL: 6-phosphogluconolactonase; AOX: alcohol oxidase; CAT: catalase; DHAK: dihydroxyacetone kinase; DHAS: dihydroxyacetone synthase; DPI: triose-phosphate isomerase; F16PA: fructose 1,6-bisphosphate aldolase; F4NR: F_{420}-dependent NADP reductase; FDH: formate dehydrogenase; FGH: S-formylglutathione hydralase; FOL: formolase; FTHF-L: formate:tetrahydrofolate ligase; G6PDH: glucose-6-phosphate dehydrogenase; GDH: S-(hydroxymethyl)glutathione dehydrogenase; GFL: S-(hydroxymethyl)glutathione formaldehyde-lyase; GHMT: glycine hydroxymethyltransferase; GLYCTK: glycerate 2-kinase; H_4MPT-FT: methenyltetrahydromethanopterin formyltransferase/hydrolase complex; H_4MPT-HL: 5,6,7,8-tetrahydromethanopterin hydro-lyase; HMT: hydroxymethyltransferase; HPR: hydroxypyruvate reductase; KDPGA: 2-keto-3-deoxygluconate-6-phosphate aldolase; MALDH: malate dehydrogenase; MCGL: malyl-CoA glyoxylate-lyase; MCL: malate:CoA ligase; MDH: methanol dehydrogenase; MH_4MPT-CH: methenyltetrahydromethanopterin cyclohydrolase; MH_4MPT-DH: methylenetetrahydromethanopterin dehydrogenase; MTHF-CH: methenyltetrahydrofolate cyclohydrolase; MTHF-DH: methylenetetrahydrofolate dehydrogenase; P3HI: 6-phospho-3-hexuloisomerase; PEPC: phosphoenolpyruvate carboxylase; PGH: phosphogluconate dehydratase; ENO: enolase/phosphopyruvate hydratase; PYK: pyruvate kinase; SGAT: serine:glyoxylate aminotransferase.

previous studies (Thauer and Shima, 2008; Haynes and Gonzalez, 2014). The different options for regeneration of fumarate include a series of reactions via TCA-cycle analogous reactions or a combination of β-oxidation and ketogenesis/GABA-metabolism. **Figure 2** gives a detailed overview of the different variations of this potential metabolic route for methane fixation. Here, nitrate respiration was assumed as a feasible way to complete the electron transport chain under anoxic conditions in the bacterial networks (Unden and Bongaerts, 1997; Nakano and Zuber, 1998; Nishimura et al., 2007; Tiemeyer et al., 2007).

AOM via reverse-methanogenesis by means of methyl-coenzyme M reductase (Mcr-AOM) was implemented as proposed by Nazem-Bokaee et al. (2016) and Bennett et al. (2018). The two branches of the pathway, which rely on an electron transport chain with iron(III) as terminal acceptor, are depicted in **Figure 3**.

It should be noted, that in **Figures 1–3** pathways were drawn out until a central metabolism metabolite (e.g., fructose-1,6-bisphosphate, pyruvate, succinate, acetyl-coenzyme A) was reached and connections to other pathways in central metabolism are indicated with double arrows. The full metabolic networks, integrated with the pathways, can be found in **Supplementary File 1**.

For chapter Potential of Different Organisms to Assimilate Additional Carbon via CO2 Co-utilization the metabolic networks were amended with established product pathway(s) for the designated target products, as described previously (Jang et al., 2012; Peralta-Yahya et al., 2012) and/or according to records in databases like KEGG (Kanehisa and Goto, 2000; Kanehisa et al., 2016, 2017) and MetaCyc (Caspi et al., 2014). All pathways can be found in **Supplementary File 1**, including details regarding the enzymes catalyzing the respective reactions and origin of the pathway.

Elementary Flux Mode Analysis

Using MATLAB® (MathWorks®) (RRID:SCR_001622) the metabolic networks were parsed with EFMTool (Terzer and Stelling, 2008; RRID:SCR_016289) into stoichiometric matrices. Metabolic solutions for each network were calculated as elementary flux modes (EFMs) using the most recent

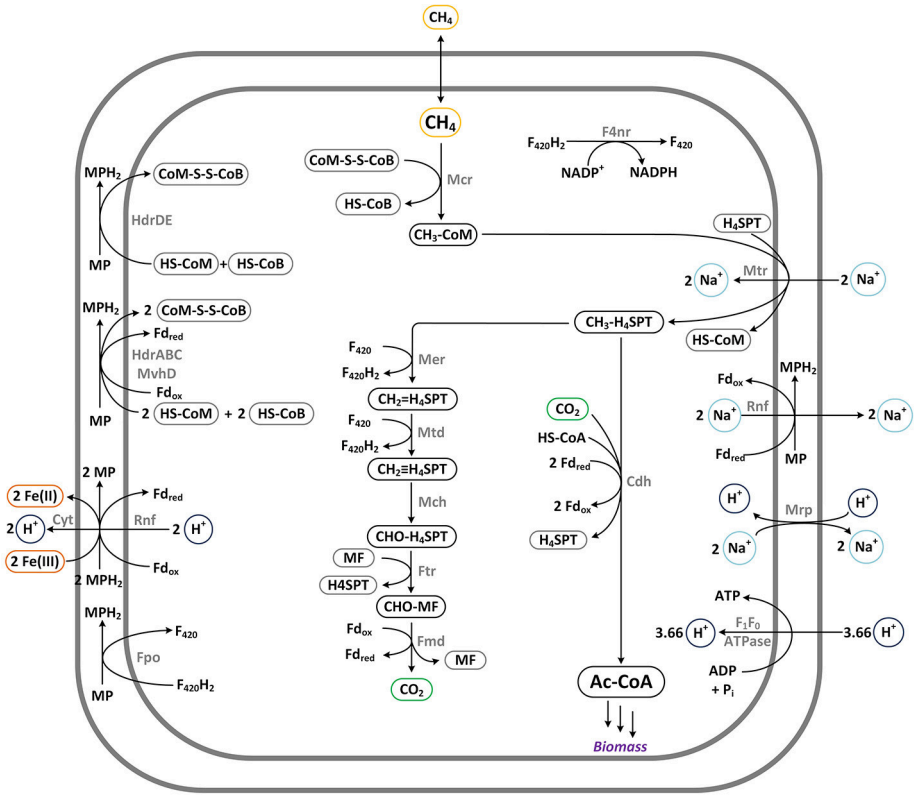

FIGURE 2 | Pathways for anaerobic methane oxidation via activation to 2-methyl-succinate: Mss-AOM. Note that this pathway requires a final electron acceptor, such as nitrate via anaerobic respiratory chain (not shown). Enzymes: BCDH: butyryl-CoA dehydrogenase; BCS: butyryl-CoA synthetase; BCT: butyryl-CoA transferase; CCH: crotonyl-CoA hydratase; CCL: citramalyl-CoA lyase; CCS: citramalyl-CoA synthetase; EMCDC: ethylmalonyl-CoA decarboxylase; HBCDH: hydroxyacyl-CoA dehydrogenase; HBCH: hydroxybutyryl-CoA hydrolase; HBCI: hydroxybutyryl-CoA isomerase; HBDH: 4-hydroxybutyrate dehydrogenase; MF: methylfumarase; MSCI: methylsuccinyl-CoA isomerase; MSCS: methylsuccinyl-CoA synthetase; MSDC: methylsuccinate decarboxylase; MSDH: methylsuccinate dehydrogenase; MSS: methylsuccinate synthase; SSADH: succinate-semialdehyde dehydrogenase; β-KAT: β-ketoacyl-thiolase.

implementation FluxModeCalculator (van Klinken and Willems Van Dijk, 2015; RRID:SCR_016290) and evaluated as described before (Averesch et al., 2016), calculating the yields by drawing carbon balances around the boundary reactions. The ratio of consumed or produced carbon dioxide to the (main) substrate was determined as the molar quotient of net CO_2-flux to other available carbon sources (most frequently methane) according to Equation (1). All calculated data and calculations based on the data can be found in **Supplementary File 1**.

$$ratio = \frac{(\text{flux}(CO_{2\text{in}}) - \text{flux}\,(CO_{2\text{out}}))\ [\text{mol}]}{(\text{flux}(CH_{4\text{in}}) - \text{flux}\,(CH_{4\text{out}}))\ [\text{mol}]} \quad (1)$$

RESULTS

Maximum Achievable Biomass Yields Via Different CH_4 Fixation Pathways

To compare the maximum achievable biomass-yields (BMY in % C-mol/C-mol) from CH_4 as sole electron and carbon source, the different pathways for aerobic and anaerobic methane oxidation were analyzed using the heterological host *E. coli* as model organism. The results are presented in **Table 1**.

When comparing the different pathways for methane catabolism pathways (see **Figures 1–3**), one universal feature can be identified: accompanying the reductive pathway for formation of carbon-carbon bonds from activated methane, there is always a second, oxidative pathway branch that ultimately forms CO_2 and provides the redox equivalents required for the reductive pathway steps. Additionally, all aerobic pathways require providing reducing equivalents for the MMO in the first pathway step (see **Figure 1**). This requirement of the key enzyme for one reducing equivalent per CH_4 limits the maximum achievable BMY via aerobic methane oxidation to 38% or lower. However, if the second pathway step, the formation of formaldehyde from methanol, could recover the electrons via a NAD-dependent enzyme (MDH) this limitation can be overcome, which is reflected in a theoretical maximum achievable BMY of 60–70% (see **Table 1**). In case of the XMP the initial step of dihydroxyacetone phosphate formation from formaldehyde is a bottleneck, as xylulose-5-phosphate needs to be regenerated. Replacing the DHA synthase with a formolase, as successfully demonstrated by Siegel et al. (Siegel et al., 2015), re-routes the pathway and eliminates this need, directly linking it to DHA, which benefits the theoretical maximum BMY.

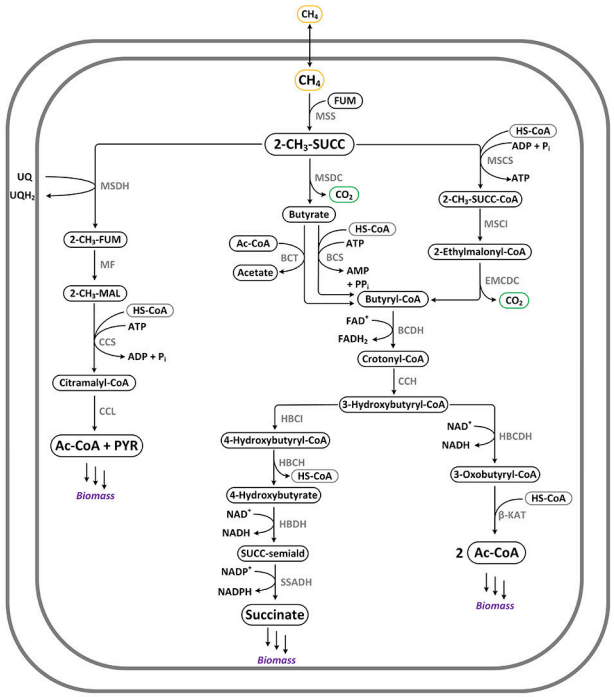

FIGURE 3 | Pathway for anaerobic methane oxidation via reverse-methanogenesis: Mcr-AOM. This pathway requires a final electron acceptor, such as iron(III) shown here. Enzymes: ATPase: ATP synthase; Cdh: CO dehydrogenase/acetyl-CoA synthase; Cyt: c-type cytochrome; F4nr: F_{420}-dependent NADP reductase; Fmd: formylmethanofuran dehydrogenase; Fpo: $F_{420}H_2$:phenazine oxidoreductase; Ftr: formylmethanofuran-H_4MPT formyltransferase; HdrABC: hydrogenase; HdrDE: CoB-CoM heterodisulfide reductase; Mch: N^5,N^{10}-methenyl-H_4MPT cyclohydrolase; Mcr: methyl-CoM reductase; Mer: N^5,N^{10}-methylene-H_4MPT reductase; Mrp: sodium/proton antiporter; Mtd: $F_{420}H_2$-dependent methylene-H_4MPT dehydrogenase; Mtr: N^5-methyl-H_4MPT:CoM methyltransferase; MvhD: heterodisulfide reductase (membrane-bound); Rnf: proton-translocating electron bifurcating oxidoreductase.

For anaerobic methane oxidation the proposed pathway via 2-methyl-succinate (Mss-AOM; **Figure 2**) and reverse-methanogenesis (Mcr-AOM; **Figure 3**) were considered. For the Mss-AOM a theoretical yield linked to respiration is given for reference, even though a feasibility of the entire pathway in one organism is regarded infeasible since the proposed glycyl-radical enzyme will require strictly anaerobic environments. For the different pathway versions of Mss-AOM only the branch via TCA-cycle analogous reactions was found feasible. This is due to decarboxylation reactions in the β-oxidation analogous pathway options, which lead to production of one CO_2 per fixed CH_4. Biomass assimilation via these pathway branches would only be feasible in combination with an efficient mechanism for CO_2 re-fixation (e.g., via RuBisCO, cf. *C. necator* BMY, **Supplementary File 1**). For the same reason, the Mss-AOM needs to recycle fumarate via the glyoxylic shunt, to compensate for the decarboxylation reactions during the TCA-cycle. The fact that this pathway needs to be operated with a different terminal electron acceptor than O_2, in this case NO_3, severely impacts the yield—otherwise it would present the most attractive option for CH_4 utilization based on stoichiometry (see **Table 1**).

Reverse-methanogenesis (Mcr-AOM) resulted in a maximum achievable BMY of 42%, which is about twice as high as the BMY for Mss-AOM with nitrate as electron acceptor. More importantly, this theoretical maximum BMY is in the same range or higher than the results for aerobic methane oxidation via MMO and Serine-cycle, RuMP or XMP/DHA-pathways in case of the natural, O_2-dependent MDH. This indicates that the AOM pathway via reverse-methanogenesis is not more restricted by stoichiometry than the aerobic options or the Mss-AOM.

Potential of Different Organisms to Assimilate Additional Carbon via CO_2 Co-utilization

Since methane is fully reduced (degree of reduction$_{(CH4)} = 8$), its assimilation in biomass as well as transformation into other hydrocarbons requires a parallel, electron accepting pathway. Here, we analyse several metabolic possibilities for microbial co-utilization of CO_2 during methane oxidation. The previous chapter, including **Figures 1**–**3**, illustrates how aerobic, as well as anaerobic methane oxidation always requires a certain amount of substrate to be oxidized in order to provide sufficient reducing equivalents for methane activation. Often oxidation in this pathway branch is complete, resulting in emission of CO_2 as by-product (degree of reduction$_{(CO2)} = 0$). We illustrate this formation of CO_2 as the ratio of net CO_2 production to the uptake of methane—CO_2:CH_4 [mol/mol] (cf. Equation 1, section Elementary Flux Mode Analysis). The rightmost column in **Table 1** shows the maximum ratios for the different pathways of microbial methane utilization applied to *E. coli*. A negative value refers to CO_2 production, while a ratio of "0" indicates that no net-flux of CO_2 is created; meaning that occurring decarboxylation reactions can be metabolically compensated for, e.g., via enzymes, such as pyruvate carboxylase. This is highly desirable, as the metabolic potential for carbon re-fixation is essential to maximize the carbon yield.

When comparing the different pathways, it appears that all aerobic pathway options inevitably will lead to CO_2 formation as by-product (for O_2-dependent MDH). The Serine cycle shows an especially high ratio of −0.262, translating to about 1 mol of CO_2 formed per 4 mol of CH_4 that are taken up. In the RuMP and XMP/DHA-pathway, potentially less carbon is "lost" as CO_2, however, complete avoidance of CO_2 formation (reflected in a ratio of "0") is only observed in case of NADH-dependent MDH for any of the aerobic pathways. Of all pathways, Mcr-AOM, seems most beneficial in this aspect as the CO_2 of its oxidative branch is directly re-fixated by adding it to the activated form of methane resulting in acetyl-CoA (see **Figure 3**). The complete reversal of methanogenesis is thermodynamically only feasible if coupled to an electron accepting pathway, in this case reduction of iron(III). If this electron accepting pathway could be provided via a carbon fixation pathway (fully or partially), the efficiency of microbial methane oxidation could potentially be further increased. Additionally, a co-fixation of CO_2 would present great environmental potential and be of particular benefit for biogas

TABLE 1 | Maximum theoretical biomass carbon yields and CO_2/substrate uptake ratios of different methane-catabolizing pathways implemented in *E. coli*, compared to glucose as natural carbon-source.

Main (redox power carrying) carbon-source (substrate)	Carbon-catabolizing pathway	Specific scenario	Maximum biomass carbon yield [%]	Maximum ratio CO_2/CH_4 [mol/mol]
Glucose	Glycolysis	–	70.2	0
Methane	Serine-pathway	O_2 dependent MDH	38.6	−0.262
		NAD dependent MDH	64.4	0
	RuMP	O_2 dependent MDH	38.2	−0.02
		NAD dependent MDH	70.2	0
	XMP/DHA-pathway	O_2 dependent MDH	30.8	−0.02
		NAD dependent MDH	61.5	0
	XMP/DHA-pathway, formolase	O_2 dependent MDH	38.1	−0.02
		NAD dependent MDH	70.7	0
	Mss-AOM via PYR + AC-CoA	O_2 respiration	73.6	0
		NO_3 respiration	21.5	−0.05
	Mss-AOM via SUCC & AC-CoA	O_2 respiration	0	N/A
		NO_3 respiration	0	N/A
	Mcr-AOM (reverse-methanogenesis)	–	42.1	0

upgrading applications (Weiland, 2010; Conrado and Gonzalez, 2014). Therefore, several metabolic options for additional CO_2 uptake were investigated.

Different microbial hosts were chosen as model organisms for CH_4-CO_2 co-utilization to evaluate the potential across several industrially relevant species: *Komagatella phaffii* (formerly *Pichia pastoris*) and *Saccharomyces cerevisiae*, *Escherichia coli*, *Bacillus subtilis, Corynebacterium glutamicum, Cupriavidus necator* (formerly *Ralstonia eutropha*), and *Clostridium autoethanogenum*. This includes eukaryotes, prokaryotes, Gram-positives and Gram-negatives, heterotrophic as well as autotrophic species (photoautotrophic organisms were not considered within this study). Exact details regarding the specific metabolism of each organism can be found in **Supplementary File 1**, while **Table 2** presents the maximum possible CO_2 uptake calculated for each case. This is again presented as maximum ratio of CO_2:CH_4 in mol/mol (positive ratio = CO_2 is fixed, negative ratio = CO_2 is produced, 0 = no net-CO_2-flux). The scenarios (C-source and pathway) that are listed in the last column represent the specific pathways, which resulted in the highest achievable CO_2 fixation in each case. A full list of results for each individual pathway and organism is included in **Supplementary File 1**.

For aerobic methane oxidation in *E. coli*, the most beneficial scenario identified above, MMO with NAD-dependent MDH, can be further improved in the case of CO_2-co utilization. The maximum ratio of 0.245 indicates that reducing equivalents can potentially be re-distributed across the metabolism to allow for additional CO_2 fixation at the theoretical maximum level of ∼1 mol CO_2 per 4 mol CH_4. The same scenario (RuMP and DHA-pathway with NAD-dependent MDH) was also found most beneficial for *B. subtilis* where it theoretically enables for CO_2-neutral CH_4-utilization. Maybe not surprisingly, most interesting scenarios are represented by organisms, which naturally inherent CO_2-fixation pathways as their major carbon metabolism: *Cupriavidus necator* and *Clostridium autoethanogenum*. The hydrogen-oxidizing bacterium *C. necator* has a very versatile metabolism, being able to switch between aerobic, anaerobic and nitrate respiration. Here, we found that if this metabolism could be paired with the ability for methane oxidation, high maximum biomass yields may be achieved. Further, CO_2 co-fixation at a maximum ratio of 0.307 was determined for the DHA-pathway featuring an NAD-dependent MDH (cf. **Table 2**). The key enzyme, which enables this high CO_2-fixation capacity is RuBisCO. The anaerobic acetogen *C. autoethanogenum*, on the other hand, uses the strict anaerobic Wood-Ljungdahl pathway for CO_2 fixation. This particular pathway was the only option found in this analysis to efficiently enable CO_2 co-utilization from reverse-methanogenesis. Since both pathways, Mcr-AOM and Wood-Ljungdahl pathway, share ferredoxin as redox carrier, electrons can be transferred most efficiently, resulting in a maximum substrate ratio of 0.875 CO_2 per CH_4 [mol/mol]. This

TABLE 2 | Overview of organisms and pathways modeled, with information on CO_2 fixation capability, including results: max.

Organism	CO_2 fixation capability	Max. biomass yield [%]	Max. ratio*	C-source/pathway
Komagataella phaffii (*Pichia pastoris*)	Pyruvate carboxylase	81.4	0	Glucose
		79.1	0	CH_4/DHA (formolase) + NAD-MDH
Saccharomyces cerevisiae	Pyruvate carboxylase	68.4	−0.851	Glucose
		67.4	0	CH_4/DHA (formolase) + NAD-MDH
Escherichia coli	Phosphoenolpyruvate carboxylase	70.2	1.2	Glucose
		70.2 70.7	0.245	CH_4/RuMP + NAD-MDH DHA (formolase) + NAD-MDH
Bacillus subtilis	Pyruvate carboxylase, phosphoenolpyruvate carboxylase	78.3	0	Glucose
		78.3	0	CH_4/RuMP + NAD-MDH CH_4/DHA (formolase) + NAD-MDH
Corynebacterium glutamicum	Pyruvate carboxylase, phosphoenolpyruvate carboxylase	68	−0.943	Glucose
		68 68.9	−0.143	CH_4/RuMP + NAD-MDH CH_4/DHA (formolase) + NAD-MDH
Cupriavidus necator (*Ralstonia eutropha*)	Pyruvate carboxylase, ribulose-1,5-bisphosphate carboxylase/oxygenase (RuBisCO)/reductive pentose phosphate cycle/Calvin–Benson cycle	73.5	1.4	Fructose
		100	0.361	$CO_2 + H_2$
		77.1	0.307	CH_4/DHA (formolase) + NAD-MDH
Clostridium autoethanogenum	Pyruvate carboxylase, reductive acetyl-CoA pathway/Wood–Ljungdahl pathway	31.9	0	Fructose
		67.3	0.5	$CO_2 + H_2$
		94.9	0.875	CH_4/Mcr-AOM

*BMY from conventional carbon-source and CH_4 as well as CO_2:substrate fixation ratio (absolute max. ratio). *Ratio is molar (e.g., mol-flux CO_2: mol-flux CH_4; in case of CO_2 being the only carbon-source, the ratio is CO_2:H_2) total CO_2 flux is calculated as CO_2-in less CO_2-out.*

theoretical transfer of electrons from methane to the carbon fixation pathway further allows a very high maximum BMY of 95% (cf. **Table 2**).

Bio-GTL: Production of (Drop-In) Fuels

The ultimate benefit of microbial methane oxidation is the potential production of liquid fuels with high specificity and at ambient temperatures and pressures (Conrado and Gonzalez, 2014). Therefore, the next step of our analysis pairs the different microbial pathways for CH_4-oxidation with production pathways for industrially relevant fuels to identify the most promising scenarios. The here investigated drop-in fuels are methanol, ethanol, butanol, *iso*-butanol, butanediol and farnesene. **Table 3** summarizes information on each target product, including the corresponding synthetic pathway(s) for each compound, which were implemented in the different metabolic networks. The three columns on the right, "PY_{max}" and "best host organism," list the most promising scenario that was determined by our analysis for each individual target product. Further, we distinguish between the different metabolic pathways for methane oxidation that were discussed in the previous chapters. The full report on all results from each individual combination is given in **Supplementary File 1**. Additionally, in **Figure 4** the distribution of EFMs is displayed for selected

TABLE 3 | Target products for methane upgrading investigated in this study.

Target product	Formula	Industrial use	Market value† [USD/kg]	Market size† [KTA]	References	Microbial product synthesis pathway	PY^{*}_{max} [%] via MMO-pathway and best host organism	PY^{*}_{max} [%] via Mss-AOM and best host organism	PY^{*}_{max} [%] via Mcr-AOM and best host organism
Methanol	CH_3OH	Fuel, antifreeze, solvent, bio-fuel production	2.6	9,000	Budzianowski, 2017	Reverse RuMP-/XMP	66.7 (any organism)	69.2 (*C. glutamicum*)	100 (*C. autoethanogenum*)
Ethanol	CH_3CH_2OH	Transportation fuel (blended in)	0.47–0.67	43,000 (fuel only)	Ghoddusi, 2017; Report, 2017	Ethanol fermentation	66.7 (any organism)	81.5 (*C. glutamicum*)	100 (*E. coli*/*C. autoethanogenum*)
Butanol	$C_4H_{10}O$	(Drop-in) fuel, solvent, paint and fragrance industry	1.2–1.4	2,800–4,000	Green, 2011; Budzianowski, 2017	(1)threonine synthesis pathway (2) Clostridial acetone–butanol–ethanol (ABE) fermentation pathway	66.7 (any organism except *K. phaffii*) ABE-pathway	85.7 (*C. glutamicum*) ABE-pathway	100 (*E. coli*/*C. autoethanogenum*) ABE-pathway
Iso-butanol	$C_4H_{10}O$	(Drop-in) fuel, precursor for chemical industry, solvent, paint and fragrance industry	1.2	552	Atsumi et al., 2008; Blombach et al., 2011; Report, 2016	Amino acid biosynthesis pathway e.g. in engineered *C. glutamicum* and *E. coli*	66.7 (any organism)	81.5 (*C. glutamicum*)	100 (*C. autoethanogenum*)
1,4-Butanediol	$C_4H_{10}O_2$	Solvent, polymer industry	1.65	2,357	Yim et al., 2011; Budzianowski, 2017	Genomatica synthetic pathway in *E. coli*	71.8 (*C. necator*)	75 (*C. glutamicum*)	100 (*C. autoethanogenum*)
2,3-butanediol	$C_4H_{10}O_2$	Food, pharma, agrochemical industry	1.65	74	Budzianowski, 2017	2,3-Butanediol pathway (from Pyruvate via Acetoin, e.g. by *Clostridium autoethanogenum*)	72.7 (*C. necator*)	89.9 (*C. glutamicum*)	100 (*C. autoethanogenum*)
farnesene	$C_{15}H_{24}$	chemical building block for solvents, emollients, vitamins	50–100	N/A	Amyris, 2018	(1)Isoprenoid biosynthesis via DXP/MEP-pathway (plants, most bacteria, and some protozoa) (2) Isoprenoid biosynthesis via mevalonate-pathway (eukaryotes, archaea, and some bacteria)	65.1 (*B. subtilis*)/65.7 (*C. neacator*)/66.7 (*C. glutamicum*) DXP/MEP-pathway	75.0 (*C. glutamicum*) mevalonate-pathway	100 (*C. autoethanogenum*) mevalonate-pathway

"Best host organism" gives the organisms with maximum theoretical product carbon yield(s), identified via elementary flux mode analysis for the three different classes CH_4-oxidizing pathways: aerobic via MMO, anaerobic via Mcr-AOM or Mss-AOM. For the PY_{max} that were achieved in each particular scenario refer to ***Supplementary File 1****.* † *Market value and size were taken or calculated from the references listed.* * *PY_{max} is the maximum achievable product carbon yield.*

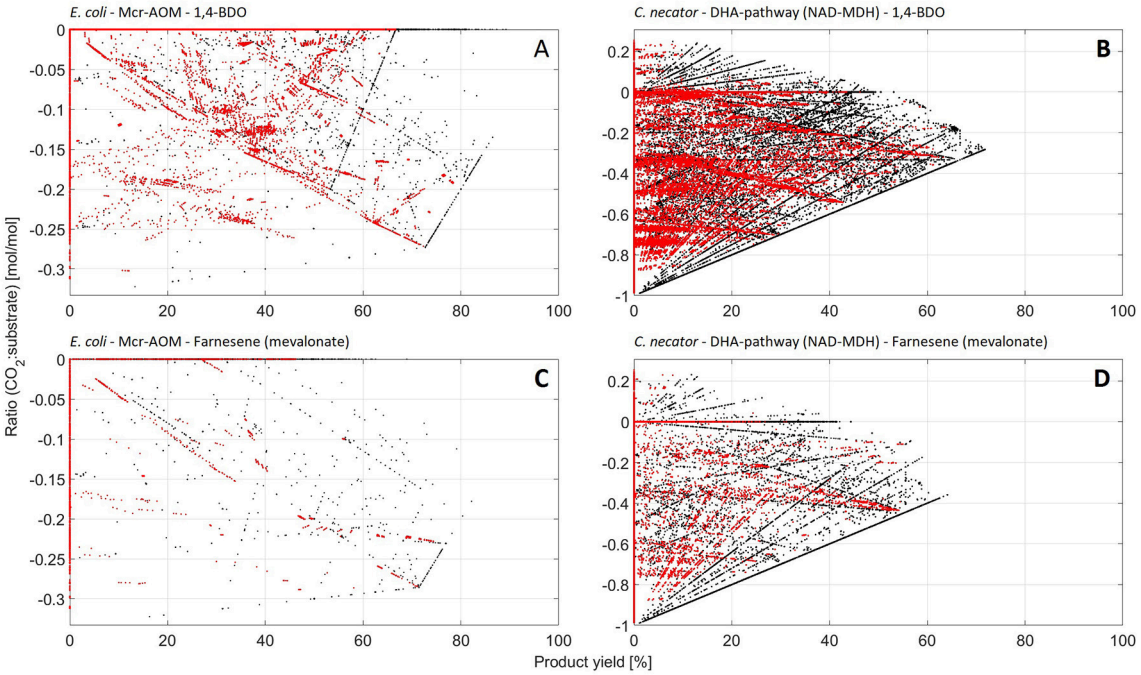

FIGURE 4 | (A–D) Distribution of elementary flux modes (EFMs) by CO_2:CH_4 uptake-ratio vs. PY for selected scenarios. **(A)**: Mcr-AOM in *E. coli*, target product 1,4-BDO; **(B)**: DHA-pathway (NAD-dependent MDH) in *C. necator*, target product 1,4-BDO; **(C)**: Mcr-AOM in *E. coli*, target product farnesene (mevalonate-pathway); **(D)**: DHA-pathway (NAD-dependent MDH) in *C. necator*, target product farnesene (mevalonate-pathway). Each dot in a plot represents one feasible steady-state flux distribution. EFMs that also allow for formation of biomass (growth) are highlighted in red.

scenarios in plots of the CO_2:CH_4-ratio vs. the PY of the individual EFMs.

Under the aspect of stoichiometric constrains as applied here, one overall best scenario and host can be identified: All here investigated compounds can be produced with a theoretical PY_{max} of 100% from methane and CO_2 via Mcr-AOM in *C. autoethanogenum*. The unique advantage of a common intracellular ferredoxin pool, accessible between the natural CO_2 fixation pathway (Wood-Ljungdahl) as well as the AOM, facilitates optimum usage of redox equivalents. As discussed under 3.2, this enables for high CO_2:CH_4 fixation ratios, which are largely in the positive range (and never lower than 0!). However, high ratios of CO_2 co-utilization and high PY are mutually exclusive. Nevertheless, this unique combination of AOM and Wood-Ljungdahl pathway presents an attractive option as production platform. Further, production via reverse-methanogenesis, Mcr-AOM, in *E. coli* shows an interesting pattern (cf. **Figure 4**), with maximum product yields of up to 100% (possible for ethanol and butanol via acetoacetyl-CoA pathway). Given the simultaneously rather low biomass yields of Mcr-AOM in *E. coli* (cf. **Table 1**; **Supplementary File 2**), this could imply that a favorable distribution of carbon between production pathways and biomass formation may be achieved.

The next best scenario for bio-GTL, evaluated by stoichiometry, is again presented by anaerobic oxidation of methane: Mss-AOM in *C. glutamicum*. Here, the PY_{max} for methanol is 69%, while for all other products PY_{max} of 75% or higher were calculated. The CO_2:CH_4 ratio for this scenario is always negative (CO_2 is being produced), however, the highest PY is always obtained at the lowest CO_2 output flux (ratio ≤ -0.1). Another promising host organism for production of fuels via the Mss-AOM is presented by the hydrogen-oxidizing bacterium *C. necator*. Theoretical achievable PY_{max} are slightly lower than in *C. glutamicum* (52% for farnesene, all others >60%), but the CO_2:CH_4 ratio can be positive, providing a promising platform for CO_2-CH_4-co-utilization. However, PY_{max} can only be reached at a negative ratio between −0.5 and −0.3 (cf. **Figure 4**).

Production via aerobic methane utilization pathways are usually limited to a maximum achievable carbon yield of 67% due to the decarboxylation steps as discussed earlier. This is also reflected in the presented analysis: the PY_{max} of aerobic methane oxidation to methanol, ethanol, butanol, *iso*-butanol and (in most cases) butanediol is limited to 67%, independent of organisms or formaldehyde assimilation pathway (cf. **Supplementary File 1**). Only *C. necator* may achieve PY_{max} above 70%, in the scenarios of butanediol production (cf. **Figure 4**), due to its efficient CO_2-re-fixation mechanism. For the production of the high value hydrocarbon building block farnesene, our analysis shows higher PY_{max} of the DXP/MEP-pathway opposing to the mevalonate-pathway (cf. **Table 3**; **Supplementary File 1**), which was expected due to the noted higher carbon efficiency of the non-mevalonate pathway (Kirby et al., 2016). Nevertheless, *C. necator* achieves an almost equivalent PY_{max} via the mevalonate-pathway (64%),

again due to its effective CO_2 (re-)fixation capability. Similar, as seen for the maximum achievable biomass yields under chapter 3.1, all PY_{max} in aerobic methane oxidation scenarios feature the NAD-dependent MDH. Given that the O_2-dependent MDH is thermodynamically greatly favored; pathways proceeding via O_2-dependent MDH will likely have higher rates. Most promising target compound here is methanol, with a PY_{max} of 50%, while all other target compounds, show PY_{max} below 36% in this scenario.

DISCUSSION

The presented analysis highlights the potential of different metabolic pathways for microbial methane utilization, which will determine future Bio-GTL processes. While the discoveries are intended to guide research efforts, it should be stressed that the presented data is theoretical and based on stoichiometry only. Therefore, the following sections discuss our results in the context of kinetic and thermodynamic limitations as well as challenges related to metabolic engineering approaches, which adds to a holistic interpretation of the study.

Challenges for Construction of Synthetic Methanotrophs, Pathway Engineering and Stoichiometric Limitations

The combination of aerobic or anaerobic pathways for methane oxidation with different anabolic pathways as discussed here, requires substantial metabolic engineering of either native methanotrophs or synthetic hosts, which present a significant challenge. Past approaches of various companies and research institutes have so far focused on aerobic methanotrophs for production applications. However, metabolic engineering of production pathways in native methylotrophs remains restricted by the limited toolset for genetic modification (Strong et al., 2015; Bennett et al., 2018). The transformation of a CH_4-oxidation pathway into an industrial organism would thus provide great advantages but has proven equally challenging. Microbial hosts, which are used in industrial scale production processes like *Escherichia coli*, *Corynebacterium glutamicum*, and *Saccharomyces cerevisiae* have been successfully engineered to utilize methanol, paving the way toward a C1-based industrial biotechnology (Schrader et al., 2009; Haynes and Gonzalez, 2014; Strong et al., 2015; Meyer et al., 2018). Introduction of a methane monooxygenase (MMO) could make them methanotrophic and open the door to many established production routes for biofuels. However, the crucial missing link, expression of fully active MMO in heterologous hosts, has not been accomplished to date (Kalyuzhnaya et al., 2015; Hwang et al., 2018). MMOs are complex proteins, soluble MMOs consist of a reductase, a hydroxylase, and a regulatory protein and despite many attempts, heterologous expression yielded only a partially active sMMO with a functional hydroxylase (West et al., 1992; Strong et al., 2015). An alternative approach is presented by P450 monooxygenases, which have been heterologically expressed to mimic the function of the MMO, however, with similarly limited success (Hwang et al., 2018). Nevertheless, an engineered BM-3 cytochrome P450 monooxygenase from *Bacillus megaterium* has been patented (Arnold et al., 2005). With the implementation of emerging new technologies that enable rapid advances in synthetic biology (CRISPR on the molecular side, and lab-automation on the operational side), breakthroughs can be expected that 1 day may allow the metabolic engineering, which is necessary for the development and construction of synthetic methylotrophs in biotechnology.

Given that the major hurdle of initial activation of methane would be overcome, our results indicate that aerobically *C. necator* theoretically allows the highest maximum CO_2:CH_4 fixation ratios. This aligns well with the observation that a *Methylacidiphilum fumariolicum* strain fixates CO_2 by means of the Calvin-cycle, in parallel to methane assimilation (Fei et al., 2014). The potential to aerobically use reducing power obtained from methane-oxidation to simultaneously fixate CO_2, has recently been demonstrated *in vivo* when *Methylobacterium extorquens* AM1 was engineered toward autotrophy to fixate CO_2 through a heterologous Calvin-cycle while growing on methanol (Schada von Borzyskowski et al., 2018). Further, our finding that the highest aerobic CO_2:CH_4-fixation ratio is obtained with the Serine-cycle, aligns with reports that α-proteobacteria can assimilate up to 50% of their biomass from CO_2, while the γ-proteobacteria can assimilate up to 15% (Trotsenko and Murrell, 2008). These co-fixation levels of CO_2 are only possible with NAD-dependent MDH (cf. **Supplementary File 2**), which is feasible in case of coupling of the MDH to pMMO via direct transfer of electrons (cf. section Thermodynamic Limitations of Aerobic and Anaerobic Oxidation of Methane; de la Torre et al., 2015).

Opposing to the efforts for engineering aerobic systems for CH_4 utilization, little research has focused on the potential of AOM as pathway for bio-GTL, due to several knowledge gaps. Even though trace methane oxidation by reverse-methanogenesis has been successfully demonstrated, optimization of the pathway remains limited due to the unavailability of pure cultures (Moran et al., 2005; Scheller et al., 2010). However, a recent synthetic biology approach successfully demonstrated anaerobic production of chemicals from methane in an engineered *Methanosarcina acetivorans* (Soo et al., 2016). Introduction of the Mcr of an unculturable ANME resulted in the first (synthetic) pure culture capable of reverse-methanogenesis. This represents a significant breakthrough toward Bio-GTL technologies since AOM pathways offer a significant carbon efficiency advantage over aerobic pathways, as shown in our analysis. A follow-up study from the same group further demonstrated co-utilization of methane and bicarbonate through the reversal of the acetoclastic-pathway in the engineered *M. acetivorans* (Nazem-Bokaee et al., 2016). This finding underlines our results regarding the benefits of possible CH_4-CO_2 co-utilization via AOM. In particular, our analysis identified the Wood-Ljungdahl pathway as potential parallel pathway to AOM. The fact that electrons from CH_4 could theoretically be efficiently conserved to act as electron carrier for CO_2 reduction presents a very promising aspect and should attract further research efforts especially since *C. autoethanogenum* has emerged as a model organism for gas fermentation and is used in industrial scale production applications (Liew et al., 2016).

Regarding the proposed pathway of Mss-AOM many knowledge gaps remain. However, the here presented analysis can allow conclusions to be drawn toward the potential stoichiometry of the pathway: in 2008 Thauer and Shima proposed two different options for carbon-cycling and regeneration of fumarate after activation of methane (Thauer and Shima, 2008). In the present study, only one of the proposed Mss-pathways has proven feasible under the given assumptions, unless a simultaneous pathway for re-fixation of CO_2 exists (e.g., RuBisCO). This finding also questions the conclusions made in a study on environmental samples of a bio-corrosive consortium, where the detection of butyric acid was interpreted as indication for activity of AOM via Mss (Duncan et al., 2009): in the proposed options for Mss-AOM, butyric acid presents an intermediate of the β-oxidation-analogous pathway branch, which has been identified as stoichiometrically infeasible (cf. **Figure 3**) in most cases. Given the predicted high carbon efficiency achievable via Mss-AOM, elucidation of the exact *in vivo* pathway is of particular interest for Bio-GTL applications.

Rate Requirements, Kinetic Considerations and Rate/Yield Trade-Off

It has previously been stated that the activity of Mcr is one to two orders of magnitude lower than that of pMMO and sMMO, respectively (Mueller et al., 2015). To achieve industrial feasibility [methane activation rate of 1 $g_{CH4}/(L \times h)$] in a bio-GTL process, and under the assumption that, in case of reverse-methanogenesis, Mcr comprises at least 20% of cellular protein (Mueller et al., 2015), this would translate to a requirement of an average cell density of 32 g_{CDW}/L. These assumptions are likely to be a fair bit too optimistic, as the below considerations illustrate:

The maximum reaction rate of limiting steps of reverse-methanogenesis have been elucidated, the lowest and therefore the bottleneck being the transfer of the methyl-group from CH_3-SCoM to THF/H_4MPT, at 9.8 ± 1.2 nmol/(min × mg) ∧ 0.6 mmol/(h × g) (Yan et al., 2018). In a rough calculation, a specific maximum rate of substrate consumption for a microbial system can be estimated: assuming a total protein concentration of 0.5 g/g_{CDW} and a maximum concentration of the respective enzyme of 1%, the maximum fraction of any given enzyme can be estimated to be 5 mg/g_{CDW} (Averesch et al., 2018). With that, a maximum specific rate of 3 $\mu mol/(g_{CDW} \times h)$ can be determined. This can be compared to established values for minimum rates to suffice standards in industry for production of biotech products. Specifically, these are a productivity in the single-digit g/(L × h) range and a minimum specific rate of 0.01 $mol/(g_{CDW} \times h)$ (Averesch and Krömer, 2018). Measured on these, the Mcr-AOM can be evaluated as "the 10,000-fold amount of biomass is needed," which means that reverse-methanogenesis is about four orders of magnitude away from operating in the range of industrial applications. However, it should be kept in mind that the thresholds presented above are accepted in the context of product formation in white biotechnology. Here, we apply these to the rate of substrate (CH_4) uptake, hence the actual product formation rate may be even lower (equal only at 100% carbon yield, while lower in any other case to account for carbon partitioning depending on the yield of the pathway/efficiency of energy conservation). On the other hand, the production rate could potentially also be higher, if the CO_2/CH_4 ratio is positive (i.e., CO_2 is a significant additional carbon-source). Nevertheless, common biotech processes rely on sugar-based carbon-sources, which, compared to methane, rank in a different price-segment, so that a gas-based processes might not have to suffice these strict standards. Additionally, utilization of a waste-stream as carbon-source, which in some cases even might be associated with a negative cost value, has the potential to change the picture, making reverse-methanogenesis still an attractive pathway for methane utilization and upgrading.

In the aerobic pathways the MMO is believed to be the rate-limiting step (Hwang et al., 2018). According to experimental data collected in BRENDA (Placzek et al., 2017), measured specific activities of sMMO span several orders of magnitude, from as low as 0.11 nmol/(min × mg) to 26.1 μmol/(min × mg) (Brenda, 2018). However, in most cases the substrate in these studies was not methane, but a longer unsaturated hydrocarbon (e.g., C_3H_x). Further, most more-recent studies report activities higher than 0.1 μmol/(min × mg), with only few publications reporting activities higher than 10 μmol/(min × mg) ∧ 0.6 mol/(h × g), which was therefore used as a "best-case scenario" to compare the aerobic pathways to reverse-methanogenesis. Based on that, the aerobic pathways are potentially three orders of magnitude faster than the Mcr-AOM and only one order of magnitude away from the established requirements for industrial viability and therefore within an achievable range. However, a further improvement of MMO activity, without changing e.g., environmental parameters, is constraint by thermodynamic limitations (section Rate Requirements, Kinetic Considerations and Rate/Yield Trade-Off).

Finally, a more global kinetic constraint of application of methanotrophs at industrial scale relates to rate issues of gas-fermentations due to poor solubility of gases and thus limited mass-transfer, outlined as one of its greatest challenges (Strong et al., 2015). Comparing solubilities of gases participating in gas-fermentations (**Table 4**), it appears that CH_4 and O_2 have similar solubilities, with the one of H_2 being orders of magnitude lower. Thus, aerobic processes would still be limited by the solubility of CH_4, however, if in an anaerobic gas fermentation H_2 could be replaced with CH_4, severe mass-transfer limitations might be overcome. Further, these constraints are not as critical for AOM (due to its metabolic rate limitations) as they are for aerobic methane oxidation, which would favor large-scale applications using AOM (Bennett et al., 2018).

Thermodynamic Limitations of Aerobic and Anaerobic Oxidation of Methane

Thermodynamically, the energy change that is associated with the activation of methane with oxygen to methanol via MMO could theoretically phosphorylate up to 14 ATP without the $\Delta_rG'^{\circ}$ becoming ≥0 [$\Delta_rG'^{m}$, which is the more relevant value for biological systems, becomes positive already at 9 ATP, as

TABLE 4 | Solubility of relevant gases in water at 30°C and atmospheric pressure.

Gas	Solubility [g/kg]
CO_2	1.25
O_2	0.036
CO	0.024
CH_4	0.019
H_2	0.00147

Values derived from Toolbox (2008).

determined with equilibrator (Flamholz et al., 2012)]—however, this energy remains unused for some reason. Potentially, it is dissipated into heat, which could be an explanation for the low rates of MMOs: avoidance of overheating. This is backed by the largely negative $\Delta H'^{\circ}$ of methanotrophic bioprocesses (−2,464 kJ/mol for butanol production via aerobic oxidation of methane), where most of the energy is lost in the form of heat, resulting in increased cooling demand (Haynes and Gonzalez, 2014).

Functionality of the NAD-dependent MDH has been evaluated in comparison to an MDH which relies on pyrroloquinoline quinone (and ultimately O_2) as electron acceptor for oxidation of methanol to formaldehyde, to determine the potential for increased carbon efficiency and energy conservation, but is thermodynamically hampered (Bennett et al., 2018). With an estimated $\Delta_r G'^{m}$ of 34.2 kJ/mol [determined with equilibrator (Flamholz et al., 2012)] the NAD-dependent MDH has limitations in the same order of magnitude as the Mcr-AOM. Here, however, a similar argument could be made as compared to the Mcr, where it has been argued that substrate concentrations, are likely orders of magnitude higher since it is a gas, thus shifting the $\Delta_r G$ into the feasible range (Thauer and Shima, 2008). For the MDH a similar gradient may be achieved, since the product concentration will always have to be very low, since formaldehyde is very toxic. Effectively this means, that when operated at highest yield, aerobic pathways may be subject to similar thermodynamic constrains as Mcr-AOM, bringing the respective maximum rates closer together. While it might be possible to further improve kinetics of the NAD-dependent MDH to a certain degree, thermodynamic limitations of an unfavored cannot be altered, unless coupled with a thermodynamically highly favored reaction, like the MMO: reportedly direct coupling of electron transfer between MDH and pMMO is possible (de la Torre et al., 2015), which could shift the $\Delta_r G$ of a NAD-dependent enzyme in the feasible range. Further, thermodynamics of the NAD-dependent MDH improve with increased temperatures, which is likely a reason for thermophily of many methanotrophs (Hwang et al., 2018).

Regarding the anaerobic pathways, it has been stated that protein engineering efforts could potentially improve the catalytic activity of the key enzyme Mcr into the range of pMMO (Mueller et al., 2015). However, this statement has to be considered with care, respecting thermodynamic constraints. Opposing to aerobic oxidation of methane via MMO, reverse-methanogenesis has the opposite issue: the $\Delta_r G'$s of the first two steps (the initial activation of CH_4 with CoM and transfer to H_4MPT) have rather largely positive values of 30 kJ/mol [with an uncertainty of ±10 (Thauer and Shima, 2008)], while the recycling of the Coenzyme M—Coenzyme B dimer even has a $\Delta_r G$ of 40 kJ/mol (Mueller et al., 2015). Further, many of the subsequent steps have a positive $\Delta_r G$ or values close enough to 0 to impose additional bottlenecks [at a $\Delta_r G$ of −1 kJ/mol, the flux-force efficacy is only 20% (Noor et al., 2014)].

Thermodynamic considerations can also be used to assess the likeliness of Mss-AOM. While there is strong indication that an alternative anaerobic pathway exists, which is based on fumarate to activate methane (Duncan et al., 2009), to date the responsible enzyme has not been identified nor has the reaction it catalyses been documented. While the reaction catalyzed by Mss has a $\Delta_r G'^{\circ}$ of −15 kJ/mol, and is thus in general thermodynamically feasible (Haynes and Gonzalez, 2014), the difference in dissociation energies of the methyl-radical and the glycyl-radical of almost 90 kJ/mol is technically too high to be overcome in a biological system (Thauer and Shima, 2008). Nevertheless, similar to Mcr glycyl-radical enzymes are functional dimers, which show half-of-the-site reactivity. Therefore, the relatively large difference might be overcome by coupling of the endergonic steps in one active site with exergonic steps of the second active site (Thauer and Shima, 2008).

Prospects of Bio-GTL Compared to Chemical GTL Technologies

In light of the slow kinetics of microbial methane oxidation, chemical and electrochemical processes are often regarded as a more promising route for methane utilization. Large-scale industrial processes for converting methane to liquid hydrocarbons are limited to two inorganic technologies: methanol-to-gasoline and Fischer–Tropsch synthesis, both of which rely on the expensive (because energy intense) intermediate production of syngas. Other chemical routes for methane activation include the direct oxidation of methane to methanol and formaldehyde, oxidative coupling of methane to ethylene, and direct conversion to aromatics and hydrogen in the absence of oxygen (Lunsford, 2000). Even though a direct activation of methane should have a distinct economic advantage over indirect syngas routes, these processes currently remain limited by low selectivity for target reactions, low conversion rates and dilute product streams (Holmen, 2009; Alvarez-Galvan et al., 2011). Biological processes for methane activation, on the other hand, may offer significant advantage by accessing high selectivity and specificity. Despite the general higher volumetric productivity of a chemical process, a biological solution could provide advantages especially for decentralized solutions due to the smaller required footprint, measured by area, which is required for product synthesis (Haynes and Gonzalez, 2014). Due to the integrated nature of bioprocesses, fewer unit operations are required, which enables profitability at smaller scales and therefore offers opportunities for new solutions especially at remote locations. This could allow for the 5% of currently flared global natural gas production to be utilized.

CONCLUSION

The specifics of a successful future Bio-GTL process remain to be elucidated, however they will inevitably depend on the microbial host organisms and its metabolic pathway features. This study presents a comprehensive, stoichiometry-based analysis of microbial pathways for aerobic and anaerobic conversion of methane to liquid fuels. The proposed combination of pathways for methane activation, CO_2 fixation and product formation require in any scenario extensive metabolic engineering, which remains a major limitation. However, recent technological advances in the field of synthetic biology give reason to believe that eventually synthetic pathways for methane utilization will be constructed, regardless of the final host organism being a native methanotroph or a model biotechnology organism.

Our analysis shows, that the low carbon efficiency of methane activation via MMO could be mitigated via a NAD-dependent MDH. However, highest product carbon yields are achievable via anaerobic pathways for methane oxidation, which proceed without de-carboxylation reactions. Especially promising seems the pairing of AOM and Wood-Ljungdahl pathway, which could allow for the efficient co-utilization of CH_4 and CO_2 for production of bio-fuels. Given the substantial knowledge gaps around the fundamentals of anaerobic methane oxidation, we deem future research efforts in this direction most necessary and auspicious.

AUTHOR CONTRIBUTIONS

NA and FK jointly designed the study, researched the data and wrote the manuscript. NA constructed the metabolic networks and performed the calculations and computational analysis. Both authors approved the final version.

ACKNOWLEDGMENTS

This research was not supported by any particular funding. Thus, the given affiliations for both authors reflect their current positions only. We would like to thank Dr. Wenyu Gu for valued feedback on the manuscript.

SUPPLEMENTARY MATERIAL

The Supplementary Material for this article can be found online at: https://www.frontiersin.org/articles/10.3389/fenrg.2018.00106/full#supplementary-material

REFERENCES

Alvarez-Galvan, M. C., Mota, N., Ojeda, M., Rojas, S., Navarro, R. M., and Fierro, J. L. G. (2011). Direct methane conversion routes to chemicals and fuels. *Catal. Today* 171, 15–23. doi: 10.1016/j.cattod.2011.02.028

Amyris (2018). *Farnesene. The renewable Hydrocarbon Building Block*. Available online at: http://farnesene.net/shop/ (Accessed May 21, 2018).

Arnold, F., Meinhold, P., Peters, M. W., Fasan, R., and Chen, M. M. Y. (2005). *Alkane Oxidation by Modified Hydroxylases*. USA patent application US20160024482A1.

Atsumi, S., Hanai, T., and Liao, J. C. (2008). Non-fermentative pathways for synthesis of branched-chain higher alcohols as biofuels. *Nature* 451, 86–89. doi: 10.1038/nature06450

Averesch, N. J., Winter, G., and Krömer, J. O. (2016). Production of para-aminobenzoic acid from different carbon-sources in engineered *Saccharomyces cerevisiae*. *Microb. Cell Fact.* 15:89. doi: 10.1186/s12934-016-0485-8

Averesch, N. J. H., and Krömer, J. O. (2018). Metabolic engineering of the shikimate pathway for production of aromatics and derived compounds – present and future strain construction strategies. *Front. Bioeng. Biotechnol.* 6:32. doi: 10.3389/fbioe.2018.00032

Averesch, N. J. H., Martínez, V. S., Nielsen, L. K., and Krömer, J. O. (2018). Toward synthetic biology strategies for adipic acid production: an *in silico* tool for combined thermodynamics and stoichiometric analysis of metabolic networks. *ACS Synth. Biol.* 7, 490–509. doi: 10.1021/acssynbio.7b00304

Beal, E. J., House, C. H., and Orphan, V. J. (2009). Manganese- and iron-dependent marine methane oxidation. *Science* 325, 184–187. doi: 10.1126/science.1169984

Bennett, R. K., Steinberg, L. M., Chen, W., and Papoutsakis, E. T. (2018). Engineering the bioconversion of methane and methanol to fuels and chemicals in native and synthetic methylotrophs. *Curr. Opin. Biotechnol.* 50, 81–93. doi: 10.1016/j.copbio.2017.11.010

Blombach, B., Riester, T., Wieschalka, S., Ziert, C., Youn, J.-W., Wendisch, V. F., et al. (2011). *Corynebacterium glutamicum* tailored for efficient isobutanol production. *Appl. Environ. Microbiol.* 77, 3300–3310. doi: 10.1128/AEM.02972-10

Boetius, A., Ravenschlag, K., Schubert, C. J., Rickert, D., Widdel, F., Gieseke, A., et al. (2000). A marine microbial consortium apparently mediating anaerobic oxidation of methane. *Nature* 407, 623–626. doi: 10.1038/35036572

Brenda (2018). *Information on EC 1.14.13.25–Methane Monooxygenase (Soluble)*. Available online at: https://www.brenda-enzymes.org/enzyme.php?ecno=1.14.13.25 (Accessed May 22, 2018).

Budzianowski, W. M. (2017). High-value low-volume bioproducts coupled to bioenergies with potential to enhance business development of sustainable biorefineries. *Renew. Sustain. Energy Rev.* 70, 793–804. doi: 10.1016/j.rser.2016.11.260

Cai, C., Leu, A. O., Xie, G. -J., Guo, J., Feng, Y., Zhao, J. -X., et al. (2018). A methanotrophic archaeon couples anaerobic oxidation of methane to Fe(III) reduction. *ISME J.* 12, 1929–1939. doi: 10.1038/s41396-018-0109-x

Caspi, R., Altman, T., Billington, R., Dreher, K., Foerster, H., Fulcher, C. A., et al. (2014). The MetaCyc database of metabolic pathways and enzymes and the BioCyc collection of pathway/genome databases. *Nucleic Acids Res.* 42, D459–D471. doi: 10.1093/nar/gkt1103

Conrado, R. J., and Gonzalez, R. (2014). Envisioning the bioconversion of methane to liquid fuels. *Science* 343, 621–623. doi: 10.1126/science.1246929

de la Torre, A., Metivier, A., Chu, F., Laurens, L. M., Beck, D. A., Pienkos, P. T., et al. (2015). Genome-scale metabolic reconstructions and theoretical investigation of methane conversion in *Methylomicrobium buryatense* strain 5G(B1). *Microb. Cell Fact.* 14:188. doi: 10.1186/s12934-015-0377-3

Duncan, K. E., Gieg, L. M., Parisi, V. A., Tanner, R. S., Tringe, S. G., Bristow, J., et al. (2009). Biocorrosive thermophilic microbial communities in alaskan north slope oil facilities. *Environ. Sci. Technol.* 43, 7977–7984. doi: 10.1021/es9013932

Ettwig, K. F., Butler, M. K., Le Paslier, D., Pelletier, E., Mangenot, S., Kuypers, M. M., et al. (2010). Nitrite-driven anaerobic methane oxidation by oxygenic bacteria. *Nature* 464, 543–548. doi: 10.1038/nature08883

Ettwig, K. F., Zhu, B., Speth, D., Keltjens, J. T., Jetten, M. S. M., and Kartal, B. (2016). Archaea catalyze iron-dependent anaerobic oxidation of methane. *Proc. Natl. Acad. Sci. U.S.A.* 113, 12792–12796. doi: 10.1073/pnas.1609534113

Fei, Q., Guarnieri, M. T., Tao, L., Laurens, L. M., Dowe, N., and Pienkos, P. T. (2014). Bioconversion of natural gas to liquid fuel: opportunities and challenges. *Biotechnol. Adv.* 32, 596–614. doi: 10.1016/j.biotechadv.2014.03.011

Flamholz, A., Noor, E., Bar-Even, A., and Milo, R. (2012). eQuilibrator—the biochemical thermodynamics calculator. *Nucleic Acids Res.* 40, D770–D775. doi: 10.1093/nar/gkr874

Ghoddusi, H. (2017). Blending under uncertainty: real options analysis of ethanol plants and biofuels mandates. *Energy Econ.* 61, 110–120. doi: 10.1016/j.eneco.2016.11.007

Green, E. M. (2011). Fermentative production of butanol—the industrial perspective. *Curr. Opin. Biotechnol.* 22, 337–343. doi: 10.1016/j.copbio.2011.02.004

Haroon, M. F., Hu, S., Shi, Y., Imelfort, M., Keller, J., Hugenholtz, P., et al. (2013). Anaerobic oxidation of methane coupled to nitrate reduction in a novel archaeal lineage. *Nature* 500, 567–570. doi: 10.1038/nature12375

Haynes, C. A., and Gonzalez, R. (2014). Rethinking biological activation of methane and conversion to liquid fuels. *Nat. Chem. Biol.* 10, 331–339. doi: 10.1038/nchembio.1509

Holmen, A. (2009). Direct conversion of methane to fuels and chemicals. *Catal. Today* 142, 2–8. doi: 10.1016/j.cattod.2009.01.004

Hwang, I. Y., Nguyen, A. D., Nguyen, T. T., Nguyen, L. T., Lee, O. K., and Lee, E. Y. (2018). Biological conversion of methane to chemicals and fuels: technical challenges and issues. *Appl. Microbiol. Biotechnol.* 102, 3071–3080. doi: 10.1007/s00253-018-8842-7

Jang, Y. S., Kim, B., Shin, J. H., Choi, Y. J., Choi, S., Song, C. W., et al. (2012). Bio-based production of C2–C6 platform chemicals. *Biotechnol. Bioeng.* 109, 2437–2459. doi: 10.1002/bit.24599

Kalyuzhnaya, M. G., Puri, A. W., and Lidstrom, M. E. (2015). Metabolic engineering in methanotrophic bacteria. *Metab. Eng.* 29, 142–152. doi: 10.1016/j.ymben.2015.03.010

Kanehisa, M., Furumichi, M., Tanabe, M., Sato, Y., and Morishima, K. (2017). KEGG: new perspectives on genomes, pathways, diseases and drugs. *Nucleic Acids Res.* 45, D353–D361. doi: 10.1093/nar/gkw1092

Kanehisa, M., and Goto, S. (2000). KEGG: Kyoto encyclopedia of genes and genomes. *Nucleic Acids Res.* 28, 27–30. doi: 10.1093/nar/28.1.27

Kanehisa, M., Sato, Y., Kawashima, M., Furumichi, M., and Tanabe, M. (2016). KEGG as a reference resource for gene and protein annotation. *Nucleic Acids Res.* 44, D457–D462. doi: 10.1093/nar/gkv1070

Kirby, J., Dietzel, K. L., Wichmann, G., Chan, R., Antipov, E., Moss, N., et al. (2016). Engineering a functional 1-deoxy-D-xylulose 5-phosphate (DXP) pathway in *Saccharomyces cerevisiae*. *Metab. Eng.* 38, 494–503. doi: 10.1016/j.ymben.2016.10.017

Koch, C., Kuchenbuch, A., Kracke, F., Bernhardt, P. V., Krömer, J., and Harnisch, F. (2017). Predicting and experimental evaluating bio-electrochemical synthesis — a case study with *Clostridium kluyveri*. *Bioelectrochemistry* 118, 114–122. doi: 10.1016/j.bioelechem.2017.07.009

Kracke, F., Virdis, B., Bernhardt, P. V., Rabaey, K., and Krömer, J. O. (2016). Redox dependent metabolic shift in *Clostridium autoethanogenum* by extracellular electron supply. *Biotechnol. Biofuels* 9:249. doi: 10.1186/s13068-016-0663-2

Liew, F., Martin, M. E., Tappel, R. C., Heijstra, B. D., Mihalcea, C., and Köpke, M. (2016). Gas fermentation—a flexible platform for commercial scale production of low-carbon-fuels and chemicals from waste and renewable feedstocks. *Front. Microbiol.* 7:694. doi: 10.3389/fmicb.2016.00694

Lopar, M., Špoljarić, I. V., Atlić, A., Koller, M., Braunegg, G., and Horvat, P. (2013). Five-step continuous production of PHB analyzed by elementary flux, modes, yield space analysis and high structured metabolic model. *Biochem. Eng. J.* 79, 57–70. doi: 10.1016/j.bej.2013.07.003

Lopar, M., Špoljarić, I. V., Cepanec, N., Koller, M., Braunegg, G., and Horvat, P. (2014). Study of metabolic network of *Cupriavidus necator* DSM 545 growing on glycerol by applying elementary flux modes and yield space analysis. *J. Ind. Microbiol. Biotechnol.* 41, 913–930. doi: 10.1007/s10295-014-1439-y

Lunsford, J. H. (2000). Catalytic conversion of methane to more useful chemicals and fuels: a challenge for the 21st century. *Catal. Today* 63, 165–174. doi: 10.1016/S0920-5861(00)00456-9

Marx, C. J., Chistoserdova, L., and Lidstrom, M. E. (2003). Formaldehyde-detoxifying role of the tetrahydromethanopterin-linked pathway in methylobacterium extorquens AM1. *J. Bacteriol.* 185, 7160–7168. doi: 10.1128/JB.185.23.7160-7168.2003

Melzer, G., Esfandabadi, M. E., Franco-Lara, E., and Wittmann, C. (2009). Flux design: *In silico* design of cell factories based on correlation of pathway fluxes to desired properties. *BMC Syst. Biol.* 3:120. doi: 10.1186/1752-0509-3-120

Meyer, F., Keller, P., Hartl, J., Gröninger, O. G., Kiefer, P., and Vorholt, J. A. (2018). Methanol-essential growth of *Escherichia coli*. *Nat. Commun.* 9:1508. doi: 10.1038/s41467-018-03937-y

Miltner, M., Makaruk, A., and Harasek, M. (2017). Review on available biogas upgrading technologies and innovations towards advanced solutions. *J. Clean. Prod.* 161, 1329–1337. doi: 10.1016/j.jclepro.2017.06.045

Moran, J. J., House, C. H., Freeman, K. H., and Ferry, J. G. (2005). Trace methane oxidation studied in several Euryarchaeota under diverse conditions. *Archaea* 1, 303–309. doi: 10.1155/2005/650670

Mueller, T. J., Grisewood, M. J., Nazem-Bokaee, H., Gopalakrishnan, S., Ferry, J. G., Wood, T. K., et al. (2015). Methane oxidation by anaerobic archaea for conversion to liquid fuels. *J. Ind. Microbiol. Biotechnol.* 42, 391–401. doi: 10.1007/s10295-014-1548-7

Nakano, M. M., and Zuber, P. (1998). Anaerobic growth of a "strict aerobe" (*Bacillus subtilis*). *Annu. Rev. Microbiol.* 52, 165–190. doi: 10.1146/annurev.micro.52.1.165

Nazem-Bokaee, H., Gopalakrishnan, S., Ferry, J. G., Wood, T. K., and Maranas, C. D. (2016). Assessing methanotrophy and carbon fixation for biofuel production by *Methanosarcina acetivorans*. *Microb. Cell Fact.* 15:10. doi: 10.1186/s12934-015-0404-4

Nishimura, T., Vertès, A. A., Shinoda, Y., Inui, M., and Yukawa, H. (2007). Anaerobic growth of *Corynebacterium glutamicum* using nitrate as a terminal electron acceptor. *Appl. Microbiol. Biotechnol.* 75, 889–897. doi: 10.1007/s00253-007-0879-y

Noor, E., Bar-Even, A., Flamholz, A., Reznik, E., Liebermeister, W., and Milo, R. (2014). Pathway thermodynamics highlights kinetic obstacles in central metabolism. *PLoS Comput. Biol.* 10:e1003483. doi: 10.1371/journal.pcbi.1003483

Peralta-Yahya, P. P., Zhang, F., Del Cardayre, S. B., and Keasling, J. D. (2012). Microbial engineering for the production of advanced biofuels. *Nature* 488, 320–328. doi: 10.1038/nature11478

Placzek, S., Schomburg, I., Chang, A., Jeske, L., Ulbrich, M., Tillack, J., et al. (2017). BRENDA in 2017: new perspectives and new tools in BRENDA. *Nucleic Acids Res.* 45, D380–D388. doi: 10.1093/nar/gkw952

Raghoebarsing, A. A., Pol, A., Van De Pas-Schoonen, K. T., Smolders, A. J. P., Ettwig, K. F., Rijpstra, W. I., et al. (2006). A microbial consortium couples anaerobic methane oxidation to denitrification. *Nature* 440, 918–921. doi: 10.1038/nature04617

Report, M. R. (2016). *Isobutanol Market Analysis by Product (Synthetic, Bio-Based), Application (Oil & Gas, Solvents & Coatings, Chemical Intermediates) and Segment Forecasts to 2022*. Available online at: https://www.grandviewresearch.com/industry-analysis/isobutanol-market (Accessed January 10, 2018).

Report, M. R. (2017). *Fuel Ethanol Market Analysis by Product (Starch-Based, Sugar-Based, Cellulosic), by Application (Conventional Vehicles, Flexible Fuel Vehicles), by Region, and Segment Forecasts, 2018–2025*. Available online at: https://www.grandviewresearch.com/industry-analysis/fuel-ethanol-market (Accessed January 10, 2018).

Schada von Borzyskowski, L., Carrillo, M., Leupold, S., Glatter, T., Kiefer, P., Weishaupt, R., et al. (2018). An engineered Calvin-Benson-Bassham cycle for carbon dioxide fixation in Methylobacterium extorquens AM1. *Metab. Eng.* 47, 423–433. doi: 10.1016/j.ymben.2018.04.003

Scheller, S., Ermler, U., and Shima, S. (2017). "Catabolic pathways and enzymes involved in anaerobic methane oxidation," in *Anaerobic Utilization of Hydrocarbons, Oils, and Lipids. Handbook of Hydrocarbon and Lipid Microbiology*, ed M. Boll (Cham: Springer), 1–29. Available online at: https://link.springer.com/referenceworkentry/10.1007%2F978-3-319-33598-8_3-1

Scheller, S., Goenrich, M., Boecher, R., Thauer, R. K., and Jaun, B. (2010). The key nickel enzyme of methanogenesis catalyses the anaerobic oxidation of methane. *Nature* 465, 606–608. doi: 10.1038/nature09015

Schrader, J., Schilling, M., Holtmann, D., Sell, D., Villela Filho, M., Marx, A., et al. (2009). Methanol-based industrial biotechnology: current status and future perspectives of methylotrophic bacteria. *Trends Biotechnol.* 27, 107–115. doi: 10.1016/j.tibtech.2008.10.009

Shima, S., Krueger, M., Weinert, T., Demmer, U., Kahnt, J., Thauer, R. K., et al. (2011). Structure of a methyl-coenzyme M reductase from Black Sea mats that oxidize methane anaerobically. *Nature* 481, 98–101. doi: 10.1038/nature10663

Siegel, J. B., Smith, A. L., Poust, S., Wargacki, A. J., Bar-Even, A., Louw, C., et al. (2015). Computational protein design enables a novel one-carbon assimilation pathway. *Proc. Natl. Acad. Sci. U.S.A.* 112, 3704–3709. doi: 10.1073/pnas.1500545112

Soo, V. W., Mcanulty, M. J., Tripathi, A., Zhu, F., Zhang, L., Hatzakis, E., et al. (2016). Reversing methanogenesis to capture methane for liquid biofuel precursors. *Microb. Cell Fact.* 15:11. doi: 10.1186/s12934-015-0397-z

Steynberg, A. (2004). "Chapter 1 – Introduction to fischer-tropsch technology," in *Studies in Surface Science and Catalysis*, Vol. 52. eds A. Steynberg and M. Dry (Elsevier), 1–63. Available online at: https://www.sciencedirect.com/science/article/pii/S0167299104804580

Strong, P. J., Xie, S., and Clarke, W. P. (2015). Methane as a resource: can the methanotrophs add value? *Environ. Sci. Technol.* 49, 4001–4018. doi: 10.1021/es504242n

Ternon, C., Grousseau, E., Gunther, J., Gorret, N., Guillouet, S., Sinskey, A., et al. (2014). Dynamic model for isopropanol production by *Cupriavidus necator*. *IFAC Proc. Vol.* 47, 4388–4393. doi: 10.3182/20140824-6-ZA-1003.02267

Terzer, M., and Stelling, J. (2008). Large-scale computation of elementary flux modes with bit pattern trees. *Bioinformatics* 24, 2229–2235. doi: 10.1093/bioinformatics/btn401

Thauer, R. K., and Shima, S. (2008). Methane as fuel for anaerobic microorganisms. *Ann. N. Y. Acad. Sci.* 1125, 158–170. doi: 10.1196/annals.1419.000

Tiemeyer, A., Link, H., and Weuster-Botz, D. (2007). Kinetic studies on autohydrogenotrophic growth of *Ralstonia eutropha* with nitrate as terminal electron acceptor. *Appl. Microbiol. Biotechnol.* 76, 75–81. doi: 10.1007/s00253-007-0983-z

Toolbox (2008). *Solubility of Gases in Water*. Available online at: https://www.engineeringtoolbox.com/gases-solubility-water-d_1148.html (Accessed May 04, 2018).

Trotsenko, Y. A., and Murrell, J. C. (2008). "Metabolic aspects of aerobic obligate methanotrophy," in *Advances in Applied Microbiology*, Vol. 63. (Academic Press), 183–229. Available online at: https://www.sciencedirect.com/science/article/pii/S0065216407000056?via%3Dihub

Unden, G., and Bongaerts, J. (1997). Alternative respiratory pathways of *Escherichia coli*: energetics and transcriptional regulation in response to electron acceptors. *Biochim. Biophys. Acta* 1320, 217–234. doi: 10.1016/S0005-2728(97)00034-0

Unrean, P. (2014). Pathway analysis of *Pichia pastoris* to elucidate methanol metabolism and its regulation for production of recombinant proteins. *Biotechnol. Prog.* 30, 28–37. doi: 10.1002/btpr.1855

Valentine, D. L., and Reeburgh, W. S. (2000). New perspectives on anaerobic methane oxidation. *Environ. Microbiol.* 2, 477–484. doi: 10.1046/j.1462-2920.2000.00135.x

van Klinken, J. B., and Willems Van Dijk, K. (2015). FluxModeCalculator: an efficient tool for large-flux mode computation. *Bioinformatics* 32, 1265–1266. doi: 10.1093/bioinformatics/btv742

Weiland, P. (2010). Biogas production: current state and perspectives. *Appl. Microbiol. Biotechnol.* 85, 849–860. doi: 10.1007/s00253-009-2246-7

West, C. A., Salmond, G. P. C., Dalton, H., and Murrell, J. C. (1992). Functional expression in *Escherichia coli* of proteins B and C from soluble methane monooxygenase of *Methylococcus capsulatus* (Bath). *Microbiology* 138, 1301–1307.

Yan, Z., Joshi, P., Gorski, C. A., and Ferry, J. G. (2018). A biochemical framework for anaerobic oxidation of methane driven by Fe(III)-dependent respiration. *Nat. Commun.* 9:1642. doi: 10.1038/s41467-018-04097-9

Yim, H., Haselbeck, R., Niu, W., Pujol-Baxley, C., Burgard, A., Boldt, J., et al. (2011). Metabolic engineering of *Escherichia coli* for direct production of 1,4-butanediol. *Nat. Chem. Biol.* 7, 445–452. doi: 10.1038/nchembio.580

Conflict of Interest Statement: The authors declare that the research was conducted in the absence of any commercial or financial relationships that could be construed as a potential conflict of interest.

frontiers in Energy Research

PERSPECTIVE
published: 05 November 2018
doi: 10.3389/fenrg.2018.00117

Microbial Interconversion of Alkanes to Electricity

*Silvan Scheller**

Department of Bioproducts and Biosystems, Aalto University, Espoo, Finland

Electricity from fuels can be produced via 2 fundamentally different methods: By burning them to spin generators, or by direct abstraction of electrons at catalysts. The future is the flame-free production of electricity via catalysis, whereby the maximal theoretical yield scales inversely proportional to the process temperature. Low temperature fuel cells are thus needed, but they are not available for hydrocarbons due to the recalcitrant C-H bonds present in alkanes. Fuel cells for alkanes typically require process temperatures higher than 600°C. The microbial pathway of anaerobic alkane oxidation, on the other side, converts alkanes reversibly to single electrons and CO_2 at temperatures as low as 4°C. In this perspective, I suggest to utilize this microbial metabolism for catalytic alkane oxidation at low temperatures, in order to convert alkanes to electricity with possibly higher thermodynamic efficiencies as current technologies. Alkane oxidation is partitioned into a biocatalytic (microbial) step to cleave the C-H bonds, and into an electrochemical step for harvest of electricity. In the biocatalytic step, the alkane is oxidized to CO_2 and the resulting electrons are loaded onto an electron carrier. Electricity is then generated from the electron-carrier via fuel cells. Due to the intrinsic reversibility of the biochemical pathway, the whole process may be reversed to convert excess electricity (e.g., from solar or wind) with CO_2 to alkanes, which is particularly interesting for the alkanes ethane, propane or butane that are easily liquefiable and storable.

Keywords: archaea and bacteria, biocatalyis, fuel conversion efficiency, electron transfer (redox reactions), microbial fuel cells (MFC), sustainable electricity production, power to gas, anaerobic oxidation of methane (AOM)

OPEN ACCESS

Edited by:
Deepak Pant,
Flemish Institute for Technological Research, Belgium

Reviewed by:
Ioannis Andrea Ieropoulos,
University of the West of England, United Kingdom
Matteo Grattieri,
University of Utah, United States

***Correspondence:**
Silvan Scheller
silvan.scheller@aalto.fi

Specialty section:
This article was submitted to Bioenergy and Biofuels, a section of the journal Frontiers in Energy Research

Received: *23 May 2018*
Accepted: *18 October 2018*
Published: *05 November 2018*

Citation:
Scheller S (2018) Microbial Interconversion of Alkanes to Electricity. Front. Energy Res. 6:117. doi: 10.3389/fenrg.2018.00117

GENERATION OF ELECTRICITY FROM FUELS

Our society got heavily dependent on un-interrupted availability of electricity, our most versatile form of energy. Production of electricity from fuels can be performed via 2 fundamentally different methods. The first and currently dominating procedure is to burn the fuel and spin generators that produce electricity. The second method, discussed in this document, relies on catalytic oxidation of the fuel thereby directly abstracting electrons as carried out in fuel cells. The thermodynamic efficiency of catalytic electricity production scales inversely with temperature: The lower the process temperature, the higher the maximum amount of electricity that can be extracted. For hydrocarbons, fuel cells typically operate at temperatures above 600°C (O'Hayre et al., 2016). Low temperature fuel cells ($T < 100$°C) exist only for hydrogen and for a few uncommon fuels, such as methanol or formic acid (Gold, 2012).

In this perspective, I discuss a possible solution for catalytic electricity production from alkanes at cold temperatures, using the recently discovered process of microbial alkane oxidation with release of single electrons. The system proposed is a derivative of a mediated microbial fuel cell. Toward the end of this document, I describe how this biochemistry can possibly be reversed to convert excess electricity (e.g., from wind or sun) to alkanes as storage compounds.

MICROBIAL ELECTRICITY PRODUCTION FROM ALKANES

Certain microbes are capable of producing or taking up single electrons (Lovley, 2012). Recently, microbes of the domain archaea from the deep-sea (**Figure 1A**) have been reported to make a living by oxidizing methane to CO_2, concomitant with transfer of electrons via electrical conductance to partner microbes that reduce sulfate (McGlynn et al., 2015; Wegener et al., 2015). Shortly after, related microbes were described carrying out the analogous reaction for the higher alkanes propane and butane (Laso-Pérez et al., 2016). In the microbial communities responsible for this process, the overall reaction of alkane oxidation with sulfate as the oxidant is partitioned such that each type of microbes carries out one half reaction (**Figure 1B**).

The microbial setup resembles a fuel cell in which archaea are the anode (red) and bacteria the cathode (green). In microbiology, this type of syntrophy is called direct-interspecies-electron transfer (Lovley, 2017). Electrical current is enabled by conductive biological structures such as multi-heme-*c*-type cytochromes (Pirbadian and El-Naggar, 2012), or different types of conductive "nano-wires" (Gorby et al., 2006; Wegener et al., 2015). Reported half reactions of alkane oxidation with release of single electrons are equations 1, 3 and 4:

(1) $CH_4 + 2\ H_2O = CO_2 + 8\ e^- + 8\ H^+$ ($E^{\circ\prime} = -245$ mV)
(2) $C_2H_6 + 4\ H_2O = 2\ CO_2 + 14\ e^- + 14\ H^+$ ($E^{\circ\prime} = -272$ mV)
(3) $C_3H_8 + 6\ H_2O = 3\ CO_2 + 20\ e^- + 20\ H^+$ ($E^{\circ\prime} = -278$ mV)
(4) $C_4H_{10} + 8\ H_2O = 4\ CO_2 + 26\ e^- + 26\ H^+$ ($E^{\circ\prime} = -280$ mV)

These reactions are the same as at anodes of solid oxide fuel cells, but they proceed at 4°C instead of at >600°C.

APPLICATION OF MICROBIAL ELECTRICITY PRODUCTION FROM ALKANES

To harvest the biochemically produced electrons, the bacteria that naturally consume them (**Figure 1B**, green) need to be replaced. The classical way is to replace the bacteria by a fuel-cell cathode in one device (bio fuel cell), in which the compartments are separated by an ion-conductive membrane (Logan et al., 2006; McAnulty et al., 2017; Schröder and Harnisch, 2017). An alternative approach is replacing the bacteria by an auxiliary redox reaction, which is described here in more detail. Such a system corresponds to a mediated microbial fuel cell, whereby microbes are used to convert the fuel into a compound that can be easily utilized in a conventional fuel cell. A soluble electron carrier (Fultz and Durst, 1982) connects the biological step of alkane oxidation with the electrochemical step of oxygen reduction, allowing the 2 half-reactions to be spatially separated. The chemically challenging step of alkane oxidation and transfer of the electron to a soluble electron carrier has been achieved for the alkane methane (Scheller et al., 2016) utilizing the electron carrier Q = 9,10-anthraquinone-2,6-disulfonate, AQDS, $E^{\circ\prime} = -186$ mV, as illustrated in **Figure 1C**. This reaction means that the fuel methane is converted to the fuel QH_2, from which electricity is harvested by a fuel cell. The homologous biochemical reaction should be possible for higher alkanes as well, but such experiments have not been reported to date.

EXAMPLE OF A TWO-STEP PROCESS FOR METHANE TO ELECTRICITY

The 2-step set-up presented here has the advantage that microbes are not directly connected to the electrode (easier to implement system and to exchange the microbes), but the disadvantage that some amount of additional energy is utilized to pump the mediator from the bioreactor to the fuel cell. A separated 2-step process is described here and not an unmediated microbial fuel cell, because there is proof of principle for the reaction shown in **Figure 1C**, unlike for such microbes directly attached to an electrode.

The overall process of methane oxidation with air, equation 5 ($E^{\circ\prime} = -0.245$ V for CH_4/CO_2 and $E^{\circ\prime} = 0.815$ V for H_2O/O_2), is divided into a biochemical reaction (equation 6) and an electrochemical reaction (equation 7).

(5) $CH_4 + 2\ O_2 = CO_2 + 2\ H_2O$ ($\Delta E^{\circ\prime} = 1.060$ V)
(6) $CH_4 + 4\ Q + 2\ H_2O = CO_2 + 4\ QH_2$ ($\Delta E^{\circ\prime} = 0.059$ V, for Q = AQDS)
(7) $4\ QH_2 + 2\ O_2 = 4\ Q + 4\ H_2O$ ($\Delta E^{\circ\prime} = 1.001$ V, for Q = AQDS)

In the biochemical reaction (equation 6), the energy carrier methane is converted into the energy carrier QH_2. Proof of concept for the biochemical reaction (equation 6) has been obtained with environmental microbes in batch mode at 1 ml scale (Scheller et al., 2016). From the energy carrier QH_2, electricity can then be harvested (equation 7), similar to flow-batteries that use the same electron carrier but Br_2/HBr at the cathode (Huskinson et al., 2014).

The overall set up may be realized by feeding a bioreactor with medium that contains dissolved methane and the soluble electron carrier (**Figure 2**). In this set-up, which has not yet been done in large scale due to lack of the biocatalyst (see "research needs"), the microbes are immobilized in a packed bed reactor. The outlet of the bioreactor contains the soluble reduced electron carrier (QH_2) and dissolved CO_2. The CO_2 is separated and used for other purposes or stored, and the reduced electron-acceptor enters a fuel cell operating with air in the cathode.

ASSESSMENT OF THERMODYNAMIC EFFICIENCY FOR METHANE TO ELECTRICITY

The overall thermodynamic efficiency depends on the maximal theoretical efficiency (see part A), and on losses (see parts B-D) as described below for the alkane methane.

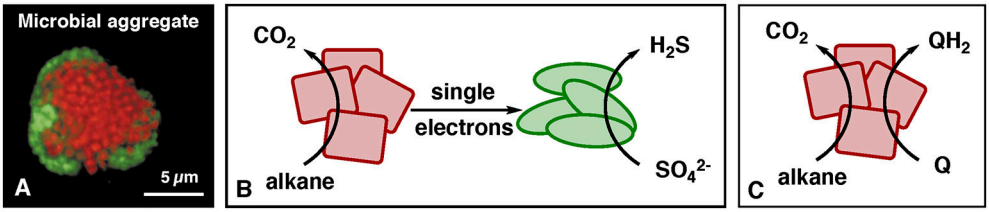

FIGURE 1 | Alkane oxidation by environmental microbes. **(A)** Microscopy picture of a microbial aggregate that performs methane oxidation coupled to sulfate reduction [from Reference (Boetius et al., 2000)]. Red microbes = methane-oxidizing archaea, green microbes = sulfate-reducing bacteria. **(B)** Process of alkane oxidation by environmental archaea (red) with electron transfer to sulfate-reducing partner bacteria (green). **(C)** Coupling of alkane oxidation with the reduction of synthetic electron carriers (Q), as demonstrated for the alkane methane (Scheller et al., 2016).

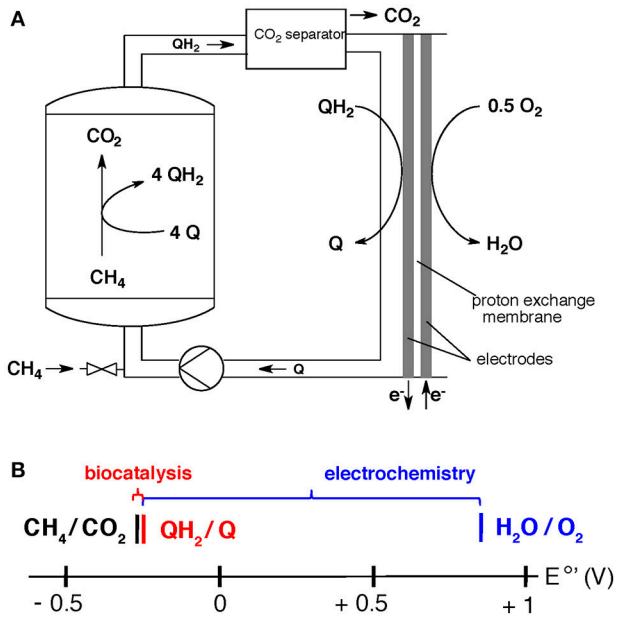

FIGURE 2 | (A) Proposed system for electricity generation from methane via a two-step process involving biocatalysis (left side) and electrochemistry (right side) (Scheller et al., 2018). **(B)** Division of energy (redox-potential difference) from methane oxidation with air (equation 5) into a biochemical step of fuel conversion (red, equation 6), followed by an electrochemical step of electricity harvest (blue, equation 7).

A) Theoretical maximum of overall process

The maximal theoretical efficiency (methane oxidation with air) corresponds to $\Delta G/\Delta H$, whereby ΔG depends on the process temperature according to equation 8:

(8) Maximal extractable electrical energy = $\Delta G = \Delta H - T\Delta S$

whereby ΔH is the enthalpy of the process ($\Delta H = -890.3$ kJ mol^{-1}) and ΔS is the reaction entropy (-242.4 J mol^{-1} K^{-1}) and T is the absolute temperature.

As ΔS is negative, more electricity can be harvested at lower temperature (ΔG is more negative). The same relation applies for higher hydrocarbons. For the lower temperature range of current solid oxide fuel cells (T = 600°C), the maximal thermodynamic efficiency ($\Delta G/\Delta H$) is 76% (equation 8 with T = 873 K). At room temperature, however, the maximal thermodynamic efficiency would be 92% (equation 8 with T = 298 K).

B) Thermodynamic losses due to two-step process

In the 2-step set-up discussed here, electricity is produced only from the electrochemical process (equation 7), which means that the difference in the redox potential of equation 6 cannot be utilized.

Equation 6 corresponds to $\Delta E^{\circ\prime} = 0.059$ V (5.6% of total energy) for Q = AQDS and standard conditions. In environmental microbes carrying out methane oxidation with sulfate *in situ*, equation 6 corresponds only to $\Delta E < 0.026$ V (ΔG for half reaction is between -5 kJ mol^{-1} and -20 kJ mol^{-1}) (Knittel and Boetius, 2009).

If an electron carrier Q with a slightly more negative redox potential would be used ($\Delta E = 0.026$ V for equation 6), as in environmental microbes, only 2.5% of the energy would be "lost" due to biocatalysis.

C) Thermodynamic efficiency of fuel cell

The fuel cell will be the main contributor to losses in efficiency in the operating system. The main reason is the high overpotential at the oxygen-reducing cathode, which depends on the current per area utilized. Such polarization effects can add up to 0.5 V under maximum power transfer (corresponding to a loss of up to 50%), a major issue that remains to be resolved. The anode process involving the artificial electron carrier is associated with low overpotentials, because compounds such as AQDS have excellent electrochemical properties (Rosso et al., 2004). For the calculation here, an efficiency of 70% is assumed.

D) Additional losses

Additional losses in the overall efficiency involve pumping the electron carrier between bioreactor and fuel cell, replacement of microbes, production costs, pressurizing methane, removal of CO_2, heat exchange. Those depend on the engineering and on the scaling of the overall system.

E) Overall assessment

The overall efficiency is the product of (A) thermodynamic efficiency 92%, (B) contribution to fuel cell: 94.4–97.5%, (C)

efficiency of fuel cell 50–70% (with current technologies), and (D) additional losses e.g., 90%. These numbers yield an overall efficiency of 39–57%.

Thus, the main losses come from the overpotential at the cathode, a general challenge in current fuel-cell research, for which solutions are needed.

ASSESSMENT OF KINETICS FOR METHANE TO ELECTRICITY

Up to date, only uncultured microbes from the environment are available for the biocatalysis of alkane to electricity conversion (see section "research needs"). Enrichment cultures of such microbes from the environment maintained at 12°C with 14 bar CH_4 catalyze specific methane oxidation rates of 1–20 mmol day^{-1} g^{-1} cell dry mass (Knittel and Boetius, 2009), assuming equal amounts of archaea and bacteria in the community. This converts to 2.3–46 mmol CH_4 per second per m^3 of living archaeal biomass (assuming dry weight = 20% of wet weight and density =1 g ml^{-1}).

If those environmental microbes would be used for the set-up described in **Figure 2**, 1 m^3 archaea cells would be required to produce an electric output of 1.2–25 kW, assuming 70% efficiency of the fuel cell (calculation: Power = 70% * rate * n * F * ΔE, with rate = 2.3–46 mmol CH_4 per second, $n = 8$, F = Faraday constant and ΔE =1.001 V for equation 7). To obtain faster rates, microbes need to be designed that possess a faster catabolism (see "research needs").

Non-biochemical kinetic limitations may arise from gas exchange to microbes or dissolution of methane, and from transfer of protons through fuel cell membrane. The electron acceptor AQDS has excellent electrochemical redox-kinetics (Rosso et al., 2004), but the oxygen reduction may be limiting, especially when the system is trimmed for high thermodynamic yields (i.e., lower current per area). The solubility of methane is about 144 mM under predicted reactor conditions [200 bar, T = 37°C, 1.0 salt concentration, according to reference (Duan and Mao, 2006)]. Higher alkanes would liquefy at higher pressures and are therefore more applicable for the reverse process.

BIOCHEMISTRY OF MICROBIAL ALKANE OXIDATION AND FORMATION

The carbon metabolism from methane to CO_2 is congruent to that of biological methane formation from CO_2, but operating in reverse direction (Hallam et al., 2004). This bi-directionality is possible because the pathway proceeds close to the thermodynamic equilibrium. Depending on the directionality, the microbial metabolism is wired differently to allow the cells to grow (Thauer et al., 2008), implying that one type of organism appears to only carry out one direction of the pathway (McGlynn, 2017; Timmers et al., 2017).

The archaeal biochemistry of converting higher alkanes to CO_2 is initiated by homologous enzymes as for methane (Laso-Pérez et al., 2016), in which the alkane is reversibly converted to an alkyl-sulfide. The downstream pathway from the alkyl-sulfide to CO_2 has not yet been fully elucidated. For the reverse reaction (conversion of CO_2 to higher alkanes), no microbes producing ethane, propane or butane are reported. According to thermodynamics, however, such metabolisms are feasible in both directions, and corresponding microbes may be genetically designed (see "research needs").

SYSTEM FOR ELECTRICITY TO ALKANES

For the alkane methane, bioelectrochemical gas generation is a vibrant research topic (Geppert et al., 2016). Current technologies utilize "classical" methanogens (Enzmann et al., 2018) as catalysts that are not adapted to carry out direct electron transfer, which might be the reason for the high overpotentials in those reactions (Geppert et al., 2016), or that they just apparently carry out direct extracellular electron transfer (Deutzmanna et al., 2015). For higher efficiencies, a methanogen able of taking up electrons directly from an electrode, or from a reduced soluble electron carrier is needed (see "research needs"). With a reduced electron carrier, the same design as in **Figure 2** can be chosen, but all the reactions operate in reverse direction (all arrows reversed), and the carrier "QH_2" requires $E^{\circ\prime}$ = ca. −304 mV (in order to provide the same potential difference, 59 mV, for the microbes as for methane oxidation).

The advantage of such a system over just making methane from electricity-derived hydrogen is that the soluble electron donor can be produced with higher efficiency than currently possible for hydrogen generation. Modifying the microbes to produce higher alkanes (see "research needs") is an attractive way to interconvert excess electricity (e.g., from wind or sun) with CO_2 to liquefiable alkanes for storage.

RESEARCH NEEDS FOR ALKANES TO ELECTRICITY

Implementation of the technology is currently hampered by the unavailability of the required microbes that are the biocatalyst. Before engineering of the application can be started, substantial research on microbial physiology is needed, including elucidation of the currently unknown biochemistry for the metabolism of higher alkanes. Enrichments of environmental microbes (e.g., of iron-reducing methanotrophs Cai et al., 2018) are under way that may be used for the system. A promising alternative to access the desired microbes is to genetic engineer them. Successful design of the microbes requires knowledge about the detailed physiology of the environmental microbes, which needs to be elucidated. With this knowledge, model microbes that grow fast on alternative substrates (e.g., on alcohols, such as methanol for the organism *M. acetivorans*) can be equipped with the metabolic capability to carry out alkane oxidation coupled to the production of QH_2. Via genetic engineering, the microbes can be tuned for faster performance to make the technology more competitive, because in the environmental system the alkane-oxidizers have only about $\Delta G = -5$ to -20 kJ mol^{-1} energy to drive the metabolism (Knittel and Boetius, 2009), but in the engineered system, more

energy can be attributed to biocatalysis. If the metabolism would be fully limited by reaction thermodynamics, every 5.7 kJ mol^{-1} in additional energy attributed to the metabolism can speed up the reaction up to a factor of 10, thus substantial rate acceleration may be possible for the electron carrier discussed (equation 6), for which $\Delta G^{\circ\prime}$ is −46 kJ mol^{-1}. The reality in environmental microbes is probably a mixture of thermodynamic and kinetic limitations, whereby the main contribution for the kinetic limitation clearly comes from alkane activation by the enzyme methyl-coenzyme M reductase (Scheller et al., 2010; Grisewood et al., 2018). The process temperature can be increased to 37°C [using the model organisms *M. acetivorans* (Nayak and Metcalf, 2017) or *M. maripaludis* (Goyal et al., 2016)], resulting in a 5–10 fold rate increase [2–3 fold per $\Delta T = 10°C$, as common for microbes (Pachepsky et al., 2014)], and the methane pressure can be increased by a factor of 10. Prediction of the rate enhancement by those modifications is difficult (Ritchie, 2018) and thus needs the modifications to be carried out experimentally. If a rate-acceleration by a factor of 100–1000 is achieved via optimized microbes, the installation volumes of the final industrial set up become industrially applicable.

RESEARCH NEEDS FOR ELECTRICITY TO ALKANES

To allow methane formation from electricity, the genes for hydrogenases in methanogens (responsible for electron transfer from H_2) need to be replaced by those encoding for multi-heme *c*-type cytochromes (to allow electron uptake). An alternative strategy could be reversing a methanotroph to generate methane, as they evolved for efficient electron transfer. Changing the primary metabolism requires changing the way cells conserve energy, which is in the beginning of being understood (McGlynn, 2017; Yan et al., 2018). Engineering of microbes to convert electricity to higher alkanes, first needs the elucidation of the currently unknown biochemical steps involved, before genetic engineering can be started. For all processes, understanding and genetic engineering of enzymes related to direct electron transfer (multi-heme *c*-type cytochromes) are crucial but currently at a very early stage of research.

CONCLUSIONS

The technology of microbial alkane to electricity interconversion is in a low technology readiness level. Current attempts of electricity to methane conversion with classical methanogens suffer from high overpotentials that are due to inefficient uptake of electrons by the methanogens involved.

By designing microbes with the desired metabolism (direct electron transfer, engineering to be able to generate higher alkanes), the technology may find industrial application in both metabolic directions: methane to electricity, and electricity to liquefiable alkanes.

Specific applications for methane to electricity may be smaller power plants, e.g., next to biogas fermenters. Electricity to liquefiable alkanes is promising for storing excess from electricity overproduction (e.g., wind or sun), or for upgrading the CO_2 from biogas plants, or by removing CO_2 from other sources.

Although new and at a very early stage, the technology described seems the first step for catalytic alkane to electricity interconversion at low temperatures and constitutes the cornerstone of a sustainable flame-free-future (Kendall, 2000) for alkane fuels.

AUTHOR CONTRIBUTIONS

The author confirms being the sole contributor of this work and has approved it for publication.

REFERENCES

Boetius, A., Ravenschlag, K., Schubert, C. J., Rickert, D., Widdel, F., Gieseke, A., et al., (2000).A marine microbial consortium apparently mediating anaerobic oxidation of methane. *Nat.* 407, 623–626. doi: 10.1038/35036572

Cai, C., Leu, A. O., Xie, G.-J., Guo, J., Feng, Y., Zhao, J.-X., et al. (2018). A methanotrophic archaeon couples anaerobic oxidation of methane to Fe(III) reduction. *ISME J.* 12, 1929–1939. doi: 10.1038/s41396-018-0109-x

Deutzmanna, J. S., Sahina, M., and Spormanna, A. M. (2015). Extracellular enzymes facilitate electron uptake in biocorrosion and bioelectrosynthesis. *MBio* 6, 1–8. doi: 10.1128/mBio.00496-15

Duan, Z., and Mao, S. (2006). A thermodynamic model for calculating methane solubility, density and gas phase composition of methane-bearing aqueous fluids from 273 to 523 K and from 1 to 2000 bar. *Geochim. Cosmochim. Acta* 70, 3369–3386. doi: 10.1016/j.gca.2006.03.018

Enzmann, F., Mayer, F., Rother, M., and Holtmann, D. (2018). Methanogens: biochemical background and biotechnological applications. *AMB Express* 8, 1–22. doi: 10.1186/s13568-017-0531-x

Fultz, M. L., and Durst, R. A. (1982). Mediator compounds for the electrochemical study of biological redox systems - a compilation. *Anal. Chim. Acta* 140, 1–18. doi: 10.1016/S0003-2670(01)95447-9

Geppert, F., Liu, D., van Eerten-Jansen, M., Weidner, E., Buisman, C., Ter Heijne, A., et al. (2016). Bioelectrochemical power-to-gas: state of the art and future perspectives. *Trends Biotechnol.* 34, 879–894. doi: 10.1016/j.tibtech.2016.08.010

Gold, S. (2012). "A low-temperature fuel cell technology for green energy, in *Handbook of Climate Change Mitigation*, eds W.-Y. Chen, J. Seiner, T. Suzuki and M. Lackner (New York, NY: Springer), 1657–1702.

Gorby, Y. A., Yanina, S., McLean, J. S., Rosso, K. M., Moyles, D., Dohnalkova, A., et al. (2006). Electrically conductive bacterial nanowires produced by *Shewanella oneidensis* strain MR-1 and other microorganisms. *Proc. Natl. Acad. Sci. U. S. A.* 103, 11358–11363. doi: 10.1073/pnas.06045 17103

Goyal, N., Zhou, Z., and Karimi, I. A. (2016). Metabolic processes of *Methanococcus maripaludis* and potential applications. *Microb. Cell Fact.* 15:107. doi: 10.1186/s12934-016-0500-0

Grisewood, M. J., Ferry, J. G., and Maranas, C. D. (2018). Computationally exploring and alleviating the kinetic bottlenecks of anaerobic methane oxidation. *Front. Environ. Sci.* 6, 1–18. doi: 10.3389/fenvs.2018. 00084

Hallam, S. J., Putnam, N., Preston, C. M., Detter, J. C., Rokhsar, D., Richardson, P. M., et al. (2004). Reverse methanogenesis: testing the hypothesis with environmental genomics. *Science* 305, 1457–1462. doi: 10.1126/science.1100025

Huskinson, B., Marshak, M. P., Suh, C., Er, S., Gerhardt, M. R., Galvin, C. J., et al. (2014). A metal-free organic-inorganic aqueous flow battery. *Nature* 505, 195–200. doi: 10.1038/nature12909

Kendall, K. (2000). Hydrocarbon fuels - Hopes for a flame-free future. *Nature* 404, 233–235. doi: 10.1038/35005191

Knittel, K., and Boetius, A. (2009). Anaerobic oxidation of methane: progress with an unknown process. *Annu. Rev. Microbiol.* 63, 311–334. doi: 10.1146/annurev.micro.61.080706.093130

Laso-Pérez, R., Wegener, G., Knittel, K., Widdel, F., Harding, K. J., Krukenberg, V., et al., (2016).Thermophilic archaea activate butane via alkyl-coenzyme M formation. *Nature* 539, 396–401. doi: 10.1038/nature20152

Logan, B. E., Hamelers, B., Rozendal, R., Schröder, U., Keller, J., Freguia, S., et al. (2006). Microbial fuel cells: methodology and technology. *Environ. Sci. Technol.* 40, 5181–5192. doi: 10.1021/es0605016

Lovley, D. R. (2012). Electromicrobiology. *Annu. Rev. Microbiol.* 66, 391–409. doi: 10.1146/annurev-micro-092611-150104

Lovley, D. R. (2017). Syntrophy goes electric: direct interspecies electron transfer. *Annu. Rev. Microbiol.* 71:annurev-micro-030117-020420. doi: 10.1146/annurev-micro-030117-020420

McAnulty, M. J., Poosarla, V. G., Kim, K.-Y., Jasso-Chávez, R., Logan, B. E., et al., Wood, T. K. (2017). Electricity from methane by reversing methanogenesis. *Nat. Commun.* 8:15419. doi: 10.1038/ncomms15419

McGlynn, S. E. (2017). Energy metabolism during anaerobic methane oxidation in ANME archaea. *Microbes Environ.* 32, 5–13. doi: 10.1264/jsme2.ME16166

McGlynn, S. E., Chadwick, G. L., Kempes, C. P. and Orphan, V. J. (2015).Single cell activity reveals direct electron transfer in methanotrophic consortia. *Nature* 526, 531–535. doi: 10.1038/nature15512

Nayak, D. D., and Metcalf, W. W. (2017). Cas9-mediated genome editing in the methanogenic archaeon *Methanosarcina acetivorans*. *Proc. Natl. Acad. Sci. U.S.A.* 114, 2976–2981. doi: 10.1073/pnas.1618596114

O'Hayre, R., Cha, S.-W., Colella, W. G., and Prinz, F. B., (2016). "Chapter 13: fuel cell system design," in *Fuel Cell Fundamentals* (Wiley-Blackwell), 447–480.

Pachepsky, Y. A., Blaustein, R. A., Whelan, G. and Shelton, D. R. (2014). Comparing temperature effects on *Escherichia coli*, Salmonella, and Enterococcus survival in surface waters. *Lett. Appl. Microbiol.* 59, 278–283. doi: 10.1111/lam.12272

Pirbadian, S., and El-Naggar, M. Y. (2012). Multistep hopping and extracellular charge transfer in microbial redox chains. *Phys. Chem. Chem. Phys.* 14, 13802–13808. doi: 10.1039/c2cp41185g

Ritchie, M. E. (2018). Reaction and diffusion thermodynamics explain optimal temperatures of biochemical reactions. *Sci. Rep.* 8, 1–10. doi: 10.1038/s41598-018-28833-9

Rosso, K. M., Smith, D. M. A., Wang, Z. M., Ainsworth, C. C. and Fredrickson, J. K. (2004). Self-exchange electron transfer kinetics and reduction potentials for anthraquinone disulfonate. *J. Phys. Chem. A* 108, 3292–3303. doi: 10.1021/jp037134u

Scheller, S., Goenrich, M., Boecher, R., Thauer, R. K., and Jaun, B. (2010). The key nickel enzyme of methanogenesis catalyses the anaerobic oxidation of methane. *Nature* 465, 606–608. doi: 10.1038/nature09015

Scheller, S., Orphan, V. J., and Yu, H. (2018). *Methane Oxidation Methods and Compositions. US Patent No* 10011813.

Scheller, S., Yu, H., Chadwick, G. L., McGlynn, S. E., and Orphan, V. J. (2016).Artificial electron acceptors decouple archaeal methane oxidation from sulfate reduction. *Science* 351, 703–707. doi: 10.1126/science.aad7154

Schröder, U., and Harnisch, F. (2017). Life electric—nature as a blueprint for the development of microbial electrochemical technologies. *Joule* 1, 244–252. doi: 10.1016/j.joule.2017.07.010

Thauer, R. K., Kaster, A.-K., Seedorf, H., Buckel, W., and Hedderich, R. (2008). Methanogenic archaea: ecologically relevant differences in energy conservation. *Nat. Rev. Microbiol.* 6, 579–591. doi: 10.1038/nrmicro1931

Timmers, P. H. A., Welte, C. U., Koehorst J. J., Plugge C. M., Jetten, M. S. M., and Stams A. J. M. (2017). Reverse methanogenesis and respiration in methanotrophic archaea. *Archaea* 2017:22. doi: 10.1155/2017/1654237

Wegener, G., Krukenberg, V., Riedel, D., Tegetmeyer, H. E. and Boetius, A. (2015). Intercellular wiring enables electron transfer between methanotrophic archaea and bacteria. *Nature* 526, 587–590. doi: 10.1038/nature15733

Yan, Z., Joshi, P., Gorski, C. A., and Ferry, J. G. (2018). A biochemical framework for anaerobic oxidation of methane driven by Fe(III)-dependent respiration. *Nat. Commun.* 9, 1–9. doi: 10.1038/s41467-018-04097-9

Conflict of Interest Statement: SS is inventor of a patent filed by California Institute of Technology, Pasadena, CA (US).

frontiers in Energy Research

ORIGINAL RESEARCH
published: 13 November 2018
doi: 10.3389/fenrg.2018.00107

Biological and Bioelectrochemical Systems for Hydrogen Production and Carbon Fixation Using Purple Phototrophic Bacteria

Ioanna A. Vasiliadou[1], Antonio Berná[2], Carlos Manchon[3], Juan A. Melero[1], Fernando Martinez[1], Abraham Esteve-Nuñez[2,3] and Daniel Puyol[1]**

[1] Department of Chemical and Environmental Technology, ESCET, Rey Juan Carlos University, Móstoles, Spain, [2] IMDEA Water, Parque Tecnológico de Alcalá, Alcalá de Henares, Spain, [3] Department of Chemical Engineering, University of Alcalá, Alcalá de Henares, Spain

Domestic and industrial wastewaters contain organic substrates and nutrients that can be recovered instead of being dissipated by emerging efficient technologies. The aim of this study was to promote bio-hydrogen production and carbon fixation using a mixed culture of purple phototrophic bacteria (PPB) that use infrared radiation in presence or absence of an electrode as electron donor. In order to evaluate the hydrogen production under electrode-free conditions, batch experiments were conducted using different nitrogen (NH_4Cl, Na-glutamate, N_2 gas) and carbon sources (malic-, butyric-, acetic- acids) under various COD:N ratios. Results suggested that the efficiency of PPB to produce biogenic H_2 was highly dependent on the substrates used. The maximum hydrogen production (H_{2_max}, 423 mLH_2/L) and production rate (H_{2_rate}, 2.71 mLH_2/Lh) were achieved using malic acid and Na-glutamate at a COD:N ratio of 100:15. Under these optimum conditions, a significant fixation of nitrogen in form of single-cell proteins (874.4 mg/L) was also detected. Under bio-electrochemical conditions using a H-cell bio-electrochemical device, the PPB were grown planktonic in the bio-cathode chamber with the optimum substrate ratio of malic acid and Na-glutamate. A redox potential of −0.5 V (vs. Ag/AgCl) under bio-electrochemical conditions produced comparable amounts of bio-hydrogen but significantly negligible traces of CO_2 as compared to the biological system (11.8 $mLCO_2/L$). This suggests that PPB can interact with the cathode to extract electrons for further CO_2 re-fixation (coming from the Krebs cycle) into the Calvin cycle, thereby improving the C usage. It has also been observed during cyclic voltammograms that a redox potential of −0.8 V favors considerably the electrons consumption by the PPB culture, suggesting that the PPB can use these electrons to increase the biohydrogen production. These results are expected to prove the feasibility of stimulating PPB through bio-electrochemical processes in the production of H_2 from wastewater resources, which is a field of special novelty and still unexplored.

Keywords: purple phototrophic bacteria, biolectrochemical, high value-added products, bio-hydrogen, carbon fixation, proteins

OPEN ACCESS

Edited by:
Sebastià Puig,
University of Girona, Spain

Reviewed by:
Ioannis Andrea Ieropoulos,
University of the West of England, United Kingdom
Matteo Grattieri,
University of Utah, United States

***Correspondence:**
Daniel Puyol
daniel.puyol@urjc.es
Abraham Esteve-Nuñez
abraham.esteve@uah.es

Specialty section:
This article was submitted to Bioenergy and Biofuels, a section of the journal Frontiers in Energy Research

Received: *15 May 2018*
Accepted: *25 September 2018*
Published: *13 November 2018*

Citation:
Vasiliadou IA, Berná A, Manchon C, Melero JA, Martinez F, Esteve-Nuñez A and Puyol D (2018) Biological and Bioelectrochemical Systems for Hydrogen Production and Carbon Fixation Using Purple Phototrophic Bacteria. Front. Energy Res. 6:107. doi: 10.3389/fenrg.2018.00107

INTRODUCTION

Typical wastewater systems entail the dissipation of the contamination. However, the high content of organics and nutrients in industrial and domestic wastewaters is a valuable resource for energy and products recovery (Puyol et al., 2017a). Hence, upgrading of existing WWTP as resource recovery systems by implementing novel technologies, are mandatory steps considering economic and environmental benefits and recent policies within the circular economy.

Among the competing technologies, the biological accumulation of nutrients and their subsequent recovery, has received great attention as an environmental friendly and certainly cost-effective process (Batstone et al., 2015). Purple phototrophic bacteria (PPB) have shown significant accumulation of organics and nutrients from wastewater through assimilative processes (Batstone et al., 2015). PPB is a group of anaerobic facultative microorganisms, which can utilize infrared light (IR) as the main energy source. The use of PPB in the Partition-Release-Recovery concept proved to be far superior to other phototrophic organisms (as algae or cyanobacteria), since they achieve high growth rates and are not inhibited by O_2 (Muñoz and Guieysse, 2006).

PPB are extremely versatile organisms due to their complex metabolic system, involving major C, N, S, P, and Fe pathways, which absorbs the IR energy through their photosystem, composed by carotenoids and bacteriochlorophyls (Hunter, 2008). Anoxygenic photosynthesis generates practically all the energy required for growth via the so-called cyclic electron flow (Klamt et al., 2008). In domestic wastewater treatment, the main metabolism follows photoheterotrophic growth on volatile fatty acids and sugars, although chemoheterotrophy (e.g., fermentation and anaerobic oxidation) can provide the necessary electrons for photoautotrophic growth (via hydrogen; Hülsen et al., 2014, 2016; Puyol et al., 2017a,b). The internal electron recycle, however, can be used for obtaining ammonium through dinitrogen gas fixation or directly dissipating electrons in the nitrogenase complex, which generates bio-hydrogen as the electron acceptor (Koku et al., 2002), or for direct internal accumulation of organic acids as poly-hydroxy-alcanoates (PHA) (Fulop et al., 2012). Moreover, the assimilative partitioning of wastewater macronutrients and organics through PPB leads to the production of one solid bacterial stream rich in proteins.

In this sense, PPB can be used for the extraction of high value-added products from waste sources, such as biofuels like bio-hydrogen, bioplastics as PHA and single-cell proteins. The metabolic pathways to obtain the valuable bioproducts are catalyzed by variant enzymes (McKinlay and Harwood, 2010). Monitoring the functionality of the involved bacteria and following-up their activity, can be of added value toward maximizing the bioproducts' formation. To add to the complexity of the above system, the end product depends greatly on the environmental conditions (IR light intensity, temperature, nutrients concentration, etc.). Thus, wastes rich in nitrogen are good sources for PPB growth producing biomass with high protein content (Verstraete et al., 2009), which can subsequently be used as additive animal food. In organic media lacking nutrients, PPB can accumulate high quantities of PHA, achieving up to 70–90% w/w (Mas and Van Gemerden, 1995). They are therefore an interesting alternative to fossil-fuels for plastics production. When the organic matter composition is quite high and is more reduced than biomass (i.e., butyrate), the excess of electrons (in absence of ammonium) are driven toward hydrogen production that can be used as a clean and renewable biofuel. Understanding the factors of importance and unraveling their relationship with the desired end bioproduct, remains one of the most important challenges in the ongoing research.

Finally, the internal electron recycling of PPB is a key issue, and an active modification of the electronic fluxes by means of artificial addition of electrons could drive toward different targeted bioproducts (Varfolomeyev, 1992). In this way, the concepts supporting microbial electrochemical technologies (METs) could be used to enhance the biochemical reactions of PPB by supplying electric current to microorganisms using electrodes as electron donors. In this context, METs have received great attention due to their potential applications in nitrate reduction (Pous et al., 2013; Tejedor et al., 2016), methanogenesis (Cheng et al., 2009) and microbial electrosynthesis (Logan and Rabaey, 2012). Likewise, the wise use of electricity to enhance PPB activity toward high value-added compounds (i.e., biohydrogen) through a bio-electrochemical system is undoubtedly an attractive challenge. PPB are highly electroactive organisms with high ability to generate bioelectricity through MFCs (Xing et al., 2008; Park et al., 2014). However, the use of electricity to enhance the PPBs metabolic activity aiming to produce high value-added bioproducts is an unexplored field with high growth potential in the short-term.

Based on the above-mentioned grounds, the aim of the present work was the assessment of PPB to enhance the formation of valuable bioproducts, such as biohydrogen, using electric and light energy as the driving forces. This was accomplished by identifying the biological and electrochemical conditions that influence the process of bio-hydrogen production from PPB. The wise use of electric energy to decontaminate wastewater and to produce bio-hydrogen is undoubtedly an attractive and novel challenge, yielding substantial ecological and economic benefits.

MATERIALS AND METHODS

Chemical Compounds and Growth Media

All the chemicals compounds used were purchased from Sigma-Aldrich. The organic compounds that were used were: L-malic acid ($C_4H_6O_5$), butyric acid ($C_4H_8O_2$), acetic acid ($C_2H_4O_2$), propionic acid ($C_3H_6O_2$) and ethanol (C_2H_6O). Stock solutions of individual organic compounds (20 gCOD/L) were prepared in ultra-pure water and stored at 4°C. The nitrogen sources used were: ammonium chloride (NH_4Cl) as inorganic N-source, L-glutamic acid monosodium salt monohydrate (Na-glutamate, $C_5H_8NNaO_4{\cdot}H_2O$) as organic N-source and nitrogen gas (N_2) as external gaseous source. Stock solutions of both organic and inorganic nitrogen sources (5 gN/L) were prepared in ultra-pure water and stored at 4°C.

Finally, macro- and micro-nutrient solutions were prepared following the recipe proposed by Ormerod et al. (1961). The

macro-nutrient solution contained 10.86 g $K_2HPO_4 \cdot 3H_2O$; 6.66 g KH_2PO_4; 2 g $MgSO_4 \cdot 7H_2O$, 0.75 g $CaCl_2 \cdot 2H_2O$; 69 mg $FeCl_2 \cdot 4H_2O$ and 0.2 g EDTA in 1 L ultra-pure water. The micro-nutrient solution contained 1.4 g H_3BO_3; 1.013 g $MnCl_2 \cdot 4H_2O$; 274 mg $(NH_4)_6Mo_7O_{24} \cdot 4H_2O$; 57 mg $ZnCl_2$; 14 mg $CuCl_2 \cdot 2H_2O$; 7.5 mg biotin and 1 g EDTA in 0.5 L ultra-pure water. The pH in all solutions was adjusted to 7.

Purple Phototrophic Bacteria (PPB) Enrichment

All experimental tests were inoculated with a mixed culture of PPB. These bacteria were enriched from a wastewater influent taken from the pilot-scale WWTP located at the Rey Juan Carlos University (Mostoles, Madrid, Spain). Enrichment was performed by inoculating a 1 L suspended growth reactor (SGR) with sludge liquor, and subsequent incubation under near infra-red (NIR) light illumination and anaerobic conditions using a synthetic wastewater (SW) as growth medium. The SW (prepared with tap water) contained the 5 different organic carbon sources (acetic acid, malic acid, propionic acid, butyric acid and ethanol) with a total COD concentration of 2 gCOD/L, 0.26 gN/L as NH_4Cl and 1 and 100 mL/L of micro- and macro-nutrient solutions, respectively. After the addition of SW the bioreactor liquor was flushed with argon gas in order to remove any presence of oxygen. The bioreactor was illuminated with LED lamps (850 nm) as IR light source. The reactor's surface was covered with UV-VIS absorbing foil (ND 1.2 299, Transformation Tubes, Banstead, UK). The foil absorbed around 90% of the wavelength below 750 nm. The average light intensity measured on the outside reactor's surface was 13 W/m^2. The PPB mixed culture was continuously stirred and incubated at room temperature (25 $\pm$ 1°C). The liquor of the reactor was refreshed every week with fresh SW (99% volume exchange) to achieve final concentrations of 2 gCOD/L and 0.26 gNH_4-N/L. The pH was weekly adjusted to 6.8 $\pm$ 0.1. The enrichment of PPB was evaluated by the detection of Bacteriochlorophylls (*BChl*) and carotenoids accumulation by performing VIS-NIR spectra analyses of the culture.

Biological Experiments

The ability of the PPB enriched culture to produce bio-hydrogen using different carbon and nitrogen sources was evaluated in batch assays. Initially, the capacity of the PPB culture to produce hydrogen using different organic and inorganic nitrogen sources was examined. The first set of experiments were conducted by using 2 gCOD/L of L-malic acid as the carbon source. Malic acid was chosen as a suitable carbon source that could favor hydrogen production by PPB (Assawamongkholsiri and Reungsang, 2015). Batch experiments were performed using: inorganic (NH_4Cl) and organic (Na-glutamate) nitrogen, both with concentrations of 75, 150, and 300 mgN/L, and finally dinitrogen gas (60 mL of N_2 in the headspace). Thereafter, two additional experiments were conducted using different carbon sources (butyric- and acetic-acid) at a concentration of 2 gCOD/L each, with 300 mgN/L of Na-glutamate as organic nitrogen source. A summary of the experimental conditions of the batch assays is shown in **Table 1**.

All the experiments were conducted in 160 mL serum bottles with a working volume of 100 mL. The reactors contained 99 mL of SW medium (prepared as described above) with the corresponding COD and N contents and were inoculated with PPB enriched culture (1% v/v inoculum). The initial pH of the medium was adjusted to 6.8 $\pm$ 0.1 using NaOH or H_2SO_4. The liquid medium of each reactor was flushed with argon for 10 min. Thereafter, the bottles were closed with rubber stoppers and capped with aluminum seals. Subsequently, the headspace of the reactors was flushed again with argon for 2 min except from the reactors where nitrogen gas was used as nitrogen source that were flushed with N_2 gas. The bottles were continuously shaken horizontally at 120 rpm at 25 $\pm$ 1°C (Orbital shaker, optic ivymen system) and illuminated at an average light intensity of 20 W/m^2 using LED lamps for 7 days. The performance for H_2 production using identical conditions but without PPB enriched culture was studied by conducting control experiments under sterilized conditions (all the glassware and media used were autoclaved). During these control experiments, no biomass growth as well as no H_2 production or acid assimilation were detected. Both the liquid and the gas media were sampled periodically to evaluate, the carbon and nitrogen assimilation, the PPB growth and the hydrogen production. All the experiments were conducted in duplicate.

Bio-Electrochemical Experiments

Bio-electrochemical experiments were performed in an H-cell device as shown in **Figure 1**. The device was consisted of two Duran glass bottles (8.6 cm diameter $\times$ 18.1 cm height) serving as two chambers. Each cell (cathode and anode) had a working volume of 500 mL. The cathode chamber was equipped with a working electrode of graphite of 10 $\times$ 100 mm and a reference electrode RE-5B Ag/AgCl. All potentials are quoted vs. Ag/AgCl. The anode chamber was equipped with a counter electrode of Ti/Pt (2.5 micro-m) 100 $\times$ 20 mm in a 10 $\times$ 5 mesh. The cathode and anode chambers were separated with a cationic membrane (RALEX, MEGA a.s., Straz pod Ralskem, Czechia). The working, counter and reference electrodes were connected to a potentiostat NEV4-V2 (Nanoelectra S.L., Alcala de Henares, Spain) with maximum current of $\pm$100 mA and compliance voltage of $\pm$10 V. A computer processed by specialized software (Potentiostat NEV4 software, Alcala de Henares, Spain) was used for the automatic recording of data.

As shown in **Figure 1**, the cathode chamber from the H-cell was employed as bio-cathode containing SW (495 ml). The bio-cathode was inoculated with PPB enriched culture (5 mL, 1% v/v inoculum). Malic acid (2 gCOD/L) and Na-glutamate at COD:N ratio of 100:15 were respectively used as carbon and nitrogen sources. The anode chamber was filled with 495 mL of tap water and 5 mL of the macro-nutrients solution. The initial pH in both chambers was adjusted to 6.8 $\pm$ 0.1. The bio-cathode was illuminated with LED lamps as NIR light source with an average light intensity of 20 W/m^2. Bio-electrochemical experiments were performed at 25 $\pm$ 1°C and the cell of bio-cathode was continuously stirred at a speed of 200 rpm. The media in both

TABLE 1 | Experimental runs of PPB biological experiments under different nitrogen and carbon sources.

ID	Carbon source	Organic acid concentration (mgCOD/L)	Nitrogen source	N concentration (mgN/L)	COD:N ratio
1	Malic acid	2,000	NH_4Cl	75	100:3.75
2	Malic acid		NH_4Cl	150	100:7.5
3	Malic acid		NH_4Cl	300	100:15
4	Malic acid	2,000	Na-glutamate	75	100:3.75
5	Malic acid		Na-glutamate	150	100:7.5
6	Malic acid		Na-glutamate	300	100:15
7	Malic acid	2,000	N_2 gas	8.8*	–
8	Butyric acid	2,000	Na-glutamate	300	100:15
9	Acetic acid	2,000	Na-glutamate	300	100:15

Based on Henry's Law and the solubility of gases.

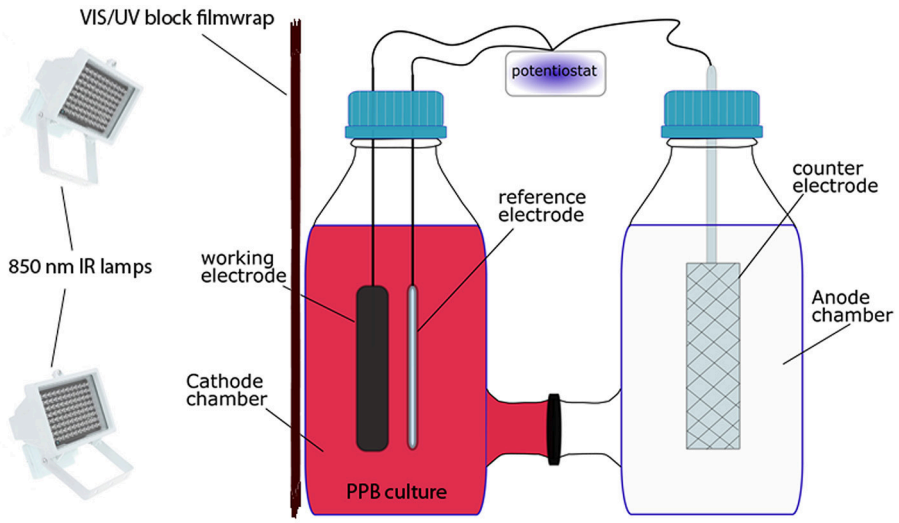

FIGURE 1 | Experimental set-up of the foto-bio-electrochemical H-cell device.

cells were flushed with argon for 20 min. Subsequently, the cells were closed with butyl septa and capped with GL45 Duran caps. The headspaces of the cells were flushed again with argon for 3 min.

Experiments were conducted by setting the potential of bio-cathode at −0.5 V in order to force the PPB culture to be adapted to the electrochemical conditions. The reaction period among the PPB culture and the bio-cathode was chosen to be 1 week, similar to the biological experiments. Control electrochemical (abiotic) experiments were conducted using the same experimental conditions without PPB biomass. In order to determine whether the PPB culture interacted with the cathode or not by means of electron acceptance from PPB, cyclic voltametry (CV) in the range of −0.8 to 0.8 V was performed during the weekly reaction process.

Analytical Methods

All parameters except total chemical oxygen demand (COD) and total Kjeldahl Nitrogen (TKN) were determined after filtering with a 0.45 μm nylon filter (Chrodisc filter/syringe, CHMLab, Barcelona, Spain). Total and soluble COD were determined using a dichromate-reflux colorimetric method (APHA, 2005). The nitrogen contents of filtered and non-filtered samples were determined by the standard Kjeldahl procedure (Gerhardt TNK, Vapodest 450, Königswinter, Germany) using 20 mL of concentrated H_2SO_4 and K_2SO_4-$CuSO_4$ as catalyst. Organic nitrogen content of PPB culture was determined as the difference between Kjeldahl nitrogen of filtered and non-filtered sample. The single cell protein (SCP) content of cell dry weight (CDW) was obtained by multiplying the obtained nitrogen value with a conversion factor of 5.33 (Salo-Vaananen and Koivistoinen, 1996). The inorganic nitrogen was analyzed as NH_4Cl using Spectroquant Ammonium Test (Merck, Darmstadt, Germany). The optical density of PPB biomass was measured at 590 nm by UV-VIS spectrophotometer (V-630, Jasco, Madrid, Spain) and the concentration of biomass was calibrated using a standard curve of PPB optical density on the basis of volatile suspended solids (gVSS/L) concentration (Vasiliadou et al., 2008). The VSS concentration (gVSS/L) was measured according to standard methods (APHA, 2005). The detection of *BChl* and carotenoids

of PPB was performed by determining the VIS-NIR spectra (400–950 nm) using a UV-vis spectrophotometer (V-630, Jasco, Madrid, Spain). The pH was measured using a pH meter (Crison GLP22, Hach Lange, Loveland, CO, USA). Illuminance was measured with a VIS-NIR spectroradiometer (STN-Bluewave-V, MTB, Madrid, Spain). The concentrations of VFAs (malic, acetic and butyric acids) in the liquid samples were analyzed using high performance liquid chromatography (HPLC) (Varian 356-LC, Agilent Technologies, Santa Clara, CA, USA), employing refractive index (RI) detector with a MetaCarb 67H 300 × 6.5 mm column (Agilent Technologies, Santa Clara, CA, USA). The oven temperature was 65°C. The mobile phase was 0.25 mM H_2SO_4 at a flow rate of 0.8 mL/min. The volume of the gas was determined by releasing pressure from the reactors headspace using a Boyle-Mariotte Apparatus (3B Scientific S.L., Hamburg, Germany). The composition of each reactors head-space was analyzed using a 7820A GC system equipped with a 3Ft 1/8 2 mm Poropak Q 80/100 SS column, a 6Ft 1/8 2 mm Poropak Q 80/100 SS column and a 6Ft 1/8 2 mm MolSieve 5A 60/80 SS column, a fitting external Luer lock and a thermal conductivity detector (TCD) (Agilent Technologies, Santa Clara, CA, USA). The mobile phase was Argon at a flow rate of 5 mL/min. The temperature of the oven and the detector were 45 and 220°C, respectively.

RESULTS AND DISCUSSION

The following section include all results generated after exploring the physiology of PPB for selecting those culture conditions, including nitrogen and carbon sources, for achieving an optimal conversion of an extracellular source of electrons into hydrogen production and CO_2 fixation.

Enrichment of a PPB Mixed Culture From Domestic Wastewater

The enrichment process was performed aiming to enhance the growth and acclimation of a mixed PPB culture from domestic wastewater, using a specific environment of NIR radiation. The organic mixture used for the enrichment was chosen on the basis that PPB can efficiently produce hydrogen from wastes that contain mixed VFAs (Wu et al., 2012). It should be noted that the optimum COD:N ratio for efficient C and N assimilation from domestic wastewater by PPB was reported to be 100:7.1 (Puyol et al., 2017b). However, during conventional DWW treatment operation, nutrients, such as N and P are usually in excess (Puyol et al., 2017b). Therefore, a COD:N ratio of 100:13.1 was chosen for the enrichment and acclimation process. Following a 2-weeks enrichment period, PPB biomass growth was evidenced through the BChl *a* accumulation as detected from the peaks with maximum absorbance at 590, 805, and 860 nm. This clearly indicated that the enrichment under anaerobic conditions and NIR light source could selectively enrich PPB from wastewater and express their photosynthetic apparatus via bacteriochlorophylls (Melnicki et al., 2008).

Figure 2 shows an example of PPB culture performance during a weekly operating cycle, after a 2-months acclimation period. **Figure 2A** shows the absorbance spectra of PPB culture aliquots that were taken at different time intervals during the weekly cycle (day 0–7). The PPB culture produced and accumulated with time BChl *a* as well as carotenoids that are naturally synthesized by photosynthetic organisms. The absorption spectrum of BChl *a* appeared in the spectral range between 560 and 930 nm, with maximum peaks at 590, 805, and 860 nm, respectively, while the spectrum of carotenoids appeared in the range between 400 and 550 nm. It has been previously reported that PPB produce molecules referred to as open-chain carotenoids and incorporate them into their photosynthetic system, such as light-harvesting complexes and the bacteriopheophytin-quinone type reaction center (Niedzwiedzki et al., 2017).

As shown in **Figure 2B**, the PPB concentration reached 750 mg/L at the end of the weekly cycle, giving a growth yield of 0.75 ± 0.05 $gCOD_{PPB}/gCOD_{VFA}$. Moreover, the removal of COD and N by PPB culture over the whole acclimation period resulted to an average COD:N of 100:10, which was higher than the optimum ratio (100:7.1) previously reported for domestic wastewater. This high ratio suggested that the PPB enriched culture may have potential for enhancing nitrogen removal in order to achieve the discharge limits for total nitrogen (Hülsen et al., 2014).

Enriched PPB biomass was used for inoculum purposes in order to study the hydrogen formation from wastewater in presence and absence of an electrode as electron donor.

Effect of Nitrogen Source on Biological Hydrogen Production by PPB

Hydrogen production under nitrogen fixation conditions is described by Equation (1) where molecular nitrogen (N_2) is converted to ammonia (NH_3) and protons (H^+) to hydrogen (H_2) (Rey et al., 2007).

$$N_2 + 8e^- + H^+ + 16ATP \rightarrow 2NH_3 + H_2 + 16ADP + 16P_i \quad (1)$$

Biological experiments were conducted in order to extract the optimum biological conditions to maximize hydrogen production while minimizing CO_2 emission. Our first approach was to analysis how biohydrogen production depended on nitrogen substrate at different concentrations by using three different N sources (ammonium, glutamate and nitrogen gas) and malic acid as a model substrate of organic carbon. Interestingly, glutamate increased PPB growth rate by 2-fold in comparison with ammonium or nitrogen gas (see **Figure S1** in Supplementary Information). This also is shown in **Table 2**, where the kinetic parameters of PPB metabolism are included.

Biohydrogen analysis revealed an interesting correlation of hydrogen with the ratio COD:N. So, hydrogen production was enhanced (451 ± 2.1 mLH_2/L) when NH_4Cl was used as inorganic nitrogen at a COD:N ratio of 100:3.75. In contrast, very low amount of hydrogen was produced when higher concentrations of NH_4Cl (COD:N of 100:7.5 and 100:15) were tested (**Figure 3A**; **Table 2**), with 95% confidence values concurring with the zero value. This, in fact, indicates that zero hydrogen production cannot be statistically discarded under these conditions. This is in agreement with the results previously

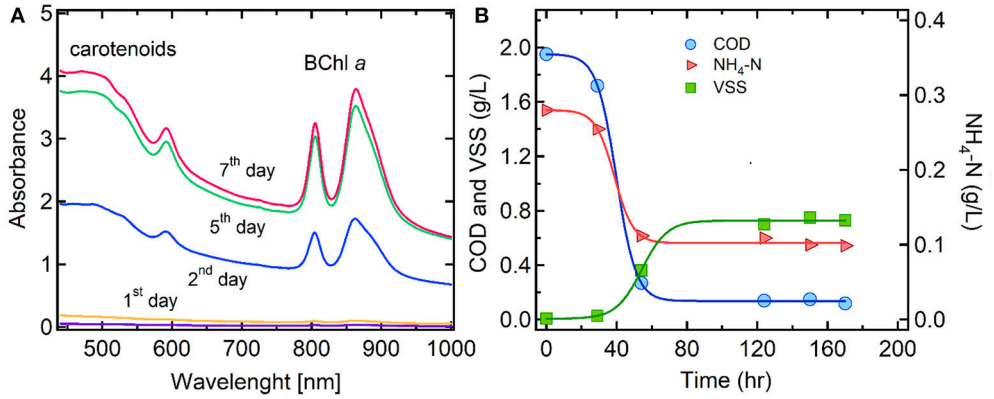

FIGURE 2 | Performance of PPB culture during a weekly operating cycle: **(A)** BChl *a* and carotenoids absorption spectra due to PPB growth, **(B)** COD and NH_4-N assimilation and PPB concentration as VSS.

TABLE 2 | Comparison of H_2 production under different nitrogen and carbon sources.

No	Sources	COD:N	R^a_{PPB} (mgVSS/Lh)	R^b_{acid} (mMacid/Lh)	$H^c_{2\_max}$ (mLH_2/L)	$H^d_{2\_rate}$ (mLH_2/Lh)	Y^e_{H2} (LH_2/g_acid)	Y^f_{molH2} (molH_2/mol_acid)
1	Malic/NH_4Cl	100:3.75	3.67 ± 0.82	0.21 ± 0.05	451.0 ± 2.1	2.63 ± 0.13	0.13 ± 0.01	0.70 ± 0.04
2	Malic/NH_4Cl	100:7.5	4.74 ± 0.84	0.19 ± 0.04	2.2 ± 2.3	(1.35 ± 1.1) ×10^{-2}	(0.59 ± 0.58) ×10^{-3}	(3.15 ± 3.18) ×10^{-3}
3	Malic/NH_4Cl	100:15	5.47 ± 1.01	0.20 ± 0.04	13.7 ± 14.5	(1.30 ± 0.7) ×10^{-2}	(0.50 ± 0.63) ×10^{-3}	(2.55 ± 2.76) ×10^{-3}
4	Malic/Na-glutamate	100:3.75	3.39 ± 0.97	0.21 ± 0.06	300.2 ± 85.0	2.06 ± 0.90	(8.75 ± 2.89) ×10^{-2}	0.47 ± 0.16
5	Malic/Na-glutamate	100:7.5	6.26 ± 2.07	0.20 ± 0.06	416.1 ± 148.2	2.57 ± 1.03	0.12 ± 0.05	0.66 ± 0.27
6	Malic/Na-glutamate	100:15	7.56 ± 1.89	0.19 ± 0.04	423.0 ± 40.9	2.71 ± 0.27	0.12 ± 0.01	0.67 ± 0.05
7	Malic/N_2 gas	–	5.57 ± 1.68	0.21 ± 0.04	12.2 ± 11.3	0.12 ± 0.05	(0.36 ± 0.39) ×10^{-2}	(1.97 ± 2.12) ×10^{-2}
8	Butyric/Na-glutamate	100:15	3.23 ± 0.18	0.06 ± 0.01	214.2 ± 7.2	1.21 ± 0.12	0.22 ± 0.02	0.79 ± 0.08
9	Acetic/Na-glutamate	100:15	3.96 ± 0.09	0.16 ± 0.0	320.4 ± 82.5	2.49 ± 0.36	0.21 ± 0.05	0.50 ± 0.13
10	Bio-electrochemical Malic/Na-glutamate*	100:15	5.91	0.17	390	2.32	0.11	0.60

*[a]PPB growth rate, [b] organic substrate assimilation rate, [c]maximum H_2 production, [d]H_2 production rate, [e,f]H_2 yield, *In the Bio-electrochemical experiments there were no replicates, so no error analysis was able to be conducted.*

reported, stating that high NH_4Cl concentration inhibits the function of the enzyme nitrogenase of PPB resulting in lower hydrogen production (Kim et al., 2012a). Alternatively, N_2 gas as a nitrogen source was used to enhance hydrogen production under nitrogen fixation conditions without repressing the expression of nitrogenase genes.

However, it was observed that the use of N_2 gas as nitrogen source did not efficiently produce H_2 (**Figure 3A**; **Table 2**). The low H_2 production rate (0.12 ± 0.05 mLH_2/Lh) observed in this experiment was probably attributed to a higher energy requirement for the process (16 ATP per mol of hydrogen produced in the nitrogen fixation case vs. 4 ATP per mol of hydrogen produced in the case of the hydrogen production with no nitrogen fixation in the nitrogenase; McKinlay and Harwood, 2010). Also, the extra consumption of reductants to conduct nitrogen fixation for the heterotrophic growth may be counteracted by an increase of the consumption of the produced H_2 in autotrophic growth mode. The absence of CO_2 evolution in the N_2 experiments confirmed such a hypothesis. The PPB culture may use the H_2 produced during the N_2 fixation to re-fixate, in the Calvin-Benson-Bassham cycle (Calvin cycle, CBB), the CO_2 produced during the malic acid assimilation. The analysis of the effect of an external electron source (e.g., from the cathode) would give light to this unsolved question and open possibilities for further research.

Finally, the results indicated that PPB culture produced large amounts of hydrogen when Na-glutamate was used as an organic nitrogen source (300–423 mLH_2/L, **Table 2**). Na-glutamate enhanced the PPB growth and hydrogen production rate (2.1–2.7 mLH_2/Lh). The results of this study are in agreement with those reported by other

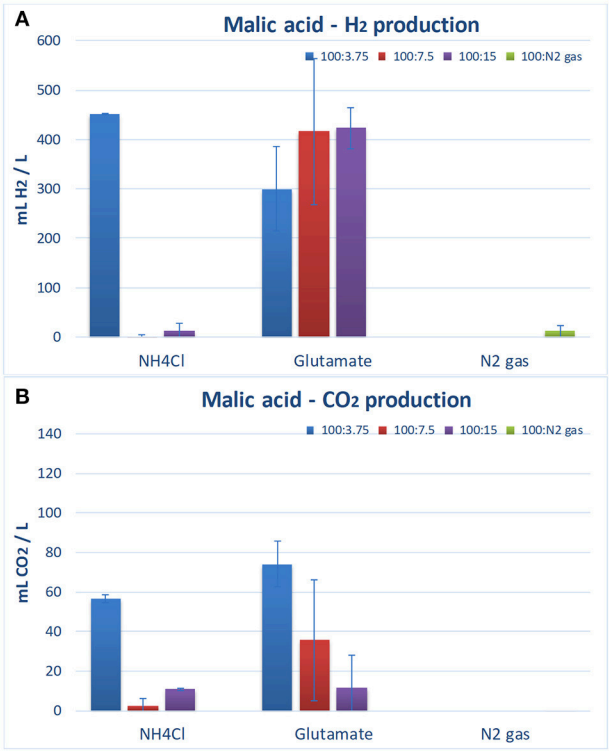

FIGURE 3 | Hydrogen **(A)** and CO_2 **(B)** production by the PPB biological activity after 1 week of reaction with different nitrogen substrates and malic acid as organic carbon source. Error bars are standard deviations from triplicate experiments.

researchers, who have shown that Na-glutamate enhances hydrogen production without inhibiting the nitrogenase enzyme (Melnicki et al., 2008; Assawamongkholsiri and Reungsang, 2015). This is due to the fact that organic nitrogen can be directly assimilated into proteins and a less complex metabolic activity is required for the production of amino acids compared to inorganic sources (Merugu et al., 2010).

Considering Na-glutamate concentration, results showed that H_2 production (mLH_2/L) as well as its production rate was increased as the organic nitrogen concentration increased, achieving a maximum H_2 production at a COD:N ratio of 100:15 (**Figure 3A**; **Table 2**). Moreover, it is noteworthy to mention that the CO_2 production was reduced as the Na-glutamate concentration increased (**Figure 3B**). Therefore, the use of Na-glutamate at COD:N ratios of 100:3.75, 100:7.5, and 100:15 resulted to the production of 74.2 ± 11.6, 35.7 ± 30.7, and 11.8 ± 16.0 $mLCO_2/L$, respectively. PPB that grow on oxidized organic substrates (as malic acid) produce CO_2 due to the oxidation of these substrates. The released CO_2 can then be fixed through the Calvin-Benson-Bassham cycle (Calvin cycle) into cell material as an electron accepting process (McKinlay and Harwood, 2010). This CO_2 fixation via the Calvin cycle enabled PPB to accept excess of electrons and to maintain redox balance and to dispose extra electrons that are generated during use of extra carbon included in Na-glutamate. Therefore, the higher Na-glutamate concentration in the medium could result in a greater CO_2 fixation and lower emission.

It should be highlighted that reducing the NH_4Cl, levels (100:3.75 ratio) resulted in a high hydrogen production (**Figure 3A**) by minimizing the inhibitory effect of this compound on the activity of nitrogenase. In contrast, same conditions resulted in a significant emission of CO_2 (56.7 ± 1.9 $mLCO_2/L$). In addition, Na-glutamate in the ratio 100:15 could favor the PPB activity toward nitrogen assimilation. In conclusion, based on the above, Na-glutamate at a COD:N ratio of 100:15 was selected as the optimum culturing conditions for maximized H_2 production with minimized CO_2 emission.

PPB Can be Cultured Under Bio-Electrochemical Conditions

Considering the importance of the internal electron recycling, an active modification of the electron fluxes through artificial addition of electrons by applying electrochemical technology may potentially enhance the PPB activity and drive toward an optimum H_2 production process. In this sense, the bio-electrochemical capability of interaction between PPB and graphite-electrode has been explored, specially emphasizing the situation when graphite electrode behaves as an electron donor to PPB (setting graphite-electrode potential at −0.5 V) aiming to increase PPB metabolic paths activity by supplying electric current. Therefore, this study focused on the analysis of a bio-electrochemical device based on PPB, using malic acid as organic source and Na-glutamate as nitrogen source, compared to electrode-free biological systems.

Figure 4 presents the cyclic voltammograms (CV) of bio-electrochemical system as well as the bare graphite-electrode as a control electrochemical process, at different time intervals during a weekly operation. The electrochemical behavior for the bare graphite-electrode in the culture media do not exhibit any electrocatalytic behavior in the whole potential range of study (−0.8 to 0.8 V). As it can be seen in **Figure 4**, the cyclic voltammograms for bare graphite-electrode (electrochemical abiotic control) has no reductive currents that can be assigned to tentative hydrogen evolution or the malic acid reduction. As expected, only capacitive currents typical from bare graphite-electrode (ideally polarizable electrode, Bard and Faulkner, 2001) were detected in absence of PPB. Only small positive currents were observed at the more positive potentials explored, 0.8 V (vs. Ag/AgCl), probably due to slight water oxidation and graphite surface oxidation. **Figure 4** shows the cyclic voltammograms for the bio-electrochemical system during the first 24 h, which are very similar to the bare graphite electrode. Only changes in the capacitive currents were observed, exhibiting a higher value for the interfacial pseudocapacitance under bio-electrochemical conditions, so suggesting an electrode surface modification by bacteria attachment. Just after inoculation no significant electroactive biofilm formed but the presence of bacteria in the interface increases the interfacial pseudocapacitance. This was

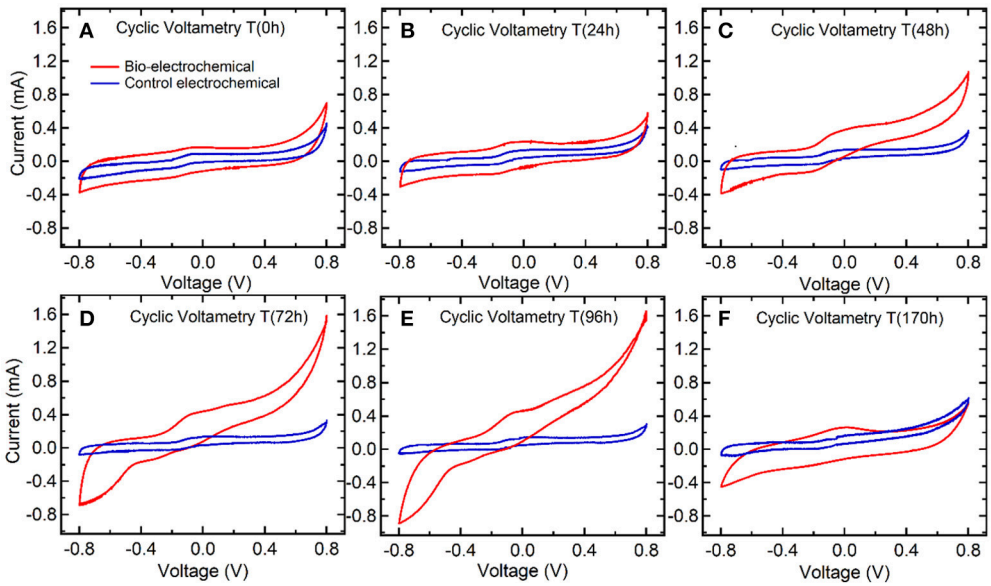

FIGURE 4 | Cyclic voltammograms at different time intervals during bio-electrochemical (red line) and control electrochemical operation (blue line).

probably due to the very low amount of PPB biomass existed at the beginning (Time 0 h) of the experiment (0.01 gVSS/L).

After 48 h of polarizing the electrode at −0.5 V (vs. Ag/AgCl), the cyclic voltammograms revealed the electroactivity of the PPB biofilm interacting with the graphite-electrode surface. These results suggested that PPB started to interact with the working electrode when sufficient amount of biomass (0.1 gVSS/L) and malic acid as carbon source were present in the cathode chamber (**Figure 5A**). It can be observed in **Figure 4C**, how the current was increased in correlation with a potential increase above 0.4 V. This result indicates that PPB biofilm used the electrode as an electron acceptor, probably for malic acid oxidation. This remarkably result indicates the use of PPB for anodic-based oxidations in MET applications. A less noticeable change in current in the negative potential region (between −0.2 and −0.8 V) is starting to develop after 48 h. In **Figure 4D** the negative currents in the potential region between −0.2 and −0.8 V results in a clear negative feature indicating processes related to the interaction of PPB with the graphite electrode as an electron donor. A detailed analysis of the cyclic voltammograms at 72 and 96 h suggests the presence of two processes responsible for the negative feature between −0.2 and −0.8 V. Two processes were may be identified: (a) between −0.2 and −0.4 V, there was a steady increase in the negative current (in absolute value), and (b) around −0.6 V there is a steep change in the slope of the negative current indicating the occurrence of a second process. In our experiments, the electrode was polarized at −0.5 V, a potential able to explore the first reductive process from electroactive PPB. Finally, it is noteworthy to mention that after the depletion of malic acid in the medium at 170 h (**Figure 5A**) the magnitude of redox reactions was changed (**Figure 4F**), showing an electrochemical behavior similar to this of Time 0 h, and suggesting low electroactivity of the PPB culture.

Effect of Carbon Source on Biological Hydrogen Production by PPB

The biological production of hydrogen by PPB was studied by testing different organic carbon sources, as malic acid, butyric acid and acetic acid, using Na-glutamate as optimum nitrogen source at a COD:N ratio of 100:15. Results indicated that the PPB culture was able to assimilate all the organic acids tested toward biomass growth as well as hydrogen production. Maximum PPB growth rate (7.56 mgVSS/Lh) was obtained when malic acid was used as compared to butyric (3.23 mgVSS/Lh) and acetic acid (3.96 mgVSS/Lh; **Table 2**). As a consequence of the higher C assimilation, the N assimilation into bacteria (as proteins) was also enhanced by using malic acid, giving a production of SCP of 874 mg/L as compared to 621 and 346 mg/L obtained with acetic and butyric acids, respectively. It was observed that the use of malic acid as carbon source achieved the highest hydrogen production (H_{2_max}, mLH_2/L) and the highest H_2 production rate (H_{2_rate}, mLH_2/Lh; **Table 2**). Malic acid has widely used as optimum carbon source for H_2 production, probably due to its capacity to directly enter the tricarboxylic acid cycle (Melnicki et al., 2008; Kim et al., 2012b; Assawamongkholsiri and Reungsang, 2015). Other evidences supporting malic acid as the optimum organic to conduct hydrogen production is shown in Supporting Information.

The experimental results obtained from the biological study (electrode-free) of hydrogen production indicated that the combination of malic acid and Na-glutamate was the optimum for maximizing the hydrogen production by PPB. The efficiency of H_2 production from the PPB mixed culture enriched in this

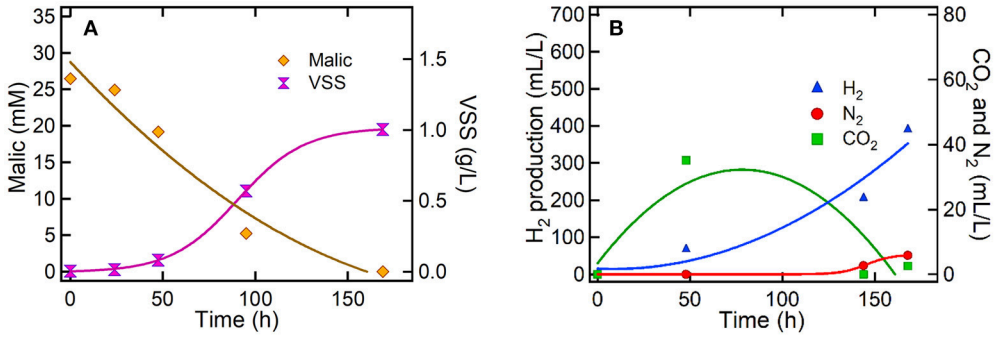

FIGURE 5 | Culture of PPB under bio-electrochemical conditions at −0.5 V (vs. Ag/AgCl) **(A)** Malic acid removal and PPB growth and **(B)** production of H_2, N_2, and CO_2.

study is comparable to those of previous studies where pure or mixed PPB cultures were used (**Table 3**). In conclusion, the high H_2 production rates achieved in this study showed that the PPB mixed culture could potentially be used for a feasible H_2 production application during wastewater treatment processes. This supports the use of malic acid and Na-glutamate as the C and N sources for the bio-electrochemical production of H_2.

Effect of Bio-Electrochemical Electron Donor on PPB for Producing Hydrogen and Fixing CO_2

Results suggested that bio-electrochemical process of PPB resulted to similar H_2 production rate and hydrogen yields (**Table 2**) compared to the PPB biological process under the same conditions. However, it was observed that after 1 week of bio-electrochemical reaction PPB fixed all the amount of CO_2 that was produced during the first 50 h (**Figure 5B**). This resulted to zero CO_2 emission as compare to the PPB biological process (see Supporting Information, **Figure S2**) that produced an average of 11.8 ± 16.0 mLCO_2/L after 1 week of biological process (**Figure 3B**). Subsequently, results suggested that CO_2 fixation was the main mechanism of PPB metabolism that was accepting electrons from the bio-cathode. This is in agreement with the negative current values observed during the bio-electrochemical process suggesting that there might be a consumption of electrons due to the PPB activity (**Figure 6**).

Figure 5 shows the malic acid assimilation, the PPB growth and the evolution of gas production during bio-electrochemical process. The bio-electrochemical setup revealed that PPB can effectively use the graphite-electrode as electron donor (**Figures 4C**-48 h, **D**-72 h, and **E**-96 h) and, subsequently, reduce the levels of CO_2. Carbon dioxide fixation is not detected in such a high extension when system was run in absence of electrode (see Supporting Information, **Figure S2**). Carbon dioxide fixation seems to occur at the origin of the **first** reductive process detected between −0.2 and −0.6 V. The extra electron source provided by the electrode promoted carbon dioxide fixation by PPB beyond the standard activity of this bacterial genus in absence of electrodes under limited electrons availability.

It is well-reported that graphite electrodes, and generally carbon electrodes, exhibit a high overpotential for hydrogen evolution and carbon dioxide reduction (Sullivan et al., 1993; DuBois, 2006; Yang et al., 2016) and therefore poor electrocatalytic properties. The standard electrode potential for carbon dioxide reduction to formic acid and oxalic acid are −0.199 and −0.590 V (Sullivan et al., 1993; Eggins et al., 1998; DuBois, 2006; Yang et al., 2016), respectively. These values are reported in the SHE scale, and taking into account that we are working in pH = 7 solutions and Ag/AgCl reference scale (ca. 0.2 V vs. SHE), the standard electrode potential has to be recalculated according to Nernst equation. Nernst equation gives an equilibrium potential of −0.716 V for formate and −0.790 V in the case of oxalate vs. Ag/AgCl. In any case, these electrode potentials are more negative than −0.5 V vs. Ag/AgCl, potential value used in this study. Furthermore, these are the thermodynamic potential values, carbon dioxide reduction has been reported on graphite electrodes taking place at potentials more negative than −0.9 V vs. Ag/AgCl (Eggins et al., 1998). Actually, this fact can be clearly observed in the electrochemical control voltammograms reported in **Figure 4**. The cyclic voltammogram corresponding to the bare graphite electrode in the same solution but in absence of PPB, displays the classical voltammogram of an ideally polarized electrode, where there are no significant faradaic currents in the whole potential range explored (0.8 to −0.8 V), as it would be expected. Only pseudocapacitive electrochemical behavior is detected in the electrode interface in absence of PPB. Regarding the previous arguments, electrochemical carbon dioxide reduction on bare graphite electrode can be discarded, and the only contribution of PPB metabolism can explain the consumption of carbon dioxide.

In contrast, at −0.5 V, the capability of hydrogen production of the bio-electrochemical system was comparable to the exhibited by PPB in absence of electrode, and no electrode potential was observed in this process. The origin of the second bio-electrochemical process developed below −0.6 V, that can be tentatively assigned to hydrogen production, will require further investigation beyond the scope of this work. The capability of PPB for using graphite-electrode as electron donor was demonstrated. The extra electron donor source can be used in

TABLE 3 | Comparison of hydrogen production rates by different cultures and systems with the one studied in the present work.

PPB culture	IR	Process mode	Carbon/Nitrogen sources	Y_{H2} (LH_2/gacid)	H_{2_rate} (mLH_2/Lh)	Y_{molH2} ($molH_2$/mol_acid)	References
Rhodospirillum rubrum *Rhodopseudomonas palustris*	60 W/m^2	Batch	Succinate/glutamate	–	21 4.3	–	Melnicki et al., 2008
Rhodobacter sphaeroides	100 W	Batch	Malate/glutamate Malate/NH_4Cl Acetate/NH_4Cl	0.541 0.224–0 0.467–0.135	5.1 4.6–0 5.8–3.3	–	Akkose et al., 2009
Rhodobacter sphaeroides	5 klux*	Continuous	Mixture of VFAs**/$(NH_4)_2SO_4$	0.185	1.125	–	Ozmihci and Kargi, 2010
Rhodopseudomonas acidophila	2,400 lux*	Batch	Acetate/nitrate Malate/nitrate Succinate/nitrate Succinate/N_2 Succinate/NH_4C	–	2.7 2.5 3.3 0.5 1.25	–	Merugu et al., 2012
Mixed culture–dominant *Rhodopseudomonas palustris*	190 W/m^2	Continuous	Mixture** of acetate, lactate, butyrate, propionate/NH_4-N	0.97	121	–	Tawfik et al., 2014
Rhodobacter sphaeroides	10 W/m^2	Batch	Succinate/$(NH_4)_2SO_4$	–	31	–	Ryu et al., 2014
Rhodobacter sp. KKU-PS1	2,500 lux*	Batch	Malate/glutamate	–	6.8	–	Assawamongkholsiri and Reungsang, 2015
Rhodopseudomonas palustris	2,000 lux*	Batch	Lactate/glutamate Butyrate/glutamate	–	8.4 19.9	2.57 4.92	Hu et al., 2017
Mixed culture	20 W/m^2	Batch	Malic acid/glutamate	0.12	2.71	0.67	This study

**Illumination intensity was calculated (1 lx = 0.0161028 W/m^2), **Dark fermentation effluent.*

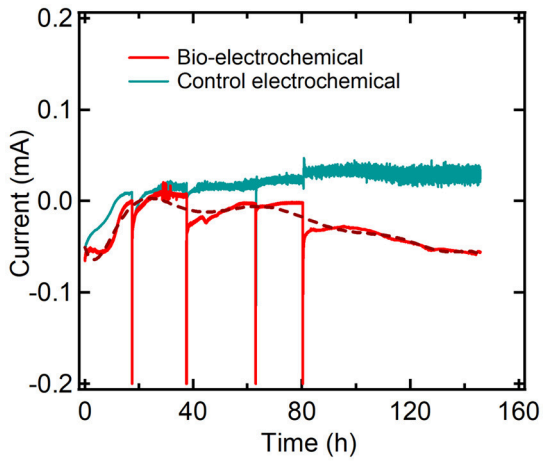

FIGURE 6 | Current evolution during bio-electrochemical and abiotic electrochemical reactions.

more than one metabolic pathway. Polarizing the electrode at −0.5 V, allows PPB to use electrode for carbon fixation reaching almost no carbon dioxide accumulation in contrast to the electrode-free biological system. This is the first study indicating that electroactive capture of CO_2 by PPB is feasible.

Finally, the SCP production achieved by PPB during the bio-electrochemical process (81% mgSCP/mgVSS) was similar to this observed by PPB growing in absence of electrodes. Therefore, the bio-electrochemical process did not seem to affect proteins yields under the experimental conditions tested.

CONCLUSIONS

This work analyzed the optimum culturing conditions for maximizing the hydrogen production by a mixed culture of purple phototrophic bacteria. In addition, the effect of a negatively polarized bio-electrochemical device on the modification of the behavior of the culture in terms of metabolic shifts and current consumption was explored. The main conclusions extracted from this work are shown below:

- Among all the conditions tested in absence of electrodes, best results on the hydrogen production have been achieved by using malic acid as a carbon source (instead of acetic and butyric) and Na-glutamate as a N source (instead of ammonium and dinitrogen gas), in a COD/N relationship of 100/15. Under these conditions, the production of CO_2 was also minimized.
- Cyclic voltammograms of the bio-electrochemical system shown the appearing of at least three potentials (two negative and one positive) with clear interaction between the PPB culture and the electrode. This makes evident the high electroactivity of PPB cultures and their potential as a MET microbial candidate.

- Negative polarization of the electrode at −0.5 V caused a detectable consumption of electrons associated with a depletion of the produced carbon dioxide, which indicates that the PPB culture was capable of using electrons from the cathode to capture the excess of C released as CO_2 during the CBB cycle. This behavior was not observed before in an indigenous (non-genetically-modified) PPB culture.
- Results presented herein have shown that further in-depth research using different conditions (other polarization of the cathode) will be of extreme benefit and may enhance the H_2 production rate.

AUTHOR CONTRIBUTIONS

IV designed and performed the experiments and wrote the manuscript, AB critically reviewed the manuscript, CM helped in the experimental stage, JM critically reviewed the manuscript, FM critically reviewed the manuscript and supervised the work, AE-N and DP designed the experiments, supervised the work, and corrected the manuscript. Both DP and AE-N are corresponding authors.

ACKNOWLEDGMENTS

IV thanks the International Excellence Campus Smart Energy Program (CEISEP) for a Post-doctoral Fellowship. Financial support of Regional Government of Madrid provided through project REMTAVARES S2013/MAE-2716 and the European Social Fund as well as Spanish Ministry of Economy are acknowledged.

SUPPLEMENTARY MATERIAL

The Supplementary Material for this article can be found online at: https://www.frontiersin.org/articles/10.3389/fenrg.2018.00107/full#supplementary-material

REFERENCES

Akkose, S., Gunduz, U., Yucel, M., and Eroglu, I. (2009). Effects of ammonium ion, acetate and aerobic conditions on hydrogen production and expression levels of nitrogenase genes in *Rhodobacter sphaeroides* O.U.00. *Int. J. Hydrog. Energy* 34, 8818–8827. doi: 10.1016/j.ijhydene.2009.08.040

APHA (2005). *Standard Methods for the Examination of Water and Wastewater*. Washington, DC: American Public Health Association.

Assawamongkholsiri, T., and Reungsang, A. (2015). Photo-fermentational hydrogen production of Rhodobacter sp. KKU-PS1 isolated from an UASB reactor. *Elec. J. Biotechnol.* 18, 221–230. doi: 10.1016/j.ejbt.2015.03.011

Bard, A. J., and Faulkner, L. R. (2001). *Electrochemical Methods. Fundamentals and Aplications*. Hoboken, NJ: John Wiley & Sons Inc.

Batstone, D. J., Hülsen, T., Mehta, C. M., and Keller, J. (2015). Platforms for energy and nutrient recovery from domestic wastewater: a review. *Chemosphere* 140, 2–11. doi: 10.1016/j.chemosphere.2014.10.021

Cheng, S., Xing, D., Call, D. F., and Logan, B. E. (2009). Direct biological conversion of electrical current into methane by electromethanogenesis. *Environ. Sci. Technol.* 43, 3953–3958. doi: 10.1021/es803531g

DuBois, D. L. (2006). "Electrochemical reactions of carbon dioxide," in *Encyclopaedia of Electrochemistry*, eds A. J. Bard, and M. Stratmann (Weinheim: Wiley-VCH), 202–225.

Eggins, B. R., Brown, E. M., O'Neill, E. A., and Grinshaw, J. (1998). Carbon dioxide fixation by electrochemical reduction in water to oxalate and glyoxylate. *Tetrahedron Lett.* 29, 945–948.

Fulop, A., Beres, R., Tengolics, R., Rakhely, G., and Kovacs, K. L. (2012). Relationship between PHA and hydrogen metabolism in the purple sulfur phototrophic bacterium *Thiocapsa roseopersicina* BBS. *Int. J. Hydrog. Energy* 37, 4915–4924. doi: 10.1016/j.ijhydene.2011.12.019

Hu, C., Choy, S. Y., and Giannis, A. (2017). Evaluation of lighting systems, carbon sources, and bacteria cultures on photofermentative hydrogen production. *Appl. Biochem. Biotechnol.* 185, 257–269. doi: 10.1007/s12010-017-2655-5

Hülsen, T., Barry, E. M., Lu, K., Puyol, D., Keller, J., and Batstone, D. J. (2016). Domestic wastewater treatment with purple phototrophic bacteria using a novel continuous photo anaerobic membrane bioreactor. *Water Res.* 100, 486–495. doi: 10.1016/j.watres.2016.04.061

Hülsen, T., Batstone, D. J., and Keller, J. (2014). Phototrophic bacteria for nutrient recovery from domestic wastewater. *Water Res.* 50, 18–26. doi: 10.1016/j.watres.2013.10.051

Hunter, C. N. (2008). *The Purple Phototrophic Bacteria*. Berlin: Springer.

Kim, M. S., Kim, D. H., and Cha, J. (2012b). Culture conditions affecting H2 production by phototrophic bacterium *Rhodobacter sphaeroides* KD131. *Int. J. Hydrog. Energy* 37, 14055–14061. doi: 10.1016/j.ijhydene.2012.06.085

Kim, M. S., Kim, D. H., Cha, J., and Lee, J. K. (2012a). Effect of carbon and nitrogen sources on photofermentative H2 production associated with nitrogenase, uptake hydrogenase activity, and PHB accumulation in Rhodobacter sphaeroides KD131. *Bioresour. Technol.* 116, 179–183. doi: 10.1016/j.biortech.2012.04.011

Klamt, S., Grammel, H., Straube, R., Ghosh, R., and Gilles, E. D., (2008). Modeling the electron transport chain of purple non-sulfur bacteria. *Mol. Syst. Biol.* 4:156. doi: 10.1038/msb4100191

Koku, H., Eroglu, I., Gunduz, U., Yucel, M., and Turker, L. (2002). Aspects of the metabolism of hydrogen production by *Rhodobacter sphaeroides*. *Int. J. Hydrogen Energ.* 27, 1315–1329. doi: 10.1016/S0360-3199(02)00127-1

Logan, B. E., and Rabaey, K. (2012). Conversion of wastes into bioelectricity and chemicals by using microbial electrochemical technologies. *Science* 337, 686–690. doi: 10.1126/science.1217412

Mas, J., and Van Gemerden, H. (1995). "Storage products in purple and green sulfur bacteria," in *Anoxygenic Photosynthetic Bacteria* (Berlin: Springer), 973–990.

McKinlay, J. B., and Harwood, C. S. (2010). Carbon dioxide fixation as a central redox cofactor recycling mechanism in bacteria. *Proc. Natl. Acad. Sci. U.S.A.* 107, 11669–11675. doi: 10.1073/pnas.1006175107

Melnicki, M. R., Bianchi, L., De Philippis, R., and Melis, A. (2008). Hydrogen production during stationary phase in purple photosynthetic bacteria. *Int. J. Hydrog. Energy* 33, 6525–6534. doi: 10.1016/j.ijhydene.2008.08.041

Merugu, R., Girisham, S., and Reddy, S. M. (2010). Bioproduction of hydrogen by *Rhodobacter capsulatus* KU002 isolated from leather industry effluents. *Int. J. Hydrog. Energy* 35, 9591–9597. doi: 10.1016/j.ijhydene.2010.06.057

Merugu, R., Rudra, M. P., Badgu, N., Girisham, S., and Reddy, S. M. (2012). Factors influencing the production of hydrogen by the purple non-sulphur phototrophic bacterium *Rhodopseudomonas acidophila* KU001. *Microb. Biotechnol.* 5, 674–678. doi: 10.1111/j.1751-7915.2012.00346.x

Muñoz, R., and Guieysse, B. (2006). Algal-bacterial processes for the treatment of hazardous contaminants: a review. *Water Res.* 40, 2799–2815. doi: 10.1016/j.watres.2006.06.011

Niedzwiedzki, D. M., Dilbeck, P. L., Tang, Q., Martin, E. C., Bocian, D. F., Hunter, C. N., et al. (2017). New insights into the photochemistry of carotenoid spheroidenone in light-harvesting complex 2 from the purple bacterium *Rhodobacter sphaeroides*. *Photosyn. Res.* 131, 291–304. doi: 10.1007/s11120-016-0322-2

Ormerod, J. G., Ormerod, K. S., and Gest, H. (1961). Light-dependent utilization of organic compounds and photoproduction of molecular hydrogen by photosynthetic bacteria; relationships with nitrogen metabolism. *Arch. Biochem. Biophys.* 94, 449–463. doi: 10.1016/0003-9861(61)90073-X

Ozmihci, S., and Kargi, F. (2010). Bio-hydrogen production by photo-fermentation of dark fermentation effluent with intermittent feeding and effluent removal. *Int. J. Hydrog. Energy* 35, 6674–6680. doi: 10.1016/j.ijhydene.2010.04.090

Park, T. J., Ding, W., Cheng, S., Brar, M. S., Ma, A. P. Y., Tun, H. M., et al. (2014). Microbial community in microbial fuel cell (MFC) medium and effluent enriched with purple photosynthetic bacterium (*Rhodopseudomonas* sp.). *AMB Express* 4:22. doi: 10.1186/s13568-014-0022-2

Pous, N., Puig, S., Coma, M., Balaguer, M. D., and Colprim, J. (2013). Bioremediation of nitrate-polluted groundwater in a microbial fuel cell. *J. Chem. Technol. Biotechnol.* 88, 1690–1696. doi: 10.1002/jctb.4020

Puyol, D., Barry, E. M., Hülsen, T., and Batstone, D. J. (2017b). A mechanistic model for anaerobic phototrophs in domestic wastewater applications: photo-anaerobic model (PAnM). *Water Res.* 116, 241–253. doi: 10.1016/j.watres.2017.03.022

Puyol, D., Batstone, D. J., Hülsen, T., Astals, S., Peces, M., and Krömer, J. O. (2017a). Resource recovery from wastewater by biological technologies: opportunities, challenges, and prospects. *Front. Microbiol.* 7:2106. doi: 10.3389/fmicb.2016.02106

Rey, F. E., Heiniger, E. K., and Harwood, C. S. (2007). Redirection of metabolism for biological hydrogen production. *Appl. Environ. Microbiol.* 73, 1665–1671. doi: 10.1128/AEM.02565-06

Ryu, M. H., Hull, N. C., and Gomelsky, M. (2014). Metabolic engineering of Rhodobacter sphaeroides for improved hydrogen production. *Int. J. Hydrog. Energy* 39, 6384–6390. doi: 10.1016/j.ijhydene.2014.02.021

Salo-Vaananen, P. P., and Koivistoinen, P. E. (1996). Determination of protein in foods: comparison of net protein and crude protein (N X 6.25) values. *Food Chem.* 51, 21–31.

Sullivan, B. P., Krist, K., and Guard, H. E., (Eds.) (1993). *Electrochemical and Electrocatalytic Reactions of Carbon Dioxide*. Amsterdam: Elsevier.

Tawfik, A., El-Bery, H., Kumari, S., and Bux, F. (2014). Use of mixed culture bacteria for photofermentive hydrogen of dark fermentation effluent. *Bioresour. Technol.* 168, 119–126. doi: 10.1016/j.biortech.2014.03.065

Tejedor, S., Baccetti de Gregoris, T., Salas, J. J., Pastor, L., and Esteve-Nu-ez, A. (2016). Integrating a microbial electrochemical system into a classical wastewater treatment configuration for removing nitrogen from low COD effluents. *Environ. Sci. Water Res. Technol.* 2, 884–896. doi: 10.1039/C6EW00100A

Varfolomeyev, S. D. (1992). Bioelectrosynthesis as an alternative to photosynthesis. *Appl. Biochem. Biotechnol. A Enz. Engin. Biotechnol.* 33, 145–155. doi: 10.1007/BF02950783

Vasiliadou, I. A., Tziotzios, G., and Vayenas, D. V. (2008). A kinetic study of combined aerobic biological phenol and nitrate removal in batch suspended growth cultures. *Int. Biodeterior. Biodegrad.* 61, 261–271. doi: 10.1016/j.ibiod.2007.09.002

Verstraete, W., Van de Caveye, P., and Diamantis, V. (2009). Maximum use of resources present in domestic "used water". *Bioresour. Technol.* 100, 5537–5545. doi: 10.1016/j.biortech.2009.05.047

Wu, T. Y., Hay, J. X. W., Kong, L. B., Juan, J. C., and Jahim, J. M. D. (2012). Recent advances in reuse of waste material as substrate to produce biohydrogen by purple non-sulfur (PNS) bacteria. *Renew Sustain Energy Rev.* 16, 3117–3122. doi: 10.1016/j.rser.2012.02.002

Xing, D., Zuo, Y., Cheng, S., Regan, J. M., and Logan, B. E. (2008). Electricity generation by *Rhodopseudomonas palustris* DX-1. *Environ. Sci. Technol.* 42, 4146–4151. doi: 10.1021/es800312v

Yang, N., Waldvogel, S. R., and Jiang, X. (2016). Electrochemistry of carbon dioxide on carbon electrodes. *Appl. Mater. Interf.* 8, 28357–28371. doi: 10.1021/acsami.5b09825

Conflict of Interest Statement: The authors declare that the research was conducted in the absence of any commercial or financial relationships that could be construed as a potential conflict of interest.

frontiers in Energy Research

ORIGINAL RESEARCH
published: 17 January 2019
doi: 10.3389/fenrg.2018.00144

Bioelectrochemical Stimulation of Electromethanogenesis at a Seawater-Based Subsurface Aquifer in a Natural Gas Field

Shun'ichi Ishii[1]*, *Hiroyuki Imachi*[1,2], *Kenjiro Kawano*[3], *Daisuke Murai*[3], *Miyuki Ogawara*[2], *Katsuyuki Uemastu*[4], *Kenneth H. Nealson*[5] and *Fumio Inagaki*[1,6,7]

[1] R&D Center for Submarine Resources, Japan Agency for Marine-Earth Science and Technology (JAMSTEC), Nankoku, Japan, [2] Department of Subsurface Geobiological Analysis and Research (D-SUGAR), Japan Agency for Marine-Earth Science and Technology (JAMSTEC), Yokosuka, Japan, [3] Kanto Natural Gas Development Co., Ltd., Mobara, Japan, [4] Marine Works Japan Co., Ltd., Yokosuka, Japan, [5] Department of Earth Science, University of Southern California, Los Angeles, CA, United States, [6] Kochi Institute for Core Sample Research, Japan Agency for Marine-Earth Science and Technology (JAMSTEC), Nankoku, Japan, [7] R&D Center for Ocean Drilling Science, Japan Agency for Marine-Earth Science and Technology (JAMSTEC), Yokohama, Japan

OPEN ACCESS

Edited by:
Deepak Pant,
Flemish Institute for Technological Research, Belgium

Reviewed by:
Kangning Zhao,
University of Wisconsin-Madison, United States
Sam Molenaar,
W&F Technologies BV, Netherlands

***Correspondence:**
Shun'ichi Ishii
sishii@jamstec.go.jp

Specialty section:
This article was submitted to Bioenergy and Biofuels, a section of the journal Frontiers in Energy Research

Received: *03 August 2018*
Accepted: *12 December 2018*
Published: *17 January 2019*

Citation:
Ishii S, Imachi H, Kawano K, Murai D, Ogawara M, Uemastu K, Nealson KH and Inagaki F (2019) Bioelectrochemical Stimulation of Electromethanogenesis at a Seawater-Based Subsurface Aquifer in a Natural Gas Field. Front. Energy Res. 6:144. doi: 10.3389/fenrg.2018.00144

In subsurface anoxic environments, microbial communities generally produce methane as an end-product to consume organic compounds. This metabolic function is a source of biogenic methane in coastal natural gas aquifers, submarine mud volcanoes, and methane hydrates. Within the methanogenic communities, hydrogenotrophic methanogens, and syntrophic bacteria are converting volatile fatty acids to methane syntrophically via interspecies hydrogen transfer. Recently, direct interspecies electron transfer (DIET) between fermentative/syntrophic bacteria and electrotrophic methanogens has been proposed as an effective interspecies metabolite transfer process to enhance methane production. In this study, in order to stimulate the DIET-associated methanogenic process at deep biosphere-aquifer systems in a natural gas field, we operated a bioelectrochemical system (BES) to apply voltage between an anode and a cathode. Two single-chamber BESs were filled with seawater-based formation water collected from an onshore natural gas well, repeatedly amended with acetate, and operated with 600 mV between electrodes for 21 months, resulting in a successful conversion of acetate to methane via electrical current consumption. One reactor yielded a stable current of ~200 mA/m^2 with a coulombic efficiency (CE) of >90%; however, the other reactor, which had been incidentally disconnected for 3 days, showed less electromethanogenic activity with a CE of only ~10%. The 16S rRNA gene-based community analyses showed that two methanogenic archaeal families, *Methanocalculaceae* and *Methanobacteriaceae*, were abundant in cathode biofilms that were mainly covered by single-cell-layered biofilm, implicating them as key players in the electromethanogenesis. In contrast, family *Methanosaetaceae* was abundant at both electrodes and the electrolyte suspension only in the reactor with less electromethanogenesis, suggesting this family was not involved in electromethanogenesis and became abundant only after the no-electron-flow event. The anodes were covered by thick biofilms with filamentous networks, with the

family *Desulfuromonadaceae* dominating in the early stage of the operation. The family *Geobacteraceae* (mainly genus *Geoalkalibacter*) became dominant during the longer-term operation, suggesting that these families were correlated with electrode-respiring reactions. These results indicate that the BES reactors with voltage application effectively activated a subsurface DIET-related methanogenic microbiome in the natural gas field, and specific electrogenic bacteria and electromethanogenic archaea were identified within the anode and/or cathode biofilms.

Keywords: microbial electrosynthesis, electromethanogenesis, extracellular electron transfer, microbial community dynamics, FIB-SEM, subsurface microbiome

INTRODUCTION

In most subsurface microbial ecosystems in oxygen-depleted organic-rich sedimentary environments, heterotrophic microbial communities generally produce methane as an end-product of the microbial respirations via CO_2 reduction. This biogeochemical ecosystem function widely occurs on Earth, including not only a wide range of terrestrial and marine environments (e.g., rice paddy soils, cow rumen, wetlands, natural forest soils, thawing permafrost, and coastal sediments; see Matthews and Fung, 1987; Bartlett and Harriss, 1993) but also anthropogenic microbial habitats (e.g., anaerobic digester, agricultural and industrial wastewaters; see Mao et al., 2015). To date, so called "biogenic methane" in anaerobic subsurface systems has been largely explored as one of the energy sources; e.g., coastal natural gas aquifers (Sano et al., 2017), submarine mud volcanoes (Ijiri et al., 2018), methane hydrates (Kvenvolden, 1995) and coal/shale beds (Inagaki et al., 2015). Activity of the naturally occurring microbial methanogenic processes is generally extraordinarily low due to the low energy availability in the deep biosphere (Lever et al., 2015). Nevertheless, several methanogens have been successfully isolated from methane hydrate-bearing sediment (Imachi et al., 2011), submarine mud volcano (Ijiri et al., 2018), and formation water from a natural gas field (Mochimaru et al., 2007). The widespread distribution of biogenic methane clearly indicates that microorganisms play an important role in biogeochemical carbon cycling on the Earth.

Within the methanogenic microbial communities, two different types of methanogenic archaea are observed as hydrogenotrophic (Equation 2) and aceticlastic (Equation 3) methanogens.

$$CH_3COO^- + 4H_2O \rightarrow 2HCO_3^- + 4H_2 + H^+ \ldots \quad \text{(syntrophic acetate oxidation)} \quad (1)$$

$$4H_2 + CO_2 \rightarrow CH_4 + 2H_2O \ldots \quad \text{(hydrogenotrophic methanogenesis)} \quad (2)$$

$$CH_3COO^- + H_2O \rightarrow CH_4 + HCO_3^- \ldots \quad \text{(aceticlastic methanogenesis)} \quad (3)$$

Hydrogenotrophic (H_2-consuming) methanogens syntrophically convert volatile fatty acids, such as acetate and propionate, to methane in conjunction with syntrophic bacteria (Equation 1 and Equation 2) (Schink, 1997). Since H_2 and formate are scavenged mainly by the CO_2 reduction of hydrogenotrophic methanogens, an efficient interspecies transfer of electron equivalents (as H_2 and formate) has been achieved by close physical contact between syntrophs and methanogens (de Bok et al., 2004; Ishii et al., 2005, 2006).

In addition to hydrogen transfer, the possibility of a syntrophic coupling through direct electron transfer (DIET) has recently reported between methanogenic/methanotrophic archaea and bacteria as well as between bacteria (Lovley, 2017; McGlynn, 2017). DIET and the associated microbial extracellular electron transfer (EET) are both known to be accelerated by metal-oxide nano-particles such as magnetite and ferrihydrite (Kato et al., 2012, 2013), suggesting that the DIET and EET could be particularly important processes in subsurface environments where metal-oxide minerals are often abundant.

In order to identify and accelerate the DIET process, a bioelectrochemical system (BES) could also be applicable by using electrodes to add voltage between electrodes (**Figure 1A**). Within the bioreactor, the electron-capturing anode enhances the EET process from electrogenic microbes to the electrode (Equation 4), while the electron-releasing cathode facilitates the EET process from the electrode to electrotrophic methanogenic microbes (Equation 5) (Logan, 2009; Rabaey and Rozendal, 2010).

$$CH_3COO^- + 4H_2O \rightarrow 2HCO_3^- + 9H^+ + 8e^- \ldots \text{(Anode)} \quad (4)$$

$$8H^+ + 8e^- + CO_2 \rightarrow CH_4 + 2H_2O \ldots \text{(Cathode)} \quad (5)$$

The biocathodic reaction to produce methane from CO_2 and electrons is called as "electromethanogenesis" (Cheng et al., 2009; Blasco-Gómez et al., 2017). In fact, electromethanogenic microbes were stimulated by electric power input to increase methane production in the anaerobic digesters (Yu et al., 2018), as well as a subsurface methanogenic microbiome from oilfield formation water (Sato et al., 2013; Kobayashi et al., 2017). Blasco-Gomez et al. reviewed the studies of electromethanogenic microbes within complex biocathodic communities and their possible methanogenic routes (Blasco-Gómez et al., 2017), concluding that further research is needed to identify the electromethanogenic processes, especially in mineral-packed subsurface methanogenic microbiomes.

In this study, in order to stimulate the subsurface DIET-associated electromethanogenic process and identify the EET-active members (**Figure 1A**), we inoculated the gas-rich

formation water samples in Minami-Kanto gas field to duplicate BES bioreactors that supplied a voltage (600 mV) continuously between an electron-accepting anode and an electron-donating cathode (**Figure 1B**). Throughout the 2 years of BES operation, we periodically analyzed both bioelectrochemical characteristics and microbial community dynamics of the anode biofilm, cathode biofilm, and planktonic cells based on 16S rRNA gene phylogeny, which were systematically integrated. The results offer new insights about how subsurface DIET-associated microbes were stimulated by the voltage input and competed against typical methanogenesis in the electromethanogenic BES bioreactor (**Figure 1A**).

MATERIALS AND METHODS

BES Bioreactor Configuration and Operation

Two single-chamber, double-electrode bioelectrochemical system (BES) bioreactors (reactors A or B) were used for enrichment of anodic electrogenic and cathodic electromethanogenic communities with voltage input between electrodes. The BES bioreactor was a bottle-type reactor (375-mL in capacity) equipped with two electrodes made of carbon cloth (3 cm × 7 cm, 42 cm^2 projected surface area; TMIL, Japan). The top of the bottle was sealed using a tight butyl-rubber stopper pierced with two Ti wires (ϕ1 mm), and the electrodes were connected by the wires (**Figure 1B**). After sterilization of the BES reactor, 190 mL of gas-associated formation water KTG1 (30.5°C, pH 7.5, conductivity 74 mS/cm, Cl^- 18.95 g/L), sampled from a production well KTG1 at the Minami-Kanto Gas field (Chiba, Japan), was anaerobically added to the duplicate BES reactors without any pretreatment in an anaerobic glove box (COY Laboratory Products, USA) equipped with Table KOACH open cleaning system (KOACH T500-F, Koken Ltd., Japan), and two electrodes were immersed in the formation water. The formation water was anaerobically sampled at the production well and stored at 4°C before use. After adding 2 mmol of sodium acetate as a carbon substrate, a multi-channel potentiostat (PS-08; Toho technical research, Japan) was used to supply a voltage of 600 mV across the electrodes, and the generated current was monitored and recorded every 5 min. The BES reactors were gently agitated with a magnetic stirrer and incubated at 30°C.

When depletion of the substrates caused the electric current to decrease, 2 mmol or 2.5 mmol of sodium acetate was re-injected. When the current-consuming performance decreased because of the accumulation of secondary metabolites and/or sodium ion, the formation water was fully discarded in the anaerobic glove box and refilled with the stored formation waters, KTG1, KTG2 (28.3°C, pH 7.5, conductivity 75 mS/cm, Cl^- 19.13 g/L) or KTG3 (19.2°C, pH 8.2, conductivity 47 mS/cm, Cl^- 11.83 g/L), which were all anaerobically sampled from different production wells in the Minami-Kanto gas field and stored at 4°C before use.

Polarization Analysis

Potential step voltammetry analyses were conducted using a potentiostat (PS-08; Toho technical research, Japan) to obtain polarization curves. The applied voltage between electrodes was changed from 0 mV to +600 mV in stepwise increments of 50 mV for 15 min or 5 min, and the corresponding current was recorded after stabilization (<1 min). An Ag/AgCl reference electrode (+200 mV vs. standard hydrogen electrode [SHE], RE-5B; BASi, USA) was placed at the side port of the BES reactors (**Figure 1B**), and the anode and cathode potentials were also recorded with a voltage logger (VR-71; T&D, Tokyo) during the step voltammetry analyses. The total time of the voltammetry analyses was 150 min for 15 min interval and 50 min for 5 min interval, respectively.

Chemical Analyses

Acetate concentrations were measured with a high-pressure liquid chromatography (HPLC) instrument equipped with a multiple wavelength detector (Class VP; Shimadzu, Japan) and a reverse-phase C18 column (TSKgel ODS-100V; Tosoh Bioscience, Japan). The eluent was 0.1% phosphoric acid at a flow rate of 1.0 mL/min. Gas production was quantified by capturing the produced gas in a 1-L aluminum gas bag (AAK-1; Asone, Japan) connected to the bioreactor with FDA viton tubing (Masterflex L/S25, Cole-Palmer, Japan) (**Figure 1B**). The methane concentration in the gas phase was monitored with a methane sensor (BCP-CH4; BlueSens, Germany) that was frequently inserted into the gas line.

Coulombic efficiency, CE (%), was calculated as $CE = C_p/C_{th} \times 100$, where C_p (C) is the total charge consumed during a single batch, and C_{th} (C) is the theoretical amount of charge allowable from either complete acetate oxidation on the anode or methane production on the cathode. The CE_{anode} (%) was calculated from the C_{th} from complete acetate oxidization (8 mmol of e^- per 1 mmol of acetate, Equation 4). The $CE_{cathode}$ (%) was calculated from the C_{th} theoretically required to produce methane from CO_2 (8 mmol of e^- per 1 mmol of CH_4, Equation 5).

Microbial Composition Analysis

Small portions of anodic and cathodic carbon cloth (6 mm × 6 mm) were collected by using ethanol-sterilized scissors in an anaerobic glove box. Planktonic cells suspended in the electrolyte solution were also collected and centrifuged to make cell pellets. Total DNA was extracted from the electrode biofilms or suspended cells by using the PowerBiofilm™ DNA Isolation Kit (MO BIO, USA) with physical disruption by bead beating for 2.5 min. PCR amplification of the small subunit (SSU) rRNA gene (V4–V5 regions) was performed using the LA Taq (TaKaRa Bio, Japan) with universal primer pair 530F/907R (Nunoura et al., 2012), which contains overhang adapters at the 5′ ends. The PCR amplification conditions have been described elsewhere (Hirai et al., 2017). After PCR amplification, PCR products were purified enzymatically (ExoSAP-IT PCR Product Cleanup Reagent; Thermo Fisher, USA). To add multiplexing indices and Illumina sequencing adapters, a second PCR amplification was performed with Ex Taq polymerase (TaKaRa Bio, Japan). The amplified products were purified with the Agencourt AMPure XP (Beckman Coulter, USA), and quantified using the Quant-iT dsDNA High-Sensitivity Assay Kit (Thermo Fisher, USA). The PCR products were subjected to DNA denaturing and sample

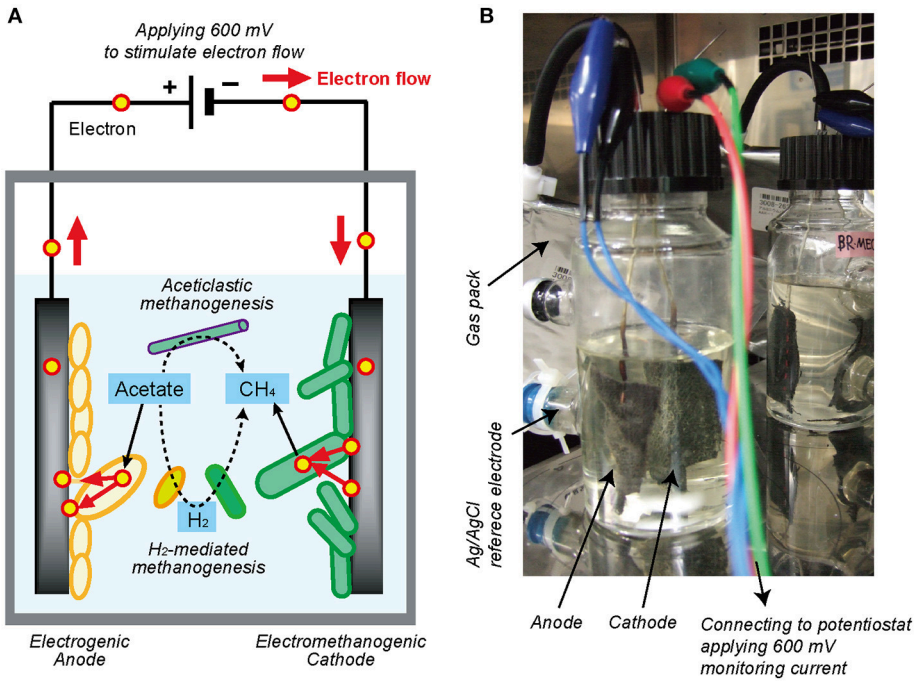

FIGURE 1 | Single-chambered bioelectrochemical system (BES) reactor used in this study. **(A)** Schematic diagram of electromethanogenesis that is stimulated by accelerating external electron flow with voltage input in a BES reactor. The EET flow for the electromethanogenesis is shown by solid arrow, while competitive methanogenic reactions are shown by dashed lines. **(B)** The single-chambered BES reactors filled with formation water at natural gas field. Anode and cathode were connected to potentiostat and apply 600 mV between them. An Ag/AgCl reference electrode was used for monitoring electrode potentials.

loading on a sequencer using MiSeq v3 reagent (Illumina, USA), and sequenced using the MiSeq platform (Illumina, USA) as the 300 bp paired end according to Illumina's standard protocol. The DNA nucleotide sequences have been deposited in the NCBI Short Read Archive under accession number SRR7990743-SRR7990766.

Analysis of SSU rRNA Gene Tag Sequencing Data

After merging paired-end reads with PEAR (Zhang et al., 2014), the regions of PCR primers were removed using Cutadapt v1.10 (Martin, 2011). Low-quality (Q score <30 in more than 3% of sequences) and short (<150 bp) reads were filtered out using a custom perl script. The SSU rRNA gene amplicon analysis was performed using the QIIME software package v1.9.1 (Caporaso et al., 2010). After the removal of chimeric sequences using USEARCH (Edgar, 2010) in QIIME, operational taxonomic units (OTUs) were selected at the 97% similarity level using UCLUST (Edgar, 2010) and were subsequently assigned to a taxon (at phylum, class, order, family, and genus levels) by comparison with the non-redundant 16S rRNA small subunit SILVA 128 database (Quast et al., 2013). Database searches for related SSU rRNA gene sequences were further conducted using the BLAST program to refer non-redundant nucleotide (nr/nt) database excluding uncultured/environmental sample sequences. Canonical correspondence analysis was performed using XLSTAT (Addinsoft, USA) to evaluate the correlations between community composition and environmental factors (Terbraak, 1986). The phylogenetic position of the OTUs was analyzed using a maximum likelihood-based phylogenetic tree created after alignment by MUSCLE in CLC Genomics Workbench version 8.5 (CLC bio, USA). Bootstrap resampling analysis for 100 replicates was performed to estimate the confidence of tree topologies. The nucleotide sequences of dominant OTUs have been deposited in the GSDB/DDBJ/EMBL/NCBI nucleotide sequence databases under accession numbers MK035761-MK035843.

Focused Ion Beam Scanning Electron Microscopy (FIB/SEM)

A small portion of carbon cloth was collected from the anodes, fixed for 2 h with 2.5% glutaraldehyde in filtered formation water, and preserved in the same fixative till post-fixation at 4°C. Samples were then washed in filtered artificial seawater and post-fixed with 2% osmium tetroxide in filtered artificial seawater for 2 h at 4°C. After the specimens were rinsed with distilled water, conductive staining was performed by incubating the specimens in 0.2% aqueous tannic acid (pH 6.8) for 30 min. After another wash with distilled water, the specimens were further stained with 1% aqueous osmium tetroxide for 1 h. Finally, the specimens were dehydrated in a graded series of ethanol, gently dried with a critical point dryer (JCPD5; JEOL, Japan), and coated with osmium using an osmium plasma coater (POC-3; Meiwafosis, Japan). SEM observations were carried out on a Helios G4 UX

(Thermo Fisher, USA), an extreme high resolution (XHR) field-emission scanning electron microscope (FE-SEM) equipped with Focused Ion Beam (FIB), at an acceleration voltage of 3 kV. The cross sectioning of the anodic and cathodic biofilms on the carbon fibers were obtained by using the FIB milling at acceleration voltage of 30 kV without deposition, and the FE-SEM observations were carried out at an acceleration voltage of 1 kV after the FIB milling.

RESULTS

Long-Term BES Enrichment and Current Generation

The gas-rich formation water sample (KTG1) was placed into two BES bioreactors where it served as a microbial inoculum as well as an electrolyte for the electromethanogenic operations. Enrichment of both electromethanogenic and electrogenic microbes was accomplished by establishing a voltage (600 mV) that was continuously applied between the cathode and the anode in each of two single-chamber BES reactors (A and B) (**Figure 1**). Current production was observed 7 days after acetate addition and stabilized at ∼1.3 mA for both reactors (**Figure 2**). During initial four months, the current production was notably unstable as the communities adapted to the electrode environment, with operational currents that fluctuated between 0.5 mA and 2.0 mA (**Table 1**). After step voltammetry analysis of reactor B at day 149, the reactor B was accidentally held at open-circuit conditions (no voltage input) for 3 days, and subsequently returned to the applied voltage operation (**Figure 2**). This EET-limited stimulus had a significant impact on the electromethanogenic production for reactor B, with a drop of current output from 1.36 mA (phase B-I) to 0.76 mA (phase B-II), indicating a lowered level of electromethanogenesis after the disconnection. However, the treatment time at phase B-II was significantly shorter than that of phase B-I (10.3 day to 3 day) (**Table 1**). These changes suggest that the different types of acetate-oxidizing methanogenesis such as hydrogen-mediated syntrophic methanogenesis (Equations 1, 2) or aceticlastic methanogenesis (Equation 3) outcompeted the EET-mediated electromethanogenesis (Equation 4, 5) in reactor B after the disconnection stimulus.

When the current output decreased during the long-term operation, the electrolyte was replaced with stored formation water in order to remove excess suspended cells and accumulated secondary metabolites. Such electrolyte replacement occurred three times for reactor A (initial replacement was to KTG1, and the other two were to KTG2), and five times for reactor B (all replacements were to KTG3), and all the treatments were carried out after the 270-day operational period. After the electrolyte replacement, current output was restored to the previously observed current output, thereafter enhanced current outputs were routinely observed (**Figure 2**).

During each batch cycle of the reactors, acetate decreased concomitantly with current output, and the current production was falling to near zero when acetate was fully consumed (**Supplementary Figure S1**). Methane concentration in the gas phase also showed consistent increase with current consumption, stopping the increase when the current output fell to near zero (**Supplementary Figure S2**). Thus, methane production was directly correlated with the current output and/or acetate degradation. The treatment time of one batch cycle was significantly correlated with the current output throughout the long-term operation for reactor A, but only phase B-I for reactor B (**Supplementary Figure S3**), which is also consistent with the notion that that current-independent acetate-consuming methanogenesis became the dominant process in reactor B after the disconnection event.

After the long-term BES operation, dense biofilms were visibly apparent at both anode and cathode surfaces (**Supplementary Figure S4**), which might lead to a reduction of current output due to an overall increase in an internal resistance by electron, proton, and substrate transport limitation (**Figure 2**). Denser biofilms were observed in less-electromethanogenic reactor B, suggesting that non-electromethanogenic cells were growing at a distance from the electrode surfaces. Red-colored biofilms were observed at only anodes in both reactors (**Supplementary Figure S4**), suggesting that the red molecules such as *c*-type cytochromes were accumulated within the electrogenic anode biofilms.

Bioelectrochemical Performance

The anodic electron-releasing and cathodic electron-capturing yields were calculated as coulombic efficiency (CE) based on the estimated half reactions of DIET (Equation 4 and Equation 5), which was found to be stable at 80–100% for both half reactions in reactor A throughout the operation (**Table 1**). These high CEs clearly indicate that almost all of electron flows were associated with the acetate oxidation by electrogenic microbes on the anode (Equation 4) and with the methane production by electromethanogenic microbes on the cathode (Equation 5). This result also suggests that other competing reactions such as typical acetate-oxidizing methanogenesis (Equations 1–3, **Figure 1A**), oxygen respiration, anaerobic respiration with soluble electron acceptors such as sulfate and nitrate, and/or anabolic biosynthesis rarely occurred in reactor A.

On the other hand, reactor B showed different trend of CEs for both half reactions after the 3-day disconnection event (**Table 1**). Before the disconnection, the CE_{anode} of reactor B was 73%; however, the CE_{anode} dropped to 15% at phase B-II and subsequent decrease to ∼10% after the 350-day BES operation. The cathodic CE showed over the 850% after phase B-IV, while another way of $CE_{cathode}$ calculation (consumed electron per methane production) showed that only 11–12% of the methane was generated via current consumption with electromethanogenic reaction in reactor B (**Table 1**). These poor CEs indicate that current-independent methanogenesis mainly carried out during the operational periods from phase B-II to phase B-V.

During the long-term operations, anodic, cathodic, and whole electrochemical cell polarization curves were determined three times via step-wise increase by 50 mV of applied voltages (**Figure 3**). The current generation trends were notably different

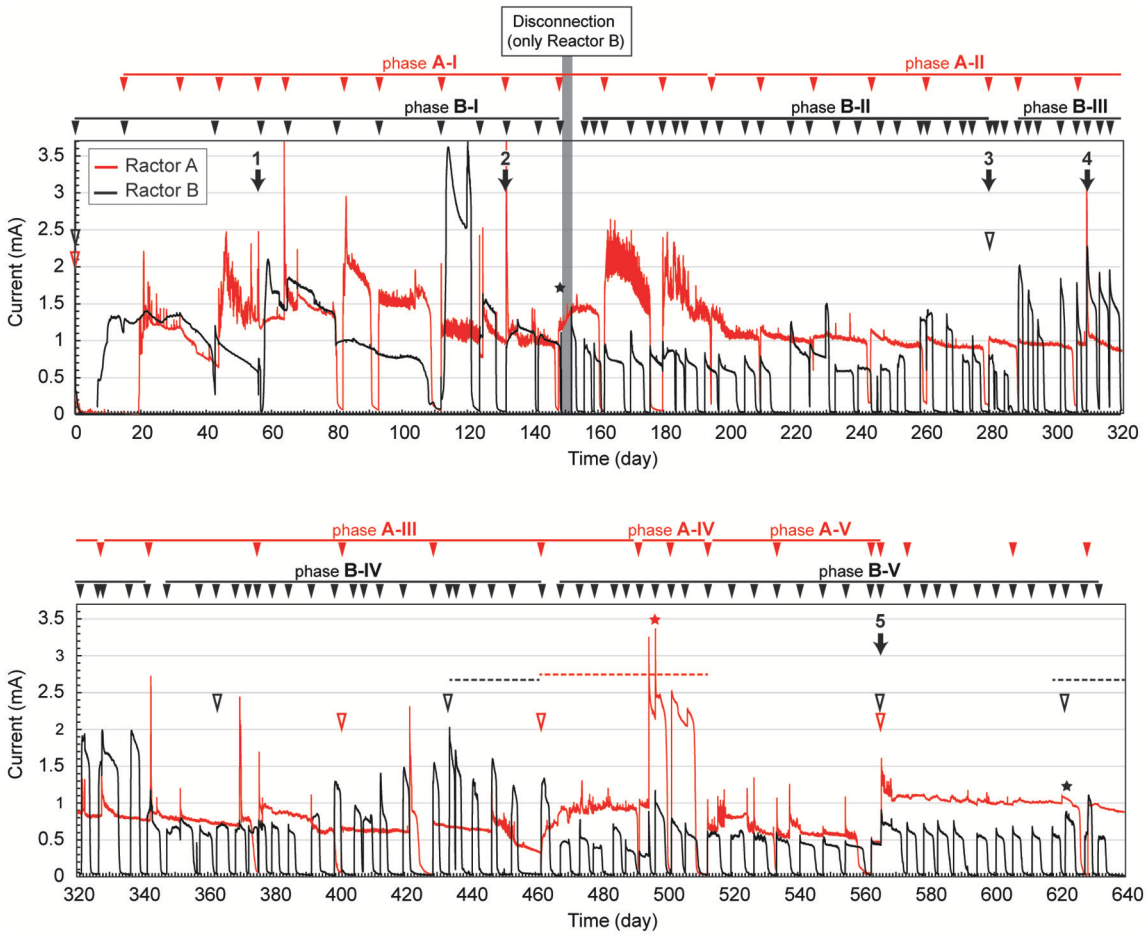

FIGURE 2 | Long-term electrical current output in duplicate BES reactors fed with acetate. Current generation with 600 mV of voltage application in duplicate single-chambered BESs is shown as red (reactor A) and black (reactor B) lines. Filled arrowheads above charts indicate feeding of acetate to the BES. Filled arrows indicate biofilm and suspension sampling for DNA extraction, and the numbers above the arrow indicate IDs for the microbial community composition analysis. Open arrowheads indicate exchange of formation water in the BESs. Stars indicate step voltammetry. Dashed lines indicate methane concentration logging. The marks with red color indicate reactor A, while marks with black color indicate reactor B.

over 300 mV of applied voltage among the three operational phases (**Figure 3A**), implying that different internal resistances were yielded by the biocatalytic features on both electrodes. Current generation was first observed at 120 mV of applied voltage, −320 mV vs. SHE of anode potential, and −440 mV vs. SHE of cathode potential, respectively (**Figure 3B**). The anode potential was stable by the −320 mV vs. SHE between 100 mV and 350 mV of applied voltage, suggesting that the anode potential was controlled by the anodic biocatalytic reaction of acetate-oxidizing electrode reduction. In fact, the operational anode potential during the batch cycle with 600 mV of applied voltage suddenly changed from −250 mV to 0 mV vs. SHE when acetate was totally consumed (**Supplementary Figure S1B**). In contrast, the cathode polarization curve showed consistent decrease with more voltage input to reach −800 mV vs. SHE, which allowed hydrogen production on the cathode. These results imply that anodic biocatalytic reaction with acetate oxidation was a key for producing hydrogen on the cathode and achieving the electromethanogenic reaction in the BES reactors.

Microbial Community Dynamics

To compare microbial community composition dynamics of the anode biofilm, cathode biofilm and planktonic cells, we conducted SSU rRNA gene-based tag-sequencing (iTAG) analysis for the samples collected at day 56 (time 1), day 132 (time 2), day 280 (time 3, only for reactor B), day 307 (time 4), and day 561 (time 5) (**Figure 2**). The iTAG analysis was also performed from the stored formation water samples KTG1, KTG2, and KTG3, which functioned as inoculum sources for the enrichments. The phylum- or class-level community compositions clearly revealed that only three taxonomic groups, *Gammaproteobacteria* (25%), *Deltaproteobacteria* (19%), and *Euryarchaeota* (19%), were highly abundant within the BES reactors (**Figure 4**). As minor members in the BES communities, *Synergistetes* (9%), *Alphaproteobacteria* (4%), and *Bacteroidetes* (4%) were also frequently seen. In total, these six taxa accounted for about 80% of the BES communities established from subsurface natural gas-associated microbiome throughout the long-term operation.

TABLE 1 | Summary of electromethanogenic profiles of BESs with 600 mV voltage input.

	REACTOR A				
Phase	**A-I**	**A-II**	**A-III**	**A-IV**	**A-V**
Periods	**day 15-195**	**day 195-376**	**day 376-492**	**day 492-513**	**day 513-561**
Cycles	**10**	**8**	**4**	**2**[a]	**2**[a]
Current (mA) ± SD	1.49 ± 0.53	0.97 ± 0.06	0.76 ± 0.14	2.17 ± 0.07	0.67 ± 0.12
Current density (mA/m^2)[b] ± SD	354 ± 126	243 ± 15	200 ± 37	571 ± 18	176 ± 32
Treatment time (Day)[c] ± SD	12.3 ± 2.9	16.3 ± 1.0	25.9 ± 2.9	7.5 ± 0.5	22.0 ± 2.0
Power input (Wh) ± SD	0.29 ± 0.05	0.24 ± 0.01	0.29 ± 0.05	0.23 ± 0.00	0.21 ± 0.00
CH_4 producing rate (ml/d)[d]	3.40[d]	2.21[d]	2.10	4.76	1.53[d]
Coulombic efficiency (%) ± SD					
Anode (e^-/acetate)	108 ± 17	93 ± 3	108 ± 24	90 ± 1	83 ± 1
Cathode (CH_4/e^-)[e]	nd	nd	85	79 ± 3	nd
	REACTOR B				
Phase	**B-I**	**B-II**	**B-III**	**B-IV**	**B-V**
Periods	**day 0-149**	**day 156-280**	**day 289-342**	**day 347-462**	**day 468-638**
Cycles	**8**	**23**	**11**	**21**	**30**
Current (mA) ± SD	1.36 ± 0.60	0.76 ± 0.20	1.54 ± 0.23	0.94 ± 0.33	0.54 ± 0.14
Current density (mA/cm^2)[b] ± SD	324 ± 143	190 ± 50	395 ± 59	247 ± 87	142 ± 37
Treatment time (Day)[c] ± SD	10.3 ± 3.6	3.3 ± 1.3	2.2 ± 0.9	2.0 ± 0.6	2.8 ± 0.7
Power input (Wh) ± SD	0.17 ± 0.09	0.04 ± 0.02	0.05 ± 0.02	0.03 ± 0.00	0.03 ± 0.00
CH_4 producing rate (ml/d)[d]	3.64[d]	1.80[d]	3.22[d]	3.69	1.67
Coulombic efficiency (%) ± SD					
Anode (e^-/acetate)	73 ± 31	15 ± 6	21 ± 7	10 ± 2	9 ± 2
Cathode (CH_4/e^-)[e]	nd	nd	nd	894 ± 93	871 ± 93
Cathode (e^-/CH_4)[e,f]	nd	nd	nd	11 ± 1	12 ± 3

[a] *Since only two cycles per the phase, median ± difference is shown.*
[b] *Current density is calculated by using projected surface area of one side of the electrodes.*
[c] *Treatment times are normalized for 2 mmol of acetate consumption per cycle.*
[d] *Estimated methane producing rate based on current and cathodic coulombic efficiency of 85%.*
[e] *nd, not determined.*
[f] *Since aceticlastic methanogenesis was occurred for reactor B, ratio of electrotrophy in methanogenesis was also shown.*

With regard to the class *Deltaproteobacteria*, only two families, *Desulfuromonadaceae* and *Geobacteraceae,* were abundant in the BES reactors, with the former dominating in the early stages of enrichment, and the *Geobacteraceae* increasing to nearly 50% at later stage of the enrichments (**Figure 4**). In phylum *Euryarchaeota*, three families, *Methanobacteriaceae*, *Methanocalculaceae,* and *Methanosaetaceae*, occupied 40–70% of the cathode biofilms after 250-day operation (**Figure 4**). Interestingly, the family *Methanosaetaceae* was only seen after the 3-day disconnection event that occurred between B2 and B3 in reactor B, and these cells were also seen in the anode biofilm and as planktonic cells. In class *Gammaproteobacteria*, ten different families were frequently shown in the BES reactors. Within them, the families *Solimonadaceae* and *Ectothiorhodospiraceae* were initially abundant in the planktonic cells to occupy over 40%. Although the families *Alteromonadaceae* and *Oceanospirillaceae* were highly dominant in the source formation waters (**Figure 4**), they were never seen as dominant forms in any of the enrichments. The portion of the two *Gammaproteobacteria* families decreased to only ∼10% after the long-term enrichment.

Correlation Between Microbial Families and Locations

Weighted canonical correspondence analysis (wCCA) is a comparative evaluation tool that can be used to represent correlations between key environmental variables, such as locations (anode, cathode or planktonic), inocula, operation time, and associated microbial taxa compositions (Ishii et al., 2013b, 2014, 2017; Suzuki et al., 2013). **Figure 5A** shows associations between the variables as five vectors and highly abundant families in reactor A with weighting by sum of relative frequencies, while **Figure 5B** shows associations between the valuables and abundant microbial families in reactor B. As expected, the relatively abundant families in the inoculated formation water (*Alteromonadaceae*, *Flavobacteriaceae, Oceanospirillaceae,* and *Rhodobacteraceae*) were not associated with neither the operational time nor any of the locations in both BES enrichments.

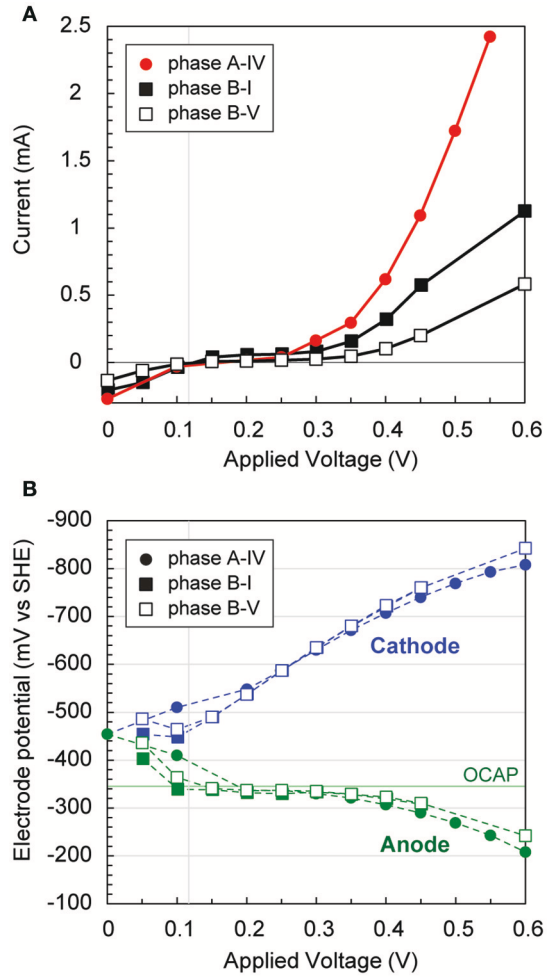

FIGURE 3 | Polarization curves via potential step voltammetry in the electromethanogenic BESs. **(A)** During potential step voltammetry, current generation after 5 min (for reactor a) or 15 min (for reactor b) with applying different voltages is plotted for different phases of the BESs (box for labels). **(B)** Anodic (blue dashed lines and blue labels) and cathodic (green dashed lines and green labels) potentials are plotted during the potential step voltammetry. OCAP indicates open circuit anode potentials.

Among the three locations, two *Deltaproteobacteria* families (*Geobacteraceae* and *Desulfuromonadaceae*) were clearly correlated with anode biofilms in both BES reactors, while family *Geobacteraceae* became more abundant with time (**Figure 5**). This trend indicates that family *Geobacteraceae* was more functional within the electrogenic anode biofilms. Two *Gammaproteobacteria* families were associated with the planktonic niche, while family *Solimonadaceae* was more frequent in reactor A and *Ectothiorhodospiraceae* was abundantly observed in reactor B. Two *Euryarchaeota* families (*Methanobacteriaceae* and *Methanocalculaceae*) were tightly associated with cathode biofilm, suggesting that these two families were both important groups for the electromethanogenic reactions on the cathode. Strikingly, we found that another *Euryarchaeota* family, *Methanosaetaceae*, which was only shown in the poorly electromethanogenic reactor B and tightly correlated with the time valuable (**Figure 5B**). This trend is consistent with what *Methanosaetaceae* microbe was only presented after the 3-day disconnection event in reactor B.

OTUs in the Electromethanogenic and Electrogenic Communities

Figure 6 shows the OTUs (>97% cut-off value) that were abundant in the three different niches in the BES reactors. The minor OTUs (i.e., lower relative abundance) are summarized in **Supplementary Table S1**. The preferable location (anode, cathode, biofilm, suspension, or source) was estimated from the wCCA diagram (**Supplementary Figure S6**) by using all 84 OTUs. These abundant OTUs occupied 84–98% of the community compositions for all thirty communities (**Supplementary Table S1**).

In class *Deltaproteobacteria, eleven* different OTUs were enriched in anode biofilms of both BES reactors, and five were relatively abundant (**Figure 6**). The dominance of these OTUs changed over time from two *Desulfuromonadaceae* OTUs (BRdel2 and BRdel3) to two *Geobacteraceae* OTUs (BRdel10 and BRdel11). From their phylogenetic positions, highly abundant *Geobacteraceae* OTUs are both affiliated to genus *Geoalkalibacter*, while the *Desulfuromonadaceae* OTUs BRdel2 and BRdel3 were not affiliated with any known genus (**Figure 7**).

In the phylum *Euryarchaeota, six* different OTUs were observed mainly in the cathodic biofilm (**Figure 6**); three of these OTUs were placed in the genus *Methanobacterium*, and one each to the genera *Methanobrevibacter*, *Methanocalculus,* and *Methanosaeta* (**Figure 8**). From them, the *Methanosaeta* OTU BReur6 was comprised over 10% at all three locations only in the reactor B after the disconnection event, which trends are likely correlated with the lower coulombic efficiency of reactor B.

In the class *Gammaproteobacteria, eighteen* different OTUs were found to be community members at source formation water and/or suspended cells in the BES reactors (**Supplementary Table S1**), while six OTUs were relatively abundant among them (**Figure 6**). Two OTUs, *Marinobacter* KTGgam8 and *Marinobacterium* KTGgam14, comprised over 40% of the inoculum community, but these OTUs decreased the frequencies in all locations of both BES reactors. Two different OTUs, *Solimonas* BRgam1 and *Thioalbus* BRgam4, were highly abundant in the planktonic niches of both BES reactors; however, both OTUs decreased their relative frequencies in later stages of the enrichment process (**Figure 6**). Thus, while diverse *Gammaproteobacteria* OTUs were introduced from the formation water, they were not seen at later stages, and it is unlikely that these taxa play an important role in electrogenic or electromethanogenic biofilms.

SEM Observation of Anodic and Cathodic Biofilms

In order to examine the morphology of EET-active anode and cathode biofilms in both BES reactors, biofilm samples were taken on day 516 (phase A-V or B-V, time 5 for the

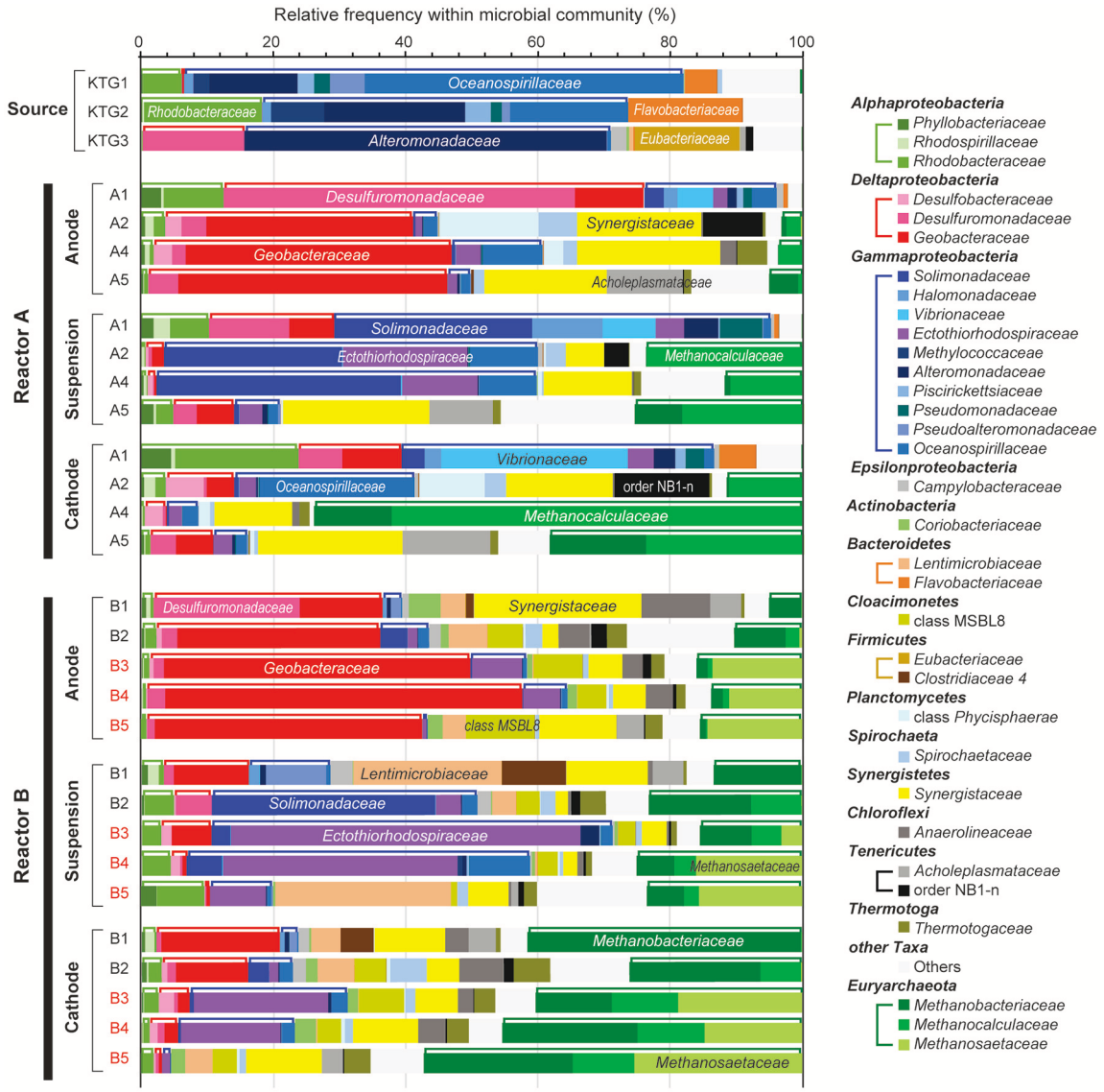

FIGURE 4 | Taxonomic distributions of 16S rRNA community profile within anode biofilm, suspension, and cathode biofilm of electromethanogenic BESs. The family-level taxonomic profiles (three unclassified families are shown by using upper level taxonomy) for anode biofilms (Anode), planktonic cell suspensions (suspension) and cathode biofilm (Cathode) within the duplicate BESs at day 56 (1), day 132 (2), day 280 (3), day 310 (4), and day 566 (5) of enrichment, and the original inoculum source of formation water at different natural gas production wells (Source). Several abundant families are also described in the bars. Class *Alphaproteobacteria*, *Deltaproteobacteria*, *Gammaproteobacteria,* and phylum *Euryarchaeota* are tied by brackets above the bars.

community analyses) and subjected to observe by using a FE-SEM. Focused ion beam (FIB) equipped with the FE-SEM was used for cutting the biofilms to observe the cross-sectional images (**Supplementary Figures S7, S8**). The electron micrographs of reactor A (**Figure 9**) and reactor B (**Figure 10**) revealed different biofilm morphologies, electrode surface structures, and cell shapes for the two reactors.

In reactor A, the anode biofilm was attached on graphite fibers in the form of big aggregates along with morphologically different microbes at the surface of the aggregates (**Figure 9A**), while the cross-sectional image showed the dense anode biofilm with thickness of 10 to 50 μm (**Supplementary Figure S7B**) and the unique rod-shaped microbe inside the biofilm (**Figure 9B**). On the other hand, the cathode biofilm was fully covered with single-layered microbes (**Figure 9D**), and three different morphologies (irregular coccoid, thin filament, and rod-shaped with a lot of membrane vesicles) were seen on the covered microbes in the vicinity of the carbon fibers (**Figure 9E**). The dense biofilms were also observed sparsely at the interspace of the graphite fiber (**Supplementary Figure S7C**). Magnified electron micrographs after FIB cutting revealed the presence of a filamentous mat structure of thin, thread-like appendages in the anode biofilms

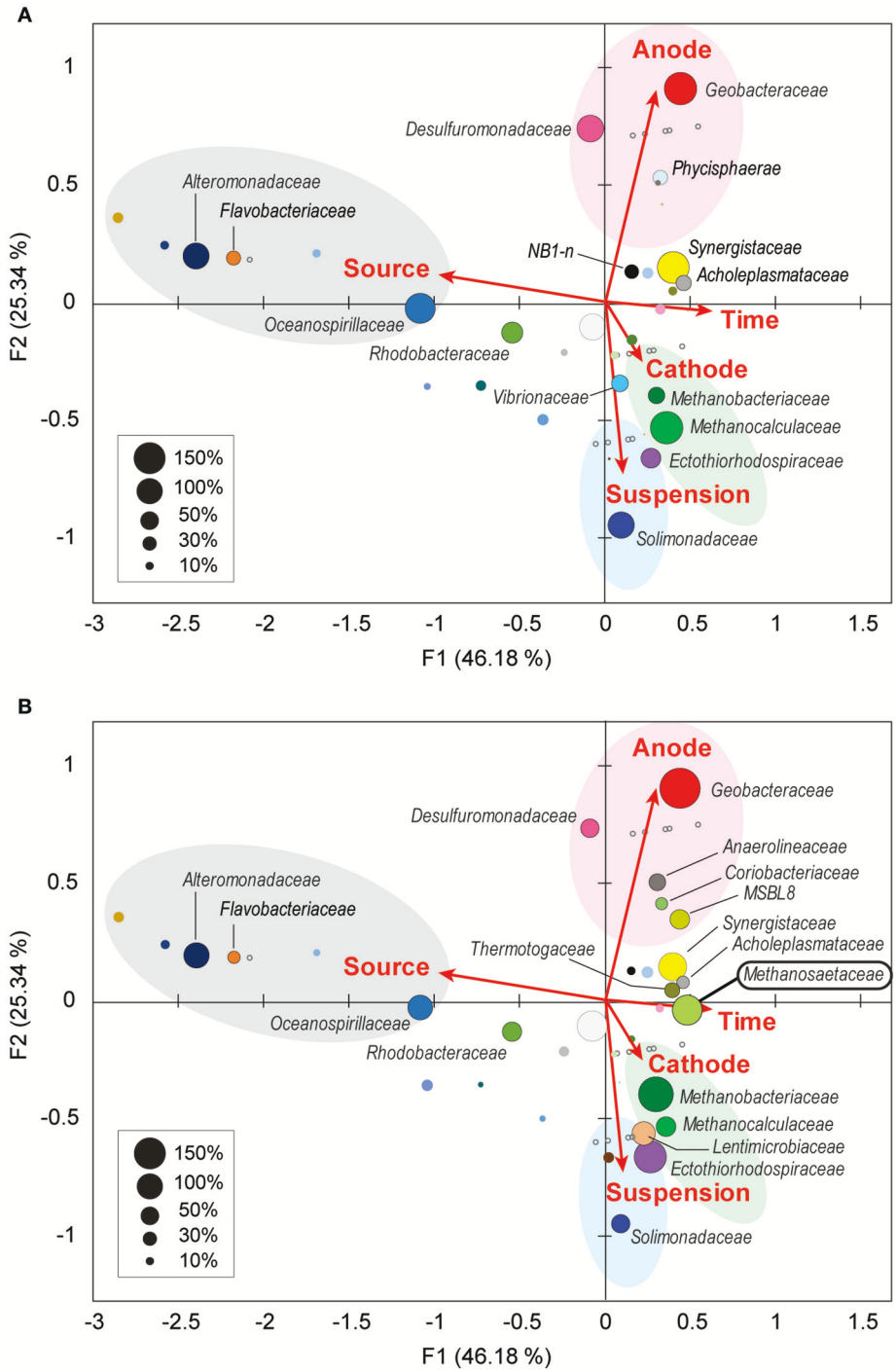

FIGURE 5 | Weighted canonical correspondence analysis (wCCA) diagram correlating microbial taxa and the environmental factors. wCCA diagrams show relationships between operational variables (red arrows) and dominant microbial taxa (filled bubbles) in BES reactor A **(A)** and reactor B **(B)**. The bubble colors indicate families that described in **Figure 4**. Bubble sizes indicate sum of relative frequencies (%) within the microbial community analyses for each reactor with the inoculated formation waters (maximum 1,500% for reactor A, and 1,800% for reactor B). Family names of the taxa of the abundant members (sum of relative frequencies over 20%) are depicted near bubbles, and the full list of the family names is shown in **Supplementary Figure S5**. Gray open circles indicate samples for microbial community analyses.

Phylum (Class) / Family	OTU ID	Source	A1			A2			A4			A5			B1			B2			B3			B4			B5			SUM (%)	Location	% match	Best matched sequence (Accesion No)
		KTG1	Anode			Anode			Anode			Anode			Anode			Anode			Anode			Anode			Anode						
		KTG2	Sus			Sus			Sus			Sus			Sus			Sus			Sus			Sus			Sus						
		KTG3	Cathode			Cathode			Cathode			Cathode			Cathode			Cathode			Cathode			Cathode			Cathode						
Alphaproteobacteria																																	
Rhodobacteraceae	BRalp7	- - -	6	5	13	1	-	1	0	-	0	-	-	-	0	1	0	2	4	2	1	2	2	0	4	1	1	6	1	53	Cathode	100	*Pseudoruegeria maritistellae* SF-16 (NR149190)
Deltaproteobacteria																																	
Desulfobacteraceae	BRdel1	- - -	-	-	-	2	0	6	3	1	3	0	-	-	15	1	1	-	0	1	1	2	2	0	1	1	0	0	0	24	Biofilm	100	*Desulfobiguntum toluenicum* 4S-CH-S3-s3 (MG264260)
	BRdel2	- - 0	40	9	5	3	-	0	-	-	-	-	-	-	2	-	1	2	-	1	0	-	0	1	-	0	-	-	-	79	Anode	98	*Desulfuromonas* sp. WB3 (KM452745)
Desulfuromonadaceae	BRdel3	- - -	13	3	2	1	-	-	-	-	-	-	-	-	7	0	0	-	0	-	-	-	-	0	-	0	-	-	-	26	Anode	93	*Desulfuromonas michiganensis* BRS1 (AF357914)
	BRdel10	- - -	-	-	-	-	-	-	-	-	-	-	-	-	12	11	18	31	5	11	46	6	2	54	1	2	40	1	0	293	Anode	100	*Geoalkalibacter subterraneus* Red1 (CP010311)
Geobacteraceae	BRdel11	- - -	10	7	9	30	2	4	40	-	-	-	-	-	0	-	-	-	-	-	-	-	-	-	-	-	-	-	-	102	Anode	98	*Geoalkalibacter subterraneus* Red1 (CP010311)
Gammaproteobacteria																																	
Solimonadaceae	BRgam1	- - -	3	30	3	0	27	1	1	37	0	-	1	0	-	-	-	4	34	3	0	3	1	0	5	0	-	-	-	154	Sus	97	*Solimonas terrae* KIS83-12 (NR125692)
Vibrionaceae	BRgam3	- - -	5	8	28	-	0	-	-	0	-	-	-	-	-	0	-	-	-	-	-	-	-	0	-	-	-	-	-	42	Cathode	100	*Vibrio alginolyticus* SNSAB08 (MH123144)
Ectothiorhodospiraceae	BRgam4	- - -	2	4	4	1	19	3	-	0	-	-	-	-	1	4	1	8	53	20	6	36	15	1	8	1	-	-	-	212	Sus	100	*Thioalbus denitrificans* Su4 (NR122087)
Alteromonadaceae	KTGam8	13 20 55	0	-	0	-	-	-	-	-	-	-	-	-	-	-	-	-	-	-	-	-	-	-	-	-	-	-	-	89	Source	100	*Marinobacter antarcticus* HEX61 (KY508320)
Oceanospirillaceae	KTGam14	47 18 0	4	1	1	0	-	0	0	6	-	1	1	1	0	1	0	0	0	0	1	0	1	9	1	-	1	-	97	Source	100	*Marinobacterium georgiense* NBRC102196 (AB681723)
	BRgam15	0 - -	0	-	-	2	10	23	9	3	2	1	0	1	-	-	-	1	2	2	0	0	2	0	1	0	0	-	0	60	Cathode	99	*Nepturomonas japonica* DL5-2-2 (KF146511)
Actinobacteria																																	
Coriobacteriaceae	BRact1	- - 0	-	-	-	-	-	-	0	-	-	-	-	0	5	0	0	1	0	2	1	0	2	1	0	3	2	0	2	22	Anode	100	Uncultured bacterium clone OTU136 (KU998399)
Bacteroidetes																																	
Lentimicrobiaceae	BRbac1	0 - -	-	-	-	-	-	-	-	-	-	0	-	-	4	22	4	6	4	6	0	-	-	0	-	0	-	-	-	46	Cathode	100	*Lentimicrobium saccharophilum* 1S-PR-S3-s2 (MG264261)
	BRbac9	- - -	-	-	-	-	-	-	-	-	-	-	-	-	-	-	-	0	0	0	-	-	-	-	-	-	3	26	4	34	Sus	95	*Lentimicrobium saccharophilum* 1S-PR-S3-s2 (MG264261)
Porphyromonadaceae	BRbac8	- - -	-	-	-	0	0	0	9	14	6	-	-	-	-	-	-	0	0	0	-	-	-	0	-	-	-	-	-	29	Cathode	98	*Petrimonas mucosa* ING2-E5A (NR148808)
Cloacimonetes																																	
class MSBL8	BRclo1	- - -	-	-	-	-	-	-	-	-	-	-	-	-	5	4	5	7	3	7	4	3	4	10	1	3	55	Biofilm	96	Uncultured bacterium clone Nit5Au0613_740 (FJ628334)		
Planctomycetes																																	
Class Phycisphaerae	BRpla1	- - -	15	0	10	3	0	1	-	-	-	-	-	-	-	-	-	-	-	-	-	-	-	0	-	-	-	-	-	30	Anode	95	Uncultured planctomycete MERTZ_21CM_213 (AF424493)
Synergistetes																																	
Synergistaceae	BRsyn1	- - -	-	-	-	12	5	11	17	8	8	18	21	21	25	12	11	1	2	3	3	3	3	4	1	7	5	2	3	207	Biofilm	92	*Thermovirga lienii* DSM 17291 (NR043522)
	BRsyn2	- - -	-	-	-	-	-	-	-	-	-	-	-	-	-	-	-	0	-	0	2	1	3	1	1	3	4	3	5	24	Biofilm	91	*Thermovirga lienii* LABEM006 (KJ576629)
Chloroflexi																																	
Anaerolineaceae	BRchl2	- - -	-	-	-	0	-	-	-	-	-	-	-	-	4	1	2	3	0	5	2	0	1	3	0	2	2	0	0	24	Anode	88	Anaerobic bacterium MO-CFX2 (AB598278)
	BRchl3	- - -	-	-	-	-	-	-	0	-	-	9	9	12	1	-	0	0	-	-	0	-	0	1	0	-	1	0	-	36	Biofilm	97	*Breveflum fermentans* CAMB-1 (LT859958)
Tenericutes																																	
order NB1-n	BRten3	- - -	-	-	-	9	4	14	0	-	-	0	-	-	-	-	-	-	-	-	-	-	-	-	-	-	-	-	-	27	Biofilm	100	Bacterium 4S-PB-a (MG264277)		
Thermotogae																																	
Thermotogaceae	BRthr1	- - -	0	0	0	5	1	2	1	1	1	0	0	1	3	4	6	2	1	3	1	1	3	3	2	4	46	Biofilm	99	*Mesotoga prima* MesG1.Ag.4.2 (NR102952)		
Euryarchaeota																																	
Methanobacteriaceae	BReur1	- - 0	-	-	-	-	-	-	-	-	-	0	-	-	1	1	7	3	4	7	1	4	6	1	2	11	0	3	15	68	Cathode	100	*Methanobacterium sp.* Mba6 (LC183834)
	BReur2	0 - -	0	-	0	-	-	-	-	0	-	-	0	-	0	0	1	0	0	2	0	2	2	0	1	1	-	2	6	21	Cathode	100	*Methanobacterium formicicum* Mb8 (JN205059)
	BReur3	- - -	0	-	0	-	-	-	1	12	-	4	7	15	-	-	-	-	-	-	-	-	-	-	-	-	-	-	1	39	Cathode	100	*Methanobacterium aarhusense* H2-LR (NR042895)
	BReur4	- - -	0	-	-	-	-	-	-	-	-	-	-	-	4	12	33	5	11	10	1	2	3	1	2	8	-	-	1	94	Cathode	100	*Methanobrevibacter arboriphilus* (AB065294)
Methanocalculaceae	BReur5	- - -	2	24	11	-	-	-	-	-	-	-	-	-	4	12	0	2	8	6	1	4	10	1	3	10	-	2	9	214	Cathode	100	*Methanocalculus pumilus* MHT-1 (NR028148)
Methanosaetaceae	BReur6	- - -	0	-	-	-	-	-	-	-	-	-	-	-	0	0	0	14	3	19	11	16	15	14	16	25	133	Biofilm	99	*Methanosaeta harundinacea* 6Ac (CP003117)		

Frequency in the community (%): 0.5 1 3 5 10 20 30

FIGURE 6 | Heatmap table of major phylotypes in the microbial communities. The major phylotypes were selected as those with frequencies that summed to over 20% in all 30 clone libraries. The calculation of frequency (%) was conducted based on **Supplemental Table S1**. Best matched sequence was identified by BLAST to nr/nt excluding Uncultured/environmental sample sequences (black letters) or including them (blue letter).

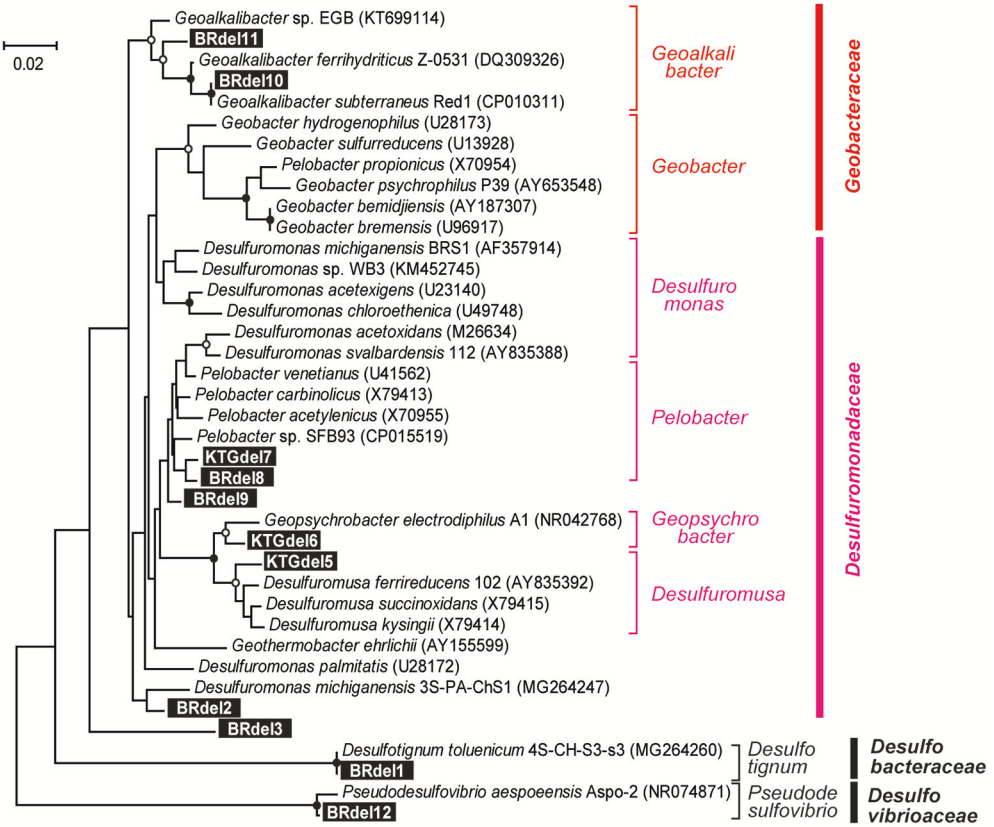

FIGURE 7 | Maximum likelihood based phylogenetic trees showing positions of major DIET-related *Deltaproteobacteria* OTUs representing anodic electrogenic microbial populations. Branch points supported with bootstrap values (100 trials) of >90% are indicated with closed circles, while those between 70 and 90% are indicated with open circles. Accession numbers of reference sequences are indicated in parentheses.

that connected microbial cells to one another, and to the anode electrode (**Figure 9C**), while the mesh-patterned structure was seen as a visible layer on the cathode surface (**Figure 9F**). These images indicate that different types of microbes performed EET process from/to the electrodes by using different ways in the BES reactor A.

In reactor B, different biofilm morphologies were observed on both anode and cathode electrodes, where the surfaces of bio-mats were fully covered by cylindrical microbes (**Supplementary Figure S8**). Below the cylindrical microbes, the egg-shaped microbes with thin filamentous appendages were abundantly observed inside the anode biofilm (**Figures 10A,B**), while the rod-shaped microbes formed an orderly single-layered biofilm onto the cathode (**Figures 10D,E**). The magnified cross-sectional image of the anode revealed the bridges between microbial cells and the electrodes by using the filamentous appendages (**Figure 10C**), while that of the cathode revealed the bridge between the rod-shaped microbe and the electrode by using polar filaments (**Figure 10F**).

The SEM observations revealed a variety of filamentous structure in the anode and cathode biofilms, and the filaments seem to be important for the EET processes between microbes and electrodes in the electromethanogenic BES reactors.

DISCUSSION

The Minami-Kanto gas field, where gases are dissolved in seawater-based formation water, is characterized by the accumulation of biogenic methane in subsurface marine turbidite sand layers interbedded with mud layers (Mochimaru et al., 2007; Katayama et al., 2015; Sano et al., 2017). Here, we report for the fist time, the long-term electromethanogenic processes at ambient temperature and associated EET-active community members enriched from subsurface microbiome in the seawater-based formation water (**Table 2**). Duplicate BES reactors were operated for 21 months, and we successfully stimulated and enriched DIET-associated members of the subsurface microbes where methane is naturally produced biologically (Mochimaru et al., 2007; Katayama et al., 2015; Sano et al., 2017). Even though three methanogenic pathways are possible when acetate was amended as a substrate to the BES operation (**Figure 1A**, Equations 1–5), EET-related electromethanogenesis was highly dominant (CE >80%) in reactor A (**Table 1**), which implies stimulation of DIET via voltage input outcompeted other two typical methanogenic pathways, hydrogenotrophic methanogenesis with syntroph and aceticlastic methanogenesis. However, in reactor B, the electromethanogenesis was remarkably limited (CE <15%) when

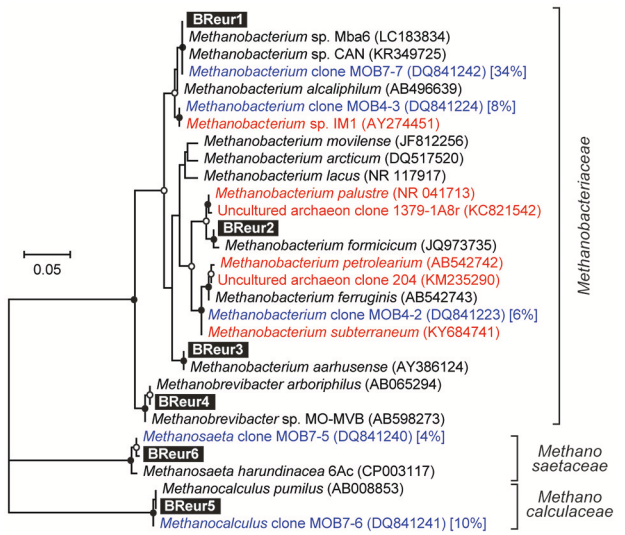

FIGURE 8 | Maximum likelihood based phylogenetic trees showing positions of major DIET-related *Euryarchaeota* OTUs representing cathodic electromethanogenic microbial populations. Branch points supported with bootstrap values (100 trials) of >90% are indicated with closed circles, while those between 70 and 90% are indicated with open circles. Accession numbers of reference sequences are indicated in parentheses. Euryarchaeal clones observed in different formation water from Minami-Kanto gas field (Mochimaru et al., 2007) were highlighted by blue letter, and the relative frequency within the formation water (%) was described after accession number. *Methanobacterium* clones observed in other electromethanogenic community or iron-oxidizing methanogenic community were highlighted by red letter.

electron flow was accidentally stopped for 3 days (**Table 1**). The electromethanogenic performance was not recovered even after re-establishment of the voltage to the electrodes, indicating that the activation of the other competitive reactions (Equations 3–5) was irreversible. The effect of no EET flow in the BES reactor and electromethanogenesis-related microbial community functions are separately discussed as below.

Effect of No Electron Flow to Electromethanogenic Community

For an electromethanogenic biocathode community, Bretschger et al reported similar trends to show 87% drop in volumetric methane production rates after 45-min open-circuit perturbation, and recovery of the electromethanogenic performance after four months under poised-potential operation (Bretschger et al., 2015). On the other hand, we have also studied the effects of open-circuit no-EET stimulus to the electrogenic communities by using state-of-the-art Meta-Omics approaches, demonstrating that EET-active microbes quickly sensed and responded to the stimulus (Ishii et al., 2013a, 2015, 2018). These previous observations suggest that EET-active microbes are quite sensitive to an open-circuit perturbation that halts EET between microbes and electrodes.

After the open-circuit event in reactor B, the abrupt increase at all locations of the relative abundances of the euryarchaeal OTU BReur6 (affiliated to the genus *Methanosaeta*) were seen (**Figure 6**). In addition, the associated abrupt drops of both anodic and cathodic CEs were only shown after the open-circuit perturbation (Table 1). The SEM images of both anodic and cathodic biofilms revealed cylindrical microbes, similar in morphology to the marine *Methanosaeta* strain (Kita et al., 2016), only in reactor B (**Supplementary Figure S8**), and the cylindrical microbes did not adhere to the electrode surface as well as EET-active biofilms (**Figure 10**). These results imply that OTU BReur6 was not involved with EET on the electrodes (**Figure 1A**). The genus *Methanosaeta* was originally reported to be a strict aceticlastic methanogen (Equation 3) (Smith and Ingram-Smith, 2007). Recently, co-cultures of *Methanosaeta harundinacea* and electrogenic *Geobacter metallireducens* were shown to convert ethanol to methane via interspecies electron and acetate transfers, suggesting that DIET is possible for at least one member of the genus *Methanosaeta* (Rotaru et al., 2014). Our results demonstrate that the enriched subsurface *Methanosaeta* OTU BReur6 did not carry out DIET or EET, leading to poor electromethanogenic performance on the cathode. The high abundance of *Methanosaeta* was only shown in reactor B, and the population did not decrease with time even after reconnection of the electric circuit (**Figures 4–6**). We suspect that the higher amounts of the aceticlastic *Methanosaeta* population will increase tolerance or accelerate their metabolic rates, and they are possible to overcome the electrode-assisted electromethanogenic metabolism in reactor B.

Electromethanogenic Microbes on Cathode Biofilm

Our community dynamics analyses and the associated wCCA diagrams clearly show that family *Methanobacteriaceae*, including genera *Methanobacterium* and *Methanobrevibacter*, were key methanogenic members responsible for the electromethanogenic reaction on the cathode (**Figures 4–6**, **Supplementary Figure S5**). Although the genus *Methanobacterium* is known as a hydrogenotrophic methanogen (Thauer et al., 2008), the genus has been frequently observed within electromethanogenic cathode biofilms that carry out methanogenesis from $e^-/H^+/CO_2$ (Siegert et al., 2015; Blasco-Gómez et al., 2017) (**Table 2**). The phylogenetic positions of the dominant *Methanobacterium* OTUs in our BES reactors revealed that the most frequently observed OTUs (BReur1 and BReur3) were different from reported electromethanogenic *Methanobacterium* microbes but close relatives of the subsurface methanogens enriched from the Minami-Kanto Gas Field (Mochimaru et al., 2007) or isolated from marine sediments (Shlimon et al., 2004) (**Figure 8**). Thus, previously unidentified subsurface electromethanogenic *Methanobacterium* microbes were enriched in our BES operation fed with seawater-based formation water from natural gas field.

The genera *Methanocalculus* and *Methanobrevibacter*, which are reported to be strictly hydrogenotrophic methanogens (Equation 1) (Thauer et al., 2008), were also abundant in cathode biofilms (**Figures 4–6**). The direct attachment on the

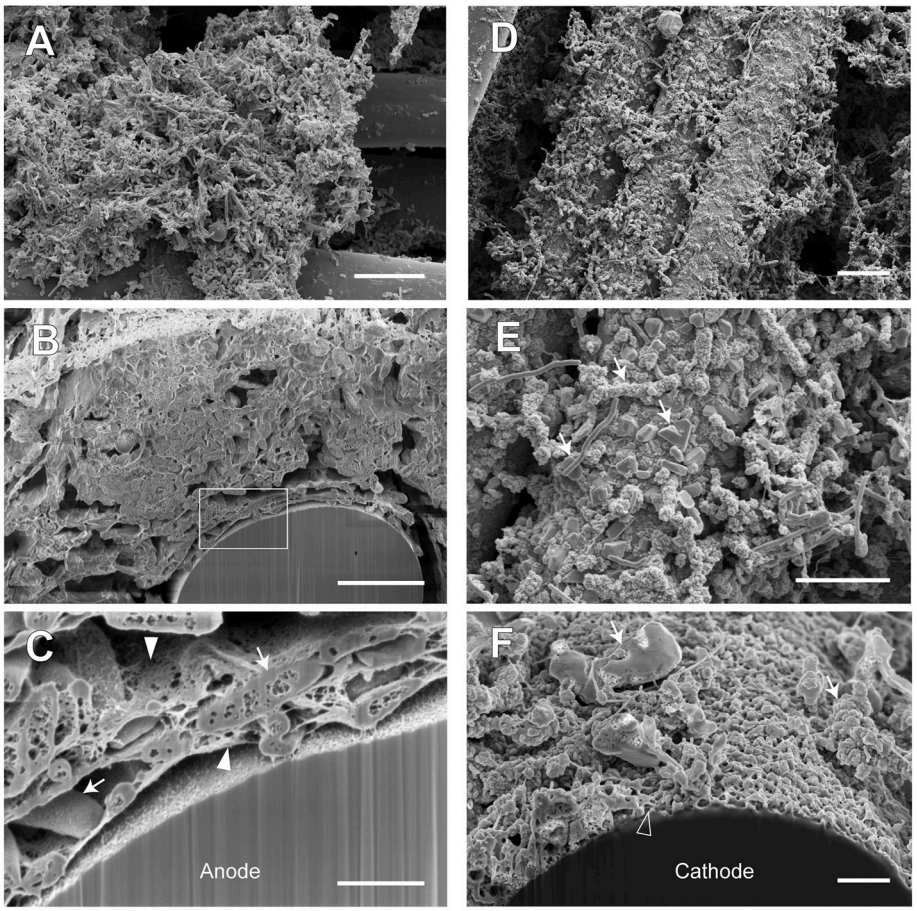

FIGURE 9 | FE-SEM images for anode and cathode biofilms adhering onto carbon cloth electrodes in the electromethanogenic BES reactor A. Anode **(A–C)** and cathode **(D–F)** samples were collected from BES reactor A after 19-month enrichment process. **B,C,F** are cross-section images of biofilms that were processed by a focused ion beam, and **(C)** shows a magnified image near electrode [rectangle region in **(B)**]. Arrows in **(C,E,F)** indicate microbes close to the electrodes. Filled arrowheads in **(C)** indicate filamentous mat structures in the anode biofilm, while open arrowhead in **(F)** indicates mesh-patterned structure in the cathode surface. Bars **(A,D)** =10 μm. Bars **(B,E)** = 5 μm. Bars **(C,F)** = 1 μm.

cathode electrode of many irregular clumps (**Figures 9E,F**) similar to *Methanocalculus* (Sorokin et al., 2015) suggests that this methanogen was playing a role in the electromethanogenic cathode of the reactor A, although this genus has not been reported in electromethanogenic communities (Blasco-Gómez et al., 2017) (**Table 2**). The phylogenetic positions of the BReur4 and BReur5 (**Figure 8**) revealed close relationship to the methanogens enriched from the Minami-Kanto Gas Field (Mochimaru et al., 2007) or isolated from sub-seafloor sediments (Imachi et al., 2011), which also implies that seawater-based formation water of the natural gas field introduced electromethanogenic archaea different from frequently observed *Methanobacterium* and *Methanothermobacter* (**Table 2**).

Two EET mechanisms have been proposed for the electromethanogenic reaction on a poised cathode electrode; one is direct electron uptake from the electrode to methanogens, the other is hydrogen/formate production on the cathode followed by a hydrogenotrophic methanogenic reaction (Blasco-Gómez et al., 2017). Our polarization analyses indicate that a cathodic potential of −800 mV vs. SHE at an input voltage of 600 mV (**Figure 3**) allowed hydrogen production on the cathode. Hydrogen-mediated methanogenesis was thereby made possible for the enriched subsurface methanogens. In contrast, the electromethanogenic biocathodes revealed single-layered biofilms anchored on the carbon fiber via filamentous appendages (**Figures 9**, **10**). The inclusion among the cathodic communities of numerous (>40%) methanogenic microbes suggests that direct electron transport from the electrode to the methanogens likely occurred in addition to hydrogen-mediated methanogenesis as reported elsewhere (Uchiyama et al., 2010; Lohner et al., 2014). Identification of the mechanism associated with the electromethanogenic reaction will require further investigation via electrochemical, biocatalytic, and MetaOmics analyses.

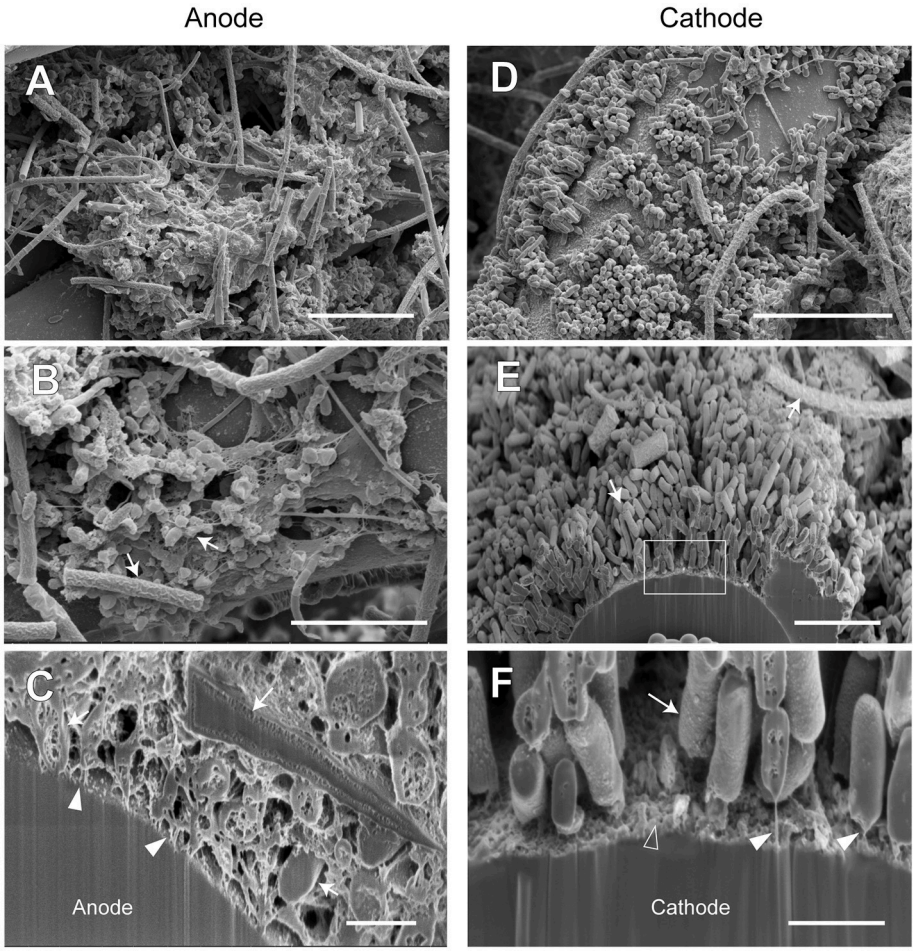

FIGURE 10 | FE-SEM images for anode and cathode biofilms adhering onto carbon cloth electrodes in the electromethanogenic BES reactor B. Anode **(A–C)** and cathode **(D–F)** samples were collected from BES reactor B after 19-month enrichment process. **B,E,F** are cross-section images of biofilms that were processed by a focused ion beam, and **(F)** shows a magnified image near electrode [rectangle region in **(E)**]. Arrows in **B,C,E,F** indicate microbes close to the electrodes. Filled arrowheads in **(C,F)** indicate filamentous structures in the anode biofilm, while open arrowhead in **(F)** indicates heterogeneous deposit on the cathode surface. Bars **(A, D)** =10 μm. Bars **(B, E)** = 5 μm. Bars **(C, F)** = 1 μm.

Acetate-Oxidizing Electrogenesis in Anode Biofilm

In the acetate-consuming electrogenic anodes, SEM images revealed remarkably thick biofilms with pili-like filamentous structures intertwined among the microbes and also between the electrode and microbes (**Figures 9**, **10**). Such morphologies have frequently been observed in EET-active anodic biofilms dominated by model acetate-oxidizing electrogenic *Geobacter* microbes (Ishii et al., 2008, 2014; Torres et al., 2009; Lovley, 2012). However, none of the abundantly observed *Deltaproteobacteria* OTUs was affiliated with genus *Geobacter* in this study (**Figure 7**). The two highly abundant OTUs in the anode biofilms were closely related to *Geoalkalibacter subterraneus*, which was isolated from a petroleum reservoir as an anaerobic metal reducing bacterium (Greene et al., 2009). The *Geoalkalibacter* microbe has also been used as a halophilic, anode-respiring bacterium for electricity production in a BES reactor with a controlling anode potential of +200 mV vs. SHE (Carmona-Martínez et al., 2013), which produced a higher current density (4.7 A/m^2) under saline conditions (3.5% NaCl) compared to the current density in this study (0.2–0.6 A/m^2, **Table 1**). The lower anode potential (−250 mV vs. SHE) in our BES reactors (**Figure 3**) and/or lower biocatalytic activity for cathodic electromethanogenic reaction may contribute to the difference.

In the early stage of the BES operation, various *Desulfuromonadaceae* OTUs dominated the electrogenic anode communities, but the two *Geoalkalibacter* OTUs subsequently became the key electrogenic microbial members (**Figures 4**–**6**). The shift of dominant *Deltaproteobacteria* members from *Desulfuromonadaceae* to *Geobacteraceae* was a common occurrence throughout community development in the BES reactors (Ishii et al., 2014, 2017). Holmes et al. reported that various *Desulfuromonas* phylotypes are enriched in an electrogenic biofilm inoculated with marine and saltmarsh sediments (Holmes et al., 2004). These features imply that these

TABLE 2 | Comparison of this work with other studies dealing with microbial community analyses in voltage-applied BESs and electromethanogenic BESs.

BES type	Applied voltage/ potential[c]	Temperature	Electrolyte	Original inocula	Current density	Anodic substrate	Dominant EET-active microbes in anode biofilm	Cathodic product	Dominant EET-active microbes in cathode biofilm[a,b]	References
Single chamber BES	600 mV	30°C	Seawater-based formation water	Natural gas field formation water	600 mA/m^2	Acetate	*Geoalkalibacter* (30–55%), *Desulfuromonas*, *Synergistaceae*	CH_4	*Methanobacterium* (10–15%), *Methanocalculus* (10–60%), *Synergistaceae*	This study
Single chamber BES	700 mV	55°C	Freshwater medium	Oil field formation water	3125 mA/m^2	Acetate	*Thermincola* (87%)	CH_4	*Methanothermobacter* (74%)[a], *Methanomethylovorans* (26%)[a]	Fu et al., 2015
High-pressure Single chamber BES	700 mV	55°C	Freshwater medium	Oil field formation water	1430 mA/m^{2d}	Acetate	*Coprothermobacter* and *Thermincola* (70%)	CH_4	*Methanothermobacter* (15%), *Thermodesulfobacteriaceae* (15%)	Kobayashi et al., 2017
Single chamber BES	1.25 V	28°C	Freshwater medium	Methophilic digestive sludge	595 mA/m^2	Acetate	*Geobacter* (23%)	CH_4	*Methanocorpusculum* (77%) [a]	Kobayashi et al., 2013
Two chamber MEC	700 mV	30°C	Freshwater medium	Anaerobic digester sludge	4250 mA/m^2	Acetate	*Geobacter* (15–45%), *Pseudomonadaceae*, *Desulfovibrio*	H_2	Pt-catalyzed	Hari et al., 2017
Two chamber BES	−500 mV vs. SHE	55°C	Freshwater medium	Oil field formation water	175 mA/m^2	Water	Abiotic	CH_4	*Methanothermobacter* (82%)[a], *Methanomethylovorans* (18%)[a]	Fu et al., 2015
Two chamber BES	−500 mV vs. SHE	25°C	Freshwater medium	Rice paddy soil	50 mA/m^2	Water	Abiotic	CH_4	*Methanobacterium* (2–25%), *Desulfovibrio* (25–60%), *Rhizobium* (5-50%)	Bretschger et al., 2015
Two chamber BES	−590 mV vs. SHE	25°C	Freshwater medium	Brewery wastewater sludge	na.	Water	Abiotic	CH_4	*Methanobacterium* (>93%)[a], *Methanobrevibacter*[a], *Sphingobacteriales* (37.7%)[b], *Spirochaetaceae*[b], *Synergistaceae*[b]	Marshall et al., 2012
Two chamber BES	−700 mV vs. SHE	nd	Freshwater medium	Activated sludge	600 mA/m^2	$K_4[Fe(II)(CN)_6]$	Abiotic	CH_4	*Methanobacterium*, *Methanobrevibacter*	Van Eerten-Jansen et al., 2013
Two chamber BES	−800 mV vs. SHE	30°C	Freshwater medium	Activated sludge	300 mA/m^2	Water	Abiotic	CH_4	*Methanobacterium*	Cheng et al., 2009

[a] *The dominant archaeal members were identified by using Archaea specific primers.*
[b] *The dominant bacterial members were identified by using Bacteria specific primers.*
[c] *Cathode potential was potentiostatically controlled in the two chamber BESs.*
[c] *The value was re-calculated from the projected surface area and the current.*

two genera, *Geoalkalibacter* and *Desulfuromonas*, likely function as an electrogenic microbe under saline conditions such as the formation waters of the natural gas field. The salinity of the formation water was seawater level (∼50 mS/cm), while that of freshwater medium was only ∼4 mS/cm (Ishii et al., 2014). This difference likely introduce *Geoalkalibacter* and *Desulfuromonas* microbes in the electrogenic anodic communities in this study instead of well-known *Geobacter* microbes (**Table 2**).

Features of Planktonic Cells

In the planktonic cells of the BES reactors and the inoculated formation waters, diverse *Gammaproteobacteria* OTUs were shown (**Figure 6**, **Supplementary Table S1**), and many of them are affiliated with well-characterized marine bacteria (Evans et al., 2008; Miyazaki et al., 2008). This result is appropriate for the enrichment process in the seawater-based formation water. Several *Gammaproteobacteria* microbes have been thoroughly studied as electrogenic microbes, including *Shewanella oneidensis* (Fredrickson et al., 2008) and *Aeromonas hydrophila* (Pham et al., 2003). In contrast, several marine *Gammaproteobacteria* species have been reported as electrotrophic members within biocathodic biofilms that consumed electrons via oxygen respiration: namely, "*Ca. Tenderia electrophaga*" in the family *Chromatiaceae* (Wang et al., 2015; Eddie et al., 2017) and *Marinobacter* spp. in the family *Alteromonadaceae* (Strycharz-Glaven et al., 2013). Although oxygen was not provided in this study, the appearance of diverse *Gammaproteobacteria* species in our BES system (**Figure 6**) suggests that they might be involved in the EET reaction by using another electron donor/acceptors.

Rare Microbial Taxa

OTUs belonging to phyla *Synergistetes*, *Chloroflexi,* and *Bacteroidetes* were frequently observed in the electromethanogenic BES reactors (**Figure 6**). The family *Synergistaceae* in phylum *Synergistetes* was abundantly observed in the reactor A, and the family has been reported as amino acid degraders (Dahle and Birkeland, 2006; Jumas-Bilak et al., 2009). Several microbes affiliated with family *Anaeroliniaceae* in phylum *Chloroflexi* were frequently observed in both anode and cathode biofilms (**Figure 6**). Members of this family are know to be fermenters, consuming sugars and/or peptides (Yamada et al., 2006), and have been documented as members of methanogenic consortia from deep subsurface microbiomes (Imachi et al., 2011) (**Supplementary Table S1**). The general role of *Bacteroidetes* (which were also commonly seen in the BES reactors) is the fermentation of sugars (Xu et al., 2003). The potential metabolic capabilities of these three taxa suggest that they may play important roles in stabilizing biofilms via degradation of cell lysate released by dead cells, secondary metabolites, and excess polysaccharide produced by other microbes.

Electromethanogenesis by Subsurface Microbiome

Deep subsurface biosphere is one of the frontiers for examining the DIET process to convert organic compounds to biogenic methane. If the DIET-related methanogenesis is occurring in subsurface environments, the process is possible to be stimulated by voltage addition in BES reactors. Recently, Sato et al. (2013) have proposed storing CO_2 in a subterranean geological reservoir and biologically converting the stored CO_2 to methane via *in situ* electromethanogenesis. Electromethanogenesis in a thermophilic, single-chamber BES under high-pressure conditions has been successfully carried out with an inoculation of subsurface microbes in the formation water from a petroleum reservoir. Electrogenic bacteria affiliated with the genus *Thermincola* were present on the anode, and a thermophilic methanogen belonging to the genus *Methanothermobacter* was present on the cathode (Kobayashi et al., 2017) (**Table 2**). The temperatures of used formation waters in this study are much lower (15–35°C) than the temperature of oil reservoir formation waters (45–91°C), while the formation waters at the Minami-Kanto gas field include a wide variety of methanogenic archaea among different production wells (Katayama et al., 2015). In this study, we identified that mesophilic subsurface methanogens affiliated with the genera *Methanobacterium* and *Methanocalculus* that enabled the electromethanogenic process to take place on the cathode, whereas the metabolism of mesophilic subsurface bacteria affiliated with the genus *Geoalkalibacter* released electrons on the anode. The taxonomic difference in the electromethanogenic enrichments between an oil reservoir and natural gas field was likely due to the different temperatures and salinity under the BES operations and/or *in situ* environments (**Table 2**).

CONCLUSION

We successfully stimulated EET-active subsurface microbes from the Minami-Kanto Gas field, and enriched the DIET-associated electromethanogenic microbes in the BES reactor. We used community dynamics and statistical analyses to correlate the genera *Methanobacterium*, *Methanobrevibacter,* and *Methanocalculus* with the electromethanogenic biocathode, while the genera *Geoalkalibacter* and *Desulfuromonas* were dominant at the acetate-oxidizing electrogenic bioanode. The genus *Methanosaeta* was a major competitor for the DIET-associated members by performing aceticlastic methanogenesis. The dominance of the *Methanosaeta* was induced by only a three day period of no-electron-flow (open circuit), and was not reversed by the voltage application during the time of our experiment. These discoveries are important for understanding the fundamental nature of EET-active communities established from an active subsurface microbiome. In addition, these DIET-associated subsurface microbiomes and the BES bioreactor system would be possible to apply bioelectrochemical power-to-gas (BEP2G), which is a potentially convenient way of storing renewable surplus electricity in the form of methane (Geppert et al., 2016). We will use MetaOmics approaches to further examine the metabolic roles and EET mechanisms in the electrogenic/electromethanogenic members (Ishii et al., 2013a, 2015, 2018), and try to apply the processes for the BEP2G in the near future.

AUTHOR CONTRIBUTIONS

SI designed and performed most of research. MO performed microbial community dynamics analysis. KU performed SEM observation. KK and DM performed formation water management. SI, HI, KN, and FI wrote the paper.

ACKNOWLEDGMENTS

We thank Takeru Ogatsu and Shoji Kunisue (Kanto Natural Gas Development Co., Ltd.) for supporting with the formation water sampling, Yuichi Hanada, Maya Hanada, Misako Utoh, and Kozue Mastuzaki for technical assistance in bioreactor construction, 16S rRNA sequencing and HPLC analyses. This work was supported by JSPS KAKENHI Grant Numbers 15H06906 and 17K19435.

SUPPLEMENTARY MATERIAL

The Supplementary Material for this article can be found online at: https://www.frontiersin.org/articles/10.3389/fenrg.2018.00144/full#supplementary-material

REFERENCES

Bartlett, K. B., and Harriss, R. C. (1993). Review and assessment of methane emissions from wetlands. *Chemosphere* 26, 261–320. doi: 10.1016/0045-6535(93)90427-7

Blasco-Gómez, R., Batlle-Vilanova, P., Villano, M., Balaguer, M. D., Colprim, J., and Puig, S. (2017). On the edge of research and technological application: a critical review of electromethanogenesis. *Int. J. Mol. Sci.* 18:874. doi: 10.3390/ijms18040874

Bretschger, O., Carpenter, K., Phan, T., Suzuki, S., Ishii, S., Grossi-Soyster, E., et al. (2015). Functional and taxonomic dynamics of an electricity-consuming methane-producing microbial community. *Bioresour. Technol.* 195, 254–264. doi: 10.1016/j.biortech.2015.06.129

Caporaso, J. G., Kuczynski, J., Stombaugh, J., Bittinger, K., Bushman, F. D., Costello, E. K., et al. (2010). QIIME allows analysis of high-throughput community sequencing data. *Nat Methods* 7, 335–336. doi: 10.1038/nmeth.f.303

Carmona-Martínez, A. A., Pierra, M., Trably, E., and Bernet, N. (2013). High current density via direct electron transfer by the halophilic anode respiring bacterium *Geoalkalibacter subterraneus*. *Phys. Chem. Chem. Phys.* 15, 19699–19707. doi: 10.1039/c3cp54045f

Cheng, S. A., Xing, D. F., Call, D. F., and Logan, B. E. (2009). Direct biological conversion of electrical current into methane by electromethanogenesis. *Environ. Sci. Technol.* 43, 3953–3958. doi: 10.1021/es803531g

Dahle, H., and Birkeland, N. K. (2006). *Thermovirga lienii* gen. nov. sp. nov. a novel moderately thermophilic, anaerobic, amino-acid-degrading bacterium isolated from a North Sea oil well. *Int. J. Syst. Evol. Microbiol.* 56, 1539–1545. doi: 10.1099/ijs.0.63894-0

de Bok, F. A., Plugge, C. M., and Stams, A. J. (2004). Interspecies electron transfer in methanogenic propionate degrading consortia. *Water Res.* 38, 1368–1375. doi: 10.1016/j.watres.2003.11.028

Eddie, B. J., Wang, Z., Hervey, W. J., Leary, D. H., Malanoski, A. P., Tender, L. M., et al. (2017). Metatranscriptomics supports the mechanism for biocathode electroautotrophy by "Candidatus *Tenderia electrophaga*". *mSystems* 2, e00002–e00017. doi: 10.1128/mSystems.00002-17

Edgar, R. C. (2010). Search and clustering orders of magnitude faster than BLAST. *Bioinformatics* 26, 2460–2461. doi: 10.1093/bioinformatics/btq461

Evans, F. F., Egan, S., and Kjelleberg, S. (2008). Ecology of type II secretion in marine gammaproteobacteria. *Environ. Microbiol.* 10, 1101–1107. doi: 10.1111/j.1462-2920.2007.01545.x

Fredrickson, J. K., Romine, M. F., Beliaev, A. S., Auchtung, J. M., Driscoll, M. E., Gardner, T. S. et al. (2008). Towards environmental systems biology of Shewanella. *Nat. Rev. Microbiol.* 6, 592–603. doi: 10.1038/nrmicro1947

Fu, Q., Kuramochi, Y., Fukushima, N., Maeda, H., Sato, K., and Kobayashi, H. (2015). Bioelectrochemical analyses of the development of a thermophilic biocathode catalyzing electromethanogenesis. *Environ. Sci. Technol.* 49, 1225–1232. doi: 10.1021/es5052233

Geppert, F., Liu, D. D., Van Eerten-Jansen, M., Weidner, E., Buisman, C., and Ter Heijne, A. (2016). Bioelectrochemical power-to-gas: state of the art and future perspectives. *Trends Biotechnol.* 34, 879–894. doi: 10.1016/j.tibtech.2016.08.010

Greene, A. C., Patel, B. K. C., and Yacob, S. (2009). *Geoalkalibacter subterraneus* sp nov., an anaerobic Fe(III)- and Mn(IV)-reducing bacterium from a petroleum reservoir, and emended descriptions of the family *Desulfuromonadaceae* and the genus *Geoalkalibacter*. *Int. J. Syst. Evol. Microbiol.* 59, 781–785. doi: 10.1099/ijs.0.001537-0

Hari, A. R., Venkidusamy, K., Katuri, K. P., Bagchi, S., and Saikaly, P. E. (2017). Temporal microbial community dynamics in microbial electrolysis cells - influence of acetate and propionate concentration. *Front. Microbiol.* 8:1371. doi: 10.3389/fmicb.2017.01371

Hirai, M., Nishi, S., Tsuda, M., Sunamura, M., Takaki, Y., and Nunoura, T. (2017). Library construction from subnanogram DNA for pelagic sea water and deep-sea sediments. *Microbes Environ.* 32, 336–343. doi: 10.1264/jsme2.ME17132

Holmes, D. E., Bond, D. R., O'neil, R. A., Reimers, C. E., Tender, L. R., and Lovley, D. R. (2004). Microbial communities associated with electrodes harvesting electricity from a variety of aquatic sediments. *Microb. Ecol.* 48, 178–190. doi: 10.1007/s00248-003-0004-4

Ijiri, A., Inagaki, F., Kubo, Y., Adhikari, R. R., Hattori, S., Hoshino, T., et al. (2018). Deep-biosphere methane production stimulated by geofluids in the Nankai accretionary complex. *Sci. Adv.* 4:eaao4631. doi: 10.1126/sciadv.aao4631

Imachi, H., Aoi, K., Tasumi, E., Saito, Y., Yamanaka, Y., Saito, Y., et al. (2011). Cultivation of methanogenic community from subseafloor sediments using a continuous-flow bioreactor. *ISME J.* 5, 1913–1925. doi: 10.1038/ismej.2011.64

Inagaki, F., Hinrichs, K. U., Kubo, Y., Bowles, M. W., Heuer, V. B., Hong, W. L., et al. (2015). Exploring deep microbial life in coal-bearing sediment down to ∼2.5 km below the ocean floor. *Science* 349, 420–424. doi: 10.1126/science.aaa6882

Ishii, S., Kosaka, T., Hori, K., Hotta, Y., and Watanabe, K. (2005). Coaggregation facilitates interspecies hydrogen transfer between *Pelotomaculum thermopropionicum* and *Methanothermobacter thermautotrophicus*. *Appl. Environ. Microbiol.* 71, 7838–7845. doi: 10.1128/AEM.71.12.7838-7845.2005

Ishii, S., Kosaka, T., Hotta, Y., and Watanabe, K. (2006). Simulating the contribution of coaggregation to interspecies hydrogen fluxes in syntrophic methanogenic consortia. *Appl. Environ. Microbiol.* 72, 5093–5096. doi: 10.1128/AEM.00333-06

Ishii, S., Suzuki, S., Norden-Krichmar, T. M., Phan, T., Wanger, G., Nealson, K. H., et al. (2014). Microbial population and functional dynamics associated with surface potential and carbon metabolism. *ISME J.* 8, 963–978. doi: 10.1038/ismej.2013.217

Ishii, S., Suzuki, S., Norden-Krichmar, T. M., Tenney, A., Chain, P. S., Scholz, M. B., et al. (2013a). A novel metatranscriptomic approach to identify gene expression dynamics during extracellular electron transfer. *Nat. Commun.* 4:1601. doi: 10.1038/ncomms2615

Ishii, S., Suzuki, S., Norden-Krichmar, T. M., Wu, A., Yamanaka, Y., Nealson, K. H., et al. (2013b). Identifying the microbial communities and operational conditions for optimized wastewater treatment in microbial fuel cells. *Water Res.* 47, 7120–7130. doi: 10.1016/j.watres.2013.07.048

Ishii, S., Suzuki, S., Tenney, A., Nealson, K. H., and Bretschger, O. (2018). Comparative metatranscriptomics reveals extracellular electron transfer pathways conferring microbial adaptivity to surface redox potential changes. *ISME J.* 12, 2844–2863. doi: 10.1038/s41396-018-0238-2.

Ishii, S., Suzuki, S., Tenney, A., Norden-Krichmar, T. M., Nealson, K. H., and Bretschger, O. (2015). Microbial metabolic networks in a complex electrogenic biofilm recovered from a stimulus-induced metatranscriptomics approach. *Sci Rep* 5:14840. doi: 10.1038/srep14840

Ishii, S., Suzuki, S., Yamanaka, Y., Wu, A., Nealson, K. H., and Bretschger, O. (2017). Population dynamics of electrogenic microbial communities in microbial fuel cells started with three different inoculum sources. *Bioelectrochemistry* 117, 74–82. doi: 10.1016/j.bioelechem.2017.06.003

Ishii, S., Watanabe, K., Yabuki, S., Logan, B. E., and Sekiguchi, Y. (2008). Comparison of electrode reduction activities of *Geobacter sulfurreducens* and an enriched consortium in an air-cathode microbial fuel cell. *Appl. Environ. Microbiol.* 74, 7348–7355. doi: 10.1128/AEM.01639-08

Jumas-Bilak, E., Roudière, L., and Marchandin, H. (2009). Description of '*Synergistetes*' phyl. nov. and emended description of the phylum '*Deferribacteres*' and of the family *Syntrophomonadaceae*, phylum '*Firmicutes*'. *Int. J. Syst. Evol. Microbiol.* 59, 1028–1035. doi: 10.1099/ijs.0.006718-0

Katayama, T., Yoshioka, H., Muramoto, Y., Usami, J., Fujiwara, K., Yoshida, S., et al. (2015). Physicochemical impacts associated with natural gas development on methanogenesis in deep sand aquifers. *ISME J.* 9, 436–446. doi: 10.1038/ismej.2014.140

Kato, S., Hashimoto, K., and Watanabe, K. (2012). Microbial interspecies electron transfer via electric currents through conductive minerals. *PNAS* 109, 10042–10046. doi: 10.1073/pnas.1117592109

Kato, S., Hashimoto, K., and Watanabe, K. (2013). Iron-oxide minerals affect extracellular electron-transfer paths of *Geobacter* spp. *Microbes Environ.* 28, 141–148. doi: 10.1264/jsme2.ME12161

Kita, A., Suehira, K., Miura, T., Okamura, Y., Aki, T., Matsumura, Y., et al. (2016). Characterization of a halotolerant acetoclastic methanogen highly enriched from marine sediment and its application in removal of acetate. *J. Biosci. Bioeng.* 121, 196–202. doi: 10.1016/j.jbiosc.2015.05.018

Kobayashi, H., Nagashima, A., Kouyama, M., Fu, Q., Ikarashi, M., Maeda, H., et al. (2017). High-pressure thermophilic electromethanogenic system producing methane at 5 MPa, 55°C. *J. Biosci. Bioeng.* 124, 327–332. doi: 10.1016/j.jbiosc.2017.04.001

Kobayashi, H., Saito, N., Fu, Q., Kawaguchi, H., Vilcaez, J., Wakayama, T., et al. (2013). Bio-electrochemical property and phylogenetic diversity of microbial communities associated with bioelectrodes of an electromethanogenic reactor. *J. Biosci. Bioeng.* 116, 114–117. doi: 10.1016/j.jbiosc.2013.01.001

Kvenvolden, K. A. (1995). A review of the geochemistry of methane in natural gas hydrate. *Organ. Geochem.* 23, 997–1008. doi: 10.1016/0146-6380(96)00002-2

Lever, M. A., Rogers, K. L., Lloyd, K. G., Overmann, J., Schink, B., Thauer, R. K., et al. (2015). Life under extreme energy limitation: a synthesis of laboratory- and field-based investigations. *FEMS Microbiol. Rev.* 39, 688–728. doi: 10.1093/femsre/fuv020

Logan, B. E. (2009). Exoelectrogenic bacteria that power microbial fuel cells. *Nat. Rev. Microbiol.* 7, 375–381. doi: 10.1038/nrmicro2113

Lohner, S. T., Deutzmann, J. S., Logan, B. E., Leigh, J., and Spormann, A. M. (2014). Hydrogenase-independent uptake and metabolism of electrons by the archaeon *Methanococcus maripaludis*. *ISME J.* 8, 1673–1681. doi: 10.1038/ismej.2014.82

Lovley, D. R. (2012). Electromicrobiology. *Annu. Rev. Microbiol.* 66, 391–409. doi: 10.1146/annurev-micro-092611-150104

Lovley, D. R. (2017). Happy together: microbial communities that hook up to swap electrons. *ISME J.* 11, 327–336. doi: 10.1038/ismej.2016.136

Mao, C. L., Feng, Y. Z., Wang, X. J., and Ren, G. X. (2015). Review on research achievements of biogas from anaerobic digestion. *Renew. Sust. Energy Rev.* 45, 540–555. doi: 10.1016/j.rser.2015.02.032

Marshall, C. W., Ross, D. E., Fichot, E. B., Norman, R. S., and May, H. D. (2012). Electrosynthesis of commodity chemicals by an autotrophic microbial community. *Appl. Environ. Microbiol.* 78, 8412–8420. doi: 10.1128/AEM.02401-12

Martin, M. (2011). Cutadapt removes adapter sequences from high-throughput sequencing reads. *EMBnet J* 17, 10–12. doi: 10.14806/ej.17.1.200

Matthews, E., and Fung, I. (1987). Methane eission from natural wetlands: global distribution, area, and environmental characteristics of sources. *Global Biogeochem. Cycles* 1, 61–86. doi: 10.1029/GB001i001p00061

McGlynn, S. E. (2017). Energy metabolism during anaerobic methane oxidation in ANME Archaea. *Microbes Environ.* 32, 5–13. doi: 10.1264/jsme2.ME16166

Miyazaki, M., Nogi, Y., Fujiwara, Y., Kawato, M., Kubokawa, K., and Horikoshi, K. (2008). *Neptunomonas japonica* sp nov., an *Osedax japonicus* symbiont-like bacterium isolated from sediment adjacent to sperm whale carcasses off Kagoshima, Japan. *Int. J. Syst. Evol. Microbiol.* 58, 866–871. doi: 10.1099/ijs.0.65509-0

Mochimaru, H., Uchiyama, H., Yoshioka, H., Imachi, H., Hoaki, T., Tamaki, H., et al. (2007). Methanogen diversity in deep subsurface gas-associated water at the Minami-kanto gas field in Japan. *Geomicrobiol. J.* 24, 93–100. doi: 10.1080/01490450701266571

Nunoura, T., Takaki, Y., Kazama, H., Hirai, M., Ashi, J., Imachi, H., et al. (2012). Microbial diversity in deep-sea methane seep sediments presented by SSU rRNA gene tag sequencing. *Microbes Environ.* 27, 382–390. doi: 10.1264/jsme2.ME12032

Pham, C. A., Jung, S. J., Phung, N. T., Lee, J., Chang, I. S., Kim, B. H., et al. (2003). A novel electrochemically active and Fe(III)-reducing bacterium phylogenetically related to *Aeromonas hydrophila*, isolated from a microbial fuel cell. *FEMS Microbiol Lett.* 223, 129–134. doi: 10.1016/S0378-1097(03)00354-9

Quast, C., Pruesse, E., Yilmaz, P., Gerken, J., Schweer, T., Yarza, P., et al. (2013). The SILVA ribosomal RNA gene database project: improved data processing and web-based tools. *Nucleic Acids Res.* 41, D590–596. doi: 10.1093/nar/gks1219

Rabaey, K., and Rozendal, R. A. (2010). Microbial electrosynthesis - revisiting the electrical route for microbial production. *Nat. Rev. Microbiol.* 8, 706–716. doi: 10.1038/nrmicro2422

Rotaru, A. E., Shrestha, P. M., Liu, F. H., Shrestha, M., Shrestha, D., Embree, M., et al. (2014). A new model for electron flow during anaerobic digestion: direct interspecies electron transfer to *Methanosaeta* for the reduction of carbon dioxide to methane. *Energy Environ. Sci.* 7, 408–415. doi: 10.1039/C3EE42189A

Sano, Y., Kinoshita, N., Kagoshima, T., Takahata, N., Sakata, S., Toki, T., et al. (2017). Origin of methane-rich natural gas at the West Pacific convergent plate boundary. *Sci. Rep.* 7:15646. doi: 10.1038/s41598-017-15959-5

Sato, K., Kawaguchi, H., and Kobayashi, H. (2013). Bio-electrochemical conversion of carbon dioxide to methane in geological storage reservoirs. *Energy Convers. Manag.* 66, 343–350. doi: 10.1016/j.enconman.2012.12.008

Schink, B. (1997). Energetics of syntrophic cooperation in methanogenic degradation. *Microb. Mol. Biol. Rev.* 61, 262–280.

Shlimon, A. G., Friedrich, M. W., Niemann, H., Ramsing, N. B., and Finster, K. (2004). Methanobacterium aarhusense sp. nov. a novel methanogen isolated from a marine sediment (Aarhus Bay, Denmark). *Int. J. Syst. Evol. Microbiol.* 54, 759–763. doi: 10.1099/ijs.0.02994-0

Siegert, M., Yates, M. D., Spormann, A. M., and Logan, B. E. (2015). Methanobacterium dominates biocathodic archaeal communities in methanogenic microbial electrolysis cells. *ACS Sustain. Chem. Eng.* 3, 1668–1676. doi: 10.1021/acssuschemeng.5b00367

Smith, K. S., and Ingram-Smith, C. (2007). Methanosaeta, the forgotten methanogen? *Trends Microbiol.* 15, 150–155. doi: 10.1016/j.tim.2007.02.002

Sorokin, D. Y., Abbas, B., Merkel, A. Y., Rijpstra, W. I., Damste, J. S., Sukhacheva, M. V., et al. (2015). *Methanosalsum natronophilum* sp. nov. and *Methanocalculus alkaliphilus* sp. nov. haloalkaliphilic methanogens from hypersaline soda lakes. *Int. J. Syst. Evol. Microbiol.* 65, 3739–3745. doi: 10.1099/ijsem.0.000488

Strycharz-Glaven, S. M., Glaven, R. H., Wang, Z., Zhou, J., Vora, G. J., and Tender, L. M. (2013). Electrochemical investigation of a microbial solar cell reveals a nonphotosynthetic biocathode catalyst. *Appl. Environ. Microbiol.* 79, 3933–3942. doi: 10.1128/AEM.00431-13

Suzuki, S., Ishii, S., Wu, A., Cheung, A., Tenney, A., Wanger, G., et al. (2013). Microbial diversity in The Cedars, an ultrabasic, ultrareducing, and low salinity serpentinizing ecosystem. *Proc. Natl. Acad. Sci. U.S.A.* 110, 15336–15341. doi: 10.1073/pnas.1302426110

Terbraak, C. J. F. (1986). Canonical correspondence-analysis - a new eigenvector technique for multivariate direct gradient analysis. *Ecology* 67, 1167–1179. doi: 10.2307/1938672

Thauer, R. K., Kaster, A. K., Seedorf, H., Buckel, W., and Hedderich, R. (2008). Methanogenic archaea: ecologically relevant differences in energy conservation. *Nat. Rev. Microbiol.* 6, 579–591. doi: 10.1038/nrmicro1931

Torres, C. I., Krajmalnik-Brown, R., Parameswaran, P., Marcus, A. K., Wanger, G., Gorby, Y. A., et al. (2009). Selecting anode-respiring bacteria based on anode potential: phylogenetic, electrochemical, and microscopic characterization. *Environ. Sci. Technol.* 43, 9519–9524. doi: 10.1021/es902165y

Uchiyama, T., Ito, K., Mori, K., Tsurumaru, H., and Harayama, S. (2010). Iron-corroding methanogen isolated from a crude-oil storage tank. *Appl. Environ. Microbiol.* 76, 1783–1788. doi: 10.1128/AEM.00668-09

Van Eerten-Jansen, M. C., Veldhoen, A. B., Plugge, C. M., Stams, A. J., Buisman, C. J., and Ter Heijne, A. (2013). Microbial community analysis of a methane-producing biocathode in a bioelectrochemical system. *Archaea* 2013:481784. doi: 10.1155/2013/481784

Wang, Z., Leary, D. H., Malanoski, A. P., Li, R. W., Hervey, W. J., Eddie, B. J., et al. (2015). A previously uncharacterized, nonphotosynthetic member of the *Chromatiaceae* is the primary CO2-fixing constituent in a self-regenerating biocathode. *Appl. Environ. Microbiol.* 81, 699–712. doi: 10.1128/AEM.02947-14

Xu, J., Bjursell, M. K., Himrod, J., Deng, S., Carmichael, L. K., Chiang, H. C., et al. (2003). A genomic view of the human-Bacteroides thetaiotaomicron symbiosis. *Science* 299, 2074–2076. doi: 10.1126/science.1080029

Yamada, T., Sekiguchi, Y., Hanada, S., Imachi, H., Ohashi, A., Harada, H., et al. (2006). Anaerolinea thermolimosa sp. nov. *Levilinea saccharolytica* gen. nov. sp. nov. and *Leptolinea tardivitalis* gen. nov. sp. nov. novel filamentous anaerobes, and description of the new classes *Anaerolineae classis* nov. and *Caldilineae classis* nov. in the bacterial phylum *Chloroflexi. Int. J. Syst. Evol. Microbiol.* 56, 1331–1340. doi: 10.1099/ijs.0.64169-0

Yu, Z., Leng, X., Zhao, S., Ji, J., Zhou, T., Khan, A., et al. (2018). A review on the applications of microbial electrolysis cells in anaerobic digestion. *Bioresour. Technol.* 255, 340–348. doi: 10.1016/j.biortech.2018.02.003

Zhang, J., Kobert, K., Flouri, T., and Stamatakis, A. (2014). PEAR: a fast and accurate Illumina Paired-End reAd mergeR. *Bioinformatics* 30, 614–620. doi: 10.1093/bioinformatics/btt593

Conflict of Interest Statement: KK and DM were employed by Kanto Natural Gas Development Co., Ltd.

The remaining authors declare that the research was conducted in the absence of any commercial or financial relationships that could be construed as a potential conflict of interest.

Advantages of publishing in Frontiers

OPEN ACCESS
Articles are free to read for greatest visibility and readership

FAST PUBLICATION
Around 90 days from submission to decision

HIGH QUALITY PEER-REVIEW
Rigorous, collaborative, and constructive peer-review

TRANSPARENT PEER-REVIEW
Editors and reviewers acknowledged by name on published articles

Frontiers
Avenue du Tribunal-Fédéral 34
1005 Lausanne | Switzerland

Visit us: www.frontiersin.org
Contact us: info@frontiersin.org | +41 21 510 17 00

REPRODUCIBILITY OF RESEARCH
Support open data and methods to enhance research reproducibility

DIGITAL PUBLISHING
Articles designed for optimal readership across devices

FOLLOW US
@frontiersin

IMPACT METRICS
Advanced article metrics track visibility across digital media

EXTENSIVE PROMOTION
Marketing and promotion of impactful research

LOOP RESEARCH NETWORK
Our network increases your article's readership